MODELING NEURODEGENERATION IN YEAST

EDITED BY: Ralf J. Braun and Sabrina Büttner
PUBLISHED IN: Frontiers in Molecular Neuroscience

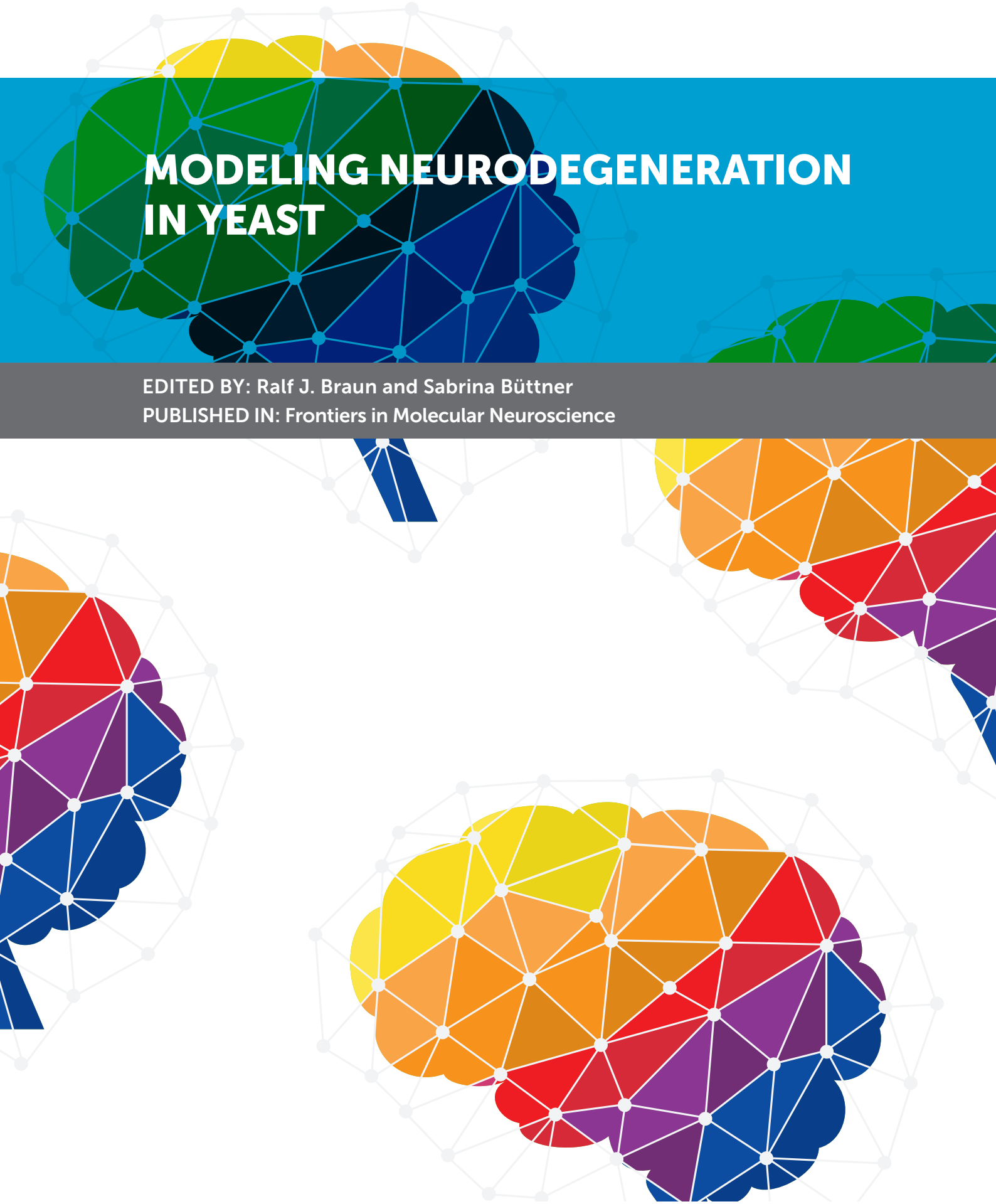

frontiers Research Topics

frontiers

ISSN 1664-8714
ISBN 978-2-88971-549-7
DOI 10.3389/978-2-88971-549-7

About Frontiers

Frontiers is more than just an open-access publisher of scholarly articles: it is a pioneering approach to the world of academia, radically improving the way scholarly research is managed. The grand vision of Frontiers is a world where all people have an equal opportunity to seek, share and generate knowledge. Frontiers provides immediate and permanent online open access to all its publications, but this alone is not enough to realize our grand goals.

Frontiers Journal Series

The Frontiers Journal Series is a multi-tier and interdisciplinary set of open-access, online journals, promising a paradigm shift from the current review, selection and dissemination processes in academic publishing. All Frontiers journals are driven by researchers for researchers; therefore, they constitute a service to the scholarly community. At the same time, the Frontiers Journal Series operates on a revolutionary invention, the tiered publishing system, initially addressing specific communities of scholars, and gradually climbing up to broader public understanding, thus serving the interests of the lay society, too.

Dedication to Quality

Each Frontiers article is a landmark of the highest quality, thanks to genuinely collaborative interactions between authors and review editors, who include some of the world's best academicians. Research must be certified by peers before entering a stream of knowledge that may eventually reach the public - and shape society; therefore, Frontiers only applies the most rigorous and unbiased reviews.
Frontiers revolutionizes research publishing by freely delivering the most outstanding research, evaluated with no bias from both the academic and social point of view. By applying the most advanced information technologies, Frontiers is catapulting scholarly publishing into a new generation.

What are Frontiers Research Topics?

Frontiers Research Topics are very popular trademarks of the Frontiers Journals Series: they are collections of at least ten articles, all centered on a particular subject. With their unique mix of varied contributions from Original Research to Review Articles, Frontiers Research Topics unify the most influential researchers, the latest key findings and historical advances in a hot research area! Find out more on how to host your own Frontiers Research Topic or contribute to one as an author by contacting the Frontiers Editorial Office: frontiersin.org/about/contact

MODELING NEURODEGENERATION IN YEAST

Topic Editors:
Ralf J. Braun, Danube Private University, Austria
Sabrina Büttner, Stockholm University, Sweden

Citation: Braun, R. J., Büttner, S., eds. (2021). Modeling Neurodegeneration in Yeast. Lausanne: Frontiers Media SA. doi: 10.3389/978-2-88971-549-7

Table of Contents

05 ***Editorial: Modeling Neurodegeneration in Yeast***
Ralf J. Braun and Sabrina Büttner

07 ***Interplay of Energetics and ER Stress Exacerbates Alzheimer's Amyloid-β (Aβ) Toxicity in Yeast***
Xin Chen, Markus M. M. Bisschops, Nisha R. Agarwal, Boyang Ji, Kumaravel P. Shanmugavel and Dina Petranovic

23 ***Q-Rich Yeast Prion [PSI+] Accelerates Aggregation of Transthyretin, a Non-Q-Rich Human Protein***
Meenakshi Verma, Amandeep Girdhar, Basant Patel, Nirmal K. Ganguly, Ritushree Kukreti and Vibha Taneja

35 ***Sumoylation Protects Against β-Synuclein Toxicity in Yeast***
Blagovesta Popova, Alexandra Kleinknecht, Patricia Arendarski, Jasmin Mischke, Dan Wang and Gerhard H. Braus

52 ***Different Expression Levels of Human Mutant Ubiquitin B^{+1} (UBB^{+1}) Can Modify Chronological Lifespan or Stress Resistance of* Saccharomyces cerevisiae**
Ana Joyce Muñoz-Arellano, Xin Chen, Andrea Molt, Eugenio Meza and Dina Petranovic

67 ***The Enzymatic Core of the Parkinson's Disease-Associated Protein LRRK2 Impairs Mitochondrial Biogenesis in Aging Yeast***
Andreas Aufschnaiter, Verena Kohler, Corvin Walter, Sergi Tosal-Castano, Lukas Habernig, Heimo Wolinski, Walter Keller, F.-Nora Vögtle and Sabrina Büttner

82 ***Yeast as a Model to Unravel Mechanisms Behind FUS Toxicity in Amyotrophic Lateral Sclerosis***
Michelle Lindström and Beidong Liu

92 ***The Insoluble Protein Deposit (IPOD) in Yeast***
Stephanie Rothe†, Abaya Prakash and Jens Tyedmers

101 ***Studying Spatial Protein Quality Control, Proteopathies, and Aging Using Different Model Misfolding Proteins in* S. cerevisiae**
Kara L. Schneider, Thomas Nyström and Per O. Widlund

114 ***Studying Huntington's Disease in Yeast: From Mechanisms to Pharmacological Approaches***
Sebastian Hofer, Katharina Kainz, Andreas Zimmermann, Maria A. Bauer, Tobias Pendl, Michael Poglitsch, Frank Madeo and Didac Carmona-Gutierrez

134 ***A Mitochondria-Associated Oxidative Stress Perspective on Huntington's Disease***
Ju Zheng, Joris Winderickx, Vanessa Franssens and Beidong Liu

144 ***ALS Yeast Models—Past Success Stories and New Opportunities***
Sonja E. Di Gregorio and Martin L. Duennwald

157 ***Exploiting Post-mitotic Yeast Cultures to Model Neurodegeneration***
Andrea Ruetenik and Antonio Barrientos

175 ***The Impact of ESCRT on $A\beta_{1-42}$ Induced Membrane Lesions in a Yeast Model for Alzheimer's Disease***
Gernot Fruhmann, Christelle Marchal, Hélène Vignaud, Mathias Verduyckt, Nicolas Talarek, Claudio De Virgilio, Joris Winderickx and Christophe Cullin

191 ***Yeast Models of Prion-Like Proteins That Cause Amyotrophic Lateral Sclerosis Reveal Pathogenic Mechanisms***
Zachary T. Monahan, Shannon N. Rhoads, Debra S. Yee and Frank P. Shewmaker

frontiers in Molecular Neuroscience

EDITORIAL
published: 01 March 2021
doi: 10.3389/fnmol.2021.645190

Editorial: Modeling Neurodegeneration in Yeast

Ralf J. Braun[1]* *and Sabrina Büttner*[2,3]*

[1] Research Division for Neurodegenerative Diseases, Center of Biosciences, Danube Private University, Krems an der Donau, Austria, [2] Department of Molecular Biosciences, The Wenner-Gren Institute, Stockholm University, Stockholm, Sweden, [3] Institute of Molecular Biosciences, University of Graz, Graz, Austria

Keywords: neurodegeneration, yeast, proteopathy, aggregation, cellular fitness

Editorial on the Research Topic

Modeling Neurodegeneration in Yeast

Most age-associated neurodegenerative disorders, including Alzheimer's, Parkinson's, Huntington's, and motoneuron disorders, are characterized by mislocalization, misfolding, and aggregation of disease-specific proteins in distinct neuronal cell populations and are therefore classified as proteopathies (Klaips et al., 2018). While diverse and partially redundant quality control mechanisms are in place to sustain proteostasis and cellular function, the accumulation of aggregation-prone proteins poses a constant burden on the proteostasis systems. With progressing cellular age, different quality control systems functionally decline, and long-lived cells such as neurons are particularly sensitive to misfolding and aggregation of proteotoxic proteins. Disease-associated oligomers and aggregates are directed to distinct protein quality control compartments, thereby compromising overall cellular fitness and survival. Proteopathies are commonly affected by disturbances of protein quality control subroutines, but also by impaired vesicle trafficking and critical mitochondrial damage. For dissecting pivotal interactions among different cellular pathways in the context of proteotoxicity, various cellular models have been established, including the baker's yeast *Saccharomyces cerevisiae* (Braun et al., 2010). *S. cerevisiae* is a genetically amenable unicellular eukaryotic model organism with a high degree of evolutionary conservation, in particular in respect to fundamental cellular processes such as protein quality control pathways, mitochondrial function and vesicle transport. Humanized yeast models based on the expression of human disease-associated aggregation-prone proteins have been successfully used to delineate molecular pathways underlying the loss of cellular fitness. In the Research Topic "*Modeling Neurodegeneration in Yeast,*" we invited researchers to critically summarize recent developments and to present novel data using yeast to study human proteopathies.

The review of Ruetenik and Barrientos provides an overview of the advantages of post-mitotic yeast cultures to model neurodegenerative protein misfolding disorders and summarizes suitable methodology. Thus, this manuscript is of special interest for people new to the field. The reviews from Schneider et al. and Rothe et al. describe the distinct cellular protein quality control compartments in which human disease-associated and aggregation-prone proteins are deposited and discuss why and in which cellular context specific proteotoxic proteins prefer distinct quality control compartments.

The reviews from Hofer et al. and Zheng et al. address yeast models for Huntington's disease (HD), for which many yeast models have been developed so far. The manuscripts give a comprehensive and critical overview of the applied yeast models expressing fragments of the human protein huntingtin, responsible for HD. They describe how these models can be used for pharmacological approaches, and include a mitochondria-associated perspective on Huntington's disease.

OPEN ACCESS

Edited and reviewed by:
David Blum,
INSERM U1172 Centre de Recherche Jean Pierre Aubert, France

***Correspondence:**
Ralf J. Braun
ralf.braun@dp-uni.ac.at
Sabrina Büttner
sabrina.buettner@su.se

Received: *22 December 2020*
Accepted: *05 February 2021*
Published: *01 March 2021*

Citation:
Braun RJ and Büttner S (2021) Editorial: Modeling Neurodegeneration in Yeast. Front. Mol. Neurosci. 14:645190. doi: 10.3389/fnmol.2021.645190

Di Gregorio et al., Monahan et al., and Lindström and Liu critically review yeast models for amyotrophic lateral sclerosis (ALS), the most common motoneuron disease. They summarize how yeast ALS models expressing the common ALS-associated proteins TDP-43 and FUS have been successfully used to unravel the molecular mechanisms underlying disease progression.

For Alzheimer's disease (AD), the Research Topic comprises three original studies. One of the pathological hallmarks of AD is the accumulation of the small hydrophobic peptide β-amyloid exerting extra- and intracellular toxicity (Goedert and Spillantini, 2006). Chen et al. and Fruhmann et al. use yeast β-amyloid models to elucidate the intricate interplay between energetics, ER stress and β-amyloid toxicity, with a particular focus on the pathophysiological membrane lesions triggered by β-amyloid. Besides β-amyloid, a mutant variant of ubiquitin, namely UBB^{+1}, accumulates in disease-affected neurons in AD. High levels of UBB^{+1} have been described to be detrimental in neurons and yeast cells (Braun et al., 2015). Using yeast expressing UBB^{+1}, Muñoz-Arellano et al. challenge this paradigm, showing that UBB^{+1} expression can induce a beneficial stress response. Thus, depending on the cellular context, UBB^{+1} may also enable the cells to cope with proteotoxic stress, which has been confirmed by a more recent study (Verheijen et al., 2020).

For Parkinson's disease (PD), two original studies are included in the Research Topic. Popova et al. provides novel insights on β-synuclein, a homolog of the PD-associated protein α-synuclein. The authors observed that β-synuclein, just as α-synuclein, triggers toxicity in yeast. Of interest, post-translational modification of β-synuclein, namely sumoylation, protects cells from this toxicity. Aufschnaiter et al. worked with another important PD-associated protein, the protein kinase LRRK2. The authors could show that the enzymatic core of this protein compromises mitochondrial function in yeast. While general mitochondrial dysfunction is a well-established hallmark for PD, this study demonstrates that LRRK2 inhibits mitochondrial biogenesis, thus providing a novel perspective on cellular demise during PD.

Finally, Verma et al. could show in their original study that the aggregation of human transthyretin is modulated by yeast prions, thereby confirming the strong interaction of this human protein with the yeast quality control system.

Collectively, this Research Topic highlights the power of yeast models to understand fundamental molecular mechanisms contributing to human proteopathies. We would like to thank all the authors and reviewers contributing to this project. We anticipate numerous novel findings, relevant for human neurodegenerative disorders, based on studies in yeast.

AUTHOR CONTRIBUTIONS

All authors listed have made a substantial, direct and intellectual contribution to the work, and approved it for publication.

REFERENCES

Braun, R. J., Büttner, S., Ring, J., Kroemer, G., and Madeo, F. (2010). Nervous yeast: modeling neurotoxic cell death. *Trends Biochem. Sci.* 35, 135–144. doi: 10.1016/j.tibs.2009.10.005

Braun, R. J., Sommer, C., Leibiger, C., Gentier, R. J. G., Dumit, V. I., Paduch, K., et al. (2015). Accumulation of basic amino acids at mitochondria dictates the cytotoxicity of aberrant ubiquitin. *Cell Rep.* 10, 1557–1571. doi: 10.1016/j.celrep.2015.02.009

Goedert, M., and Spillantini, M. G. (2006). A century of Alzheimer's disease. *Science* 314, 777–781. doi: 10.1126/science.1132814

Klaips, C. L., Jayaraj, G. G., and Hartl, F. U. (2018). Pathways of cellular proteostasis in aging and disease. *J. Cell Biol.* 217, 51–63. doi: 10.1083/jcb.201709072

Verheijen, B. M., Lussier, C., Müller-Hübers, C., Garruto, R. M., Oyanagi, K., Braun, R. J., et al. (2020). Activation of the unfolded protein response and proteostasis disturbance in parkinsonism-dementia of guam. *J. Neuropathol. Exp. Neurol.* 79, 34–45. doi: 10.1093/jnen/nlz110

Conflict of Interest: The authors declare that the research was conducted in the absence of any commercial or financial relationships that could be construed as a potential conflict of interest.

frontiers in Molecular Neuroscience

ORIGINAL RESEARCH
published: 27 July 2017
doi: 10.3389/fnmol.2017.00232

Interplay of Energetics and ER Stress Exacerbates Alzheimer's Amyloid-β (Aβ) Toxicity in Yeast

*Xin Chen[1‡], Markus M. M. Bisschops[1†‡], Nisha R. Agarwal[2†], Boyang Ji[1], Kumaravel P. Shanmugavel[2] and Dina Petranovic[1,3]**

[1] Division of Systems and Synthetic Biology, Department of Biology and Biological Engineering, Chalmers University of Technology, Gothenburg, Sweden, [2] Division of Chemical Biology, Department of Biology and Biological Engineering, Chalmers University of Technology, Gothenburg, Sweden, [3] Novo Nordisk Foundation Center for Biosustainability, Chalmers University of Technology, Gothenburg, Sweden

OPEN ACCESS

Edited by:
Ralf J. Braun, University of Bayreuth, Germany

Reviewed by:
Julia Ring, University of Graz, Austria
Vanessa Franssens, KU Leuven, Belgium
Bruce Morgan, Kaiserslautern University of Technology, Germany

***Correspondence:**
Dina Petranovic
dina.petranovic@chalmers.se

†Present Address:
Markus M. M. Bisschops, Department of Biotechnology, Delft University of Technology, Delft, Netherlands;
Nisha R. Agarwal, Department of Chemistry and Chemical Biology, Biointerfaces Institute, McMaster University, Hamilton, Ontario, CA, Canada

‡*These authors have contributed equally to this work.*

Received: *04 April 2017*
Accepted: *06 July 2017*
Published: *27 July 2017*

Citation:
Chen X, Bisschops MMM, Agarwal NR, Ji B, Shanmugavel KP and Petranovic D (2017) Interplay of Energetics and ER Stress Exacerbates Alzheimer's Amyloid-β (Aβ) Toxicity in Yeast. Front. Mol. Neurosci. 10:232. doi: 10.3389/fnmol.2017.00232

Alzheimer's disease (AD) is a progressive neurodegeneration. Oligomers of amyloid-β peptides (Aβ) are thought to play a pivotal role in AD pathogenesis, yet the mechanisms involved remain unclear. Two major isoforms of Aβ associated with AD are Aβ40 and Aβ42, the latter being more toxic and prone to form oligomers. Here, we took a systems biology approach to study two humanized yeast AD models which expressed either Aβ40 or Aβ42 in bioreactor cultures. Strict control of oxygen availability and culture pH, strongly affected chronological lifespan and reduced variations during cell growth. Reduced growth rates and biomass yields were observed upon Aβ42 expression, indicating a redirection of energy from growth to maintenance. Quantitative physiology analyses furthermore revealed reduced mitochondrial functionality and ATP generation in Aβ42 expressing cells, which matched with observed aberrant mitochondrial structures. Genome-wide expression level analysis showed that Aβ42 expression triggered strong ER stress and unfolded protein responses. Equivalent expression of Aβ40, however, induced only mild ER stress, which resulted in hardly affected physiology. Using AD yeast models in well-controlled cultures strengthened our understanding on how cells translate different Aβ toxicity signals into particular cell fate programs, and further enhance their potential as a discovery platform to identify possible therapies.

Keywords: amyloid-β, Alzheimer's disease, energetics, ER stress, yeast

INTRODUCTION

Alzheimer's disease (AD) is the most common form of neurodegenerative disorder, and its incidence is projected to rise due to the increasing life expectancy (Wyss-Coray, 2016). Due to incomplete knowledge on the underlying mechanisms that lead to cellular dysfunction in AD, it is difficult to design effective therapies. Accumulation of amyloid-β (Aβ) plaques in the brain is a key neuropathological feature of AD (Hardy and Selkoe, 2002). Aβ peptides (ranging in length from 39 to 43 amino acids) are generated by amyloidogenic processing of the transmembrane amyloid precursor protein (APP; Selkoe, 2001). Differential cleavage of APP produces two major Aβ peptide isoforms, Aβ40 and Aβ42, of which Aβ40 is most abundantly produced, but Aβ42 is the predominant isoform found in AD plaques (Younkin, 1998). Aβ42 is also more hydrophobic and prone to aggregation than Aβ40 (Jarrett et al., 1993). Increasing evidence suggests that oligomeric

species of Aβ are the most toxic forms (McLean et al., 1999; Shankar et al., 2008) and the accumulation of intracellular Aβ42 oligomers may be an early event in AD pathogenesis (Gouras et al., 2005).

The strong conservation of the cellular protein quality control system between yeast and human, combined with its genetic accessibility and ease of manipulation and cultivation, make the yeast *Saccharomyces cerevisiae* a powerful model organism to study protein-misfolding pathologies caused by Aβ (Khurana and Lindquist, 2010). Over the past two decades, several humanized yeast models have been developed to study Aβ toxicity (Fruhmann et al., 2017). The earlier models have been successfully used to monitor aggregation patterns of Aβ (Bagriantsev and Liebman, 2006; von der Haar et al., 2007), but failed to recapitulate its toxic effects. More recently developed models illustrated the importance of intracellular trafficking for Aβ toxicity (Treusch et al., 2011; D'Angelo et al., 2013). In neurons, APP is processed to generate Aβ peptides through the secretory pathway as well as the endocytic pathway (Thinakaran and Koo, 2008). This progression through different intracellular organelles and vesicles has been recapitulated in yeast by fusion of the Aβ peptide to secretion signal sequences, i.e., the Kar2 or α-prepro targeting signals (Treusch et al., 2011; D'Angelo et al., 2013). Expression of human Aβ peptides with the ER Kar2 signal ensures that Aβ peptides transit through the secretory pathway and are eventually exported from the cytoplasm. However, the yeast cell wall prevents secreted Aβ from diffusing away, and Aβ peptides re-enter into the cell through endocytosis (Treusch et al., 2011). Similar to observations in human neurons and other AD model organisms (Luheshi et al., 2007), Aβ42 peptides form more oligomers than Aβ40 and exhibit an increased cellular toxicity in yeast (Treusch et al., 2011). These models captured important aspects of Aβ toxicity and identified the yeast homologs of phosphatidylinositol binding clathrin assembly protein (*PICALM*) and other endocytic factors to be involved in Aβ toxicity (Treusch et al., 2011; D'Angelo et al., 2013; Verduyckt et al., 2016).

Although these models capture the cellular trafficking processes essential to Aβ toxicity, the heterologous Aβ expression in yeast is different from native expression in human neurons. In humanized yeast models, expression of Aβ peptides is often under control of a strong inducible promotor, whereas the production in neurons is constitutively. This inducible type of expression allows for well-timed induction of acute cytotoxicity, but is accompanied by a drastic change in carbon-source and hence metabolism, and excludes capturing effects of cellular aging or cumulative effects on toxicity. To avoid these drawbacks, we developed a continuous and tightly regulated Aβ expression model, which mimicked the chronic cytotoxicity that occurs during AD progression better. In our model, we successfully expressed human Aβ peptides (Aβ40 and Aβ42) in a constitutive manner, resulting in a shorter chronological life span (CLS) and increased oxidative stress. Furthermore, strong links between mitochondrial dysfunction and reduced proteasome activity were observed upon mild expression of Aβ42 peptide (Chen and Petranovic, 2015). Here, we take advantage of this improved humanized yeast model to further exploit the effects of Aβ on cellular functioning, viability and energetics following a systems biology approach.

The complexity of AD is illustrated by the continued interplay of unbalanced networks and homeostatic networks in neurons (Castrillo and Oliver, 2015). To capture these dynamics at the molecular and cellular level, time-course analyses of yeast Aβ models are needed. A crucial prerequisite to extract relevant information from the large amount of data obtained (e.g., genome-wide expression profile analysis), is minimization of confounding variables. The widely used shake-flask or tube cultures suffer from several important drawbacks, including lack of online monitoring and continuous control of cultivation parameters (Klöckner and Büchs, 2012), that influence cell growth and physiology and thus hinder data interpretation (Burtner et al., 2011). Therefore, we considered bioreactors an optimal system in which parameters can be continuously monitored and controlled. In addition, analysis of in- and off-gas compositions, aids in evaluating the energetic efficiencies of growth. Monitoring these parameters is relevant for *S. cerevisiae* as a model organism to estimate the interplay of metabolism, energetics, and mitochondrial functions. The typical growth curve consists of an initially predominantly fermentative, fast exponential growth phase (EX) until glucose is exhausted. Then it is followed by slower, fully respiratory growth on ethanol, glycerol, and organic acids during the post-diauxic shift phase (PD). Finally, growth is arrested due to depletion of extracellular carbon sources and the culture enters stationary phase (SP). Transition through these phases heavily depends on culture conditions (Herman, 2002) and strongly influences cell survival during SP (Bisschops et al., 2015). Although bioreactor cultivation offers strong advantages over more simple culture techniques, it is rarely applied in studies of humanized yeast models.

Subjecting our improved humanized Aβ yeast model to strictly controlled and monitored bioreactor environments, allow us, for the first time, to study how cell physiology and genome-wide expression levels are affected by different Aβ variants over time (**Figure 1**). By controlling the culture parameters, we reduced the number of irrelevant and sidetracking variables and produced a considerable amount of genome-wide and physiological information concerning the energetic consequences of Aβ expression, as well as revealing how these different Aβ toxic isoforms interfered with cellular metabolism and stress response pathways, causing pronounced physiological effects.

MATERIALS AND METHODS

Yeast Strains and Plasmids

The auxotrophic yeast *S. cerevisiae* strain CEN.PK.113-5D (*MATa ura3-52 HIS3*, *LEU2 TRP1 MAL2-8^c SUC2*; kindly provided by Dr. P. Kötter, University of Frankfurt, Germany; Entian and Kötter, 2007) was used as a host strain in this study. The host strain was transformed with the plasmids for constitutive and equivalent expression of Aβ42 and Aβ40, under control of the *GPD1* promoter: p416GPD-Aβ42 and p416GPD-Aβ40, respectively. The detailed construction of these plasmids and

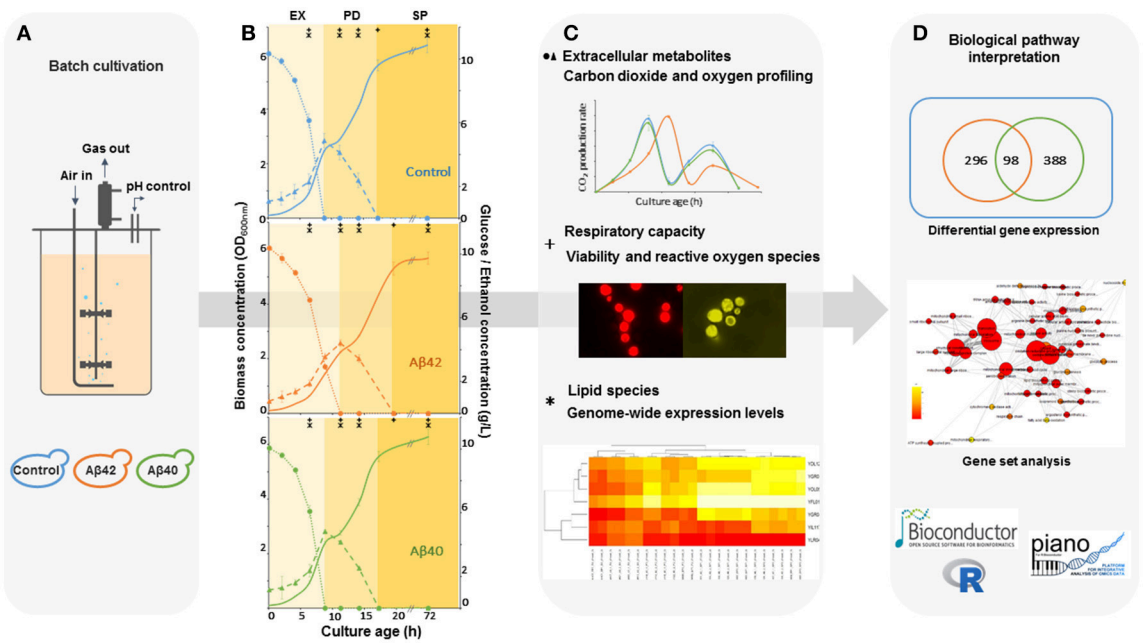

FIGURE 1 | Schematic workflow for the integrated analysis of Aβ-induced cytotoxicity in *S. cerevisiae*. **(A)** Batch cultures of control, Aβ42 and Aβ40 expressing strains were grown and compared in well-controlled bioreactors. **(B)** Biomass, glucose (•), and ethanol (Δ) concentrations were measured and used to divide growth into exponential (EX), post-diauxic shift (PD), and stationary phases (SP). Time-points of specific analyses mentioned in **(C)** are indicated by $^{+}$ and *. **(C)** Samples were taken for analysis of physiology, lipidome, and transcriptome during different growth phases. **(D)** The data obtained were collected and integrated, resulting in an overall biological interpretation of intracellular Aβ toxicity.

strains has been reported previously (Chen and Petranovic, 2015). Both Aβ constructs consist of the Kar2 signal sequence (42 amino acids) in front of Aβ42 or Aβ40 sequence, as described previously (Treusch et al., 2011).

Batch Cultivation

Strains were grown in defined minimal medium as described previously (Chen and Petranovic, 2015), containing per liter: 10 g glucose, 5 g $(NH_4)_2SO_4$, 3 g KH_2PO_4, 0.5 g $MgSO_4.7H_2O$, 125 µl antifoam 204 (Sigma-Aldrich, USA), trace metals solution, and vitamins. Trace metals and vitamins solutions were prepared as described previously (Jensen et al., 2014). Batch fermentations were performed at 30°C in 1.2-l bioreactors (DasGip, Germany) with a working volume of 700 ml. Cultures were operated with 800 rpm agitation and 1 vvm gas flow of either pure dried air (aerobic) or dried air mixed with nitrogen gas to obtain a mixture containing 2% oxygen (micro-aerobic). Culture pH was measured with a pH sensor (Mettler Toledo, Switzerland) and maintained at 5.0 by automated addition of 2 M KOH or 2 M H_2SO_4. The CO_2 and O_2 concentrations in the exhaust gas were analyzed real-time with a GA4 gas analyzer (DasGip, Germany).

Determination of Biomass and Extracellular Metabolites

Biomass and extracellular metabolites were determined as described previously (Zhou et al., 2016). Biomass concentrations were measured as the optical density at 600 nm (OD_{600}) and cell dry weight (CDW). CDW was measured by filtering 5 ml of culture samples over a pre-weighted, pre-dried 0.45 µm nitrocellulose filter (Sartorius Stedim, Germany), microwave drying of the filter plus biomass and determining the increase in weight of the dried filter. During the different growth phases, OD/CDW ratios were constant (1.45 ± 0.04 OD/g l^{-1}). Extracellular glucose, ethanol, glycerol and acetate concentrations were analyzed on an Ultimate 3000 HPLC (Dionex, Sunnyvale, USA) equipped with an Aminex HPX-87H column (Bio Rad, USA). The column was eluted at 45°C using 5 mM H_2SO_4 at a flow rate of 0.6 ml min^{-1}.

Glycogen and Trehalose Assays

Ten OD_{600} of cells were harvested by centrifugation at 2,000 × *g* for 5 min at 4°C, and washed once in ice-cold distilled water. Cell pellets were resuspended in boiling 0.25 M Na_2CO_3 solution and processed as described previously (Parrou and François, 1997). Glycogen and trehalose were converted into glucose with amyloglucosidase (Sigma-Aldrich) and trehalase (Sigma-Aldrich), respectively, in acidic environment (pH 5.2). Glucose levels were determined enzymatically using a Glucose (HK) assay kit (Sigma-Aldrich).

Viability and Reactive Oxygen Species (ROS) Measurement

Viability and intracellular ROS were measured by propidium iodide (PI, Thermo Fisher Scientific, USA) and dihydrorhodamine 123 (DHR123, Sigma-Aldrich, USA) staining respectively, as described previously (Chen and Petranovic,

2015). For the staining, 0.5 OD_{600} of cells were taken at different phases and incubated with 0.5 μg ml^{-1} of PI or 5 μM of DHR123 for 20 min. Cells were analyzed with a Guava flow cytometer (Merck, Germany) using a 488 nm laser for excitation. Fluorescence was detected with a 690/50 filter for PI or a 525/30 nm filter for rhodamine 123. Five thousand cells were analyzed for each sample. Two populations could be distinguished based on fluorescence intensity. Positively stained cells fall within the more fluorescent population (mean fluorescence 5–100 times higher). Results are shown as the fractions stained positively by PI or DHR123.

Determination of Respiratory Capacity

Five OD_{600} of cells were harvested, washed twice in distilled water and resuspended in PBS before measurement. Oxygen consumption was measured at 30°C in a 1 ml temperature controlled closed chamber with a Clark oxygen electrode (Gilson) as described previously (Albers et al., 2007). One milliliter of PBS was added to the chamber and incubated until baseline (100% dissolved O_2) was stable. One OD_{600} of cells were added to the chamber to measure the endogenous oxygen consumption rate. When the rate was stable, 25 mM of glucose was added to the chamber to obtain the initial oxygen consumption rate with glucose. Sodium thiosulfate (NaS_2O_3) was used for the zero-point calibration of the sensors. Oxygen consumption rates were determined from the slope of a plot of oxygen concentration vs. time and expressed as mM/OD/h.

Non-linear Microscopy

One OD_{600} of cells were harvested during PD. Mitochondria were stained with 1 μg ml^{-1} Rhodamine 123 (Rh123, Sigma-Aldrich, USA) for 30 min and washed once in PBS. One OD_{600} of cells was harvested during EX for lipid droplets measurement. Non-linear microscopy was applied to detect lipid droplets and mitochondria signals as described previously (Mertz, 2004). Two laser beams, 817 (5 mW) and 1,064 nm (6 mW) of synchronized pico-second pulse trains were spatially and temporally overlapped to be coupled into an inverted Nikon microscope (Eclipse TE2000-E microscope). CARS and TPEF signals were generated in live yeast cells to monitor lipid droplets and Rh123 stained mitochondria, respectively. The laser beams were focused on the samples using a 40x objective (Nikon Plan Fluor N.A. 1.3, working distance 0.21 mm). CARS and TPEF signals were collected in forward and epi-direction, respectively, with a high NA lens with a 661/20 and 514/30 or 609/45 filter into a single photon counting (SPC) photomultiplier tube (HPM-100-40, Becker & Hickl GmbH). Z-stacks were acquired for each sample with 0.2 μm step size for a maximum of 10 μm sample thickness. Each single acquisition in the z-stack was taken in 1 sec with a resolution of 256 pixels for a 34.4 μm field of view. The images were opened in ImageJ and then processed in Imaris (Bitplane software for image processing). The lipid quantification for control and Aβ42 expressing cells was done by ImageJ and GIMP (GNU Image Manipulation Program). Statistics was performed for 10 images of each strain. The quantities were determined from the CARS channel in which lipids were detected. The channel was turned into a binary color format (0 and 1) in GIMP first for lipids and their area in each slice (Li, i = slice number) was calculated using ImageJ. Subsequently cell areas in each slice (Ci, i = slice number) were also calculated. The ratio of the summation of lipid area / summation of cell area gave the value of lipid content in a cell as shown in Equation 1. The distance between slices (Δz) was canceled out since it was constant for all cells.

$$\frac{\sum_i Li}{\sum_i Ci} = Volume\ of\ lipids\ in\ a\ given\ cell\ volume \quad (1)$$

Transcriptome Analysis

Samples for microarray analysis were taken from duplicate cultures during EX, PD, SP1, and SP2, respectively. Samples of cells were frozen rapidly in liquid nitrogen to prevent mRNA turnover (Piper et al., 2002). Total RNA was extracted using the RNeasy Mini Kit (QIAGEN, Germany) with a FastPrep homogenizer (MP Biomedicals, USA) to disrupt cells. Quality of total RNA was assessed by an Agilent 2100 bioanalyzer (Agilent Technologies, USA). Further RNA preparation and hybridization of biotin-conjugated aRNA fragments to Yeast Genome 2.0 Arrays (Affymetrix GeneChip, USA) was performed by the Bioinformatics and Expression Analysis core facility (BEA) of the Karolinska Institute, Sweden. Microarray data are deposited at the Genome Expression Omnibus website (GEO, http://www.ncbi.nlm.nih.gov/geo/) with series number GSE94793. Raw RNA data (CEL files) were preprocessed by Bioconductor and R version 3.2.3. The PIANO package was used for gene ontology (GO) terms and gene set analysis (GSA; Väremo et al., 2013). Only gene sets significantly enriched by distinctly up or down-regulated genes ($p < 0.05$) were considered in this study. The KEGG pathway and Gene Ontology functional categories enrichment analysis were used to investigate the transcriptional regulation of lipogenesis by using online software tool David (Database for Annotation, Visualization, and Integrated Discovery, http://david.abcc.ncifcrf.gov; Huang et al., 2008). Adjusted $P < 0.05$ and fold changes <0.81 or >1.2 were used as thresholds to identify significantly differentially expressed genes. Pheatmap package (https://cran.r-project.org/web/packages/pheatmap/index.html) was used to generate clustered heatmaps of gene sets.

Quantitative Real-Time PCR (qPCR)

qPCR was performed as previously described (Liu et al., 2016). cDNA was synthesized from 1 μg of total RNA using the QuantiTect Reverse Transcription Kit (QIAGEN, Germany). Two microliters of synthesized cDNA were used as the template for qPCR with the DyNAmo Flash SYBR Green qPCR kit (Thermo Fisher Scientific, USA). Housekeeping gene *ACT1* was used as a reference gene to normalize RNA levels. Used primer sets are listed in **Table S4**.

Lipid Extraction and HPLC-CAD Analysis

Lipid extraction and separation were performed as described previously (Khoomrung et al., 2013). Ten micrograms of freeze-dried cells were mixed with 7 ml of chloroform:methanol (2:1, v/v) solution in extraction tubes containing 50 μg of

cholesterol as internal standard. Each tube was vigorously vortexed and placed in microwave reaction vessel (12 × 3cm I.D., 0.5 cm thickness, Milestone Stard D, Italy) which was heated to 60°C within 6 min and kept at 60°C for 10 min. After the sample was cooled down to room temperature, 1.7 ml of NaCI was added and the tube was vortexed vigorously. Thereafter, the sample was centrifuged at 1,912 *g* for 10 min and the organic phase was transferred into a clean extraction tube. Organic solvent was evaporated and residues dissolved in 200 μl of chloroform:methanol (2:1, v/v) for HPLC-CAD analysis (Corona, USA). Lipid peaks were identified based on the spectrum of a standard mix (SE, TAG, CH, ES, PA, CL, PE, PC, PS, and PI). Quantification of lipids was performed using serial dilutions of the standard mix from concentrations of 10–1,000 μg ml^{-1}. The average $\log_{10}$ of peak area was plotted against $\log_{10}$ of concentration. Correlation (r^2) was determined for all standard curves by linear regression.

Statistical Analyses

Significance of differences observed in physiological parameters between strains were determined using two-tailed, student *t*-tests. Cultures were independent replicates and, as parameters were determined using identical procedures, student *t*-tests were performed as two-sample with equal variance. Unless specified explicitly, three independent replicate cultures of the Aβ42 and control strains and two independent replicate cultures of the Aβ40 strain were analyzed under both fully aerated and micro-aerobic conditions. $P < 0.05$ was considered to indicate significant differences. Values are represented as mean ± SEM.

RESULTS

Physiological Characterization of Humanized Yeast Aβ Strains in Controlled Bioreactor Cultures

To determine the effects of human Aβ peptides on *S. cerevisiae* growth characteristics, strains constitutively expressing either human Aβ42 or Aβ40 peptide (hereafter referred to as Aβ42 and Aβ40 strain) or carrying the empty vector (control strain) were grown in well-aerated bioreactors using glucose as carbon-source (**Figures 1A,B**). Physiological parameters from these cultures are presented in **Table 1**. The maximal specific growth rate of the Aβ42 strain was 17% lower than that of the control and Aβ40 strains ($p < 0.0003$), in accordance with our previous report (Chen and Petranovic, 2015). The Aβ42 strain also showed a less pronounced but significantly decreased maximal glucose uptake rate ($p = 0.02$), which was reflected by 15% reduced biomass yield during EX ($p < 0.02$). Maximal ethanol production rates were not significantly altered ($p > 0.4$) during EX. On the contrary, we observed substantially increased production of two fermentation products: glycerol and acetate (**Table 1**). Glycerol yields were increased in both Aβ strains ($p < 0.01$), but was highest in the Aβ42 strain (2.7-fold compared to control strain, $p < 0.00005$). Despite the well-aerated conditions, the Aβ42 strain also produced more acetate than control and Aβ40 strains (1.28- and 1.21-fold compared to control and Aβ40 strains, respectively, $p < 0.01$). Overall these results suggest an altered redox-cofactor balancing in the heterologous Aβ42 expressing strain (Bakker et al., 2001). During SP, cells rely heavily on the storage carbohydrates glycogen and trehalose as energy sources. No significant differences in the accumulation of glycogen were observed among these strains (**Figure S1A**). Levels of trehalose were significantly higher in the Aβ42 strain during PD and SP1 (when extracellular carbon source was depleted; **Figure S1B**), which may be linked to its alternative role in stress-resistance. Trehalose can stabilize proteins in their native folding during heat shock and reduce the aggregation of denatured proteins in yeast cells (Singer and Lindquist, 1998). Reduced viable cell fractions might explain reduced growth and substrate consumption rates in the Aβ42 strain. However, viability analysis showed that fractions of dead cells were low for all strains during different phases (<2.5%). The slightly, yet significantly, elevated fractions of dead cells in Aβ42 cultures ($p < 0.007$, **Figure S2A**), did not fully explain the observed differences in fermentation kinetics.

Aβ42 Expression Strongly Affects Mitochondrial Functionality

Mitochondria are pivotal to the survival of cells, including neurons, due to their role in energy metabolism. The increased glycerol production in the Aβ42 strain suggested that the surplus of NADH produced in anabolism, could not be completely reoxidized by mitochondrial respiration (**Table 1**). Despite the differences in glycerol and acetate production, the maximal oxygen uptake rates during the fully respiratory PD phase were surprisingly similar for both Aβ strains, yet lower than

TABLE 1 | The physiological parameters of all strains during aerobic batch cultivation.

Strain	μ_{max} [a] (/h)	$r_{glucose,max}$ [b] (g/g/h)	$Y^{c}_{X/S}$ (g/g)	$Y^{d}_{glycerol/S}$ (mCmol/Cmol)	$C^{e}_{acetate,max}$ (mmol/L)	$r^{f}_{ethanol,max}$ (g/g/h)	Respiratory quotient[g]	$r^{h}_{O2,max}$ (mmol/g/h)
Control	0.368 ± 0.002	2.34 ± 0.05	0.39 ± 0.01	13.5 ± 1.5	3.6 ± 0.2	0.24 ± 0.02	0.42 ± 0.01	8.2 ± 0.5
Aβ40[i]	0.366 ± 0.004	2.27 ± 0.09	0.40 ± 0.03	20.4* ± 0.5	3.8 ± 0.2	0.25 ± 0.01	0.44 ± 0.01	7.4 ± 0.2
Aβ42	0.304* ± 0.003	2.18* ± 0.05	0.36* ± 0.01	35.3* ± 1.4	4.6* ± 0.1	0.22 ± 0.01	0.40 ± 0.02	7.5 ± 0.2

Values are represented as the average of three independent biological replicates ± SEM. The asterisk (*) indicates significant different values from the control strain parameters ($p < 0.05$). a, Maximal biomass-specific growth rate on glucose; b, Maximal biomass-specific glucose uptake rate; c, Final biomass yields on substrate; d, Glycerol yields on glucose; e, Maximal acetate concentrations; f, Maximal biomass-specific ethanol consumption rate during PD; g, Respiratory quotient, the ratio of carbon dioxide produced over oxygen consumed during PD; h, Maximal biomass-specific oxygen uptake rate during PD; i, Average values from biological duplicates.

control strain (**Table 1**). These observations suggested that not consumption of oxygen *per se*, but rather its usage was affected specifically by Aβ42 expression. Together with our previous observations that the respiratory rate of the Aβ42 strain was significantly reduced in ethanol-grown cultures (Chen and Petranovic, 2015), this suggests that the toxicity triggered by Aβ42 might involve reduced mitochondrial functionality. To further test this, we evaluated the respiratory capacity of all strains during different growth phases. During EX no significant differences were observed between strains, which matched with fermentation being the main catabolic pathway at this phase. However, during the subsequent phases (PD and SP1), the respiratory capacity of the Aβ42 strain was significantly decreased compared to both other strains ($p < 0.05$, **Figure 2A**). Impaired mitochondrial function can lead to excess reactive oxygen species (ROS) production which contributes to AD pathology (Livnat-Levanon et al., 2014). In the Aβ42 strain, the ROS-positive fractions were significantly increased during phases of high metabolic activity, i.e., EX and PD, compared to the other strains ($p < 0.003$, **Figure S2B**). To investigate if these physiological indications of mitochondrial dysfunction coincided with aberrant mitochondrial structures, we stained the mitochondria with Rhodamine 123 and employed TPEF (two-photon excited fluorescence) microscopy to investigate the morphology in fully respiratory growing cells. Control cells exhibited continuous mitochondrial structures (networks), whereas Aβ42 expressing cells displayed a more fragmented structure of mitochondria (**Figure 2C** and **Videos S1**, **S2**). Such fragmented structures of mitochondria were previously observed in aged yeast cells and could enhance the turn-over of damaged mitochondria by mitophagy (Mao and Klionsky, 2013; Breitenbach et al., 2014).

Oxygen-Limited Conditions Enhance Impact of Aβ42 Expression on Physiology

The affected mitochondrial functionality is likely to have a more severe impact on cells under oxygen-limited conditions. Oxygen limitation is common due to increased oxygen-requirements during PD in less-controlled cultivations, such as shake-flasks, in which oxygen-transfer rates are lower (Anderlei and Büchs, 2001). We also noticed this effect by the differences in viability of the same Aβ42 strain reported here (**Figure S1**) and previously in shake-flasks (Chen and Petranovic, 2015). In standard bioreactor cultures, the dissolved oxygen levels were maintained above 30% of saturation at all time, but to test the combinatorial effect of oxygen limitation and Aβ peptides expression on cell physiology, oxygen-limited cultivations were also performed. To this end, the oxygen concentration in the inflowing gas was reduced to 2%, leading to dissolved oxygen levels below 1% of saturation. The reduced dissolved oxygen levels only reduced the maximal

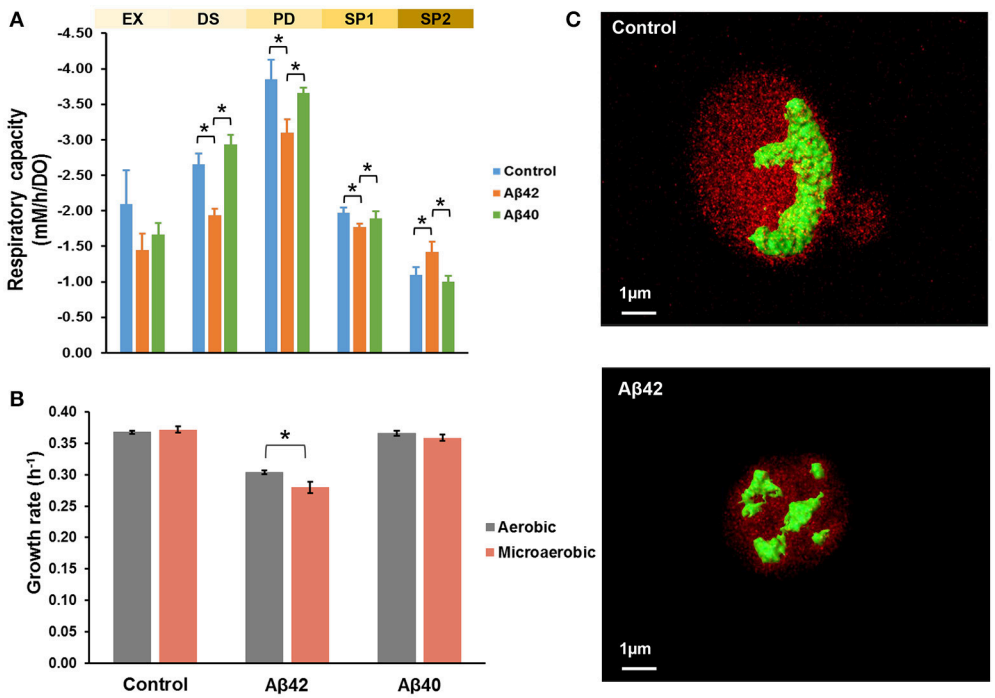

FIGURE 2 | Aβ42 expression causes abnormal mitochondrial functionality and morphology. **(A)** Respiratory capacity was measured during EX, diauxic shift (DS), PD, early SP (SP1), and late SP (SP2) phases. Measurements were performed in duplicate (Aβ40) or triplicate (control and Aβ42) during EX, DS, SP1, and SP2 phases. During PD phase, measurements were done in quadruplicate (Aβ40 strain) or sextuplicate (control and Aβ42 strains), when cells solely relied on respiration. **(B)** Comparison of growth rates between aerobic and microaerobic conditions in bioreactors. **(C)** TPEF microscopy images of representative mitochondrial morphology in PD from control and Aβ42-expressing cells. Mitochondria were stained by Rhodamine 123 and are shown in green. The background fluorescence of cells is shown in red and is indicative of the cell volume. Data shown are average values ± SEM, of triplicate (Aβ42 and control) or duplicate (Aβ40) independent biological replicates. The asterisk (*) indicates significant differences ($p < 0.05$).

growth rate of the Aβ42 strain on glucose significantly (8% reduction, $p < 0.05$) and did not significantly affect growth of control and Aβ40 strains (**Figure 2B**). Similarly, total biomass yields were only significantly reduced in the Aβ42 strain (13% reduction, $p = 0.05$; **Table S1**). Under well-aerated, standard conditions, we observed differences in maximal oxygen uptake rates between Aβ42 and control strains (**Table 1**). When the oxygen supply was severely limited, oxygen uptake rates were also restricted and differences between strains were absent (**Table S1**). However, despite these equal oxygen consumption rates, the Aβ42 strain produced less carbon dioxide as shown by the almost one-third reduction in respiratory quotient (defined as the ratio of carbon dioxide produced/oxygen consumed) compared to control strain ($p < 0.05$, **Table S1**). This indicates an altered usage of the oxygen consumed by the Aβ42 strain, likely due to less efficient respiration. In addition to these effects on physiology, oxygen limitation also resulted in a doubling of the fraction of dead cells in all strains (<6%; **Figure S2A**). The ROS-positive fractions were similar compared to well-aerated conditions for all strains during EX and PD, but lower during SP, likely due to reduced oxygen availability (**Figure S2B**).

Oxygen limitation may thus contribute to enhanced cell death, however the drastic effect of Aβ42 expression on CLS observed in shake-flask cultures (Chen and Petranovic, 2015) was not observed in oxygen-limited bioreactor cultures. Only 5.25 ± 0.44 and 2.39 ± 0.64% of cells were identified as dead in Aβ42 and control cultures, respectively, during SP2, i.e., 2 days after extracellular carbon source exhaustion (**Figure S2A**), in contrast to 37.15 ± 1.21 and 14.06 ± 1.82%, respectively, in shake-flask cultures (Chen and Petranovic, 2015). A putative explanation could be the different glucose concentrations in the medium used for bioreactors and shake-flask cultivations, i.e., 10 g L^{-1} instead of 20 g L^{-1}, respectively. Shake flask cultures grown in medium containing 10 g L^{-1} of glucose which is identical to the medium used in bioreactor cultures, revealed indeed a strong effect on viability. The higher initial glucose concentration resulted in a strongly reduced CLS, i.e., the fractions of dead cells were 5–7 fold higher during SP2 for the different strains (**Figures S3A,B**). Both initial glucose concentrations are generally not considered to induce calorie restriction related hormesis effects, but strongly affect other culture parameters in stationary phase. When using 10 g L^{-1} of glucose the pH dropped to only 4.5, instead of to 3.1, when 20 g L^{-1} of glucose was used (**Figures S3C,D**). Final cell concentrations correlated with initial glucose concentrations (**Figures S3E,F**). The acidic environment poses a strong stress on cells and can result in reduced CLS. An additional confounding factor were higher acetate levels in shake-flask cultures, which were highest for the Aβ42 strain on 20 g L^{-1} glucose (**Figure S4**). Altogether oxygen limitation, low pH-values and high acetate concentrations may contribute to the strongly reduced viability and CLS of all strains and especially of the Aβ42 strain in less-controlled shake-flasks environment. These effects are smaller in bioreactor cultures, because oxygen is not limited and a decrease in pH is prevented by online-monitoring and automated titration of base.

Global Transcriptional Response to Aβ Expression

To understand the mechanisms behind the phenotypic changes in Aβ42 and Aβ40 strains, gene expression levels during EX, PD, SP1, and SP2 were quantified using microarrays. The global expression pattern was characterized using principal component analysis (PCA). PCA resulted in strong grouping of biological replicates, indicative of a high degree of reproducibility. The first and second PCA components clearly separated all of samples from different growth phases by their gene expression profiles (**Figure 3A** and **Figure S5**). To further examine the extent of changes in each phase, we performed pair-wise comparisons

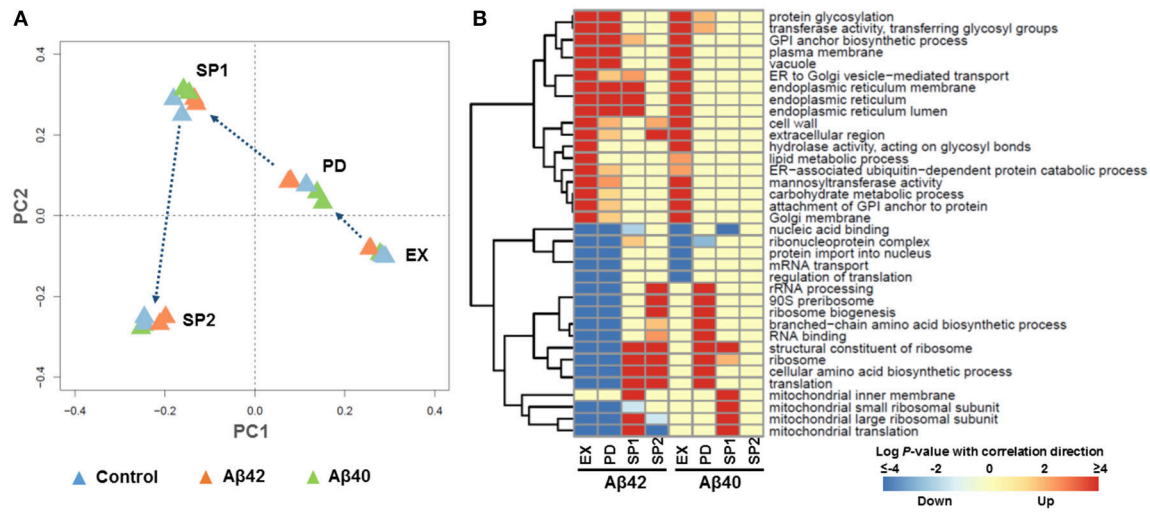

FIGURE 3 | Global transcriptional response to Aβ expression. **(A)** Principle Component Analysis (PCA). Each triangle represents one biological replicate. **(B)** The most strongly enriched GO terms of biological processes in Aβ42 and Aβ40 strains, compared to the control strain ($p < 0.005$) during EX, PD, SP1, and SP2, with red color indicating up-regulated processes and blue indicating down-regulated processes. For the complete gene set analysis results, see **Figures S7**, **S8**.

between the strains at each time-point. The expression of 472, 394, 391, and 280 genes was significantly different (adjusted $p < 0.001$) during EX, PD, SP1, and SP2, respectively, between the Aβ42 strain and the control strain (**Figure S6A**). Although the physiology of the Aβ40 strain was not notably different from the control strain, expression of 89, 486, and 1,118 genes was significantly different (adjusted $p < 0.001$) during EX, PD, and SP1, respectively. No significantly changed genes were identified later in SP2 between Aβ40 and control strains (**Figure S6B**). Of note, the overlap in differentially expressed genes was <20% between Aβ42 and Aβ40 strains during all phases, suggesting that different biological processes were influenced (**Figure S6C**).

To gain more insight in biological processes affected by Aβ42 and Aβ40 expression, gene set analysis (GSA) was performed on the significantly differentially expressed genes. Significant enrichment of 126 and 129 gene sets was identified ($p < 0.005$) among genes differentially expressed in Aβ42 and Aβ40 strains, respectively compared to the control strain. The complete list of gene sets can be found in **Figures S7**, **S8**. The most significantly enriched gene sets are shown in **Figure 3B** for both Aβ strains. Gene sets associated with protein processing (post-translational modifications, transport, and degradation), such as, "endoplasmic reticulum (ER)," "protein glycosylation," "vacuole" were enriched with up-regulated genes during EX, PD, and SP1 in the Aβ42 strain, but only during EX in the Aβ40 strain. Gene sets related to protein synthesis such as, "ribosome," "translation," "mitochondrial translation," and "cellular amino acid biosynthetic process," were enriched with down-regulated genes in the Aβ42 strain during EX and PD. Remarkably, these genes were up-regulated in the Aβ42 strain compared to the control strain during SP. The expression profiles of these protein synthesis related genes were studied throughout the different culture phases. This revealed that for genes, whose expression was higher in the Aβ42 strain than control strain in SP, this was due to a less pronounced decrease in expression (data not shown). These protein synthesis-related gene sets were enriched with up-regulated genes in the Aβ40 strain especially in PD. This opposite regulation of these genes clearly indicated different responses to Aβ42 and Aβ40 expression. For illustration, the genes involved in amino acid biosynthesis pathways of which expression levels were significantly changed can be found in **Figure S9** and **Table S2**. In addition to these processes directly involved in protein synthesis and processing, transcription related gene sets such as, "nucleic acid binding," "protein import into nucleus," "ribonucleoprotein complex," and "mRNA transport" were enriched with down-regulated genes in both Aβ strains.

Aβ42 Expression Induces Strong ER Stress Response

As a key component of cellular proteostasis, the ER is responsible for processing of one-third of cellular proteins and harbors an elaborate protein quality control system (PQC) to eliminate misfolded proteins by degradation (Cao and Kaufman, 2012). However, an overload of the PQC machinery results in an ER stress response (ESR) and activates the unfolded protein response (UPR; Scheper and Hoozemans, 2015). In the Aβ42 strain, most genes involved in "response to stress" were significantly higher expressed, including *HAC1*, the key regulator of UPR. In response to ER stress, *HAC1* ($HAC1^u$) mRNA is spliced to *HAC1* ($HAC1^s$) to initiate synthesis of the active transcription activator Hac1p which induces expression of over 300 of UPR target genes (Travers et al., 2000). The ratio of $HAC1^s/HAC1^u$ was 19, 17, and 13-fold higher in the Aβ42 strain compared to the control strain during EX, PD, and SP1, respectively (**Figure S10A**). Induction of UPR target genes results in the biosynthesis of chaperones, and other factors involved in the secretory pathway, and ER associated degradation (ERAD) to restore ER homeostasis. The gene sets related to protein processing were strongly triggered upon expression of Aβ42 (**Figure 4**). Genes encoding "folding" chaperones such as, *KAR2*, *SIL1*, *SCJ1*, *JEM1*, and disulfide bond formation enzymes *PDI1* and *ERO1* were indeed all found significantly up-regulated (**Figure 4**). Higher transcription levels of *PDI1* and *ERO1* were verified by qPCR (**Figures S10B,C**). Genes encoding proteins involved in processes throughout the secretory pathway including translocation, glycosylation, GPI (Glycosylphosphatidylinositol) biosynthesis, trafficking between ER and Golgi, ER associated degradation (ERAD), and vacuole were also significantly higher expressed in the Aβ42 strain (**Figure 4**). Besides ERAD, which is the predominant cellular mechanism to degrade misfolded proteins under ER stress, autophagy can also be activated when the amount of misfolded proteins exceeds the ER capacity (Bernales et al., 2006). In line with this, the Aβ42 strain expressed the autophagy related genes *ATG8*, *ATG22*, *ATG34*, *NVJ1*, and *ATG19* to a higher extent (**Figure 4**).

In the Aβ40 strain, changes in expression levels of genes involved in protein processing were less pronounced (**Figure S11**). The ratio of $HAC1^s/HAC1^u$ in the Aβ40 strain was only 5.8-fold higher than control strain in EX. qPCR confirmed that transcript levels of *PDI1* and *ERO1* were not significantly changed (**Figure S10**). The distributions of significantly differentially expressed genes between Aβ42 and Aβ40 strains are shown in **Figure S12** ($p < 0.05$). All differentially expressed genes involved in protein processing are listed in **Table S3**.

Aβ42 Expression Increases Lipid Synthesis

It was previously shown that ER stress and activation of UPR pathways play a critical role in lipid metabolism in different model organisms (Hetz, 2012). GSA revealed that the gene sets related to "lipid metabolic process" were overrepresented with up-regulated genes in both Aβ strains during EX. More specifically, gene sets involved in "glycerolipid biosynthesis process," "phospholipid biosynthetic process," "glycerophospholipid biosynthetic process," and "lipid biosynthetic process" were strongly overrepresented among up-regulated genes in the Aβ42 strain during EX, compared to the control strain. Similar results were also found for the Aβ40 strain. However, for the Aβ40 strain, the enrichment was less strong and the amounts of significantly up-regulated genes involved in each processes were, respectively, 30, 34, 31, and 42% lower than for the Aβ42 strain (**Figure 5A**). The expression level of *INO1*, the gene encoding an important regulator in lipid metabolism in yeast (Henry et al., 2012), was significantly

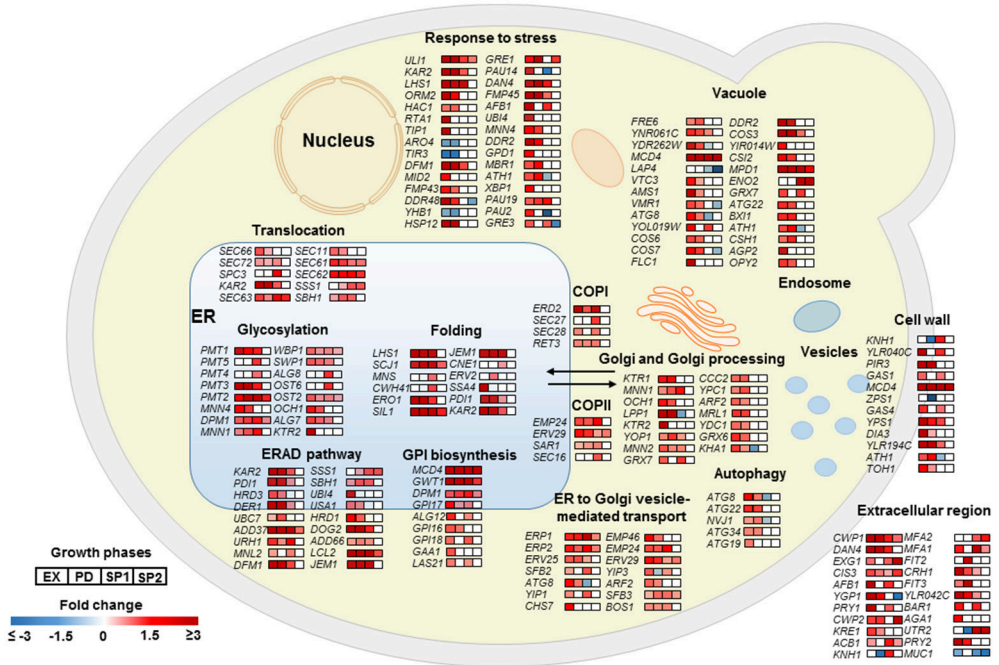

FIGURE 4 | Transcriptional profiles of differentially expressed genes encoding proteins involved in protein secretory and metabolic processes in the Aβ42 strain. Changes in gene expression are shown as fold changes compared to the control strain during EX, PD, SP1, and SP2.

increased in the Aβ42 strain during EX (data not shown). To see whether the different expression patterns led to alterations in cellular lipid composition, we measured different lipid classes dynamically in all three strains. The major lipid constituents of *S. cerevisiae*: storage lipids, phospholipids, and sterols were analyzed. Compared to the control strain, the levels of all lipid categories were significantly increased during EX and PD in the Aβ42 strain. The differences were most pronounced during EX. In the Aβ40 strain, only phospholipids showed a slight but significant increase during EX and PD compared to control strain (**Figure 5B**). To gain insight in the structural storage of lipids we monitored the three-dimensional distribution and amounts of lipids stored at the single-cell level (which usually coalesce into lipid droplets) by CARS (coherent anti-Stokes Raman scattering) microscopy in exponentially growing cells. CARS can probe and image lipid structures by vibrations between carbon and hydrogen bonds and hence no fluorescent labels or tags are needed. The average lipid droplet volume was 1.6-fold larger in the Aβ42 strain ($0.078 \pm 0.032\ \mu m^3$) than in the control strain ($0.048 \pm 0.028\ \mu m^3$; **Figure S13**). CARS images showed that the lipid droplets in control cells were numerous and smaller in sizes, whereas they tended to accumulate and form larger drops in Aβ42 expressing cells (**Figure 5C** and **Videos S3**, **S4**).

DISCUSSION

Humanized yeast models have been exploited to investigate protein functions and cellular pathways implicated in neurodegenerative disorders including Huntington's disease (Giorgini et al., 2005), Parkinson's disease (Outeiro and Lindquist, 2003), and AD (Zhang et al., 1994). To study the cytotoxicity of Aβ peptides in AD, several yeast models have been explored (Verduyckt et al., 2016), of which only recent models recapitulate important aspects of Aβ cytotoxicity by including intracellular trafficking (Treusch et al., 2011; D'Angelo et al., 2013). To overcome a major disadvantage of these models, i.e., the use of inducible promoters resulting in strong acute cytotoxicity, we recently presented an improved yeast model in which human Aβ peptides are constitutively expressed, only moderately affecting growth. To our knowledge all studies with these and similar models have been carried out in uncontrolled cultivation systems, such as, shake-flask, tubes, or 96-well plates due to their ease and scalability. However, these cultures present a highly dynamic environment, with changes in nutrient and metabolite levels, pH, and oxygen availability (Büchs, 2001), that strongly influence the growth of Crabtree-positive *S. cerevisiae*. In contrast, the stable (controlled) environments in bioreactor cultures are well defined and highly reproducible. In this paper, we dynamically elucidate the effects of different human Aβ peptides expression on yeast physiology and transcriptome by using bioreactor cultures. This allowed partial confirmation of earlier observation on the role of Aβ peptides in AD pathology (Treusch et al., 2011; Nair et al., 2014; Chen and Petranovic, 2015), but also revealed remarkable differences and increased our knowledge on the mechanistic principles behind cytotoxicity of different Aβ peptides.

Both shake-flask and bioreactor cultures displayed a reduction in the maximal growth rate of the Aβ42 strain (Chen and

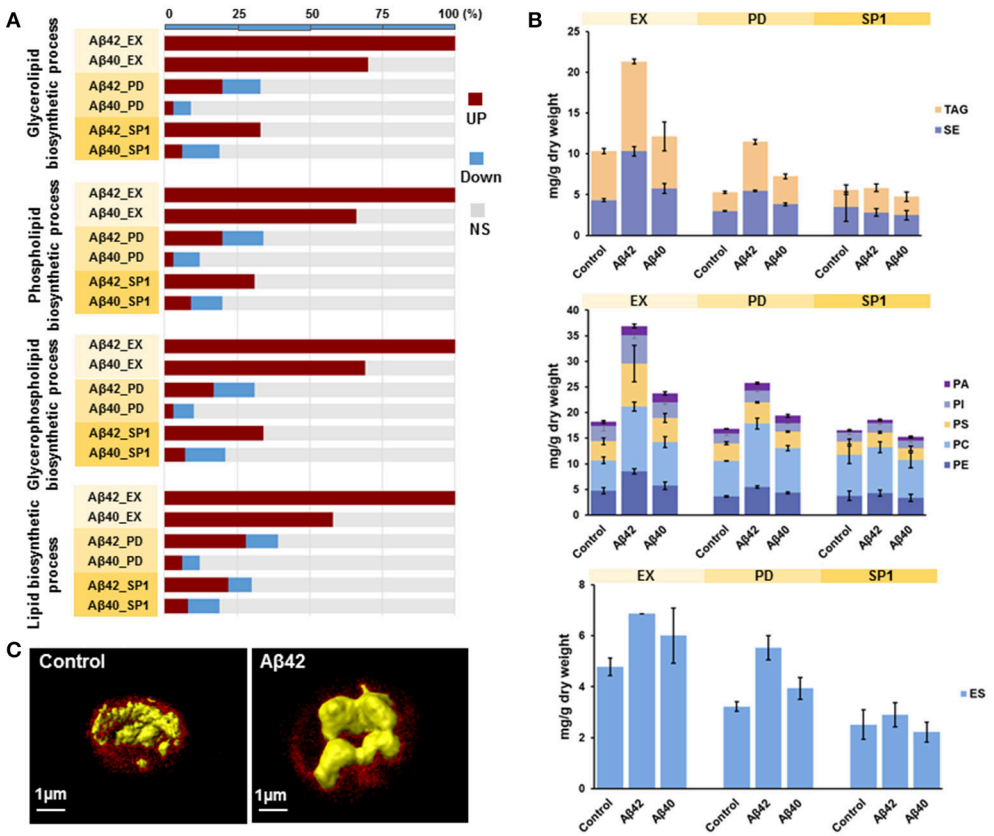

FIGURE 5 | Aβ42 expression results in increased lipid synthesis. **(A)** For significantly enriched GO terms involved in lipid biosynthetic processes, the percentages of genes that are either higher (red), lower (blue), or not significantly (NS, gray) differentially expressed in both Aβ strains during EX, PD, and SP1 are shown. **(B)** Cellular concentrations of storage lipids, phospholipids and ergosterol were measured by HPLC-CAD in all strains. TAG, Triacylglycerols; SE, steryl esters; PA, phosphatidic acid; PI, phosphatidylinositol; PS, phosphatidylserine; PC, phosphatidylcholine; PE, phosphatidylethanolamine; ES, sterol ergosterol. **(C)** CARS microscopy visualization of lipid droplets (in yellow) during EX in control and Aβ42-expressing cells. The background fluorescence of cells is shown in red and is indicative of the cell volume.

Petranovic, 2015). However, the previously observed drastic effect on CLS was significantly reduced in bioreactor cultures, which underlines the importance of culture conditions in aging and aging-related disease models (Longo et al., 2012). There may be several reasons for the observed difference in CLS between the two experimental set-ups. First and likely foremost, the well-controlled environment reduced additional stresses on cells. As illustrated by the comparison of aerobic and micro-aerobic conditions in bioreactor cultures, sufficient availability of oxygen had a beneficial effect on CLS (**Figure S2A**). An additional important parameter kept constant in bioreactor cultures was pH. Neuronal excitability is highly susceptible to fluctuations of intracellular and extracellular pH (Ruffin et al., 2014). One of the main clinical presentations of AD includes signs of decreased brain pH (Demetrius and Simon, 2012). The combination of low pH and presence of toxic peptides might contribute to neuronal cell death. As we confirmed in our yeast model, in non-pH-controlled shake-flask cultures, the acidity of medium increases due to both ammonium consumption and the production of acids, such as acetic acid and CO_2 (Fraenkel, 1982; Burtner et al., 2009). The degree of acidification depends on medium composition and strain. In our study, an increase in initial glucose concentration from 10 to 20 g L^{-1} resulted in a more than 10-fold increase in proton concentration (**Figures S3C,D**). Virtually all cellular processes are dependent on intracellular pH (Orij et al., 2012), for example acidification of the cytosol is an early event to regulate caspase-dependent apoptosis in yeast (Matsuyama et al., 2000), and collapse of intracellular pH homeostasis shifts the model of cell death from apoptosis to necrosis in *Caenorhabditis elegans* (Syntichaki et al., 2005). Depending on the extracellular pH, cells invest significant amounts of energy to keep intracellular pH homeostasis to maintain viability (Della-Bianca et al., 2014). Increased energy expenditure in acidified non-controlled cultures negatively influences viability, as other studies showed that CLS can be enhanced by buffering the culture pH (Fabrizio et al., 2004). And these effects might be even stronger in already challenged Aβ42 expressing cells. In addition to contributing to low pH, organic acids have been shown to affect cell performance in specific manners (Abbott et al., 2007). Especially acetic acid is a potent cell-stressor that has been shown to induce lysosomal apoptotic pathway either in

a mitochondria-independent or dependent way (Marques et al., 2013; Oliveira et al., 2015). Under bioreactor conditions less acetate was produced by all strains than in shake-flask cultures (**Figure S4** and **Table 1**). Higher initial glucose concentrations also led to higher acetate levels, especially for the Aβ42 strain. Overall the reduced oxygen availability, low pH, and increased acetate levels cause additional stress and strongly affect survival of Aβ42 expressing cells.

Human brain activity corresponds to a high fraction of total energy consumption, and neurons strongly depend on mitochondria due to a limited glycolytic capacity (Moreira et al., 2009). Mitochondrial dysfunction leads to energy metabolism abnormalities that endanger normal neuron functioning and contribute to AD pathology. In yeast expressing Aβ42, lower growth rates and reduced biomass yields were observed (**Table 1**). This reflects a redirection of energy from growth to maintenance, i.e., processes aimed at maintaining cell integrity and functioning that do not lead to an increase in biomass. In addition, it also points at reduced ATP generation from the energy sources consumed as indicated by reduced oxygen consumption rates and lower respiratory quotient (**Figure 2A** and **Table S1**). Reduced energy metabolism in the diseased brain is one of best documented abnormalities in AD (Moreira et al., 2007). In fact, the low glucose baseline metabolism and its decline during aging are viewed as sensitive measures and being increasingly adopted to assist diagnosis in cognitive decline (Shokouhi et al., 2013; Yamane et al., 2014). Several groups reported that Aβ peptides accumulate in mitochondria and directly interact with several mitochondrial proteins (Manczak et al., 2006; Pagani and Eckert, 2011; Pavlov et al., 2011). The interaction of Aβ peptides with Aβ-binding alcohol dehydrogenase (ABAD) in mitochondria promotes leakage of ROS, mitochondrial dysfunction and cell death in AD patients and transgenic mice (Lustbader et al., 2004). The interaction of Aβ peptides with mitochondria appears to affect a multitude of different functions in AD, including respiration, detoxification of ROS, and organellar morphology (Rhein et al., 2009; Yao et al., 2009; Selfridge et al., 2013). Here, we observed similar responses specifically in yeast cells expressing the more toxic Aβ42 peptide. With TPEF microscopy, aberrant fragmented mitochondrial structures were detected in the Aβ42 strain. In brain tissue from AD patients and neuronal cells expressing mutant APP, similar fragmented mitochondria and structural changes have been observed (Hirai et al., 2001; Wang et al., 2008).

Genome wide expression level analysis revealed that both Aβ peptides expression induced ESR, although the Aβ40 strain did not show significant physiological changes (**Figure 3B**). Studies proposed an important role for ER stress in AD pathogenesis by acting as a mediator of Aβ neurotoxicity (Umeda et al., 2011; Hoozemans et al., 2012). Aβ furthermore triggers ER stress-specific apoptosis through caspase-12 and caspase-4 (Nakagawa et al., 2000; Hitomi et al., 2004). ER stress results in activation of UPR, one of stress response pathways, which aims to restore ER homeostasis (Cao and Kaufman, 2012). In yeast, the UPR is regulated solely by the Ire1 pathway which is conserved from yeast to mammals (Iwawaki et al., 2001). In response to ER stress, activated Ire1p splices $HAC1^u$ to $HAC1^s$ to initiate synthesis of Hac1p which translocates into nucleus to regulate expression of UPR target genes (Mori et al., 2000). The different ratio of $HAC1^s/HAC1^u$ in Aβ42 and Aβ40 strains suggested that the expression of these variants results in a different extent of ER stress and consequently UPR. This is in accordance with previous findings in yeast, which show that UPR signaling can be modulated through differential target gene expression depending on the nature of stress (Thibault et al., 2011). The different nature of the two Aβ peptides investigated here, showed that Aβ40 triggered a mild response, and Aβ42 resulted in a stronger stress affecting many aspects of the physiology of the cells. Decreasing the ER protein load is the first attempt of UPR to restore proteostasis. In our study, the processes involved in protein folding/maturation, ER-to-Golgi trafficking and ERAD were significantly upregulated in both Aβ strains initiating from EX, though at different levels. In addition to ERAD, autophagy was activated only in the Aβ42 strain, which suggested that the amounts of misfolded or aggregated proteins exceed the ER capacity (**Figure 4**). Global transcription, translation, and amino acid synthesis were repressed in response to Aβ42 expression (**Figure 3B** and **Figure S7**). By these responses, the

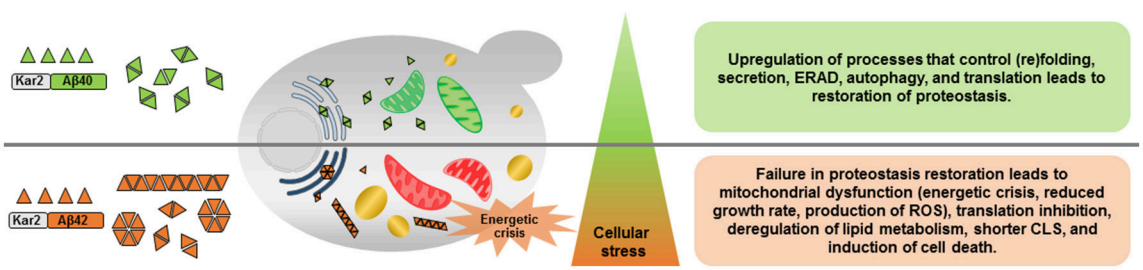

FIGURE 6 | Schematic overview of the effects of constitutive expression of Aβ40 or Aβ42 peptides. Aβ40 and Aβ42 differ in potential to form aggregates resulting in different levels of ER stress and induction of the unfolded protein response (UPR). Constitutive expression of Aβ40, induces mild ER stress and subsequent activation of the UPR recovers proteome homeostasis (proteostasis) by promoting protein (re)folding, protein quality control, and degradation mechanisms. Aβ42 peptides, on the contrary, result in prolonged ER stress and the strongly activated UPR fails to buffer the misfolded protein load, leading to cellular dysfunction and a shorter chronological life span (CLS). ERAD, ER-associated degradation; ROS, reactive oxygen species; Green mitochondria, functional; Red mitochondria, dysfunctional; Light blue ER, mild ER stress; Dark blue ER, strong ER stress; Yellow, lipid droplets.

influx of new proteins into ER can be reduced, whereas the efflux is increased. The large fraction of nuclear-DNA encoded mitochondrial proteins is processed through the ER. Reduced mitochondrial protein biogenesis and turn-over can result in increased dysfunction, thereby linking the UPR with energy metabolism. Mitochondria furthermore communicate directly with ER through MAM (mitochondria-associated ER membranes) to regulate several fundamental cellular processes (Csordás et al., 2006; Rowland and Voeltz, 2012). This crosstalk between ER and mitochondria may have a role in facilitating stress response and UPR (Bernales et al., 2012; Stoica et al., 2014; Paillusson et al., 2016). However, these processes were up-regulated in the Aβ40 strain during PD, which suggested the cells started to re-establish homeostasis within the ER (**Figure 3B** and **Figure S8**). When the buffering capacity of UPR proves inadequate to restore ER proteostasis, the pathway switches from an adaptation program to apoptosis to remove irreversibly damaged cells (Rutkowski et al., 2006; Szegezdi et al., 2006). This is reflected by the significantly elevated fractions of dead cells in Aβ42 strain cultures, compared to cultures of control and Aβ40 strains (**Figure S2A**).

Recently, it was found that ER stress and UPR activation regulate cellular processes beyond ER protein folding and play crucial roles in lipid metabolism by controlling the transcriptional regulation of lipogenesis in the liver (Lee et al., 2008; Zhang et al., 2011). We found that at the transcript level, genes involved in lipid biosynthesis were higher expressed in both Aβ strains compared to the control strain during EX (**Figure 5A**). UPR regulates inositol, an important regulator of lipid metabolism in yeast, which plays a key role in phospholipid biosynthesis required for membranes (Jesch et al., 2005). The expression levels of *INO1*, the gene encoding the enzyme that catalyzes the rate-limiting step in *de novo* synthesis of inositol (Henry et al., 2012), was significantly increased in the Aβ42 strain during EX. Moreover, the tight link between lipid synthesis and UPR was shown previously by the induction of UPR upon *OPI3* or *INO1* deletion (Jonikas et al., 2009). We used lipidomics to quantify the lipid and sterol components and it showed a significant increase in phospholipids and storage lipids during growth phases in the Aβ42 strain (**Figure 5B**). This result was further supported by CARS microscopy, which showed significantly larger lipid drops in the Aβ42 strain compared to the control strain during EX (**Figure 5C**). Links between lipid metabolism and AD have been previously proposed, since the initial observation that feeding rabbits with a cholesterol-enriched diet leads to Aβ accumulation (Sparks et al., 1994). Nowadays several studies provide substantial evidence that aberrant lipid metabolism is closely connected to Aβ modulation during the pathogenesis of AD in humans (Wood, 2012; Walter and van Echten-Deckert, 2013). Apolipoprotein E (ApoE) is the strongest known genetic risk factor for the most common late-onset sporadic AD (Corder et al., 1993; Strittmatter et al., 1993), which might impair Aβ clearance and increase its aggregation in the brain (Bales et al., 1997; Holtzman et al., 2000; Verghese et al., 2013). Moreover, alterations in membrane lipid composition, including cholesterol and sphingolipids may also affect Aβ generation and aggregation properties (Simons et al., 1998; Sawamura et al., 2004). Conversely, Aβ can influence lipid homeostasis by modulating lipid metabolic enzymes and directly binding to membrane lipids (Cutler et al., 2004; Grimm et al., 2005). Our study demonstrated that Aβ-induced ER stress might be an additional mechanism contributing to the increased brain cholesterol content observed in AD.

Overall, this study provided highly informative data regarding changes in cellular metabolic activity and energy metabolism as consequences of different Aβ peptides expression. The expression of Aβ40 and Aβ42 peptides also caused different levels of ER stress which tightly regulates the amplitude and kinetics of UPR signaling to decide different cell fates (**Figure 6**). Due to the emerging role of UPR in diverse disease conditions, such as, cancer, diabetes, and neurodegeneration, understanding how the UPR interacts with other cellular regulations is fundamental for the identification of future points of intervention in many important and to date often incurable human diseases.

AUTHOR CONTRIBUTIONS

XC, MB, and DP designed research; XC and MB performed and analyzed batch cultivation, extracellular metabolites, mitochondrial bioenergetics, molecular, and cellular experiments. NA performed Non-linear microscopy experiments. KS prepared cells for Non-linear microscopy experiments. XC, MB, and BJ analyzed microarray data. XC, MB, and DP wrote the manuscript, with contributions from NA and BJ.

FUNDING

This work was funded by grants from Novo Nordisk Foundation (21210022).

ACKNOWLEDGMENTS

DP would like to dedicate the paper to the memory of Prof. Susan Lindquist, a dear friend, mentor, and colleague whose work on humanized yeast models and proteostasis continues to inspire us. XC and MB are grateful to Dr. Mingtao Huang, Dr. Zhiwei Zhu, and Dr. Leif Väremo for valuable discussions and comments on the manuscript. NA is grateful to Prof. Annika Enejder for providing the non-linear microscopy lab. We thank the Bioinformatics and Expression Analysis core facility (BEA) at the Karolinska Institute for help with microarray.

SUPPLEMENTARY MATERIAL

The Supplementary Material for this article can be found online at: http://journal.frontiersin.org/article/10.3389/fnmol.2017.00232/full#supplementary-material

Figure S1 | Cellular reserve carbohydrate concentrations in batch cultures. Cellular contents of glycogen **(A)** and trehalose **(B)** are measured during PD, SP1, and SP2 phases under aerobic condition. Results represent average values ± SEM, of triplicate (Aβ42 and control) or duplicate (Aβ40) independent biological replicates. The asterisk (*) indicates significant differences ($p < 0.001$).

Figure S2 | Fractions of dead cells and reactive oxygen species (ROS) positive cells as function of age in aerobic and microaerobic cultures. **(A)** Cells were stained with PI and analyzed by flow cytometry, PI-positive cells are considered dead. **(B)** Cells were stained with DHR123 and analyzed by flow cytometry. Strongly fluorescent cells (i.e., 5–100 times more fluorescent than low fluorescent cells) are considered ROS positive. Insert shows the values for the first three growth phases in detail. Full lines and dotted lines indicate aerobic or microaerobic conditions, respectively.

Figure S3 | Comparison of fractions of dead cells **(A,B)**, pH **(C,D)**, and cell growth **(E,F)** between 1 and 2% glucose cultures grown in shake flasks.

Figure S4 | Quantification and comparison of acetate production under different culture conditions after glucose exhaustion (diauxic shift, DS).

Figure S5 | Principle Component Analysis (PCA). Histogram of variance for each PC shows that the first two PCs capture the largest variance of dataset, which are 70% (PC1) and 19.8% (PC2), respectively.

Figure S6 | The Venn diagrams show distribution of significantly differentially expressed genes between Aβ42 and control strains **(A)**, Aβ40 and control strains **(B)**, Aβ42 and Aβ40 strains **(C)** during different growth phases ($p < 0.001$).

Figure S7 | The significantly enriched GO terms in Aβ42 strain among genes differentially expressed compared to control strain ($p < 0.001$).

Figure S8 | The significantly enriched GO terms in Aβ40 strain among genes differentially expressed compared to control strain ($p < 0.001$).

Figure S9 | Schematic overview of significantly changed genes in amino acid biosynthetic pathways in Aβ42 strain **(A)** and Aβ40 strain **(B)** compared to control strain. Differences in gene expression levels are shown as fold changes compared to control strain during EX, PD, SP1, and SP2 phases ($p < 0.05$).

Figure S10 | qPCR analysis of $HAC1^S/HAC1^U$ ratio **(A)**, *PDI1* **(B)**, and *ERO1* **(C)** mRNA levels in all strains from EX, PD, and SP1 phases. Results are average values ± SEM, of triplicate (Aβ42 and control) or duplicate (Aβ40) independent biological replicates. The asterisk (*) indicates significant differences ($p < 0.05$).

Figure S11 | Transcriptional profiles of differentially expressed genes related to protein secretory and metabolic processes in Aβ40 strain compared to control strain. Changes in gene expressions are shown as fold changes compared to control strain during EX, PD, SP1, and SP2.

Figure S12 | The Venn diagrams show distribution of significantly differentially expressed genes in protein secretory and metabolic processes between Aβ42 and Aβ40 strains during EX **(A)**, PD **(B)**, and SP1 **(C)** phases ($p < 0.05$).

Figure S13 | Quantitative analysis of CARS microscopy images presenting the contents of lipids in control and Aβ42 expressing cells during EX. Ten images were analyzed for each strain. Each image contains one or more cells. The value of lipid content was calculated by the ratio of summation over stacks of lipids area/summation over stacks of cell area. The average lipid content was higher in Aβ42 strain ($0.078 \pm 0.032\ \mu m^3$) than in control strain ($0.048 \pm 0.028\ \mu m^3$).

Table S1 | Physiological parameters of micro-aerobic batch cultures.

Table S2 | Genes with significantly different expression in amino acid biosynthetic pathways (Aβ42 strain vs. control strain).

Table S3 | Genes with significantly different expression in protein secretory and metabolic processes (Aβ40 strain vs. control strain).

Table S4 | Primer-sets used for qPCR.

Video S1 | 3D movie of a representative image of mitochondrial structure in control cell. Mitochondria were stained with Rhodamine 123 and shown in green. Red shows the background of TPEF microscopy and is indicative of cell volume.

Video S2 | 3D movie of a representative image of mitochondrial structure in Aβ42-expressing cells. Mitochondria were stained with Rhodamine 123 and shown in green. Red shows the background of TPEF microscopy and is indicative of cell volume.

Video S3 | 3D movie of a representative image of lipid drops in control cell. Yellow, lipid drops; red, background of CARS microscopy to indicate the cell volume.

Video S4 | 3D movie of a representative images of lipid drops in Aβ42-expressing cells. Yellow, lipid drops; red, background of CARS microscopy to indicate the cell volume.

REFERENCES

Abbott, D. A., Knijnenburg, T. A., De Poorter, L. M. I., Reinders, M. J. T., Pronk, J. T., and van Maris, A. J. A. (2007). Generic and specific transcriptional responses to different weak organic acids in anaerobic chemostat cultures of *Saccharomyces cerevisiae*. *FEMS Yeast Res.* 7, 819–833. doi: 10.1111/j.1567-1364.2007.00242.x

Albers, E., Larsson, C., Andlid, T., Walsh, M. C., and Gustafsson, L. (2007). Effect of nutrient starvation on the cellular composition and metabolic capacity of *Saccharomyces cerevisiae*. *Appl. Environ. Microbiol.* 73, 4839–4848. doi: 10.1128/AEM.00425-07

Anderlei, T., and Büchs, J. (2001). Device for sterile online measurement of the oxygen transfer rate in shaking flasks. *Biochem. Eng. J.* 7, 157–162. doi: 10.1016/S1369-703X(00)00116-9

Bagriantsev, S., and Liebman, S. (2006). Modulation of Abeta42 low-n oligomerization using a novel yeast reporter system. *BMC Biol.* 4:32. doi: 10.1186/1741-7007-4-32

Bakker, B. M., Overkamp, K. M., van Maris, A. J. A., Kötter, P., Luttik, M. A. H., Pronk, J. T., et al. (2001). Stoichiometry and compartmentation of NADH metabolism in *Saccharomyces cerevisiae*. *FEMS Microbiol. Rev.* 25, 15–37. doi: 10.1111/j.1574-6976.2001.tb00570.x

Bales, K. R., Verina, T., Dodel, R. C., Du, Y., Altstiel, L., Bender, M., et al. (1997). Lack of apolipoprotein E dramatically reduces amyloid [β]-peptide deposition. *Nat. Genet.* 17, 263–264. doi: 10.1038/ng1197-263

Bernales, S., McDonald, K. L., and Walter, P. (2006). Autophagy counterbalances endoplasmic reticulum expansion during the unfolded protein response. *PLoS Biol.* 4:e423. doi: 10.1371/journal.pbio.0040423

Bernales, S., Morales Soto, M., and McCullagh, E. (2012). Unfolded protein stress in the endoplasmic reticulum and mitochondria: a role in neurodegeneration. *Front. Aging Neurosci.* 4:5. doi: 10.3389/fnagi.2012.00005

Bisschops, M. M. M., Vos, T., Moreno-Martinez, R., De La Torre-Cortes, P., Pronk, J. T., and Daran-Lapujade, P. (2015). Oxygen availability strongly affects chronological lifespan and thermotolerance in batch cultures of *Saccharomyces cerevisiae*. *Microb. Cell* 2, 429–444. doi: 10.15698/mic2015.11.238

Breitenbach, M., Rinnerthaler, M., Hartl, J., Stincone, A., Vowinckel, J., Breitenbach-Koller, H., et al. (2014). Mitochondria in ageing: there is metabolism beyond the ROS. *FEMS Yeast Res.* 14, 198–212. doi: 10.1111/1567-1364.12134

Büchs, J. (2001). Introduction to advantages and problems of shaken cultures. *Biochem. Eng. J.* 7, 91–98. doi: 10.1016/S1369-703X(00)00106-6

Burtner, C. R., Murakami, C. J., Kennedy, B. K., and Kaeberlein, M. (2009). A molecular mechanism of chronological aging in yeast. *Cell Cycle* 8, 1256–1270. doi: 10.4161/cc.8.8.8287

Burtner, C. R., Murakami, C. J., Olsen, B., Kennedy, B. K., and Kaeberlein, M. (2011). A genomic analysis of chronological longevity factors in budding yeast. *Cell Cycle* 10, 1385–1396. doi: 10.4161/cc.10.9.15464

Cao, S. S., and Kaufman, R. J. (2012). Unfolded protein response. *Curr. Biol.* 22, R622–R626. doi: 10.1016/j.cub.2012.07.004

Castrillo, J. I., and Oliver, S. G. (2015). "Systems biology of multifactorial diseases: Alzheimer's disease," in *Systems Biology of Alzheimer's Disease*, eds J. I. Castrillo and S. G. Oliver (New York, NY: Humana Press), 3–48.

Chen, X., and Petranovic, D. (2015). Amyloid-β peptide-induced cytotoxicity and mitochondrial dysfunction in yeast. *FEMS Yeast Res.* 15:fov061. doi: 10.1093/femsyr/fov061

Corder, E., Saunders, A., Strittmatter, W., Schmechel, D., Gaskell, P., Small, G., et al. (1993). Gene dose of apolipoprotein E type 4 allele and the risk of Alzheimer's disease in late onset families. *Science* 261, 921–923. doi: 10.1126/science.8346443

Csordás, G., Renken, C., Várnai, P., Walter, L., Weaver, D., Buttle, K. F., et al. (2006). Structural and functional features and significance of the physical linkage between ER and mitochondria. *J. Cell Biol.* 174, 915–921. doi: 10.1083/jcb.200604016

Cutler, R. G., Kelly, J., Storie, K., Pedersen, W. A., Tammara, A., Hatanpaa, K., et al. (2004). Involvement of oxidative stress-induced abnormalities in ceramide and cholesterol metabolism in brain aging and Alzheimer's disease. *Proc. Natl. Acad. Sci. U.S.A.* 101, 2070–2075. doi: 10.1073/pnas.0305799101

D'Angelo, F., Vignaud, H., Di Martino, J., Salin, B., Devin, A., Cullin, C., et al. (2013). A yeast model for amyloid-β aggregation exemplifies the role of membrane trafficking and PICALM in cytotoxicity. *Dis. Model. Mech.* 6, 206–216. doi: 10.1242/dmm.010108

Della-Bianca, B. E., De Hulster, E., Pronk, J. T., van Maris, A. J., and Gombert, A. K. (2014). Physiology of the fuel ethanol strain *Saccharomyces cerevisiae* PE-2 at low pH indicates a context-dependent performance relevant for industrial applications. *FEMS Yeast Res.* 14, 1196–1205. doi: 10.1111/1567-1364.12217

Demetrius, L. A., and Simon, D. K. (2012). An inverse-Warburg effect and the origin of Alzheimer's disease. *Biogerontology* 13, 583–594. doi: 10.1007/s10522-012-9403-6

Entian, K.-D., and Kötter, P. (2007). "25 yeast genetic strain and plasmid collections," in *Methods in Microbiology*, eds S. Ian and J. R. S. Michael (Cambridge, MA: Academic Press), 629–666.

Fabrizio, P., Battistella, L., Vardavas, R., Gattazzo, C., Liou, L.-L., Diaspro, A., et al. (2004). Superoxide is a mediator of an altruistic aging program in *Saccharomyces cerevisiae*. *J. Cell Biol.* 166, 1055–1067. doi: 10.1083/jcb.200404002

Fraenkel, D. (1982). *Carbohydrate Metabolism.* Cold Spring Harbor, CA: Cold Spring Harbor Press.

Fruhmann, G., Seynnaeve, D., Zheng, J., Ven, K., Molenberghs, S., Wilms, T., et al. (2017). Yeast buddies helping to unravel the complexity of neurodegenerative disorders. *Mech. Ageing Dev.* 161, 288–305. doi: 10.1016/j.mad.2016.05.002

Giorgini, F., Guidetti, P., Nguyen, Q., Bennett, S. C., and Muchowski, P. J. (2005). A genomic screen in yeast implicates kynurenine 3-monooxygenase as a therapeutic target for Huntington's disease. *Nat. Genet.* 37, 526–531. doi: 10.1038/ng1542

Gouras, G. K., Almeida, C. G., and Takahashi, R. H. (2005). Intraneuronal Aβ accumulation and origin of plaques in Alzheimer's disease. *Neurobiol. Aging* 26, 1235–1244. doi: 10.1016/j.neurobiolaging.2005.05.022

Grimm, M. O. W., Grimm, H. S., Patzold, A. J., Zinser, E. G., Halonen, R., Duering, M., et al. (2005). Regulation of cholesterol and sphingomyelin metabolism by amyloid-[β] and presenilin. *Nat. Cell Biol.* 7, 1118–1123. doi: 10.1038/ncb1313

Hardy, J., and Selkoe, D. J. (2002). The amyloid hypothesis of Alzheimer's disease: progress and problems on the road to therapeutics. *Science* 297, 353–356. doi: 10.1126/science.1072994

Henry, S. A., Kohlwein, S. D., and Carman, G. M. (2012). Metabolism and regulation of glycerolipids in the yeast *Saccharomyces cerevisiae*. *Genetics* 190, 317–349. doi: 10.1534/genetics.111.130286

Herman, P. K. (2002). Stationary phase in yeast. *Curr. Opin. Microbiol.* 5, 602–607. doi: 10.1016/S1369-5274(02)00377-6

Hetz, C. (2012). The unfolded protein response: controlling cell fate decisions under ER stress and beyond. *Nat. Rev. Mol. Cell Biol.* 13, 89–102. doi: 10.1038/nrm3270

Hirai, K., Aliev, G., Nunomura, A., Fujioka, H., Russell, R. L., Atwood, C. S., et al. (2001). Mitochondrial abnormalities in Alzheimer's disease. *J. Neurosci.* 21, 3017–3023.

Hitomi, J., Katayama, T., Eguchi, Y., Kudo, T., Taniguchi, M., Koyama, Y., et al. (2004). Involvement of caspase-4 in endoplasmic reticulum stress-induced apoptosis and Aβ-induced cell death. *J. Cell Biol.* 165, 347–356. doi: 10.1083/jcb.200310015

Holtzman, D. M., Bales, K. R., Tenkova, T., Fagan, A. M., Parsadanian, M., Sartorius, L. J., et al. (2000). Apolipoprotein E isoform-dependent amyloid deposition and neuritic degeneration in a mouse model of Alzheimer's disease. *Proc. Natl. Acad. Sci. U.S.A.* 97, 2892–2897. doi: 10.1073/pnas.050004797

Hoozemans, J. J. M., Van Haastert, E. S., Nijholt, D. A. T., Rozemuller, A. J. M., and Scheper, W. (2012). Activation of the unfolded protein response is an early event in Alzheimer's and Parkinson's disease. *Neurodegenerative Dis.* 10, 212–215. doi: 10.1159/000334536

Huang, D. W., Sherman, B. T., and Lempicki, R. A. (2008). Systematic and integrative analysis of large gene lists using DAVID bioinformatics resources. *Nat. Protoc.* 4, 44–57. doi: 10.1038/nprot.2008.211

Iwawaki, T., Hosoda, A., Okuda, T., Kamigori, Y., Nomura-Furuwatari, C., Kimata, Y., et al. (2001). Translational control by the ER transmembrane kinase/ribonuclease IRE1 under ER stress. *Nat. Cell Biol.* 3, 158–164. doi: 10.1038/35055065

Jarrett, J. T., Berger, E. P., and Lansbury, P. T. (1993). The carboxy terminus of the .beta. amyloid protein is critical for the seeding of amyloid formation: implications for the pathogenesis of Alzheimer's disease. *Biochemistry* 32, 4693–4697. doi: 10.1021/bi00069a001

Jensen, N. B., Strucko, T., Kildegaard, K. R., David, F., Maury, J., Mortensen, U. H., et al. (2014). EasyClone: method for iterative chromosomal integration of multiple genes in *Saccharomyces cerevisiae*. *FEMS Yeast Res.* 14, 238–248. doi: 10.1111/1567-1364.12118

Jesch, S. A., Zhao, X., Wells, M. T., and Henry, S. A. (2005). Genome-wide analysis reveals inositol, not choline, as the major effector of Ino2p-Ino4p and unfolded protein response target gene expression in yeast. *J. Biol. Chem.* 280, 9106–9118. doi: 10.1074/jbc.M411770200

Jonikas, M. C., Collins, S. R., Denic, V., Oh, E., Quan, E. M., Schmid, V., et al. (2009). Comprehensive characterization of genes required for protein folding in the endoplasmic reticulum. *Science* 323, 1693–1697. doi: 10.1126/science.1167983

Longo, V. D., Shadel, G. S., Kaeberlein, M., and Kennedy, B. (2012). Replicative and chronological aging in *Saccharomyces cerevisiae*. *Cell Metab.* 16, 18–31. doi: 10.1016/j.cmet.2012.06.002

Khoomrung, S., Chumnanpuen, P., Jansa-Ard, S., Ståhlman, M., Nookaew, I., Borén, J., et al. (2013). Rapid quantification of yeast lipid using microwave-assisted total lipid extraction and HPLC-CAD. *Anal. Chem.* 85, 4912–4919. doi: 10.1021/ac3032405

Khurana, V., and Lindquist, S. (2010). Modelling neurodegeneration in *Saccharomyces cerevisiae*: why cook with baker's yeast? *Nat. Rev. Neurosci.* 11, 436–449. doi: 10.1038/nrn2809

Klöckner, W., and Büchs, J. (2012). Advances in shaking technologies. *Trends Biotechnol.* 30, 307–314. doi: 10.1016/j.tibtech.2012.03.001

Lee, A.-H., Scapa, E. F., Cohen, D. E., and Glimcher, L. H. (2008). Regulation of hepatic lipogenesis by the transcription factor XBP1. *Science* 320, 1492–1496. doi: 10.1126/science.1158042

Liu, G., Bergenholm, D., and Nielsen, J. (2016). Genome-wide mapping of binding sites reveals multiple biological functions of the transcription factor Cst6p in *Saccharomyces cerevisiae*. *MBio* 7:e00559–16. doi: 10.1128/mBio.00559-16

Livnat-Levanon, N., Kevei, E., Kleifeld, O., Krutauz, D., Segref, A., Rinaldi, T., et al. (2014). Reversible 26S proteasome disassembly upon mitochondrial stress. *Cell Rep.* 7, 1371–1380. doi: 10.1016/j.celrep.2014.04.030

Luheshi, L. M., Tartaglia, G. G., Brorsson, A. C., Pawar, A. P., Watson, I. E., Chiti, F., et al. (2007). Systematic *in vivo* analysis of the intrinsic determinants of amyloid β pathogenicity. *PLoS Biol.* 5:e290. doi: 10.1371/journal.pbio.0050290

Lustbader, J. W., Cirilli, M., Lin, C., Xu, H. W., Takuma, K., Wang, N., et al. (2004). ABAD directly links Aß to mitochondrial toxicity in Alzheimer's disease. *Science* 304, 448–452. doi: 10.1126/science.1091230

Manczak, M., Anekonda, T. S., Henson, E., Park, B. S., Quinn, J., and Reddy, P. H. (2006). Mitochondria are a direct site of Aβ accumulation in Alzheimer's disease neurons: implications for free radical generation and oxidative damage in disease progression. *Hum. Mol. Genet.* 15, 1437–1449. doi: 10.1093/hmg/ddl066

Mao, K., and Klionsky, D. J. (2013). Participation of mitochondrial fission during mitophagy. *Cell Cycle* 12, 3131–3132. doi: 10.4161/cc.26352

Marques, C., Oliveira, C. S. F., Alves, S., Chaves, S. R., Coutinho, O. P., Corte-Real, M., et al. (2013). Acetate-induced apoptosis in colorectal carcinoma cells involves lysosomal membrane permeabilization and cathepsin D release. *Cell Death Dis.* 4, e507. doi: 10.1038/cddis.2013.29

Matsuyama, S., Llopis, J., Deveraux, Q. L., Tsien, R. Y., and Reed, J. C. (2000). Changes in intramitochondrial and cytosolic pH: early events that

modulate caspase activation during apoptosis. *Nat. Cell Biol.* 2, 318–325. doi: 10.1038/35014006

McLean, C. A., Cherny, R. A., Fraser, F. W., Fuller, S. J., Smith, M. J., Konrad, V., et al. (1999). Soluble pool of Aβ amyloid as a determinant of severity of neurodegeneration in Alzheimer's disease. *Ann. Neurol.* 46, 860–866. doi: 10.1002/1531-8249(199912)46:6<860::AID-ANA8>3.0.CO;2-M

Mertz, J. (2004). Nonlinear microscopy: new techniques and applications. *Curr. Opin. Neurobiol.* 14, 610–616. doi: 10.1016/j.conb.2004.08.013

Moreira, P. I., Duarte, A. I., Santos, M. S., Rego, A. C., and Oliveira, C. R. (2009). An integrative view of the role of oxidative stress, mitochondria and insulin in Alzheimer's disease. *J. Alzheimers Dis.* 16, 741–761. doi: 10.3233/JAD-2009-0972

Moreira, P. I., Nunomura, A., Honda, K., Aliev, G., Casadesus, G., Zhu, X., et al. (2007). "The key role of oxidative stress in Alzheimer's disease," in *Oxidative Stress and Neurodegenerative Disorders,* ed S. H. Parvez (Amsterdam: Elsevier Science B.V.), 267–281.

Mori, K., Ogawa, N., Kawahara, T., Yanagi, H., and Yura, T. (2000). mRNA splicing-mediated C-terminal replacement of transcription factor Hac1p is required for efficient activation of the unfolded protein response. *Proc. Natl. Acad. Sci. U.S.A.* 97, 4660–4665. doi: 10.1073/pnas.050010197

Nair, S., Traini, M., Dawes, I. W., and Perrone, G. G. (2014). Genome-wide analysis of *Saccharomyces cerevisiae* identifies cellular processes affecting intracellular aggregation of Alzheimer's amyloid-β42: importance of lipid homeostasis. *Mol. Biol. Cell* 25, 2235–2249. doi: 10.1091/mbc.E13-04-0216

Nakagawa, T., Zhu, H., Morishima, N., Li, E., Xu, J., Yankner, B. A., et al. (2000). Caspase-12 mediates endoplasmic-reticulum-specific apoptosis and cytotoxicity by amyloid-β. *Nature* 403, 98–103. doi: 10.1038/47513

Oliveira, C. S. F., Pereira, H., Alves, S., Castro, L., Baltazar, F., Chaves, S. R., et al. (2015). Cathepsin D protects colorectal cancer cells from acetate-induced apoptosis through autophagy-independent degradation of damaged mitochondria. *Cell Death Dis.* 6, e1788. doi: 10.1038/cddis.2015.157

Orij, R., Urbanus, M. L., Vizeacoumar, F. J., Giaever, G., Boone, C., Nislow, C., et al. (2012). Genome-wide analysis of intracellular pH reveals quantitative control of cell division rate by pHc in *Saccharomyces cerevisiae*. *Genome Biol.* 13:R80. doi: 10.1186/gb-2012-13-9-r80

Outeiro, T. F., and Lindquist, S. (2003). Yeast cells provide insight into alpha-synuclein biology and pathobiology. *Science* 302, 1772–1775. doi: 10.1126/science.1090439

Pagani, L., and Eckert, A. (2011). Amyloid-Beta interaction with mitochondria. *Int. J. Alzheimer's Dis.* 2011:925050. doi: 10.4061/2011/925050

Paillusson, S., Stoica, R., Gomez-Suaga, P., Lau, D. H. W., Mueller, S., Miller, T., et al. (2016). There's something wrong with my MAM; the ER–mitochondria axis and neurodegenerative diseases. *Trends Neurosci.* 39, 146–157. doi: 10.1016/j.tins.2016.01.008

Parrou, J. L., and François, J. (1997). A simplified procedure for a rapid and reliable assay of both glycogen and trehalose in whole yeast cells. *Anal. Biochem.* 248, 186–188. doi: 10.1006/abio.1997.2138

Pavlov, P. F., Wiehager, B., Sakai, J., Frykman, S., Behbahani, H., Winblad, B., et al. (2011). Mitochondrial γ-secretase participates in the metabolism of mitochondria-associated amyloid precursor protein. *FASEB J.* 25, 78–88. doi: 10.1096/fj.10-157230

Piper, M. D. W., Daran-Lapujade, P., Bro, C., Regenberg, B., Knudsen, S., Nielsen, J., et al. (2002). Reproducibility of oligonucleotide microarray transcriptome analyses: an interlaboratory comparison using chemostat cultures of *Saccharomyces cerevisiae*. *J. Biol. Chem.* 277, 37001–37008. doi: 10.1074/jbc.M204490200

Rhein, V., Song, X., Wiesner, A., Ittner, L. M., Baysang, G., Meier, F., et al. (2009). Amyloid-β and tau synergistically impair the oxidative phosphorylation system in triple transgenic Alzheimer's disease mice. *Proc. Natl. Acad. Sci. U.S.A.* 106, 20057–20062. doi: 10.1073/pnas.0905529106

Rowland, A. A., and Voeltz, G. K. (2012). Endoplasmic reticulum-mitochondria contacts: function of the junction. *Nat. Rev. Mol. Cell Biol.* 13, 607–625. doi: 10.1038/nrm3440

Ruffin, V. A., Salameh, A. I., Boron, W. F., and Parker, M. D. (2014). Intracellular pH regulation by acid-base transporters in mammalian neurons. *Front. Physiol.* 5:43. doi: 10.3389/fphys.2014.00043

Rutkowski, D. T., Arnold, S. M., Miller, C. N., Wu, J., Li, J., Gunnison, K. M., et al. (2006). Adaptation to ER stress is mediated by differential stabilities of pro-survival and pro-apoptotic mRNAs and proteins. *PLoS Biol.* 4:e374. doi: 10.1371/journal.pbio.0040374

Sawamura, N., Ko, M., Yu, W., Zou, K., Hanada, K., Suzuki, T., et al. (2004). Modulation of amyloid precursor protein cleavage by cellular sphingolipids. *J. Biol. Chem.* 279, 11984–11991. doi: 10.1074/jbc.M309832200

Scheper, W., and Hoozemans, J. J. M. (2015). The unfolded protein response in neurodegenerative diseases: a neuropathological perspective. *Acta Neuropathol.* 130, 315–331. doi: 10.1007/s00401-015-1462-8

Selfridge, J. E., Lezi, E., Lu, J., and Swerdlow, R. H. (2013). Role of mitochondrial homeostasis and dynamics in Alzheimer's disease. *Neurobiol. Dis.* 51, 3–12. doi: 10.1016/j.nbd.2011.12.057

Selkoe, D. J. (2001). Alzheimer's disease: genes, proteins, and therapy. *Physiol. Rev.* 81, 741–766.

Shankar, G. M., Li, S., Mehta, T. H., Garcia-Munoz, A., Shepardson, N. E., Smith, I., et al. (2008). Amyloid-[β] protein dimers isolated directly from Alzheimer's brains impair synaptic plasticity and memory. *Nat. Med.* 14, 837–842. doi: 10.1038/nm1782

Shokouhi, S., Claassen, D., Kang, H., Ding, Z., Rogers, B., Mishra, A., et al. (2013). Longitudinal progression of cognitive decline correlates with changes in the spatial pattern of brain 18F-FDG pet. *J. Nuclear Med.* 54, 1564–1569. doi: 10.2967/jnumed.112.116137

Simons, M., Keller, P., De Strooper, B., Beyreuther, K., Dotti, C. G., and Simons, K. (1998). Cholesterol depletion inhibits the generation of β-amyloid in hippocampal neurons. *Proc. Natl. Acad. Sci. U.S.A.* 95, 6460–6464. doi: 10.1073/pnas.95.11.6460

Singer, M. A., and Lindquist, S. (1998). Multiple effects of trehalose on protein folding *in vitro* and *in vivo*. *Mol. Cell* 1, 639–648. doi: 10.1016/S1097-2765(00)80064-7

Sparks, D. L., Scheff, S. W., Hunsaker, J. C. III, Liu, H., Landers, T., and Gross, D. R. (1994). Induction of Alzheimer-like β-amyloid immunoreactivity in the brains of rabbits with dietary cholesterol. *Exp. Neurol.* 126, 88–94. doi: 10.1006/exnr.1994.1044

Stoica, R., De Vos, K. J., Paillusson, S., Mueller, S., Sancho, R. M., Lau, K.-F., et al. (2014). ER–mitochondria associations are regulated by the VAPB–PTPIP51 interaction and are disrupted by ALS/FTD-associated TDP-43. *Nat. Commun.* 5:3996. doi: 10.1038/ncomms4996

Strittmatter, W. J., Saunders, A. M., Schmechel, D., Pericak-Vance, M., Enghild, J., Salvesen, G. S., et al. (1993). Apolipoprotein E: high-avidity binding to β-amyloid and increased frequency of type 4 allele in late-onset familial Alzheimer disease. *Proc. Natl. Acad. Sci. U.S.A.* 90, 1977–1981. doi: 10.1073/pnas.90.5.1977

Syntichaki, P., Samara, C., and Tavernarakis, N. (2005). The vacuolar H^+-ATPase mediates intracellular acidification required for neurodegeneration in *C. elegans*. *Curr. Biol.* 15, 1249–1254. doi: 10.1016/j.cub.2005.05.057

Szegezdi, E., Logue, S. E., Gorman, A. M., and Samali, A. (2006). Mediators of endoplasmic reticulum stress-induced apoptosis. *EMBO Rep.* 7, 880–885. doi: 10.1038/sj.embor.7400779

Thibault, G., Ismail, N., and Ng, D. T. W. (2011). The unfolded protein response supports cellular robustness as a broad-spectrum compensatory pathway. *Proc. Natl. Acad. Sci. U.S.A.* 108, 20597–20602. doi: 10.1073/pnas.1117184109

Thinakaran, G., and Koo, E. H. (2008). Amyloid precursor protein trafficking, processing, and function. *J. Biol. Chem.* 283, 29615–29619. doi: 10.1074/jbc.R800019200

Travers, K. J., Patil, C. K., Wodicka, L., Lockhart, D. J., Weissman, J. S., and Walter, P. (2000). Functional and genomic analyses reveal an essential coordination between the unfolded protein response and ER-associated degradation. *Cell* 101, 249–258. doi: 10.1016/S0092-8674(00)80835-1

Treusch, S., Hamamichi, S., Goodman, J. L., Matlack, K. E. S., Chung, C. Y., Baru, V., et al. (2011). Functional links between Aβ toxicity, endocytic trafficking and Alzheimer's disease risk factors in yeast. *Science* 334, 1241–1245. doi: 10.1126/science.1213210

Umeda, T., Tomiyama, T., Sakama, N., Tanaka, S., Lambert, M. P., Klein, W. L., et al. (2011). Intraneuronal amyloid β oligomers cause cell death via endoplasmic reticulum stress, endosomal/lysosomal leakage, and mitochondrial dysfunction *in vivo*. *J. Neurosci. Res.* 89, 1031–1042. doi: 10.1002/jnr.22640

Väremo, L., Nielsen, J., and Nookaew, I. (2013). Enriching the gene set analysis of genome-wide data by incorporating directionality of gene expression

and combining statistical hypotheses and methods. *Nucleic Acids Res.* 41, 4378–4391. doi: 10.1093/nar/gkt111

Verduyckt, M., Vignaud, H., Bynens, T., Van Den Brande, J., Franssens, V., Cullin, C., et al. (2016). "Yeast as a model for Alzheimer's disease: latest studies and advanced strategies," in *Systems Biology of Alzheimer's Disease*, eds J. I. Castrillo and S. G. Oliver (New York, NY: Humana Press), 197–215.

Verghese, P. B., Castellano, J. M., Garai, K., Wang, Y., Jiang, H., Shah, A., et al. (2013). ApoE influences amyloid-β (Aβ) clearance despite minimal apoE/Aβ association in physiological conditions. *Proc. Natl. Acad. Sci. U.S.A.* 110, E1807–E1816. doi: 10.1073/pnas.1220484110

von der Haar, T., Jossé, L., Wright, P., Zenthon, J., and Tuite, M. F. (2007). Development of a novel yeast cell-based system for studying the aggregation of Alzheimer's disease-associated Aβ peptides *in vivo*. *Neurodegenerative Dis.* 4, 136–147. doi: 10.1159/000101838

Walter, J., and van Echten-Deckert, G. (2013). Cross-talk of membrane lipids and Alzheimer-related proteins. *Mol. Neurodegener.* 8, 34–34. doi: 10.1186/1750-1326-8-34

Wang, X., Su, B., Siedlak, S. L., Moreira, P. I., Fujioka, H., Wang, Y., et al. (2008). Amyloid-β overproduction causes abnormal mitochondrial dynamics via differential modulation of mitochondrial fission/fusion proteins. *Proc. Natl. Acad. Sci. U.S.A.* 105, 19318–19323. doi: 10.1073/pnas.0804871105

Wood, P. L. (2012). Lipidomics of Alzheimer's disease: current status. *Alzheimer's Res. Ther.* 4, 5–5. doi: 10.1186/alzrt103

Wyss-Coray, T. (2016). Ageing, neurodegeneration and brain rejuvenation. *Nature* 539, 180–186. doi: 10.1038/nature20411

Yamane, T., Ikari, Y., Nishio, T., Ishii, K., Ishii, K., Kato, T., et al. (2014). Visual-statistical interpretation of 18F-FDG-PET images for characteristic Alzheimer patterns in a multicenter study: inter-rater concordance and relationship to automated quantitative evaluation. *Am. J. Neuroradiol.* 35, 244–249. doi: 10.3174/ajnr.A3665

Yao, J., Irwin, R. W., Zhao, L., Nilsen, J., Hamilton, R. T., and Brinton, R. D. (2009). Mitochondrial bioenergetic deficit precedes Alzheimer's pathology in female mouse model of Alzheimer's disease. *Proc. Natl. Acad. Sci. U.S.A.* 106, 14670–14675. doi: 10.1073/pnas.0903563106

Younkin, S. G. (1998). The role of Aβ42 in Alzheimer's disease. *J. Physiol. Paris* 92, 289–292. doi: 10.1016/S0928-4257(98)80035-1

Zhang, H., Komano, H., Fuller, R. S., Gandy, S. E., and Frail, D. E. (1994). Proteolytic processing and secretion of human beta-amyloid precursor protein in yeast. Evidence for a yeast secretase activity. *J. Biol. Chem.* 269, 27799–27802.

Zhang, K., Wang, S., Malhotra, J., Hassler, J. R., Back, S. H., Wang, G., et al. (2011). The unfolded protein response transducer IRE1α prevents ER stress-induced hepatic steatosis. *EMBO J.* 30, 1357–1375. doi: 10.1038/emboj.2011.52

Zhou, Y. J., Buijs, N. A., Zhu, Z., Qin, J., Siewers, V., and Nielsen, J. (2016). Production of fatty acid-derived oleochemicals and biofuels by synthetic yeast cell factories. *Nat. Commun.* 7:11709. doi: 10.1038/ncomms11709

Conflict of Interest Statement: The authors declare that the research was conducted in the absence of any commercial or financial relationships that could be construed as a potential conflict of interest.

frontiers in Molecular Neuroscience

ORIGINAL RESEARCH
published: 13 March 2018
doi: 10.3389/fnmol.2018.00075

Q-Rich Yeast Prion [*PSI*$^+$] Accelerates Aggregation of Transthyretin, a Non-Q-Rich Human Protein

Meenakshi Verma[1,2], *Amandeep Girdhar*[3], *Basant Patel*[3], *Nirmal K. Ganguly*[2], *Ritushree Kukreti*[1] *and Vibha Taneja*[2]*

[1] Genomics and Molecular Medicine, Institute of Genomics and Integrative Biology, Council of Scientific & Industrial Research (CSIR), New Delhi, India, [2] Department of Research, Sir Ganga Ram Hospital, New Delhi, India, [3] Department of Biotechnology, IIT Hyderabad, New Delhi, India

Interactions amongst different amyloid proteins have been proposed as a probable mechanism of aggregation and thus an important risk factor for the onset as well as progression of various neurodegenerative disorders including Alzheimer's, Parkinson's, Huntington's, and Amyotrophic Lateral Sclerosis. Evidences suggest that transthyretin (TTR), a plasma protein associated with transthyretin amyloidosis or familial polyneuropathy (FAP) interacts with heterologous amyloid proteins including amyloid beta and islet amyloid polypeptide. In addition, recent clinical studies have revealed the presence of systemic polyneuropathy associated with FAP mutations in patients with spinocerebral ataxia, amyotrophic lateral sclerosis, and new familial systematic prion disease. Hence, it is important to investigate the interactions amongst different amyloid proteins to gain better insight into the pathology of amyloid disorders. Yeast has been an excellent model system to study interaction/ cross-seeding between heterologous amyloid proteins, more because of presence of endogenous yeast prions. Here, we examined interactions of non-glutamine (non-Q)-rich transthyretin, with glutamine (Q)-rich yeast prion protein Sup35. We established aggregation of an engineered double (F87M/L110M) mutant M-TTR-GFP in yeast. This mutant is monomeric and readily formed aggregates compared to WT-TTR-GFP in yeast at acidic pH. Interestingly, aggregation of M-TTR-GFP was significantly enhanced in presence of [*PSI*$^+$], an endogenous prion form of Sup35. Different variants of [*PSI*$^+$] seeded M-TTR-GFP with different efficiencies and curing of [*PSI*$^+$] (losing the prion form) in these strains reduced aggregation. Moreover, overexpression of prion domain of Sup35 fused to RFP (NM-RFP) also increased M-TTR-GFP aggregation. M-TTR-GFP and NM-RFP aggregates co-localized in perivacuolar and juxtranuclear region. Sup35 protein was even immunocaptured in M-TTR-GFP aggregates. However, M-TTR-GFP overexpression did not induce Sup35 aggregation. Thus, it appears to be a unidirectional interaction between these two amyloid proteins. However, no affect on M-TTR-GFP aggregation was observed due to another yeast prion, [*PIN*$^+$]. Our findings thus show the molecular interaction of transthyretin with yeast prion and support that sequence similarity is not the prime requirement for heterologous amyloid interactions.

Keywords: amyloid aggregation, cross-seeding, transthyretin, Sup35 protein, yeast prion [*PSI*$^+$]

OPEN ACCESS

Edited by:
Sabrina Büttner,
Stockholm University, Sweden

Reviewed by:
Mick Tuite,
University of Kent, United Kingdom
Anita L. Manogaran,
Marquette University, United States

***Correspondence:**
Vibha Taneja
vibha.taneja@sgrh.com

Received: *22 September 2017*
Accepted: *26 February 2018*
Published: *13 March 2018*

Citation:
Verma M, Girdhar A, Patel B, Ganguly NK, Kukreti R and Taneja V (2018) Q-Rich Yeast Prion [PSI$^+$] Accelerates Aggregation of Transthyretin, a Non-Q-Rich Human Protein. Front. Mol. Neurosci. 11:75. doi: 10.3389/fnmol.2018.00075

INTRODUCTION

Transthyretin amyloidosis (ATTR) is one of the most common forms of hereditary systemic amyloidosis caused due to abnormal accumulation of transthyretin protein (TTR) in various organs/tissues. More than 100 point mutations in TTR have been associated with the disease. Even the wild type TTR has an intrinsic propensity to form aggregates and cause late onset of the sporadic form of ATTR. TTR is a tetramer in its native state and the point mutations destabilize the tetramer into monomers which undergo conformational changes (Hammarström et al., 2002). These misfolded monomers self-assemble to form a seed or nuclei during the lag phase. This seed serves as a template to recruit more misfolded monomers/conformers and catalyze its own polymerization. Therefore, the formation of nuclei or seed is considered as the time-limiting step in the process of fibrillization. The introduction of preformed "seed" can reduce or eliminate the lag phase and accelerate fibrillization. Evidences suggest that this "seed" could be homologous or heterologous in nature (Jarrett and Lansbury, 1993; Morales et al., 2009, 2013). The evidence for cross seeding of TTR was first suggested by an *in vitro* experiment, where addition of IAPP fibrils enhanced TTR aggregation (Westermark and Westermark, 2008). Further, several reports showed interaction of TTR with other amyloid proteins including Aβ (Schwarzman et al., 1994; Choi et al., 2007; Wati et al., 2009) and α-synuclein (Guerreiro et al., 2012). Recently, a new familial form of human prion disease defined as PrP systemic amyloidosis has been reported to show clinical overlap with familial amyloid polyneuropathy, which is known to be associated with TTR mutations (Mead et al., 2013; Mead and Reilly, 2015).

Yeast has served as an excellent model system to investigate homologous and heterologous seeding amongst amyloid proteins. Interestingly, yeast has endogenous prions (Wickner, 1994; Wickner et al., 1995; Patino et al., 1996; Liebman and Derkatch, 1999; Du et al., 2008; Patel et al., 2009), which interact with heterologous prions and other amyloid proteins, thus providing the proof of concept of cross-seeding hypothesis. Endogenous glutamine-rich (Q-rich) yeast prions promote or inhibit induction of other Q-rich yeast prions (Derkatch et al., 2001; Schwimmer and Masison, 2002; Bradley and Liebman, 2003; Kryndushkin et al., 2008; Yang et al., 2013; Du and Li, 2014; Ripaud et al., 2014). In addition, yeast prions have been shown to promote aggregation of other polyQ proteins such as huntingtin, a human amyloid protein (Meriin et al., 2002; Derkatch et al., 2004; Zhao et al., 2012; Kantcheva et al., 2014). Increasing line of evidence now shows interactions amongst Q-rich and non-Q-rich amyloid proteins also. Non-Q-rich human insulin, Ig light chain and yeast prion Mod5 promote Q-rich Sup35 aggregation though with varying intensities (Derkatch et al., 2004; Arslan et al., 2015). Even Q-rich yeast prion [PIN^+] enhanced aggregation of non-Q/N rich fungal prion protein Het-s (Taneja et al., 2007). Evidences also indicate that some of the interactions between amyloid proteins are reciprocal (both amyloid proteins can promote aggregation of each other) whereas some are unidirectional (one amyloid protein promotes aggregation of the second amyloid protein but not vice-a-versa) (O'Nuallain et al., 2004; Westermark and Westermark, 2008).

Similar to strains of mammalian prion protein (Safar et al., 1998; Jones and Surewicz, 2005), yeast prions are known to exist as biological variants, which exhibit variable phenotype, aggregation and seeding/ cross-seeding abilities (Derkatch et al., 1996; Schlumpberger et al., 2001; Uptain et al., 2001). Variants of yeast prions, [PSI^+] and [PIN^+], have been well studied. Distinct variants of [PSI^+] have been classified as strong [PSI^+] or weak [PSI^+] based on different functional activity and ability to form aggregates (Derkatch et al., 1996; Zhou et al., 1999). Furthermore, these prion variants have been shown to interact differently with other amyloid proteins. Variants of the [PIN^+] prion induce [PSI^+] with different efficiencies (Bradley et al., 2002). These differences amongst the prion variants can probably be explained by the ability of a protein to misfold into a range of conformers giving rise to different aggregated forms (Krishnan and Lindquist, 2005; Tanaka et al., 2006; Toyama et al., 2007).

Accumulating evidences suggest interactions amongst different heterologous amyloid proteins to be one of the risk factors in the pathogenesis of amyloid disorders. Hence, it is important to investigate how presence of one amyloid disease might influence the onset and progression of another. Examining the molecular interactions between heterologous amyloid proteins will help to gain better insight into disease pathology. In this study, we created transthyretin aggregation model in yeast and examined the interaction of TTR with endogenous yeast prion proteins. We observed that Q-rich yeast prion protein Sup35 directly interacts and enhances aggregation of non-Q-rich TTR. However, similar to previous report (Derkatch et al., 2004), overexpression of TTR did not induce Sup35 aggregation indicating a unidirectional interaction among them. Our findings suggest that not just sequence similarity but conformational fold may promote interactions among heterologous amyloid proteins and hence, support the cross-seeding hypothesis for the onset of aggregation and disease progression.

MATERIALS AND METHODS

Yeast Strains, Media, and Plasmids

Yeast strains VL1, a [psi^-][PIN^+]; VL2, a [psi^-][pin^-]; VL3, a weak [PSI^+][pin^-]; VL4, a strong [PSI^+][pin^-] in 74-D694 background (*ade1-14 ura3-52 leu2-3, 112 trp1-289, his3-200*) were a kind gift from Dr. Susan Liebman. L2723, a *SUP35* deletion strain (*sup35*Δ:LEU2) episomally expressing full length (*N-MRF*) Sup35 (pRS313-N-MRF, *HIS*) in 74-D694 was also a gift from Dr. Liebman's lab (Bagriantsev and Liebman, 2006). As described by them, a control strain was generated by replacing the pRS313-N-MRF with plasmid pRS316-MRF expressing only the C-domain of Sup35 (MRF). W303, a wild type (*leu2-3,112 trp1-1 can1-100 ura3-1 ade2-1 his3-11,15*) yeast strain was also used.

Yeast cells were grown in standard media. Rich media contained either 1 or 0.25% yeast extract, 2% peptone and 2%

Abbreviations: TTR, transthyretin; WT-TTR, wild type transthyretin; M-TTR, monomeric transthyretin; AB, amyloid beta; GFP, green fluorescence protein; GuHCl, guanidine hydrochloride.

dextrose. Synthetic minimal media contained all amino acids except those used for selection and 2% dextrose (*SD*). For overexpression constructs dextrose was replaced with raffinose (2%) and galactose (3%) (SRaf+Gal) in minimal media. To examine the effect of pH, media pH was adjusted to 4.2 with HCl and 6.5 with NaOH. Yeast transformations were done by lithium acetate protocol (Gietz and Woods, 2002).

The plasmid, pRS316-MRF, expressing only the C-domain of Sup35 and another plasmid pNM-RFP for overexpression of prion domain (NM) of Sup35 fused to RFP were again a gift from Dr. Susan Liebman. The wild type TTR-GFP fusion construct was generated by amplifying the full length human transthyretin cDNA from pDNR-LIB clone and inserting it upstream of GFP in a centromeric plasmid, pRS316CG. WT-TTR-GFP fusion fragment was then amplified and cloned at BamHI site in pRS424-GAL1, a 2 micron expression vector to generate pWT-TTR-GFP. Plasmid pM-TTR-GFP was obtained by introducing two point mutations simultaneously; methionine substitution at phenylalanine 87 position (F87M) and methionine substitution at leucine 110 position (L110M) in WT-TTR-GFP using QuickChange site-directed mutagenesis procedure from Stratagene (Cat# 200516). A vector control (pGFP) was created by digesting pWT-TTR-GFP with SacII enzyme and subcloning the GFP fragment at SacII site in pRS424-GAL1 vector. All the clones were verified by restriction digestion and DNA sequencing.

Quantification of Amyloid Aggregates in Yeast by Fluorescent Microscopy

Different yeast strains were transformed with either TTR-GFP overexpression constructs alone or co-transformed with plasmids expressing N-MRF or MRF. Cells were grown in synthetic glucose selection media and reinnoculated in inducing media. (SRaf+Gal) TTR aggregates were analyzed after 72 h using a Nikon Ti-E inverted fluorescent microscope. For each transformant, six or more microscopic visual fields were randomly selected and cells with aggregates and diffused GFP expression were manually counted. More than 600 cells were counted per transformant and three independent transformants were analyzed for each construct.

Determining the Native State of TTR-GFP in Yeast

Yeast cells overexpressing WT-TTR-GFP or M-TTR-GFP were harvested after 24 h of incubation in the inducing media and lysed using 1X lysis buffer (50 mM TrisCl, 50 mM KCl, 10 mM $MgCl_2$, 5% glycerol). Cell lysates were normalized for total protein and incubated at 37 and 95°C in non-denaturing sample buffer without β-mercaptoethanol and resolved on 12% SDS-PAGE. The blot was probed using anti-GFP antibody (Cat# G6795, Sigma).

Centrifugation Assay to Analyze the Distribution of Overexpressed WT-TTR-GFP and M-TTR-GFP in Yeast

Cell lysates were normalized for total protein at 100 μg/μl and 1 mg of total protein was centrifuged at 40,000 rpm for 3 h at 4°C. Supernatant fraction was aspirated and the pellet fraction was resuspended in the same volume (100 μl) of 1X lysis buffer as the supernatant. Equal volumes of supernatant and pellet fractions were loaded. Total protein loaded was one-tenth of the normalized protein for both the samples. The total, supernatant and pellet fractions were resolved on 10% SDS-PAGE, immunoblotted and probed using anti GFP antibody.

Determining the Effect of Overexpression of WT-TTR-GFP and M-TTR-GFP on Cell Viability in Yeast

Effect of over-expression of WT-TTR-GFP and M-TTR-GFP was measured by spotting serial dilutions of exponentially growing liquid cultures. Yeast cells with WT-TTR-GFP or M-TTR-GFP were grown in raffinose media till early log phase (0.3–0.4). The cultures were normalized to 0.2 OD and 5-fold serial dilutions were prepared (5^{-1}, 5^{-2}, 5^{-3}, and 5^{-4}). 5 μl of each dilution was spotted on glucose (uninduced media) and galactose (inducing media) selection plates and incubated at 30°C for 2–3 days.

Determining the Affect of pH of the Media on Intracellular pH of the Yeast Cells

Yeast cells were grown in SD media maintained at different pH at 30°C for 24 and 36 h. Cells were harvested, washed and incubated with 500 nM of Lysotracker Red DND-99 (Cat# L7528) at 30°C for 30 min in their respective media. Cells were washed and visualized using confocal laser scanning microscope Leica TCS SP8. Images were processed using LAS X 3.1.1 software.

Examining the Expression Levels of WT-TTR-GFP and M-TTR-GFP

Protein levels of the WT-TTR-GFP and M-TTR-GFP in yeast were determined by lysing the cells, normalizing the total protein and immunoblotting using anti-GFP antibody under the defined experimental conditions (different pH, yeast strain variants). GAPDH was used as the endogenous loading control.

Examining Cellular Localization and Interaction of TTR Aggregates With Sup35 Aggregates

Yeast cells expressing M-TTR-GFP aggregates were stained with, 4,6-diamidino-2-phenylindole (DAPI), a nuclear DNA-binding dye and FM4-64, an endocytic vesicle and vacuolar membrane dye. For nuclear staining, cells were fixed with 10% formaldehyde for 2 h, washed with phosphate-buffered saline (PBS), permeabilized by incubation in 70% ethanol for 30 min at room temperature. Cells were washed again and incubated with DAPI (1 μg/ml) for 10 min and visualized. For vacuolar staining, cells were incubated with 8 μM FM4-64 in YPD for 15 min at 30°C. Cells were washed and further incubated for 60 min in fresh YPD and then visualized under fluorescent microscope.

Colocalization of M-TTR-GFP aggregates and Sup35 aggregates were monitored by co-transforming M-TTR-GFP and prion domain (NM) of Sup35 fused with RFP (NM-RFP). Colocalization was evaluated visually, quantitatively and statistically. Cells from independent transformants were

analyzed under fluorescent microscope (Nikon Ti, 100X with oil immersion) for aggregates after 72 h under FITC (GFP) and TRITC (RFP) channels and images were captured separately for both the channels. Colocalization was analyzed by merging the images from two channels using NIS-Elements AR 3.2. Cells with M-TTR-GFP, NM-RFP or both M-TTR-GFP/NM-RFP aggregates were manually counted to calculate the percentage of cells showing colocalized aggregates. The degree of colocalization between the fluorophore conjugated proteins (M-TTR-GFP and NM-RFP) was quantified by calculating Pearson's correlation coefficient using Coloc2 Fiji pluggin of the ImageJ software.

Examine the Effect of TTR Aggregation on Sup35 by Red/White Color Plate Assay

To determine the effect of M-TTR on aggregation of Sup35, M-TTR-GFP construct was transformed in Δ *sup35* strain maintained by either N-MRF (expressing full length Sup35 where N is the prion domain) or MRF (expressing only functional domain of Sup35). This strain also has an *ade1* mutation which encodes for a premature stop codon. Cells were grown in SRaf+Gal selection media, normalized at 0.2 OD and 5 μl of each culture was spotted on 1/4 YPD agar plates and adenine deficient (-Ade) plates. Growth on -Ade plates was monitored after incubating at 30°C for 3 days. The color saturation on YPD medium was observed after incubation at 30°C for 2 days and then at 4°C for 3 days. If Sup35 protein which is a translation termination factor is functional, it terminates the translation of *ADE1* gene at the premature stop codon which results in accumulation of a red pigment giving red coloration to yeast cells on rich media and reduced or no growth on media lacking adenine. However, if Sup35 is in the aggregated form and its function is impaired, it leads to read-through of the premature stop codon and synthesis of full length Ade1 protein. There is no accumulation of red pigment, yeast cells appear white on rich media and grow on media lacking adenine.

Curing of Yeast Prions by Subculturing Yeast Cells on Guanidine Hydrochloride Media

Transformants expressing M-TTR-GFP in different variants of yeast prions: [*psi*$^-$], weak [*PSI*$^+$], strong [*PSI*$^+$], [*pin*$^-$], and [*PIN*$^+$] were cured of the prions by subculturing the cells 4 to 5 times on YPD plate containing 5 mM guanidine hydrochloride (GuHCl) at 30°C till the colonies turned red from pink or white on YPD plates.

Examining the Interaction of M-TTR-GFP and Endogenous Sup35 Aggregates in Yeast by Co-immunoprecipitation

The imunoprecipitation was performed according to the Catch and Release kit protocol (Cat#17-500). Briefly, the protein was isolated from weak [*PSI*$^+$] cells over-expressing either M-TTR-GFP fusion protein or GFP alone by standard glass bead method using 1X lysis buffer (100 mM Tris Cl, 100 mM KCl, 20 mM $MgCl_2$ and 10% glycerol) and total protein was estimated by BCA pierce kit (Cat# 23225). 1 mg of total lysate was incubated with 10 μl of anti-GFP antibodies (Cat# G1544) on column containing resin for overnight at 4°C in continuous rotation. Following incubation, the resin in the column was washed twice with 1X wash buffer to remove non-specifically bound proteins. Immunoprecipitated protein complexes were eluted with hot (95°C) 1X denaturing elution buffer, resolved by 10% SDS-polyacrylamide gels, and analyzed by immunoblotting using antibodies against the Sup35 (BE4, a polyclonal antibody, was a kind gift from Susan Liebman) and GFP (monoclonal antibody, Sigma Cat# 6795).

Statistical Analysis

Statistical analysis was performed using SPSS software for Windows, version 17.0 (SPSS, Chicago, Illinois). Data was checked for normality and two-tailed *t*-test was applied to determine the statistical significance and *p*-value less than 0.05 was considered to be significant.

RESULTS

An Engineered Double Mutant TTR (M-TTR-GFP) Is Monomeric in Yeast and Forms Enhanced Aggregation Compared to Wild Type TTR (WT-TTR-GFP)

To investigate TTR aggregation, wild type TTR was fused to GFP (WT-TTR-GFP) and overexpressed in yeast as described in Materials and Methods section. On overexpression of WT-TTR-GFP, most of the cells showed diffused fluorescence and only 5–7% of cells showed dot-like visible aggregates (**Figures 1A,B**). Since destabilization of TTR tetramer to monomer is important for aggregation, the native state of WT-TTR-GFP was analyzed. WT-TTR-GFP appeared to migrate as a higher molecular weight species at ∼120 KDa (**Figure 1C**, lane 3). It is possible that in yeast WT-TTR-GFP exists as either trimer or tetramer that dissociates into trimer under our experimental conditions (2% SDS without β-mercaptoethanol at 37°C). These higher molecular weight species dissociated into monomer when incubated at 95°C (**Figure 1C**, lane 5). Another possibility is that these higher molecular weight species occur due to interaction of TTR with other cellular components. However, we reasoned it to be a trimer because trimer species have been shown to populate in the serum (Cubedo et al., 2012). Moreover, WT-TTR tetramers are formed by sequential addition of monomers; and trimer intermediates have been observed *in vitro* (Wiseman et al., 2005).

We then introduced two previously (Jiang et al., 2001) defined point mutations, F87M at the monomer-monomer and L110M at the dimer-dimer interface of WT-TTR, which destabilizes the TTR tetramer. As expected, this engineered double mutant, M-TTR-GFP, existed as monomer in yeast (**Figure 1C**, lane 2) and did not migrate at higher molecular weight. On overexpression of M-TTR-GFP, no aggregation of M-TTR-GFP was observed at 24 h and very minute dot-like aggregates start appearing between 36 and 48 h (Figure S1). The aggregates became clearly visible at ∼72 h of incubation

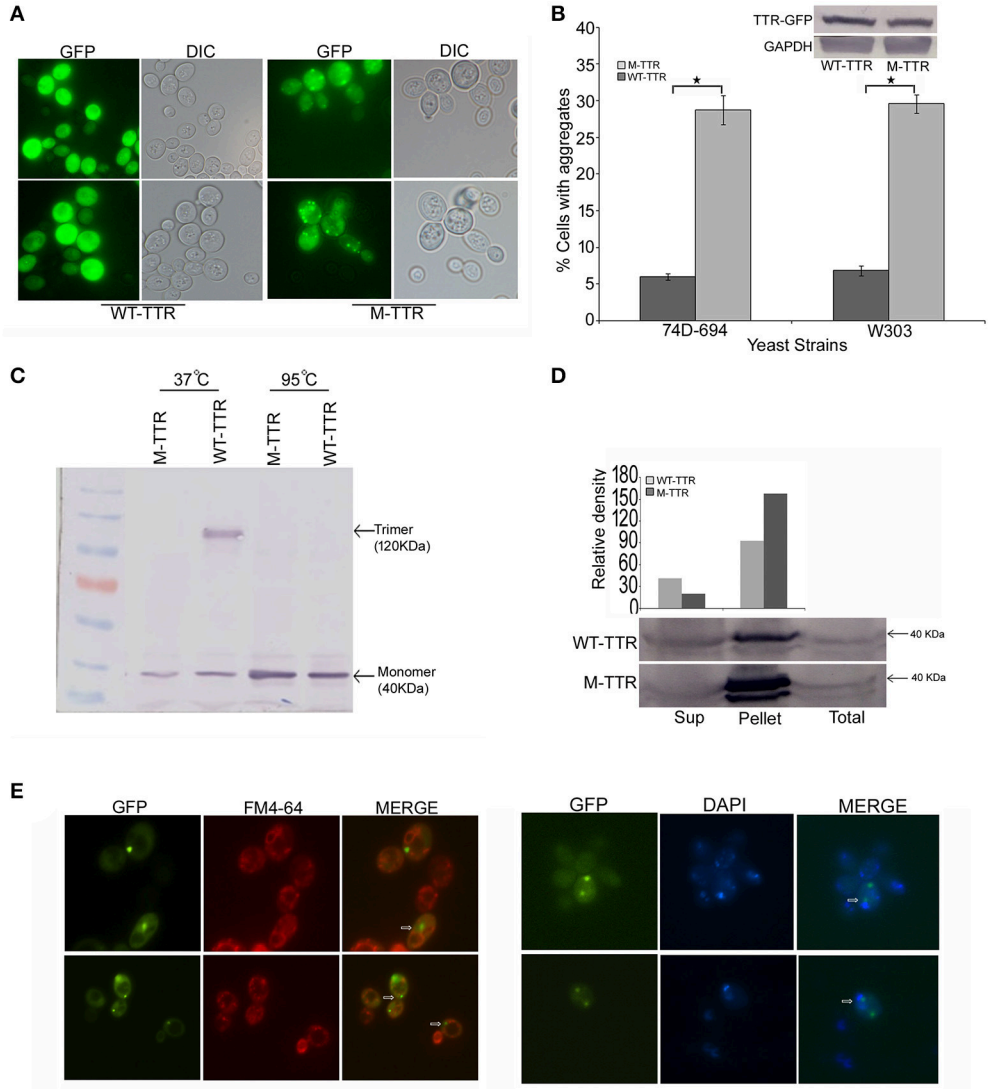

FIGURE 1 | Aggregation and native state of WT-TTR and M-TTR in yeast. **(A)** The microscopic images of TTR aggregation state in yeast cells overexpressing WT-TTR-GFP and M-TTR-GFP after incubation for 72 h at 30°C. **(B)** The aggregate formation due to overexpression of WT-TTR-GFP and M-TTR-GFP was quantified in 74D-694 and W303 strains by calculating percentage of cells with aggregates. Three independent transformants and more than 600 cells were analyzed for each construct. Error bars represent standard errors of the mean of the three transformants. The significant difference in aggregation between WT-TTR-GFP and M-TTR-GFP was analyzed by using two-tailed *t*-test (*depicts *p*-value < 0.05). The inset on top shows the equal protein levels of WT-TTR-GFP and M-TTR-GFP as determined by immunoblotting with anti-GFP antibody. **(C)** Western blot showing the native state of WT-TTR-GFP and M-TTR-GFP in yeast. Cells expressing the two GFP fusion constructs were harvested after 24 h, lysed and the lysates were incubated under non-denaturing (37°C and without β-ME) and denaturing (95°C with β-ME) conditions. Samples were resolved on 10% SDS-PAGE and immunoblotted using anti-GFP antibody. **(D)** Centrifugation assay showing the distribution of WT-TTR-GFP and M-TTR-GFP in supernatant (Sup) and pellet fraction. Cells expressing the WT-TTR-GFP and M-TTR-GFP were harvested after 72 h and protein was isolated. Total protein was normalized before subjecting to centrifugation and equal volumes of all the fractions were loaded. The fractions were resolved on 10% SDS and probed using anti-GFP antibody. One tenth of total protein has been used as a loading control. **(E)** Cellular localization of M-TTR-GFP aggregates was analyzed by staining cells overexpressing M-TTR-GFP aggregates with FM4-64 (vacuolar) and DAPI (nuclear) dye. The images of same cells were captured under FITC and DAPI filters. The images were merged to analyze the localization of M-TTR-GFP aggregates. The white arrows in the merged panel shows the aggregates localized near the vacuole (FM4-64) and nucleus (DAPI).

in inducing media under fluorescent microscope. A significant ($p < 0.05$) and approximately 5-fold increase in percentage of cells with dot-like visible aggregates compared to WT-TTR-GFP in two different (74D-694 and W303) yeast backgrounds (**Figures 1A,B**) was observed at 72 h. It is important to point out that more WT-TTR-GFP protein was present in the insoluble pellet fraction compared to supernatant suggesting presence of non-visible higher molecular weight species on overexpression of WT-TTR-GFP. These higher molecular weight species are the biochemical aggregates which are not visible using microscopic

techniques and may include aggregation intermediates. However, M-TTR-GFP fractionated more than 2-fold in the pellet as compared to the WT-TTR-GFP (**Figure 1D**). It was further ensured that the increase in aggregation was not due to any difference in the expression levels of WT-TTR-GFP and M-TTR-GFP (**Figure 1B**, inset). The effect of aggregates on viability of yeast was monitored by dilution spotting and 7-AAD staining. No effect on growth or viability of yeast cells was observed on either episomal or stable overexpression of WT-TTR-GFP or M-TTR-GFP (data not shown). Thus, TTR-GFP aggregates appeared to be non-toxic in yeast.

Further, to visualize the cellular localization of M-TTR-GFP aggregates, cells overexpressing M-TTR-GFP were stained with FM4-64 (vacuolar staining dye) and DAPI (nucleolar staining dye). Similar to several other amyloid proteins, bigger M-TTR-GFP aggregates were observed at periphery of vacuole and smaller aggregates near the nucleus (Braun et al., 2010) (**Figure 1E**).

The pH has been previously shown to be a factor that triggers tetramer dissociation, partial unfolding and aggregation of TTR *in vitro* (Jiang et al., 2001; Lim et al., 2013; Xue et al., 2014). It has been earlier contested and demonstrated that intracellular pH of yeast is altered by the external pH (Slavík, 1983; Thevelein et al., 1987). We also analyzed the affect of pH of media on the intracellular pH of yeast cells using Lysotracker Red probe which is an acidotropic probe and commonly used to stain acidic organelles. At external pH 7.4, vacuoles, the acidic compartment of yeast, were stained in all the cells and no cytoplasmic staining was observed. At pH 6.5, vacuoles were stained in more than 80% of the cells and cytoplasmic staining was observed in approximately 20% of the cells. Interestingly, at pH 4.2, more than 90% of the cells showed cytoplasmic staining suggesting the acidic nature of the cell interior (**Figure 2C**). There was no difference in Lysotracker staining after culturing for 24 or 36 h in media with different pH.

To monitor whether pH of the media has any effect on TTR aggregation in yeast, cells expressing either WT-TTR-GFP or M-TTR-GFP constructs were grown in inducing media with different pH. The percentage of cells exhibiting M-TTR-GFP aggregates was significantly reduced by 4-fold at higher pH compared to acidic pH (**Figure 2A**). Even, the WT-TTR-GFP aggregates were completely abolished at pH 6.5. It was also ascertained that the difference in aggregation at two different pHs was not due to different expression levels (**Figure 2A**, inset) or cell death as monitored by dilution spotting (**Figure 2B**) and 7-AAD staining (data not shown). Thus, WT-TTR-GFP or M-TTR-GFP aggregation in yeast is susceptible to acidic pH and recapitulates the *in vitro* scenario.

[*PSI*$^+$], an Endogenous Prion Form of Sup35 Enhances Visible M-TTR-GFP Aggregates

Endogenous yeast prions have been suggested to interact with other amyloid proteins. [*PSI*$^+$] is a phenotypic trait of endogenous prion form of Sup35p and exists as different variants in yeast (Uptain et al., 2001) whereas [*psi*$^-$] represents the non-prion form of Sup35p. In order to determine the interaction of TTR with yeast prion protein Sup35, we examined the effect of variants of [*PSI*$^+$] on M-TTR-GFP aggregation. A significant ($p < 0.05$) 2-fold increase in cells with visible M-TTR-GFP aggregates was observed in weak [*PSI*$^+$] and more than 1.5-folds in strong [*PSI*$^+$] as compared to [*psi*$^-$] strain (**Figure 3A**, dark gray bars). Again, the difference in aggregation was not due to any significant change in expression levels of M-TTR-GFP in the different strains (**Figure 3A**, left inset).

To confirm that the enhanced aggregation of TTR is solely due to presence of [*PSI*$^+$], endogenous prion was cured from these transformants by passaging 8–10 times on guanidine hydrochloride (GuHCl) plates. Curing of [*PSI*$^+$] leads to the elimination of prion and was monitored by change in coloration from white/pink ([*PSI*$^+$]) to red as in ([*psi*$^-$]) strain (**Figure 3A** right inset). After curing of the prion, the expression of M-TTR-GFP was re-induced in these [*psi*$^-$] cells. Interestingly, M-TTR-GFP aggregation was remarkably reduced on losing the prion form of Sup35. (**Figure 3A**, light gray bars). This data indicates that yeast prion, [*PSI*$^+$] is able to promote M-TTR-GFP aggregation.

Additionally, we overexpressed M-TTR-GFP in another [*PSI*$^+$] *sup35*Δ *ade1-14* strain maintained by full length Sup35 expressed on a plasmid (N-MRF). The control non-prion form of this strain was maintained by expressing only the functional domain (MRF) but lacking the prion (N) domain of Sup35. Even in this strain background, a significant ($p < 0.05$) 2-fold increase in cells with visible aggregates of M-TTR-GFP was observed in the presence of aggregated N-MRF [*PSI*$^+$] as compared to soluble MRF strain (**Figure 3B**, upper panel). This again supported the interaction amongst these two heterologous amyloid proteins lacking any sequence similarity. We further exploited this experimental set up to examine if overexpression of M-TTR-GFP cures [*PSI*$^+$]. On overexpressing GFP alone, N-MRF [*PSI*$^+$] strain is white or pink in color on YPD media and grows on -Ade media whereas cells expressing the functional, non-aggregated MRF domain of Sup35 are red on YPD and do not grow on -Ade media (**Figure 3B**, lower panel). On overexpression of M-TTR-GFP, however, no change in the color of the N-MRF expressing cells on rich media or growth on -Ade media (**Figure 3B**, lower panel) was observed. Thus, it appears that M-TTR-GFP is not able to cure the yeast prion, [*PSI*$^+$].

To further verify whether these two heterologous amyloid aggregates are merely sharing the common cellular space or they exhibit any direct interaction, M-TTR-GFP fusion protein was overexpressed in a weak [*PSI*$^+$] strain and M-TTR-GFP aggregates were pulled down using anti-GFP antibody. Sup35 protein co-immunoprecipated with M-TTR-GFP aggregates but was not pulled down from the cells overexpressing GFP alone as the control (**Figure 3C**). This observation suggests that Sup35 directly interacts with M-TTR aggregates.

In addition to [*PSI*$^+$], another yeast prion [*PIN*$^+$] was also examined for its effect on M-TTR aggregation. [*PIN*$^+$] is the prion form of Rnq1 and has been shown to induce [*PSI*$^+$] and Htt aggregation in yeast. However, we did not observe any significant

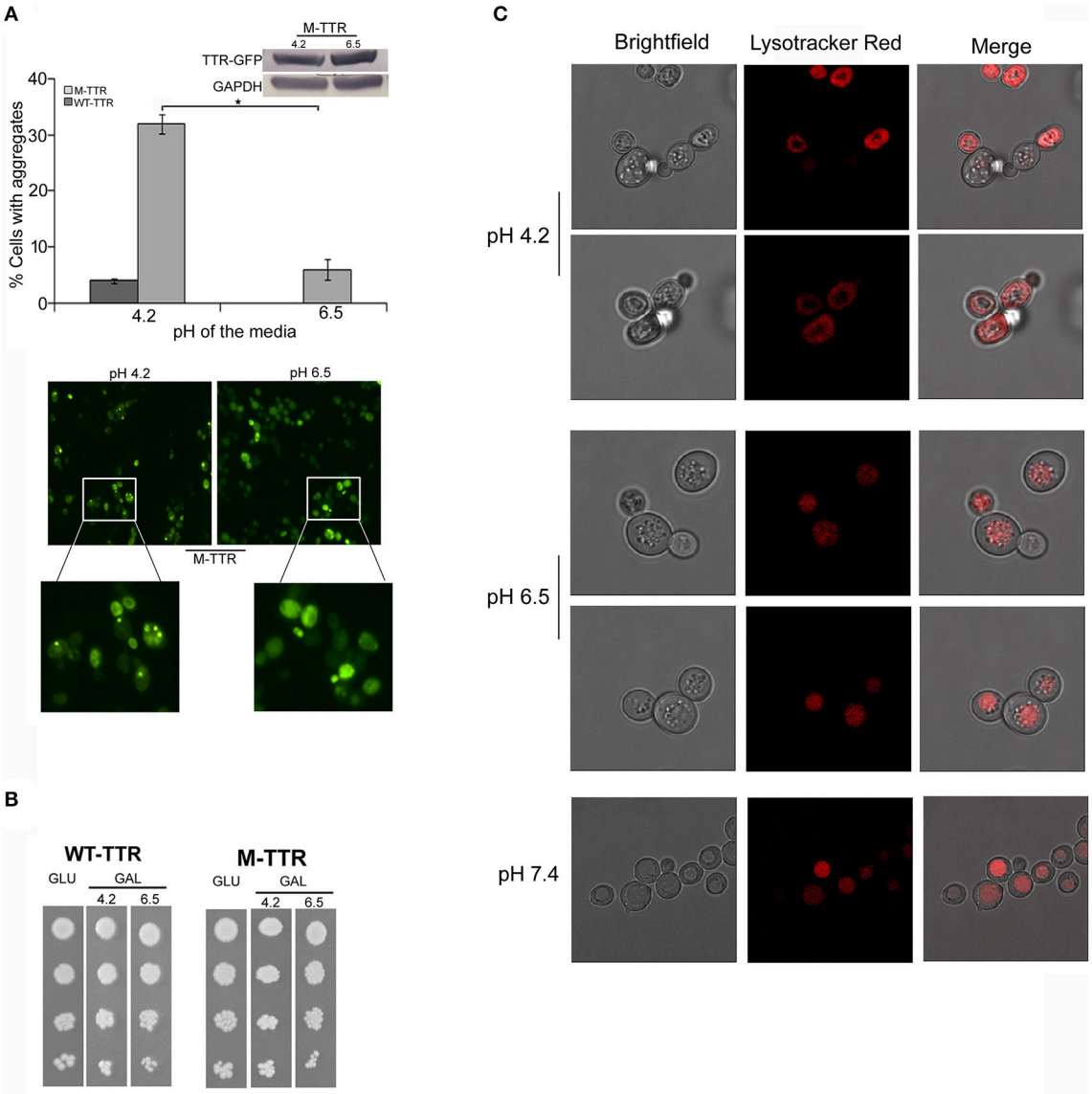

FIGURE 2 | Effect of pH of the inducing media on TTR aggregation. **(A)** The effect of pH on TTR aggregation in yeast was assessed by overexpressing cells with WT-TTR-GFP or M-TTR-GFP in inducing media at pH 4.2 and pH 6.5. The percentage of cells with aggregates was counted manually under the microscope. Three independent transformants for each construct were analyzed under both conditions. Error bars in each graph represent standard errors of the mean of triplicates. To assess the significance of difference in aggregation of M-TTR-GFP at pH 4.2 and pH 6.5, two-tailed *t*-test was performed (*depicts *p*-value < 0.05). Equal levels of M-TTR-GFP protein at different pH were determined by immunoblotting with anti-GFP antibody. The lower panel shows a representative microscopic image of yeast cells with M-TTR-GFP aggregates at pH 4.2 and pH 6.5. **(B)** The viability of cells overexpressing M-TTR-GFP at pH 4.2 and 6.5 was determined by serial dilution spotting on inducing media (upper panel). **(C)** The microscopic images showing staining of acidic regions in the cells grown in media for 24 h with different pH using Lysotracker Red DND. Images were captured using confocal microscope Leica TCS SP8 and processed using LAS X 3.1.1 software.

difference in the percentage of cells with M-TTR-GFP aggregates in [*PIN*$^+$] and [*pin*$^-$] cells (**Figure 3D**).

Overexpressed Prion (NM) Domain of Sup35 Enhances M-TTR-GFP Aggregation

To verify the inducing effect of Sup35 on M-TTR aggregation, we co-overexpressed M-TTR-GFP and prion (NM) domain of Sup35 fused to RFP (NM-RFP) in a [*psi*$^-$] [*PIN*$^+$] strain. A 2-fold increase in M-TTR-GFP aggregation was observed in the presence of overexpressed NM-RFP (∼21%) as compared to RFP (∼10%). On analyzing the cells for aggregates, single, two and multiple dots were observed for M-TTR-GFP and peripheral rings, lines and dots for NM-RFP as tabulated in **Table 1**. In about 8% of the cells, both M-TTR-GFP and NM-RFP aggregates were present and more than 90% of these cells showed colocalization. The M-TTR-GFP dots colocalized with dot-, line- (at the ends) and peripheral ring/mesh-like aggregates of NM-RFP (**Figure 4**). The Pearson's correlation coefficient (R^2) ranged from

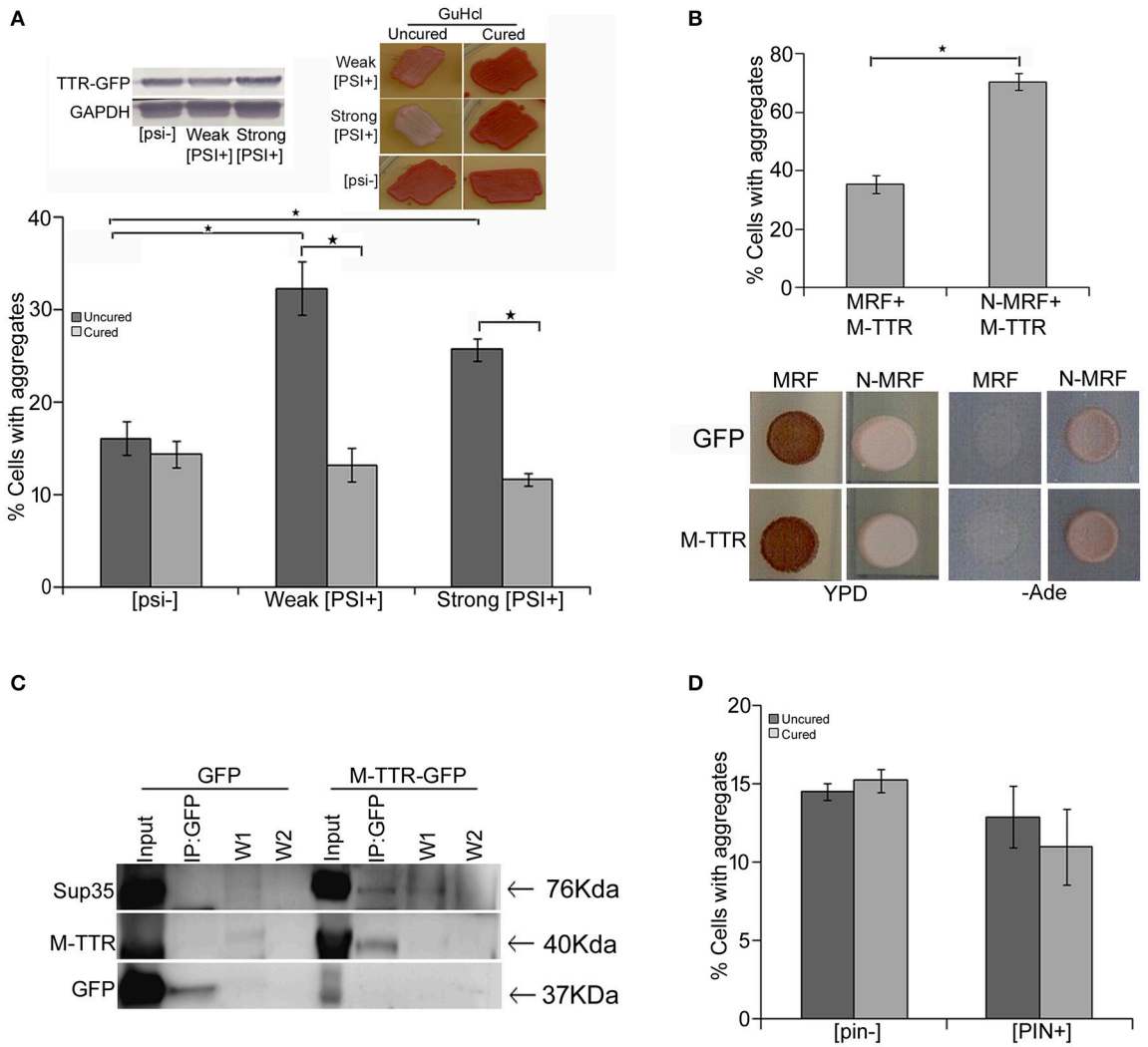

FIGURE 3 | Effect of endogenous prion strains on M-TTR aggregation. **(A)** The effect of endogenous prion, [*PSI*$^+$], on M-TTR aggregation was analyzed by manually counting percentage of cells with M-TTR-GFP aggregates (under the microscope) in [*psi*$^-$] (non-prion) and weak and strong variants of [*PSI*$^+$], depicted as uncured strains in the graph. Left inset: Equal levels of M-TTR-GFP protein in different strains were determined by immunobloting using anti-GFP antibody. M-TTR-GFP aggregation was again determined after curing the [*PSI*$^+$] prion in these strains by passaging on GuHCL (right inset), depicted as cured in the graph. Error bars represent standard errors of the mean of three independent transformants. The significant difference in aggregation between [*PSI*$^+$] variants and [*psi*$^-$] as well as between uncured and cured strains was assessed by using two-tailed *t*-test (*depicts *p*-value < 0.05). **(B)** Upper panel: Percentage of cells with M-TTR-GFP aggregates were analyzed in a [*PSI*$^+$] *sup35*Δ *ade1-14* strain maintained by either expression of full length (N-MRF) or the functional domain (MRF) lacking the prion (N) domain of Sup35. The strain expressing MRF could not propagate [*PSI*$^+$]. Aggregation counting for all the experiments was done for atleast three independent transformants for each sample. Error bars represent standard errors of the mean of triplicates. To assess the significant difference in M-TTR-GFP aggregation between N-MRF and MRF expressing cells, two-tailed *t*-test was performed (*depicts *p*-value < 0.05). Lower panel: The effect of M-TTR-GFP in curing [*PSI*$^+$] prion was analyzed by co-overexpressing M-TTR-GFP and N-MRF in [*PSI*$^+$] *sup35*Δ *ade1-14* and spotting on rich media (YPD) and media lacking adenine (-Ade). Cells were examined for any change in coloration from white/pink (prion) to red (non-prion) on rich media and growth on -Ade media. M-TTR-GFP co-expressed with MRF (soluble functional domain of Sup35) and GFP alone co-expressed with MRF as well as N-MRF were used as controls. **(C)** Direct interaction of heterologous aggregates was examined by pull down of Sup35 with M-TTR-GFP aggregates. A weak [*PSI*$^+$] strain overexpressing M-TTR-GFP fusion protein were lysed and incubated with anti-GFP antibody conjugated beads in a column. Cells overexpressing GFP were used as a control. Total protein of M-TTR-GFP and GFP lysates were normalized before incubation with the anti-GFP beads. The incubation complexes were washed twice (W1 and W2) and co-precipitated protein was eluted (IP:GFP) and resolved on 10% SDS-PAGE. Blot was probed with anti-GFP and anti-Sup35 (BE4) antibodies. Input fraction is 100 μg of the total protein lysates. **(D)** The effect of endogenous yeast prion [*PIN*$^+$] on M-TTR aggregation was also analyzed by counting the percentage of cells with M-TTR-GFP aggregates in [*pin*$^-$] (non-prion) and [*PIN*$^+$] (prion) form of Rnq1. Aggregation counting was done for three independent transformants for each. Error bars represent standard errors of the mean of triplicates. The significance of difference in M-TTR-GFP aggregation between [*PIN*$^+$] and [*pin*$^-$] samples was analyzed by using two-tailed *t*-test (*depicts *p*-value < 0.05).

TABLE 1 | Enumeration of colocalization of M-TTR-GFP and NM-RFP aggregates.

% Cells with visible aggregates		% Cells with both M-TTR-GFP and NM-RFP aggregates	% Cells with co-localization
M-TTR-GFP aggregates 10.2% single dot 4.5% two dots 6.5% multiple dots	21.2	8.2%	94% of the cells with both the aggregates
NM-RFP aggregates 3% peripheral rings 0.7% lines 7.2% dots	10.9		

Total number of cells analyzed for co-localization (n) = 610.

0.5 (for rings and lines) to 0.95 (for dots) and suggested a positive correlation of colocalization. No correlation was found between M-TTR-GFP and cytoplasmic expression of RFP alone (**Figure 4**). This co-localization again supports the probability of interaction between the two amyloid proteins. However, we again did not notice any significant increase in aggregation of NM-RFP (data not shown) due to the overexpression of M-TTR-GFP compared to GFP. This finding is consistent with the earlier report where addition of wild type TTR fibrils did not accelerate aggregation of Sup35-NM-YFP (Derkatch et al., 2004). Thus, the interaction of M-TTR and Sup35-NM appears to be unidirectional where overexpression of NM-RFP enhances M-TTR-GFP aggregation but not vice-a versa.

DISCUSSION

Tetramer dissociation of native TTR to monomers has been demonstrated to be the rate-limiting step for aggregation. In our study, wild type TTR fused to GFP exists majorly as trimer or tetramer in yeast and did not readily form visible aggregates, which is consistent with a previous observation by Gomes et al. (2012). Further, *in vitro* experiments have established that partial denaturation of transthyretin under acidic conditions cause structural changes, yielding a conformational intermediate that can self-assemble to form aggregates (McCutchen et al., 1993; Lai et al., 1996; Jiang et al., 2001; Lim et al., 2013). Here, we observed that an engineered monomeric variant of transthyretin (M-TTR) readily forms aggregates in yeast when cultured in acidic media. Interestingly, these aggregates diminished significantly at near physiological pH of the media. It is noteworthy that external pH has been shown to have effect on the cytoplasmic pH in yeast (Slavík, 1982, 1983; Valli et al., 2005). Our data also supports that when pH of the media is acidic, the cell interior also becomes acidic. Thus, aggregation of M-TTR in yeast recapitulated the *in vitro* aggregation (Jiang et al., 2001). We further exploited M-TTR aggregation model in yeast to examine the interaction of TTR with yeast prions.

Co-existence of different amyloid proteins and presence of overlapping clinico-pathological features can be probably explained by interaction among heterologous amyloid proteins. It is evident from past many studies that aggregates of one protein can accelerate or inhibit the *de novo* appearance of other amyloid proteins. Most of the earlier studies suggested sequence similarity to be the determining factor for interaction amongst heterologous amyloid proteins (Krebs et al., 2004). However, over the years, several evidences indicate that efficacy of cross-seeding does not correlate linearly with the sequence similarities. Mutant Aβ amyloid protein that differs at one amino acid is not able to seed aggregation of wild type Aβ40 (O'Nuallain et al., 2004). Interactions among Q-rich and non-Q-rich yeast or fungal prion proteins [(Sup35 and Mod5) and (Rnq1 and Het-s)] have also been demonstrated (Taneja et al., 2007; Arslan et al., 2015). Clinically, oligomerization of α-synuclein that is associated with Parkinson's disease has been observed in amyloid plaques in Alzheimer's (Hamilton, 2000), Huntington's (Charles et al., 2000), and ATTR (Guerreiro et al., 2012). In this study, we investigated the interaction between human TTR, a non-Q-rich amyloid protein and yeast prion protein Sup35 in the yeast model. Despite no sequence similarity, [PSI^+], the endogenous prion form of Sup35 significantly enhanced aggregation of the engineered monomeric TTR-GFP. Further, variants of [PSI^+] have been suggested to have different structural organizations and seed amyloid proteins with varying degrees. We also observed that different variants of [PSI^+] seed M-TTR with different efficiencies. Loss of [PSI^+] variants reduced the aggregation of M-TTR-GFP and thereby showed that enhanced aggregation was infact due to presence of heterologous seeds of [PSI^+]. Increase in aggregation of M-TTR-GFP on overexpression of the prion (NM) domain of Sup35 further suggested the interaction between these two amyloid proteins. Our data also showed direct interaction between them as Sup35 was immunocaptured with M-TTR-GFP. Even the aggregation of WT-TTR-GFP, which showed very low aggregation, was enhanced in the presence of [PSI^+] (data not shown).

Similar to Sup35 aggregates, M-TTR-GFP aggregates were also observed in the perivacuolar or juxtranuclear region in the cell. It can be debated that existing in the same cellular niche might be increasing the probability of interaction between these two heterologous amyloid proteins. However, another Q-rich yeast prion [PIN^+], which is known to seed [PSI^+] (Derkatch et al., 2001) and other heterologous amyloid proteins (Meriin et al., 2002; Derkatch et al., 2004; Taneja et al., 2007), despite being localized in the same spatial compartments in the cell, did not cause any significant effect on M-TTR-GFP aggregation. This brings to the possibility that resemblance of structural fold between the heterologous seed and misfolded soluble monomer of the protein to be seeded may influence the interaction and determine the seeding efficiency. Recent evidences suggest vast structural diversity among amyloid proteins and even the same polypeptide can adopt different conformation that give rise to different variants or strains as observed for prions. Hence, further structural insight may help in addressing the interaction between heterologous amyloid proteins and its role in genesis and progression of various amyloid disorders.

Additionally, our study highlights non-reciprocity in heterologous seeding. We did not observe any effect of M-TTR-GFP on Sup35 aggregation as previously shown by

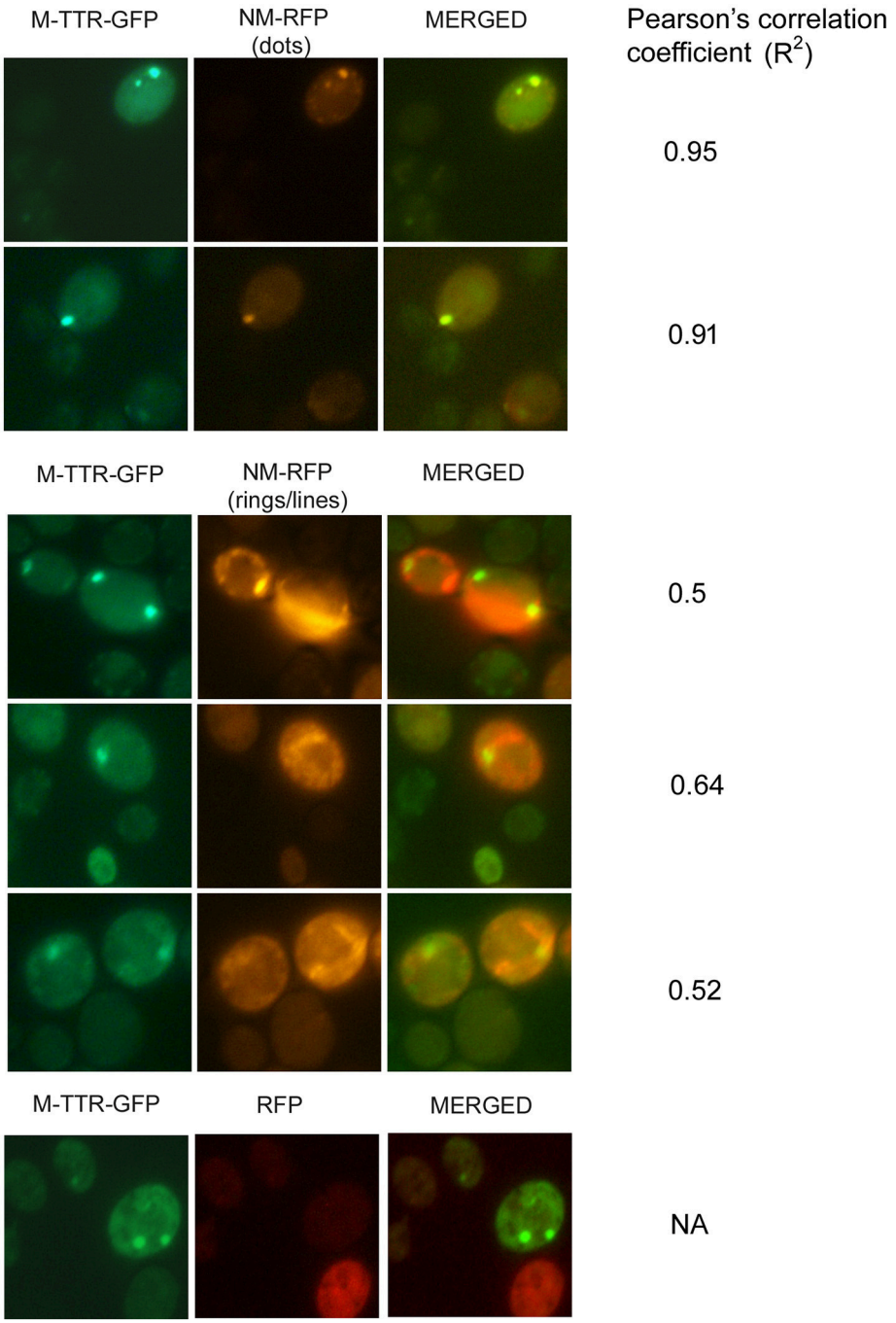

FIGURE 4 | Colocalization of M-TTR-GFP and Sup35 aggregates. The microscopic images showing colocalization of M-TTR-GFP dots and Sup35 dots-, lines-, ring/mesh- like aggregates on co-overexpression of M-TTR-GFP and NM domain of Sup35 fused to RFP (NM-RFP) in yeast cells. Images were captured under FITC (GFP) and TRITC (RFP) channels and merged using NIS-Elements AR3.2 software. Pearson's correlation coefficient was determined using Coloc2.

Derkatch et al. (2004). They observed occasional colocalization of Sup35 (NM-YFP) with WT-TTR aggregates but WT-TTR aggregates did not promote the [*PSI*$^+$] induction. They stated that colocalization in the same cellular niche does not necessarily suggest interaction amongst the two amyloid proteins. However, our data suggests that this colocalization of M-TTR-GFP and NM-RFP (Sup35) results in unidirectional interaction which promotes M-TTR-GFP aggregation but not vice-a-versa. This lack of reciprocity in seeding has been documented for other amyloid proteins including Aβ and IAPP (O'Nuallain et al., 2004) and TTR and IAPP (Westermark and Westermark, 2008). Thus, we believe that the detailed structural determination

of TTR and Sup35 may reveal an important aspect of cross seeding efficiencies. Further, targeting M-TTR to a different cellular compartment might help to establish that colocalization and direct interaction with Sup35 aggregates enhances M-TTR aggregation.

Thus, our findings provide evidence for interaction of transthyretin, a non-Q-rich amyloid protein with a Q-rich heterologous yeast prion protein that can be further explored for their relevance in the clinical scenario. Such interactions between heterologous amyloid proteins may explain how occurrence of one amyloid disorder could induce the development of another amyloid disorder. While our finding that Sup35 directly interacts with M-TTR aligns with the cross-seeding model, however the alternate possibility of indirect sequestration of cellular factors could not be ruled out. Since cellular pathways controlling aggregate formation appear to be conserved from yeast to mammals, therefore evaluating titration of other cellular factors during heterologous interaction might provide new approach for amyloid disease intervention.

AUTHOR CONTRIBUTIONS

MV and VT: Conceived and designed the experiments; MV and AG: Performed the experiments; MV, AG, RK, NG, and VT: Analyzed the data; MV and BP: Interpretation of data; MV, RK, and VT: Wrote the manuscript; RK, BP, and NG: Critically reviewed the paper.

ACKNOWLEDGMENTS

VT acknowledges the funding from Innovative Young Biotechnology Award 2007, Department of Biotechnology, India. MV acknowledges the Senior Research Fellowship from the Indian Council of Medical Research. We are also thankful to Dr. Bhupesh Taneja for healthy discussions and valuable suggestions during the preparation of manuscript. We are also thankful to Vishal Chauhan for critically reading the manuscript. We are also thankful to Swarna Naidu, Abhishek Vats, and Kavita Pahuja for their help in the initial experimentation. We would also like to acknowledge Dr. C.V. Srikanth, Dr. Selvapandiyan, and Gayatri for providing certain reagents.

SUPPLEMENTARY MATERIAL

The Supplementary Material for this article can be found online at: https://www.frontiersin.org/articles/10.3389/fnmol.2018.00075/full#supplementary-material

REFERENCES

Arslan, F., Hong, J. Y., Kanneganti, V., Park, S. K., and Liebman, S. W. (2015). Heterologous aggregates promote de novo prion appearance via more than one mechanism. *PLoS Genet.* 11:e1004814. doi: 10.1371/journal.pgen.1004814

Bagriantsev, S., and Liebman, S. (2006). Modulation of $A\beta_{42}$ low-n oligomerization using a novel yeast reporter system. *BMC Biol.* 4:32. doi: 10.1186/1741-7007-4-32

Bradley, M. E., Edskes, H. K., Hong, J. Y., Wickner, R. B., and Liebman, S. W. (2002). Interactions among prions and prion "strains" in yeast. *Proc. Natl. Acad. Sci. U.S.A.* 99(Suppl. 4), 16392–16399. doi: 10.1073/pnas.152330699

Bradley, M. E., and Liebman, S. W. (2003). Destabilizing interactions among [PSI(+)] and [PIN(+)] yeast prion variants. *Genetics* 165, 1675–1685.

Braun, R. J., Büttner, S., Ring, J., Kroemer, G., and Madeo, F. (2010). Nervous yeast: modeling neurotoxic cell death. *Trends Biochem. Sci.* 35, 135–144. doi: 10.1016/j.tibs.2009.10.005

Charles, V., Mezey, E., Reddy, P. H., Dehejia, A., Young, T. A., Polymeropoulos, M. H., et al. (2000). Alpha-synuclein immunoreactivity of huntingtin polyglutamine aggregates in striatum and cortex of Huntington's disease patients and transgenic mouse models. *Neurosci. Lett.* 289, 29–32. doi: 10.1016/S0304-3940(00)01247-7

Choi, S. H., Leight, S. N., Lee, V. M., Li, T., Wong, P. C., Johnson, J. A., et al. (2007). Accelerated Abeta deposition in APPswe/PS1deltaE9 mice with hemizygous deletions of TTR (transthyretin). *Neuroscience.* 27, 7006–7010. doi: 10.1523/JNEUROSCI.1919-07.2007

Cubedo, J., Padró, T., Alonso, R., Cinca, J., Mata, P., and Badimon, L. (2012). Differential proteomic distribution of TTR (pre-albumin) forms in serum and HDL of patients with high cardiovascular risk. *Atherosclerosis* 222, 263–269. doi: 10.1016/j.atherosclerosis.2012.02.024

Derkatch, I. L., Bradley, M. E., Hong, J. Y., and Liebman, S. W. (2001). Prions affect the appearance of other prions: the story of [PIN$^+$]. *Cell* 106, 171–182. doi: 10.1016/S0092-8674(01)00427-5

Derkatch, I. L., Chernoff, Y. O., Kushnirov, V. V., Inge-Vechtomov, S. G., and Liebman, S. W. (1996). Genesis and variability of *[PSI]* prion factors in *Saccharomyces cerevisiae*. *Genetics* 144, 1375–1386.

Derkatch, I. L., Uptain, S. M., Outeiro, T. F., Krishnan, R., Lindquist, S. L., and Liebman, S. W. (2004). Effects of Q/N-rich, polyQ, and non-polyQ amyloids on the de novo formation of the [PSI+] prion in yeast and aggregation of Sup35 *in vitro*. *Proc. Natl. Acad. Sci. U.S.A.* 101, 12934–12939. doi: 10.1073/pnas.0404968101

Du, Z., and Li, L. (2014). Investigating the interactions of yeast prions: [SWI+], [PSI+], and [PIN+]. *Genetics* 197, 685–700. doi: 10.1534/genetics.114.163402

Du, Z., Park, K. W., Yu, H., Fan, Q., and Li, L. (2008). Newly identified prion linked to the chromatin-remodeling factor Swi1 in *Saccharomyces cerevisiae*. *Nat. Genet.* 40, 460–465. doi: 10.1038/ng.112

Gietz, R. D., and Woods, R. A. (2002). Transformation of yeast by lithium acetate/single-stranded carrier DNA/polyethylene glycol method. *Meth. Enzymol.* 350, 87–96. doi: 10.1016/S0076-6879(02)50957-5

Gomes, R. A., Franco, C., Da Costa, G., Planchon, S., Renaut, J., Ribeiro, R. M., et al. (2012). The proteome response to amyloid protein expression *in vivo*. *PLoS ONE* 7:e50123. doi: 10.1371/journal.pone.0050123

Guerreiro, A., da Costa, G., Gomes, R. A., Ribeiro-Silva, C., Gilberto, S., Mateus, E., et al. (2012). α-Synuclein aggregation in the saliva of familial transthyretin amyloidosis: a potential biomarker. *Amyloid* 19, 74–80. doi: 10.3109/13506129.2012.668500

Hamilton, R. L. (2000). Lewy bodies in Alzheimer's disease: a neuropathological review of 145 cases using alpha-synuclein immunohistochemistry. *Brain Pathol.* 10, 378–384. doi: 10.1111/j.1750-3639.2000.tb00269.x

Hammarström, P., Jiang, X., Hurshman, A. R., Powers, E. T., and Kelly, J. W. (2002). Sequence-dependent denaturation energetics: a major determinant in amyloid disease diversity. *Proc. Natl. Acad. Sci. U.S.A.* 99, 16427–16432. doi: 10.1073/pnas.202495199

Jarrett, J. T., and Lansbury, P. T. Jr. (1993). Seeding "one-dimensional crystallization" of amyloid: a pathogenic mechanism in Alzheimer's disease and scrapie? *Cell* 73, 1055–1058.

Jiang, X., Smith, C. S., Petrassi, H. M., Hammarström, P., White, J. T., Sacchettini, J. C., et al. (2001). An engineered transthyretin monomer that is nonamyloidogenic unless it is partially denatured. *Biochemistry* 40, 11442–11452. doi: 10.1021/bi011194d

Jones, E. M., and Surewicz, W. K. (2005). Fibril conformation as the basis of species- and strain-dependent seeding specificity of mammalian prion amyloids. *Cell* 121, 63–72. doi: 10.1016/j.cell.2005.01.034

Kantcheva, R. B., Mason, R., and Giorgini, F. (2014). Aggregation-prone proteins modulate huntingtin inclusion body formation in yeast. *PLoS Curr*. 6:ecurrents.hd.501008f3051342c9a5c0cd0f3a5bf3a4. doi: 10.1371/currents.hd.501008f3051342c9a5c0cd0f3a5bf3a4

Krebs, M. R., Morozova-Roche, L. A., Daniel, K., Robinson, C. V., and Dobson, C. M. (2004). Observation of sequence specificity in the seeding of protein amyloid fibrils. *Protein Sci.* 13, 1933–1938. doi: 10.1110/ps.04707004

Krishnan, R., and Lindquist, S. L. (2005). Structural insights into a yeast prion illuminate nucleation and strain diversity. *Nature* 435, 765–772. doi: 10.1038/nature03679

Kryndushkin, D. S., Shewmaker, F., and Wickner, R. B. (2008). Curing of the [URE3] prion by Btn2p, a Batten disease-related protein. *EMBO J.* 27, 2725–2735. doi: 10.1038/emboj.2008.198

Lai, Z., Colón, W., and Kelly, J. W. (1996). The acid-mediated denaturation pathway of transthyretin yields a conformational intermediate that can self-assemble into amyloid. *Biochemistry* 35, 6470–6482. doi: 10.1021/bi952501g

Liebman, S. W., and Derkatch, I. L. (1999). The yeast [PSI+] prion: making sense of nonsense. *J. Biol. Chem.* 274, 1181–1184. doi: 10.1074/jbc.274.3.1181

Lim, K. H., Dyson, H. J., Kelly, J. W., and Wright, P. E. (2013). Localized structural fluctuations promote amyloidogenic conformations in transthyretin. *J. Mol. Biol.* 425, 977–988. doi: 10.1016/j.jmb.2013.01.008

McCutchen, S. L., Colon, W., and Kelly, J. W. (1993). Transthyretin mutation Leu-55-Pro significantly alters tetramer stability and increases amyloidogenicity. *Biochemistry* 32, 12119–12127. doi: 10.1021/bi00096a024

Mead, S., Gandhi, S., Beck, J., Caine, D., Gajulapalli, D., Carswell, C., et al. (2013). A novel prion disease associated with diarrhea and autonomic neuropathy. *N. Engl. J. Med.* 369, 1904–1914. doi: 10.1056/NEJMoa1214747

Mead, S., and Reilly, M. M. (2015). A new prion disease: relationship with central and peripheral amyloidoses. *Nat. Rev. Neurol.* 11, 90–97. doi: 10.1038/nrneurol.2014.263

Meriin, A. B., Zhang, X., He, X., Newnam, G. P., Chernoff, Y. O., and Sherman, M. Y. (2002). Huntington toxicity in yeast model depends on polyglutamine aggregation mediated by a prion-like protein Rnq1. *J. Cell Biol.* 157, 997–1004. doi: 10.1083/jcb.200112104

Morales, R., Green, K. M., and Soto, C. (2009). Cross currents in protein misfolding disorders: interactions and therapy. *CNS Neurol. Disord. Drug Targets* 8, 363–371. doi: 10.2174/187152709789541998

Morales, R., Moreno-Gonzalez, I., and Soto, C. (2013). Cross-seeding of misfolded proteins: implications for etiology and pathogenesis of protein misfolding diseases. *PLoS Pathog.* 9:e1003537. doi: 10.1371/journal.ppat.1003537

O'Nuallain , B., Williams, A. D., Westermark, P., and Wetzel, R. (2004). Seeding specificity in amyloid growth induced by heterologous fibrils. *J. Biol. Chem.* 279, 17490–17499. doi: 10.1074/jbc.M311300200

Patel, B. K., Gavin-Smyth, J., and Liebman, S. W. (2009). The yeast global transcriptional co-repressor protein Cyc8 can propagate as a prion. *Nat. Cell Biol.* 11, 344–349. doi: 10.1038/ncb1843

Patino, M. M., Liu, J. J., Glover, J. R., and Lindquist, S. (1996). Support for the prion hypothesis for inheritance of a phenotypic trait in yeast. *Science* 273, 622–626.

Ripaud, L., Chumakova, V., Antonin, M., Hastie, A. R., Pinkert, S., Körner, R., et al. (2014). Overexpression of Q-rich prion-like proteins suppresses polyQ cytotoxicity and alters the polyQ interactome. *Proc. Natl. Acad. Sci. U.S.A.* 111, 18219–18224. doi: 10.1073/pnas.1421313111

Safar, J., Wille, H., Itri, V., Groth, D., Serban, H., Torchia, M., et al. (1998). Eight prion strains have PrP(Sc) molecules with different conformations. *Nat. Med.* 4, 1157–1165. doi: 10.1038/2654

Schlumpberger, M., Prusiner, S. B., and Herskowitz, I. (2001). Induction of distinct [URE3] yeast prion strains. *Mol. Cell. Biol.* 21, 7035–7046. doi: 10.1128/MCB.21.20.7035-7046.2001

Schwarzman, A. L., Gregori, L., Vitek, M. P., Lyubski, S., Strittmatter, W. J., Enghilde, J. J., et al. (1994). Transthyretin sequesters amyloid beta protein and prevents amyloid formation. *Proc. Natl. Acad. Sci. U.S.A.* 91, 8368–8372. doi: 10.1073/pnas.91.18.8368

Schwimmer, C., and Masison, D. C. (2002). Antagonistic interactions between yeast [PSI(+)] and [URE3] prions and curing of [URE3] by Hsp70 protein chaperone Ssa1p but not by Ssa2p. *Mol. Cell. Biol.* 22, 3590–3598. doi: 10.1128/MCB.22.11.3590-3598.2002

Slavík, J. (1982). Intracellular pH of yeast cells measured with fluorescent probes. *FEBS Lett.* 140, 22–26. doi: 10.1016/0014-5793(82)80512-7

Slavík, J. (1983). Intracellular pH topography: determination by a fluorescent probe. *FEBS Lett.* 156, 227–230. doi: 10.1016/0014-5793(83)80501-8

Tanaka, M., Collins, S. R., Toyama, B. H., and Weissman, J. S. (2006).The physical basis of how prion conformations determine strain phenotypes. *Nature* 442, 585–589. doi: 10.1038/nature04922

Taneja, V., Maddelein, M. L., Talarek, N., Saupe, S. J., and Liebman, S. W. (2007). A non-Q/N-rich prion domain of a foreign prion, [Het-s], can propagate as a prion in yeast. *Mol. Cell* 27, 67–77. doi: 10.1016/j.molcel.2007.05.027

Thevelein, J. M., Beullens, M., Honshoven, F., Hoebeeck, G., Detremerie, K., den Hollander, J. A., et al. (1987). Regulation of the cAMP level in the yeast *Saccharomyces cerevisiae*: intracellular pH and the effect of membrane depolarizing compounds. *J. Gen. Microbiol.* 133, 2191–2196. doi: 10.1099/00221287-133-8-2191

Toyama, B. H., Kelly, M. J., Gross, J. D., and Weissman, J. S. (2007). The structural basis of yeast prion strain variants. *Nature* 449, 233–237. doi: 10.1038/nature06108

Uptain, S. M., Sawicki, G. J., Caughey, B., and Lindquist, S. (2001). Strains of [*PSI*(+)] are distinguished by their efficiencies of prion-mediated conformational conversion. *EMBO J.* 20, 6236–6245. doi: 10.1093/emboj/20.22.6236

Valli, M., Sauer, M., Branduardi, P., Borth, N., Porro, D., and Mattanovich, D. (2005). Intracellular pH distribution in Saccharomyces cerevisiae cell populations, analyzed by flow cytometry. *Appl. Environ. Microbiol.* 71, 1515–1521. doi: 10.1128/AEM.71.3.1515-1521.2005

Wati, H., Kawarabayashi, T., Matsubara, E., Kasai, A., Hirasawa, T., Kubota, T., et al. (2009). Transthyretin accelerates vascular Abeta deposition in a mouse model of Alzheimer's disease. *Brain Pathol.* 19, 48–57. doi: 10.1111/j.1750-3639.2008.00166.x

Westermark, G. T., and Westermark, P. (2008). Transthyretin and amyloid in the islets of Langerhans in type-2 diabetes. *Exp. Diabetes Res.* 2008:429274. doi: 10.1155/2008/429274

Wickner, R. B. (1994). [URE3] as an altered URE2 protein: evidence for a prion analog in *Saccharomyces cerevisiae*. *Science* 264, 566–569. doi: 10.1126/science.7909170

Wickner, R. B., Masison, D. C., and Edskes, H. K. (1995). [PSI] and [URE3] as yeast prions. *Yeast* 11, 1671–1685. doi: 10.1002/yea.320111609

Wiseman, R. L., Powers, E. T., and Kelly, J. W. (2005). Partitioning conformational intermediates between competing refolding and aggregation pathways: insights into transthyretin amyloid disease. *Biochemistry* 44, 16612–16623. doi: 10.1021/bi0511484

Xue, Q., Zheng, Q. C., Zhang, J. L., Cui, Y. L., Chu, W. T., and Zhang, H. X. (2014). Mutation and low pH effect on the stability as well as unfolding kinetics of transthyretin dimer. *Biophys. Chem.* 189, 8–15. doi: 10.1016/j.bpc.2014.02.002

Yang, Z., Hong, J. Y., Derkatch, I. L., and Liebman, S. W. (2013). Heterologous gln/asn-rich proteins impede the propagation of yeast prions by altering chaperone availability. *PLoS Genet.* 9:e1003236. doi: 10.1371/journal.pgen.1003236

Zhao, X., Park, Y. N., Todor, H., Moomau, C., Masison, D., Eisenberg, E., et al. (2012). Sequestration of Sup35 by aggregates of huntingtin fragments causes toxicity of [PSI+] yeast. *J. Biol. Chem.* 287, 23346–23355. doi: 10.1074/jbc.M111.287748

Zhou, P., Derkatch, I. L., Uptain, S. M., Patino, M. M., Lindquist, S., and Liebman, S. W. (1999). The yeast non-Mendelian factor [ETA+] is a variant of [PSI+], a prion-like form of release factor eRF3. *EMBO J.* 18, 1182–1191. doi: 10.1093/emboj/18.5.1182

Conflict of Interest Statement: The authors declare that the research was conducted in the absence of any commercial or financial relationships that could be construed as a potential conflict of interest.

frontiers in Molecular Neuroscience

ORIGINAL RESEARCH
published: 27 March 2018
doi: 10.3389/fnmol.2018.00094

Sumoylation Protects Against β-Synuclein Toxicity in Yeast

*Blagovesta Popova[1,2], Alexandra Kleinknecht[1,2], Patricia Arendarski[1], Jasmin Mischke[1], Dan Wang[1] and Gerhard H. Braus[1,2]**

[1]Department of Molecular Microbiology and Genetics and Göttingen Center for Molecular Biosciences (GZMB), Institute for Microbiology and Genetics, Universität Göttingen, Göttingen, Germany, [2]Center for Nanoscale Microscopy and Molecular Physiology of the Brain (CNMPB), Göttingen, Germany

Aggregation of α-synuclein (αSyn) plays a central role in the pathogenesis of Parkinson's disease (PD). The budding yeast *Saccharomyces cerevisiae* serves as reference cell to study the interplay between αSyn misfolding, cytotoxicity and post-translational modifications (PTMs). The synuclein family includes α, β and γ isoforms. β-synuclein (βSyn) and αSyn are found at presynaptic terminals and both proteins are presumably involved in disease pathogenesis. Similar to αSyn, expression of βSyn leads to growth deficiency and formation of intracellular aggregates in yeast. Co-expression of αSyn and βSyn exacerbates the cytotoxicity. This suggests an important role of βSyn homeostasis in PD pathology. We show here that the small ubiquitin-like modifier SUMO is an important determinant of protein stability and βSyn-induced toxicity in eukaryotic cells. Downregulation of sumoylation in a yeast strain, defective for the SUMO-encoding gene resulted in reduced yeast growth, whereas upregulation of sumoylation rescued growth of yeast cell expressing βSyn. This corroborates a protective role of the cellular sumoylation machinery against βSyn-induced toxicity. Upregulation of sumoylation significantly reduced βSyn aggregate formation. This is an indirect molecular process, which is not directly linked to βSyn sumoylation because amino acid substitutions in the lysine residues required for βSyn sumoylation decreased aggregation without changing yeast cellular toxicity. αSyn aggregates are more predominantly degraded by the autophagy/vacuole than by the 26S ubiquitin proteasome system. We demonstrate a vice versa situation for βSyn, which is mainly degraded in the 26S proteasome. Downregulation of sumoylation significantly compromised the clearance of βSyn by the 26S proteasome and increased protein stability. This effect is specific, because depletion of functional SUMO did neither affect βSyn aggregate formation nor its degradation by the autophagy/vacuolar pathway. Our data support that cellular βSyn toxicity and aggregation do not correlate in their cellular impact as for αSyn but rather represent two distinct independent molecular functions and molecular mechanisms. These insights into the relationship between βSyn-induced toxicity, aggregate formation and degradation demonstrate a significant distinction between the impact of αSyn compared to βSyn on eukaryotic cells.

Keywords: beta-synuclein, Parkinson's disease, sumoylation, posttranslational modification, yeast, proteasome, autophagy, aggregation

OPEN ACCESS

Edited by:
Sabrina Büttner,
Stockholm University, Sweden

Reviewed by:
Martin Lothar Duennwald,
University of Western Ontario, Canada
Bing Zhou,
Tsinghua University, China

***Correspondence:**
Gerhard H. Braus
gbraus@gwdg.de

Received: *13 December 2017*
Accepted: *09 March 2018*
Published: *27 March 2018*

Citation:
Popova B, Kleinknecht A, Arendarski P, Mischke J, Wang D and Braus GH (2018) Sumoylation Protects Against β-Synuclein Toxicity in Yeast.
Front. Mol. Neurosci. 11:94.
doi: 10.3389/fnmol.2018.00094

INTRODUCTION

Parkinson's disease (PD) is characterized by loss of dopaminergic neurons in the *substantia nigra* in the midbrain and formation of intracellular protein inclusions called Lewy bodies (Kalia and Lang, 2015). Loss of dopaminergic neurons leads to dopamine depletion and results in a wide range of motoric and non-motoric symptoms. One of the major components of Lewy bodies is the small and highly abundant protein α-synuclein (αSyn; Spillantini et al., 1998). αSyn is part of a family of proteins that includes also β-synuclein (βSyn) and γ-synuclein (γSyn). αSyn and βSyn are localized predominantly at presynaptic nerve terminals, whereas γSyn is abundant in the peripheral nervous system (Li et al., 2002; Mori et al., 2002). Synuclein family members share a highly conserved N-terminal domain and a more divergent and highly acidic C-terminal domain. αSyn and βSyn are closely related to each other and their sequences share 62% homology (George, 2002). The most notable difference between the two proteins is that βSyn lacks 11 residues in the central most hydrophobic region, referred to as non-amyloid-β component (NAC) region, involved in fibril formation and aggregation. All three synucleins are intrinsically unstructured when isolated under physiological conditions and adopt helical structures in their N-terminal domains upon binding to lipid vesicles (Sung and Eliezer, 2006; Ducas and Rhoades, 2012).

αSyn is implicated as prime contributor of PD development as it is associated with familial and sporadic forms of PD. The protein has a strong propensity to self-assemble into oligomeric protofibrils that can further mature into different types of fibrils and insoluble aggregates (Villar-Piqué et al., 2015). The abnormal accumulation of the protein is partly triggered by gene duplications or even triplications as well as missense mutations (Polymeropoulos et al., 1997; Krüger et al., 1998; Singleton et al., 2003; Zarranz et al., 2004). Aggregation of αSyn is assumed to constitute the central pathological process in synucleinopathies. One of the critical factors that affect αSyn aggregation process is the protein level in the cell, which depends on the rate of its turnover. αSyn can be degraded both by ubiquitin-proteasome system (UPS) and the autophagy/lysosome pathway (Webb et al., 2003; Xilouri et al., 2013). Inhibition of protein degradation pathways resulting in inefficient protein clearance leads to accumulation of pathological αSyn species and is sufficient to trigger neurotoxicity (Xilouri et al., 2013; Vilchez et al., 2014). Therefore, understanding of αSyn turnover mechanism is an essential aspect to uncover the pathological mechanism of PD.

αSyn undergoes numerous post-translational modifications (PTMs) such as phosphorylation, ubiquitination, sumoylation, nitration or acetylation (Giasson et al., 2000; Shimura et al., 2001; Fujiwara et al., 2002; Hasegawa et al., 2002; Dorval and Fraser, 2006; Kleinknecht et al., 2016; de Oliveira et al., 2017). PTMs influence αSyn aggregation and toxicity and in addition modulate the degradation of the protein by different proteolytic pathways (Popova et al., 2015). The small ubiquitin-like modifier SUMO is covalently conjugated to target proteins and modulates a number of cellular processes. Many PD-associated proteins are SUMO-modified, highlighting the importance of this PTM in neurodegeneration (Eckermann, 2013). αSyn is a substrate of SUMO1, one of the four SUMO isoforms in human (Dorval and Fraser, 2006). Sumoylation of αSyn negatively regulates αSyn aggregation by promoting protein solubility (Krumova et al., 2011).

The yeast *Saccharomyces cerevisiae* is a valuable model system for studying protein misfolding and cellular pathways associated with protein quality control systems due to the high conservation of functions with higher eukaryotes including humans (Menezes et al., 2015). Heterologous expression of αSyn in yeast results in aggregate formation and dose-dependent cytotoxicity, recapitulating central features of PD (Outeiro and Lindquist, 2003; Petroi et al., 2012). Yeast was employed to investigate the role of PTMs for αSyn aggregate clearance. Recent study demonstrated that αSyn is sumoylated in yeast and that the cellular mechanism of sumoylation is conserved from yeast to human (Shahpasandzadeh et al., 2014). The distribution of αSyn to different cellular degradation pathways was dependent on a complex cross-talk between sumoylation and phosphorylation at Serine 129 (S129).

The other two members of synuclein family have been less well studied until recently due to lack of genetic links to PD. Initial reports suggested βSyn as a negative regulator of αSyn aggregation (Hashimoto et al., 2001; Uversky et al., 2002; Fan et al., 2006). Recent results revealed that βSyn can act as a neurodegeneration-inducing factor and can cause cell loss when expressed in rat brains (Taschenberger et al., 2013). This suggests a role of βSyn in the pathogenesis of PD. V70M or P123H mutations in βSyn were linked to cases of dementia with Lewy bodies (DLB; Ohtake et al., 2004) and were suggested to be involved in lysosomal pathology (Wei et al., 2007). Expression of P123H βSyn in transgenic mouse resulted in progressive neurodegeneration that acted synergistically with overexpression of αSyn (Fujita et al., 2010). These studies revealed an emerging role of βSyn in a broad range of α-synucleinopathies. However, the molecular mechanism of this role remains poorly studied.

Recently, yeast was used as a reference cell to investigate the cellular effects of βSyn. Expression of βSyn but not γSyn was toxic to yeast cells and resulted in formation of cytosolic inclusions, similar to those formed by αSyn (Tenreiro et al., 2016). βSyn can induce cell death by mechanisms associated with vesicular trafficking impairment or oxidative stress, similarly as it is described for αSyn toxicity. Co-expression of αSyn and βSyn enhanced the cytotoxicity due to increased dosage of toxic species in an additive manner. Both different synucleins were able to form heterodimers in yeast as well as in human cells. These findings emphasize pathogenesis-related cellular role of βSyn, suggesting that increased levels of βSyn enhance αSyn-induced cytotoxicity due to dosage effects. The molecular mechanisms that control βSyn turnover in the cell are yet elusive.

In contrast to αSyn, PTM of βSyn are hardly studied. βSyn has been found to be phosphorylated at S118 *in vitro* and *in vivo* (Nakajo et al., 1993; Mbefo et al., 2010), however other PTMs were not yet reported. Since αSyn and βSyn proteins are highly similar, there have to be differences in their molecular behavior that might explain their differential contribution to neurodegeneration.

We used yeast as a reference cell to exploit the molecular mechanisms that affect βSyn turnover in the cell. We showed that SUMO is an important modulator of protein stability. βSyn is sumoylated in yeast at three lysine residues and sumoylation supports aggregate formation. The exchange of the codons for the sumoylation sites decreased βSyn aggregate formation but did not change cellular cytotoxicity monitored as yeast growth. However, downregulation of the entire cellular sumoylation pool drastically enhanced βSyn-induced cytotoxicity. We demonstrate in yeast cells that intact sumoylation machinery is prerequisite for the degradation of soluble as well as aggregated βSyn protein. βSyn is degraded mainly by the 26S proteasome, in contrast to αSyn that is degraded predominantly by the autophagy/vacuolar pathway. These findings reveal distinct molecular mechanisms of protein turnover for βSyn in comparison to αSyn.

MATERIALS AND METHODS

Plasmid Construction, Yeast Strains, Transformation and Growth Conditions

Plasmids and *Saccharomyces cerevisiae* strains are listed in **Tables 1**, **2**. Yeast plasmids expressing *SNCB-GFP* fusion were cloned into the *Sma*I site of the integrative plasmids pRS304 or pRS306 using GENEART Seamless cloning and assembly kit (Life technologies). The βSyn mutant constructs were generated by site-directed mutagenesis of the corresponding plasmids. All constructs were verified by DNA sequencing.

The *GAL1-SNCB*-GFP was integrated into the mutated *ura3-1* locus of *S. cerevisiae* W303-1A strain using an intact *URA3* gene on the corresponding integrative plasmid for selection. The number of the integrated copies was determined by Southern hybridization as described previously (Petroi et al., 2012). The *GAL1::SNCB* or its derivatives were integrated into the *trp1-1* locus.

S. cerevisiae strains W303-1A, $smt3^{ts}$ and $ulp1^{ts}$ were used for transformations performed by standard lithium acetate protocol (Gietz et al., 1992). All strains were grown in Synthetic complete medium (SC; Guthrie and Fink, 1991) lacking the nutrient amino acid corresponding to the marker, and supplemented with 2% raffinose or 2% glucose. αSyn or βSyn expression was induced by shifting yeast cells cultivated overnight in raffinose to 2% galactose-containing medium (OD_{600} = 0.1).

TABLE 1 | Plasmids used in this study.

Name	Description	Source
p426	*URA3*, 2 μm, pUC origin, AmpR	Mumberg et al. (1994)
pRS304	*TRP1*, pUC origin, AmpR	Sikorski and Hieter (1989)
pRS306	*URA3*, pUC origin, AmpR	Sikorski and Hieter (1989)
pME3759	p426-*GAL1-GFP*	Petroi et al. (2012)
pME3763	p426-*GAL1::SNCA::GFP*	Petroi et al. (2012)
pME4102	p426-*GAL1::SNCB::GFP*	Tenreiro et al. (2016)
pME4103	p426-*GAL1::SNCG::GFP*	Tenreiro et al. (2016)
pME4624	p426-*GAL1::SNCB^{K12R}::GFP*	This study
pME4625	p426-*GAL1::SNCB^{K85R}::GFP*	This study
pME4626	p426-*GAL1::SNCB^{K94R}::GFP*	This study
pME4627	p426-*GAL1::SNCB$^{K85R\ K94R}$::GFP*	This study
pME4628	p426-*GAL1::SNCB$^{K12\ K85R\ K94R}$::GFP*	This study
pME4629	pRS304-*GAL1::SNCB*	This study
pME4630	pRS304-*GAL1::SNCB^{K12R}*	This study
pME4631	pRS304-*GAL1::SNCB^{K85R}*	This study
pME4632	pRS304-*GAL1::SNCB^{K94R}*	This study
pME4633	pRS304-*GAL1*::*SNCB$^{K85R\ K94R}$*	This study
pME4634	pRS304-*GAL1*::SNCB$^{K12R\ K85R\ K94R}$	This study
pME4635	pRS306-*GAL1::SNCB::GFP*	This study

Spotting Assay

For growth test on solid medium, yeast cells were pre-grown in minimal medium containing 2% raffinose lacking the corresponding marker to mid-log phase. Cells were normalized to equal densities, serially diluted 10-fold starting with an OD_{600} of 0.1, and spotted on SC-plates containing either 2% glucose or 2% galactose and lacking in corresponding marker. $smt3^{ts}$ mutant cells were incubated at permissive temperature (25°C) and restrictive temperature (30°C). After 3 days incubation the plates were photographed.

TABLE 2 | Yeast strains used in this study.

Name	Genotype	Source
W303-1A	*MATa; ura3-1; trp1-1; leu2-3_112; his3-11; ade2-1; can1-100*	EUROSCARF
RH3465	W303 containing *GAL1::GFP* in *ura3* locus	Petroi et al. (2012)
RH3468	W303 containing three genomic copies of *GAL1::SNCA^{WT}::GFP* in *ura3* locus	Petroi et al. (2012)
$ulp1^{ts}$	ulp1ts-333	Li and Hochstrasser (1999)
RH3603	$ulp1^{ts}$ containing YIplac211-*ADH-His6-SMT3* in *his3* locus	Shahpasandzadeh et al. (2014)
$smt3^{ts}$	S542: *MAT α, smt3-331*	Dieckhoff et al. (2004)
RH3700	W303 containing one genomic copy of *GAL1::SNCB^{WT}::GFP* in *ura3* locus	This study
RH3701	W303 containing two genomic copies of *GAL1::SNCB^{WT}::GFP* in *ura3* locus	This study
RH3702	W303 containing three genomic copies of *GAL1::SNCB^{WT}::GFP* in *ura3* locus	This study
RH3703	RH3603 containing *GAL1::SNCB^{WT}* in *trp1* locus	This study
RH3704	RH3603 containing *GAL1::SNCB^{K12R}* in *trp1* locus	This study
RH3705	RH3603 containing *GAL1::SNCB^{K85R}* in *trp1* locus	This study
RH3706	RH3603 containing *GAL1::SNCB^{K94R}* in *trp1* locus	This study
RH3707	RH3603 containing *GAL1::SNCB$^{K85R\ K94R}$* in *trp1* locus	This study
RH3708	RH3603 containing *GAL1::SNCB$^{K12R\ K85R\ K94R}$* in *trp1* locus	This study
RH 3709	$smt3^{ts}$ containing one genomic copy of *GAL1::SNCB^{WT}::GFP* in *ura3* locus	This study
RH 3710	$smt3^{ts}$ containing one genomic copy of *GAL1::SNCB$^{K12R\ K85R\ K94R}$::GFP* in *ura3* locus	This study

Growth Analysis in Liquid Culture

For growth tests in liquid cultures, cells were pre-grown in 2% raffinose-containing selective SC medium until logarithmic growth phase and inoculated in 2% galactose-containing SC medium to equal densities of OD_{600} = 0.1. Optical density measurements of 150 µl cell cultures were performed in quadruplicates in 96-well plates for 24 h using a microplate reader with temperature control and continuous shaking (Infinite M200, Tecan).

Fluorescence Microscopy and Quantifications

Wild type (W303-1A) yeast cells harboring βSyn were grown in SC selective medium containing 2% raffinose at 30°C and *smt3*^{ts} mutant cells at 25°C overnight, and transferred to 2% galactose containing medium for induction of βSyn expression for 6 h. *smt3*^{ts} mutant cells were induced at 25°C or 30°C. Fluorescent images were obtained with Zeiss Observer. Z1 microscope (Zeiss) equipped with a CSU-X1 A1 confocal scanner unit (YOKOGAWA), QuantEM:512SC digital camera (Photometrics) and SlideBook 6.0 software package (Intelligent Imaging Innovations). For quantification of aggregation at least 200 cells were counted per strain and per experiment. The number of cells presenting inclusions was referred to the total number of cells counted. The values are mean of at least three independent experiments.

Immunoblotting

Wild type (W303-1A) yeast cells harboring βSyn were pre-grown at 30°C in SC selective medium containing 2% raffinose. Cells were transferred to SC medium containing 2% galactose at OD_{600} = 0.1 to induce the *GAL1* promoter for 6 h. *smt3*^{ts} or *ulp1*^{ts} cells harboring βSyn were pre-incubated at 25°C and later transferred to either 25°C or 30°C. Total protein extracts were prepared and the protein concentrations were determined with a Bradford assay. Forty microgram of each protein were subjected to 12% SDS-polyacrylamide gel electrophoresis and transferred to a nitrocellulose membrane. Membranes were probed with βSyn rabbit monoclonal antibody (abcam, UK), GFP rat monoclonal antibody (Chromotek, Germany), SUMO rabbit polyclonal antibody (Rockland Immunochemicals Inc., USA) or ubiquitin mouse monoclonal antibody for detection of poly-ubiquitinated and ubiquitinated proteins (clone P4D1-A11, Millipore). GAPDH mouse monoclonal antibody (Thermo Fisher Scientific, USA) was used as loading controls. Pixel density values for Western quantification were obtained from TIFF files generated from digitized X-ray films (KODAK) and analyzed with the ImageJ software (NIH, Bethesda, MD, USA). Before comparison, sample density values were normalized to the corresponding loading control.

Ultracentrifugation and Fractionation

The sedimentation assay, extraction of SDS-soluble and insoluble βSyn protein fractions were performed as described (Alberti et al., 2010) with modifications. Equal number of yeast cells corresponding to total OD = 10 were collected by centrifugation and resuspended in lysis buffer (50 mM Tris-HCl pH 7.5, 1 mM EDTA, 5 mM DTT, 1× protease inhibitor mix (Roche). The cells were lysed by shaking with glass beads at 4°C. The crude lysate was centrifuged for 5 min at 500 *g* to pellet the cell debris. Two-hundred microliter of each cleared lysate was centrifuged at 100,000 *g* for 30 min. The supernatant was designated as soluble protein. The pellet was washed three times with the lysis buffer, resuspended in 200 µl lysis buffer containing 2% SDS and incubated on ice for 30 min. The suspension was centrifuged for 30 min at 100,000 *g* and the supernatant was labeled as SDS-soluble protein fraction. The pellet was washed three times with lysis buffer, resuspended in 200 µl 6 M urea and designated as SDS-insoluble fraction. Equal amount from each fraction (20 µl) was analyzed by SDS-PAGE and Western blotting.

Flow Cytometry

Cells were grown as above and protein expression was induced as described for 6 h. Before measuring, cells were re-suspended in 50 mM trisodium citrate buffer, pH 7.0. Flow cytometry analysis was performed on a BD FACSCANTO II (Becton Dickinson). Fifty thousand events were counted for each experiment. Data analysis was performed using the BD FACSDIVA software (Becton Dickinson). Representative examples that are shown in the Figures were repeated at least three times. Yeast cell membrane integrity was analyzed with PI staining. Yeast cells were incubated with 12.5 µg/ml PI for 30 min. As a positive control, cells were boiled for 10 min at 95°C.

Promoter Shut-Off Assay and Chemical Treatments

Yeast cells carrying βSyn were pre-grown in selective SC medium containing 2% raffinose overnight and shifted to 2% galactose-containing selective SC medium to induce the βSyn expression for 4 h. Afterwards, cells were shifted to SC medium supplemented with 2% glucose to shut-off the promoter. For experiments with temperature sensitive yeast strain *smt3*^{ts}, pre-incubation was performed at 25°C. Induction of βSyn expression and the promoter shut-off assay were performed at 25°C and 30°C. Five hours after promoter shut-off, cells were visualized by fluorescence microscopy. The reduction of number of cells displaying βSyn inclusions was recorded. To study the lysosome/vacuole degradation pathway (autophagy) phenylmethanesulfonyl fluoride (PMSF) in ethanol (EtOH) was applied to the suspension in a final concentration of 1 mM. For impairment of the proteasomal degradation system Carbobenzoxyl-leucinylleucinyl-leucinal (MG132) dissolved in dimethyl sulfoxide (DMSO) was added to the cell suspension in a final concentration of 75 µM. Drug treatment was conducted concomitantly with the shift to glucose-supplemented medium. In parallel, equal volume of DMSO or EtOH was applied to the control cells. For drug treatment with MG132 induction-medium containing galactose and shut-off-medium containing glucose was supplemented with 0.003% SDS and 0.1% proline.

Ni^{2+}-NTA Affinity Chromatography

ulp1^{ts} mutant cells carrying *GAL1-SNCB* integrations and His6-tagged Smt3 (*His6-SMT3*) were pre-grown in 200 ml SC

medium containing 2% raffinose at 30°C overnight. Total cells harvested by centrifugation were transferred to 2 l YEPD liquid medium containing 2% galactose for 12 h induction. Cells were collected and lysed by 25 ml 1.85 M NaOH containing 7.5% ß-mercaptoethanol for 10 min on ice. Proteins were precipitated in 25 ml 50% trichloroacetic acid (TCA), washed with 100% cold acetone, and suspended in 25 ml buffer A (6 M guanidine HCl, 100 mM sodium phosphate, 10 mM Tris/HCl, pH 8.0) and rotated for 1 h at 25°C. The supernatant was cleared by centrifugation; the pH was adjusted to 7.0 by 1 M Tris base and supplemented with imidazole to final concentration of 20 mM. After equilibration of the His GraviTrap column (GE Healthcare Life Science, Buckinghamshire, United Kingdom) with 5 ml of buffer A containing 20 mM imidazole, proteins were applied to the column and the flow-through fraction was collected for analysis. The column was washed with buffer A supplemented with 20 mM imidazole and then with buffer B (8 M Urea, 100 mM sodium phosphate, 10 mM Tris, pH 6.3). Then the column was washed with buffer C (50 mM Tris pH 8.0, 300 mM NaCl, 20 mM imidazole). Finally, the proteins were eluted four times with 1 ml of 200 mM imidazole resolved in buffer C. Protein concentration in the eluted fractions was determined with Bradford assay.

Statistical Analysis

Data were analyzed using GraphPad Prism 5 (San Diego, CA, USA) Software and were presented as mean ± SEM of at least three independent experiments. The significance of differences was calculated using Students *t*-test and One-way Anova test. P value < 0.05 was considered to indicate a significant difference.

RESULTS

βSyn Has a Higher Toxicity Threshold Than αSyn When Expressed in Yeast

We evaluated the impact of αSyn, βSyn and γSyn GFP-tagged proteins on growth of *Saccharomyces cerevisiae* cells. The expression was controlled by the *GAL1* promoter, which can be repressed in the presence of glucose and induced in the presence of galactose. High level expression from 2μ plasmid of αSyn resulted in the described growth impairment (Outeiro and Lindquist, 2003; Petroi et al., 2012). Cells expressing βSyn were also inhibited in growth, whereas expression of γSyn resulted in wild type yeast growth similar of GFP control (Tenreiro et al., 2016; **Figure 1A**). Fluorescent microscopy was used to assess, whether the synuclein-induced growth inhibition is accompanied with aggregate formation. αSyn and βSyn expression resulted in formation of similar cytoplasmic inclusions (**Figure 1B**). Quantification of the cells displaying inclusions revealed similar percentages of αSyn and βSyn expressing cells with inclusions 6 h after induction of protein expression, whereas γSyn expressing cells did not exhibit formation of aggregates (**Figure 1C**).

Previous studies revealed that a threshold level for αSyn-induced toxicity was reached if expression was driven by three genomic copies of the αSyn encoding gene (Petroi et al., 2012). We aimed to characterize the threshold for βSyn-induced toxicity. Strains were constructed with single, double or triple integrations of βSyn-encoding genes at the single *ura3* locus. Growth assays revealed no growth inhibition by expression of βSyn from single, double or triple genomic copies. In contrast cells expressing αSyn from three copies were impaired in growth (**Figure 1D**). This growth phenotype correlated with increased aggregate formation. Expression from one copy of βSyn did not result in aggregate formation. Two copies of αSyn and βSyn had lower percentages of cells with aggregates, whereas expression from three copies of αSyn gene resulted in 91% of cells displaying aggregates in comparison with 24% of cells expressing βSyn (**Figure 1E**). The measured differences in toxicity were not due to different protein levels of the two variants, as observed with Western hybridization after 6 h induction of expression (**Figures 1F,G**).

The solubility of βSyn in strains differing in the potential for aggregate formation was analyzed. Cells, expressing βSyn from two or three genomic copies and cells, overexpressing βSyn from 2μ plasmid were used. Crude protein extracts were prepared from equal number of cells 6 h after induction of protein expression. The protein extracts were subjected to fractionation to produce soluble, SDS-soluble and SDS-insoluble fractions (**Figures 1H,I**). Comparison of the different βSyn fractions revealed significant increase towards SDS-insoluble fraction in cells, displaying higher aggregate formation. The results illustrate a direct correlation between βSyn aggregation and the accumulation of insoluble protein species, suggesting that the observed fluorescent foci are indicative for βSyn aggregate formation.

These results demonstrate that expression from three copies of βSyn encoding gene is below the toxicity threshold. βSyn is less toxic with a higher threshold for cytotoxicity and aggregate formation than αSyn.

βSyn Is Sumoylated in Yeast at Three Lysine Residues Within SUMO Consensus Motifs

αSyn was shown to be efficiently sumoylated in human cells lines and the major sumoylation sites are conserved from yeast to human (Krumova et al., 2011; Shahpasandzadeh et al., 2014). We examined, whether βSyn is sumoylated in yeast cells. *In silico* analysis with SUMOplot analysis predicted three putative SUMO consensus motifs at lysine residues 12, 85 or 94 (K12, K85, K94; **Table 3**). A temperature-sensitive strain deficient for the gene, encoding the SUMO-deconjugation isopeptidase (*ulp1^{ts}*) that expressed His_6-tagged yeast SUMO protein Smt3 (Petroi et al., 2012) was used for enrichment of SUMO-conjugates (**Figure 2A**). βSyn was expressed in the *ulp1^{ts}-SMT3-His6* strain and SUMO-conjugates were enriched by Ni^{2+}-NTA affinity chromatography under denaturing conditions. Immunoblotting analysis with βSyn antibody revealed SUMO-modified βSyn protein with an apparent molecular mass of ∼35 kDa (**Figure 2B**) that could be separated from the non-modified 15 kDa βSyn protein.

In order to map the sumoylation sites of βSyn, mutants with single (K12R; K85R; K94R), double (K85/K94R) and triple

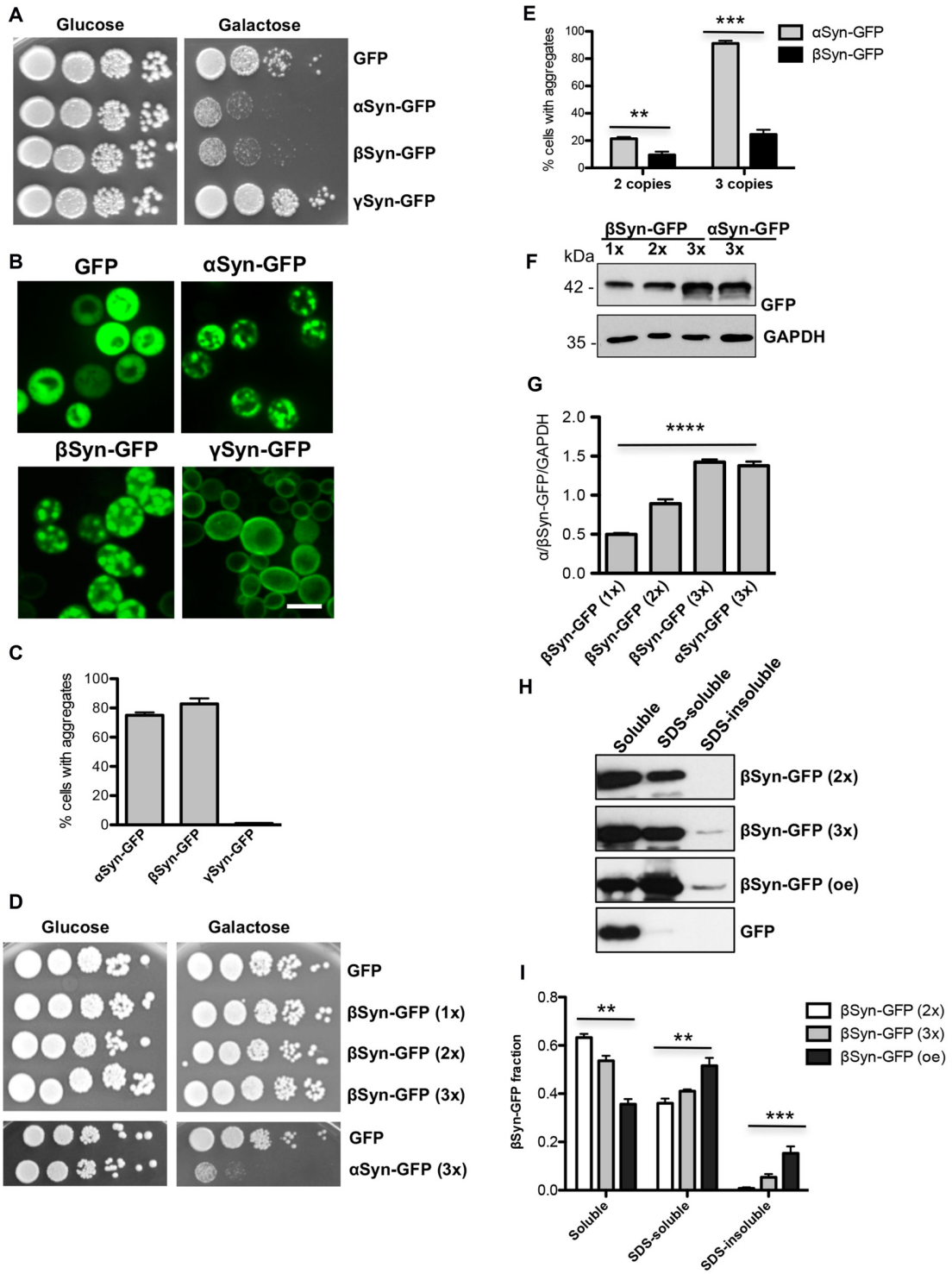

FIGURE 1 | β-synuclein (βSyn)-GFP expression impairs yeast growth. **(A)** Wild type yeast cells (W303) were transformed with a high copy plasmid carrying α-synuclein (αSyn)-GFP, βSyn-GFP and γ-synuclein (γSyn)-GFP under the control of *GAL1*. GFP expressing cells, expressed from the same promoter, served as control. Yeast cells were spotted in 10-fold dilutions on selection plates containing glucose (*GAL1* promoter "OFF") or galactose (*GAL1* promoter "ON"). **(B)** Live-cell fluorescence microscopy of yeast cells expressing *GAL1*-driven synuclein isoforms from 2μ plasmids. Yeast cells, pre-grown to mid-log phase, were induced in galactose-containing medium and examined for aggregates at 6 h of induction. Scale bar—5 μM. **(C)** Aggregate quantification of yeast cells, expressing synuclein-GFP isoforms. For each strain, the number of cells displaying cytoplasmic foci is presented as percent of the total number of cells. For quantification of

(*Continued*)

FIGURE 1 | Continued
aggregation at least 200 cells were counted per strain and per experiment. The results are mean from at least five independent experiments ± SD. **(D)** Spotting assay of yeast cells expressing one (1x), two (2x) or three (3x) copies of βSyn and three copies of αSyn. Yeast cells, expressing GFP were used as a control. The yeast cells were spotted in 10-fold dilutions on selective SC-Ura plates containing 2% glucose and 2% galactose. **(E)** Aggregate quantification of yeast cells, expressing two or three copies of genes, encoding αSyn-GFP and βSyn-GFP at 6 h of induction. Expression of βSyn-GFP from a single copy gene did not result in aggregate formation. Significance of differences was calculated with *t*-test (**$p < 0.01$; ***$p < 0.001$; $n = 3$). **(F)** Western blot analysis of crude protein extracts of GFP-tagged proteins, expressed from one, two or three copies of βSyn and three copies of αSyn encoding genes, respectively. GAPDH was used as a loading control. **(G)** Densitometric analysis of the immunodetection of βSyn-GFP relative to the GAPDH loading control. Significance of differences was calculated with One-way Anova test (****$p < 0.0001$; $n = 3$). **(H)** Distribution of βSyn-GFP levels across different solubility fractions. Yeast cells, expressing βSyn-GFP from two (2x) or three (3x) genomic copies or overexpressing (oe) the protein from high copy plasmid were induced for 6 h in galactose medium. Starting from equal number of cells, crude protein extracts were prepared and fractionated by ultracentrifugation to produce soluble, SDS-soluble and SDS-insoluble fractions. Fractionation of GFP was performed as a control. Equal amounts from all fractions were analyzed by immunoblotting with βSyn or GFP antibody. **(I)** Densitometric analysis of the immunodetection of βSyn-GFP. The relative ratio of each βSyn fraction is normalized to the sum of the three fractions. Significance of differences was calculated with One-way Anova test (**$p < 0.01$; ***$p < 0.001$; $n = 4$).

TABLE 3 | β-synuclein (βSyn) putative sumoylation sites.

Position	Group	Score
K86	AATGL **VKRE** EFPTD	0.93
K95	EFPTD **LKPE** EVAQE	0.91
K12	KGLSM **AKEG** VVAAA	0.62

The score represents the probability for the SUMO consensus sequence (bold) to be involved in SUMO conjugation. The lysine acceptor site is underlined.

(K12/K85/K94R) lysine substitutions of the three putative βSyn sumoylation sites were generated. The βSyn lysine mutants were expressed in *ulp1^{ts}-SMT3-His6* strain and SUMO-conjugates were purified by Ni^{2+}-NTA pull-down as above. Single substitutions of each codon for putative sumoylation site, as well as double substitutions (K85/K94R) did not result in loss of the 35 kDa band. Only when all three putative SUMO-acceptor sites were mutated simultaneously (K12/K85/K94R), complete abolishment of sumoylation was observed (**Figure 2C**). These results support that βSyn sumoylation *in vivo* comprises all three K12, K85 and K94 lysine residues, which are embedded in a SUMO consensus motif.

Loss of Sumoylation of βSyn Reduces Inclusion Formation Without Reducing Cytotoxicity

We examined whether modification of βSyn as a direct SUMO target affects βSyn-induced growth inhibition in yeast. Wild type βSyn, the single lysine mutants (K12R; K85R; K94R), as well as the triple lysine mutant (K12/K85/K94R) were expressed in yeast. The effect of abolishing the sumoylation acceptor sites of βSyn on yeast growth was examined with spotting test (**Figure 3A**). Yeast cells were inhibited in growth and no significant differences were observed, when single SUMO acceptor sites or all three SUMO acceptor sites were substituted. Growth in liquid medium resulted in similar effects (**Figures 3B,C**). Cells, expressing βSyn or sumoylation deficient mutants revealed reduced growth in comparison to the GFP control, however no significant differences in growth were observed among the βSyn variants. Immunoblotting analysis revealed that all proteins were expressed at similar levels after 6 h induction of expression (**Figures 3D,E**). Fluorescent microscopy studies were performed to assess the aggregate formation of different βSyn variants. Quantification of the number of cells with inclusions revealed a significant reduction in cells displaying K12R, as well as K12/K85/K94R mutants (**Figures 3F,G**). In order to assess, whether the differences in aggregate formation correlate with changes in cytotoxicity, propidium iodide (PI) staining for membrane permeability was performed as a sensitive method for quantification of yeast viability. Flow cytometry measurements of cells, expressing βSyn and K12/K85/K94R, showed a significantly increased number of PI-positive cells in comparison to the GFP control (**Figures 3H,I**). No significant differences between cells expressing βSyn and the triple lysine mutant were observed. These data correlate with the results from the growth assays and reveal that SUMO modifications of βSyn enhances aggregate formation of the protein without significantly affecting cell growth and viability. This suggests that βSyn aggregate formation and cytotoxicity are part of different molecular mechanisms.

Sumoylation Protects Against βSyn-Induced Toxicity

The finding that SUMO modification at βSyn acceptor sites did not change cytotoxicity suggested that sumoylation of additional target proteins or cellular pathways might be involved in cytoprotection against βSyn-induced toxicity. We assessed the effect of sumoylation on βSyn-induced toxicity using a yeast strain with a temperature sensitive SUMO-encoding gene (*smt3^{ts}*). Growth of yeast *smt3^{ts}* cells at restrictive temperature (30°C) results in accumulation of non-functional SUMO-conjugates (Dieckhoff et al., 2004; Shahpasandzadeh et al., 2014). A growth assay was performed with cells, expressing βSyn or K12/K85/K94R mutant from high copy plasmid at permissive temperature (25°C) and restrictive temperature (30°C; **Figure 4A**). Impairment of sumoylation at 30°C only slightly affected growth of the control strain expressing GFP, whereas expression of βSyn or K12/K85/K94R mutants resulted in drastic growth inhibition under these conditions. Importantly, at permissive temperature cells that were not depleted of functional SUMO were less affected by expression of βSyn and derivatives. Mutant *smt3^{ts}* yeast strains with single integration of βSyn or 3xK/R-encoding genes at the *ura3* locus were constructed. Expression from single copy of βSyn or K12/K85/K94R-encoding gene is lower than the toxicity threshold (**Figure 1D**). Accordingly, growth assays revealed no retardation at 25°C (**Figure 4B**). Inhibition of sumoylation at 30°C slightly affected growth of the strains expressing βSyn or K12/K85/K94R. Quantitative growth assays in liquid cultures

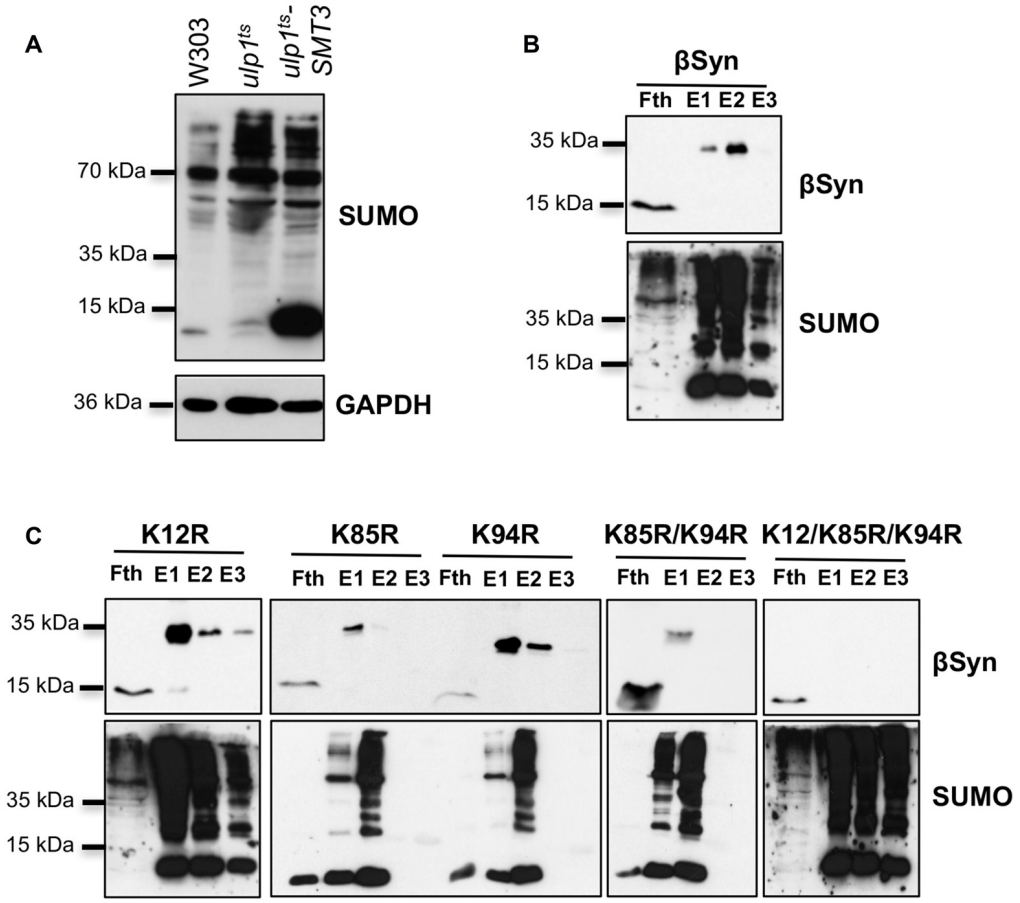

FIGURE 2 | βSyn is sumoylated in yeast. **(A)** Enrichment of sumoylated conjugates in *ulp1*^{ts} strain, expressing *SMT3-HIS6*. Western blot analysis of the total protein extract from the *ulp1*^{ts} strain, deficient in SUMO-deconjugation, expressing His-tagged *SMT3*. *ulp1*^{ts} and W303 were used as controls. SUMO-conjugated proteins were detected using specific SUMO antibody. GAPDH served as a loading control. **(B)** Ni^{2+} pull-down of *ulp1*^{ts}*-SMT3-His6* strain expressing *GAL1*-driven βSyn. Fth: flow-through; E1: Elution 1; E2: Elution 2; E3: Elution 3. The same membrane was stripped and probed with SUMO antibody verifying the Ni^{2+} pull-down. Modified βSyn migrates at ∼35 kDa. Unmodified βSyn migrates at ∼15 kDa. **(C)** Ni^{2+} pull-down of *ulp1*^{ts}*-SMT3-His6* strain expressing βSyn sumoylation deficient mutants K12R, K85R, K94R, K85R/K94R and K12R/K85/K94R.

were performed with the *smt3*^{ts} yeast cells, expressing βSyn or K12/K85/K94R from single gene copy (**Figures 4C,D**). Analysis of the growth rate revealed significant differences in growth compared to the GFP control when sumoylation is impaired. These results indicated gain of βSyn toxicity in strains expressing non-toxic levels of βSyn or K12/K85/K94R under conditions of impaired sumoylation. This suggests a protective role of sumoylation for βSyn-induced toxicity that is not dependent on direct modification of the protein.

Next, we examined whether increased sumoylation affects βSyn-induced cytotoxicity. We used the *ulp1*^{ts} strain, defective for SUMO de-conjugation, to enrich the pool of sumoylated proteins. Expression of βSyn or K12/K85/K94R resulted in significantly reduced growth inhibition (**Figure 4E**). This result revealed that up-regulation of sumoylation partially rescues the growth defect of yeast cells, expressing βSyn.

We tested, whether there is a correlation between growth inhibition and aggregate formation of βSyn and K12/K85/K94R variant. Aggregate formation was followed by life-cell microscopy and the number of cells with aggregates was counted (**Figure 4F**). Expression of βSyn variants in *smt3*^{ts} cells in presence or absence of functional SUMO did not result in changes of the percentage of cells with aggregates 6 h after induction (**Figure 4G**). However, expression of βSyn and K12/K85/K94R in *ulp1*^{ts} cells resulted in complete loss of aggregation after 6 h of induction and increased cytoplasmic staining (**Figures 4F,H**). Formation of aggregates was observed as late as 24 h after protein induction and there was a strong decrease of the percentage of cells with aggregates in comparison with *smt3*^{ts} background (**Figure 4G**) or wild type W303 background (**Figure 1C**).

Our findings support a complex interplay between sumoylation, βSyn-induced cytotoxicity and aggregate formation. Downregulation of functional cellular SUMO pools strongly inhibits yeast growth without affecting efficient aggregate formation. In contrast, higher levels of sumoylated

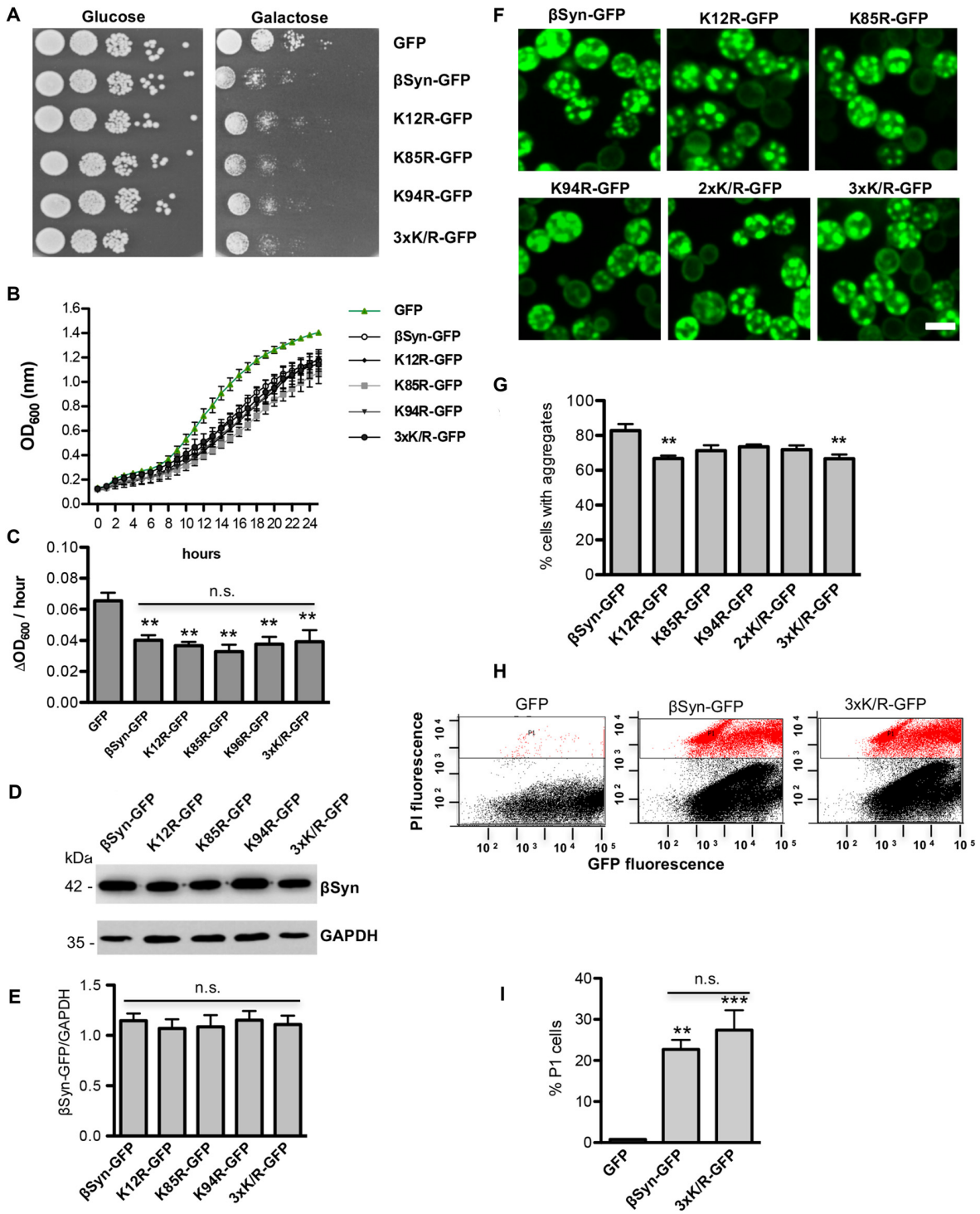

FIGURE 3 | High-copy expression of βSyn-GFP variants in yeast. **(A)** Spotting assay of yeast cells expressing *GAL1*-driven GFP-tagged βSyn and βSyn SUMOylation deficient mutants K12R, K85R, K94R, K85R/K94R (2xK/R) or K12R/K85R/K94R (3xK/R) from 2μ plasmids. GFP expressing plasmid was used as a control. Yeast cells were spotted in 10-fold dilutions on selective plates containing 2% glucose (*GAL1* "OFF") or 2% galactose (*GAL1* "ON"). **(B)** Growth analysis of yeast cells from **(A)** in galactose-containing medium for 24 h. **(C)** Growth rate of yeast cells from **(B)** in logarithmic phase. Significance of differences to the GFP control was calculated with *t*-test (**$p < 0.01$; $n = 4$). One-way Anova test revealed no significant differences among the βSyn variants. **(D)** Western blot analysis of protein crude extracts from **(A)** after 6 h induction in galactose-containing medium. GAPDH served as a loading control. **(E)** Densitometric analysis of the immunodetection of

(*Continued*)

FIGURE 3 | Continued
βSyn-GFP relative to the GAPDH loading control. One-way Anova test revealed no significant differences among the βSyn variants ($n = 3$). **(F)** Live-cell fluorescence microscopy of yeast cells expressing *GAL1*-driven βSyn-GFP variants from 2μ plasmids. Yeast cells, pre-grown to mid-log phase, were induced in galactose-containing medium and examined for aggregates at 6 h of induction. Scale bar – 5 μM. **(G)** Aggregate quantification of yeast cells, expressing βSyn-GFP variants. For quantification of aggregation at least 200 cells were counted per strain and per experiment. The results are mean from at least four independent experiments ± SD. Significance of differences was calculated with *t*-test (**$p < 0.01$ vs. βSyn). **(H)** Propidium iodide (PI) fluorescence intensity of cells expressing βSyn, 3xK/R and GFP (control) after 20 h induction of expression, assessed by flow cytometry analysis. **(I)** Quantification of PI-positive yeast cells with higher fluorescent intensities (P1) than the background is presented. Significance of differences to the GFP control was calculated with *t*-test (**$p < 0.01$; ***$p < 0.001$; $n = 4$).

proteins by inhibition of SUMO de-conjugation enzymes prevented aggregate formation but still caused significant cellular growth inhibition. These effects are not dependent on direct sumoylation of βSyn, since the growth and aggregation propensity of βSyn and K12/K85/K94R-expressing cells is influenced similarly. The results suggest an indirect effect of SUMO on βSyn-induced cytotoxicity by modification of other SUMO-target proteins that affect the aggregation or cytotoxicity of βSyn.

βSyn Aggregates Are Cleared Mainly By the 26S Proteasome

Both autophagy and UPS are implicated in degradation of αSyn and manifestation of PD. Inefficient protein clearance may lead to accumulation of toxic protein species and is sufficient to trigger neurotoxicity (Xilouri et al., 2013). In yeast, autophagy represents the major pathway for degradation of αSyn aggregates (Petroi et al., 2012; Tenreiro et al., 2014) and this process is promoted by sumoylation (Shahpasandzadeh et al., 2014).

We assessed the mechanism of βSyn aggregate clearance mediated by the autophagy/vacuolar and the ubiquitin-proteasome pathways. The impact of blocking these systems by drug treatments was studied. Expression of βSyn and K12/K85/K94R in *smt3*^{ts} cells was induced for 4 h at permissive (25°C; +SUMO) or restrictive temperature (30°C; −SUMO). Promoter shut-off was achieved by shifting the cells to glucose-containing medium that represses the *GAL1* promoter. PMSF was used as an inhibitor of autophagy/vacuolar pathway as described previously (Petroi et al., 2012; Kleinknecht et al., 2016; **Figure 5A**). Cells were imaged 5 h after promoter shut-off. Inhibition of autophagy resulted in increased number of cells with βSyn or K12/K85/K94R aggregates relative to the control. This suggests that the autophagy/vacuolar pathway contribute to βSyn aggregate clearance. Inhibition of sumoylation resulted in similar aggregate clearance.

The contribution of the UPS to βSyn degradation was analyzed by inhibiting this system with the proteasome inhibitor MG132 (**Figure 5B**). In the presence of functional SUMO, there was almost two-fold increase of cells with βSyn aggregates in comparison to the control, when the proteasome is not inhibited. These data suggest a major contribution of the UPS to βSyn or K12/K85/K94R aggregate clearance. In contrast to autophagy, downregulation of sumoylation had a significant impact on the aggregate clearance by the proteasome, diminishing the contribution of this system on βSyn aggregate clearance.

These results suggest that βSyn aggregates in yeast are cleared mainly by the proteasome with a smaller contribution of autophagy/vacuolar pathway. The proteasomal clearance of βSyn aggregates is not significantly affected by direct sumoylation of βSyn lysine residues. Downregulation of sumoylation significantly reduces βSyn aggregate clearance by the proteasome, however, does not affect the autophagy/vacuolar mediated aggregate clearance.

Sumoylation Affects βSyn Protein Turnover

We next analyzed the effect of sumoylation on the protein stability of βSyn and K12/K85/K94R by promoter shut-off experiments. The contribution of the autophagy/vacuole and the proteasome pathway was examined as described above by inhibiting each system with drug treatment. Protein expression was induced for 4 h in galactose medium, then the cells were shifted to glucose medium (*GAL1*-"OFF") and protein crude extracts were prepared 6 h after promoter shut-off. Assays were performed in W303 wild type, *smt3*^{ts} and *ulp1*^{ts} strains at restrictive temperature (30°C). Immunoblotting analysis was performed and steady-state levels of βSyn variants were quantified (**Figure 6**). Inhibition of autophagy/vacuolar pathway by PMSF did not result in changes of βSyn or K12/K85/K94R protein levels in wild type W303 background in comparison to the control (**Figures 6A,B**). Impairment of functional SUMO (*smt3*^{ts}) did not significantly affect the protein levels of both βSyn variants, when autophagy was inhibited. However, inhibition of the vacuolar/autophagy pathway resulted in significant increases of the protein levels of both βSyn variants, when the pool of sumoylated proteins was up-regulated in *ulp1*^{ts} strain.

In contrast to autophagy, inhibition of the proteasome with MG132 in presence of functional SUMO in yeast wild type background had a strong impact on the protein stability (**Figures 6C,D**). Increased protein levels of both βSyn variants were detected in comparison to the control, suggesting involvement of the UPS in degradation of βSyn and K12/K85/K94R proteins. Importantly, impairment of functional SUMO in *smt3*^{ts} strain did not alter ßSyn protein levels 6 h after promoter shut-off, when the proteasome was impaired, indicating that inhibition of sumoylation suppressed the proteasomal degradation of βSyn and K12/K85/K94R derivative. Proteasome impairment resulted in significantly compromised degradation of the proteins in *ulp1*^{ts} strain, when the pool of sumoylated proteins is up-regulated, revealing the major impact of the proteasome and functional sumoylation machinery on βSyn degradation.

These findings suggest that the 26S-proteasome represents the major pathway for degradation of βSyn in the cells. Functional sumoylation machinery is required for the efficient degradation of the protein by the 26S-proteasome, indicating a cross-talk between sumoylation and UPS in βSyn protein homeostasis. This process is not dependent on direct SUMO modification of βSyn at K12, K85 or K94 acceptor sites. Sumoylation promotes

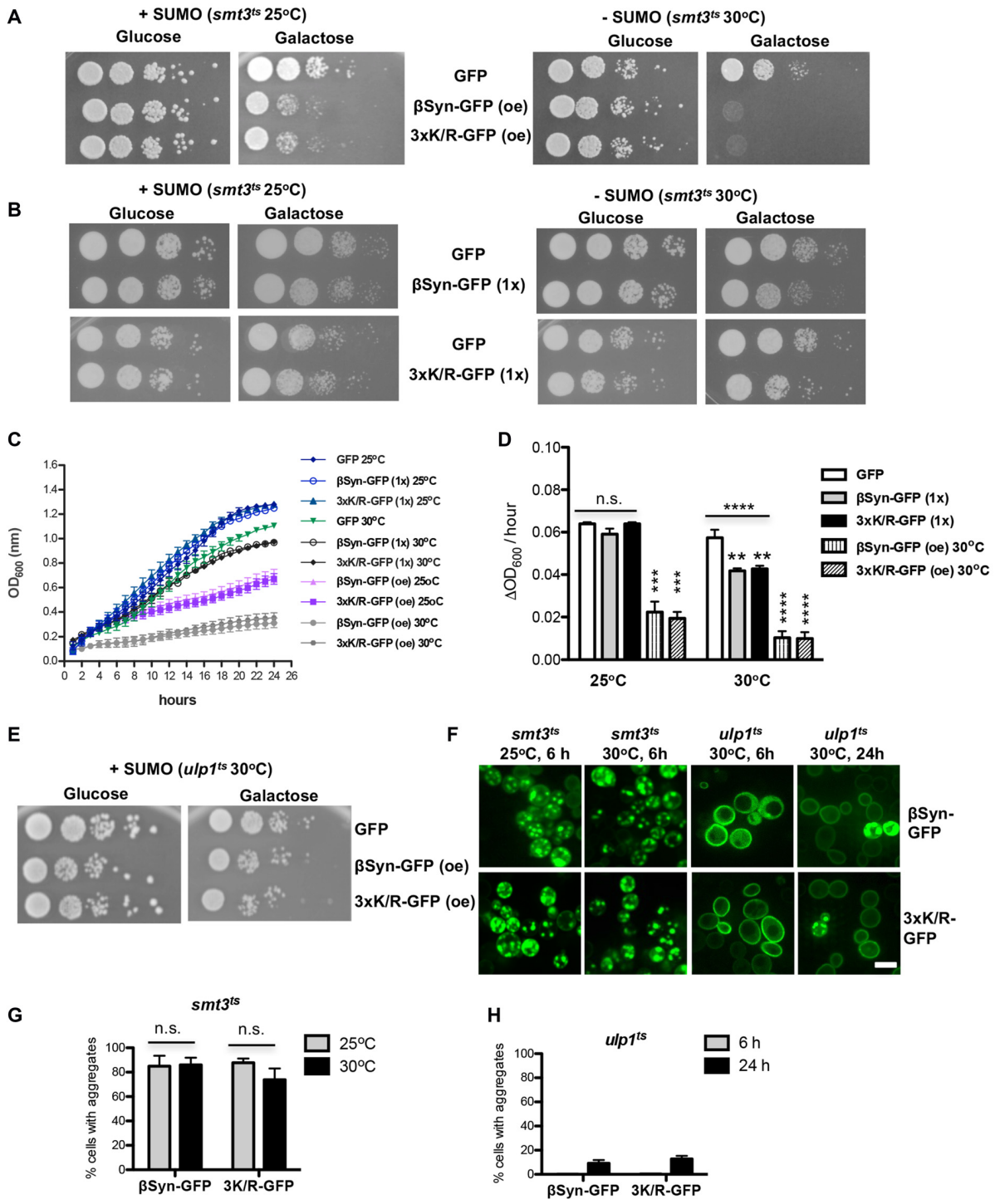

FIGURE 4 | Impairment of sumoylation increases βSyn-GFP induced toxicity. **(A)** Spotting assay of *smt3*^{ts} mutant strain expressing βSyn-GFP and 3xK/R-GFP at permissive (25°C; +SUMO) or restrictive temperature (30°C; −SUMO). *GAL1*-driven synucleins are expressed from 2μ plasmid (oe-overexpression). GFP, expressed from the same promoter, is used as a control. Yeast cells were spotted in 10-fold dilutions on selection plates containing glucose (*GAL1* promoter "OFF") or galactose (*GAL1* promoter "ON"). **(B)** Spotting assay of *smt3*^{ts} mutant strain expressing one copy (1x) of βSyn-GFP or 3xK/R-GFP. Yeast cells, expressing GFP were used as a control. **(C)** Growth analysis of yeast cells from **(A,B)** in galactose-containing medium for 24 h at the indicated temperatures. **(D)** Growth rate of yeast cells in logarithmic phase. Significance of differences was calculated with One-way Anova test or *t*-test, relative to the GFP control (**$p < 0.01$; ***$p < 0.001$; ****$p < 0.0001$; $n = 4$). **(E)** Spotting assay of *ulp1*^{ts} mutant strain expressing βSyn-GFP and 3xK/R-GFP from 2μ plasmid at 30°C. **(F)** Live-cell fluorescence

(*Continued*)

FIGURE 4 | Continued
microscopy of yeast cells expressing *GAL1*-driven synuclein isoforms from 2μ plasmids in *smt3*^{ts} strain and *ulp1*^{ts} strain. Yeast cells, pre-grown to mid-log phase, were induced in galactose-containing medium and examined for aggregates at indicated temperatures and hours after induction. Scale bar—5 μM. **(G)** Aggregate quantification of yeast cells, expressing synuclein-GFP isoforms in *smt3*^{ts} strain at 25°C and 30°C. For each strain, the number of cells displaying cytoplasmic foci is presented as percent of the total number of cells. The results are mean from at least four independent experiments ± SD. **(H)** Aggregate quantification of yeast cells, expressing synuclein-GFP isoforms in *ulp1*^{ts} strain 6 h and 24 h after induction of protein expression.

the proteasomal degradation of βSyn. Up-regulation of the sumoylation pool promotes in addition the degradation by autophagy/vacuole.

Downregulation of Sumoylation Increases the Accumulation of Ubiquitinated Cellular Proteins

Sumoylation is involved in protein homeostasis by its interplay with the UPS (Liebelt and Vertegaal, 2016). It was examined, whether compromised degradation of βSyn by the proteasome is connected to misregulation of UPS when cellular sumoylation is decreased. We followed the accumulation of ubiquitinated substrates in yeast cells in presence and absence of βSyn expression and tested if downregulation of the cellular pool of functional SUMO affects the levels of ubiquitin conjugates. Immunoblotting analysis was performed with protein extracts from yeast cells, expressing βSyn, K12/K85/K94R or empty vector control (**Figure 7A**). Inhibition of sumoylation in *smt3*^{ts} strain revealed accumulation of ubiquitinated proteins, whereas up-regulation of the sumoylation pool by inhibition of the SUMO de-conjugation resulted in similar levels of ubiquitinated proteins as in W303 wild type yeast cells (**Figure 7B**). Expression of βSyn variants did not affect the accumulation of ubiquitinated proteins in comparison to the empty vector control. Importantly, the steady-state levels of βSyn variants differed between the yeast strains. Expression of βSyn or K12/K85/K94R in *smt3*^{ts} cells resulted in significantly increased protein accumulation in comparison to the wild type W303 strain (**Figure 7C**), whereas up-regulation of the sumoylation in *ulp1*^{ts} cells decreased the protein levels. The increased protein levels correlated with accumulation of ubiquitinated substrates in *smt3*^{ts} cells.

These findings showed that reduction of available functional SUMO has a strong impact on the steady-state levels of ubiquitin conjugates, including proteasomal degradation. This presumably leads to accumulation of soluble βSyn protein in the cell and supports that sumoylation protects against βSyn-induced toxicity by promoting the degradation of soluble as well as aggregated protein.

DISCUSSION

The budding yeast *Saccharomyces cerevisiae* was used as a prototypic eukaryotic cell to investigate the mechanism of βSyn turnover and the effect of sumoylation on βSyn-induced cytotoxicity, aggregation and protein stability. Accumulating evidence suggested that besides αSyn, also βSyn is involved in the pathogenesis of aggregopathies such as PD. In the current study, we analyzed βSyn lysine residues required for covalent attachment of SUMO, as well as the effect of the cellular sumoylation pool on βSyn-induced toxicity, aggregate formation and stability.

Initial reports on βSyn in double transgenic mice suggested that βSyn is less prone to aggregation than αSyn and may counteract the αSyn aggregation (Hashimoto et al., 2001). Recent studies reported that βSyn contributes to neuronal degeneration and suggest a possible toxic gain-of-function of βSyn. It was shown that βSyn forms Proteinase K resistant aggregates in primary cultured neurons and dopaminergic neurons in rat brains and to cause neurotoxicity (Taschenberger et al., 2013). Importantly, this effect was

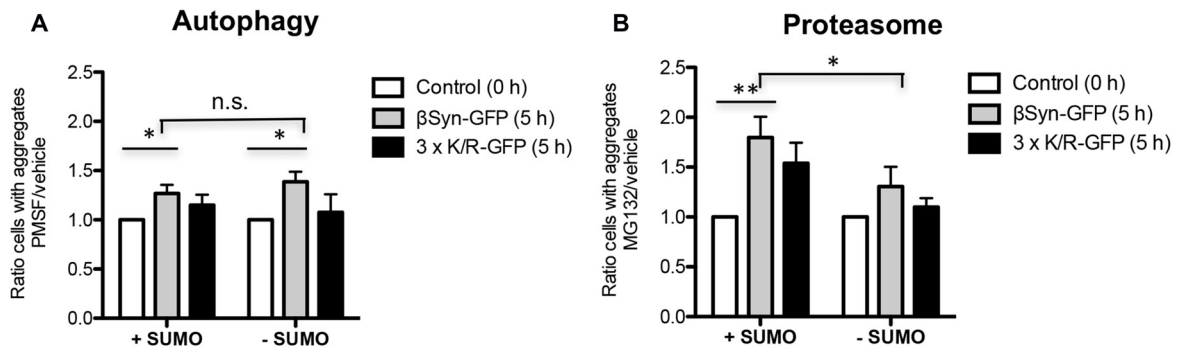

FIGURE 5 | βSyn aggregate clearance after promoter shut-off. Quantification of cells displaying aggregates of βSyn-GFP or 3xK/R-GFP upon inhibition of autophagy by phenylmethanesulfonyl fluoride (PMSF) **(A)** or proteasome by MG132 **(B)**. Yeast cells were incubated in 2% galactose-containing media for 4 h either at permissive (25°C; +SUMO) or restrictive temperature (30°C; −SUMO) and shifted to 2% glucose-containing media supplemented with 1 mM PMSF dissolved in EtOH **(A)** or 75 μM MG132, dissolved in dimethyl sulfoxide (DMSO) **(B)**. Control cells were supplemented with vehicles only (EtOH or DMSO). Cells with aggregates were counted after 5 h *GAL1*-promoter shut-off and presented as a ratio to the control. Significance of differences was calculated with *t*-test (*$p < 0.05$; **$p < 0.01$; $n = 4$).

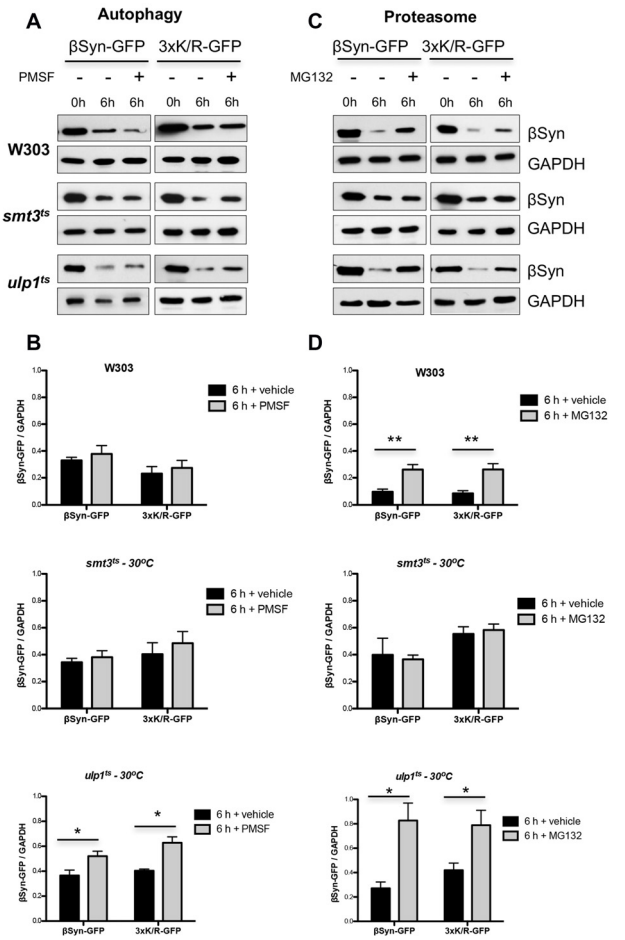

FIGURE 6 | Effect of sumoylation on βSyn protein stability. Yeast cells, expressing βSyn-GFP or 3xK/R-GFP variant in the indicated strains were induced for 4 h in galactose medium (*GAL1* "ON") and then transferred to glucose containing medium (*GAL1* "OFF"). The glucose medium was supplemented with 1 mM PMSF **(A)** or 75 μM MG132 **(C)**. Immunoblotting analysis was performed at the indicated time points after promoter shut-off with βSyn antibody and GAPDH as a loading control. A representative result is shown from at least three independent experiments. **(B,D)** Densitometric analysis of the immunodetection of βSyn relative to the GAPDH loading control. Significance of differences was calculated with *t*-test (*$p < 0.05$; **$p < 0.01$; $n = 3$).

dependent on the accumulation of the protein over time and after 8 weeks of βSyn overexpression, similar neurodegenerative effect to that of αSyn was observed. Another study reported on two mutations of βSyn, P123H and V70M, linked to DLB that may stimulate neurodegeneration in transgenic mice by itself or via αSyn aggregation (Fujita et al., 2010). These studies reveal that βSyn may possess gain-of-function pathogenic properties on its own or act synergistically with αSyn and that alteration of βSyn levels in the cell might play a role in a broad range of synucleinopathies.

Budding yeast is an established model system to study the molecular mechanisms of PD and other synucleinopathies (Menezes et al., 2015; Popova et al., 2015). Expression of human αSyn in yeast induces growth inhibition and aggregate formation, similar to the pathology of the disease (Outeiro and Lindquist, 2003; Petroi et al., 2012). Recently, yeast was used to investigate the molecular mechanism of βSyn-induced toxicity (Tenreiro et al., 2016). Expression of βSyn was toxic and resulted in formation of cellular aggregates resembling the αSyn aggregates. βSyn expression induced defects in similar pathways as αSyn, including ER-to-Golgi trafficking defects and increased oxidative stress. Importantly, co-expression of αSyn and βSyn resulted in formation of heterodimers and enhanced toxicity due to additive accumulation of toxic protein species. Co-expression of αSyn and βSyn strongly inhibited yeast vegetative growth, preventing the in-depth analysis of the molecular effects of α/ßSyn co-expression (Tenreiro et al., 2016).

The increase in αSyn-mediated cytotoxicity is dose-dependent resulting in a threshold for toxicity (Outeiro and Lindquist, 2003; Petroi et al., 2012). The thresholds for βSyn and αSyn mediated toxicity differed considerably in yeast. Three copies of the *GAL1* promoter driven αSyn gene integrated into the yeast genome inhibited cellular growth (Petroi et al., 2012), but three copies with the same promoter for βSyn were not sufficient for a significant growth effect. Overexpression of βSyn significantly inhibited yeast growth and induced formation of cellular aggregation, similar to αSyn, corroborating that βSyn has a higher threshold for toxicity and aggregation than αSyn.

PTMs including phosphorylation, ubiquitination, nitration, glycosylation, acetylation or sumoylation play an important role in regulation of αSyn function and stability (Giasson et al., 2000; Shimura et al., 2001; Fujiwara et al., 2002; Hasegawa et al., 2002; Dorval and Fraser, 2006; de Oliveira et al., 2017). Sumoylation can change sub-cellular protein localization, alter protein-protein interactions or change the solubility of the protein. Sumoylation is a dynamic process and the levels of sumoylated proteins are regulated by different stresses (Enserink, 2015). Sumoylation is directly involved in maintaining protein homeostasis and is closely linked to neurodegeneration, exhibiting a protective role against αSyn-induced toxicity and inclusion formation in yeast (Shahpasandzadeh et al., 2014).

Three lysine residues within consensus SUMO motifs are used for PTM of βSyn in yeast. Inhibition of sumoylation at the single K12 site as well as at all three SUMO sites resulted in decreased aggregate formation, suggesting that sumoylation promotes aggregation. The results are based on mutagenesis analysis changing the codons for the consensus sumoylation sites of βSyn. Cell growth or viability was not affected when sumoylation was inhibited. This supports that βSyn mediated aggregate formation and cytotoxicity represent unlinked molecular functions. Global inhibition of the cellular sumoylation resulted in significant increase in βSyn-induced toxicity without changes in aggregate formation. Functional sumoylation therefore protects yeast cells against βSyn-induced toxicity without affecting the aggregate propensity of the protein (**Figure 8**). In line with our observations, expression of V70M and P123H βSyn mutants, which are associated with sporadic and familial cases of DLB, increased the aggregate formation without enhancing the toxicity in yeast (Tenreiro et al., 2016). Accumulated βSyn may undergo additional PTMs such as

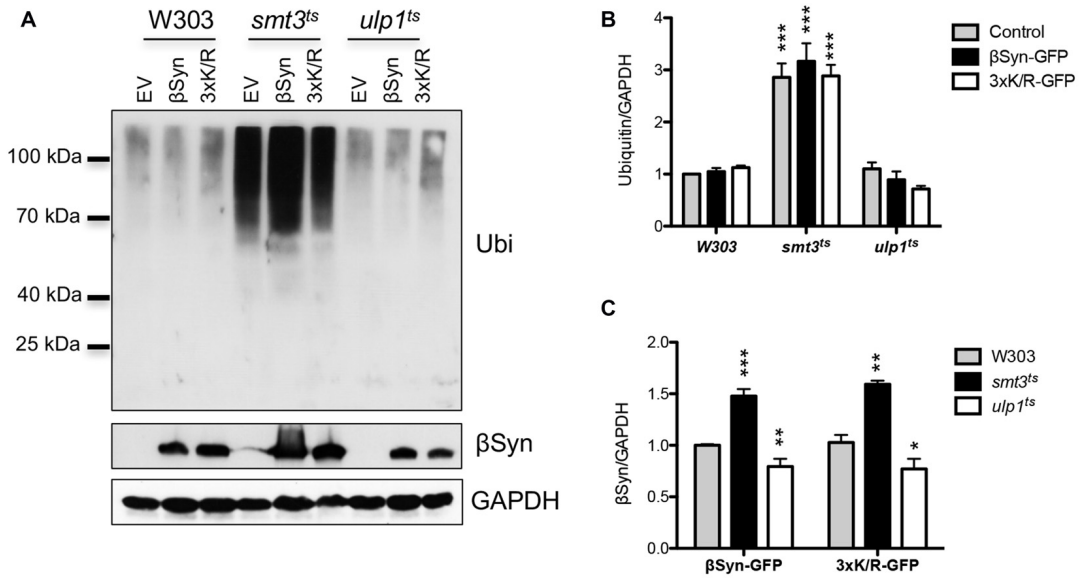

FIGURE 7 | Interplay between sumoylation and ubiquitination. **(A)** Western blot analysis of crude protein extracts from yeast cell, expressing βSyn-GFP and 3xK/R-GFP mutant in W303, *smt3*^{ts} and *ulp1*^{ts} strains at 30°C, probed with ubiquitin antibody, detecting poly- and mono-ubiquitinated proteins. The same membrane was stripped and probed with βSyn antibody. GAPDH was used as a loading control. **(B)** Densitometric analysis of the immunodetection of ubiquitin or βSyn **(C)**, relative to the GAPDH loading control. Significance of differences was calculated with *t*-test (***$p < 0.001$; **$p < 0.01$; *$p < 0.05$ vs. W303 wild type background; $n = 3$).

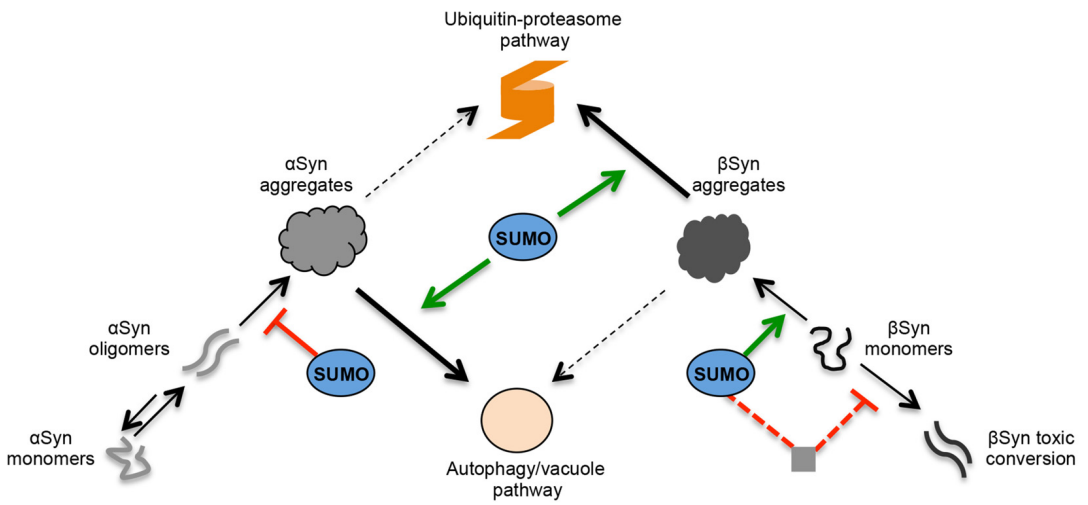

FIGURE 8 | Role of SUMO in the regulation of αSyn and βSyn turnover and toxicity in yeast. Schematic representation of αSyn and βSyn aggregation pathways. Under pathological conditions, αSyn can undergo oligomerization. A dynamic equilibrium exists between monomeric and multimeric forms of αSyn. The oligomeric species represent intermediates of the aggregation process and are suggested to be the most toxic forms of αSyn. SUMO exhibits a protective role against αSyn-induced toxicity. Sumoylation increases the solubility αSyn and decreases the aggregation of the protein. In contrast, βSyn aggregate formation and cytotoxicity are part of different molecular mechanisms. A fraction of accumulated βSyn might gradually undergo structural conversion and form toxic oligomers or fibrils. In contrast to αSyn, these might not be intermediate species in the aggregation process but might be part of an independent molecular pathway. Sumoylation of βSyn promotes the aggregate formation of the protein without affecting the cytotoxicity. The presence of functional cellular sumoylation machinery protects against βSyn toxicity independently of βSyn sumoylation. Sumoylation of additional target proteins or cellular pathways might be involved in the cytoprotection by inhibiting the formation of βSyn toxic species. αSyn and βSyn aggregates are cleared predominantly by two different pathways. The main pathway for αSyn aggregate clearance is autophagy, whereas ubiquitin-proteasome system (UPS) is the major degradation pathway for βSyn aggregates. Autophagy/vacuolar pathway has a minor contribution to βSyn aggregate clearance. Presence of functional SUMO protects against βSyn as well as αSyn toxicity by promoting the degradation of the proteins. Sumoylated αSyn is primarily targeted to the autophagy pathway, whereas presence of functional SUMO promotes the degradation of βSyn monomers and βSyn aggregates by the ubiquitin-proteasome pathway.

phosphorylation or acetylation and gain pathogenic properties. A fraction of βSyn might adopt a different structure and form toxic oligomers or fibrils. In contrast to αSyn this might not necessarily lead to aggregates. The cellular environment might be relevant, because it is known that βSyn can form fibrils at mild acidic pH as a result of pH dysregulation due to oxidative stress or in acidic organelles such as endosomes or lysosomes/vacuoles (Moriarty et al., 2017). Alteration of βSyn may enhance synergistically the toxicity of αSyn and promote PD pathology. Another possible explanation is that the disintegration between toxicity and aggregation is due to the co-existence of toxic aggregates and non-toxic "protective" aggregates. Sumoylation might protect against cytotoxicity by promoting the conversion of toxic into protective aggregates.

The protective role of sumoylation against αSyn-induced toxicity is significantly different from βSyn. Sumoylation increases the solubility αSyn and thereby decreases the aggregation of the protein (Krumova et al., 2011). In contrast to βSyn, direct modification of αSyn by SUMO at the conserved modification sites K96 and K102 reduced the formation of inclusions and simultaneously protected against cytotoxicity. Therefore, sumoylation promotes βSyn but reduces αSyn aggregation. In contrast, the cellular sumoylation machinery is equally important for protection against βSyn as well as αSyn, because inhibition of cellular sumoylation had a similar negative impact on growth of yeast cells expressing either βSyn or αSyn (Shahpasandzadeh et al., 2014).

One of the major factors that lead to PD pathogenesis is decreased degradation of αSyn protein by one of the two major proteolytic systems—the autophagy/lysosome system or UPS (Xilouri et al., 2013; Vilchez et al., 2014). This contributes to increased protein levels and aggregation. Yeast has been extensively used for examination of αSyn degradation due to the high conservation of functions and pathways, involved in protein quality control between yeast and higher eukaryotes, including humans. Autophagy is the major pathway for αSyn aggregate clearance in yeast (Petroi et al., 2012; Tenreiro et al., 2014). Sumoylation of αSyn promoted aggregate clearance by autophagy, whereas phosphorylation at S129 triggered increased ubiquitination and degradation of the protein by the UPS (Shahpasandzadeh et al., 2014). Here, we demonstrated that UPS is the major degradation pathway, responsible for clearance of βSyn aggregates. Sumoylation promoted the aggregate clearance by the UPS significantly, whereas autophagy/vacuolar pathway had a minor contribution to βSyn aggregate clearance that was not dependent on a functional sumoylation pool (**Figure 8**). These results indicate that αSyn and βSyn aggregates have different mechanisms for aggregate clearance.

The effect of SUMO on βSyn protein stability is consistent with the aggregate clearance assays. Inhibition of the proteasome significantly increased the level of βSyn. Downregulation of sumoylation stabilized the βSyn protein and abolished its degradation through the UPS, whereas upregulation of the sumoylation had an opposite effect on protein stability. Similarly, sumoylation promotes the degradation of soluble αSyn monomers in yeast that occurs through both degradation pathways (Shahpasandzadeh et al., 2014). These findings highlight the complex regulative role of SUMO in balancing the protein levels of αSyn and βSyn.

Autophagy and the ubiquitin-dependent degradation pathways do not act independently from each other. In the process of selective autophagy, ubiquitination can target proteins not only to the 26S-proteasome but also for autophagic degradation (Kirkin et al., 2009). Inactive 26S-proteasomes can be degraded by the autophagy in a newly discovered pathway termed "proteaphagy" (autophagy of proteasomes), initially described in plants and yeast (Marshall et al., 2015, 2016) and recently reported in mammalian cells (Cohen-Kaplan et al., 2016). Inactivation of UPS is one of the major causes for PD pathology. A proposed mechanism for UPS dysfunction is the direct binding of soluble oligomeric or aggregated species of αSyn with the 26S-proteasome that inhibit its activity (Xilouri et al., 2013). Thus, a possible scenario for αSyn clearance is degradation of the protein together with the inactive proteasomes via the proteaphagy pathway. βSyn has no direct effect on the 26S ubiquitin-dependent degradation and does not bind to the 26S proteasome (Snyder et al., 2005). Thus, higher protein loads of βSyn can be processed by the 26S-proteasome. This might account for the different involvement of the two degradation pathways in the clearance of αSyn and βSyn.

An important contribution of SUMO to protein homeostasis is its interplay with the UPS (Liebelt and Vertegaal, 2016). SUMO-acceptor lysine residues can be targets for ubiquitin conjugation. Thus, sumoylation can directly antagonize the degradation by UPS by a competition with ubiquitin at the same lysine residues, as first shown for IκB-α (Desterro et al., 1998), or can function cooperatively with ubiquitination in a sequential cycle that regulates the function, localization and stability of the protein, as reported for PCNA (Hoege et al., 2002). SUMO can also function as a recognition signal for SUMO-targeted ubiquitin ligases, thus mediating ubiquitin-dependent degradation by the proteasome (Uzunova et al., 2007; Tatham et al., 2008). Downregulation of sumoylation in our studies resulted in significant accumulation of ubiquitinated conjugates and increased levels of βSyn protein in the cell. Expression of βSyn did not affect the steady-state levels of ubiquitin conjugates, consistent with previous findings (Snyder et al., 2005). This indicates that elevated levels of soluble βSyn may account for the increased βSyn-induced toxicity and sumoylation has a protective role by promoting the degradation of the protein.

The complex functional interaction of SUMO and the UPS may also contribute to off-target effects of sumoylation on βSyn protein stability and toxicity. Sumoylation might regulate protein stability or function of additional target proteins and thus indirectly affect the cytotoxicity of βSyn (**Figure 8**). The off-target effect of SUMO may co-exist with the direct effect of sumoylation on βSyn toxicity. It should be noted that the analysis of temperature sensitive mutant strains can evoke additional indirect effects on βSyn protein quality control.

In this study, we provide evidence that the molecular basis of βSyn-induced cytotoxicity and accumulation in the cell is not directly linked to βSyn aggregate formation.

Aggregate formation and cytotoxicity are both linked to sumoylation. Sumoylation determines the accumulation of βSyn and therefore its cytotoxicity. Our data strongly support that the major molecular pathway involved in βSyn turnover and clearance of soluble as well as aggregated proteins is the 26S proteasome.

AUTHOR CONTRIBUTIONS

BP and GHB designed the research. BP, AK, PA, JM and DW performed and analyzed the experiments. BP and GHB wrote the manuscript, with contributions from AK.

FUNDING

This work was funded by the Deutsche Forschungsgemeinschaft (DFG) Research Center Nanoscale Microscopy and Molecular Physiology of the Brain (CNMPB), Göttingen, Germany.

ACKNOWLEDGMENTS

We thank Maria Meyer and Katharina Ziese-Kubon for excellent technical assistance. We thank Kai Heimel for reading of the manuscript.

REFERENCES

Alberti, S., Halfmann, R., and Lindquist, S. (2010). Biochemical, cell biological, and genetic assays to analyze amyloid and prion aggregation in yeast. *Methods Enzymol.* 470, 709–734. doi: 10.1016/s0076-6879(10)70030-6

Cohen-Kaplan, V., Livneh, I., Avni, N., Fabre, B., Ziv, T., Kwon, Y. T., et al. (2016). p62- and ubiquitin-dependent stress-induced autophagy of the mammalian 26S proteasome. *Proc. Natl. Acad. Sci. U S A* 113, E7490–E7499. doi: 10.1073/pnas.1615455113

de Oliveira, R. M., Vicente Miranda, H., Francelle, L., Pinho, R., Szegö, É. M., Martinho, R., et al. (2017). The mechanism of sirtuin 2-mediated exacerbation of α-synuclein toxicity in models of Parkinson disease. *PLoS Biol.* 15:e2000374. doi: 10.1371/journal.pbio.2000374

Desterro, J. M., Rodriguez, M. S., and Hay, R. T. (1998). SUMO-1 modification of IκBα inhibits NF-κB activation. *Mol. Cell* 2, 233–239. doi: 10.1016/S1097-2765(00)80133-1

Dieckhoff, P., Bolte, M., Sancak, Y., Braus, G. H., and Irniger, S. (2004). Smt3/SUMO and Ubc9 are required for efficient APC/C-mediated proteolysis in budding yeast. *Mol. Microbiol.* 51, 1375–1387. doi: 10.1046/j.1365-2958.2003.03910.x

Dorval, V., and Fraser, P. E. (2006). Small ubiquitin-like modifier (SUMO) modification of natively unfolded proteins tau and α-synuclein. *J. Biol. Chem.* 281, 9919–9924. doi: 10.1074/jbc.M510127200

Ducas, V. C., and Rhoades, E. (2012). Quantifying interactions of β-synuclein and γ-synuclein with model membranes. *J. Mol. Biol.* 423, 528–539. doi: 10.1016/j.jmb.2012.08.008

Eckermann, K. (2013). SUMO and Parkinson's disease. *Neuromolecular Med.* 15, 737–759. doi: 10.1007/s12017-013-8259-5

Enserink, J. M. (2015). Sumo and the cellular stress response. *Cell Div.* 10:4. doi: 10.1186/s13008-015-0010-1

Fan, Y., Limprasert, P., Murray, I. V. J., Smith, A. C., Lee, V. M. Y., Trojanowski, J. Q., et al. (2006). β-synuclein modulates α-synuclein neurotoxicity by reducing α-synuclein protein expression. *Hum. Mol. Genet.* 15, 3002–3011. doi: 10.1093/hmg/ddl242

Fujita, M., Sugama, S., Sekiyama, K., Sekigawa, A., Tsukui, T., Nakai, M., et al. (2010). A β-synuclein mutation linked to dementia produces neurodegeneration when expressed in mouse brain. *Nat. Commun.* 1:110. doi: 10.1038/ncomms1101

Fujiwara, H., Hasegawa, M., Dohmae, N., Kawashima, A., Masliah, E., Goldberg, M. S., et al. (2002). α-Synuclein is phosphorylated in synucleinopathy lesions. *Nat. Cell Biol.* 4, 160–164. doi: 10.1038/ncb748

George, J. M. (2002). The synucleins. *Genome Biol.* 3, reviews3002.1–reviews3002.6.

Giasson, B. I., Duda, J. E., Murray, I. V., Chen, Q., Souza, J. M., Hurtig, H. I., et al. (2000). Oxidative damage linked to neurodegeneration by selective α-synuclein nitration in synucleinopathy lesions. *Science* 290, 985–989. doi: 10.1126/science.290.5493.985

Gietz, D., St Jean, A., Woods, R. A., and Schiestl, R. H. (1992). Improved method for high efficiency transformation of intact yeast cells. *Nucleic Acids Res.* 20:1425. doi: 10.1093/nar/20.6.1425

Guthrie, C., and Fink, G. R. (1991). Guide to yeast genetics and molecular biology. *Methods Enzymol.* 194, 1–863. doi: 10.1016/s0076-6879(00)x0276-5

Hasegawa, M., Fujiwara, H., Nonaka, T., Wakabayashi, K., Takahashi, H., Lee, V. M., et al. (2002). Phosphorylated α-synuclein is ubiquitinated in α-synucleinopathy lesions. *J. Biol. Chem.* 277, 49071–49076. doi: 10.1074/jbc.M208046200

Hashimoto, M., Rockenstein, E., Mante, M., Mallory, M., and Masliah, E. (2001). β-Synuclein inhibits α-synuclein aggregation: a possible role as an anti-parkinsonian factor. *Neuron* 32, 213–223. doi: 10.1016/S0896-6273(01)00462-7

Hoege, C., Pfander, B., Moldovan, G.-L. L., Pyrowolakis, G., and Jentsch, S. (2002). RAD6-dependent DNA repair is linked to modification of PCNA by ubiquitin and SUMO. *Nature* 419, 135–141. doi: 10.1038/nature00991

Kalia, L. V., and Lang, A. E. (2015). Parkinson's disease. *Lancet* 386, 896–912. doi: 10.1016/S0140-6736(14)61393-3

Kirkin, V., McEwan, D. G., Novak, I., and Dikic, I. (2009). A role for ubiquitin in selective autophagy. *Mol. Cell* 34, 259–269. doi: 10.1016/j.molcel.2009.04.026

Kleinknecht, A., Popova, B., Lázaro, D. F., Pinho, R., Valerius, O., Outeiro, T. F., et al. (2016). C-terminal tyrosine residue modifications modulate the protective phosphorylation of serine 129 of α-synuclein in a yeast model of Parkinson's disease. *PLoS Genet.* 12:e1006098. doi: 10.1371/journal.pgen.1006098

Krüger, R., Kuhn, W., Müller, T., Woitalla, D., Graeber, M., Kösel, S., et al. (1998). Ala30Pro mutation in the gene encoding α-synuclein in Parkinson's disease. *Nat. Genet.* 18, 106–108. doi: 10.1038/ng0298-106

Krumova, P., Meulmeester, E., Garrido, M., Tirard, M., Hsiao, H. H., Bossis, G., et al. (2011). Sumoylation inhibits α-synuclein aggregation and toxicity. *J. Cell Biol.* 194, 49–60. doi: 10.1083/jcb.201010117

Li, J., Henning Jensen, P., and Dahlström, A. (2002). Differential localization of α-, β- and γ-synucleins in the rat CNS. *Neuroscience* 113, 463–478. doi: 10.1016/s0306-4522(02)00143-4

Li, S.-J., and Hochstrasser, M. (1999). A new protease required for cell-cycle progression in yeast. *Nature* 398, 246–251. doi: 10.1038/18457

Liebelt, F., and Vertegaal, A. C. O. (2016). Ubiquitin-dependent and independent roles of SUMO in proteostasis. *Am. J. Physiol. Cell Physiol.* 311, C284–C296. doi: 10.1152/ajpcell.00091.2016

Marshall, R. S., Li, F., Gemperline, D. C., Book, A. J., and Vierstra, R. D. (2015). Autophagic degradation of the 26S proteasome is mediated by the dual ATG8/ubiquitin receptor RPN10 in arabidopsis. *Mol. Cell* 58, 1053–1066. doi: 10.1016/j.molcel.2015.04.023

Marshall, R. S., McLoughlin, F., and Vierstra, R. D. (2016). Autophagic turnover of inactive 26S proteasomes in yeast is directed by the ubiquitin receptor Cue5 and the Hsp42 chaperone. *Cell Rep.* 16, 1717–1732. doi: 10.1016/j.celrep.2016.07.015

Mbefo, M. K., Paleologou, K. E., Boucharaba, A., Oueslati, A., Schell, H., Fournier, M., et al. (2010). Phosphorylation of synucleins by members of the Polo-like kinase family. *J. Biol. Chem.* 285, 2807–2822. doi: 10.1074/jbc.M109.081950

Menezes, R., Tenreiro, S., Macedo, D., Santos, C. N., and Outeiro, T. F. (2015). From the baker to the bedside: yeast models of Parkinson's disease. *Microb. Cell* 2, 262–279. doi: 10.15698/mic2015.08.219

Mori, F., Tanji, K., Yoshimoto, M., Takahashi, H., and Wakabayashi, K. (2002). Immunohistochemical comparison of α- and β-synuclein in adult rat central nervous system. *Brain Res.* 941, 118–126. doi: 10.1016/s0006-8993(02)02643-4

Moriarty, G. M., Olson, M. P., Atieh, T. B., Janowska, M. K., Khare, S. D., and Baum, J. (2017). A pH dependent switch promotes β-synuclein fibril formation via glutamate residues. *J. Biol. Chem.* 292, 16368—16379. doi: 10.1074/jbc.M117.780528

Mumberg, D., Müller, R., Funk, M., Müller, R., and Funk, M. (1994). Regulatable promoters of Saccharomyces cerevisiae: comparison of transcriptional activity and their use for heterologous expression. *Nucleic Acids Res.* 22, 5767–5768. doi: 10.1093/nar/22.25.5767

Nakajo, S., Tsukada, K., Omata, K., Nakamura, Y., and Nakaya, K. (1993). A new brain-specific 14-kDa protein is a phosphoprotein. Its complete amino acid sequence and evidence for phosphorylation. *Eur. J. Biochem.* 217, 1057–1063. doi: 10.1111/j.1432-1033.1993.tb18337.x

Ohtake, H., Limprasert, P., Fan, Y., Onodera, O., Kakita, A., Takahashi, H., et al. (2004). β-synuclein gene alterations in dementia with Lewy bodies. *Neurology* 63, 805–811. doi: 10.1212/01.WNL.0000139870.14385.3C

Outeiro, T. F., and Lindquist, S. (2003). Yeast cells provide insight into α-synuclein biology and pathobiology. *Science* 302, 1772–1775. doi: 10.1126/science.1090439

Petroi, D., Popova, B., Taheri-Talesh, N., Irniger, S., Shahpasandzadeh, H., Zweckstetter, M., et al. (2012). Aggregate clearance of α-synuclein in Saccharomyces cerevisiae depends more on autophagosome and vacuole function than on the proteasome. *J. Biol. Chem.* 287, 27567–27579. doi: 10.1074/jbc.M112.361865

Polymeropoulos, M. H., Lavedan, C., Leroy, E., Ide, S. E., Dehejia, A., Dutra, A., et al. (1997). Mutation in the α-synuclein gene identified in families with Parkinson's disease. *Science* 276, 2045–2047. doi: 10.1126/science.276.5321.2045

Popova, B., Kleinknecht, A., and Braus, G. (2015). Posttranslational modifications and clearing of α-synuclein aggregates in yeast. *Biomolecules* 5, 617–634. doi: 10.3390/biom5020617

Shahpasandzadeh, H., Popova, B., Kleinknecht, A., Fraser, P. E., Outeiro, T. F., and Braus, G. H. (2014). Interplay between sumoylation and phosphorylation for protection against α-synuclein inclusions. *J. Biol. Chem.* 289, 31224–31240. doi: 10.1074/jbc.M114.559237

Shimura, H., Schlossmacher, M. G., Hattori, N., Frosch, M. P., Trockenbacher, A., Schneider, R., et al. (2001). Ubiquitination of a new form of α-synuclein by parkin from human brain: implications for Parkinson's disease. *Science* 293, 263–269. doi: 10.1126/science.1060627

Sikorski, R. S., and Hieter, P. (1989). A system of shuttle vectors and yeast host strains designed for efficient manipulation of DNA in Saccharomyces cerevisiae. *Genetics* 122, 19–27.

Singleton, A. B., Farrer, M., Johnson, J., Singleton, A., Hague, S., Kachergus, J., et al. (2003). α-Synuclein locus triplication causes Parkinson's disease. *Science* 302:841. doi: 10.1126/science.1090278

Snyder, H., Mensah, K., Hsu, C., Hashimoto, M., Surgucheva, I. G., Festoff, B., et al. (2005). β-Synuclein reduces proteasomal inhibition by α-synuclein but not γ-synuclein. *J. Biol. Chem.* 280, 7562–7569. doi: 10.1074/jbc.M412887200

Spillantini, M. G., Crowther, R. A., Jakes, R., Hasegawa, M., and Goedert, M. (1998). α-Synuclein in filamentous inclusions of Lewy bodies from Parkinson's disease and dementia with lewy bodies. *Proc. Natl. Acad. Sci. U S A* 95, 6469–6473. doi: 10.1073/pnas.95.11.6469

Sung, Y.-H., and Eliezer, D. (2006). Secondary structure and dynamics of micelle bound β- and γ-synuclein. *Protein Sci.* 15, 1162–1174. doi: 10.1110/ps.051803606

Taschenberger, G., Toloe, J., Tereshchenko, J., Akerboom, J., Wales, P., Benz, R., et al. (2013). β-synuclein aggregates and induces neurodegeneration in dopaminergic neurons. *Ann. Neurol.* 74, 109–118. doi: 10.1002/ana.23905

Tatham, M. H., Geoffroy, M.-C., Shen, L., Plechanovova, A., Hattersley, N., Jaffray, E. G., et al. (2008). RNF4 is a poly-SUMO-specific E3 ubiquitin ligase required for arsenic-induced PML degradation. *Nat. Cell Biol.* 10, 538–546. doi: 10.1038/ncb1716

Tenreiro, S., Reimão-Pinto, M. M., Antas, P., Rino, J., Wawrzycka, D., Macedo, D., et al. (2014). Phosphorylation modulates clearance of α-synuclein inclusions in a yeast model of Parkinson's disease. *PLoS Genet.* 10:e1004302. doi: 10.1371/journal.pgen.1004302

Tenreiro, S., Rosado-Ramos, R., Gerhardt, E., Favretto, F., Magalhães, F., Popova, B., et al. (2016). Yeast reveals similar molecular mechanisms underlying α- and β-synuclein toxicity. *Hum. Mol. Genet.* 25, 275–290. doi: 10.1093/hmg/ddv470

Uversky, V. N., Li, J., Souillac, P., Millett, I. S., Doniach, S., Jakes, R., et al. (2002). Biophysical properties of the synucleins and their propensities to fibrillate: inhibition of α-synuclein assembly by β- and γ-synucleins. *J. Biol. Chem.* 277, 11970–11978. doi: 10.1074/jbc.M109541200

Uzunova, K., Göttsche, K., Miteva, M., Weisshaar, S. R., Glanemann, C., Schnellhardt, M., et al. (2007). Ubiquitin-dependent proteolytic control of SUMO conjugates. *J. Biol. Chem.* 282, 34167–34175. doi: 10.1074/jbc.M706505200

Vilchez, D., Saez, I., and Dillin, A. (2014). The role of protein clearance mechanisms in organismal ageing and age-related diseases. *Nat. Commun.* 5:5659. doi: 10.1038/ncomms6659

Villar-Piqué, A., Lopes da Fonseca, T., and Outeiro, T. F. (2015). Structure, function and toxicity of α-synuclein: the Bermuda triangle in synucleinopathies. *J. Neurochem.* 139, 240–255. doi: 10.1111/jnc.13249

Webb, J. L., Ravikumar, B., Atkins, J., Skepper, J. N., and Rubinsztein, D. C. (2003). α-Synuclein is degraded by both autophagy and the proteasome. *J. Biol. Chem.* 278, 25009–25013. doi: 10.1074/jbc.M300227200

Wei, J., Fujita, M., Nakai, M., Waragai, M., Watabe, K., Akatsu, H., et al. (2007). Enhanced lysosomal pathology caused by β-synuclein mutants linked to dementia with Lewy bodies. *J. Biol. Chem.* 282, 28904–28914. doi: 10.1074/jbc.M703711200

Xilouri, M., Brekk, O. R., and Stefanis, L. (2013). α-synuclein and protein degradation systems: a reciprocal relationship. *Mol. Neurobiol.* 47, 537–551. doi: 10.1007/s12035-012-8341-2

Zarranz, J. J., Alegre, J., Gómez-Esteban, J. C., Lezcano, E., Ros, R., Ampuero, I., et al. (2004). The new mutation, E46K, of α-synuclein causes Parkinson and Lewy body dementia. *Ann. Neurol.* 55, 164–173. doi: 10.1002/ana.10795

Conflict of Interest Statement: The authors declare that the research was conducted in the absence of any commercial or financial relationships that could be construed as a potential conflict of interest.

frontiers in Molecular Neuroscience

ORIGINAL RESEARCH
published: 08 June 2018
doi: 10.3389/fnmol.2018.00200

Different Expression Levels of Human Mutant Ubiquitin B^{+1} (UBB^{+1}) Can Modify Chronological Lifespan or Stress Resistance of *Saccharomyces cerevisiae*

Ana Joyce Muñoz-Arellano[1†], *Xin Chen*[1,2†], *Andrea Molt*[1‡], *Eugenio Meza*[1] *and Dina Petranovic*[1,2*]

[1]*Division of Systems and Synthetic Biology, Department of Biology and Biological Engineering, Chalmers University of Technology, Gothenburg, Sweden,* [2]*Novo Nordisk Foundation Center for Biosustainability, Chalmers University of Technology, Gothenburg, Sweden*

OPEN ACCESS

Edited by:
Ralf J. Braun,
University of Bayreuth, Germany

Reviewed by:
Fred Van Leeuwen,
Maastricht University, Netherlands
Bert M. Verheijen,
Utrecht University, Netherlands
Nico P. Dantuma,
Karolinska Institutet (KI), Sweden

***Correspondence:**
Dina Petranovic
dina.petranovic@chalmers.se

†These authors have contributed equally to this work.

‡Present address:
Andrea Molt,
Fine Chemicals and Biocatalysis Research, BASF SE, Ludwigshafen, Germany

Received: *14 December 2017*
Accepted: *18 May 2018*
Published: *08 June 2018*

Citation:
Muñoz-Arellano AJ, Chen X, Molt A, Meza E and Petranovic D (2018) Different Expression Levels of Human Mutant Ubiquitin B^{+1} (UBB^{+1}) Can Modify Chronological Lifespan or Stress Resistance of Saccharomyces cerevisiae. Front. Mol. Neurosci. 11:200. doi: 10.3389/fnmol.2018.00200

The ubiquitin-proteasome system (UPS) is the main pathway responsible for the degradation of misfolded proteins, and its dysregulation has been implicated in several neurodegenerative diseases, including Alzheimer's disease (AD). UBB^{+1}, a mutant variant of ubiquitin B, was found to accumulate in neurons of AD patients and it has been linked to UPS dysfunction and neuronal death. Using the yeast *Saccharomyces cerevisiae* as a model system, we constitutively expressed UBB^{+1} to evaluate its effects on proteasome function and cell death, particularly under conditions of chronological aging. We showed that the expression of UBB^{+1} caused inhibition of the three proteasomal proteolytic activities (caspase-like (β1), trypsin-like (β2) and chymotrypsin-like (β5) activities) in yeast. Interestingly, this inhibition did not alter cell viability of growing cells. Moreover, we showed that cells expressing UBB^{+1} at lower level displayed an increased capacity to degrade induced misfolded proteins. When we evaluated cells during chronological aging, UBB^{+1} expression at lower level, prevented cells to accumulate reactive oxygen species (ROS) and avert apoptosis, dramatically increasing yeast life span. Since proteasome inhibition by UBB^{+1} has previously been shown to induce chaperone expression and thus protect against stress, we evaluated our UBB^{+1} model under heat shock and oxidative stress. Higher expression of UBB^{+1} caused thermotolerance in yeast due to induction of chaperones, which occurred to a lesser extent at lower expression level of UBB^{+1} (where we observed the phenotype of extended life span). Altering UPS capacity by differential expression of UBB^{+1} protects cells against several stresses during chronological aging. This system can be valuable to study the effects of UBB^{+1} on misfolded proteins involved in neurodegeneration and aging.

Keywords: UBB^{+1}, proteasome, Alzheimer's disease, aging, cell death, yeast

Abbreviations: AD, Alzheimer's disease; AZE, L-azetidine-2-carboxylic acid; CLS, chronological life span; DHR123, dihydrorhodamine 123; HSPs, heat shock proteins; PI, propidium iodide; PS, phosphatidylserine; ROS, reactive oxygen species; TUNEL, terminal deoxynucleotidyl transferase dUTP nick end labeling; UPS, ubiquitin proteasome system.

INTRODUCTION

The ubiquitin proteasome system (UPS) is the principal proteolytic pathway that degrades proteins in a regulated manner. Its substrates are targeted for degradation by ubiquitin, a 76-amino-acid polypeptide that is covalently attached to one or more lysine residues of cellular proteins in a process called ubiquitylation. Protein ubiquitylation is mediated by an enzymatic cascade consisting of ubiquitin activating (E1), conjugating (E2) and ligating (E3) enzymes which generates a polyubiquitin chain that functions as the degradation signal. The ubiquitin-conjugated proteins are subsequently recognized and degraded by the 26S proteasome to short peptides, while reusable ubiquitin is released by deubiquitinating enzymes (DUBs; Welchman et al., 2005).

The UPS is involved in a variety of cellular functions such as intracellular signaling, regulation of cell cycle and induction of apoptosis (Hershko and Ciechanover, 1998). Deficiencies in either ubiquitin or proteasome, unless timely corrected, can cause cellular dysfunction or death. An example that ubiquitin itself can be a cause of UPS impairment is the aberrant ubiquitin UBB^{+1}. This mutant ubiquitin results from a dinucleotide "deletion" probably occurring during transcription near the 3' mRNA end, at the first of three ubiquitin repeats of ubiquitin B gene *UBB* (van Leeuwen et al., 1998a). This process, termed molecular misreading (van Leeuwen et al., 2000), preferentially occurs at sequence repeats like GAGAG with 1:10^5 frequency in different cell types. The aberrant mRNA results in the translation of UBB^{+1}, which has a 20 amino acid C-terminal extension, with the rest of the protein being identical to ubiquitin (van Leeuwen et al., 1998b). Due to this modification, the C-terminal glycine, which is essential for the role in conjugation of substrates, is missing. Thus, UBB^{+1} cannot be conjugated to targets, but itself is ubiquitylated at lysines 29 and 48 and further degraded by the proteasome (Lam et al., 2000; Lindsten et al., 2002). Although UBB^{+1} is successfully degraded under normal conditions when its levels are very low in the cells (Lindsten et al., 2002), it tends to accumulate specifically in affected cells in several neurodegenerative diseases characterized by the presence of misfolded proteins, such as Alzheimer's disease (AD) and Huntington's disease (van Leeuwen et al., 1998b; de Pril et al., 2004), as well as in some non-neuronal pathologies such as liver pathologies (French et al., 2001; Wu et al., 2002) and sporadic inclusion body myositis muscle fibers (Fratta et al., 2004). Shabek et al. showed that the polyubiquitin chain on UBB^{+1} increases its affinity for the proteasome, and because UBB^{+1} cannot be efficiently degraded, it inhibits degradation of other ubiquitin-dependent proteasome substrates (Shabek et al., 2009). Moreover Krutauz et al. demonstrated that extended ubiquitin variants affect the ubiquitin-dependent turnover by inhibiting deubiquitination activity of proteasome associated DUBs (Krutauz et al., 2014). Thus, when UBB^{+1} accumulates to higher levels, under conditions where the capacity of UPS is challenged, this can result in a positive feedback loop in which the already compromised UPS is further inhibited due to the accumulated UBB^{+1} (Verhoef et al., 2009). Hence, the presence of UBB^{+1} in human tissue serves as a reporter for UPS impairment (Fischer et al., 2003). Since elevated levels of UBB^{+1} inhibit the UPS (Lindsten et al., 2002; Hope et al., 2003), cells can be driven to cell cycle arrest, neuritic beading, mitochondrial stress and apoptosis (De Vrij et al., 2001; Lindsten et al., 2002; Hope et al., 2003; Tan et al., 2007). Studies in HeLa cells and cortex slice cultures expressing UBB^{+1} showed that there is a dose-dependent shift in UBB^{+1} properties from UPS substrate to UPS inhibitor with increasing expression levels (van Tijn et al., 2007). In human neuroblastoma cells, induction of UBB^{+1} causes proteasome inhibition as well as induction of heat shock proteins (HSPs), the latter presumably promoting the observed resistance to oxidative stress (Hope et al., 2003). Hence, in this model the protective effect of HSPs is bigger than the deleterious inhibition of proteasome by UBB^{+1}.

UBB^{+1} transgenic mouse lines have been established with post-natal neuronal expression of UBB^{+1} (Fischer et al., 2009). These mice showed increased levels of ubiquitylated proteins in the cortex, at least 20% decreased proteasome activity, expression changes in proteins similar to the proteomic profiles of AD brain as well as the deficit in contextual memory. The same mouse line has been used in a study where in addition to UBB^{+1} also expanded huntingtin constructs were expressed using a lentiviral system (de Pril et al., 2010). This resulted in increased neuronal inclusion formation demonstrating that UBB^{+1} transgenic mice are more vulnerable to toxic protein accumulation. Similar results were observed by Tank and True expressing a protein analogous to UBB^{+1}, Ub^{ext}, in baker's yeast. They found out that UBB^{+1} causes UPS impairment and makes cells more susceptible to toxic protein aggregates (Tank and True, 2009).

Although UBB^{+1} has been studied in several *in vivo* models, the exact molecular mechanism for UBB^{+1}-mediated UPS dysfunction and its contribution to cell death in AD is still unclear. Using a yeast model, Braun et al. (2015a,b) showed that UBB^{+1} expressed from a high-copy vector under the control of an inducible promoter leads to UPS impairment, mitochondrial dysfunction and toxic impairment of the basic amino acids synthesis. Yeast *S. cerevisiae* is a suitable model for aging and cell death studies, including apoptosis and necrosis, as well as for the study of protein quality control mechanisms, which are key cellular processes involved in neurodegeneration and are well conserved between yeast and higher eukaryotes (Khurana and Lindquist, 2010). In this study, we constitutively expressed UBB^{+1} at lower and higher expression levels under different conditions, including those of chronological aging. We aimed at modeling conditions that would occur naturally in aging neurons and evaluated the effects on proteasome function and cell death. We showed that UBB^{+1} inhibited all three types of proteolytic subunits of the proteasome. However the constitutive expression of low level of UBB^{+1} increased cellular resistance to misfolded proteins and moreover prevented cells from accumulating reactive oxygen species (ROS) during aging, delayed cell death and increased chronological life span (CLS). On the other hand high UBB^{+1} expression besides causing proteasomal inhibition, conferred resistance to heat shock stress in exponential phase, and this did not affect cell survival under aging conditions.

MATERIALS AND METHODS

Plasmids and Strains

Plasmids and strains used and constructed in this study are listed in **Table 1**. Plasmid p413TEF CEN (Mumberg et al., 1995) is a centromeric plasmid (1–2 copies) that carries the marker genes *HIS3* and *ampC*, for maintenance and propagation in *S. cerevisiae* and *Escherichia coli*, respectively (**Figure 1B**). This plasmid has a multicloning site flanked by the constitutive promoter of translation elongation factor 1α (TEF1) and cytochrome c terminator (CYC1). The p423 TEF 2μ plasmid (**Figure 1B**) shares the same features as p413 TEF CEN but it is a high copy number plasmid, due to its episomal autonomous origin of replication (Mumberg et al., 1995). To create the p413TEF UBB^{+1} and p423TEF UBB^{+1} plasmids, human *UBB*$^{+1}$ gene was synthesized by DNA2.0 Inc. with a yeast Kozak sequence (Hamilton et al., 1987) at the 5' end, and the *UBB*$^{+1}$ codons were optimized for efficient expression in *S. cerevisiae*. The synthetic gene coding was inserted into pJ204 plasmid resulting in pJ204:28004-UBB^{+1}. Then UBB^{+1} was subcloned from pJ204:28004-UBB^{+1} into p413TEF CEN and p423TEF 2μ plasmids. Constructed plasmids were purified and verified by restriction analysis and sequencing (GATC Biotech AB, Sweden).

Eshcerichia coli DH5α strain (*fhuA2*Δ (*argF-lacZ*) *U169 phoA glnV44* Φ80Δ (*lacZ*)*M15 gyrA96 recA1 relA1 endA1 thi-1 hsdR17*; Inoue et al., 1990) was used for cloning. The *S. cerevisiae* strains used in this study were derivatives of haploid CEN.PK113-11C (*MATa his3*Δ1 *ura 3-52 MAL-8c SUC2*). *S. cerevisiae* CEN.PK 113-11C was transformed with purified p413TEF CEN, p423TEF 2μ, p413TEF UBB^{+1} and p423TEF UBB^{+1} by standard procedures (Gietz and Woods, 2002) to generate the strains Low_EP, High_EP, Low_UBB^{+1} and High_UBB^{+1}, respectively (**Table 1**). Transformants were selected on synthetic minimal medium lacking histidine (SD-His^{-}). The presence of *UBB*$^{+1}$ gene in the resulting yeast strains was verified by PCR (Fisher Scientific, Sweden).

For *Atg1* deletion, the knockout cassette was constructed with a PCR amplified KanMX marker (from pUG6 plasmid) including approximately 500 bp upstream and downstream of the *Atg1* locus. The CEN.PK 113-11C strain was transformed with this cassette. Correct integration in the genome was confirmed by PCR (unpublished data).

Cultivation Medium and Growth Conditions

Unless otherwise indicated, strains were grown in synthetic drop-out medium containing yeast nitrogen base without aminoacids (Formedium, Hunstanton, England) and a complete supplement amino acid mixture lacking histidine (SD-His^{-}; Formedium, England), with 2% glucose as carbon source. Strains were grown on SD-His^{-} plates for 2–3 days at 30°C or in liquid SD-His^{-} medium (either in tube or shake flasks with a 1:5 medium/volume flask ratio) at 30°C with 200 rpm shaking.

Initial innoculation of the liquid SD- His^{-} medium was at OD_{600} of 0.15. The growth was monitored by measuring OD_{600} every 90 min during the first 12 h and at different time points of stationary phase.

All experiments were performed with samples from at least two independent transformants, and in triplicate, unless specified.

Verification of *UBB*$^{+1}$ Gene Transcription by RT-PCR

Strains Low_EP, High_EP, Low_UBB^{+1} and High_UBB^{+1} were grown in SD- His^{-} medium overnight. At OD_{600} ∼2.5, cells were harvested and total RNA was extracted with the waterbath method (Li et al., 2009). After verifying concentration and quality of RNA samples, 1 μg of each RNA sample was treated with RNase-free DNase I (Qiagen, Sweden) according to the manufacturer's instructions. First-strand cDNA synthesis was performed with 1 μg of DNase treated RNA using random hexamers and RevertAid H Minus M-MuLV Reverse Transcriptase (Thermo Fisher Scientific, Sweden) according to the manufacturer's instructions. Subsequently, multiplex PCR was carried out for *UBB*$^{+1}$ and *ACT1* genes using Phusion High-Fidelity DNA polymerase (Thermo Fisher Scientific, Sweden). Housekeeping gene *ACT1* was used as a reference gene to normalize RNA levels.

Verification of UBB^{+1} Translation by Western Blot

Protein extraction for exponential phase cells was performed as described previously (Chen and Petranovic, 2015). Five OD_{600} of cells were spun down and resuspended in 200 μl of lysis buffer containing 50 mM HEPES (pH 7.5), 150 mM NaCl, 2.5 mM EDTA, 1% Triton X-100 with Complete Mini Protease Inhibitor (Roche, Switzerland). Two-hundred microliter of glass beads (MP Biomedicals, USA) was added to the lysis buffer, then the cells were mechanically disrupted at 4°C for 3 min on the FastPrep homogenizer (MP Biomedicals, USA). Afterwards, samples were centrifuged and the supernatant was collected as lysate. BCA protein assay kit (Thermo Scientific, USA) was used to measure protein concentrations in the lysate and 30 μg of protein for each sample was loaded on a 4%–12% Bis-Tris gel (Invitrogen, USA).

Protein extraction from stationary phase cells was done according to Kushnirov (Kushnirov, 2000), in 50 μl reducing ClearPAGE^{TM} LDS Sample Buffer (VWR international AB, Sweden). Samples were heated for 10 min at 70°C. About 10 μl of protein extract (0.6 OD_{600}) was loaded per lane of 4%–12% Bis-Tris gel (Invitrogen, USA). After electrophoresis, proteins were transferred onto 0.2 micron PVDF membrane (BioRad, USA) using a semi-dry transfer system (Towbin et al., 1979; Kyhse-Andersen, 1984). Monoclonal antibodies against UBB^{+1} (Ub^{+1} 40B3, Santa Cruz Biotechnology, Sweden) and GAPDH (Santa Cruz Biotechnology, Sweden) were used for Western blot. Enhanced chemiluminescence signals were detected using the ECL Prime reagent (GE Healthcare, USA) and the ChemiDoc XRS imaging system (BioRad, USA).

Proteasome Activity Measurements

Luminescence activity measurements of the chymotrypsin-, caspase- and trypsin-like proteolytic activities of 20S proteasome

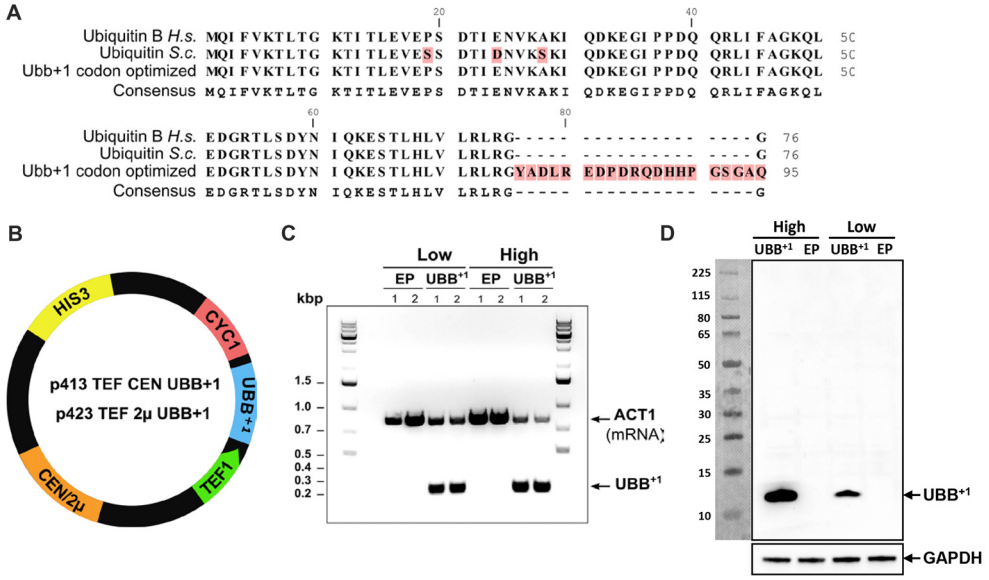

FIGURE 1 | Human UBB^{+1} expression in yeast *S. cerevisiae*. **(A)** Alignment of ubiquitin protein sequences from human (Ubiquitin B *H.s.*), yeast (Ubiquitin *S.c.*) and *UBB*$^{+1}$ codon optimized for expression in yeast. The UBB^{+1} protein sequence is depicted with the 20 amino acid C-terminal extension. **(B)** Schematic map of the *UBB*$^{+1}$ expression plasmids. *HIS3* stands for histidine auxotrophic marker, *CEN* or 2μ is the origin of replication, *TEF1* is the promoter sequence and *CYC1* is the terminator sequence. **(C)** RT-PCR verifies the transcription of *UBB*$^{+1}$ in Low and High_UBB^{+1} strains. The controls carried empty plasmid (EP) without *UBB*$^{+1}$ gene. Housekeeping gene *ACT1* was used as a reference gene. **(D)** Western blot analysis of UBB^{+1} expression from exponential growth cells, using the anti-ub^{+1} antibody. Expression of UBB^{+1} (12 kDa) is indicated by an arrow.

were performed using the Proteasome-Glo^{TM} Cell-Based Assay from Promega according to the manufacturer's instructions (Promega Biotech, Sweden). The Proteasome-GloTM Cell-Based Reagents each contains a specific luminogenic proteasome substrate in a buffer optimized for cell permeabilization, proteasome activity and luciferase activity. The specific proteasome can recognize and cleave luminogenic substrates, resulting in a luminescent signal that is proportional to the amount of proteasome activity in cultured cells. One-hundred microliter of SD-His^{-} medium containing defined numbers of cells (20,000, 40,000 and 80,000) was mixed with 100 μl of Cell-Based Reagent and incubated for 20 min at room temperature. Luminescence was recorded using the FLUOstar Galaxy plate reader from BMG Labtechnologies (Sweden). Every sample was measured in duplicate on two independent transformants and in three independent experiments.

In order to exclude that the detected signal resulted from non-proteasome specific cleavage of the aminoluciferin substrates, in a parallel experiment the samples were incubated with the proteasome inhibitor epoxomicin for 1 h before measurement. Since no significant luminescence was detected in the presence of epoxomicin, the signals detected in the

TABLE 1 | Plasmids and strains used in this study.

Plasmids or strains	Relevant genotype	Reference
Plasmids		
pJ204:28004-UBB^{+1}	*UBB*$^{+1}$ Amp^{R} (*bla*)	This work
p413TEF CEN	CEN *HIS3* P_{TEF1}/T_{CYC1} Amp^{R} (*bla*)	Mumberg et al. (1995)
p423TEF 2μ	2μ *HIS3* P_{TEF1}/T_{CYC1} Amp^{R} (*bla*)	Mumberg et al. (1995)
p413TEF CEN UBB^{+1}	CEN *HIS3* P_{TEF1}-*UBB*$^{+1}$-T_{CYC1} Amp^{R} (*bla*)	This work
p423TEF 2μ UBB^{+1}	2μ *HIS3* P_{TEF1}-*UBB*$^{+1}$-T_{CYC1} Amp^{R} (*bla*)	This work
***S. cerevisiae* strains**		
CEN.PK113-11C	MATa *his*3Δ1 *ura 3-52* MAL-8c SUC2	van Dijken et al. (2000)
Low_EP	CEN.PK113-11C, p413TEF CEN	This work
Low_UBB^{+1}	CEN.PK113-11C, p413TEF CEN UBB^{+1}	This work
High_EP	CEN.PK113-11C, p423TEF 2μ	This work
High_UBB^{+1}	CEN.PK113-11C, p423TEF 2μ UBB^{+1}	This work
*atg1*Δ	CEN.PK113-11C Δ*Atg1*	This work
*atg1*Δ_Low_UBB^{+1}	CEN.PK113-11C Δ*Atg1*, p413TEF CEN UBB^{+1}	This work
Escherichia coli		
DH5α	*fhuA2*Δ (*argF-lacZ*) *U169 phoA glnV44* Φ80Δ (*lacZ*)*M15 gyrA96 recA1 relA1 endA1 thi-1 hsdR17*	Bryant (1988)

samples without epoxomicin were attributed to the activity of 20S proteasome.

Cell Survival and Viability Assays

Strains were grown overnight in SD-His$^-$ medium. Cultures were diluted to OD_{600} 0.15 in 6 ml of SD-His$^-$ medium and incubated until $\Delta OD_{600} \approx 1.0$. Samples were collected in exponential phase or on days 3, 6, 9 and 14 (i.e., days after start of incubation). For the spot-assay, cells were pelleted, resuspended in water (to OD_{600} 0.2) and diluted in 10-fold series (10^{-1}, 10^{-2}, 10^{-3}). 4.5 μl of each suspension was spotted on SD-His$^-$ plates.

To assess the cell resistance to oxidative stress or heat shock, cells were incubated for 4 h in liquid SD-His$^-$ medium supplemented with hydrogen peroxide at a final concentration of 20 mM (Sigma-Aldrich, Sweden) or incubated at 52°C for 2 h. Cell survival was analyzed by spot-assay after 3–4 days of incubation at 30°C.

Yeast cell viability was determined by staining with the fluorescent vital dye FUN-1 [2-chloro-4-(2,3-dihydro-3-methyl-(benzo-1,3-thiazol-2-yl)-methylidene)-1-phenylquinolinium iodide] (Life Technologies Europe BV, Sweden). Cells were harvested, washed and suspended in 10 mM HEPES buffer (2% glucose) with 15 μM FUN-1 and 25 μM Calcofluor White M2R (Life Technologies Europe BV, Sweden). Cells were then incubated at 30°C for 30 min protected from light before analysis by fluorescence microscopy using TL-DIC, FLUO-GFP, FLUO-RFP and FLUO-A4 settings. Metabolically active cells are able to transport and concentrate the dye in the vacuole where it forms structures in the shape of red bars or rods. Metabolically non-active cells give out a uniform glow, due to the non-specific distribution of the dye.

Every sample was measured in duplicate on two independent transformants and in three independent experiments.

Inducing Protein Misfolding With L-Azetidine-2-Carboxylic Acid

L-azetidine-2-carboxylic acid (AZE, Aze or AZC) is a proline analog, that is incorporated into the proteins during translation, causing changes in protein conformation, and eventually misfolding (Zagari et al., 1990). Cells were grown overnight in SD-His$^-$ medium, diluted to OD_{600} 0.15 in 6 ml and incubated at 30°C. At $OD_{600} \approx 1$, AZE (Sigma-Aldrich, Sweden) was added to the culture to a final concentration of 30 mM. After 3 h of incubation, cells were pelleted and diluted to OD_{600} 0.2 in 1 ml of water. Serial dilutions (10^{-1}, 10^{-2}, 10^{-3}) were used for spot-assays on SD-His$^-$ plates. Growth was recorded after 2–3 days of incubation at 30°C.

For continuous treatment with AZE, cells were collected and diluted as before and spotted on SD-His$^-$ plates containing 2, 4 and 7 mM AZE, respectively. Growth was recorded after 2–3 days of incubation at 30°C.

The viability was also measured by colony forming units (CFU). Cells were serially diluted in SD-His$^-$ medium to 4×10^3 cells/ml. One-hundred microliter of diluted cells was plated on SD-His$^-$ plates, which were incubated at 30°C for 2–4 days. Viability of control strains was considered to be the initial survival (100%). Every sample was measured in duplicate on two independent transformants and in three independent experiments.

Assessing the Apoptotic Markers

The production of ROS was measured using dihydrorhodamine 123 (DHR123, Sigma-Aldrich, Sweden). Cells were collected at selected time points, washed and suspended in 50 mM sodium citrate buffer with (pH 5.0) 50 μM of DHR 123 and then incubated for 20 min at room temperature before analysis by fluorescent microscopy using YFP settings. Cells showing an intense fluorescence were treated as ROS accumulating cells.

Cell membrane integrity was assessed by detecting loss of membrane asymmetry by exposed phosphatidylserine (PS), using Annexin V labeling (Life Technologies Europe BV, Sweden) and assessing membrane rupture by using propidium iodide (PI, Life Technologies Europe BV, Sweden). Cells were washed in sorbitol buffer (sorbitol 1.2 M, KH_2PO_4 35 mM and $MgCl_2$ 0.5 mM pH 6.8) and digested with 120 U/ml lyticase (Sigma-Aldrich, Sweden) for 2 h at 28°C (Madeo et al., 1997; Herker et al., 2004). After the incubation, cells were harvested by centrifugation (5000 rpm, 1 min), washed twice with 1 ml of cold PBS buffer (137 mM NaCl, 2.7 mM KCl, 10 mM Na_2HPO_4 and 1.76 mM KH_2PO_4, pH 7.4) and resuspended in Annexin-binding buffer (Life Technologies Europe BV, Sweden). Finally, 3 μl of Alexa Fluor 488 Annexin V and 1 μl of PI (100 μg/ml) were added to 100 μl of cell suspension and then incubated for 15 min at room temperature, protected from light. Finally the cells were centrifuged (5000 rpm, 1 min) and resuspended in 20 μl of Annexin-binding buffer for examination and analysis using a fluorescence microscope with FLUO-GFP and FLUO-RFP settings. Cells showing green fluorescence are apoptotic cells (PS externalization-positive), cells showing red fluorescence are necrotic cells (PI-positive) and cells showing fluorescence with both filters, are late apoptotic cells.

To analyze ***DNA breakage***, terminal deoxynucleotidyl transferase dUTP nick end labeling (TUNEL) assay was performed using the *in situ* Cell Death Detection kit (Roche AB, Sweden), as described previously (Madeo et al., 1999). Yeast cells were washed with PBS buffer, fixed with 3.7% formaldehyde and digested with 120 U/ml of lyticase for 40 min at 30°C. The cells were then harvested, washed with SPM buffer (sorbitol 1.2 M, KH_2PO_4 50 mM and $MgCl_2$ 1 mM pH 7.3) and transferred to a polylysine-coated slide. The slides were rinsed three times with PBS and incubated with permeabilization solution (0.1% sodium citrate, 0.1% Triton X-100) for 2 min at 4°C. After rinsing twice with PBS, 50 μl of TUNEL reaction mixture was added to the slide and incubated at 30°C for 60 min. For co-staining with DAPI (Life Technologies Europe BV, Sweden), 1 μl of DAPI (1 mg/ml) was added 5 min before the incubation time ended. Finally the slides were washed twice with PBS and mounting medium was added to analyze by fluorescence microscopy with FLUO-A4 and FLUO-GFP settings and DNA breakage could be visualized as fluorescence.

In vivo detection of Caspase–like activity was done with 5×10^6 cells taken on 6, 9 and 14 days of incubation, which were washed in PBS and resuspended in 200 μl of PBS containing 10 μM of a caspase substrate FITC-VAD-FMK (CaspACE FITC-

VAD-FMK *in situ* marker, Promega Biotech, Sweden) and PI, to identify cells with ruptured plasma membrane indicating necrotic cell death, to a final concentration of 50 ng/ml. After incubation for 20 min (protected from light) at room temperature and with low agitation, cells were centrifuged and washed twice with PBS. Finally cells were centrifuged and resuspended in the remaining buffer. Stained cells were analyzed by fluorescence microscopy with FLUO-GFP and FLUO-RFP settings, and the bound marker is localized by fluorescence.

Fluorescence Microscopy

Images from stained cells were taken on an inverted Leica AF 6000 fluorescence microscope (Wetzlar, Germany) with a HCX PL APO CS 100.0x1.40 OIL objective, captured with a DFC 360 FX camera, and analyzed with Leica Application Suite software. Quantitative determinations involved the analysis of at least 600 cells per sample from three independent experiments. Brightness and gain settings were adjusted to avoid background noise and discard false positives during the counting.

Real-Time PCR Analysis of Chaperone Expression

UBB^{+1} expressing cells and control cells were grown in liquid selective medium at 30°C. Cell samples were taken on exponential phase (OD_{600} of 1.0), days 1 and 3 of incubation. Total RNA was extracted using the RNeasy® kit (QIAGEN, Sweden) following manufacturer's instructions. The synthesis of first strand cDNA was performed using 1 μg of total RNA and following the QuantiTec Reverse Transcription (QIAGEN, Sweden) manufacturer's protocol. The primers were designed using the Primer3 software and synthesized by Sigma-Aldrich Company (Sigma-Aldrich, Sweden). The DyNAmo™ ColorFlash SYBR® Green qPCR Kit (Thermo Fisher Scientific, Sweden) and the Mx3005P Agilent Technologies equipment (Agilent Technologies, Sweden) were used for the QPCR assay. *DAL81* snd *SPC10* were used as reference genes to normalize the RNA levels. The relative transcription levels were calculated using the $\Delta\Delta Ct$ method. Results are from three independent experiments, performed duplicate per experiment. The data analysis was performed using the MX pro QPCR software.

Statistical Analyses

Significance of differences observed between strains were determined using two-tailed, student *t*-tests. Unless specified explicitly, three independent replicates on two independent transformants were analyzed. Values were represented as mean ± SEM. $P < 0.05$ was considered to indicate significant difference.

RESULTS

Expression of Human UBB^{+1} in Yeast *S. cerevisiae*

The DNA sequence coding for the human UBB^{+1} protein was codon-optimized for efficient expression in yeast *S. cerevisiae*. In order to ensure the transcription and translation of the correct mutated version, the GU nucleotides that are deleted during spontaneous and random molecular misreading of the native *UBB* gene in human cells, were omitted in the synthetic version, giving rise to the mutated *UBB*$^{+1}$ gene (**Figure 1A** and **Supplementary Figure S1**). This *UBB*$^{+1}$ gene was cloned into either the single- (centromeric, CEN) or multi-copy (2μ) yeast expression vectors, under the constitutive *TEF1* promoter, giving rise to p413TEF CEN UBB^{+1} and p423TEF 2μ UBB^{+1} plasmids, respectively (Mumberg et al., 1995), enabling its constitutive expression (**Figure 1B**). Yeast wild type strain CEN.PK 113-11C, a host for heterologous protein production (van Dijken et al., 2000), was transformed with the UBB^{+1} CEN or 2μ plasmids to generate the Low_UBB^{+1} and High_UBB^{+1} strains, respectively. Control strains (Low_EP and High_EP) were generated by transforming CEN.PK 113-11C with the empty CEN or 2μ plasmids (EP), without the *UBB*$^{+1}$ gene. Transcription of *UBB*$^{+1}$ was verified by RT-PCR (**Figure 1C**) and expression of UBB^{+1} protein was confirmed by Western blot (**Figure 1D**).

Expression of UBB^{+1} Reduces the Proteolytic Activities of the 20S Proteasome

It has been previously shown that overexpression of UBB^{+1} reduces the activity of the UPS in HeLa and human neuroblastoma SH-SY5Y cell lines (Lindsten et al., 2002; Verhoef et al., 2009). We measured the three proteolytic activities of the 20S proteasome i.e., the caspase-like (β1), trypsin-like (β2) and chymotrypsin-like (β5) proteases activities in exponential Low_UBB^{+1} and High_UBB^{+1} strains, and corresponding controls. To this purpose luminogenic peptide substrates for the individual 20S proteolytic activities were used: Z-norleucine-proline-norleucine-aspartate-aminoluciferin, Z-leucine-arginine-arginine-aminoluciferin and Succinyl-leucine-leucine-valine-tyrosine-aminoluciferin for the caspase-like, trypsin-like and chymotrypsin-like activities, respectively. We found that both low and high UBB^{+1} expression caused a decrease in all three proteolytic activities of the proteasome ($p < 0.05$) when compared with its respective controls (**Figures 2A–C**). In the High_UBB^{+1} strain, the caspse-, trypsin- and chymotrypsin-like activities decreased up to 32%, 10% and 35%, respectively. The activities of these three proteases in Low_UBB^{+1} strain were reduced by 38%, 12% and 30%.

In order to evaluate the effects of a reduced proteasomal activity on cell growth due to UBB^{+1} expression, UBB^{+1} and control strains were cultured in liquid SD-His^{-} medium. Cell growth was followed during exponential phase and cell viability was measured in exponential and stationary phases by spotting on SD-His^{-} plates. Specific growth rate was determined for each strain from the maximal slope on logarithmic scale (μmax). Each experiment was conducted by triplicate on three independent experiments. While low UBB^{+1} expression did not affect exponential growth in liquid culture ($\mu = 0.39$), the High_UBB^{+1} strain had a significantly reduced growth rate up to 16% ($\mu = 0.32$) as compared to its control ($\mu = 0.38$; **Figure 2D**). Moreover, cells expressing UBB^{+1} at lower level reached a higher cellular density after 1 day of incubation (OD_{600}

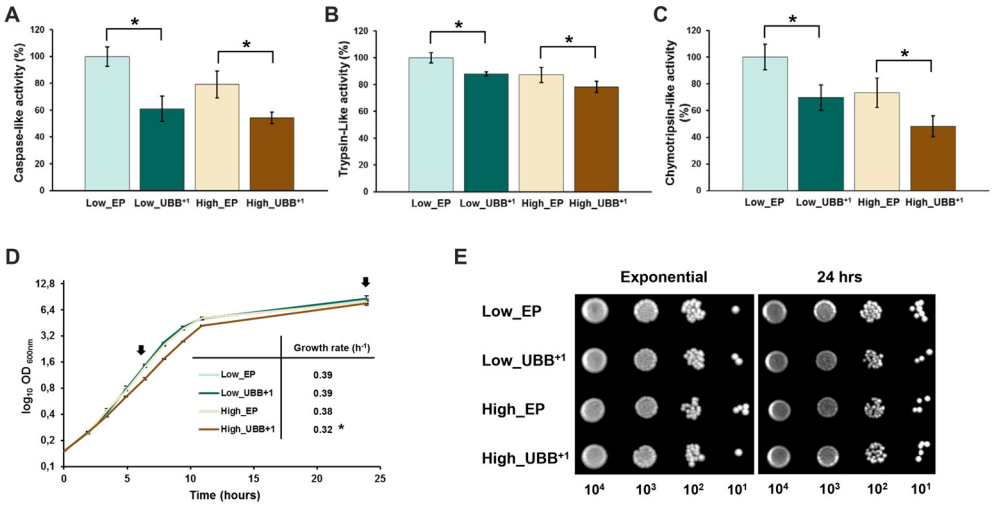

FIGURE 2 | UBB^{+1} inhibits the proteolytic activities of the 20S proteasome and affects exponential growth. The luminescent assays were performed individually to measure the caspase-like, trypsin-like and chymotrypsin-like protease activities associated with the proteasome complex in cultured cells. Luminescence activity measurements of the **(A)** caspase-, **(B)** trypsin-and **(C)** chymotrypsin-like proteolytic activities of the 20S proteasome are shown. The data shown are average values of three independent experiments ± SEM. The asterisk (*) indicates significant differences ($p < 0.05$). UBB^{+1} strains were compared with its respective controls (Low_EP and High_EP). **(D)** The specific growth rate was determined from the maximal slope on logarithmic scale (μmax). The data represents an average of three independent experiments from two different colonies for each strain. Low UBB^{+1} expression did not affect cell growth while high UBB^{+1} expression slightly reduced growth rate (*$p < 0.05$). Arrows indicated the time points when samples were taken for spot survival assay **(E)** of control strains (Low_EP and High_EP) and UBB^{+1} expressing strains (Low_UBB^{+1} and High_UBB^{+1}).

8.6 ± 0.2) as compared to controls (OD_{600} 7.9 ± 0.3) and the high_UBB^{+1} strain (OD_{600} 7.5 ± 0.25; **Figure 2D**). From the serial spot dilution assay, no difference on survival was observed on exponentially growing cells and 1 day old stationary cells expressing UBB^{+1} (**Figure 2E**).

Low UBB^{+1} Expression Increases Cellular Tolerance to Chemically Induced Protein Misfolding

We investigated how exponentially growing cells, with a reduced proteasomal capacity, coped with misfolding burden, by generating misfolded proteins using amino acid analogs. The UPS is the main protein degradation pathway that eliminates misfolded or damaged proteins and its dysfunction may lead to protein accumulation, aggregation and neurodegeneration in mouse brain neurons (Bedford et al., 2008). To test the tolerance to protein misfolding stress, we challenged UBB^{+1} expressing cells with AZE. AZE is an analog of proline, whose structural difference results in changes in torsion angles, the direction of turns of the protein backbone, and cis-trans isomerizations in the random newly synthesized polypeptides that incorporate AZE instead of proline, inducing general misfolding stress (Tsai et al., 1990; Baeza et al., 2008). We incubated exponentially growing cells with 30 mM AZE for 3 h, then cells were diluted and spotted on standard plates. After 3 days of incubation, we observed that all strains were affected and no significant difference in survival was observed between UBB^{+1} strains and controls (**Figure 3A**). The number of viable cells was determined using CFU, which showed similar results to spot assay (**Supplementary Figure S2A**). We also observed a decreased viability in high_UBB^{+1} strain compared to its control strain (**Supplementary Figure S2A**).

A second experiment was conducted where cells were grown in liquid medium and spotted on plates containing different concentrations of AZE. Interestingly, the Low_UBB^{+1} strain showed better survival, as compared to controls and High_UBB^{+1} strain (**Figure 3B** and **Supplementary Figure S2B**). The expression of UBB^{+1} protein was also confirmed by Western blot during different concentrations of AZE treatment (**Supplementary Figure S3**). This shows that low UBB^{+1} expression, although inhibited the core proteolytical activities of the proteasome during exponential growth, increases the cellular capacity to cope with misfolded proteins during a prolonged misfolding stress.

Low UBB^{+1} Expression Prolongs CLS of *S. cerevisiae*

Successful handling of misfolded proteins declines with age which thus contributes to protein accumulation and aggregation, a common feature of neurodegenerative diseases (Basaiawmoit and Rattan, 2010). We tested whether Low_UBB^{+1} cells could deal more efficiently with aging stress conditions. To evaluate the effect of UBB^{+1} expression during aging, cells were grown in liquid SD-His^{-} medium. Sampling was conducted in the exponential phase (OD_{600} of 1.0), and on days 3, 6, 9 and 14, after the inoculation (**Figure 4A**). Cell viability was assessed by taking identical amounts of cells (OD_{600} 0.2) to make serial dilutions and spot onto SD-His^{-} plates.

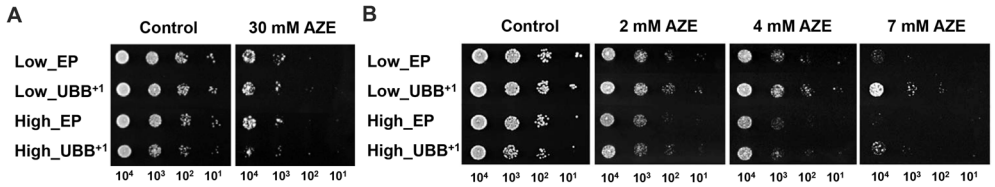

FIGURE 3 | Low UBB^{+1} expression increases cellular tolerance to misfolded proteins. Spot tests to analyze the effect of chemically induced protein misfolding on survival of UBB^{+1} expressing strains and control strains. **(A)** Exponential cells, incubated for 3 h with 30 mM L-azetidine-2-carboxylic acid (AZE), were 10-fold serial diluted and spotted on selective plates. The control cultures were left untreated. **(B)** Exponential cells were spotted in 10-fold serial dilutions on plates containing 2 mM, 4 mM and 7 mM of AZE, respectively. Every sample was measured in duplicate on two independent transformants and in three independent experiments.

We found that Low_UBB^{+1} strain was much more viable after 14 days, when compared to controls and the High_UBB^{+1} strain (**Figure 4B**). This was supported by FUN1 staining, which is a vital dye that passively diffuses into the cytoplasm and gives a diffused green fluorescence. In the living cells the dye is transported to the vacuole where it creates compact foci with a striking red fluorescence, thus reducing the diffuse green cytoplasmic fluorescence. Formation of the fluorescent red cylindrical intravacuolar structures (CIVS) requires both plasma membrane integrity and metabolic activity. Controls and cells expressing UBB^{+1} at higher level showed a similar reduction in viability ($p < 0.05$) from day 9 as compared to the Low_UBB^{+1} strain (**Figure 4C**). The average viability for the Low_UBB^{+1} strain at day 14 was above 70%, while cells expressing higher level of UBB^{+1} and controls had the average viability below 10% (**Figure 4C**). During CLS, the expression of UBB^{+1} protein was confirmed by Western blot on day 3 and day 9 (**Supplementary Figure S4**).

UBB^{+1} Prevents the Accumulation of ROS and Decreases Apoptotic and Necrotic Cell Death During Chronological Aging

Deficiencies in either ubiquitin or proteasome can lead to the accumulation and aggregation of misfolded proteins with lethal consequences. It has been reported that proteasomal inhibition by UBB^{+1} overexpression contributes to proteotoxic stress, neuritic beading of mitochondria (Tan et al., 2007), cellular dysfunction and apoptotic cell death in HeLa and SH-SY5Y neuroblastoma cells (de Pril et al., 2004). In order to investigate the implications of UBB^{+1} expression in oxidative stress and cellular death, we measured the levels of intracellular ROS by using DHR123, where the nonfluorescent DHR is

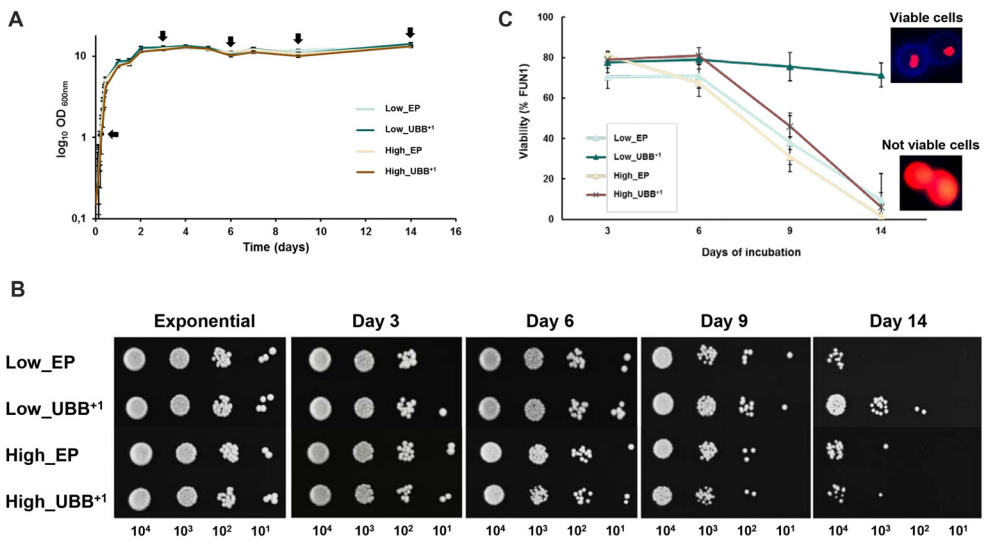

FIGURE 4 | Low UBB^{+1} expression prolongs the CLS of *S. cerevisiae*. **(A)** Effect of UBB^{+1} expression on cell growth during chronological aging. All strains maintained similar biomass during stationary phase. Sampling for further analyses was performed at the indicated time points (black arrows). **(B)** Spot tests of Low_UBB^{+1}, High_UBB^{+1} and control strains to investigate long time survival. 0.2 OD_{600} of cells were diluted in 10-fold series (10^{-1}, 10^{-2}, 10^{-3}) and spotted on selective plates from the indicated days. **(C)** Percentage of cell viability was determined by FUN1 staining. Above 70% of the cells expressing Low_UBB^{+1} remained viable after 14 days of incubation. Representative images of metabolically viable cells and non-viable cells stained with FUN1 are shown. Viable cells showed concentrated red staining in vacuole while non-viable cells showed uniform red glow. Samples were measured in duplicate on two independent transformants and in three independent experiments.

converted to the fluorescent product rhodamine 123 by the interaction with superoxides. ROS accumulated at very low levels during the first 6 days of incubation in all strains (between 11% and 13%; **Figure 5A**). As expected, controls showed an increased accumulation of ROS after 9 days of incubation since the generation of ROS is the first apoptotic trigger during chronological aging of yeast (Herker et al., 2004). Interestingly, a lower production of ROS was observed in Low_UBB^{+1} strain where the generation and accumulation of ROS were prevented after 9 and 14 days of incubation (**Figure 5A**).

Since ROS are the major inducers of apoptosis, we investigated whether lower ROS observed in the Low_UBB^{+1} strain correlated with reduced cell death. We focused on PS externalization, DNA fragmentation and the activation of caspase, as the markers of cell death. PS is actively maintained on the inner leaflet of the plasma membrane. In apoptotic cells externalization of the PS indicates the loss of plasma membrane asymmetry, which can be detected on the surface of the cell by Annexin V staining. After 9 days in culture, 17% of control cells and 16% of high UBB^{+1} expressing cells were positive in the Annexin V test, while only 8% of cells expressing low UBB^{+1} showed fluorescence (**Figure 5B**). After 14 days, the difference between strains was less prominent (**Figure 5B**).

DNA fragmentation is identified by the TUNEL assay, which is used for labeling DNA nick-ends (both single- and double-strand DNA breaks). In exponential phase and during

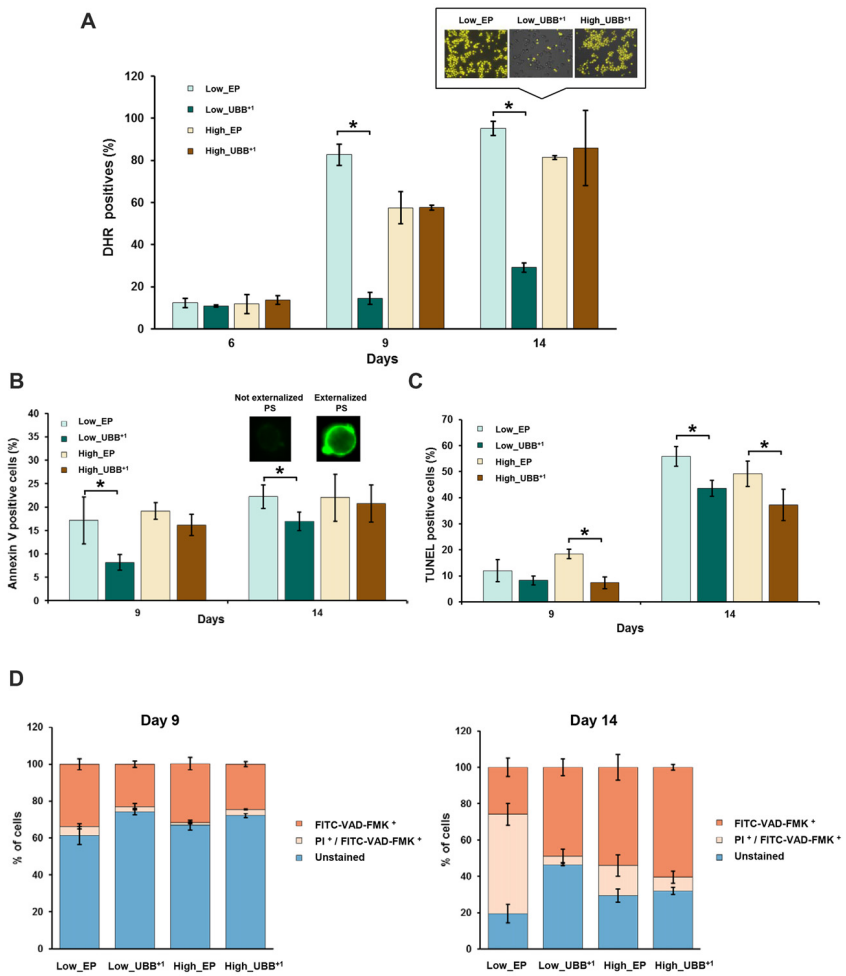

FIGURE 5 | UBB^{+1} expression decreases cell death during chronological aging. **(A)** UBB^{+1} expressing cells and controls were stained with DHR 123 to determine the percentage of reactive oxygen species (ROS)-positive cells at different time points. Compared to control strain, low UBB^{+1} expression prevented cells to accumulate ROS at day 9 and day 14 (*$p < 0.05$). Representative images of DHR 123 stained cells from day 14 are shown. Cells showing an intense yellow fluorescence were counted as ROS accumulating cells. **(B)** Annexin V and **(C)** TUNEL assays were performed in UBB^{+1} expressing cells and controls to determine the percentages of cells exhibing phosphatidylserine (PS) externalization and DNA fragmentation after 9 and 14 days of incubation. UBB^{+1} expression, particularly at low levels, reduced the ocurrence of these apoptotic markers as compared to its control strain. **(D)** Stained cells with FITC-VAD-FMK and propidium iodide (PI) to determine the caspase-like activity and membrane integrity. Low levels of UBB^{+1} delays apoptosis on aged cells. After 14 days of incubation, controls showed a greater portion of cells in secondary necrotic stage or cells already dead as compared to low UBB^{+1} expressing cells, whose membrane integrity remains intact. The data shown were representative of average values ± SEM, of three independent experiments.

first 6 days of incubation, all strains were negative in the TUNEL assay. After 9 days of incubation, 7%–8% of cells expressing UBB^{+1} showed fragmented DNA while slightly more cells (12%–18%) were positive in controls (**Figure 5C**). After 14 days of incubation, substantially more cells in controls exhibited DNA fragmentation (49%–56%) while 37% of cells expressing UBB^{+1} at high level were TUNEL positive, and 43% of UBB^{+1} at low expression displayed fragmented DNA (**Figure 5C**).

We finally measured the activation of caspases. In yeast, caspase-like activity contributes to apoptotic cell death under a variety of stimuli (Madeo et al., 2002, 2004), although caspase-independent apoptotic pathways have also been identified (Liang et al., 2008). It has been demonstrated previously, in human mononuclear cells from peripheral-blood that apoptotic cell death resulting from proteasome inhibition requires caspase activation in most cases (Pérez-Galán et al., 2006). To evaluate whether UBB^{+1} expression has an effect on caspase activation, we used FITC-VAD-FMK that can diffuse into the permeabilized cells and bind to activated caspases, allowing its identification by fluorescence microscopy. Co-staining with PI was performed to identify cells with ruptured plasma membrane, indicating necrotic cell death. Cells that are positive for the FITC-VAD-FMK assay alone, are considered induced apoptosis. Those that are positive in the PI assay are necrotic with ruptured plasma membrane and those positive in both assays, are late apoptotic. An increased number of cells showed caspase activation after 9 days, 32%–34% for the controls and 23% and 25% for Low_UBB^{+1} and High_UBB^{+1} strains, respectively (**Figure 5D**).

On 14-days old cells, the major caspase activity was measured in UBB^{+1} expressing cells (49% and 61% for low and high UBB^{+1} expressing cells, respectively) as compared to their respective controls (26% and 54%). However, co-staining with PI

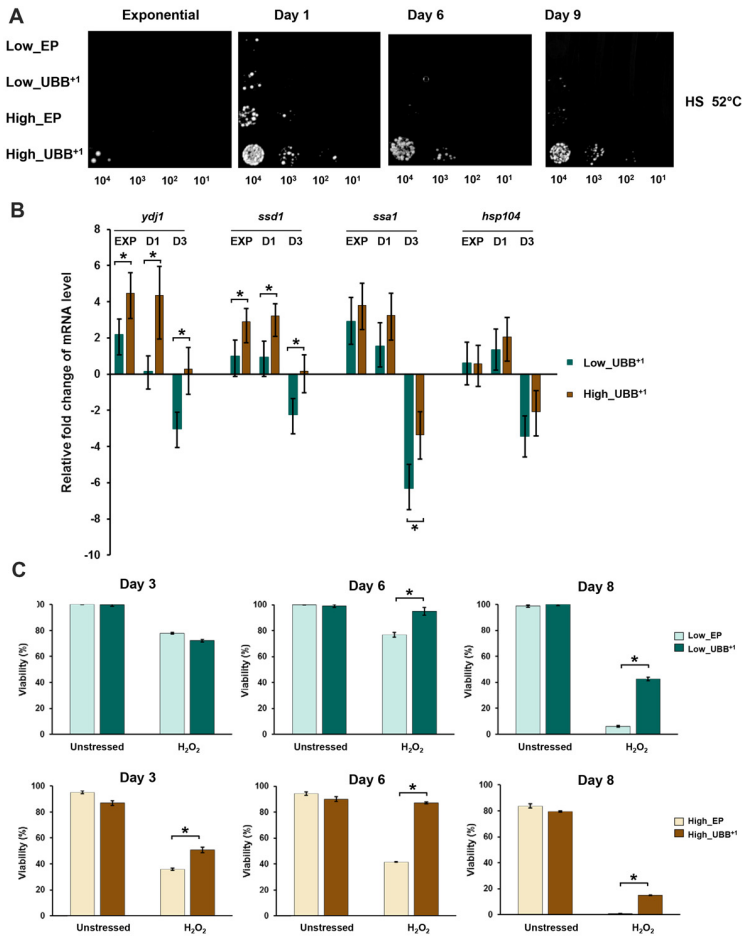

FIGURE 6 | High UBB^{+1} expression increases yeast resistance to heat shock. **(A)** Spot assay of UBB^{+1} strains and control strains after heat shocked at 52°C for 2 h. Compared to other strains, high UBB^{+1} expression increased cell resistance to heat shock. **(B)** qPCR analysis of chaperone transcripts in low and high UBB^{+1} expression strains from exponential phase, day 1 and day 3. Both low and high levels of UBB^{+1} expression significantly increased the transcript levels of *Ydj1*, *Ssd1* and *Ssa1* genes in exponential phase and day 1. Comparing to Low_UBB^{+1} strain, the transcription levels of *Ydj1* and *Ssd1* were significantly higher in High_UBB^{+1} strain. The levels of these chaperone transcripts were significantly decreased after 3 days. **(C)** Viability of stationary cells exposed to 20 mM H_2O_2. Both of low and high UBB^{+1} expression increased cell resistance to oxidative stress. Results are average values ± SEM of biological triplicates. The asterisk (*) indicates significant differeces ($p < 0.05$).

revealed that a large portion of control cells (17%–55%) stained for both FITC-VAD-FMK and PI while only 5%–7% of cells expressing UBB^{+1} were actually dead (**Figure 5D**). Additionally, and in accordance to our previous results on survival assay, a significant portion of cells expressing low level of UBB^{+1} remained unstained (46%) on day 14 (**Figure 5D**), demonstrating a beneficial effect on longevity.

High UBB^{+1} Expression Increases Resistance to Heat Shock and Oxidative Stress

A previous work in human neuroblastoma cells has reported the induction of heat-shock proteins caused by expression of UBB^{+1}, which also promotes resistance to oxidative stress (Hope et al., 2003). In yeast cells, proteasomal inhibition confers thermotolerance due to the induction of chaperone expression and trehalose accumulation (Lee and Goldberg, 1998). We measured trehalose content in different strains under stress and control conditions and did not find significant differences (data not shown). We evaluated whether the proteasomal inhibition caused by UBB^{+1} induced a heat shock response protecting cells from stress. We evaluated the thermotolerance of UBB^{+1} expressing cells, in exponential phase (6 h) and on days 1, 6 and 9, respetively, by incubation of the liquid culture at 52°C for 2 h. 0.2 OD_{600} of cells were sampled, serially diluted and spotted on SD-His^{-} plates. After 3 days of incubation at 30°C, we observed that stationary cells (1, 6 and 9-days old cells) expressing UBB^{+1} at higher level were able to tolerate better to the heat stress, compared to controls and Low_UBB^{+1} cells (**Figure 6A**).

The transcription of chaperone genes (*Ydj1-Hsp40*, *Ssa1-Hsp70*, *Ssd1* and *Hsp104*) relevant for yeast thermotolerance was measured by real-time PCR. The trancription levels were compared between the UBB^{+1} expressing cells and its corresponding controls from samples taken from exponential phase (6 h), day 1 and 3, respectively. We observed that both low and high levels of UBB^{+1} expression significantly increased the transcript levels of *Ydj1*, *Ssd1* and *Ssa1* genes in exponential phase and day 1 ($p < 0.05$). Moreover, the transcription levels of *Ydj1* and *Ssd1* were significantly higher in the high UBB^{+1} expression strain, compared to low UBB^{+1} expresssion strain ($p < 0.05$). Interestingly, the levels of these chaperone transcripts were significantly decreased after 3 days ($p < 0.05$) and this was more pronounced in the low UBB^{+1} expressing strain (**Figure 6B**).

Since the induction of chaperones promoted resistance to oxidative stress, we exposed stationary cells (3, 6 and 8 days-old) to 20 mM H_2O_2. Better coping with oxidative stress was observed in both Low_UBB^{+1} and High_UBB^{+1} strains as compared to controls, particularly in aging cells (**Figure 6C**). There was no significant difference in exponentially growing cells (data not shown).

Low UBB^{+1} Expression Increases Resistance to Misfolded Proteins in Autophagy Defective Cells

The UPS and autophagy machinery are two major protein degradation systems in cells. Several studies have suggested a functional cross-talk and it has been demonstrated that inhibition of UPS by proteasome inhibitors can activate autophagy. Autophagy induced by proteasome inhibition was shown to be important for controlling endoplasmic reticulum stress and reducing cell death in cancer cells (Ding et al., 2007). We tested if the autophagosomal pathway contributed to protect cells from toxicity under misfolding protein stress on cells expressing low level of UBB^{+1}, where proteasomal activity was reduced. The *Atg1* gene, required for autophagosome, was deleted to generate cells defective in autophagy (unpublished data). The *atg1*Δ cells expressing UBB^{+1} and controls were grown in liquid medium and then diluted and spotted on plates containing 2, 4 and 7 mM of AZE, respectively. We observed a lower survival on cells defective in autophagy (*atg1*Δ) as compared to controls (**Figure 7** and **Supplementary Figure S5**). Surprisingly, the expression of low UBB^{+1} increased the cellular capacity to cope with misfolded proteins on both WT and *atg1*Δ background, in 2 mM and 4 mM AZE (**Figure 7**). However, at the higher concentration of AZE tested (7 mM) only the UBB^{+1} strain (without the *Atg1* deletion) was able to thrive (**Figure 7** and **Supplementary Figure S5**). This suggests that the autophagosomal pathway might be relevant for cell survival in some conditions but is not crucial in exponentially growing cells, during prolonged general misfolding stress induced by 4 mM AZE, when UBB^{+1} was present.

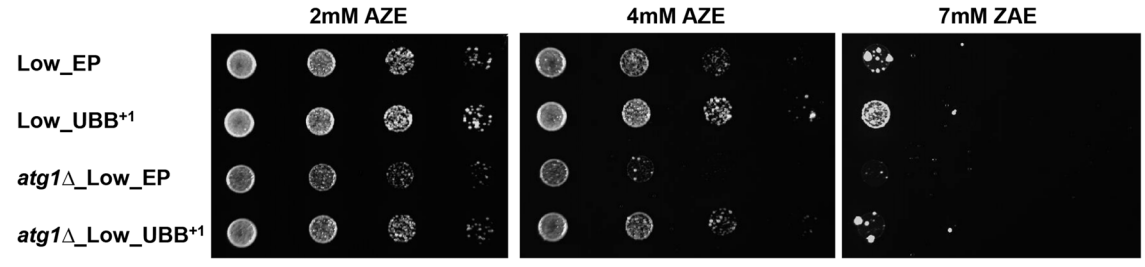

FIGURE 7 | Exponentially growing Low UBB^{+1} expression resists to AZE-induced protein misfolding stress under autophagy defective background. Spot assay of Low_EP, Low_UBB^{+1}, *atg1*Δ_Low_EP and *atg1*Δ_Low_UBB^{+1} cells on different concentrations of AZE. The expression of UBB^{+1} increased the cellular capacity to cope with misfolding protein stress in the absense of the autophagic pathway. Every sample was measured in duplicate on two independent transformants and in three independent experiments.

DISCUSSION

In this study we present a yeast UBB^{+1} model, with the ubiquitin mutant expressed constitutively at two levels. We used this system to explore the role of proteasome impairment and cell death by UBB^{+1} accumulation. It has been documented that the accumulation of UBB^{+1} protein is among hallmarks of several neurodegenerative diseases, including AD and other tauopathies (van Leeuwen et al., 1998b; Fischer et al., 2003). Studies in neuron cells have shown that UBB^{+1} can be further degraded by the proteasome, but it acts as a potent proteasomal inhibitor when it accumulates at high concentrations (Lam et al., 2000; Lindsten et al., 2002). Moreover, some reports showed that the proteasome activity is decreased in AD, reinforcing the idea that the accumulation of UBB^{+1} is related to proteasomal dysfunction (Keller et al., 2000). By measuring the proteolytic activities of the 20S proteasome in our yeast model, we demonstrated that expression of UBB^{+1}, either at low or high levels, inhibited the caspase-, trypsin- and chymotrypsin-like proteases (**Figures 2A–C**). Although high UBB^{+1} expression caused a decrease in the growth rate of dividing cells, it did not affect cell survival of dividing cells, which reached similar biomass after 24 h in culture (**Figures 2D,E**).

Since proteasome dysfunction can lead to protein accumulation and aggregation with detrimental consequences, we evaluated the cellular tolerance to misfolded proteins in the presence of UBB^{+1}. Surprisingly, low UBB^{+1} expression increased the tolerance to misfolded proteins when cells were challenged with AZE (**Figure 3**). Because neurodegenerative diseases, including AD and Huntington's disease, are age-related disorders, we evaluated the effect of UBB^{+1} on chronologically aged cells and we found that low UBB^{+1} expression could extend yeast life span (**Figure 4**).

The impairment of proteosomal activity by UBB^{+1} overexpression has been shown to be detrimental to the neuronal cell cultures leading to mitochondrial stress (Tan et al., 2007) and triggering apoptosis (De Vrij et al., 2001). Based on our results, the constitutive low expression of UBB^{+1} in yeast decreased the levels of ROS (**Figure 5A**), which normally accumulates during aging. Consequently, UBB^{+1} expression caused a delay of apoptotic and necrotic cell death (**Figure 5**). High and induced expression of UBB^{+1} was found in different models to be toxic (Tank and True, 2009). Braun et al. showed that when UBB^{+1} was expressed from a high-copy vector under the control of an inducible promotor, the cytotoxicity (as shown by CFU, oxidative stress) occurred in the stationary phase (post-mitotic cells) and the toxic effects were observed 2 or 3 days after the induction (which was in exponential phase; Braun et al., 2015a). In our work, the expression of UBB^{+1} was constitutive which allowed the cells to adapt for example by overexpressing chaperones hence providing some cytoprotective functions. Our constitutive UBB^{+1} model seemed to produce enough of UBB^{+1} to cause some proteasomal inhibition, and a potentially protective response but not enough to be detrimental.

Hope et al. reported that in their human neuroblastoma cell model UBB^{+1} causes proteasome inhibition and induces the expression of HSPs, protecting cells against heat and oxidative stress conditions (Hope et al., 2003). Similarly in yeast, the exposure to proteasome inhibitors causes the expression of HSPs and the accumulation of trehalose conferring thermotolerance to *S. cerevisiae* (Lee and Goldberg, 1998). We demonstrated that high UBB^{+1} expression induced the transcription of HSPs in yeast and, in accordance to previous findings, increased the tolerance to oxidative stress (**Figure 6**). The induction of HSPs was observed in early time points (logarithmic phase and day 1), suggesting its activation as an initial protective mechanism to counteract with protein misfolding after stress. The up-regulation of Hsp104 and Ydj1 upon proteasomal inhibition and its involvement in increased resistance to high temperature of yeast is well documented (Lee and Goldberg, 1998). Our data showed a greater up-regulation of HSPs transcripts, particularly of *Ydj1*, in the presence of high levels of UBB^{+1} and consequently an increased resistance to heat shock in that strain (**Figure 6B**). Although trehalose has been reported to accumulate upon proteasomal inhibition having additive effects in causing thermotolerance, we did not observe any difference in the cellular content of this disaccharide upon UBB^{+1} expression (data not shown). Based on our test with the *Atg1* deletion mutant, we proposed that autophagy is not a crucial pathway for UBB^{+1} mediated survival during AZE-induced misfolding stress in exponentially growing cells.

The cell resistance to several stresses such as protein misfolding, oxidative stress and heat, induced by differential expression of UBB^{+1}, is most probably not just due to the induction of chaperones or the autophagosomal pathway, but also to the participation of other cytoprotective mechanisms. In yeast cells (Tank and True, 2009) has shown that blocking ubiquitination of Ub^{ext} (a protein analogous to UBB^{+1}) or weakening its interactions with other ubiquitin-processing proteins reduces the UPS impairment. Therefore, the interaction of Ub^{ext} with more than one protein is crucial to elicit impairment of the UPS (Tank and True, 2009). Another study showed that the accumulation of UBB^{+1} may be due to the inefficient hydrolysis of the C-terminus of UBB^{+1} by the UCHL3 under oxidative stress in AD (Dennissen et al., 2011). UBB^{+1} has been implicated to mediate neurodegeneration via interaction with other components of the UPS (Ko et al., 2010). The UBB^{+1} can serve as an inhibitor of DUB by binding to the Ubp6, the primary enzymes responsible for the disassembly of Lys48 linkages at proteasome (Krutauz et al., 2014). The UBB^{+1} can also be ubiquitylated by unusual ubiquitin-conjugating enzyme E2-25K and E3 ligating enzyme TRIP12 and HUWE1. The interation between E2-25K and UBB^{+1} is critical for the accumulation of UBB^{+1}-anchored polyubiquitin, which results in proteasome inhibition and cell death (Ko et al., 2010).

We proposed that our UBB^{+1} yeast model might benefit to elucidate the contribution of different factors that together with UBB^{+1} may contribute to the disease initiation and/or progression (**Supplementary Figure S6**). Conservation of cellular protein quality control systems between yeast and human cells, makes yeast a useful model to study misfolding

diseases. Humanized yeast models have been exploited to investigate pathological proteins and pathways for example, in Huntington's disease (Giorgini et al., 2005), Parkinson's disease (Outeiro and Lindquist, 2003) and AD (Chen et al., 2017). It is possible that the yeast discovery and validation platforms will provide new knowledge and tools for the identification of therapeutic strategies against neurodegenerative or other misfolding diseases (Chung et al., 2013; Tardiff et al., 2013).

AUTHOR CONTRIBUTIONS

AJM-A, AM, XC, EM and DP designed the experiments. AJM-A, AM, EM and XC performed the experiments. AJM-A, AM, XC and DP analyzed the data and wrote the manuscript.

FUNDING

This work was funded by Knut and Alice Wallenberg Foundation, Chalmers Foundation, Kristina Stenborg Foundation and Novo Nordisk Foundation (award id: 21210022).

ACKNOWLEDGMENTS

We would also like to thank Prof. Jens Nielsen at Chalmers for continuous support on this project, and dedicate this work to the memory of Prof. Susan Lindquist who has been a continuous supporter of our UBB^{+1} work.

SUPPLEMENTARY MATERIAL

The Supplementary Material for this article can be found online at: https://www.frontiersin.org/articles/10.3389/fnmol.2018.00200/full#supplementary-material

FIGURE S1 | Alignment of ubiquitin RNA sequences among human (Ubiquitin B *H.s.*), yeast (Ubiquitin *S.c.*) and *UBB*$^{+1}$ codon optimized for expression in yeast.

FIGURE S2 | CFU measurement of cellular survival under different concentrations of AZE treatment. **(A)** Exponential cells were incubated with 30 mM AZE for 3 h and plated on SD-His$^-$ plates. **(B)** Exponential cells were plated on SD-His$^-$ plates containing 2 mM, 4 mM and 7 mM of AZE, respectively. Results are average values ± SEM of biological triplicates.

FIGURE S3 | Western blot analysis of UBB^{+1} expression under different concentrations of AZE treatment. GAPDH was used as a loading control.

FIGURE S4 | Western blot analysis of UBB^{+1} expression during CLS on day 3 and day 9. GAPDH was used as a loading control.

FIGURE S5 | CFU measurement of cellular survival under different concentrations of AZE treatment. Exponential cells were plated on SD-His$^-$ plates containing 2 mM, 4 mM and 7 mM of AZE, respectively. Results are average values ± SEM of biological triplicates.

FIGURE S6 | (A) Construction of the strains using a one copy or multicopy plasmid for the expression of the codon optimized UBB^{+1} sequence. **(B)** Evaluation of the strains on exponential phase. **(C)** Evaluation of the strains on stationary phase. Viability and the ocurrence of cell death markers were measured at the indicated time points. **(D)** Evaluations of the strains under stress conditions. Stress was induced either in liquid medium or on agar plates. The percentages shown are the results by comparing the UBB^{+1} strains with their respective controls.

REFERENCES

Baeza, J. L., Gerona-Navarro, G., Pérez De Vega, M. J., García-López, M. T., Gonzalez-Muñiz, R., and Martín-Martínez, M. (2008). Azetidine-derived amino acids versus proline derivatives. Alternative trends in reverse turn induction. *J. Org. Chem.* 73, 1704–1715. doi: 10.1021/jo701746w

Basaiawmoit, R. V., and Rattan, S. I. (2010). Cellular stress and protein misfolding during aging. *Methods Mol. Biol.* 648, 107–117. doi: 10.1007/978-1-60761-756-3_7

Bedford, L., Hay, D., Devoy, A., Paine, S., Powe, D. G., Seth, R., et al. (2008). Depletion of 26S proteasomes in mouse brain neurons causes neurodegeneration and Lewy-like inclusions resembling human pale bodies. *J. Neurosci.* 28, 8189–8198. doi: 10.1523/JNEUROSCI.2218-08.2008

Braun, R. J., Sommer, C., Leibiger, C., Gentier, R. J., Dumit, V. I., Paduch, K., et al. (2015a). Modeling non-hereditary mechanisms of Alzheimer disease during apoptosis in yeast. *Microb. Cell* 2, 136–138. doi: 10.15698/mic2015.04.199

Braun, R. J., Sommer, C., Leibiger, C., Gentier, R. J., Dumit, V. I., Paduch, K., et al. (2015b). Accumulation of basic amino acids at mitochondria dictates the cytotoxicity of aberrant ubiquitin. *Cell Rep.* 10, 1557–1571. doi: 10.1016/j.celrep.2015.02.009

Bryant, F. R. (1988). Construction of a recombinase-deficient mutant recA protein that retains single-stranded DNA-dependent ATPase activity. *J. Biol. Chem.* 263, 8716–8723.

Chen, X., Bisschops, M. M. M., Agarwal, N. R., Ji, B., Shanmugavel, K. P., and Petranovic, D. (2017). Interplay of energetics and ER stress exacerbates Alzheimer's amyloid-β (Aβ) toxicity in yeast. *Front. Mol. Neurosci.* 10:232. doi: 10.3389/fnmol.2017.00232

Chen, X., and Petranovic, D. (2015). Amyloid-β peptide-induced cytotoxicity and mitochondrial dysfunction in yeast. *FEMS Yeast Res.* 15:fov061. doi: 10.1093/femsyr/fov061

Chung, C. Y., Khurana, V., Auluck, P. K., Tardiff, D. F., Mazzulli, J. R., Soldner, F., et al. (2013). Identification and rescue of α-synuclein toxicity in Parkinson patient-derived neurons. *Science* 342, 983–987. doi: 10.1126/science.1245296

de Pril, R., Fischer, D. F., Maat-Schieman, M. L., Hobo, B., de Vos, R. A., Brunt, E. R., et al. (2004). Accumulation of aberrant ubiquitin induces aggregate formation and cell death in polyglutamine diseases. *Hum. Mol. Genet.* 13, 1803–1813. doi: 10.1093/hmg/ddh188

de Pril, R., Hobo, B., van Tijn, P., Roos, R. A., van Leeuwen, F. W., and Fischer, D. F. (2010). Modest proteasomal inhibition by aberrant ubiquitin exacerbates aggregate formation in a Huntington disease mouse model. *Mol. Cell. Neurosci.* 43, 281–286. doi: 10.1016/j.mcn.2009.12.001

De Vrij, F. M., Sluijs, J. A., Gregori, L., Fischer, D. F., Hermens, W. T., Goldgaber, D., et al. (2001). Mutant ubiquitin expressed in Alzheimer's disease causes neuronal death. *FASEB J.* 15, 2680–2688. doi: 10.1096/fj.01-0438com

Dennissen, F. J., Kholod, N., Hermes, D. J., Kemmerling, N., Steinbusch, H. W., Dantuma, N. P., et al. (2011). Mutant ubiquitin (UBB^{+1}) associated with neurodegenerative disorders is hydrolyzed by ubiquitin C-terminal hydrolase L3 (UCH-L3). *FEBS Lett.* 585, 2568–2574. doi: 10.1016/j.febslet.2011.06.037

Ding, W. X., Ni, H. M., Gao, W., Yoshimori, T., Stolz, D. B., Ron, D., et al. (2007). Linking of autophagy to ubiquitin-proteasome system is important for the regulation of endoplasmic reticulum stress and cell viability. *Am. J. Pathol.* 171, 513–524. doi: 10.2353/ajpath.2007.070188

Fischer, D. F., de Vos, R. A., van Dijk, R., de Vrij, F. M., Proper, E. A., Sonnemans, M. A., et al. (2003). Disease-specific accumulation of mutant ubiquitin as a marker for proteasomal dysfunction in the brain. *FASEB J.* 17, 2014–2024. doi: 10.1096/fj.03-0205com

Fischer, D. F., van Dijk, R., van Tijn, P., Hobo, B., Verhage, M. C., van der Schors, R. C., et al. (2009). Long-term proteasome dysfunction in the mouse

brain by expression of aberrant ubiquitin. *Neurobiol. Aging* 30, 847–863. doi: 10.1016/j.neurobiolaging.2008.06.009

Fratta, P., Engel, W. K., Van Leeuwen, F. W., Hol, E. M., Vattemi, G., and Askanas, V. (2004). Mutant ubiquitin UBB^{+1} is accumulated in sporadic inclusion-body myositis muscle fibers. *Neurology* 63, 1114–1117. doi: 10.1212/01.WNL.0000138574.56908.5d

French, B. A., van Leeuwen, F., Riley, N. E., Yuan, Q. X., Bardag-Gorce, F., Gaal, K., et al. (2001). Aggresome formation in liver cells in response to different toxic mechanisms: role of the ubiquitin-proteasome pathway and the frameshift mutant of ubiquitin. *Exp. Mol. Pathol.* 71, 241–246. doi: 10.1006/exmp.2001.2401

Gietz, R. D., and Woods, R. A. (2002). Transformation of yeast by lithium acetate/single-stranded carrier DNA/polyethylene glycol method. *Methods Enzymol.* 350, 87–96. doi: 10.1016/s0076-6879(02)50957-5

Giorgini, F., Guidetti, P., Nguyen, Q., Bennett, S. C., and Muchowski, P. J. (2005). A genomic screen in yeast implicates kynurenine 3-monooxygenase as a therapeutic target for Huntington disease. *Nat. Genet.* 37, 526–531. doi: 10.1038/ng1542

Hamilton, R., Watanabe, C. K., and de Boer, H. A. (1987). Compilation and comparison of the sequence context around the AUG startcodons in *Saccharomyces cerevisiae* mRNAs. *Nucleic Acids Res.* 15, 3581–3593. doi: 10.1093/nar/15.8.3581

Herker, E., Jungwirth, H., Lehmann, K. A., Maldener, C., Fröhlich, K. U., Wissing, S., et al. (2004). Chronological aging leads to apoptosis in yeast. *J. Cell Biol.* 164, 501–507. doi: 10.1083/jcb.200310014

Hershko, A., and Ciechanover, A. (1998). The ubiquitin system. *Annu. Rev. Biochem.* 67, 425–479. doi: 10.1146/annurev.biochem.67.1.425

Hope, A. D., de Silva, R., Fischer, D. F., Hol, E. M., van Leeuwen, F. W., and Lees, A. J. (2003). Alzheimer's associated variant ubiquitin causes inhibition of the 26S proteasome and chaperone expression. *J. Neurochem.* 86, 394–404. doi: 10.1046/j.1471-4159.2003.01844.x

Inoue, H., Nojima, H., and Okayama, H. (1990). High efficiency transformation of *Escherichia coli* with plasmids. *Gene* 96, 23–28. doi: 10.1016/0378-1119(90)90336-p

Keller, J. N., Hanni, K. B., and Markesbery, W. R. (2000). Impaired proteasome function in Alzheimer's disease. *J. Neurochem.* 75, 436–439. doi: 10.1046/j.1471-4159.2000.0750436.x

Khurana, V., and Lindquist, S. (2010). Modelling neurodegeneration in Saccharomyces cerevisiae: why cook with baker's yeast? *Nat. Rev. Neurosci.* 11, 436–449. doi: 10.1038/nrn2809

Ko, S., Kang, G. B., Song, S. M., Lee, J. G., Shin, D. Y., Yun, J. H., et al. (2010). Structural basis of E2–25K/UBB^{+1} interaction leading to proteasome inhibition and neurotoxicity. *J. Biol. Chem.* 285, 36070–36080. doi: 10.1074/jbc.M110.145219

Krutauz, D., Reis, N., Nakasone, M. A., Siman, P., Zhang, D., Kirkpatrick, D. S., et al. (2014). Extended ubiquitin species are protein-based DUB inhibitors. *Nat. Chem. Biol.* 10, 664–670. doi: 10.1038/nchembio.1574

Kushnirov, V. V. (2000). Rapid and reliable protein extraction from yeast. *Yeast* 16, 857–860. doi: 10.1002/1097-0061(20000630)16:9<857::aid-yea561>3.0.co;2-b

Kyhse-Andersen, J. (1984). Electroblotting of multiple gels: a simple apparatus without buffer tank for rapid transfer of proteins from polyacrylamide to nitrocellulose. *J. Biochem. Biophys. Methods* 10, 203–209. doi: 10.1016/0165-022x(84)90040-x

Lam, Y. A., Pickart, C. M., Alban, A., Landon, M., Jamieson, C., Ramage, R., et al. (2000). Inhibition of the ubiquitin-proteasome system in Alzheimer's disease. *Proc. Natl. Acad. Sci. U S A* 97, 9902–9906. doi: 10.1073/pnas.170173897

Lee, D. H., and Goldberg, A. L. (1998). Proteasome inhibitors cause induction of heat shock proteins and trehalose, which together confer thermotolerance in Saccharomyces cerevisiae. *Mol. Cell Biol.* 18, 30–38. doi: 10.1128/mcb.18.1.30

Li, J., Liu, J., Wang, X., Zhao, L., Chen, Q., and Zhao, W. (2009). A waterbath method for preparation of RNA from Saccharomyces cerevisiae. *Anal. Biochem.* 384, 189–190. doi: 10.1016/j.ab.2008.09.021

Liang, Q., Li, W., and Zhou, B. (2008). Caspase-independent apoptosis in yeast. *Biochim. Biophys. Acta* 1783, 1311–1319. doi: 10.1016/j.bbamcr.2008.02.018

Lindsten, K., de Vrij, F. M., Verhoef, L. G., Fischer, D. F., van Leeuwen, F. W., Hol, E. M., et al. (2002). Mutant ubiquitin found in neurodegenerative disorders is a ubiquitin fusion degradation substrate that blocks proteasomal degradation. *J. Cell Biol.* 157, 417–427. doi: 10.1083/jcb.200111034

Madeo, F., Fröhlich, E., and Fröhlich, K. U. (1997). A yeast mutant showing diagnostic markers of early and late apoptosis. *J. Cell Biol.* 139, 729–734. doi: 10.1083/jcb.139.3.729

Madeo, F., Fröhlich, E., Ligr, M., Grey, M., Sigrist, S. J., Wolf, D. H., et al. (1999). Oxygen stress: a regulator of apoptosis in yeast. *J. Cell Biol.* 145, 757–767. doi: 10.1083/jcb.145.4.757

Madeo, F., Herker, E., Maldener, C., Wissing, S., Lächelt, S., Herlan, M., et al. (2002). A caspase-related protease regulates apoptosis in yeast. *Mol. Cell* 9, 911–917. doi: 10.1016/s1097-2765(02)00501-4

Madeo, F., Herker, E., Wissing, S., Jungwirth, H., Eisenberg, T., and Frohlich, K. U. (2004). Apoptosis in yeast. *Curr. Opin. Microbiol.* 7, 655–660. doi: 10.1016/j.mib.2004.10.012

Mumberg, D., Müller, R., and Funk, M. (1995). Yeast vectors for the controlled expression of heterologous proteins in different genetic backgrounds. *Gene* 156, 119–122. doi: 10.1016/0378-1119(95)00037-7

Outeiro, T. F., and Lindquist, S. (2003). Yeast cells provide insight into α-synuclein biology and pathobiology. *Science* 302, 1772–1775. doi: 10.1126/science.1090439

Pérez-Galán, P., Roué, G., Villamor, N., Montserrat, E., Campo, E., and Colomer, D. (2006). The proteasome inhibitor bortezomib induces apoptosis in mantle-cell lymphoma through generation of ROS and Noxa activation independent of p53 status. *Blood* 107, 257–264. doi: 10.1182/blood-2005-05-2091

Shabek, N., Herman-Bachinsky, Y., and Ciechanover, A. (2009). Ubiquitin degradation with its substrate, or as a monomer in a ubiquitination-independent mode, provides clues to proteasome regulation. *Proc. Natl. Acad. Sci. U S A* 106, 11907–11912. doi: 10.1073/pnas.0905746106

Tan, Z., Sun, X., Hou, F. S., Oh, H. W., Hilgenberg, L. G., Hol, E. M., et al. (2007). Mutant ubiquitin found in Alzheimer's disease causes neuritic beading of mitochondria in association with neuronal degeneration. *Cell Death Differ.* 14, 1721–1732. doi: 10.1038/sj.cdd.4402180

Tank, E. M., and True, H. L. (2009). Disease-associated mutant ubiquitin causes proteasomal impairment and enhances the toxicity of protein aggregates. *PLoS Genet.* 5:e1000382. doi: 10.1371/journal.pgen.1000382

Tardiff, D. F., Jui, N. T., Khurana, V., Tambe, M. A., Thompson, M. L., Chung, C. Y., et al. (2013). Yeast reveal a "druggable" Rsp5/Nedd4 network that ameliorates α-synuclein toxicity in neurons. *Science* 342, 979–983. doi: 10.1126/science.1245321

Towbin, H., Staehelin, T., and Gordon, J. (1979). Electrophoretic transfer of proteins from polyacrylamide gels to nitrocellulose sheets: procedure and some applications. *Proc. Natl. Acad. Sci. U S A* 76, 4350–4354. doi: 10.1073/pnas.76.9.4350

Tsai, F. H., Overberger, C. G., and Zand, R. (1990). Synthesis and peptide-bond orientation in tetrapeptides containing L-azetidine-2-carboxylic acid and L-proline. *Biopolymers* 30, 1039–1049. doi: 10.1002/bip.360301105

van Dijken, J. P., Bauer, J., Brambilla, L., Duboc, P., Francois, J. M., Gancedo, C., et al. (2000). An interlaboratory comparison of physiological and genetic properties of four Saccharomyces cerevisiae strains. *Enzyme Microb. Technol.* 26, 706–714. doi: 10.1016/s0141-0229(00)00162-9

van Leeuwen, F. W., Burbach, J. P., and Hol, E. M. (1998a). Mutations in RNA: a first example of molecular misreading in Alzheimer's disease. *Trends Neurosci.* 21, 331–335. doi: 10.1016/s0166-2236(98)01280-6

van Leeuwen, F. W., de Kleijn, D. P., van den Hurk, H. H., Neubauer, A., Sonnemans, M. A., Sluijs, J. A., et al. (1998b). Frameshift mutants of β amyloid precursor protein and ubiquitin-B in Alzheimer's and Down patients. *Science* 279, 242–247. doi: 10.1126/science.279.5348.242

van Leeuwen, F. W., Fischer, D. F., Benne, R., and Hol, E. M. (2000). Molecular misreading. A new type of transcript mutation in gerontology. *Ann. N Y Acad. Sci.* 908, 267–281. doi: 10.1111/j.1749-6632.2000.tb06654.x

van Tijn, P., de Vrij, F. M., Schuurman, K. G., Dantuma, N. P., Fischer, D. F., van Leeuwen, F. W., et al. (2007). Dose-dependent inhibition of proteasome activity by a mutant ubiquitin associated with neurodegenerative disease. *J. Cell Sci.* 120, 1615–1623. doi: 10.1242/jcs.03438

Verhoef, L. G., Heinen, C., Selivanova, A., Halff, E. F., Salomons, F. A., and Dantuma, N. P. (2009). Minimal length requirement for proteasomal degradation of ubiquitin-dependent substrates. *FASEB J.* 23, 123–133. doi: 10.1096/fj.08-115055

Welchman, R. L., Gordon, C., and Mayer, R. J. (2005). Ubiquitin and ubiquitin-like proteins as multifunctional signals. *Nat. Rev. Mol. Cell Biol.* 6, 599–609. doi: 10.1038/nrm1700

Wu, S. S., de Chadarevian, J. P., McPhaul, L., Riley, N. E., van Leeuwen, F. W., and French, S. W. (2002). Coexpression and accumulation of ubiquitin +1 and ZZ proteins in livers of children with α_1-antitrypsin deficiency. *Pediatr. Dev. Pathol.* 5, 293–298. doi: 10.1007/s10024-001-0202-3

Zagari, A., Némethy, G., and Scheraga, H. A. (1990). The effect of the L-azetidine-2-carboxylic acid residue on protein conformation. I. Conformations of the residue and of dipeptides. *Biopolymers* 30, 951–959. doi: 10.1002/bip.360300909

Conflict of Interest Statement: The authors declare that the research was conducted in the absence of any commercial or financial relationships that could be construed as a potential conflict of interest.

frontiers in Molecular Neuroscience

ORIGINAL RESEARCH
published: 21 June 2018
doi: 10.3389/fnmol.2018.00205

The Enzymatic Core of the Parkinson's Disease-Associated Protein LRRK2 Impairs Mitochondrial Biogenesis in Aging Yeast

*Andreas Aufschnaiter[1†], Verena Kohler[1†], Corvin Walter[2,3], Sergi Tosal-Castano[4], Lukas Habernig[4], Heimo Wolinski[1], Walter Keller[1], F.-Nora Vögtle[2] and Sabrina Büttner[1,4]**

[1]Institute of Molecular Biosciences, University of Graz, Graz, Austria, [2]Institute of Biochemistry and Molecular Biology, ZBMZ, Faculty of Medicine, University of Freiburg, Freiburg, Germany, [3]Faculty of Biology, University of Freiburg, Freiburg, Germany, [4]Department of Molecular Biosciences, The Wenner-Gren Institute, Stockholm University, Stockholm, Sweden

Mitochondrial dysfunction is a prominent trait of cellular decline during aging and intimately linked to neuronal degeneration during Parkinson's disease (PD). Various proteins associated with PD have been shown to differentially impact mitochondrial dynamics, quality control and function, including the leucine-rich repeat kinase 2 (LRRK2). Here, we demonstrate that high levels of the enzymatic core of human LRRK2, harboring GTPase as well as kinase activity, decreases mitochondrial mass via an impairment of mitochondrial biogenesis in aging yeast. We link mitochondrial depletion to a global downregulation of mitochondria-related gene transcripts and show that this catalytic core of LRRK2 localizes to mitochondria and selectively compromises respiratory chain complex IV formation. With progressing cellular age, this culminates in dissipation of mitochondrial transmembrane potential, decreased respiratory capacity, ATP depletion and generation of reactive oxygen species. Ultimately, the collapse of the mitochondrial network results in cell death. A point mutation in LRRK2 that increases the intrinsic GTPase activity diminishes mitochondrial impairment and consequently provides cytoprotection. In sum, we report that a downregulation of mitochondrial biogenesis rather than excessive degradation of mitochondria underlies the reduction of mitochondrial abundance induced by the enzymatic core of LRRK2 in aging yeast cells. Thus, our data provide a novel perspective for deciphering the causative mechanisms of LRRK2-associated PD pathology.

Keywords: LRRK2, Parkinson's disease, neurodegeneration, mitochondria, complex IV, cell death, yeast, aging

OPEN ACCESS

Edited by:
David Blum, Institut National de la Santé et de la Recherche Médicale (INSERM), France

Reviewed by:
Giovanni Piccoli, University of Trento, Italy
Emmanuel Brouillet, Commissariat à l'Energie Atomique et aux Energies Alternatives (CEA), France

***Correspondence:**
Sabrina Büttner
sabrina.buettner@su.se

[†]These authors have contributed equally to this work.

Received: *29 March 2018*
Accepted: *22 May 2018*
Published: *21 June 2018*

Citation:
Aufschnaiter A, Kohler V, Walter C, Tosal-Castano S, Habernig L, Wolinski H, Keller W, Vögtle F-N and Büttner S (2018) The Enzymatic Core of the Parkinson's Disease-Associated Protein LRRK2 Impairs Mitochondrial Biogenesis in Aging Yeast. Front. Mol. Neurosci. 11:205. doi: 10.3389/fnmol.2018.00205

INTRODUCTION

Parkinson's disease (PD) is a neurodegenerative disorder of multifactorial etiology with genetics, environmental toxins and age as determinant risk factors. While the majority of PD cases are sporadic, various monogenic forms of PD have been identified (Thomas and Beal, 2007; Klein and Westenberger, 2012; Hernandez et al., 2016). Accumulating evidence points towards shared

Abbreviations: $\Delta\Psi_m$, mitochondrial transmembrane potential; COR, C-terminal-of-ROC; DHE, dihydroethidium; Eth, ethidium; GFP, green fluorescent protein; IMS, intermembrane space; LRRK2, leucine-rich repeat kinase 2; OM, outer (mitochondrial) membrane; PD, Parkinson's disease; PI, propidium iodide; ProtK, proteinase K; ROC, Ras-of-complex; ROS, reactive oxygen species.

cellular pathways driving sporadic and familial PD pathology (Klein and Westenberger, 2012). Consistently, several genes causative for familial PD have also been shown to constitute risk factors for the development of sporadic PD. Importantly, impairment of mitochondrial function is a reoccurring phenotype in PD. Samples derived from sporadic PD patients display respiratory chain complex I deficiency (Schapira et al., 1990; Parker et al., 2008). Similarly, mutations in genes associated with both autosomal recessive and dominant familial PD interfere with mitochondrial function, in particular mitochondrial quality control, at different levels and in diverse model systems (Larsen et al., 2018). Thus, unraveling the link between PD and mitochondrial dysfunction is fundamental to understand disease development.

The most prevalent genetic cause of both familial and sporadic PD is linked to sequence variations in the gene encoding the leucine-rich repeat kinase 2 (LRRK2; Klein and Westenberger, 2012; Hernandez et al., 2016). LRRK2 has been proposed to function in a wide variety of cellular processes, including vesicle trafficking and endocytosis, autophagy, regulation of the retromer complex as well as mitochondrial function and, in turn, dysregulation of these processes is reported for diverse PD-associated LRRK2 mutations (Wallings et al., 2015). Still, the molecular mechanisms of its physiological and pathological mode of action are mostly unknown. LRRK2 is a large, multifunctional protein with several domains, including distinct protein-protein interaction domains and an enzymatic core composed of a Ras-of-complex (ROC) GTPase, an associated C-terminal-of-ROC (COR) domain and a serine/threonine protein kinase (Islam and Moore, 2017). The most frequent pathogenic mutations in LRRK2, such as R1441C/G/H, Y1699C, G2019S and I2020T, are located within its catalytic core and affect its enzymatic activity. The GTPase and the kinase activity mutually influence each other, but their interplay as well as their specific contribution to neurotoxicity are not fully understood yet. Whereas kinase hyperactivation (G2019S and I2020T) as well as decreased activity of the GTPase (R1441C/G/H and Y1699C) are linked to PD, enhanced GTPase activity as seen for the synthetic R1398L mutant or the R1398H variant in humans reduce toxic consequences mediated by LRRK2 or the risk for onset of PD, respectively (Chen et al., 2011; Ross et al., 2011; Heckman et al., 2014; Nguyen and Moore, 2017; Ramírez et al., 2017).

Several *in vivo* and *in vitro* models display distinct mitochondrial abnormalities upon high levels of LRRK2 variants, but the effects of particular point mutations on the observed mitochondrial changes remain controversial (Mortiboys et al., 2010; Cooper et al., 2012; Godena et al., 2014; Thomas et al., 2016; Schwab et al., 2017). Common phenotypes observed in most studies include a decrease in mitochondrial transmembrane potential, alterations of mitochondrial trafficking and a depletion of mitochondria, specifically within neurites. This reduction of mitochondrial mass has been attributed to either increased retrograde trafficking of mitochondria (Schwab et al., 2017), to inhibition of both anterograde and retrograde trafficking (Godena et al., 2014; Thomas et al., 2016), or to excessive mitochondrial degradation via autophagy (Cherra et al., 2013). Other studies observed no effect on mitochondrial content but a dissipation of mitochondrial transmembrane potential, resulting in a depletion of cellular ATP levels (Mortiboys et al., 2010; Papkovskaia et al., 2012). Thus, the effects of LRRK2 on mitochondrial function seem to be rather pleiotropic. Interestingly, genetically enforcing mitochondrial biogenesis has been recently shown to alleviate LRRK2-induced degeneration in a *Drosophila* model for PD (Ng et al., 2017). Yet it has not been analyzed whether defects in mitochondrial biogenesis represent a causative factor for the LRRK2-triggered decrease in mitochondrial mass.

Here, we establish an aging yeast model for LRRK2 cytotoxicity and show that expression of the enzymatic core of LRRK2, consisting of its ROC, COR and kinase domain, hereafter referred to as $LRRK2^{RCK}$, decreases mitochondrial mass via an impairment of mitochondrial biogenesis prior to the induction of age-dependent cell death. We link mitochondrial depletion to a specific downregulation of mitochondria-related gene transcripts and identify complex IV deficiency as early event in $LRRK2^{RCK}$-triggered cellular demise.

MATERIALS AND METHODS

Saccharomyces cerevisiae Strains and Genetics

All experiments were performed in *Saccharomyces cerevisiae* BY4741 (MAT**a**; *his3*Δ1; *leu2*Δ0; *met15*Δ0; *ura3*Δ0) obtained from Euroscarf and experiments shown in **Figures 3G–I** were additionally performed in *S. cerevisiae* W303 (MAT**a**; *leu2–3,112*; *trp1–1*; *can1–100*; *ura3–1*; *ade2–1*). Plasmids for heterologous expression of the enzymatic core of human wild type LRRK2 ($LRRK2^{RCK}$), the $R1389L^{RCK}$ mutant form with enhanced GTPase activity, and the $G2019S^{RCK}$ variant with increased kinase activity were kindly provided by Darren J. Moore (Xiong et al., 2010). ß-galactosidase (LacZ) expressed from the same plasmid was used as a control. $LRRK2^{RCK}$ variants and LacZ harbored a C-terminal V5 tag and were expressed under the control of a GAL1 promoter from a pYES2/CT plasmid. C-terminally mCherry-tagged versions of these proteins were constructed by PCR-amplification of mCherry, restriction digest with *Xba*I and *Pme*I and ligation into the existing pYES2/CT plasmids encoding the $LRRK2^{RCK}$ variants. mCherry expressed from a pYES2/CT plasmid was used as a control for microscopic analyses, and was cloned by PCR amplification of mCherry, restriction digest with *Bam*HI and *Not*I and ligation into the pYES2/CT plasmid. All oligonucleotides used in this study are listed in Supplementary Table S1. Standard lithium acetate method was used for yeast transformation (Gietz and Woods, 2002). Genomically modified strains were created by homologous recombination as previously described (Janke et al., 2004). All strains used in this study are listed in Supplementary Table S2. After plasmid transformation or genomic modification, at least four different clones were tested to rule out clonogenic variations.

Media and Culturing Conditions

All strains were grown at 28°C and 145 rpm in synthetic complete (SC) medium, consisting of 0.17% yeast nitrogen base (Difco, BD Biosciences), 0.5% $(NH_4)_2SO_4$ and 30 mg/l of all amino acids (except 80 mg/l histidine and 200 mg/l leucine) and 30 mg/l adenine with 2% D-glucose (SCD), or 2% D-galactose (SCG) for GAL1-driven expression of LacZ and $LRRK2^{RCK}$ variants. Media were prepared using double distilled water and autoclaved for 25 min at 121°C, 210 kPa. Amino acids were sterilized separately as 10× stocks and admixed to the media after autoclaving. Full media (YEPD) contained 1% yeast extract (Bacto, BD Biosciences), 2% peptone (Bacto, BD Biosciences) and 4% D-glucose. For solid media, 2% agar was admixed and hygromycin (300 mg/l), nourseothricin (100 mg/l) or geneticin (300 mg/l) was added after autoclaving when required to select for transformants.

For chronological aging experiments, overnight cultures grown in SCD media for 16–20 h were used to inoculate 10 ml SCD in 100 ml baffled Erlenmeyer flasks to an OD_{600} of 0.1. Cells were further grown to an OD_{600} of 0.3, collected by centrifugation (5 min, 2300 rcf), and resuspended in 10 ml SCG media to induce GAL1-dependent expression. Aliquots were taken at indicated time points to study survival and mitochondrial abundance, morphology and function. To analyze exponential growth after induction of galactose-driven expression, OD_{600} was measured every 2 h for 24 h on a Beckman coulter DU 730 Life Science UV/VIS Spectrophotometer.

Analysis of Cell Death

Loss of membrane integrity was determined with propidium iodide (PI) staining as previously described (Aufschnaiter et al., 2017). In brief, $2*10^6$ cells were harvested in 96-well plates at indicated time points and resuspended in 250 µl of phosphate buffered saline (PBS, 25 mM potassium phosphate, 0.9% NaCl; adjusted to pH 7.2) containing 100 µg/l PI. After incubation for 10 min at room temperature (RT) in the dark, cells were washed once in 250 µl PBS and subsequently analyzed via flow cytometry (BD LSR Fortessa; 30,000 cells were evaluated with BD FACSDivia software) and/or fluorescence microscopy.

To discriminate between necrotic and early/late apoptotic cell death, AnnexinV/PI co-staining was applied as described previously (Büttner et al., 2007, 2011). $2*10^7$ cells were harvested, washed once in digestion buffer (35 mM K_3PO_4, 0.5 mM $MgCl_2$, 1.2 M sorbitol; adjusted to pH 6.8) and subsequently resuspended in 330 µl of the same buffer. After addition of 2.5 µl Lyticase (1000 U/ml) and 15 µl Glucoronidase/Arylsulfatase (4.5 U/ml), cells were incubated at 28°C and 145 rpm for about 1 h to digest the cell wall. Spheroplasts were carefully washed in 500 µl digestion buffer, resuspended in 30 µl staining buffer (10 mM HEPES, 140 mM NaCl, 5 mM $CaCl_2$, 0.6 M sorbitol; adjusted to pH 7.4) containing PI and AnnexinV-FITC (Roche) and incubated for 20 min at RT in the dark. 250 µl staining buffer were added to each sample and cells were evaluated via flow cytometry and fluorescence microscopy.

To measure clonogenic survival, the cell number of each culture was determined with a CASY cell counting device (Schärfe Systems) and 500 cells were plated on agar plates with YEPD media. Plates were incubated at 28°C for 2 days and colony forming units (cfu) were analyzed with Fiji software (Schindelin et al., 2012).

Measurement of Oxidative Stress and Mitochondrial Transmembrane Potential in Whole Cells

Oxidative stress was monitored via the reactive oxygen species (ROS) driven conversion of non-fluorescent dihydroethidium (DHE) to fluorescent ethidium (Eth; Büttner et al., 2007). Briefly, $2*10^6$ cells were harvested in 96-well plates at indicated time points. Cells were then resuspended in 250 µl of PBS containing 2.5 mg/l DHE and incubated for 5 min at RT in the dark. After washing once with PBS, cells were analyzed via flow cytometry. Of note, dead cells, accumulating the fluorescent dye, were excluded from the analysis (gating strategy is depicted in **Figure 3C**) and the mean fluorescence intensity of living cells was quantified. Results are presented as fold of control cells expressing LacZ on day one. Mitochondrial transmembrane potential ($\Delta\Psi_m$) was determined with the fluorescent dye Mitotracker CMXRos (Thermo Fisher Scientific). For this purpose, $2*10^6$ cells were harvested and resuspended in 250 µl PBS containing 200 nM Mitotracker CMXRos. After incubation for 10 min at RT in the dark, cells were washed once in PBS and quantified via flow cytometry and analyzed with confocal microscopy.

Determination of Cellular Oxygen Consumption and ATP Levels

Oxygen consumption of yeast cells was measured with a Fire-Sting optical oxygen sensor system (Pyro Science) at indicated time points. To that end, 2 ml of culture were directly transferred into glass tubes, hermetically sealed and immediately used for the analysis. Oxygen concentration was measured for a period of at least 2 min and the slope of the regression line was calculated. The number of cells was assessed directly from the measurement tubes with a CASY cell counting device and the percentage of dead cells was analyzed via flow cytometric quantification of PI-stained cells as described above. Oxygen consumption per living cell was then calculated, and results were normalized to control cells and depicted as fold values.

To quantify cellular ATP levels, 1 ml of culture was harvested and ATP was extracted with the hot ethanol method. In brief, cells were flash frozen in liquid nitrogen, resuspended in 0.5 ml BES buffer (75% EtOH, 10 mM $(NH_4)_2SO_4$) and incubated for 3 min at 90°C. Samples were then centrifuged for 20 min at 4°C with 16,100 rcf and diluted 20-fold in Tris buffer (20 mM; pH 8). The ATP content of the extracts was quantified with a luminescent ATP detection assay kit (Abcam). For that, 150 µl of sample were transferred into a low-bind 96-well plate and incubated for 5 min for adaption

to RT. 50 µl of supplied substrate solution were added and incubated for 5 min in the dark. The assay plate was placed into a GloMax Multi detection system (Promega) and incubated for further 10 min to allow dark adaption. Luminescence was then measured via integration of the signal over 10 s. The number of living cells was simultaneously quantified as described above to calculate the ATP content of living cells. Results are depicted as fold values via normalization to control cells expressing LacZ.

Fluorescence Microscopy

Specimen were prepared on agar slides to immobilize yeast cells. Epifluorescence microscopy was performed with a Zeiss Axioskop with appropriate filter settings. For visualization of mitochondrial morphology and colocalization studies, yeast cells were analyzed with a Leica SP5 confocal microscope equipped with a Leica HCX PL APO 63× NA 1.4 oil immersion objective. Green fluorescent protein (GFP) was excited at 488 nm and emission was measured between 500 nm and 530 nm. To exclude dead cells from the analysis of mitochondrial morphology, cells were counterstained with PI as described above, excited at 563 nm and detected between 590 nm and 650 nm. Z-stacks were acquired using 63 × 63 × 125 (x/y/z) nm sampling. Microscopic pictures were analyzed and processed with the open-source software Fiji (Schindelin et al., 2012). To reduce image noise in z-stacks, 3-dimensional Gaussian filtering ($x\sigma = y\sigma = z\sigma = 1$) was applied, followed by background subtraction (rolling ball radius = 100 pixels). Three-dimensional data was projected using the maximum-intensity projection method. Pictures within an experiment were captured and processed in the same way.

For quantification of colocalization, the Pearson correlation coefficient (PCC) as well as the threshold-corrected Manders' coefficient M1 (overlap of GFP signal with mCherry-tagged $LRRK2^{RCK}$ variants) and M2 (overlap of mCherry-tagged $LRRK2^{RCK}$ variants with GFP signal) were calculated using the Fiji plugin JACoP (Bolte and Cordelières, 2006). Depicted M1 and M2 coefficients used a threshold value, which was determined with Fiji applying the Mean method. Picture pre-processing was performed as described above. For each strain and expression type, at least 120 cells from three different clones were analyzed ($n = 3$) and means ± SEM are presented.

Subcellular Fractionation

Subcellular fractionation experiments were adapted from Klasson et al. (1999). Cells equivalent to an OD_{600} of 200 were harvested at day one, flash frozen in liquid nitrogen and stored at −80°C until lysis. Samples were thawed on ice and resuspended in ice-cold water with 10 mM NaN_3 and centrifuged for 10 min at 500 rcf. Cells were then resuspended in 0.5 ml lysis buffer (10 mM MOPS, 0.8 M sorbitol, 2 mM EDTA, 1 mM phenylmethylsulfonyl fluoride, 1× cOmplete protease inhibitor cocktail (Roche); adjusted to pH 7.2) and approx. 500 µl glass beads (500 µm diameter) were added. Mechanical lysis was performed in three cycles of 1 min. Unlysed cells and cell debris were removed by two centrifugation steps for 5 min at 2400 rcf. The supernatant was carefully loaded on a sucrose step gradient (60%, 54%, 48%, 42%, 36%, 30%, 24%, 18% and 12% (w/v), each 1 ml) and centrifuged for 3 h at 4°C with 150,000 rcf (Beckman coulter LE-80K centrifuge, SW 41 Ti Swinging-Bucket Rotor, 34,000 rpm). Fractions of 1 ml were collected manually from top to bottom, 1 ml 50% trichloroacetic acid was added and incubated for 5 min on ice. After centrifugation (15 min, 16,100 rcf, 4°C), samples were rinsed once in 1 ml of 1 M Tris (untitrated) and resuspended in 150 µl of non-reducing Laemmli buffer (50 mM Tris-HCl, 2% SDS, 10% glycerol, 0.1% bromophenol blue; adjusted to pH 6.8). 50 µl of samples were used for immunoblotting as described below.

Immunoblotting

Cells equivalent to an OD_{600} of 3 were harvested at indicated time points. For lysis, pellets were resuspended in 200 µl of 0.1 M NaOH and incubated for 5 min at RT with 1400 rpm shaking. Samples were then centrifuged with 1500 rcf for 5 min, resuspended in 150 µl reducing Laemmli buffer (50 mM Tris-HCl, 2% SDS, 10% glycerol, 0.1% bromophenol blue, 100 mM 2-mercaptoethanol; adjusted to pH 6.8) and incubated for 5 min at RT with 1400 rpm shaking. Prior to SDS-PAGE, samples were heated for 10 min to 65°C and centrifuged for 1 min with 16,100 rcf. 15 µl of supernatant was applied for standard SDS-PAGE and immunoblotting was performed using standard protocols. For detection, antibodies against the GFP-epitope (Roche; 11814460001), V5-epitope (Thermo Fisher Scientific; MA5–1525), glyceraldehyde 3-phosphate dehydrogenase (GAPDH; Thermo Fisher Scientific; MA5–15738), Por1 (Thermo Fisher Scientific; 16G9E6BC4) and histone H3 (Abcam; ab1791) were used. Furthermore, antibodies against Mdh1, Tom22, Pma1, Ssa1, Vam3, Sec61, Cox1, Cox3, Cox4, Cox6, Sdh1, Tom70, Tim44, Atp14, Tim54, Mcr1, Tim22, Tim21 and Mas1, which were generated by injecting rabbits with recombinantly expressed and purified proteins, were applied. Peroxidase conjugated secondary antibodies against rabbit (Sigma; A0545) or mouse (Sigma; A9044) were used for chemiluminescence detection.

To analyze $LRRK2^{RCK}$ oligomers, semi-native immunoblots were applied as recently described (Aufschnaiter et al., 2017). Cells equivalent to an OD_{600} of 8 were prepared as described above with non-reducing Laemmli buffer. Polyacrylamide gels without SDS were used for electrophoresis, which was performed at 4°C. For detection of all immunoblots, a ChemiDoc™ Touch Imaging System (Bio-Rad) was used and densitometric quantification was performed with ImageLab 5.2 Software (Bio-Rad). All indicated molecular weights shown in immunoblots represent the apparent molecular weights (kDa), determined with a PageRuler prestained protein ladder (Thermo Fisher Scientific) or a Spectra™ Multicolor High Range Protein Ladder (Thermo Fisher Scientific), as stated by the manufactures migration patterns.

Quantitative Real-Time PCR

For quantification of mRNA levels, total RNA was isolated from yeast cultures. To that end, cells equivalent to an OD_{600} of 3 were

harvested at indicated time points and resuspended in 1 ml of TRIzol reagent (Thermo Fisher Scientific). Approximately 200 µl of glass beads (500 µm diameter) were added and cells were mechanically lysed in three cycles of 1 min. Subsequent steps were performed as described in the manufacturer's manual. RNA integrity was visualized by agarose-gel electrophoresis (adapted from Aranda et al., 2012). Residual DNA was removed with the DNA-free Kit (Ambion) and the RNA concentration was determined with a NanoDrop 1000 Spectrophotometer. Reverse transcription of 3.5 µg isolated RNA was performed with the FIREScript RT cDNA synthesis kit (Solis Biodyne) using the supplied random hexamer primers. After dilution of the resulting cDNA, q-RT-PCR was performed with the 5× HOT FirePol EvaGreen qPCR Supermix (Solis Biodyne). All primers used for q-RT-PCR are listed in Supplementary Table S1. All primers showed an efficiency between 90% and 110%, as assessed with standard curve experiments. To measure gene expression levels, cDNA was utilized in duplicate for q-RT-PCR and the relative gene expression levels were calculated with the comparative C_T method (Livak and Schmittgen, 2001) with normalization to *UBC6* as housekeeping gene.

Isolation and Purification of Mitochondria

Mitochondria from *S. cerevisiae* strains were isolated by differential centrifugation (Meisinger et al., 2006). Briefly, yeast cells were grown on SCG medium at 28°C for around 19 h until an OD_{600} of 1.5–2 was reached. The cultures were harvested and afterwards incubated for 20 min in pre-warmed dithiothreitol (DTT) buffer (0.1 M Tris-H_2SO_4, 10 mM DTT; adjusted to pH 9.4). After centrifugation, the pellet was resuspended in zymolyase buffer (20 mM potassium phosphate buffer, 1.2 M sorbitol; adjusted to pH 7.4) containing 4 mg zymolyase per gram wet weight of the cells and incubated for 30–45 min to generate spheroplasts. Spheroplasts were washed and resuspended at 7 ml/g cells in ice-cold homogenization buffer (10 mM Tris-HCl, 0.6 M sorbitol, 1 mM EDTA, 1 mM phenylmethylsulfonyl fluoride (PMSF), 0.2% (w/v) bovine serum albumin (BSA); adjusted to pH 7.4) and were broken on ice with 30 strokes using a tight-fitting glass douncer with a Teflon pistil. Cell debris and unbroken cells were removed via two times centrifugation (5 min, 2000 rcf, 4°C). The mitochondrial fraction was isolated by centrifugation (15 min, 16,800 rcf, 4°C) and 25 µl aliquots were immediately snap-frozen in liquid nitrogen. Protein concentration was determined with a Bradford assay (Roti-Quant™, Roth) against bovine γ-globulin standard (Bio-Rad) according to the manufacturer's instructions.

Measurement of Mitochondrial Transmembrane Potential in Isolated Mitochondria

Isolated mitochondria were used to measure $\Delta\Psi_m$ via fluorescence reduction. 30 µg of crude mitochondria were resuspended in 3 ml membrane potential buffer (20 mM potassium phosphate buffer, 0.6 M sorbitol, 10 mM $MgCl_2$, 0.5 mM EDTA, 5 mM L-malate, 5 mM succinate, 0.1% (w/v) BSA; adjusted to pH 7.2) containing 2 µM 3,3′-dipropylthiadicarbocyanine iodide ($DiSC_3$, stored in ethanol). Immediately, the absorption (excitation 622 nm, emission 670 nm) was recorded with a luminescence spectrometer (Aminco Bowman 2, Thermo Electron) until a distribution equilibrium was generated. By adding 1 µM valinomycin the $\Delta\Psi_m$ was disrupted and the total fluorescence was measured. Data were analyzed with FL WinLab (PerkinElmer).

Blue-Native-PAGE and Mitochondrial ATPase Activity Staining

Mitochondrial protein complexes were investigated by solubilizing 80 µg mitochondria in digitonin buffer (20 mM Tris-HCl, 1% (w/v) digitonin, 10% (v/v) glycerol, 0.1 mM EDTA, 50 mM NaCl, 1 mM PMSF; adjusted to pH 7.4) on ice for 15 min. Afterwards, samples were centrifuged (15 min, 16,100 rcf, 4°C) and the supernatant was analyzed on a 4%–10% gradient Blue-Native-PAGE, followed by immunodecoration, which was performed according to standard protocols. The molecular weight of the standard proteins from the HMW Native Marker Kit (GE Healthcare) is depicted for all Blue-Native blots.

For mitochondrial ATPase activity staining, 80 µg mitochondria were lysed in digitonin buffer and protein complexes were separated using Blue-Native-PAGE. The gel was washed in distilled H_2O for 20 min and immediately incubated in ATP-buffer (50 mM glycine, 20 mM ATP, 5 mM $MgCl_2$; adjusted to pH 8.4 with NaOH) for 20 min. The gel was transferred into a 10% (w/v) $CaCl_2$ solution and incubated until calcium phosphate precipitation was visible, washed with distilled H_2O, before documentation was carried out by using the LAS4000 camera system (Fujifilm).

Outer Mitochondrial Membrane Integrity Test

40 µg of mitochondria were diluted in 100 µl SEM buffer (10 mM MOPS, 250 mM sucrose, 1 mM EDTA; adjusted to pH 7.2) and treated with 0, 10 or 20 µg/ml proteinase K on ice. After 10 min PMSF was added to samples to a final concentration of 2.5 mM and incubated for further 10 min. Mitochondria were washed with SEM buffer and resuspended in Laemmli buffer (120 mM Tris-HCl, 20% (v/v) glycerol, 4% (w/v) SDS, 0.001% (w/v) bromophenol blue; 3% (v/v) β-mercaptoethanol; pH 6.8). Samples were analyzed by SDS-PAGE and immunoblotting, according to standard protocols.

Statistical Analysis

To analyze the effect of dependent variables across the type of expression (between-subject factor) and along time (within-subject factor), a two-way mixed-design analysis of variance (ANOVA) with a Bonferroni *post hoc* test was applied. To disprove the null-hypothesis (no difference between conditions) in non-time-depending experiments, a one-way ANOVA corrected with a Bonferroni *post hoc* test for one variable (type

of expression) was performed. A Student's *t*-test was applied to compare between two groups. Significances are indicated with asterisks: $^{***}p < 0.001$, $^{**}p < 0.01$, $^{*}p < 0.05$, not significant (n.s.) $p > 0.05$. Final results of experiments, performed at multiple time points, are visualized as fold-values normalized to control cells at the earliest time point shown. Statistical analysis was performed with Origin Pro 2016 (OriginLab) and figures were prepared with Origin Pro 2016 and Adobe Illustrator CS6 (Adobe).

RESULTS

Cellular Age Is a Decisive Factor for LRRK2^{RCK}-Induced Death

Within the last 15 years, numerous humanized yeast models for neurodegeneration have been developed, not only successfully recapitulating basic characteristics of diverse neurotoxic proteins, but also providing new insights into the molecular pathways and determinants underlying disease pathology that subsequently were found to be conserved across species (Braun et al., 2010; Oliveira et al., 2017; Tenreiro et al., 2017). While the heterologous expression of the enzymatic core of LRRK2 in dividing yeast cells has been shown to cause growth arrest and defects in vesicular trafficking (Xiong et al., 2010), nothing is known about its effect on post-mitotic yeast cells. Thus, we established a setup that allowed us to analyze LRRK2-mediated changes in stationary, aging cells. Here, the galactose-driven expression of a truncated version of LRRK2, ranging from amino acid 1300–2163 and containing its ROC, COR and kinase domain (LRRK2^{RCK}, **Figure 1A**) did not affect exponential growth (**Figure 1B**). Instead, upon entry into stationary phase, LRRK2^{RCK} triggered a progressive loss of survival starting at day 3 as determined by flow cytometric quantification of membrane rupture (**Figure 1C**) and clonogenic assays monitoring the abundance of viable cells (**Figure 1D**). The point mutation R1398L partly prevented, but not completely inhibited LRRK2^{RCK} cytotoxicity. This mutation has been shown to convey higher GTPase activity (Xiong et al., 2010), and an exchange at the R1398 residue has been identified as the functional variant in a human haplotype that is protective against PD (Ross et al., 2011; Heckman et al., 2014). Expression of a protein of comparable size (ß-galactosidase, LacZ) did not affect survival during aging compared to the empty vector control (**Figure 1C**) and was used as control for further experiments. The pathogenic point mutation G2019S, which has been shown to increase kinase activity (West et al., 2005), seemed to slightly enforce LRRK2^{RCK}-mediated cell death, however without reaching statistical significance (Supplementary Figures S1A–G).

To discriminate between necrotic and early/late apoptotic cell death, we performed AnnexinV/PI co-staining, demonstrating that LRRK2^{RCK}-mediated age-dependent death displays phenotypic manifestation of both apoptosis and necrosis (**Figures 1E,F** and Supplementary Figures S1D–F). Conclusively, the R1398L^{RCK} mutant displayed reduced cytotoxicity, which was not due to decreased stability or expression of this variant as shown by immunoblots decorated with an antibody against the C-terminal V5 tag of the proteins (**Figure 1G**). In addition, these experiments revealed the presence of dimeric and trimeric species of LRRK2^{RCK} variants already on day 1 (**Figure 1G** and Supplementary Figure S1G).

Thus, LRRK2^{RCK} triggers age-dependent cell death that can be partly prevented by a mutation conferring increased GTPase activity and, comparable to full-length LRRK2 in mammalian cells (Islam and Moore, 2017), dimerizes in yeast.

LRRK2^{RCK} Localizes to Mitochondria and the Plasma Membrane

A broad cellular localization has been reported for LRRK2, ranging from microtubules, membranes and diverse vesicular structures to mitochondria (Biskup et al., 2006; Berger et al., 2010; Ramírez et al., 2017). We analyzed the localization of C-terminally mCherry-tagged LRRK2^{RCK} and R1398L^{RCK} in yeast strains expressing endogenously GFP-tagged marker proteins for different organelles with three-dimensional confocal laser scanning microscopy. In accordance with its localization in higher eukaryotic cells, we find a portion of LRRK2^{RCK} (and of the R1398L^{RCK} variant) associated with the plasma membrane, as revealed by simultaneous visualization of GFP-labeled Pma1, the major plasma membrane H^+-ATPase (**Figure 2A**). However, the majority of LRRK2^{RCK} accumulated at intracellular structures that neither co-localized with vacuoles, visible due to the transport of Pma1-GFP to the vacuole for subsequent degradation (Chang and Fink, 1995; Henderson et al., 2014; **Figure 2A**), nor the nucleus, visualized by a histone-GFP chimera (Supplementary Figure S2A). Instead, these structures co-localized with Om45, a protein of the outer mitochondrial membrane (**Figure 2B**). Quantitative analysis of microscopic pictures confirmed that the majority of the LRRK2^{RCK}-mCherry signal overlapped with the Om45-GFP signal (M2 = 0.74) and, to a lower extend, also with Pma1-GFP (M2 = 0.17, please see Supplementary Figure S2B for detailed quantification). Of note, Pma1 exhibited a raft-like distribution at the plasma membrane as shown in **Figure 2A** and reported previously (Spira et al., 2012). While also LRRK2^{RCK} localized in distinct clusters at the plasma membrane (**Figure 2A**), Pma1 and LRRK2^{RCK} spots appeared rather separated and the quantification of Pma1 and LRRK2^{RCK} colocalization might thus underestimate the actual portion of this protein at the plasma membrane. In line with studies reporting severe impairment of mitochondrial morphology upon expression of full-length LRRK2 or its pathogenic variants (Ramonet et al., 2011; Su and Qi, 2013), the yeast mitochondrial network appeared fragmented and aggregated upon LRRK2^{RCK} expression (**Figure 2B**). Next, we subjected cells expressing V5-tagged LRRK2^{RCK} to subcellular fractionation. LRRK2^{RCK} showed a broad distribution, and the most prominent bands were detectable in mitochondrial and plasma membrane fractions, confirming the microscopy results (**Figure 2C**). Furthermore, we could detect LRRK2^{RCK} in isolated mitochondria (**Figure 2D**). Treatment of these

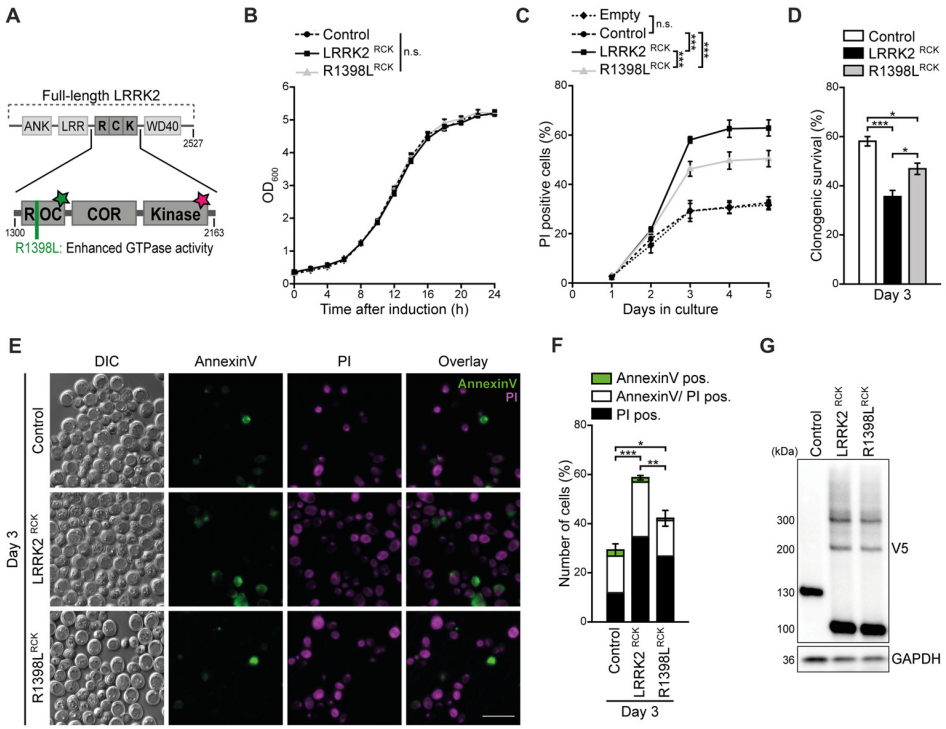

FIGURE 1 | LRRK2^{RCK} triggers death of aging yeast cells. **(A)** Scheme of truncated leucine-rich repeat kinase 2 (LRRK2) constructs used in this study. The enzymatic core of human LRRK2 (amino acids 1300–2163) containing the Ras-of-complex (ROC) GTPase, the C-terminal-of-ROC (COR) and the protein kinase domain, was expressed in yeast cells during chronological aging under the control of a GAL1 promoter. The wild type form of truncated LRRK2 (hereinafter referred as LRRK2^{RCK}) and the point mutant R1398L^{RCK} with higher GTPase activity were used. The green star indicates GTPase activity, the star in magenta represents kinase activity. **(B)** Growth of control cells expressing LacZ compared to cells expressing LRRK2^{RCK} and the R1398L^{RCK} variant. OD_{600} was measured in intervals of 2 h starting from the induction of galactose-driven expression. Means ± SEM; $n = 4$. **(C)** Flow cytometric quantification of loss of membrane integrity as indicated with propidium iodide (PI) staining of cells as described in **(B)**. In addition, cells harboring the empty vector were analyzed to validate the suitability of LacZ expression as a control. Significances represent simple main effects between different expression types at each time point. Significances shown are valid for day 3–5. Means ± SEM; $n = 4$. **(D)** Clonogenic survival on day 3 of chronological aging determined by counting colony forming units (cfu) after plating 500 cells with indicated expression types on YEPD agar plates. Means ± SEM; $n = 8$. **(E,F)** AnnexinV/PI co-staining on day 3 of aging. Representative epifluorescence micrographs **(E)** and flow cytometric quantification **(F)** are shown. Scale bar represents 10 μm. Means ± SEM; $n = 4$. For AnnexinV/PI staining at earlier time points, please see Supplementary Figures S1D,E. **(G)** Immunoblot analysis of protein extracts from cells as described in **(B)**. Blots were probed with antibodies directed against the V5-epitope to detect V5-tagged LacZ, LRRK2^{RCK} and R1398L^{RCK}, and against glyceraldehyde 3-phosphate dehydrogenase (GAPDH) as a loading control. $^{***}p < 0.001$, $^{**}p < 0.01$, $^{*}p < 0.05$, n.s. not significant.

mitochondrial fractions with proteinase K demonstrated that LRRK2^{RCK}, similar to the intermembrane space (IMS) control protein Mcr1, was not accessible to the protease, indicating that LRRK2^{RCK} resides within mitochondria. In sum, these data suggest an association of LRRK2^{RCK} with the plasma membrane and mitochondria.

Mitochondrial Function Is Impaired Upon LRRK2^{RCK} Expression

We further analyzed mitochondrial functionality in respect to respiration, generation of ROS and transmembrane potential. Measurement of cellular oxygen consumption via a Fire-Sting optical oxygen sensor system revealed a drop of respiration caused by LRRK2^{RCK} on day 2. While control cells displayed a massive increase in oxygen consumption with progressing age, reflecting the induction of the aerobic metabolism after the diauxic shift, this boost in respiration was reduced in cells expressing LRRK2^{RCK} (**Figure 3A**). The ROS-driven conversion of non-fluorescent dihydroethidium (DHE) to fluorescent ethidium (Eth) demonstrated that enhanced oxygen consumption of control cells was accompanied by an increase in oxidative stress (**Figure 3B**). While LRRK2^{RCK} expressing cells exhibited lower respiratory activity, the production of ROS was still enhanced compared to control cells on day 2, suggesting a dysfunction in oxidative phosphorylation. Dead cells, which randomly accumulate the dye, were excluded from the analysis as depicted in **Figure 3C**. Quantification of total cellular ATP content revealed reduced ATP levels upon prolonged expression of LRRK2^{RCK} (**Figure 3D**). The R1398L point mutation mitigated the LRRK2^{RCK}-driven effects on respiration, oxidative stress and cellular ATP levels (**Figures 3A–D**). Moreover, mitochondrial transmembrane potential ($\Delta\Psi_m$) assessed by microscopy and flow cytometry on day 2 of aging was reduced upon LRRK2^{RCK} expression, whereas these changes were less pronounced in R1398L^{RCK} expressing cells (**Figures 3E,F**).

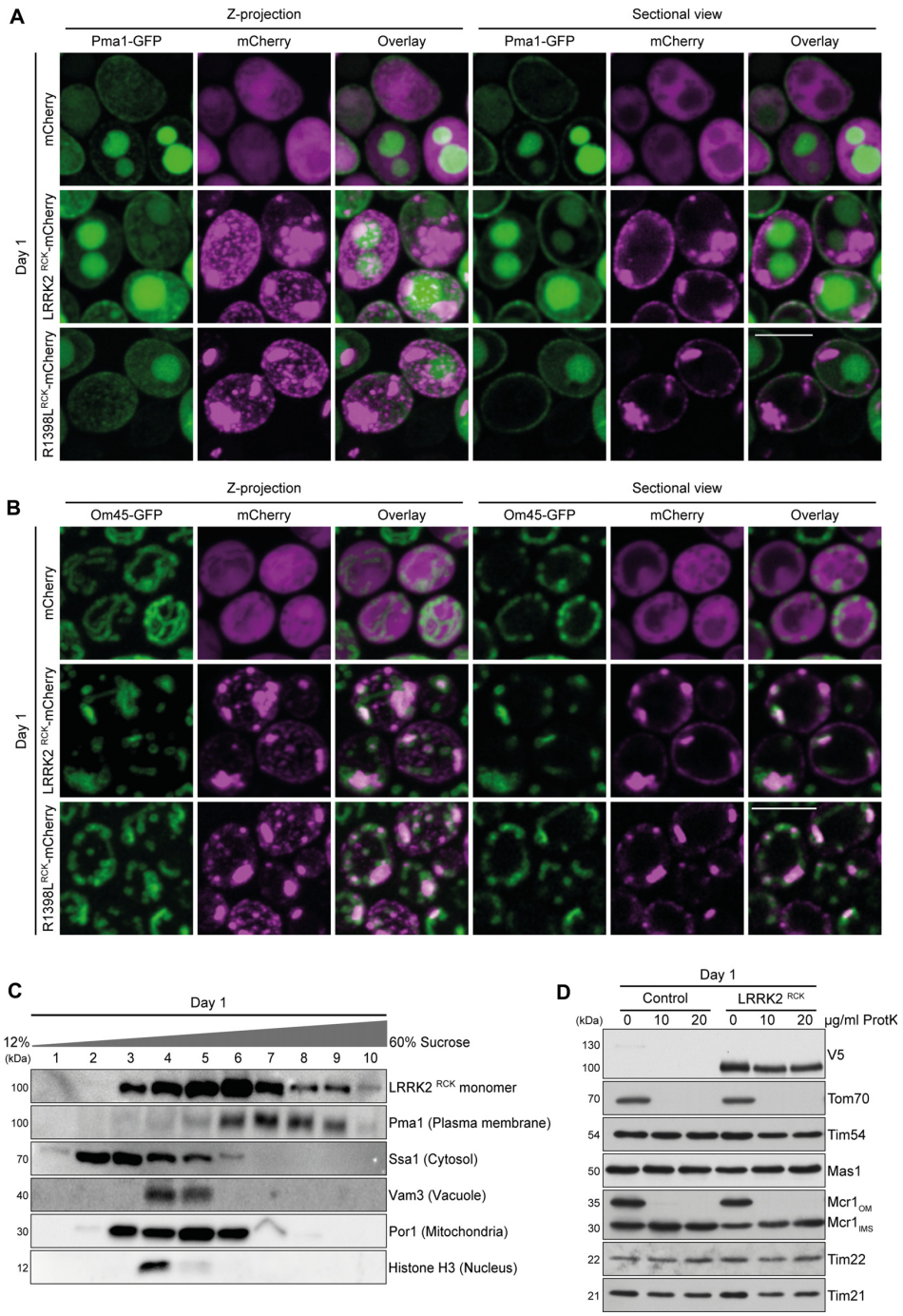

FIGURE 2 | LRRK2^{RCK} localizes in mitochondria and at the plasma membrane. **(A)** Representative confocal micrographs of strains harboring endogenously green fluorescent protein (GFP)-tagged Pma1 expressing mCherry alone or fused to LRRK2^{RCK} and R1398L^{RCK} on day 1 of aging. Z-projections of three-dimensional stacks as well as a representative section are shown. Scale bar represents 5 µm. For quantification of colocalization and confocal micrographs of strains harboring GFP-tagged Htb2, please see Supplementary Figures S2A,B. **(B)** Representative confocal micrographs of strains harboring endogenously GFP-tagged Om45, expressing the constructs as described in **(A)**. Z-projections of three-dimensional stacks as well as a representative section are shown. Scale bar represents 5 µm. For quantification of colocalization please see Supplementary Figure S2B. **(C)** Representative immunoblots of subcellular fractionation of whole cell extracts on 12%–60% step sucrose gradients. Collected fractions were analyzed by immunoblotting. Blots were probed with antibodies directed against the V5-epitope to detect V5-tagged LRRK2^{RCK}, and against organelle-specific marker proteins as indicated. **(D)** Immunoblot analysis of purified mitochondria obtained from cells expressing LRRK2^{RCK} or LacZ on day 1. Prior to SDS-PAGE, samples were treated with depicted concentrations of proteinase K (ProtK). Blots were probed with antibodies directed against the V5-epitope, the outer mitochondrial membrane protein Tom70, the inner mitochondrial membrane proteins Tim54, Tim22 and Tim21, the mitochondrial matrix localized protease Mas1, as well as Mcr1, located in the outer membrane (OM) and intermembrane space (IMS).

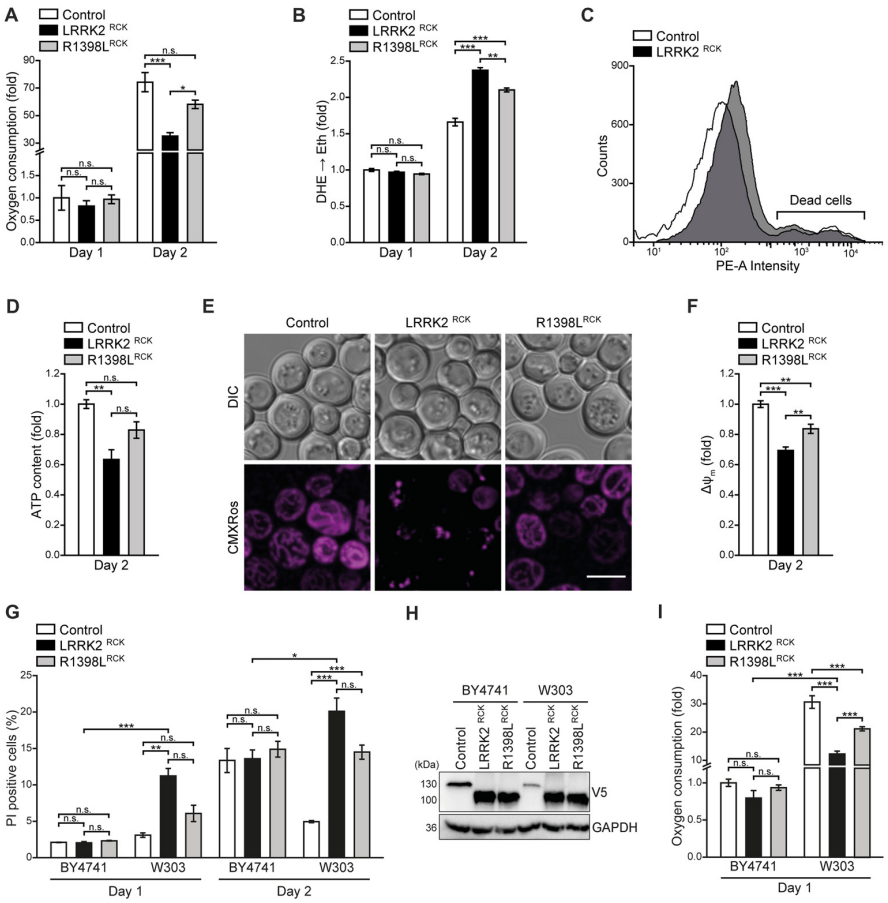

FIGURE 3 | LRRK2^{RCK} impairs mitochondrial function. **(A)** Oxygen consumption determined with a Fire-Sting optical oxygen sensor system in cells expressing LacZ, LRRK2^{RCK} or R1398L^{RCK} on day 1 and 2 of aging. Oxygen consumption was normalized to living cells and subsequently depicted as fold of control cells. Means ± SEM; $n = 4$. **(B,C)** Flow cytometric quantification of the reactive oxygen species (ROS)-driven conversion of non-fluorescent dihydroethidium (DHE) to fluorescent ethidium (Eth) in cells described in **(A)**. Mean fluorescence intensities are shown as fold of control cells on day 1 **(B)**. Dead cells, which accumulated Eth due to a loss of membrane integrity, were excluded from the analysis as shown in **(C)**. Means ± SEM; $n = 4$. **(D)** Quantification of ATP content from cells described in **(A)** on day 2 of aging. Values were normalized to living cells and subsequently depicted as fold of control cells. Means ± SEM; $n = 4$. **(E,F)** Analysis of the mitochondrial transmembrane potential ($\Delta\Psi_m$) with Mitotracker CMXRos on day 2 of aging. Representative confocal micrographs **(E)** and flow cytometric quantification of the mean fluorescence intensity **(F)** are shown. Values for $\Delta\Psi_m$ were normalized to control cells. Scale bar represents 5 μm. Means ± SEM; $n = 4$. **(G)** Flow cytometric quantification of loss of membrane integrity as indicated with PI staining of BY4741 and W303 strains expressing LacZ, LRRK2^{RCK} or R1398L^{RCK} on day 1 and day 2 of aging. Means ± SEM; $n = 4$. **(H)** Immunoblot analysis of protein extracts from cells as described in **(G)**. Blots were probed with antibodies directed against the V5-epitope and against GAPDH as loading control. **(I)** Oxygen consumption determined with a Fire-Sting optical oxygen sensor system in cells as described in **(G)** on day 1 of aging experiments. Normalization was performed as described in **(A)**. Means ± SEM; $n = 4$. $^{***}p < 0.001$, $^{**}p < 0.01$, $^{*}p < 0.05$, n.s. not significant.

To further elucidate the relation between mitochondrial dysfunction and cell death caused by LRRK2^{RCK}, we compared the so-far used BY4741 strain to the more respiratory active strain W303. In the W303 background, LRRK2^{RCK} triggered cell death already on day 1, despite comparable LRRK2^{RCK} expression levels in BY4741 and W303 strains (**Figures 3G,H**). Respiration was increased 30-fold in control cells of the W303 strain compared to BY4741 control cells (**Figure 3I**), suggesting that cells with high respiratory activity are particularly sensitive to LRRK2^{RCK}. Again, the R1398L^{RCK} variant displayed reduced cytotoxicity. In sum, LRRK2^{RCK} disrupts mitochondrial respiration, leading to oxidative stress and energy depletion.

LRRK2^{RCK} Reduces Mitochondrial Abundance

The decrease in respiratory capacity and cellular ATP levels prompted us to analyze mitochondrial morphology and abundance at early time points during aging using microscopy and flow cytometry. While only a mild impairment of the mitochondrial appearance was visible after entry into stationary phase (Supplementary Figure S3A), we observed a severely aggregated and fragmented mitochondrial network on day 2 of LRRK2^{RCK} expression, thus preceding the onset of LRRK2^{RCK}-induced cell death (**Figure 4A**). These effects were again less prominent in cells expressing R1398L^{RCK}. Consistently, flow

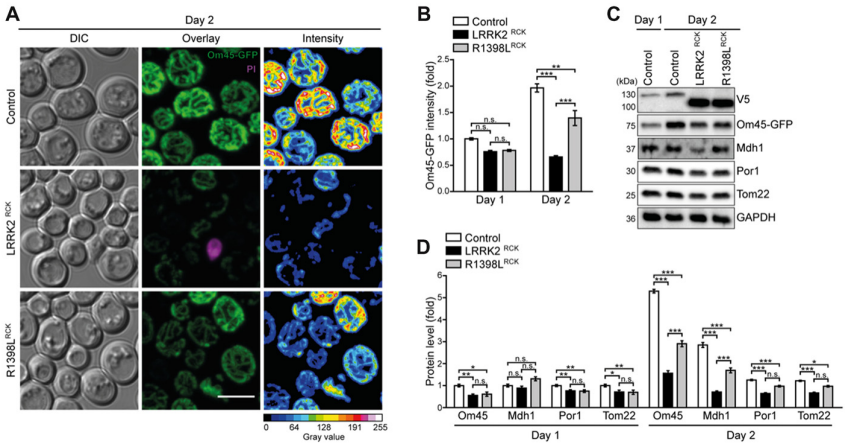

FIGURE 4 | Mitochondrial morphology and abundance is impaired by LRRK2^{RCK}. **(A,B)** Analysis of cells harboring endogenously GFP-tagged Om45 expressing LacZ, LRRK2^{RCK} or R1398L^{RCK}. Representative confocal micrographs on day 2 **(A)** and flow cytometric quantification of Om45-GFP fluorescence signal at day 1 and 2 **(B)** are shown. Dead cells were excluded via PI counterstaining. Values were normalized to control cells on day 1. Scale bar represents 5 μm. Means ± SEM; $n = 4$. For confocal micrographs of Om45-GFP strains on day 1, please see Supplementary Figure S3A. **(C,D)** Immunoblot analysis of extracts from cells as described in **(A)**. Representative immunoblots **(C)** and densitometric quantification **(D)** are shown. Blots were probed with antibodies directed against the V5- and the GFP-epitopes, against the mitochondrial proteins Mdh1, Por1 and Tom22, and against glyceraldehyde 3-phosphate dehydrogenase (GAPDH) as loading control. Values were normalized to the respective signals from control cells on day 1. Means ± SEM; $n \geq 6$. For immunoblot analysis of Om45-GFP cells on day 1, and of Tim44-GFP strains, please see Supplementary Figures S3B–E. $^{***}p < 0.001$, $^{**}p < 0.01$, $^{*}p < 0.05$, n.s. not significant.

cytometric quantification of Om45-GFP fluorescence intensity indicated a prominent reduction of mitochondrial mass starting on day 2 (**Figure 4B**). Control cells increased their Om45-GFP levels between day 1 and day 2, reflecting the augmentation of mitochondrial mass after the diauxic shift, when cells rely on respiration for energy production. This increase was absent in cells expressing LRRK2^{RCK}. Similar results were obtained using endogenously GFP-tagged Tim44, a component of the translocase of the inner mitochondrial membrane, as readout (Supplementary Figure S3B). Immunoblot analysis was used to determine the protein levels of Om45-GFP and Tim44-GFP and confirmed these results. The reduction of several additional mitochondrial proteins demonstrated a general decrease of mitochondrial abundance induced by LRRK2^{RCK}, again less prominent for the R1398L^{RCK} mutant (**Figures 4C,D**; for immunoblots on day 1 and quantification of Tim44-GFP levels, please see Supplementary Figures S3C–E), while the pathogenic G2019S^{RCK} variant impaired mitochondrial abundance to a similar extend than the wild type LRRK2^{RCK} (Supplementary Figures S4A,B).

The observed depletion of mitochondria might underlie the decrease in respiration and ATP levels, and our data points towards inefficient replenishment of the mitochondrial population when cells need to adapt their metabolism to respiration.

LRRK2^{RCK} Inhibits Mitochondrial Biogenesis

Reduced mitochondrial abundance upon LRRK2^{RCK} expression might be due to excessive mitochondrial degradation or to insufficient mitochondrial biosynthesis. To evaluate the contribution of increased mitochondrial degradation via selective autophagy (mitophagy) to mitochondrial depletion, we monitored Om45-GFP intensity as a readout for mitochondrial mass in strains lacking Atg11, an essential adapter protein for selective autophagic processes, including mitophagy. While the absence of Atg11 amplified mitochondrial mass in general, it did not affect the LRRK2^{RCK}-driven reduction of Om45-GFP signal, indicating that the loss of mitochondrial mass is not due to mitochondrial degradation via mitophagy (**Figure 5A**). Examining cytotoxicity in cells devoid of Atg11 as well as in strains lacking Atg32, a mitochondrial outer membrane (OM) protein crucial for the initiation of mitophagy, or Atg1, an essential component of the general autophagic machinery, demonstrated that LRRK2^{RCK}-mediated death of aging cells was unaltered in these mutants (**Figure 5B**). Next, we determined the levels of several mitochondria-related transcripts upon expression of LRRK2^{RCK}. This revealed a transcriptional downregulation of a diverse set of mitochondrial proteins, including *OM45*, the mitochondrial malate dehydrogenase *MDH1*, the porin *POR1*, and a subunit of respiratory chain complex IV, *COX4* (**Figure 5C**). The levels of *HAP4*, an important transcription factor required for reprogramming yeast cells from fermentation to respiration (Buschlen et al., 2003), were also reduced. Interestingly, we found LRRK2^{RCK} to upregulate mRNA levels for *PGC1* encoding the phosphatidylglycerol phospholipase C that regulates mitochondrial phosphatidylglycerol content to ensure proper mitochondrial function and morphology (Simocková et al., 2008; Pokorná et al., 2016). Thus, LRRK2^{RCK} does not affect mitophagic degradation but globally impairs mitochondrial biogenesis and this can, at least in part, be explained by changed transcription.

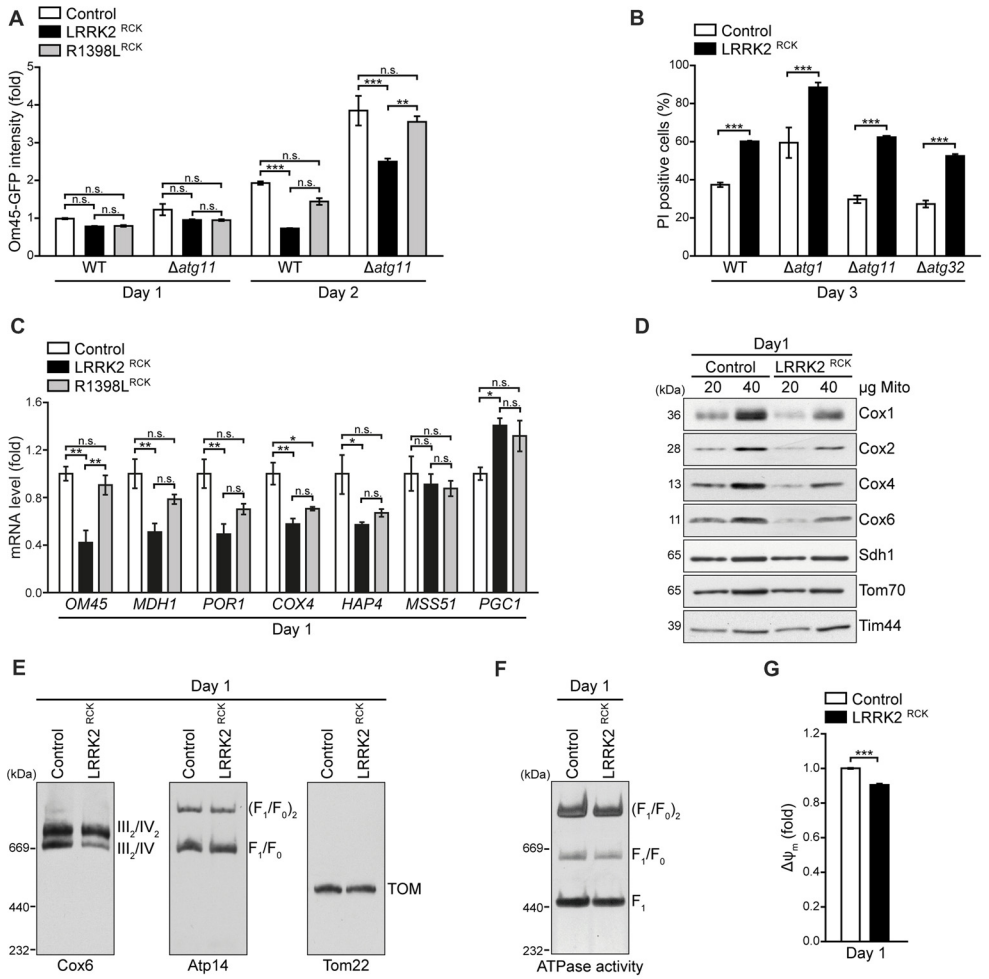

FIGURE 5 | LRRK2^{RCK} compromises mitochondrial biogenesis and complex IV assembly. **(A)** Flow cytometric quantification of wild type and *ATG11* deletion strains harboring Om45-GFP and expressing LacZ, LRRK2^{RCK} or R1398L^{RCK} on day 1 and 2 of aging. Dead cells were excluded via PI counterstaining. Values were normalized to control cells on day 1. Means ± SEM; $n = 4$. **(B)** Flow cytometric quantification of PI-stained wild type and *ATG1*, *ATG11* and *ATG32* deletion strains expressing LacZ or LRRK2^{RCK} on day 3 of aging. Means ± SEM; $n = 4$. **(C)** q-RT-PCR to determine mRNA levels of indicated mitochondria-related transcripts in cells expressing LacZ, LRRK2^{RCK} or R1398L^{RCK}. Normalization was performed using mRNA levels of *UBC6*. Means ± SEM; $n = 4$. **(D)** Immunoblot analysis of mitochondria isolated from cells expressing LacZ or LRRK2^{RCK} on day 1. Blots were probed with antibodies directed against the respiratory chain complex IV components Cox1, Cox2, Cox4 and Cox6, as well as Sdh1 (subunit of complex II), Tom70 (outer mitochondrial membrane) and Tim44 (inner mitochondrial membrane). **(E)** Immunoblots of Blue-Native-PAGE with samples described in **(D)**. Blots were probed with antibodies against Cox6 (complex III/IV), Atp14 (complex V) and Tom22 (translocase of outer membrane (TOM) complex). **(F)** In-gel ATPase activity assay of samples described in **(D)**. **(G)** Measurement of mitochondrial transmembrane potential ($\Delta\Psi_m$) in mitochondria isolated from cells described in **(D)**. Values for $\Delta\Psi_m$ were normalized to mitochondria from control cells. Means ± SEM; $n = 3$. $^{***}p < 0.001$, $^{**}p < 0.01$, $^{*}p < 0.05$, n.s. not significant.

LRRK2^{RCK} Causes Misassembly of the Respiratory Chain Complex IV

While the reduced respiration as well as the drop of ATP levels most probably arise from a general decrease in mitochondrial mass, the LRRK2^{RCK}-driven accumulation of ROS (**Figure 3B**) points to additional defects in oxidative phosphorylation in the residual mitochondrial population. Therefore, we purified mitochondria and analyzed the levels of mitochondrial proteins early after entry into the post-mitotic state (day 1). While the levels of Sdh1, a subunit of the respiratory chain complex II, and of Tom70 and Tim44 as outer and inner mitochondrial membrane proteins, respectively, were unchanged, we observed a reduction of all tested components of the respiratory chain complex IV (cytochrome c oxidase) upon LRRK2^{RCK} expression (**Figure 5D**). Moreover, Blue-Native PAGE demonstrated that LRRK2^{RCK} selectively impaired the assembly of complex IV. In contrast, the translocase of the outer membrane (TOM complex) as well as assembly and ATPase activity of complex V (mitochondrial F_1F_0 ATP synthase) were not affected by LRRK2^{RCK} (**Figures 5E,F**). Notably, while the outer mitochondrial membrane was intact (**Figure 2D**), mitochondria purified from cells expressing LRRK2^{RCK} displayed a slight dissipation of $\Delta\Psi_m$ compared to mitochondria from control cells (**Figure 5G**), most likely a

result of impaired complex IV assembly. Thus, already early during aging, LRRK2^{RCK} selectively compromises complex IV formation, with subsequent consequences for mitochondrial function and generation of ROS.

DISCUSSION

PD-associated neurotoxic consequences of LRRK2 are thought to be due to a gain-of-function of the protein, emanating from pathogenic mutations (e.g., G2019S with increased kinase activity) or from elevated protein loads, particularly found in brains of patients in early stages of PD (Dzamko et al., 2017). Mitochondrial dysfunction and reduced mitochondrial mass have been frequently reported upon dysregulation of LRRK2 and have mostly been attributed to excessive mitochondrial degradation (Cherra et al., 2013). Using aging yeast cells, we show that LRRK2^{RCK} diminishes mitochondrial biogenesis and provide insights into the progressive decline of mitochondrial function as a consequence of cellular age. While heterologous expression of LRRK2^{RCK} in proliferating yeast has been shown to arrest growth (Xiong et al., 2010), we established a model in which LRRK2^{RCK} does not affect proliferation but impacts cellular fitness in stationary phase, recapitulating the situation in post-mitotic cells such as neurons (Carmona-Gutierrez and Büttner, 2014).

Based on our findings, we propose the following sequence of events resulting in death of aging cells: LRRK2^{RCK} is targeted to mitochondria and causes a specific decrease in the levels of complex IV components. In consequence, complex IV is insufficiently assembled and $\Delta\Psi_m$ starts to dissipate, while the ATPase activity of complex V remains unaffected. Moreover, a transcriptional downregulation of diverse mitochondrial gene products becomes evident. This happens shortly after entry into a post-mitotic state, where cells induce the amplification of mitochondrial mass to adjust to the need for respiration as energy source. With progressing age, these early defects culminate in: (i) a reduction of mitochondrial mass, (ii) insufficient respiratory capacity, (iii) a further drop in $\Delta\Psi_m$, (iv) mitochondrial fragmentation, (v) decreased cellular ATP content, and (vi) oxidative stress. Ultimately, these LRRK2^{RCK}-mediated changes lead to cell death (**Figure 6**). While our results clearly link LRRK2^{RCK}-induced cellular demise to defects in complex IV and a reduction of mitochondrial biogenesis, further research is needed to establish the precise sequence of events. The complex IV deficiency might very well represent an early manifestation of the decrease in mitochondria-related gene transcripts, including *COX4*. Vice versa, it is also feasible that mitochondria-resident LRRK2^{RCK} directly targets complex IV and that this in turn activates mitochondria-to-nucleus signaling, thereby altering transcription.

So far, rather pleiotropic effects of LRRK2 on mitochondria were observed, ranging from no alteration of mitochondrial content but dissipation of $\Delta\Psi_m$ (Mortiboys et al., 2010; Papkovskaia et al., 2012) to a reduction of mitochondrial

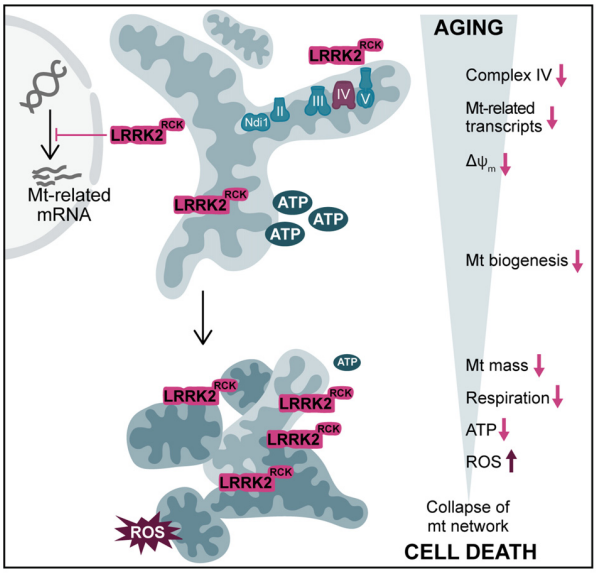

FIGURE 6 | Overview of LRRK2^{RCK}-induced mitochondrial dysfunction in yeast. In post-mitotic yeast cells, LRRK2^{RCK} (magenta) is targeted to mitochondria, leading to misassembly of respiratory chain complex IV (cytochrome c oxidase). Transcription of mitochondria (mt)-related gene products is reduced and a dissipation of the mitochondrial transmembrane potential ($\Delta\Psi_m$) can be observed. With increasing age, cells display a prominent decrease in mt mass and a concomitant drop in respiratory activity and ATP levels. In addition, mitochondrial dysfunction leads to enhanced production of ROS. This culminates in the collapse of the mt network, ultimately resulting in cell death.

mass within neurites via either increased retrograde trafficking (Schwab et al., 2017), decreased anterograde trafficking (Godena et al., 2014; Thomas et al., 2016), or excessive degradation of mitochondria via mitophagy (Cherra et al., 2013). Although, enforcing mitochondrial biogenesis via activation of the PGC-1α ortholog in *Drosophila melanogaster* resulted in a reduction of PD phenotypes induced by Parkin and LRRK2 (Ng et al., 2017), LRRK2-mediated effects on mitochondrial biogenesis remained unexplored. In our experiments, genetic inactivation of mitophagy did neither prevent the loss of mitochondrial mass nor cytotoxicity driven by LRRK2^{RCK}. Instead, we find a downregulation of various mitochondrial transcripts, including *HAP4*, the transcriptional activator of global respiratory gene expression. In consequence, this entails inefficient amplification of mitochondrial mass to increase respiratory capacity in stationary phase. These data establish inhibition of mitochondrial biogenesis rather than enhanced mitochondrial degradation as primary cause for the drop in mitochondrial abundance upon LRRK2^{RCK} expression.

Several studies show that LRRK2 influences transcription (Dorval and Hébert, 2012), but the mechanistic details of these changes and their contribution to PD pathology remain elusive. Interestingly, LRRK2-mediated transcriptional alterations are also associated with Crohn's disease, a type of inflammatory bowel disease (Liu et al., 2011), and LRRK2 alleles contributing to both PD and Crohn's

disease have been identified (Hui et al., 2018). Mice lacking LRRK2 display enhanced nuclear translocation of the nuclear factor of activated T cells (NFAT), suggesting that a physiological function of LRRK2 is to regulate the cellular distribution and thus activity of NFAT and that loss of this regulation contributes to the progression of Crohn's disease (Liu et al., 2011). In addition, genome-wide mRNA profiling identified transcriptional changes for both LRRK2 deficiency and pathogenic mutation, showing differential gene expression profiles for a wide range of cellular processes, including ribosomal/translational function, glycolysis, ubiquitination and oxidative phosphorylation (Nikonova et al., 2012). Thus, it is feasible that LRRK2 modulates the nuclear translocation or activity of distinct transcription factors, such as regulators of *HAP4*, resulting in decreased mitochondrial biogenesis. On the other hand, early and subtle mitochondrial damage by LRRK2 might interfere with the expression of mitochondria-encoded proteins, culminating in the observed complex IV misassembly which in consequence might also trigger a compensatory downregulation of nuclear-encoded mitochondria-related transcripts.

Whereas in proliferating yeast cells a cytosolic localization of $LRRK2^{RCK}$ has been reported (Xiong et al., 2010), we find $LRRK2^{RCK}$ and the $R1398L^{RCK}$ variant associated with mitochondria and the plasma membrane in post-mitotic cells, recapitulating the localization of full-length LRRK2 in higher eukaryotic systems (Biskup et al., 2006; Berger et al., 2010; Ramírez et al., 2017). While proteinase K treatment of isolated mitochondria suggests that $LRRK2^{RCK}$ resides within these organelles, this might also reflect proteinase K-resistant $LRRK2^{RCK}$ aggregates attached to the outer mitochondrial membrane. Further analyses are needed to determine the exact localization of distinct $LRRK2^{RCK}$ species in or at mitochondria and how this relates to decreased complex IV abundance and assembly. Interestingly, mRNA levels of the *PGC1* gene, which encodes a phosphatidylglycerol phospholipase, were upregulated in response to $LRRK2^{RCK}$ expression. Pgc1 is important to maintain balanced ratios of anionic phospholipids ensuring proper mitochondrial function and morphology, and deletion of *PGC1* has been shown to increase complex IV activity (Pokorná et al., 2016). Thus, the $LRRK2^{RCK}$-mediated upregulation of *PGC1* might contribute to the misassembly of complex IV in aging yeast.

Notably, while the $G2019S^{RCK}$ variant triggered cell death comparable to the wild type form of $LRRK2^{RCK}$, the $R1398L^{RCK}$ point mutant displayed decreased cytotoxicity, indicating a cytoprotective role of high GTPase activity (Xiong et al., 2010; Biosa et al., 2013; Nguyen and Moore, 2017). Though genetic variations at the R1398 site have been shown to decrease the risk to develop PD (Ross et al., 2011; Heckman et al., 2014), the differential contribution of the two enzymatic activities of LRRK2 to the neurodegenerative processes during PD is not fully understood and might be rather complex. GTP-binding as well as GTP-hydrolysis of the ROC domain has been shown to regulate kinase activity, and vice versa, the kinase of LRRK2 autophosphorylates distinct sites in the ROC domain, thereby driving GTP-hydrolysis (Biosa et al., 2013). In addition, this intricate regulation of the two catalytic functions is likely modulated by distinct effector proteins and the specific cellular context (Liu et al., 2018). Interestingly, LRRK2 toxicity in neurons depends on the presence of α-synuclein (Skibinski et al., 2014), and vice versa rats devoid of LRRK2 are more vulnerable to dopaminergic neurodegeneration caused by high levels of α-synuclein (Daher et al., 2014), providing evidence for an interplay between these two PD-associated proteins and a function of LRRK2 that can counteract α-synuclein-associated neurodegeneration. As α-synuclein also has been shown to compromise mitochondrial function, the modulation of mitochondrial biogenesis via LRRK2 might thus impact distinct aspects of α-synuclein-driven cellular demise.

In sum, we show that inhibition of mitochondrial biogenesis rather than increased mitochondrial degradation is causative for the $LRRK2^{RCK}$-mediated decline in mitochondrial mass. With progressing cellular age, $LRRK2^{RCK}$ triggers a sequence of events that includes distinct transcriptional alterations and a drop in complex IV abundance, followed by a decrease in mitochondrial transmembrane potential and respiration, accumulation of ROS and a breakdown of the mitochondrial network, ultimately resulting in cell death.

AUTHOR CONTRIBUTIONS

AA, VK and SB conceptualized the study and analyzed the data and wrote the manuscript. AA, VK, CW, ST-C and LH performed the experiments. F-NV and WK analyzed and discussed the data and gave conceptual advice. SB supervised the study. All authors commented on the manuscript, read and approved the final version.

FUNDING

This work was supported by the Austrian Science Fund FWF (P27183-B24 to SB and P27383-B2 to WK), the Swedish Research Council Vetenskapsrådet (2015-05468), Åke Wiberg Stiftelse (M16-0130), Carl Tryggers Stiftelse för Vetenskaplig Forskning (CTS16:85), Deutsche Forschungsgemeinschaft (RTG 2202 to CW), and the Emmy Noether Programm (to F-NV). We thank Tobias Eisenberg for help with statistical analysis, Claes Andréasson and Chris Meisinger for critical reading of the manuscript and Darren J. Moore for sharing LRRK2 plasmids.

SUPPLEMENTARY MATERIAL

The Supplementary Material for this article can be found online at: https://www.frontiersin.org/articles/10.3389/fnmol.2018.00205/full#supplementary-material

REFERENCES

Aranda, P. S., LaJoie, D. M., and Jorcyk, C. L. (2012). Bleach gel: a simple agarose gel for analyzing RNA quality. *Electrophoresis* 33, 366–369. doi: 10.1002/elps.201100335

Aufschnaiter, A., Habernig, L., Kohler, V., Diessl, J., Carmona-Gutierrez, D., Eisenberg, T., et al. (2017). The coordinated action of calcineurin and cathepsin D protects against α-synuclein toxicity. *Front. Mol. Neurosci.* 10:207. doi: 10.3389/fnmol.2017.00207

Berger, Z., Smith, K. A., and Lavoie, M. J. (2010). Membrane localization of LRRK2 is associated with increased formation of the highly active lrrk2 dimer and changes in its phosphorylation. *Biochemistry* 49, 5511–5523. doi: 10.1021/bi100157u

Biosa, A., Trancikova, A., Civiero, L., Glauser, L., Bubacco, L., Greggio, E., et al. (2013). GTPase activity regulates kinase activity and cellular phenotypes of Parkinson's disease-associated LRRK2. *Hum. Mol. Genet.* 22, 1140–1156. doi: 10.1093/hmg/dds522

Biskup, S., Moore, D. J., Celsi, F., Higashi, S., West, A. B., Andrabi, S. A., et al. (2006). Localization of LRRK2 to membranous and vesicular structures in mammalian brain. *Ann. Neurol.* 60, 557–569. doi: 10.1002/ana.21019

Bolte, S., and Cordelières, F. P. (2006). A guided tour into subcellular colocalization analysis in light microscopy. *J. Microsc.* 224, 213–232. doi: 10.1111/j.1365-2818.2006.01706.x

Braun, R. J., Büttner, S., Ring, J., Kroemer, G., and Madeo, F. (2010). Nervous yeast: modeling neurotoxic cell death. *Trends Biochem. Sci.* 35, 135–144. doi: 10.1016/j.tibs.2009.10.005

Buschlen, S., Amillet, J. M., Guiard, B., Fournier, A., Marcireau, C., and Bolotin-Fukuhara, M. (2003). The *S. cerevisiae* HAP complex, a key regulator of mitochondrial function, coordinates nuclear and mitochondrial gene expression. *Comp. Funct. Genomics* 4, 37–46. doi: 10.1002/cfg.254

Büttner, S., Eisenberg, T., Carmona-Gutierrez, D., Ruli, D., Knauer, H., Ruckenstuhl, C., et al. (2007). Endonuclease G regulates budding yeast life and death. *Mol. Cell* 25, 233–246. doi: 10.1016/j.molcel.2006.12.021

Büttner, S., Ruli, D., Vögtle, F.-N., Galluzzi, L., Moitzi, B., Eisenberg, T., et al. (2011). A yeast BH3-only protein mediates the mitochondrial pathway of apoptosis. *EMBO J.* 30, 2779–2792. doi: 10.1038/emboj.2011.197

Carmona-Gutierrez, D., and Büttner, S. (2014). The many ways to age for a single yeast cell. *Yeast* 31, 289–298. doi: 10.1002/yea.3020

Chang, A., and Fink, G. R. (1995). Targeting of the yeast plasma membrane [H+]ATPase: a novel gene AST1 prevents mislocalization of mutant ATPase to the vacuole. *J. Cell Biol.* 128, 39–49. doi: 10.1083/jcb.128.1.39

Chen, L., Zhang, S., Liu, Y., Hong, H., Wang, H., Zheng, Y., et al. (2011). LRRK2 R1398H polymorphism is associated with decreased risk of Parkinson's disease in a Han Chinese population. *Parkinsonism Relat. Disord.* 17, 291–292. doi: 10.1016/j.parkreldis.2010.11.012

Cherra, S. J., Steer, E., Gusdon, A. M., Kiselyov, K., and Chu, C. T. (2013). Mutant LRRK2 elicits calcium imbalance and depletion of dendritic mitochondria in neurons. *Am. J. Pathol.* 182, 474–484. doi: 10.1016/j.ajpath.2012.10.027

Cooper, O., Seo, H., Andrabi, S., Guardia-Laguarta, C., Graziotto, J., Sundberg, M., et al. (2012). Pharmacological rescue of mitochondrial deficits in iPSC-derived neural cells from patients with familial Parkinson's disease. *Sci. Transl. Med.* 4:141ra90. doi: 10.1126/scitranslmed.3003985

Daher, J. P. L., Volpicelli-Daley, L. A., Blackburn, J. P., Moehle, M. S., and West, A. B. (2014). Abrogation of α-synuclein-mediated dopaminergic neurodegeneration in LRRK2-deficient rats. *Proc. Natl. Acad. Sci. U S A* 111, 9289–9294. doi: 10.1073/pnas.1403215111

Dorval, V., and Hébert, S. S. (2012). LRRK2 in transcription and translation regulation: relevance for Parkinson's disease. *Front. Neurol.* 3:12. doi: 10.3389/fneur.2012.00012

Dzamko, N., Gysbers, A. M., Bandopadhyay, R., Bolliger, M. F., Uchino, A., Zhao, Y., et al. (2017). LRRK2 levels and phosphorylation in Parkinson's disease brain and cases with restricted Lewy bodies. *Mov. Disord.* 32, 423–432. doi: 10.1002/mds.26892

Gietz, R. D., and Woods, R. A. (2002). Transformation of yeast by lithium acetate/single-stranded carrier DNA/polyethylene glycol method. *Meth. Enzymol.* 350, 87–96. doi: 10.1016/s0076-6879(02)50957-5

Godena, V. K., Brookes-Hocking, N., Moller, A., Shaw, G., Oswald, M., Sancho, R. M., et al. (2014). Increasing microtubule acetylation rescues axonal transport and locomotor deficits caused by LRRK2 Roc-COR domain mutations. *Nat. Commun.* 5:5245. doi: 10.1038/ncomms6245

Heckman, M. G., Elbaz, A., Soto-Ortolaza, A. I., Serie, D. J., Aasly, J. O., Annesi, G., et al. (2014). The protective effect of LRRK2 p.R1398H on risk of Parkinson's disease is independent of MAPT and SNCA variants. *Neurobiol. Aging* 35, 266.e5–266.e14. doi: 10.1016/j.neurobiolaging.2013.07.013

Henderson, K. A., Hughes, A. L., and Gottschling, D. E. (2014). Mother-daughter asymmetry of pH underlies aging and rejuvenation in yeast. *Elife* 3:e03504. doi: 10.7554/eLife.03504

Hernandez, D. G., Reed, X., and Singleton, A. B. (2016). Genetics in Parkinson disease: mendelian versus non-mendelian inheritance. *J. Neurochem.* 139, 59–74. doi: 10.1111/jnc.13593

Hui, K. Y., Fernandez-Hernandez, H., Hu, J., Schaffner, A., Pankratz, N., Hsu, N.-Y., et al. (2018). Functional variants in the LRRK2 gene confer shared effects on risk for Crohn's disease and Parkinson's disease. *Sci. Transl. Med.* 10:eaai7795. doi: 10.1126/scitranslmed.aai7795

Islam, M. S., and Moore, D. J. (2017). Mechanisms of LRRK2-dependent neurodegeneration: role of enzymatic activity and protein aggregation. *Biochem. Soc. Trans.* 45, 163–172. doi: 10.1042/BST20160264

Janke, C., Magiera, M. M., Rathfelder, N., Taxis, C., Reber, S., Maekawa, H., et al. (2004). A versatile toolbox for PCR-based tagging of yeast genes: new fluorescent proteins, more markers and promoter substitution cassettes. *Yeast* 21, 947–962. doi: 10.1002/yea.1142

Klasson, H., Fink, G. R., and Ljungdahl, P. O. (1999). Ssy1p and Ptr3p are plasma membrane components of a yeast system that senses extracellular amino acids. *Mol. Cell. Biol.* 19, 5405–5416. doi: 10.1128/mcb.19.8.5405

Klein, C., and Westenberger, A. (2012). Genetics of Parkinson's disease. *Cold Spring Harb. Perspect. Med.* 2:a008888. doi: 10.1101/cshperspect.a008888

Larsen, S. B., Hanss, Z., and Krüger, R. (2018). The genetic architecture of mitochondrial dysfunction in Parkinson's disease. *Cell Tissue Res.* doi: 10.1007/s00441-017-2768-8 [Epub ahead of print].

Liu, Z., Bryant, N., Kumaran, R., Beilina, A., Abeliovich, A., Cookson, M. R., et al. (2018). LRRK2 phosphorylates membrane-bound Rabs and is activated by GTP-bound Rab7L1 to promote recruitment to the trans-Golgi network. *Hum. Mol. Genet.* 27, 385–395. doi: 10.1093/hmg/ddx410

Liu, Z., Lee, J., Krummey, S., Lu, W., Cai, H., and Lenardo, M. J. (2011). The kinase LRRK2 is a regulator of the transcription factor NFAT that modulates the severity of inflammatory bowel disease. *Nat. Immunol.* 12, 1063–1070. doi: 10.1038/ni.2113

Livak, K. J., and Schmittgen, T. D. (2001). Analysis of relative gene expression data using real-time quantitative PCR and the 2-ΔΔCT method. *Methods* 25, 402–408. doi: 10.1006/meth.2001.1262

Meisinger, C., Pfanner, N., and Truscott, K. N. (2006). "Isolation of yeast mitochondria," in *Yeast Protocols*, ed. W. Xiao (New Jersey, NJ: Humana Press), 33–40.

Mortiboys, H., Johansen, K. K., Aasly, J. O., and Bandmann, O. (2010). Mitochondrial impairment in patients with Parkinson disease with the G2019S mutation in LRRK2. *Neurology* 75, 2017–2020. doi: 10.1212/WNL.0b013e3181ff9685

Ng, C. H., Basil, A. H., Hang, L., Tan, R., Goh, K. L., O'Neill, S., et al. (2017). Genetic or pharmacological activation of the *Drosophila* PGC-1α ortholog spargel rescues the disease phenotypes of genetic models of Parkinson's disease. *Neurobiol. Aging* 55, 33–37. doi: 10.1016/j.neurobiolaging.2017.03.017

Nguyen, A. P. T., and Moore, D. J. (2017). Understanding the GTPase activity of LRRK2: regulation, function, and neurotoxicity. *Adv. Neurobiol.* 14, 71–88. doi: 10.1007/978-3-319-49969-7_4

Nikonova, E. V., Xiong, Y., Tanis, K. Q., Dawson, V. L., Vogel, R. L., Finney, E. M., et al. (2012). Transcriptional responses to loss or gain of function of the leucine-rich repeat kinase 2 (LRRK2) gene uncover biological processes modulated by LRRK2 activity. *Hum. Mol. Genet.* 21, 163–174. doi: 10.1093/hmg/ddr451

Oliveira, A. V., Vilaça, R., Santos, C. N., Costa, V., and Menezes, R. (2017). Exploring the power of yeast to model aging and age-related neurodegenerative disorders. *Biogerontology* 18, 3–34. doi: 10.1007/s10522-016-9666-4

Papkovskaia, T. D., Chau, K.-Y., Inesta-Vaquera, F., Papkovsky, D. B., Healy, D. G., Nishio, K., et al. (2012). G2019S leucine-rich repeat kinase 2 causes uncoupling protein-mediated mitochondrial depolarization. *Hum. Mol. Genet.* 21, 4201–4213. doi: 10.1093/hmg/dds244

Parker, W. D., Parks, J. K., and Swerdlow, R. H. (2008). Complex I deficiency in Parkinson's disease frontal cortex. *Brain Res.* 1189, 215–218. doi: 10.1016/j.brainres.2007.10.061

Pokorná, L., Čermáková, P., Horváth, A., Baile, M. G., Claypool, S. M., Griač, P., et al. (2016). Specific degradation of phosphatidylglycerol is necessary for proper mitochondrial morphology and function. *Biochim. Biophys. Acta* 1857, 34–45. doi: 10.1016/j.bbabio.2015.10.004

Ramírez, M. B., Lara Ordóñez, A. J., Fdez, E., Madero-Pérez, J., Gonnelli, A., Drouyer, M., et al. (2017). GTP binding regulates cellular localization of Parkinson's disease-associated LRRK2. *Hum. Mol. Genet.* 26, 2747–2767. doi: 10.1093/hmg/ddx161

Ramonet, D., Daher, J. P. L., Lin, B. M., Stafa, K., Kim, J., Banerjee, R., et al. (2011). Dopaminergic neuronal loss, reduced neurite complexity and autophagic abnormalities in transgenic mice expressing G2019S mutant LRRK2. *PLoS One* 6:e18568. doi: 10.1371/journal.pone.0018568

Ross, O. A., Soto-Ortolaza, A. I., Heckman, M. G., Aasly, J. O., Abahuni, N., Annesi, G., et al. (2011). Association of LRRK2 exonic variants with susceptibility to Parkinson's disease: a case-control study. *Lancet. Neurol.* 10, 898–908. doi: 10.1016/S1474-4422(11)70175-2

Schapira, A. H. V., Cooper, J. M., Dexter, D., Clark, J. B., Jenner, P., and Marsden, C. D. (1990). Mitochondrial complex I deficiency in Parkinson's disease. *J. Neurochem.* 54, 823–827. doi: 10.1111/j.1471-4159.1990.tb02325.x

Schindelin, J., Arganda-Carreras, I., Frise, E., Kaynig, V., Longair, M., Pietzsch, T., et al. (2012). Fiji: an open-source platform for biological-image analysis. *Nat. Methods* 9, 676–682. doi: 10.1038/nmeth.2019

Schwab, A. J., Sison, S. L., Meade, M. R., Broniowska, K. A., Corbett, J. A., and Ebert, A. D. (2017). Decreased sirtuin deacetylase activity in LRRK2 G2019S iPSC-derived dopaminergic neurons. *Stem Cell Reports* 9, 1839–1852. doi: 10.1016/j.stemcr.2017.10.010

Simocková, M., Holic, R., Tahotná, D., Patton-Vogt, J., and Griac, P. (2008). Yeast Pgc1p (YPL206c) controls the amount of phosphatidylglycerol via a phospholipase C-type degradation mechanism. *J. Biol. Chem.* 283, 17107–17115. doi: 10.1074/jbc.M800868200

Skibinski, G., Nakamura, K., Cookson, M. R., and Finkbeiner, S. (2014). Mutant LRRK2 toxicity in neurons depends on LRRK2 levels and synuclein but not kinase activity or inclusion bodies. *J. Neurosci.* 34, 418–433. doi: 10.1523/JNEUROSCI.2712-13.2014

Spira, F., Mueller, N. S., Beck, G., von Olshausen, P., Beig, J., and Wedlich-Söldner, R. (2012). Patchwork organization of the yeast plasma membrane into numerous coexisting domains. *Nat. Cell Biol.* 14, 640–648. doi: 10.1038/ncb2487

Su, Y. C., and Qi, X. (2013). Inhibition of excessive mitochondrialfissionreduced aberrant autophagy and neuronal damage caused by LRRK2 G2019S mutation. *Hum. Mol. Genet.* 22, 4545–4561. doi: 10.1093/hmg/ddt301

Tenreiro, S., Franssens, V., Winderickx, J., and Outeiro, T. F. (2017). Yeast models of Parkinson's disease-associated molecular pathologies. *Curr. Opin. Genet. Dev.* 44, 74–83. doi: 10.1016/j.gde.2017.01.013

Thomas, B., and Beal, M. F. (2007). Parkinson's disease. *Hum. Mol. Genet.* 16, R183–R194. doi: 10.1093/hmg/ddm159

Thomas, J. M., Li, T., Yang, W., Xue, F., Fishman, P. S., and Smith, W. W. (2016). 68 and FX2149 attenuate mutant LRRK2–R1441C-induced neural transport impairment. *Front. Aging Neurosci.* 8:337. doi: 10.3389/fnagi.2016.00337

Wallings, R., Manzoni, C., and Bandopadhyay, R. (2015). Cellular processes associated with LRRK2 function and dysfunction. *FEBS J.* 282, 2806–2826. doi: 10.1111/febs.13305

West, A. B., Moore, D. J., Biskup, S., Bugayenko, A., Smith, W. W., Ross, C. A., et al. (2005). Parkinson's disease-associated mutations in leucine-rich repeat kinase 2 augment kinase activity. *Proc. Natl. Acad. Sci. U S A* 102, 16842–16847. doi: 10.1073/pnas.0507360102

Xiong, Y., Coombes, C. E., Kilaru, A., Li, X., Gitler, A. D., Bowers, W. J., et al. (2010). GTPase activity plays a key role in the pathobiology of LRRK2. *PLoS Genet.* 6:e1000902. doi: 10.1371/journal.pgen.1000902

Conflict of Interest Statement: The authors declare that the research was conducted in the absence of any commercial or financial relationships that could be construed as a potential conflict of interest.

frontiers in Molecular Neuroscience

REVIEW
published: 28 June 2018
doi: 10.3389/fnmol.2018.00218

Yeast as a Model to Unravel Mechanisms Behind FUS Toxicity in Amyotrophic Lateral Sclerosis

Michelle Lindström[1] *and Beidong Liu*[1,2,3]*

[1]*Department of Chemistry and Molecular Biology, University of Gothenburg, Gothenburg, Sweden,* [2]*State Key Laboratory of Subtropical Silviculture, School of Forestry and Biotechnology, Zhejiang A&F University, Hangzhou, China,* [3]*Center for Large-scale cell-based screening, Faculty of Science, University of Gothenburg, Gothenburg, Sweden*

Fused in sarcoma (FUS) is a multifunctional DNA/RNA-binding protein predominantly localized in the cell nucleus. However, FUS has been shown to accumulate and form aggregates in the cytoplasm when mislocalized there due to mutations. These FUS protein aggregates are known as pathological hallmarks in a subset of amyotrophic lateral sclerosis (ALS) and frontotemporal lobar degeneration (FTLD) cases. In this review, we discussed recent research developments on elucidating the molecular mechanisms behind FUS protein aggregation and toxicity. We mainly focus on studies using the budding yeast (*Saccharomyces cerevisiae*) as a model system, especially on results acquired from yeast genome-wide screens addressing FUS aggregation and toxicity. Human homologs of the FUS toxicity suppressors, identified from these studies, indicate a strong relevance and correlation to a human disease model. By using yeast as a FUS cytotoxicity model these studies provided valuable clues on potential novel targets for therapeutic intervention in ALS.

Keywords: yeast, ALS, FUS, aggregates, protein toxicity

OPEN ACCESS

Edited by:
Sabrina Büttner,
Stockholm University, Sweden

Reviewed by:
Mauro Cozzolino,
Istituto di Farmacologia Traslazionale (IFT), Italy
Karim Mekhail,
University of Toronto, Canada

***Correspondence:**
Beidong Liu
beidong.liu@cmb.gu.se

Received: *15 April 2018*
Accepted: *05 June 2018*
Published: *28 June 2018*

Citation:
Lindström M and Liu B (2018) Yeast as a Model to Unravel Mechanisms Behind FUS Toxicity in Amyotrophic Lateral Sclerosis. Front. Mol. Neurosci. 11:218. doi: 10.3389/fnmol.2018.00218

INTRODUCTION

Amyotrophic lateral sclerosis (ALS), also known as Lou Gehrig's disease, is a progressive and eventually fatal neurodegenerative disorder with characteristics including loss of upper and lower motor neuron functions, leading to muscular weakness. The cell death seen in the motor neurons of ALS patients occurs with the accumulation of misfolded protein depositions in motor neurons and oligodendrocytes, as well as neuroinflammation (Sreedharan and Brown, 2013). Approximately 10% of all ALS cases are inherited as an autosomal trait (familial ALS, fALS), whereas most cases of ALS are sporadic (sALS). In ALS pathology, certain proteins have been more implicated than others, e.g., SOD1 (Cu-Zn superoxide dismutase 1), TAR-DNA-binding protein-43 kDa (TDP-43) and fused in sarcoma/translocated in sarcoma (FUS/TLS) (Shaw et al., 2001; Guerrero et al., 2016).

The *FUS* gene is located on chromosome 16 and encodes for a 526 amino acid protein which belongs to the family of FET (FUS/EWS/TAF15)/TET (TLS/EWS/TAF15) proteins (Rabbitts et al., 1993; Tan and Manley, 2009). FUS is a DNA/RNA-binding protein with gene regulatory functions including DNA repair, transcriptional control, RNA splicing and mRNA transport to the cytoplasm. FUS shares many similar structures and functions with TDP-43, another DNA/RNA-binding protein, including similar roles in disease induction (Law et al., 2006; Nolan et al., 2016; Ederle and Dormann, 2017).

In many cell types, FUS and TDP-43 are ubiquitously expressed throughout both the cytoplasm and the nucleus and shown to shuttle between these locations. The mechanism behind this shuttling is still not fully explained (Zinszner et al., 1997; Andersson et al., 2008). However, the wild-type FUS protein is predominantly located in the nucleus of neurons and glial cells but when mutated it has been found to accumulate into cytoplasmic aggregates, in synergy with ALS pathology. FUS is thereby lost from the nucleus, most likely resulting in the loss of the normal nuclear protein functions and/or gain of new toxic functions in the cytoplasm (Ling et al., 2013; Ederle and Dormann, 2017). FUS aggregates have been implicated in 7.5% of fALS and <1% of sALS cases, as well as in rare forms of frontotemporal lobar degeneration (FTLD; Kwiatkowski et al., 2009; Vance et al., 2009; Tarlarini et al., 2015). Not only mutated FUS has been implicated in the progression of neurodegenerative diseases, wild-type FUS has also been observed to abnormally aggregate and contribute to a disease phenotype. This has been seen in e.g., most TDP-43- and tau-negative FTLD cases, as well as in some cases of juvenile ALS with basophilic inclusions and a subtype of FTLD-FUS, also with basophilic inclusion bodies (Huang et al., 2010; Urwin et al., 2010; Matsumoto et al., 2015). Furthermore, studies show that FUS strongly interacts with pathological neuronal intranuclear inclusions found in the brains of patients with Huntington disease (HD), spinocerebellar ataxia and dentatorubral-pallidoluysian atrophy (Doi et al., 2010; Woulfe et al., 2010).

Yeast Models of Neurodegeneration

The simple and well-characterized model organism *Saccharomyces cerevisiae* has been extensively used when studying the mechanisms behind, and impact of protein misfolding and aggregation, typical neurodegenerative disease phenotypes (Outeiro and Lindquist, 2003; Sun et al., 2011). There are many advantages to working with yeast, such as a fully sequenced genome, facilitated genetic manipulations and the existence of a high number (approx. 20%) of orthologous gene families linked to human diseases (Tenreiro et al., 2013). Moreover, many of the complex processes and pathways coupled to protein folding diseases are preserved in yeast and can therefore be studied in this more accessible model (Heinicke et al., 2007). In accordance, *Saccharomyces cerevisiae* contains no FUS homolog, but many cellular pathways coupled to FUS are shared between human and budding yeast cells (Ju et al., 2011).

Yeast gene-to-gene and genome-wide high-throughput screening techniques have played a fundamental and pioneering role in describing protein localization, deletion and over-expression phenotypes as well as identifying modifiers of protein-associated toxicity, thereby contributing to our present understanding of pathways involved in the most prominent human neurodegenerative diseases (Krobitsch and Lindquist, 2000; Outeiro and Lindquist, 2003; Ju et al., 2011; Sun et al., 2011). For instance, yeast models of Parkinson's disease (PD) and Huntington disease (HD) have uncovered many of the mechanisms behind the toxic aggregation of mutated huntingtin (htt), implicated in HD, and α-synuclein, one of the proteins behind the cytoplasmic inclusions found in PD. It has been shown that α-synuclein induces dose-dependent toxicity, whereas in the case of huntingtin, yeast studies have further validated discoveries indicating that longer polyglutamine stretches in htt increase the tendency of the protein to form insoluble inclusions (Krobitsch and Lindquist, 2000; Outeiro and Lindquist, 2003; Tenreiro et al., 2013). Similarly, yeast genome-wide expression studies focusing on Sen1, the yeast homolog to human Senataxin, implicated in amyotrophic lateral sclerosis 4, have uncovered that mutated SEN1 results in growth defects and increased cellular reactive oxygen species levels (Sariki et al., 2016). Large-scale yeast screenings utilizing gene deletion, and gene over-expression libraries have been frequently employed in neurodegenerative research. For instance, when uncovering that pathways involved in lipid metabolism, vesicular transport and vacuolar degradation harbor proteins that work as potential enhancers and suppressors of α-synuclein toxicity, whereas the kynurenine pathway works as a modifier of htt toxicity (Willingham et al., 2003; Giorgini et al., 2005; Zabrocki et al., 2008). Notably, yeast high-throughput screens are a convenient first approach to the discovery of new mechanisms behind disease progression, followed by validation in more complex animal models and finally a potential discovery of new candidate therapeutic targets (Tenreiro et al., 2013).

In the following, we review recent research developments concerning the DNA/RNA-binding protein FUS and its role in ALS pathogenesis and progression. We focus on research using the yeast system; however, studies in other model systems are also discussed (see outline in **Figure 1**).

DOMAINS REQUIRED FOR FUS AGGREGATION

It has been shown that most FUS mutations coupled to ALS reside in certain distinct domains of *FUS*, such as the N-terminal prion-like domain, including a portion of the glycine-rich region and the nonclassical C-terminal nuclear localization signal (NLS) (Lagier-Tourenne et al., 2010). Other domains present in FUS are the conserved RNA-recognition motif (RRM), the C2/C2 zinc finger motif as well as several arginine-glycine-glycine (RGG)-repeat regions (Burd and Dreyfuss, 1994; Morohoshi et al., 1998; Yoshizawa et al., 2018). The DNA/RNA-binding ability of FUS is enabled through the zinc finger motif, the RRM region, and the RGG regions (Burd and Dreyfuss, 1994; Iko et al., 2004; Ederle and Dormann, 2017). As previously mentioned, a prion-like domain, i.e., a region enriched in polar amino acids (glutamine, glycine, serine and tyrosine, QGSY) has been identified in FUS. These regions are common in RNA-binding proteins and are hypothesized to drive protein aggregation in neurons (Cushman et al., 2010; Gitler and Shorter, 2011; King et al., 2012).

Yeast studies have shown that full-length FUS assemble into multiple cytoplasmic inclusions in yeast (Ju et al., 2011; Kryndushkin et al., 2011; Sun et al., 2011). However, in order to uncover the exact sequence regions and domains required for FUS aggregation and cytotoxicity in *S. cerevisiae*, the aggregation and intracellular location of constructed FUS truncations coupled to a fluorescent tag, have been studied. It

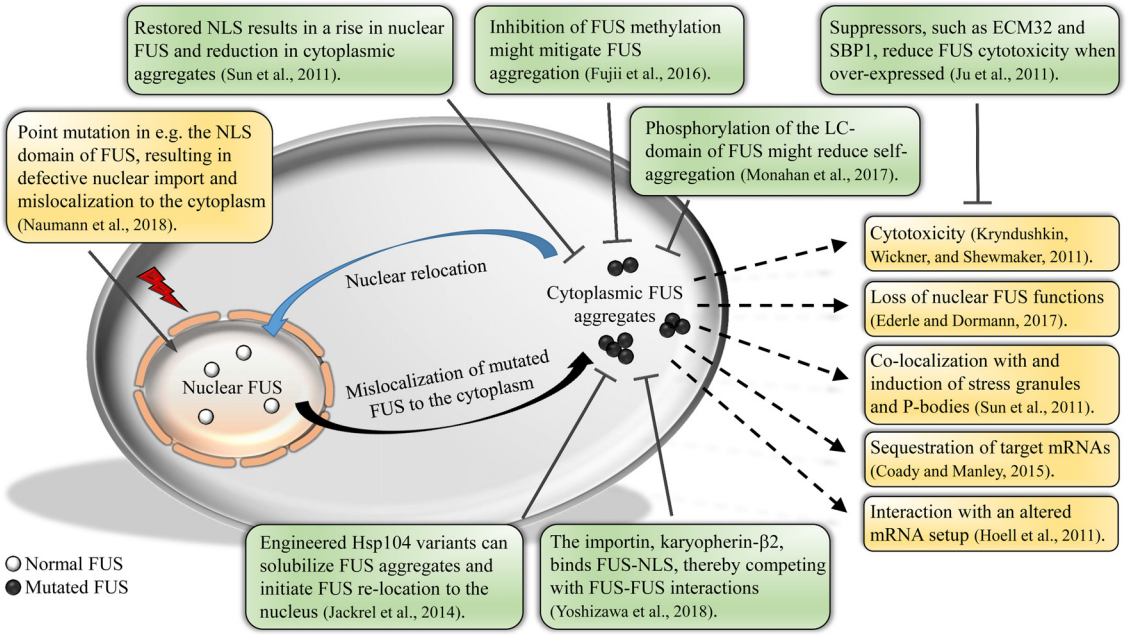

FIGURE 1 | Impact of fused in sarcoma (FUS) mislocalization and aggregation. Normal FUS is predominantly localized to the nucleus. Due to defective methylation of the protein or mutations in the nuclear localization signal (NLS), FUS will mislocalize to the cytoplasm, forming aggregates. Cytoplasmic FUS aggregation could result in various unfavorable outcomes, e.g., cytotoxicity and altered mRNA interactions of FUS. Studies show that a relocation of FUS back into the nucleus is possible by e.g., restoring the NLS or various post-translational modifications, thereby reducing the amount of aggregated FUS and cytotoxicity. Further, studies have uncovered new potential suppressors of FUS cytotoxicity, as well as engineered disaggregases that solubilize aggregated FUS.

has been shown that FUS constructs missing the C-terminal part, including the NLS and the RGG-regions, localize to the nucleus. However, already when only adding back one of the RGG-regions (amino acids 371–422), clear cytoplasmic aggregation of FUS could be seen. In other words, the RGG domain is required for cytoplasmic aggregation of FUS (Sun et al., 2011). Furthermore, constructs containing all domains except the prion-like N-terminal QGSY-region induced only diffuse cytoplasmic staining of FUS with a few small cytoplasmic foci. The QGSY-region of *FUS* is therefore needed for full aggregation to occur but not enough to cause cytoplasmic aggregation in itself (Sun et al., 2011). Studies in insect cells further support the conclusion that the N-terminal prion-like domain is essential for the forming of FUS inclusions (Patel et al., 2015).

A similar approach has also been performed with focus on TDP-43 where it was found that the C-terminal prion-like domain, the region containing most of the ALS-linked mutations in *TDP-43*, was necessary for, and even increase, TDP-43 aggregation and toxicity (Johnson et al., 2008; Cushman et al., 2010). In addition to the C-terminal prion-like domain being necessary for aggregation and toxicity of TDP-43, a portion from RRM2 (RNA recognition motif 2) is also required (Johnson et al., 2008). However, when the entire C-terminal part including the RRM region was deleted in *FUS*, it resulted in nuclear localization of the FUS protein, indicating that this domain is not needed for cytoplasmic aggregation of FUS in yeast (Sun et al., 2011).

In order to establish whether the same FUS domains are needed for aggregation in a mammalian cell model, the previously mentioned full-length FUS and some of the FUS constructs were transfected into COS-7 cells (Sun et al., 2011). In accordance with the yeast results, the FUS deletion constructs missing the C-terminal part, including the RGG region (amino acids 371–422), localized to the nucleus, even though they did not contain the NLS, indicating that other sequences also enable nuclear import of FUS. Furthermore, when adding back the RGG region (amino acids 371–422), FUS aggregated in the cytoplasm of COS-7 cells, as observed in yeast. It has therefore been proposed that domains needed for FUS aggregation in yeast are also needed for aggregation in mammalian cells (Sun et al., 2011). However, in contrast to what has been seen in yeast cells, full-length FUS almost always localizes to the nucleus in mammalian cells, rarely forming transient cytoplasmic foci (Kwiatkowski et al., 2009; Vance et al., 2009; Dormann et al., 2010). Nonetheless, studies show that this is due to differences in the nuclear import process of yeast and mammalian cells (Ju et al., 2011).

Upon stress, phase separation of FUS is important in order for the protein to associate with cytoplasmic stress granules, a normal and reversible process in healthy cells. Studies in mammalian cells have shown that assemblies of FUS are dynamic and turn over quickly as well as always relax into a spherical shape upon fusion, indicators of phase separation into a state called liquid droplets (Patel et al., 2015). Moreover, an atomic force microscopy-infrared nanospectroscopy approach has suggested

that FUS liquid-liquid phase separation is guided by cation-π interactions between tyrosine residues in the LC-domain and arginine residues in the RGG domains. The strength of these interactions is regulated by arginine methylation, where hypomethylation of selected FUS arginines has been shown to drive FUS condensation into stable intermolecular β-sheet-rich hydrogel structures (Qamar et al., 2018).

Furthermore, studies indicate that over prolonged time, FUS liquid droplets convert to an aggregated fibrous state, a process hastened by ALS-linked mutations in the prion-like domain of FUS. As previously mentioned, studies in insect cells indicate that the formation of liquid droplets is dependent on the N-terminal prion-like LC-domain of FUS (Patel et al., 2015). In addition, data from solid-state nuclear magnetic resonance methods illustrate the mechanism of the FUS LC-domain in the formation of the FUS fibril cores. The study shows that out of the 214 residues found in the LC-domain, only a 57 residue-segment composes the fibril core while the remainder of the segment is dynamically disordered. The LC-domain of FUS does not display any hydrophobic interactions within the core (Murray et al., 2017).

Protein aggregation and toxicity can be enhanced by certain domains in other aggregation prone proteins in the cell. Such as the yeast protein RNQ1, which contains a Q/N-rich region (glutamines and asparagines). Its aggregated prion form has been reported to significantly enhance aggregation of other Q/N-rich proteins, such as huntingtin (Meriin et al., 2002). No increase in FUS aggregation has been found when the aggregated prion form of RNQ1 is present, in accordance with the small Q/N-region of FUS. However, it has been proposed that the prion form of RNQ1 could enhance the toxicity caused by FUS even though not affecting the aggregation (Park et al., 2018). Furthermore, transgenic mouse models have shown that when wild-type human FUS is over-expressed, the mice develop an aggressive phenotype with increased cytoplasmic expression of FUS in the brain and motor neurons, pathological features seen in ALS and FTLD patients (Mitchell et al., 2013). In addition, transgenic rats over-expressing the wild-type human FUS protein do not show any symptoms at a young age but display cognitive deficiencies when older, due to significant neuronal loss, displaying a resemblance to some ALS and FTLD phenotypes (Huang et al., 2011). These discoveries indicate that over-expression of wild-type FUS is sufficient to promote vast neuron death and thereby aid in augmenting a neurodegenerative disease phenotype (Huang et al., 2011; Mitchell et al., 2013).

To summarize, in order for FUS to form distinct cytoplasmic aggregates in yeast, both sequences in the N-terminal and the C-terminal parts are required. Specifically, the N-terminal prion-like domain and at least the 371–422 RGG domain (Sun et al., 2011; Patel et al., 2015). There are indications that TDP-43 and FUS, even though they are both RNA-binding proteins with many similarities in structure and function, aggregate and develop their disease phenotypes via distinct mechanisms (Johnson et al., 2008). The aggregation pattern of full-length FUS in yeast cells can be of convenience in ALS research, since the physical protein aggregation mimics the FUS aggregation seen in ALS pathology (Kwiatkowski et al., 2009; Vance et al., 2009). Even though the same mutations are not present, the cellular impact of FUS aggregation can still be studied, in addition to being coupled to findings regarding pathological wild-type FUS aggregation.

FUS AGGREGATION CAUSES CYTOTOXICITY

FUS forms cytoplasmic inclusions when present in yeast but are these aggregates also toxic? Yeast screening assays have identified which human RNA-binding proteins, containing RRMs, aggregate and are toxic at high expression levels in yeast. Out of 132 tested proteins, 35 aggregated and were toxic, including TDP-43 and FUS. Furthermore, some of these proteins also shared the feature of having a prion-like domain. In other words, FUS expression, just like TDP-43 expression, is cytotoxic and correlates with the protein aggregation in the cytoplasm (Kryndushkin et al., 2011; Sun et al., 2011; Park et al., 2018). However, a mouse model expressing a human truncation mutation, associated with early onset ALS (20 years of age), at physiological levels, has been shown to induce adult onset motor neuron loss in the absence of FUS protein aggregates (Devoy et al., 2017). Furthermore, in a *Drosophila* FUS transgenic model, neither wild-type FUS nor ALS-linked FUS mutants formed any cytoplasmic inclusions even though high toxicity was observed. It was suggested that nuclear localization of FUS was necessary for FUS toxicity to occur, whereas the formation of cytoplasmic FUS inclusions was not (Xia et al., 2012).

In accordance with previous studies focusing on sequence domains required for FUS aggregation, the same approach has been carried out to pinpoint which FUS domains are needed for toxicity to occur in yeast. Studies have shown that a decrease in toxicity often occurs with a decline in the aggregation capacity of truncated FUS constructs. When removing segments from either terminal domain of *FUS*, the toxicity is dampened in yeast (Kryndushkin et al., 2011; Sun et al., 2011). Complementary to what has been observed regarding domains needed for FUS aggregation, most of the prion-like N-terminal QGSY-region is also required for enabling FUS toxicity in yeast, but not enough to confer toxicity by itself. Similar results have been achieved with TDP-43 (Sun et al., 2011). For toxicity to occur, the 371–422 RGG domain of FUS seems to be required for FUS cytotoxicity. However, the extreme C-terminal domain with the last 25 amino acids, where most ALS-linked FUS mutations reside, is not necessary for the toxicity effect. When comparing toxicity caused by full-length FUS and FUS constructs missing the last 25 amino acids, it has been shown that the construct is slightly more toxic. In other words, when the N-terminal part and at least the RGG domain (amino acids 371–422) were present, a rise in toxicity could be observed with each add-back at the C-terminal part of FUS (Sun et al., 2011). Furthermore, by disrupting the RNA binding capacity of FUS, a mitigation of FUS toxicity has been seen in yeast but no effect on the cytoplasmic aggregation. This indicates that the RRM region contributes to toxicity in yeast, likely through RNA binding. However, in contrast to what has been seen in TDP-43, adding back the RRM

region to the prion-like N-terminal of FUS, does not result in toxicity (Sun et al., 2011).

To summarize, for FUS toxicity to occur in yeast, the prion-like N-terminal, the RRM and the RGG domain (amino acids 371–422) are required, and additional C-terminal sequences are further needed to reach full toxicity (Kryndushkin et al., 2011; Sun et al., 2011). It is still not completely clear whether the FUS misbehavior and consequential ALS pathology are due to a toxic gain or loss of FUS function. Furthermore, the exact role and necessity of FUS aggregation, in the induction of toxicity, is also not yet fully explained. However, when comparing with TDP-43, it seems as if FUS aggregation and toxicity in yeast is carried out in a more complex and multi-domain process, since regions in both the N- and C-terminal parts of FUS are needed for full toxicity.

IMPAIRED NUCLEAR IMPORT RESULTS IN FUS AGGREGATION

FUS is a predominantly intranuclear protein. However, during stress, such as heat shock and oxidative stress, FUS can exit and assemble in perinuclear stress granules, and in time re-enter the nucleus. In order for FUS to re-enter the nucleus, the conserved extreme C-terminal NLS of FUS needs to be recognized by a nuclear transport receptor called transportin 1/karyopherin-β2 (Bosco et al., 2010; Dormann et al., 2012).

The importin karyopherin-β2 has been shown to inhibit FUS liquid-liquid phase separation by interacting with and tightly binding the NLS of FUS (Guo et al., 2018; Hofweber et al., 2018; Yoshizawa et al., 2018). Karyopherin-β2 has also been shown to dissolve and reverse phase-separated liquids and fibrillary hydrogels of FUS, by engaging the NLS and LC domains (Guo et al., 2018). Biochemical and nuclear magnetic resonance analysis have further uncovered the occurrence of weak interactions of karyopherin-β2 with multiple other FUS regions, which are also known to promote phase separation. In the proposed model, karyopherin-β2 binds the FUS-NLS with high-affinity, thereby bringing the proteins together, enabling the weak interactions to take place and thereby compete with FUS-FUS interactions, resulting in regulation of FUS inclusion formation and dynamics (Yoshizawa et al., 2018). Moreover, it has been shown that karyopherin-β2, in addition to suppressing FUS phase separation, also hampers the association of FUS with stress granules. However, ALS-linked mutations in the FUS-NLS decreases the chaperone ability of karyopherin-β2, an indication of the further importance of the NLS beyond its role as an import signal (Hofweber et al., 2018).

The FUS-NLS has a non-classical proline-tyrosine (PY) rich domain (PY-NLS). It has been shown that the majority of fALS-associated mutations in *FUS* occur within the NLS, thereby affecting the nuclear import, which correlates with the nuclear import being impaired in some ALS cases. Studies show that FUS is redistributed and recruited into cytoplasmic SGs as a result of an impaired nuclear transport pathway and weakened karyopherin-β2 binding, leading to the production of toxic and insoluble aggregates in neuronal cells (Dormann et al., 2010; Ju et al., 2011; Hofweber et al., 2018). Further studies in human induced pluripotent stem cells derived from motor neurons show that mutations in *FUS*-NLS result in a defective DNA damage response signaling, eventually leading to cytoplasmic FUS mislocalization and aggregation (Naumann et al., 2018).

Yeast also has the same PY-type nuclear localization system as FUS but deviations in the recognition signal results in the mentioned cytoplasmic mislocalization of FUS in yeast, i.e., both ALS-linked mutant FUS and full-length FUS mislocalize to the cytoplasm and are equally toxic in yeast due to a non-functional NLS (Ju et al., 2011). Yeast studies have shown that upon replacement of the non-functional NLS of FUS constructs with a, in yeast, functioning recognition sequence, nuclear localization of FUS can be seen, followed by a reduction in cytotoxicity. In other words, a non-functional FUS-NLS will result in increased toxicity (Ju et al., 2011). This further supports the findings showing that a mislocalization of FUS is essential for the increase in cytotoxicity in yeast (Dormann et al., 2010; Sun et al., 2011). When largely restricting FUS to the nucleus, by fusing a strong heterologous NLS to the N-terminal region of the protein, a considerably lower toxicity level was observed in yeast cells. Even though some cytoplasmic localization of FUS was still present, the now predominantly nuclear FUS resulted in the elimination of cytoplasmic aggregation (Sun et al., 2011). Interestingly, it has been shown that two components, NSR1 and NUP84 (human homologs; NCL and NUP107), related to the nuclear import/export machinery suppress FUS toxicity in yeast when deleted (Sun et al., 2011).

In summary, some ALS-linked FUS mutations have been shown to disrupt the nuclear import process, a behavior resembling the impaired FUS nuclear shuttling seen in some ALS cases, thereby resulting in toxic FUS aggregation in the cytoplasm (Sreedharan and Brown, 2013). However, studies show that when restoring the defective recognition sequence and function of the NLS, FUS relocates back to the nucleus, thereby decreasing the cytotoxicity (Ju et al., 2011; Sun et al., 2011).

IMPACT OF POST-TRANSLATIONAL MODIFICATIONS ON FUS AGGREGATION

FUS normally becomes arginine-methylated by protein arginine methyltransferase 1 (PRMT1). Extensive dimethylation in the RGG domains of FUS has been found to possibly affect the shuttling and cellular localization of FUS, since dimethylation functions as a signal for nuclear/cytoplasmic translocation of RNA binding proteins (Pahlich et al., 2006; Du et al., 2011; Ju et al., 2011; Fujii et al., 2016). Since the arginine methylations are implicated in the shuttling of FUS, arginine methylation may play a role in the toxicity caused by FUS. Moreover, while inclusions found in ALS-FUS patients contain methylated FUS, it is not present in FTLD-FUS patients (Fujii et al., 2016).

Ju and colleagues explored the possible role of yeast arginine methyl transferases on FUS localization and toxicity upon deletion of either of the major yeast arginine methyl transferases. They found that neither deletion nor over-expression of the arginine methyltransferases, nor the introduction of chemicals

known to inhibit the activity of arginine methyltransferases resulted in any effects on FUS aggregation and toxicity levels in yeast (Ju et al., 2011). Another study, in a mammalian cell system, showed that by treating mammalian cells with adenosine dialdehyde, a global methyl transferase inhibitor, the mislocalization and aggregation of FUS mutant was mitigated. Even though this study also showed that excessive treatment with a methylation inhibitor could result in intranuclear aggregation of the FUS mutant, they found that at appropriate levels, inhibition of methylation could mitigate the cytoplasmic mislocalization of the FUS mutant (Fujii et al., 2016). However, in accordance with what has been seen in FTLD patients, other studies have shown that loss of FUS arginine methylation induces liquid-liquid phase separation and stress granule association of FUS, possibly contributing to FUS aggregation. Moreover, in FTLD-FUS patients it has been noted that karyopherin-β2 is aggregated and the arginine methylation needed for FUS-karyopherin-β2 interaction is lost (Hofweber et al., 2018).

As mentioned before, FUS consists of an N-terminal QGSY-rich low-complexity (LC) region (prion-like domain), which has been proposed to drive the formation of reversible liquid droplet structures of FUS (Murakami et al., 2015; Patel et al., 2015). ALS-linked mutations in the LC-domain have been shown to further induce phase transition into irreversible fibrillary hydrogels of FUS, which further induce neurotoxicity in a *C. elegans* model (Murakami et al., 2015). The same domain has also been seen to enable FUS self-assembly in the nucleus of mammalian cells, a critical process required for chromatin-binding and gene regulation. These FUS functions are impaired when ALS-linked mutations are present, such mutations can disrupt the FUS aggregation and subsequent chromatin binding (Yang et al., 2014). Furthermore, when FUS becomes phosphorylated in the LC-domain, the protein's aggregation-prone behavior becomes mitigated and a disruption of the phase separation is observed. Upon phosphorylation, interactions between LC-domains of FUS proteins can be prevented and thereby hinder any self-aggregation of FUS into pathological inclusions. This change in behavior, which is due to alterations in the biophysical properties of the LC, has been seen in both human and yeast cell models where a subsequent reduction of FUS cytotoxicity was found (Monahan et al., 2017; Murray et al., 2017).

FUS INDUCES STRESS GRANULE AND P-BODY FORMATION

Stress granules and processing bodies (P-bodies) play vital roles in RNA regulation and processing. RNAs and RNA-binding proteins are incorporated into these structures by highly conserved pathways found in both yeast and humans (Buchan et al., 2008). Heat shock, oxidative stress and other stress situations result in TDP-43 and FUS being localized into these temporary structures, and FUS accumulation in stress granules is a reversible process in healthy neurons (Colombrita et al., 2009; Bosco et al., 2010; Freibaum et al., 2010; Dormann and Haass, 2011). Moreover, mammalian cells studies show that depending on the type of stress the cell is being subjected to, FUS will localize to various compartments, i.e., at DNA lesions upon DNA damage and in stress granules upon heat stress (Patel et al., 2015).

Even though ALS-linked FUS mutants associate with stress granules, FUS was not observed to be significantly associated with P-bodies in mammalian cells, similarly to previous TDP-43 results. ALS-linked FUS mutants displayed increased association with stress granules, contrary to what had been noted for wild-type FUS (Colombrita et al., 2009; Bosco et al., 2010). Furthermore, mutated FUS has been found able to bind and sequester wild-type FUS into stress granules, which might indicate a possible link to its effect on ALS pathogenesis (Guerrero et al., 2016).

In order to test whether stress granule and P-body formations in yeast are coupled to, and perhaps induced by, FUS Sun et al. (2011) expressed yellow fluorescent protein tagged FUS (FUS-YFP) in a yeast model with tagged SG and P-body markers. The study showed that the expression of FUS did indeed induce the formation of both SGs and P-bodies. In addition, FUS physically co-localized with these cellular compartments, just as they do in inclusions of fALS-FUS patients (Sun et al., 2011; Deng et al., 2014). In other words, FUS is able to induce, as well as localize to, RNA granules in yeast, just as in human cells.

During impaired nuclear transport, FUS is recruited into SGs, following redistribution to the cytoplasm (Dormann et al., 2010). Poly-A binding protein 1 (PABP1) was identified as an interacting partner of FUS in mammalian cells. The mutant FUS inclusions co-localized with PABP1-foci, while no such co-localization could be observed between wild-type FUS and PABP1-foci (Gal et al., 2011). In addition, ALS-FUS inclusions have been seen to co-localize with the stress granule marker Ataxin-2, a protein involved in mRNA regulation and stress granule formation, in spinal cord tissue of ALS patients (Elden et al., 2010). It has also been proposed that even though FUS accumulation in stress granules is a reversible and normally occurring phenomenon in healthy neurons, it could advance to harmful aggregation of FUS in stress granules during chronic stress (Ling et al., 2013). The above-mentioned studies provide evidence that stress granules and P-bodies are coupled to FUS functions, indicating an interesting correlation between mutant FUS, stress granules and ALS pathology.

FUS MUTANTS DISPLAY ALTERED RNA INTERACTIONS

Many FUS functions involve the binding of RNA, including thousands of pre-mRNAs, with a preference for long introns (Fujii et al., 2005). It has been shown that FUS is able to interact directly with RNA via hydrogen bonds and ring stacking. This contact is enabled through the most conserved region of FUS, the RNA-binding domain (Burd and Dreyfuss, 1994). Other domains have also been observed to bind RNA or increase the RNA affinity, e.g., the zinc finger domain and the RGG motifs (Iko et al., 2004). ALS mutations in *FUS* have been seen to affect the expression of its target genes, i.e., by sequestering these

target mRNAs within the insoluble cytoplasmic FUS aggregates (Coady and Manley, 2015). In HEK293 cells, ALS-linked human FUS mutants uniquely targeted an overrepresented group of transcripts, originating from endoplasmic reticulum and ubiquitin-proteasome-linked gene types. The mutant FUS variants did not display any impaired RNA-binding capabilities but showed a striking change in binding patterns and an increase in unique targets compared to proteins in the FET family (Hoell et al., 2011). The identification of RNA targets and effects of both mutant and wild-type FUS provides insights into the systems and mechanisms underlying the aggregation and toxicity of FUS.

FUS TOXICITY SUPPRESSORS

An interesting question regarding FUS toxicity is whether there are any potential suppressors in the cell that could counteract the toxicity caused by mislocalized FUS. In order to answer this question, Ju and colleagues performed a genome-wide screen using a yeast model (over-expression library), where over 5000 genes were each transformed into a yeast strain expressing an integrated and moderately toxic FUS. The outcome of this screen was the identification of five yeast genes (*ECM32*, *NAM8*, *SBP1*, *SKO1* and *VHR1*) that were able to rescue the FUS toxicity when over-expressed. All the suppressors were DNA/RNA binding proteins, like FUS, and had not been implicated as suppressors of toxicity caused by other neurodegenerative diseases proteins, indicating that these proteins are specific to FUS (Ju et al., 2011).

The identified suppressors were only capable of partially suppressing the toxic FUS effects on yeast growth, and they did not alter the expression level, the location of FUS, or the inclusion formation (Ju et al., 2011). Out of the five screen hits, extracellular mutant 32 (ECM32) was found to have a human homolog, human up-frameshift protein 1 (hUPF1), which has been shown to be involved in mRNA quality control and surveillance, and also found to localize to P-bodies and cytoplasmic granules (Ohnishi et al., 2003; Isken and Maquat, 2008; Ju et al., 2011). Further study showed that the over-expression of *hUPF1*, and of *hUPF2* (physical interaction partner of *hUPF1*), also rescued FUS toxicity in yeast (Ju et al., 2011). The potential mechanism underlying the rescue ability of these expressed genes probably involves compensation or restoration of essential cellular functions disturbed by the FUS toxicity. One such possible disturbance could be that the deviance in FUS behavior results in RNA and/or other molecules become sequestered, thereby disrupting normal RNA functions. For instance, hUPF1 plays a vital role in mRNA surveillance and RNA quality control, functions that might enable the rescue seen here (Isken and Maquat, 2008; Ju et al., 2011).

When conducting a similar genome-wide yeast over-expression screen, Sun et al. (2011) found 24 suppressors and 10 enhancers of FUS toxicity, including the same five suppressor hits also identified by Ju et al. (2011). The largest class of genes uncovered in the screen included RNA-binding proteins, in accordance with the results by Ju et al. (2011), and proteins involved in RNA metabolism. Moreover, three stress granule components, translation initiation factors (Tif2 and Tif3) and Pab1, were isolated as FUS toxicity suppressors. Pab1 is involved in stress granule formation in yeast and has a human homolog, called PABP1, mentioned earlier as a FUS-interactor in mammalian cells (Gal et al., 2011). This indicates that stress granule components might play a key role in reducing FUS toxicity.

It has been shown that over-expression of FUS in yeast results in toxicity as well as inhibition of the ubiquitin proteasome system. This phenotype can be relieved by over-expression of the heat shock protein 40 chaperone, Sis1. This was done without altering the FUS levels in the yeast cells (Park et al., 2018). In accordance, Jackrel et al. (2014) conducted a study to test the effect of protein disaggregases when attempting to eliminate misfolded toxic protein conformers. They aimed at engineering heat shock protein 104 (Hsp104) variants that would reverse the protein misfolding seen in neurodegenerative disorders. The modifications to Hsp104, a conserved hexameric AAA+ protein disaggregase from *S. cerevisiae*, would enhance Hsp104 and thereby eliminate substrates implicated in ALS (Jackrel et al., 2014; Torrente et al., 2016). Under normal conditions, Hsp104 solubilizes disordered aggregates and amyloids, restoring the native protein conformation, but displays very limited activity against human neurodegenerative disease proteins. Upon *HSP104* gene deletion, no changes in FUS aggregation nor toxicity has been observed (Shorter, 2008; Vashist et al., 2010; Kryndushkin et al., 2011). Jackrel and colleagues developed yeast platform methods which enabled them to screen large libraries of Hsp104 variants for abilities in suppressing toxicity caused by protein misfolding. The result was a series of reprogrammed and enhanced Hsp104 variants that not only reversed FUS aggregation and toxicity but also restored correct FUS localization, thereby restoring proteostasis. Furthermore, engineered Hsp104 variants have been shown to also mitigate neurodegeneration in a *C. elegans* model (Jackrel et al., 2014).

The suppressors identified in these genome-wide screens illuminate the cellular pathways linked to abnormal FUS aggregation and thereby propose new potential therapeutic targets.

CONCLUDING REMARKS

Although the simple yeast system does not display all of the cellular processes found in human cells, many essential cellular functions are shared. Conveniently, several pathways associated with neurodegeneration are conserved between yeast and humans and have therefore been crucial when establishing yeast as a model for protein mislocalization and aggregation in neurodegenerative diseases. Despite some clear differences between yeast and mammalian cell functions, such as wild-type FUS locating to the cytoplasm or the nucleus, the yeast system has proven to be a highly useful model of FUS cytoplasmic aggregation and toxicity, critical pathological events in ALS. In accordance, the yeast studies discussed in this review have uncovered several conserved molecular mechanisms behind FUS protein misfolding, such as sequence domains required

for aggregation and toxicity, as well as subsequent impact on other cellular pathways, such as RNA metabolism and stress granule formation. Studies show that the toxicity caused by FUS could be a result of misfolded proteins surviving the protein control system and consequentially disturbing the normal cellular functions. Such a disturbance might be a sequestration of proteins and/or RNAs by the cytoplasmic aggregation of FUS, thereby displaying a gained toxic ability. But also, the loss of normal FUS functions in the nucleus, such as RNA processing, imply a loss of function affecting the cell. However, there are studies indicating that cytoplasmic aggregation of FUS might not at all be needed for FUS toxicity to occur in mammalian systems.

Moreover, yeast has served as an optimal platform for isolating FUS toxicity suppressors from large libraries, and uncovered possible candidate genes with human homologs, which strongly indicate that yeast can serve as a proper model for studying FUS cytotoxicity. Further developing genome-wide genetic and phenomic approaches can be used to address remaining challenges in understanding the FUS-ALS pathogenesis, such as identification and characterization of the altered protein and RNA interactions affected by FUS mutants, as well as characterizing the genetic susceptibility and environmental triggers of the disease. By identifying the molecular pathways underlying ALS and the role of external environmental factors in disease development, new therapeutic approaches and disease prevention methods could be uncovered.

AUTHOR CONTRIBUTIONS

BL conceived and outlined the paper. ML wrote the manuscript with the help from BL.

FUNDING

This work was supported by grants from the Swedish Cancer Society (CAN 2012/601, CAN 2015/406 and CAN 2017/643, to BL), the Swedish Natural Research Council (VR 2011-5923 and VR 2015-04984, to BL), and the Carl Trygger Foundation (CTS 14: 295, to BL). Additional support came from the People Programme (Marie Curie Actions) of the European Union's Seventh Framework Programme (FP7/2007–2013) under REA grant agreement n°608743.

REFERENCES

Andersson, M. K., Ståhlberg, A., Arvidsson, Y., Olofsson, A., Semb, H., Stenman, G., et al. (2008). The multifunctional FUS, EWS and TAF15 proto-oncoproteins show cell type-specific expression patterns and involvement in cell spreading and stress response. *BMC Cell Biol.* 9:37. doi: 10.1186/1471-2121-9-37

Bosco, D. A., Lemay, N., Ko, H. K., Zhou, H., Burke, C., Kwiatkowski, T. J. Jr., et al. (2010). Mutant FUS proteins that cause amyotrophic lateral sclerosis incorporate into stress granules. *Hum. Mol. Genet.* 19, 4160–4175. doi: 10.1093/hmg/ddq335

Buchan, J. R., Muhlrad, D., and Parker, R. (2008). P bodies promote stress granule assembly in *Saccharomyces cerevisiae*. *J. Cell Biol.* 183, 441–455. doi: 10.1083/jcb.200807043

Burd, C. G., and Dreyfuss, G. (1994). Conserved structures and diversity of functions of RNA-binding proteins. *Science* 265, 615–621. doi: 10.1126/science.8036511

Coady, T. H., and Manley, J. L. (2015). ALS mutations in TLS/FUS disrupt target gene expression. *Genes Dev.* 29, 1696–1706. doi: 10.1101/gad.267286.115

Colombrita, C., Zennaro, E., Fallini, C., Weber, M., Sommacal, A., Buratti, E., et al. (2009). TDP-43 is recruited to stress granules in conditions of oxidative insult. *J. Neurochem.* 111, 1051–1061. doi: 10.1111/j.1471-4159.2009.06383.x

Cushman, M., Johnson, B. S., King, O. D., Gitler, A. D., and Shorter, J. (2010). Prion-like disorders: blurring the divide between transmissibility and infectivity. *J. Cell Sci.* 123, 1191–1201. doi: 10.1242/jcs.051672

Deng, H., Gao, K., and Jankovic, J. (2014). The role of FUS gene variants in neurodegenerative diseases. *Nat. Rev. Neurol.* 10, 337–348. doi: 10.1038/nrneurol.2014.78

Devoy, A., Kalmar, B., Stewart, M., Park, H., Burke, B., Noy, S. J., et al. (2017). Humanized mutant FUS drives progressive motor neuron degeneration without aggregation in 'FUSDelta14' knockin mice. *Brain* 140, 2797–2805. doi: 10.1093/brain/awx248

Doi, H., Koyano, S., Suzuki, Y., Nukina, N., and Kuroiwa, Y. (2010). The RNA-binding protein FUS/TLS is a common aggregate-interacting protein in polyglutamine diseases. *Neurosci. Res.* 66, 131–133. doi: 10.1016/j.neures.2009.10.004

Dormann, D., Madl, T., Valori, C. F., Bentmann, E., Tahirovic, S., Abou-Ajram, C., et al. (2012). Arginine methylation next to the PY-NLS modulates Transportin binding and nuclear import of FUS. *EMBO J.* 31, 4258–4275. doi: 10.1038/emboj.2012.261

Dormann, D., and Haass, C. (2011). TDP-43 and FUS: a nuclear affair. *Trends Neurosci.* 34, 339–348. doi: 10.1016/j.tins.2011.05.002

Dormann, D., Rodde, R., Edbauer, D., Bentmann, E., Fischer, I., Hruscha, A., et al. (2010). ALS-associated fused in sarcoma (FUS) mutations disrupt Transportin-mediated nuclear import. *EMBO J.* 29, 2841–2857. doi: 10.1038/emboj.2010.143

Du, K., Arai, S., Kawamura, T., Matsushita, A., and Kurokawa, R. (2011). TLS and PRMT1 synergistically coactivate transcription at the survivin promoter through TLS arginine methylation. *Biochem. Biophys. Res. Commun.* 404, 991–996. doi: 10.1016/j.bbrc.2010.12.097

Ederle, H., and Dormann, D. (2017). TDP-43 and FUS en route from the nucleus to the cytoplasm. *FEBS Lett.* 591, 1489–1507. doi: 10.1002/1873-3468.12646

Elden, A. C., Kim, H. J., Hart, M. P., Chen-Plotkin, A. S., Johnson, B. S., Fang, X., et al. (2010). Ataxin-2 intermediate-length polyglutamine expansions are associated with increased risk for ALS. *Nature* 466, 1069–1075. doi: 10.1038/nature09320

Freibaum, B. D., Chitta, R. K., High, A. A., and Taylor, J. P. (2010). Global analysis of TDP-43 interacting proteins reveals strong association with RNA splicing and translation machinery. *J. Proteome Res.* 9, 1104–1120. doi: 10.1021/pr901076y

Fujii, R., Okabe, S., Urushido, T., Inoue, K., Yoshimura, A., Tachibana, T., et al. (2005). The RNA binding protein tls is translocated to dendritic spines by mGluR5 activation and regulates spine morphology. *Curr. Biol.* 15, 587–593. doi: 10.1016/j.cub.2005.01.058

Fujii, S., Takanashi, K., Kitajo, K., and Yamaguchi, A. (2016). Treatment with a global methyltransferase inhibitor induces the intranuclear aggregation of ALS-linked FUS mutant *in vitro*. *Neurochem. Res.* 41, 826–835. doi: 10.1007/s11064-015-1758-z

Gal, J., Zhang, J., Kwinter, D. M., Zhai, J., Jia, H., Jia, J., et al. (2011). Nuclear localization sequence of FUS and induction of stress granules by ALS mutants. *Neurobiol. Aging* 32, 2323.e27–2323.e40. doi: 10.1016/j.neurobiolaging.2010.06.010

Giorgini, F., Guidetti, P., Nguyen, Q., Bennett, S. C., and Muchowski, P. J. (2005). A genomic screen in yeast implicates kynurenine 3-monooxygenase as a therapeutic target for Huntington disease. *Nat. Genet.* 37, 526–531. doi: 10.1038/ng1542

Gitler, A. D., and Shorter, J. (2011). RNA-binding proteins with prion-like domains in ALS and FTLD-U. *Prion* 5, 179–187. doi: 10.4161/pri.5.3.17230

Guerrero, E. N., Wang, H., Mitra, J., Hegde, P. M., Stowell, S. E., Liachko, N. F., et al. (2016). TDP-43/FUS in motor neuron disease: complexity and challenges. *Prog. Neurobiol.* 145–146, 78–97. doi: 10.1016/j.pneurobio.2016.09.004

Guo, L., Kim, H. J., Wang, H., Monaghan, J., Freyermuth, F., Sung, J. C., et al. (2018). Nuclear-import receptors reverse aberrant phase transitions of RNA-binding proteins with prion-like domains. *Cell* 173, 677.e20–692.e20. doi: 10.1016/j.cell.2018.03.002

Heinicke, S., Livstone, M. S., Lu, C., Oughtred, R., Kang, F., Angiuoli, S. V., et al. (2007). The princeton protein orthology database (P-POD): a comparative genomics analysis tool for biologists. *PLoS One* 2:e766. doi: 10.1371/journal.pone.0000766

Hoell, J. I., Larsson, E., Runge, S., Nusbaum, J. D., Duggimpudi, S., Farazi, T. A., et al. (2011). RNA targets of wild-type and mutant FET family proteins. *Nat. Struct. Mol. Biol.* 18, 1428–1431. doi: 10.1038/nsmb.2163

Hofweber, M., Hutten, S., Bourgeois, B., Spreitzer, E., Niedner-Boblenz, A., Schifferer, M., et al. (2018). Phase separation of FUS is suppressed by its nuclear import receptor and arginine methylation. *Cell* 173, 706.e13–719.e13. doi: 10.1016/j.cell.2018.03.004

Huang, C., Zhou, H., Tong, J., Chen, H., Liu, Y. J., Wang, D., et al. (2011). FUS transgenic rats develop the phenotypes of amyotrophic lateral sclerosis and frontotemporal lobar degeneration. *PLoS Genet.* 7:e1002011. doi: 10.1371/journal.pgen.1002011

Huang, E. J., Zhang, J., Geser, F., Trojanowski, J. Q., Strober, J. B., Dickson, D. W., et al. (2010). Extensive FUS-immunoreactive pathology in juvenile amyotrophic lateral sclerosis with basophilic inclusions. *Brain Pathol.* 20, 1069–1076. doi: 10.1111/j.1750-3639.2010.00413.x

Iko, Y., Kodama, T. S., Kasai, N., Oyama, T., Morita, E. H., Muto, T., et al. (2004). Domain architectures and characterization of an RNA-binding protein, TLS. *J. Biol. Chem.* 279, 44834–44840. doi: 10.1074/jbc.M408552200

Isken, O., and Maquat, L. E. (2008). The multiple lives of NMD factors: balancing roles in gene and genome regulation. *Nat. Rev. Genet.* 9, 699–712. doi: 10.1038/nrg2402

Jackrel, M. E., DeSantis, M. E., Martinez, B. A., Castellano, L. M., Stewart, R. M., Caldwell, K. A., et al. (2014). Potentiated Hsp104 variants antagonize diverse proteotoxic misfolding events. *Cell* 156, 170–182. doi: 10.1016/j.cell.2013.11.047

Johnson, B. S., McCaffery, J. M., Lindquist, S., and Gitler, A. D. (2008). A yeast TDP-43 proteinopathy model: exploring the molecular determinants of TDP-43 aggregation and cellular toxicity. *Proc. Natl. Acad. Sci. U S A* 105, 6439–6444. doi: 10.1073/pnas.0802082105

Ju, S., Tardiff, D. F., Han, H., Divya, K., Zhong, Q., Maquat, L. E., et al. (2011). A yeast model of FUS/TLS-dependent cytotoxicity. *PLoS Biol.* 9:e1001052. doi: 10.1371/journal.pbio.1001052

King, O. D., Gitler, A. D., and Shorter, J. (2012). The tip of the iceberg: RNA-binding proteins with prion-like domains in neurodegenerative disease. *Brain Res.* 1462, 61–80. doi: 10.1016/j.brainres.2012.01.016

Krobitsch, S., and Lindquist, S. (2000). Aggregation of huntingtin in yeast varies with the length of the polyglutamine expansion and the expression of chaperone proteins. *Proc. Natl. Acad. Sci. U S A* 97, 1589–1594. doi: 10.1073/pnas.97.4.1589

Kryndushkin, D., Wickner, R. B., and Shewmaker, F. (2011). FUS/TLS forms cytoplasmic aggregates, inhibits cell growth and interacts with TDP-43 in a yeast model of amyotrophic lateral sclerosis. *Protein Cell* 2, 223–236. doi: 10.1007/s13238-011-1525-0

Kwiatkowski, T. J. Jr., Bosco, D. A., Leclerc, A. L., Tamrazian, E., Vanderburg, C. R., Russ, C., et al. (2009). Mutations in the FUS/TLS gene on chromosome 16 cause familial amyotrophic lateral sclerosis. *Science* 323, 1205–1208. doi: 10.1126/science.1166066

Lagier-Tourenne, C., Polymenidou, M., and Cleveland, D. W. (2010). TDP-43 and FUS/TLS: emerging roles in RNA processing and neurodegeneration. *Hum. Mol. Genet.* 19, R46–R64. doi: 10.1093/hmg/ddq137

Law, W. J., Cann, K. L., and Hicks, G. G. (2006). TLS, EWS and TAF15, a model for transcriptional integration of gene expression. *Brief. Funct. Genomic. Proteomic.* 5, 8–14. doi: 10.1093/bfgp/ell015

Ling, S. C., Polymenidou, M., and Cleveland, D. W. (2013). Converging mechanisms in ALS and FTD: disrupted RNA and protein homeostasis. *Neuron* 79, 416–438. doi: 10.1016/j.neuron.2013.07.033

Matsumoto, A., Suzuki, H., Fukatsu, R., Shimizu, H., Suzuki, Y., and Hisanaga, K. (2015). An autopsy case of frontotemporal lobar degeneration with the appearance of fused in sarcoma inclusions (basophilic inclusion body disease) clinically presenting corticobasal syndrome. *Neuropathology* 36, 77–87. doi: 10.1111/neup.12232

Meriin, A. B., Zhang, X., He, X., Newnam, G. P., Chernoff, Y. O., and Sherman, M. Y. (2002). Huntingtin toxicity in yeast model depends on polyglutamine aggregation mediated by a prion-like protein Rnq1. *J. Cell Biol.* 157, 997–1004. doi: 10.1083/jcb.200112104

Mitchell, J. C., McGoldrick, P., Vance, C., Hortobagyi, T., Sreedharan, J., Rogelj, B., et al. (2013). Overexpression of human wild-type FUS causes progressive motor neuron degeneration in an age- and dose-dependent fashion. *Acta Neuropathol.* 125, 273–288. doi: 10.1007/s00401-012-1043-z

Monahan, Z., Ryan, V. H., Janke, A. M., Burke, K. A., Rhoads, S. N., and Zerze, G. H. (2017). Phosphorylation of the FUS low-complexity domain disrupts phase separation, aggregation, and toxicity. *EMBO J.* 36, 2951–2967. doi: 10.15252/embj.201696394

Morohoshi, F., Ootsuka, Y., Arai, K., Ichikawa, H., Mitani, S., Munakata, N., et al. (1998). Genomic structure of the human RBP56/hTAFII68 and FUS/TLS genes. *Gene* 221, 191–198. doi: 10.1016/s0378-1119(98)00463-6

Murakami, T., Qamar, S., Lin, J. Q., Schierle, G. S., Rees, E., Miyashita, A., et al. (2015). ALS/FTD mutation-induced phase transition of FUS liquid droplets and reversible hydrogels into irreversible hydrogels impairs RNP granule function. *Neuron* 88, 678–690. doi: 10.1016/j.neuron.2015.10.030

Murray, D. T., Kato, M., Lin, Y., Thurber, K. R., Hung, I., McKnight, S. L., et al. (2017). Structure of FUS protein fibrils and its relevance to self-assembly and phase separation of low-complexity domains. *Cell* 171, 615.e16–627.e16. doi: 10.1016/j.cell.2017.08.048

Naumann, M., Pal, A., Goswami, A., Lojewski, X., Japtok, J., Vehlow, A., et al. (2018). Impaired DNA damage response signaling by FUS-NLS mutations leads to neurodegeneration and FUS aggregate formation. *Nat. Commun.* 9:335. doi: 10.1038/s41467-017-02299-1

Nolan, M., Talbot, K., and Ansorge, O. (2016). Pathogenesis of FUS-associated ALS and FTD: insights from rodent models. *Acta Neuropathol. Commun.* 4:99. doi: 10.1186/s40478-016-0358-8

Ohnishi, T., Yamashita, A., Kashima, I., Schell, T., Anders, K. R., Grimson, A., et al. (2003). Phosphorylation of hUPF1 induces formation of mRNA surveillance complexes containing hSMG-5 and hSMG-7. *Mol. Cell* 12, 1187–1200. doi: 10.1016/s1097-2765(03)00443-x

Outeiro, T. F., and Lindquist, S. (2003). Yeast cells provide insight into α-synuclein biology and pathobiology. *Science* 302, 1772–1775. doi: 10.1126/science.1090439

Pahlich, S., Zakaryan, R. P., and Gehring, H. (2006). Protein arginine methylation: cellular functions and methods of analysis. *Biochim. Biophys. Acta* 1764, 1890–1903. doi: 10.1016/j.bbapap.2006.08.008

Park, S. K., Arslan, F., Kanneganti, V., Barmada, S. J., Purushothaman, P., Verma, S. C., et al. (2018). Overexpression of a conserved HSP40 chaperone reduces toxicity of several neurodegenerative disease proteins. *Prion* 12, 16–22. doi: 10.1080/19336896.2017.1423185

Patel, A., Lee, H. O., Jawerth, L., Maharana, S., Jahnel, M., Hein, M. Y., et al. (2015). A liquid-to-solid phase transition of the ALS protein FUS accelerated by disease mutation. *Cell* 162, 1066–1077. doi: 10.1016/j.cell.2015.07.047

Qamar, S., Wang, G., Randle, S. J., Ruggeri, F. S., Varela, J. A., Lin, J. Q., et al. (2018). FUS phase separation is modulated by a molecular chaperone and methylation of arginine cation-π interactions. *Cell* 173, 720.e15–734.e15. doi: 10.1016/j.cell.2018.03.056

Rabbitts, T. H., Forster, A., Larson, R., and Nathan, P. (1993). Fusion of the dominant negative transcription regulator CHOP with a novel gene FUS by translocation t(12;16) in malignant liposarcoma. *Nat. Genet.* 4, 175–180. doi: 10.1038/ng0693-175

Sariki, S. K., Sahu, P. K., Golla, U., Singh, V., Azad, G. K., and Tomar, R. S. (2016). Sen1, the homolog of human Senataxin, is critical for cell survival through regulation of redox homeostasis, mitochondrial function, and the TOR pathway in Saccharomyces cerevisiae. *FEBS J.* 283, 4056–4083. doi: 10.1111/febs.13917

Shaw, C. E., Al-Chalabi, A., and Leigh, N. (2001). Progress in the pathogenesis of amyotrophic lateral sclerosis. *Curr. Neurol. Neurosci. Rep.* 1, 69–76. doi: 10.1007/s11910-001-0078-7

Shorter, J. (2008). Hsp104: a weapon to combat diverse neurodegenerative disorders. *Neurosignals* 16, 63–74. doi: 10.1159/000109760

Sreedharan, J., and Brown, R. H. Jr. (2013). Amyotrophic lateral sclerosis: problems and prospects. *Ann. Neurol.* 74, 309–316. doi: 10.1002/ana.24012

Sun, Z., Diaz, Z., Fang, X., Hart, M. P., Chesi, A., Shorter, J., et al. (2011). Molecular determinants and genetic modifiers of aggregation and toxicity for the ALS disease protein FUS/TLS. *PLoS Biol.* 9:e1000614. doi: 10.1371/journal.pbio.1000614

Tan, A. Y., and Manley, J. L. (2009). The TET family of proteins: functions and roles in disease. *J. Mol. Cell Biol.* 1, 82–92. doi: 10.1093/jmcb/mjp025

Tarlarini, C., Lunetta, C., Mosca, L., Avemaria, F., Riva, N., Mantero, V., et al. (2015). Novel FUS mutations identified through molecular screening in a large cohort of familial and sporadic amyotrophic lateral sclerosis. *Eur. J. Neurol.* 22, 1474–1481. doi: 10.1111/ene.12772

Tenreiro, S., Munder, M. C., Alberti, S., and Outeiro, T. F. (2013). Harnessing the power of yeast to unravel the molecular basis of neurodegeneration. *J. Neurochem.* 127, 438–452. doi: 10.1111/jnc.12271

Torrente, M. P., Chuang, E., Noll, M. M., Jackrel, M. E., Go, M. S., and Shorter, J. (2016). Mechanistic insights into Hsp104 potentiation. *J. Biol. Chem.* 291, 5101–5115. doi: 10.1074/jbc.m115.707976

Urwin, H., Josephs, K. A., Rohrer, J. D., Mackenzie, I. R., Neumann, M., Authier, A., et al. (2010). FUS pathology defines the majority of tau- and TDP-43-negative frontotemporal lobar degeneration. *Acta Neuropathol.* 120, 33–41. doi: 10.1007/s00401-010-0698-6

Vance, C., Rogelj, B., Hortobágyi, T., De Vos, K. J., Nishimura, A. L., Sreedharan, J., et al. (2009). Mutations in FUS, an RNA processing protein, cause familial amyotrophic lateral sclerosis type 6. *Science* 323, 1208–1211. doi: 10.1126/science.1165942

Vashist, S., Cushman, M., and Shorter, J. (2010). Applying Hsp104 to protein-misfolding disorders. This paper is one of a selection of papers published in this special issue entitled 8th International Conference on AAA Proteins and has undergone the Journal's usual peer review process. *Biochem. Cell Biol.* 88, 1–13. doi: 10.1139/o09-121

Willingham, S., Outeiro, T. F., DeVit, M. J., Lindquist, S. L., and Muchowski, P. J. (2003). Yeast genes that enhance the toxicity of a mutant huntingtin fragment or α-synuclein. *Neurotoxicology* 302, 1769–1772. doi: 10.1126/science.1090389

Woulfe, J., Gray, D. A., and Mackenzie, I. R. (2010). FUS-immunoreactive intranuclear inclusions in neurodegenerative disease. *Brain Pathol.* 20, 589–597. doi: 10.1111/j.1750-3639.2009.00337.x

Xia, R., Liu, Y., Yang, L., Gal, J., Zhu, H., and Jia, J. (2012). Motor neuron apoptosis and neuromuscular junction perturbation are prominent features in a *Drosophila* model of Fus-mediated ALS. *Mol. Neurodegener.* 7:10. doi: 10.1186/1750-1326-7-10

Yang, L., Gal, J., Chen, J., and Zhu, H. (2014). Self-assembled FUS binds active chromatin and regulates gene transcription. *Proc. Natl. Acad. Sci. U S A* 111, 17809–17814. doi: 10.1073/pnas.1414004111

Yoshizawa, T., Ali, R., Jiou, J., Fung, H. Y. J., Burke, K. A., Kim, S. J., et al. (2018). Nuclear import receptor inhibits phase separation of FUS through binding to multiple sites. *Cell* 173, 693.e22–705.e22. doi: 10.1016/j.cell.2018.03.003

Zabrocki, P., Bastiaens, I., Delay, C., Bammens, T., Ghillebert, R., Pellens, K., et al. (2008). Phosphorylation, lipid raft interaction and traffic of α-synuclein in a yeast model for Parkinson. *Biochim. Biophys. Acta* 1783, 1767–1780. doi: 10.1016/j.bbamcr.2008.06.010

Zinszner, H., Sok, J., Immanuel, D., Yin, Y., and Ron, D. (1997). TLS (FUS) binds RNA *in vivo* and engages in nucleo-cytoplasmic shuttling. *J. Cell Sci.* 110, 1741–1750.

Conflict of Interest Statement: The authors declare that the research was conducted in the absence of any commercial or financial relationships that could be construed as a potential conflict of interest.

frontiers in Molecular Neuroscience

MINI REVIEW
published: 12 July 2018
doi: 10.3389/fnmol.2018.00237

The Insoluble Protein Deposit (IPOD) in Yeast

*Stephanie Rothe†, Abaya Prakash† and Jens Tyedmers**

Department of Medicine I and Clinical Chemistry, Heidelberg University Hospital, Heidelberg, Germany

The appearance of protein aggregates is a hallmark of several pathologies including many neurodegenerative diseases. Mounting evidence suggests that the accumulation of misfolded proteins into inclusions is a secondary line of defense when the extent of protein misfolding exceeds the capacity of the Protein Quality Control System, which mediates refolding or degradation of misfolded species. Such exhaustion can occur during severe proteotoxic stress, the excessive occurrence of aggregation prone protein species, e.g., amyloids, or during ageing. However, the machinery that mediates recognition, recruitment and deposition of different types of misfolded proteins into specific deposition sites is only poorly understood. Since emerging principles of aggregate deposition appear evolutionarily conserved, yeast represents a powerful model to study basic mechanisms of recognition of different types of misfolded proteins, their recruitment to the respective deposition site and the molecular organization at the corresponding site. Yeast possesses at least three different aggregate deposition sites, one of which is a major deposition site for amyloid aggregates termed Insoluble PrOtein Deposit (IPOD). Due to the link between neurodegenerative disease and accumulation of amyloid aggregates, the IPOD is of particular interest when we aim to identify the molecular mechanisms that cells have evolved to counteract toxicity associated with the occurrence of amyloid aggregates. Here, we will review what is known about IPOD composition and the mechanisms of recognition and recruitment of amyloid aggregates to this site in yeast. Finally, we will briefly discuss the possible physiological role of aggregate deposition at the IPOD.

Keywords: yeast (*Saccharomyces cerevisiae*), amyloid aggregates, neurodegenerative disease, insoluble protein deposit (IPOD), phagophore assembly site (PAS), actin, vesicular transport, Atg9 vesicles

OPEN ACCESS

Edited by:
Ralf J. Braun,
University of Bayreuth, Germany

Reviewed by:
Daniel Kaganovich,
Hebrew University of Jerusalem, Israel
Frank Shewmaker,
Uniformed Services University, United States

***Correspondence:**
Jens Tyedmers
jens.tyedmers@med.uni-heidelberg.de

†These authors have contributed equally to this work.

***Received:** 13 April 2018*
***Accepted:** 18 June 2018*
***Published:** 12 July 2018*

Citation:
Rothe S, Prakash A and Tyedmers J (2018) The Insoluble Protein Deposit (IPOD) in Yeast. Front. Mol. Neurosci. 11:237. doi: 10.3389/fnmol.2018.00237

INTRODUCTION

The Protein Quality Control System, comprising molecular chaperones and proteolytic machineries, ensures that proteins reach and maintain their native state. It recognizes misfolded species and either reverts them to the native state or eliminates them (Bukau et al., 2006; Hartl and Hayer-Hartl, 2009). However, when the generation of misfolded proteins exceeds the capacity of those systems, they accumulate and can coalesce into aggregates. Aggregates can be structurally very diverse. They range from more amorphously appearing aggregates with a low degree of structured elements to those with a high degree of structure such as amyloid aggregates (Kikis et al., 2010; Tyedmers et al., 2010a; Hipp et al., 2014). Amyloids are highly ordered, insoluble fibrous aggregates with a very high content of β-strands being oriented perpendicularly to the fibril axis. Their occurrence is a hallmark of several fatal neurodegenerative diseases (Knowles et al., 2014). It is currently still under debate why amyloid aggregates can become detrimental to the cell, but it

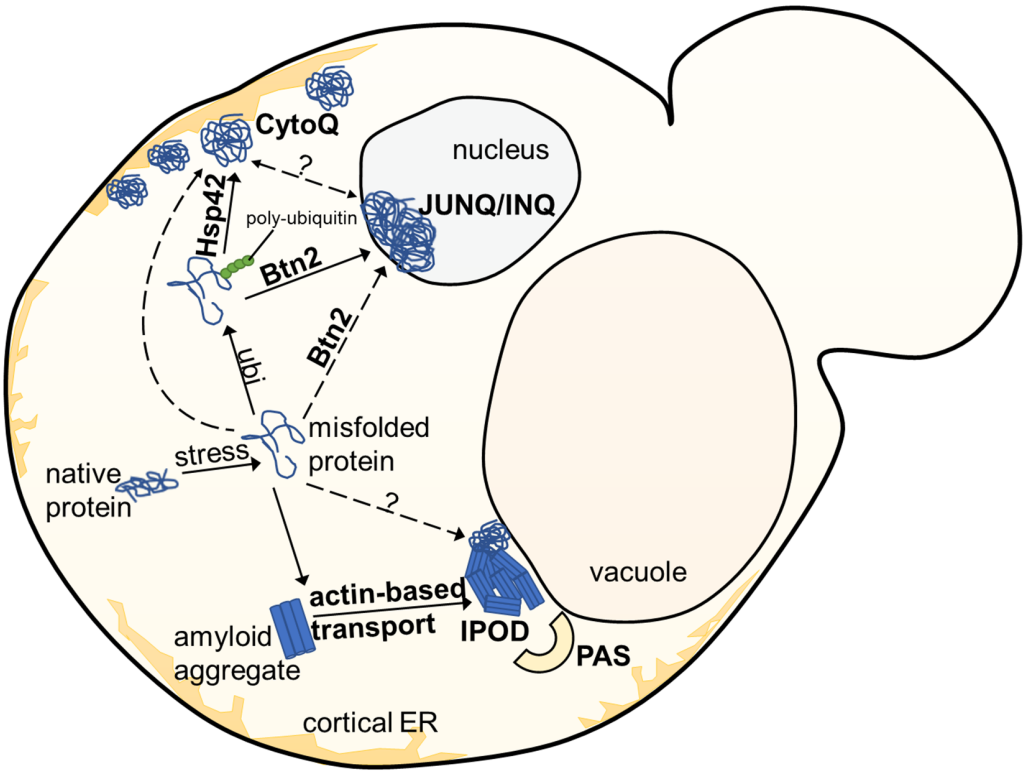

FIGURE 1 | Overview of aggregate deposition sites in the yeast *S. cerevisiae*. Upon exposure to stress, misfolded or damaged proteins are targeted for either degradation or refolding, aided by molecular chaperones. Soluble protein aggregates are either targeted to the JUNQ/INQ compartment by the nuclear sorting factor Btn2, or to the peripherally localized Q-Bodies/CytoQ by the cytosolic Hsp42. Amyloidogenic aggregates accumulate predominantly at the perivacuolar insoluble protein deposit (IPOD) site adjacent to the Phagophore Assembly Site (PAS), targeted by an actin-based transport machinery, which has not yet been completely elucidated.

was suggested that one determinant is the capacity of the aggregates to promote aberrant protein interactions that can capture other essential cellular proteins (Olzscha et al., 2011; Park et al., 2013; Hipp et al., 2014). Thus, mounting evidence supports the hypothesis that the sequestration of aggregates including amyloids into specialized deposition sites is a key defensive strategy for protecting the cell from harmful interactions. In case of amyloidogenic proteins, sequestration may limit templated conversion of other protein molecules into the amyloid form (Kopito, 2000; Arrasate et al., 2004; Tanaka et al., 2004; Tyedmers et al., 2010a; Olzscha et al., 2011; Holmes et al., 2014). Not surprisingly then, aggregate deposition sites have evolved very early during evolution and hence exist in simple eukaryotes such as yeast as well as in humans (Kaganovich et al., 2008; Tyedmers et al., 2010a; Sontag et al., 2014; Miller et al., 2015b).

In yeast, several often spatially separated deposition sites have been described (**Figure 1**). Those comprise: (i) the "JUxtaNuclear Quality Control Compartment (JUNQ)" (Kaganovich et al., 2008); (ii) the "IntraNuclear Quality Control Compartment (INQ)" (Gallina et al., 2015; Miller et al., 2015a); (iii) the "Insoluble PrOtein Deposit (IPOD)" (Kaganovich et al., 2008); (iv) peripheral aggregates (Specht et al., 2011; Malinovska et al., 2012; Shiber et al., 2013); (v) stress foci (Spokoini et al., 2012); and (vi) "Q-Bodies" (Escusa-Toret et al., 2013). The latter three structures were suggested to represent the same structure. It was simply discovered and named differently by different laboratories. It was therefore proposed to rename these structures as "CytoQ" (Miller et al., 2015a). The JUNQ and INQ compartments are formed under similar conditions by similar model substrates but differ in their cellular localization. While the JUNQ displays a perinuclear localization in an indentation of the nuclear envelope (Kaganovich et al., 2008), the INQ is an intranuclear site (Gallina et al., 2015; Miller et al., 2015a). It is currently under debate whether they represent identical or independent structures (Miller et al., 2015b; Hill et al., 2017; Sontag et al., 2017). Specific nuclear proteins have been identified to accumulate strictly at the INQ, which could be a future tool to test whether JUNQ and INQ are identical or different structures (Gallina et al., 2015). CytoQ, JUNQ and INQ appear predominantly during proteotoxic stress and harbor misfolded cytosolic and nuclear proteins that are more soluble and exchange rapidly with the surrounding cellular environment, whereas the IPOD seems to harbor predominantly less soluble, terminally aggregated misfolded proteins. The IPOD forms also under non-stress conditions and is described primarily as a depository for amyloid aggregates. However, it can also harbor non-amyloid substrates (Kaganovich et al., 2008; Sontag et al., 2014; Miller et al., 2015b; Hill et al., 2017). **Figure 2** gives an

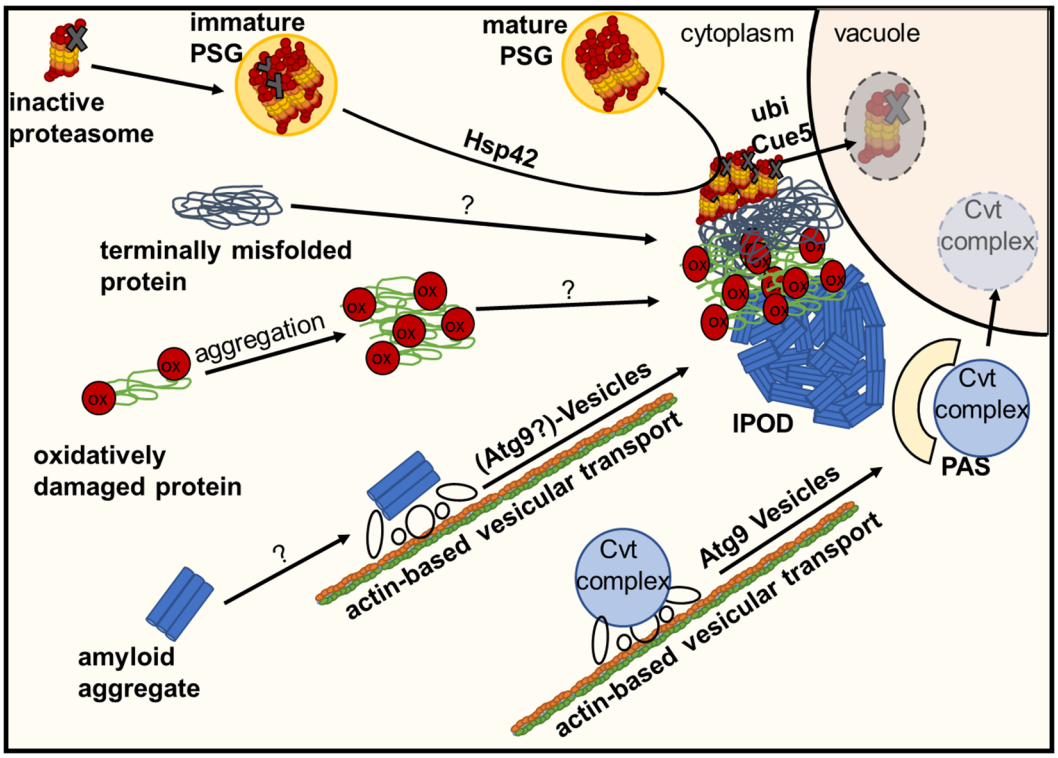

FIGURE 2 | Deposition of damaged or inactive proteins, amyloids or protein complexes at the IPOD. Inactive proteasomes associated with Proteasome Storage Granules (PSGs) are known to accumulate at the IPOD in a Hsp42-dependent manner. Amyloid aggregates are targeted there by an actin-based transport machinery which overlaps with the recruitment machinery for vacuolar hydrolase precursors and their specific receptor (Cvt complex) to the pre-autophagosomal structure (PAS) via Atg9 vesicles, where these precursors are packaged into cytoplasm-to-vacuole vesicles for delivery to the lumen of the vacuole. It is hypothesized that large terminally misfolded proteins and oxidatively damaged proteins also accumulate at the IPOD in an as yet unknown manner.

overview of the different substrate classes deposited at the IPOD. Since especially amyloids are associated with many late-onset neurodegenerative diseases, we will focus on the IPOD, and refer to other review articles for more detailed descriptions on JUNQ, INQ and CytoQ (Sontag et al., 2014, 2017; Miller et al., 2015b; Hill et al., 2017).

COMPOSITION OF THE INSOLUBLE PROTEIN DEPOSIT (IPOD)

The perivacuolar IPOD (Kaganovich et al., 2008; Tyedmers et al., 2010b) is located directly adjacent to the pre-autophagosomal structure (PAS; Suzuki and Ohsumi, 2010) where the cell initiates biogenesis of autophagosomes and Cytoplasm-to-vacuole targeting (Cvt) vesicles. The IPOD was described first by Frydman and co-workers (Kaganovich et al., 2008) as a deposition site for terminally aggregated proteins. Substrate proteins accumulating here comprise amorphously aggregated, terminally misfolded proteins such as ubc9ts and VHL on the one hand and amyloidogenic proteins on the other hand. Ubc9ts is a thermosensitive variant of the SUMO-conjugating enzyme Ubc9 (Tongaonkar et al., 1999) whereas VHL is the heterologously expressed "Von Hippel-Lindau tumor supressor (VHL)" that fails to properly fold in yeast (McClellan et al., 2005). It should be noted that these model substrates partitioned not only to the IPOD, but also to the JUNQ, INQ and CytoQs (Kaganovich et al., 2008; Specht et al., 2011; Escusa-Toret et al., 2013; Miller et al., 2015a), which makes it difficult to use them as a clear-cut marker for the IPOD. This is even more relevant when one considers that CytoQs, whose formation is strictly dependent on Hsp42, present initially upon stress as multiple foci that coalesce later into very few larger ones, and under impaired proteasomal activity even into a single perivacuolar deposition that could represent the IPOD (Spokoini et al., 2012). In contrast, amyloidogenic proteins appear to be targeted exclusively to the IPOD and are often used to define a single perivacuolar inclusion as IPOD (Kaganovich et al., 2008; Tyedmers et al., 2010b; Malinovska et al., 2012). These include the yeast prions Rnq1, Ure2 and Sup35. They accumulate at the IPOD constitutively without any external stress when overproduced (Kaganovich et al., 2008; Tyedmers et al., 2010b; Saibil et al., 2012). Additional potential prion proteins (Alberti et al., 2009) that often form a single inclusion resembling the IPOD are Mot3, Lsm4 and Nrp1 (Winkler et al., 2012). Moreover, the amyloid forming "huntingtin exon1 with expanded polyglutamine and polyproline domains (Htt103Q)" is deposited at this site (Kaganovich et al., 2008; Kryndushkin et al., 2012). Additional substrates for the IPOD

may include proteins that are particularly sensitive to the oxidative modification of carbonylation. Since they were found to partially co-localize with the IPOD after oxidative stress, it was suggested that they were deposited here due to oxidative damage (Tyedmers et al., 2010b). Interestingly, the major cytosolic peroxiredoxin in yeast, Tsa1, was found to be necessary to recruit Hsp70 chaperones and Hsp104 to H_2O_2-induced aggregates accumulating in inclusions such as JUNQ- and IPOD (Hanzen et al., 2016), further supporting a possible role of the IPOD in handling protein aggregates during oxidative stress. Furthermore, GFP fusions of proteins that are known to form inclusions in patients with amyotrophic lateral sclerosis (ALS), namely optineurin (OPTN)-GFP and an N-terminal GFP fusion of Fus1, were found to often form single inclusions co-localizing with the bonafide IPOD substrates Rnq1-GFP and Htt103Q (Kryndushkin et al., 2012). These substrates did not form amyloids in the corresponding study. In addition, it has also been reported that proteasome storage granules (PSGs) associate transiently with the IPOD upon their formation under environmental stress conditions (Peters et al., 2015, 2016). PSGs initially contain functional proteasomes as well as damaged ones. However, during transient co-localization with the IPOD, the damaged proteasomes are sorted from the PSGs to the IPOD in an Hsp42-dependent manner, while the mature PSGs, containing only functional proteasomes, dissociate from the IPOD. The proteasomes remaining at the IPOD are further heavily ubiquitinated and removed from the cell by a selective autophagic mechanism termed proteaphagy, which requires the ubiquitin receptor Cue5 (Peters et al., 2015, 2016; Marshall et al., 2016).

Thus, the fate of defective proteasomes that accumulate only transiently at the IPOD is turnover by proteaphagy. For other substrates, much less is known about their fate. For the amyloid forming fusion protein of the prion domain of Sup35 and GFP (PrD-GFP), it was shown in pulse-chase type of experiments that the protein slowly decays from the IPOD in an Hsp104 and proteasome dependent manner. Although a contribution of autophagy on turnover of PrD-GFP residing at the IPOD could not be excluded, there was no direct evidence found for this (Kumar et al., 2016). Along these lines, the yeast metacaspase Mca1 was found to localize to JUNQ and IPOD-like inclusions to counteract accumulation of terminally misfolded and aggregated proteins in an Hsp104 and proteasome-dependent manner (Hill et al., 2014).

Morphologically, IPODs consisting of the prion domain of Sup35 or GFP-fusions thereof, have been studied with different electron microscopy-based methods. This revealed that the prion amyloids in the IPODs display arrays of aligned bundles of regularly spaced fibrils without any bordering structures (Kawai-Noma et al., 2010; Tyedmers et al., 2010a; Saibil et al., 2012; O'Driscoll et al., 2015). Molecular chaperones show a non-uniform distribution within the IPOD. The chaperone Hsp104 is often found in an arrangement around the periphery of the IPOD (Kaganovich et al., 2008; O'Driscoll et al., 2015). Its presence there might reflect its roles in the disaggregation or fragmentation of prion aggregates (Paushkin et al., 1996; Kryndushkin et al., 2003; Shorter and Lindquist, 2004; Satpute-Krishnan et al., 2007; Tyedmers et al., 2010b; Winkler et al., 2012). The Hsp70 chaperones Ssa1 and Ssa2 and their co-chaperone Sis1 are very abundant within the IPOD (Bagriantsev et al., 2008; Saibil et al., 2012). Furthermore, it was found that manipulations of the Hsp70 chaperone machinery caused remodeling of the aggregates in the IPOD with a higher presence of non-fibrillar amorphous structures (O'Driscoll et al., 2015). Therefore, molecular chaperones have important roles in determining the structural organization of fibrils in the IPOD.

IPOD-like inclusions also exist in mammalian cells and have been characterized as dense, immobile, stable compartments, which are not initially ubiquitinated (Kaganovich et al., 2008; Hipp et al., 2012; Weisberg et al., 2012). In yeast, JUNQ and IPOD inclusions are tethered to organelles and dependent on a functional cytoskeleton, whereas the mammalian IPOD does not appear to be specifically associated with the cytoskeleton or the microtubule organizing center (MTOC). (Ogrodnik et al., 2014). Furthermore, additional mammalian aggregate deposition sites such as the aggresome exist where amyloid aggregates accumulate. For a more detailed view on these compartments, we refer to additional reviews (Tyedmers et al., 2010a; Amen and Kaganovich, 2015; Sontag et al., 2017).

SUBSTRATE TARGETING TO THE IPOD

Targeting of Non-amyloid Substrates to the IPOD

As mentioned before, the IPOD harbors different classes of substrates, but not all of them require the same targeting signals. For the aggregation prone non-amyloid substrate OPTN-GFP, the expression levels influence its targeting efficiency to the IPOD, as higher expression levels of the construct caused appearance of additional aggregate foci next to a major IPOD deposition site (Kryndushkin et al., 2012). This predicts that the capacity for recruitment to and/or accumulation of substrates at the IPOD is limited. Furthermore, the orientation of the GFP tag influenced targeting, as despite similar expression levels, a GFP-OPTN fusion was more efficiently targeted as compared to a C-terminal OPTN-GFP fusion (Kryndushkin et al., 2012). Interestingly, a similar observation was made with Fus1-GFP: whereas Fus1-GFP formed multiple cytoplasmic foci, the corresponding N-terminal GFP-Fus1 fusion was targeted efficiently to the IPOD (Kryndushkin et al., 2011, 2012). A similar dependency on the flanking regions of an IPOD substrate was observed for different variants of Htt103Q. While the protein often aggregated in one major focus in the presence of for example a flanking poly-proline stretch, its absence caused the protein to form dispersed foci in the cytoplasm (Duennwald et al., 2006; Kaganovich et al., 2008; Wang et al., 2009; Kryndushkin et al., 2012). Although the identity of the single inclusion of Htt103Q as IPOD is still under debate, together these data suggest that there are intrinsic features in the substrates that have to

be accessible to allow for efficient IPOD targeting. Whether these features may represent particular substrate conformations or binding sites for specific targeting factors remain to be elucidated.

Despite this progress in understanding determining features in the substrate, knowledge about unique targeting factors for the IPOD is very limited. In this regard, it is discussed controversially whether two confirmed targeting factors for the JUNQ/INQ and Q-Bodies/CytoQ, namely Btn2 and Hsp42, may also be involved in targeting of substrates to the IPOD. For OPTN-GFP, a co-localization with Btn2 in the major deposition site was observed. However, a direct interaction between OPTN-GFP and Btn2 was not found. Furthermore, depletion of Btn2 caused only a slight reduction in OPTN-GFP targeting to the IPOD, but did not abolish it (Kryndushkin et al., 2012). For amyloids, partial co-localization with Btn2 was also observed (Alberti, 2012; Kryndushkin et al., 2012; Malinovska et al., 2012), however Btn2 deletion showed no discernible defects in localizing amyloid aggregates to the IPOD (Alberti, 2012). Therefore, Btn2 is currently considered mostly as a targeting factor for misfolded proteins to the JUNQ/INQ (Alberti, 2012; Miller et al., 2015b).

The small heat shock protein Hsp42 has been identified as a general targeting factor for the Q-Body/CytoQ compartment (Specht et al., 2011; Escusa-Toret et al., 2013; Miller et al., 2015a). Interestingly, it was also crucial for targeting of inactive proteasomes to the IPOD (Alberti, 2012; Marshall et al., 2016; Peters et al., 2016).

Targeting of Amyloid Substrates to the IPOD

Although Hsp42 and Btn2 have been implicated in targeting of selective substrates to the IPOD, their deletion did not affect targeting of amyloid substrates to the IPOD (Specht et al., 2011; Alberti, 2012; Escusa-Toret et al., 2013). In contrast, a possible link between a Ubiquitin-Proteasome-System component, namely the E3 ubiquitin ligase Ltn1, and deposition of amyloidogenic huntingtin aggregates into single large inclusions representing the IPOD was observed. Ltn1, also known as a key factor for targeting aborted translation products for proteasomal destruction, was found to stimulate accumulation of Htt103Q with a polyproline stretch at the IPOD. It was suggested that an intermediate range of Hsf1 activity was crucial and may regulate actin cytoskeleton dynamics and thereby affect sequestration of Htt103Q aggregates through Ltn1 (Yang et al., 2016). This possible dependency of substrate recruitment on actin cytoskeleton dynamics is in agreement with another study reporting that amyloid targeting to the IPOD was strongly reduced by depletion of proteins that function in actin cable-based transport processes, such as the motor protein Myo2 and tropomyosin (Kumar et al., 2016, 2017). An intact actin cytoskeleton is also required for aggregate targeting to the JUNQ/INQ (Specht et al., 2011) and asymmetric inheritance of protein aggregates (Ganusova et al., 2006; Liu et al., 2010, 2011; Chernova et al., 2011; Song et al., 2014). On a side note, an involvement of microtubules in the formation of JUNQ/INQ and IPOD depositions was initially suggested (Kaganovich et al., 2008), but turned out to be due to an unspecific effect of the microtubule-depolymerizing drug benomyl used in these experiments (Specht et al., 2011). Taken together, a role of the actin cytoskeleton in IPOD targeting of amyloids was consistent with previous findings. In contrast, an involvement of several proteins known to act in vesicular transport and fusion events in amyloid targeting to the IPOD (Kumar et al., 2016, 2017) was initially rather surprising. In more detail, it was found that depletion of the SNARE disassembly factor Sec18, the Sec14 and Sec21 proteins as well as deletion of the dynamin-like small GTPase Vps1 prevented accumulation of model amyloids at the IPOD but resulted reversibly in multiple smaller aggregates dispersed throughout the cytoplasm, that were interpreted as transport intermediates (Kumar et al., 2016, 2017). Strikingly, the dependency on these factors for proper amyloid targeting to the IPOD mirrored the requirements for faithful targeting of preApe1 to the perivacuolar Phagophore Assembly Site (PAS; Monastyrska et al., 2009; Lynch-Day and Klionsky, 2010; Suzuki, 2013) directly adjacent to the IPOD (Kaganovich et al., 2008; Tyedmers et al., 2010b). PreApe1 is a vacuolar precursor aminopeptidase present in large oligomeric complexes. For its recruitment to the PAS, where it is packed into autophagosome-like vesicles for delivery to the vacuolar lumen, it is attached to the outside of small transport vesicles termed Atg9 vesicles that move along actin cables (He et al., 2006). Interestingly, depleting components of this actin-cable based vesicular recruitment system did not only abolish proper accumulation of preApe1 at the PAS and amyloid aggregates at the IPOD, respectively, but both substrates co-localized with each other as multiple transport intermediates. These accumulations also harbored Myo2 and Atg9, the marker protein for Atg9 vesicles. Thus, it was hypothesized that the recruitment machinery for amyloid aggregates overlaps with that for preApe1 and involves Atg9- or related vesicles that move along actin cables with the aid of Myo2 (Kumar et al., 2016, 2017). How can a possible recruitment of amyloid aggregates on (Atg9) vesicles be reconciled with the observed effects for depletion of Sec14, 18, 21 and Vps1? Atg9 vesicles originate from the Golgi and are stored in cytoplasmic reservoirs as vesicles and tubular structures that can be activated for their rapid recruitment to the PAS if needed (Mari et al., 2010; Ohashi and Munro, 2010; Yamamoto et al., 2012). Atg9 vesicle-based transport requires several SNARE proteins (Nair and Klionsky, 2011; Nair et al., 2011). Hence, depleting Sec18, which is crucial for SNARE protein function (Mayer et al., 1996), would disturb faithful recruitment of Atg9 vesicles including their cargos to the PAS or the adjacent IPOD. Sec14 is a phosphatidylinositol/phosphatidylcholine (PI/PC) transfer protein that transfers PI lipid from the ER to the Golgi, where PI is phosphorylated to generate phosphatidylinositol-4-phosphate (PI4P; Bankaitis et al., 1990; Hama et al., 1999; Grabon et al., 2015). The pool of PI4P in turn regulates the extent to which Golgi-derived secretory vesicles can be formed (Hama et al., 1999; Grabon et al., 2015). In fact, it was demonstrated that reducing PI4P formation blocks anterograde

transport of Atg9 vesicles from the Golgi to the PAS (Wang et al., 2012). Vps1 is one of three dynamin-like proteins in yeast. Dynamins are involved in membrane fusion and fission events (Williams and Kim, 2014). Strikingly, the mammalian dynamin 2 (DNM2) was recently shown to be involved in the generation of Atg9 containing vesicles (Takahashi et al., 2016). Although such a role has not been confirmed for Vps1, it seems possible that Vps1 is also involved in Atg9 vesicle biogenesis in yeast. The last protein whose depletion resulted in impaired recruitment of amyloid aggregates to the IPOD was the COPI vesicle component Sec21, which was shown recently to influence dynamics of Golgi cisternae (Ishii et al., 2016). Although this is purely speculative, interfering with Sec21 function may potentially also affect Atg9 vesicle biogenesis at the Golgi.

In summary, these data indicate that vesicle-based transport along actin cables plays an important role in recruitment of amyloids to the IPOD. This rather new concept of aggregates hitchhiking vesicular transport routes was also proposed by Nystroem and co-workers when they observed that deletion or overexpression of components of the vacuole inheritance machinery or endocytic vesicles, among them Vps1 and the myosin dependent adaptor protein Vac17, impaired or enhanced, respectively, recruitment of heat induced and Hsp104 bound aggregates to a perivacuolar inclusion site reminiscent of the IPOD (Hill et al., 2016).

PHYSIOLOGICAL ROLE OF AGGREGATE DEPOSITION INTO THE IPOD

Sequestration Function

A general function of aggregate deposition into specialized deposition sites may be sequestration, either temporal, as anticipated for the JUNQ/INQ, or prolonged as thought for the IPOD (Sontag et al., 2014; Miller et al., 2015b). As shown particularly for amyloid aggregates, their deposition may reduce harmful aberrant interactions with other cellular proteins (Olzscha et al., 2011; Park et al., 2013). This sequestration function was further substantiated by the observation that the toxicity associated with accumulating amyloidogenic proteins inversely correlated with the degree of organization: deposition into few to a single inclusion such as the IPOD was associated with less toxicity as compared to accumulation into multiple aggregate foci (Duennwald et al., 2006; Wang et al., 2009; Kryndushkin et al., 2012).

Asymmetric Inheritance of Aggregates

Protein aggregates have been identified as aging factors that are inherited asymmetrically between mother and daughter cells. This refers to both amyloid aggregates as well as non-amyloid ones. Different principles that contribute to this asymmetry emerged, which may not be mutually exclusive (Tyedmers et al., 2010a; Nyström and Liu, 2014; Hill et al., 2017; Sontag et al., 2017). One of these mechanisms comprise the deposition of aggregates into quality control compartments such as JUNQ/INQ or IPOD, which were observed to stay in mother cells during division (Kaganovich et al., 2008; Tyedmers et al., 2010b; Spokoini et al., 2012; Hill et al., 2017). Consequently, deposition contributes to achieving damage asymmetry.

Prion Induction

Deposition of specifically prion aggregates at the IPOD may aid another function, namely prion formation and propagation (Tyedmers et al., 2008, 2010b; Tyedmers, 2012). This hypothesis was based on the observation that a specific prion induction intermediate intersected with the IPOD (Tyedmers et al., 2010b; Saibil et al., 2012). It was discussed that misfolded species of the Sup35 prion protein ([PSI^+]) in the non-prion state may be targeted to the IPOD for sequestration during proteotoxic stress. At the IPOD, Sup35 molecules get into contact with their inducer prion, [RNQ^+] (Tyedmers et al., 2010b; Tyedmers, 2012) known to be present here as well (Kaganovich et al., 2008), and can adopt the prion conformation. However, other studies found that conversion to the prion state does not necessarily need to take place at the IPOD, but can also happen in the cell periphery, for example through association with actin patches (Ganusova et al., 2006; Mathur et al., 2010; Chernova et al., 2011). Most recently, it was suggested that induction of the [PSI^+] prion through misfolded Sup35p molecules damaged by oxidative stress requires an active actin cytoskeleton and deposition at the IPOD, whereas prion induction by overexpression of the [PSI^+] prion determinant Sup35 does not have these requirements (Speldewinde et al., 2017).

OUTLOOK

During the past years, it became more and more obvious that protein aggregation is not a random process but represents a second line of defense. It involves a sophisticated cellular machinery that comes into play when the cellular protein quality control systems to either refold or degrade misfolded proteins are overwhelmed. In such a situation, different types of misfolded or aberrantly folded proteins are deposited into different specialized aggregate deposition sites. This implies that the cell must be able to recognize and direct different types of misfolded proteins to the respective deposition site, and recent evidence suggests that deposition at the appropriate site can be crucial for the fidelity of the cell (Weisberg et al., 2012; Wolfe et al., 2013). Deciphering the cellular machinery and involved factors that handle amyloid aggregates will shed light into their potential role in neurodegenerative diseases. This becomes even more crucial when one considers that IPOD-like structures were described in mammalian cells as well.

Moreover, IPODs that function in sequestration of misfolded proteins and amyloids, prion induction and asymmetric distribution of aggregates during cell division, might have another potential role in the yeast cell: the IPOD may also represent a sorting center for large aggregates and high molecular weight protein complexes destined for autophagic

turnover. This hypothesis originates from the observation that the substrates ranging from amyloids, terminally misfolded proteins, carbonylated, oxidatively damaged proteins (Nyström, 2005) and defective and inactive proteasomes are all large structures. Furthermore, the cell accumulates large multimeric complexes of vacuolar precursor hydrolases on transit to the vacuolar lumen via the Cvt-pathway (Lynch-Day and Klionsky, 2010; Suzuki, 2013) directly next to the IPOD. Future studies have to confirm or reject such a possible role.

AUTHOR CONTRIBUTIONS

JT conceptualized and wrote the manuscript. SR wrote the manuscript and designed the figures. AP wrote the manuscript.

FUNDING

This study was supported by a grant from the Deutsche Forschungsgemeinschaft to JT (TY93/1-2).

ACKNOWLEDGMENTS

We would also like to acknowledge financial support by Deutsche Forschungsgemeinschaft within the funding program Open Access Publishing, by the Baden-Württemberg Ministry of Science, Research and the Arts and by Ruprecht-Karls-Universität Heidelberg. Furthermore, we would like to thank Prof. Bernd Bukau and members of his lab and Prof. Peter P. Nawroth and members of his lab for helpful discussions during the project.

REFERENCES

Alberti, S. (2012). Molecular mechanisms of spatial protein quality control. *Prion* 6, 437–442. doi: 10.4161/pri.22470

Alberti, S., Halfmann, R., King, O., Kapila, A., and Lindquist, S. (2009). A systematic survey identifies prions and illuminates sequence features of prionogenic proteins. *Cell* 137, 146–158. doi: 10.1016/j.cell.2009.02.044

Amen, T., and Kaganovich, D. (2015). Dynamic droplets: the role of cytoplasmic inclusions in stress, function, and disease. *Cell. Mol. Life Sci.* 72, 401–415. doi: 10.1007/s00018-014-1740-y

Arrasate, M., Mitra, S., Schweitzer, E. S., Segal, M. R., and Finkbeiner, S. (2004). Inclusion body formation reduces levels of mutant huntingtin and the risk of neuronal death. *Nature* 431, 805–810. doi: 10.1038/nature02998

Bagriantsev, S. N., Gracheva, E. O., Richmond, J. E., and Liebman, S. W. (2008). Variant-specific [PSI^+] infection is transmitted by Sup35 polymers within [PSI^+] aggregates with heterogeneous protein composition. *Mol. Biol. Cell* 19, 2433–2443. doi: 10.1091/mbc.E08-01-0078

Bankaitis, V. A., Aitken, J. R., Cleves, A. E., and Dowhan, W. (1990). An essential role for a phospholipid transfer protein in yeast Golgi function. *Nature* 347, 561–562. doi: 10.1038/347561a0

Bukau, B., Weissman, J., and Horwich, A. (2006). Molecular chaperones and protein quality control. *Cell* 125, 443–451. doi: 10.1016/j.cell.2006.04.014

Chernova, T. A., Romanyuk, A. V., Karpova, T. S., Shanks, J. R., Ali, M., Moffatt, N., et al. (2011). Prion induction by the short-lived, stress-induced protein Lsb2 is regulated by ubiquitination and association with the actin cytoskeleton. *Mol. Cell* 43, 242–252. doi: 10.1016/j.molcel.2011.07.001

Duennwald, M. L., Jagadish, S., Muchowski, P. J., and Lindquist, S. (2006). Flanking sequences profoundly alter polyglutamine toxicity in yeast. *Proc. Natl. Acad. Sci. U S A* 103, 11045–11050. doi: 10.1073/pnas.0604547103

Escusa-Toret, S., Vonk, W. I., and Frydman, J. (2013). Spatial sequestration of misfolded proteins by a dynamic chaperone pathway enhances cellular fitness during stress. *Nat. Cell Biol.* 15, 1231–1243. doi: 10.1038/ncb2838

Gallina, I., Colding, C., Henriksen, P., Beli, P., Nakamura, K., Offman, J., et al. (2015). Cmr1/WDR76 defines a nuclear genotoxic stress body linking genome integrity and protein quality control. *Nat. Commun.* 6:6533. doi: 10.1038/ncomms7533

Ganusova, E. E., Ozolins, L. N., Bhagat, S., Newnam, G. P., Wegrzyn, R. D., Sherman, M. Y., et al. (2006). Modulation of prion formation, aggregation, and toxicity by the actin cytoskeleton in yeast. *Mol. Cell. Biol.* 26, 617–629. doi: 10.1128/mcb.26.2.617-629.2006

Grabon, A., Khan, D., and Bankaitis, V. A. (2015). Phosphatidylinositol transfer proteins and instructive regulation of lipid kinase biology. *Biochim. Biophys. Acta* 1851, 724–735. doi: 10.1016/j.bbalip.2014.12.011

Hama, H., Schnieders, E. A., Thorner, J., Takemoto, J. Y., and DeWald, D. B. (1999). Direct involvement of phosphatidylinositol 4-phosphate in secretion in the yeast *Saccharomyces cerevisiae*. *J. Biol. Chem.* 274, 34294–34300. doi: 10.1074/jbc.274.48.34294

Hanzen, S., Vielfort, K., Yang, J., Roger, F., Andersson, V., Zamarbide-Fores, S., et al. (2016). Lifespan control by redox-dependent recruitment of chaperones to misfolded proteins. *Cell* 166, 140–151. doi: 10.1016/j.cell.2016.05.006

Hartl, F. U., and Hayer-Hartl, M. (2009). Converging concepts of protein folding *in vitro* and *in vivo*. *Nat. Struct. Mol. Biol.* 16, 574–581. doi: 10.1038/nsmb.1591

He, C., Song, H., Yorimitsu, T., Monastyrska, I., Yen, W. L., Legakis, J. E., et al. (2006). Recruitment of Atg9 to the preautophagosomal structure by Atg11 is essential for selective autophagy in budding yeast. *J. Cell Biol.* 175, 925–935. doi: 10.1083/jcb.200606084

Hill, S. M., Hanzén, S., and Nyström, T. (2017). Restricted access: spatial sequestration of damaged proteins during stress and aging. *EMBO Rep.* 18, 377–391. doi: 10.15252/embr.201643458

Hill, S. M., Hao, X., Grönvall, J., Spikings-Nordby, S., Widlund, P. O., Amen, T., et al. (2016). Asymmetric inheritance of aggregated proteins and age reset in yeast are regulated by Vac17-dependent vacuolar functions. *Cell Rep.* 16, 826–838. doi: 10.1016/j.celrep.2016.06.016

Hill, S. M., Hao, X., Liu, B., and Nyström, T. (2014). Life-span extension by a metacaspase in the yeast *Saccharomyces cerevisiae*. *Science* 344, 1389–1392. doi: 10.1126/science.1252634

Hipp, M. S., Park, S. H., and Hartl, F. U. (2014). Proteostasis impairment in protein-misfolding and -aggregation diseases. *Trends Cell Biol.* 24, 506–514. doi: 10.1016/j.tcb.2014.05.003

Hipp, M. S., Patel, C. N., Bersuker, K., Riley, B. E., Kaiser, S. E., Shaler, T. A., et al. (2012). Indirect inhibition of 26S proteasome activity in a cellular model of Huntington's disease. *J. Cell Biol.* 196, 573–587. doi: 10.1083/jcb.201110093

Holmes, W. M., Klaips, C. L., and Serio, T. R. (2014). Defining the limits: protein aggregation and toxicity *in vivo*. *Crit. Rev. Biochem. Mol. Biol.* 49, 294–303. doi: 10.3109/10409238.2014.914151

Ishii, M., Suda, Y., Kurokawa, K., and Nakano, A. (2016). COPI is essential for Golgi cisternal maturation and dynamics. *J. Cell Sci.* 129, 3251–3261. doi: 10.1242/jcs.193367

Kaganovich, D., Kopito, R., and Frydman, J. (2008). Misfolded proteins partition between two distinct quality control compartments. *Nature* 454, 1088–1095. doi: 10.1038/nature07195

Kawai-Noma, S., Pack, C. G., Kojidani, T., Asakawa, H., Hiraoka, Y., Kinjo, M., et al. (2010). *In vivo* evidence for the fibrillar structures of Sup35 prions in yeast cells. *J. Cell Biol.* 190, 223–231. doi: 10.1083/jcb.201002149

Kikis, E. A., Gidalevitz, T., and Morimoto, R. I. (2010). Protein homeostasis in models of aging and age-related conformational disease. *Adv. Exp. Med. Biol.* 694, 138–159. doi: 10.1007/978-1-4419-7002-2_11

Knowles, T. P., Vendruscolo, M., and Dobson, C. M. (2014). The amyloid state and its association with protein misfolding diseases. *Nat. Rev. Mol. Cell Biol.* 15, 384–396. doi: 10.1038/nrm3810

Kopito, R. R. (2000). Aggresomes, inclusion bodies and protein aggregation. *Trends Cell Biol.* 10, 524–530. doi: 10.1016/s0962-8924(00)01852-3

Kryndushkin, D. S., Alexandrov, I. M., Ter-Avanesyan, M. D., and Kushnirov, V. V. (2003). Yeast [PSI^+] prion aggregates are formed by

small Sup35 polymers fragmented by Hsp104. *J. Biol. Chem.* 278, 49636–49643. doi: 10.1074/jbc.M307996200

Kryndushkin, D., Ihrke, G., Piermartiri, T. C., and Shewmaker, F. (2012). A yeast model of optineurin proteinopathy reveals a unique aggregation pattern associated with cellular toxicity. *Mol. Microbiol.* 86, 1531–1547. doi: 10.1111/mmi.12075

Kryndushkin, D., Wickner, R. B., and Shewmaker, F. (2011). FUS/TLS forms cytoplasmic aggregates, inhibits cell growth and interacts with TDP-43 in a yeast model of amyotrophic lateral sclerosis. *Protein Cell* 2, 223–236. doi: 10.1007/s13238-011-1525-0

Kumar, R., Nawroth, P. P., and Tyedmers, J. (2016). Prion aggregates are recruited to the insoluble protein deposit (IPOD) via myosin 2-based vesicular transport. *PLoS Genet.* 12:e1006324. doi: 10.1371/journal.pgen.1006324

Kumar, R., Neuser, N., and Tyedmers, J. (2017). Hitchhiking vesicular transport routes to the vacuole: amyloid recruitment to the Insoluble Protein Deposit (IPOD). *Prion* 11, 71–81. doi: 10.1080/19336896.2017.1293226

Liu, B., Larsson, L., Caballero, A., Hao, X., Oling, D., Grantham, J., et al. (2010). The polarisome is required for segregation and retrograde transport of protein aggregates. *Cell* 140, 257–267. doi: 10.1016/j.cell.2009.12.031

Liu, B., Larsson, L., Franssens, V., Hao, X., Hill, S. M., Andersson, V., et al. (2011). Segregation of protein aggregates involves actin and the polarity machinery. *Cell* 147, 959–961. doi: 10.1016/j.cell.2011.11.018

Lynch-Day, M. A., and Klionsky, D. J. (2010). The Cvt pathway as a model for selective autophagy. *FEBS Lett.* 584, 1359–1366. doi: 10.1016/j.febslet.2010.02.013

Malinovska, L., Kroschwald, S., Munder, M. C., Richter, D., and Alberti, S. (2012). Molecular chaperones and stress-inducible protein-sorting factors coordinate the spatiotemporal distribution of protein aggregates. *Mol. Biol. Cell* 23, 3041–3056. doi: 10.1091/mbc.E12-03-0194

Mari, M., Griffith, J., Rieter, E., Krishnappa, L., Klionsky, D. J., and Reggiori, F. (2010). An Atg9-containing compartment that functions in the early steps of autophagosome biogenesis. *J. Cell Biol.* 190, 1005–1022. doi: 10.1083/jcb.200912089

Marshall, R. S., McLoughlin, F., and Vierstra, R. D. (2016). Autophagic turnover of inactive 26S proteasomes in yeast is directed by the ubiquitin receptor Cue5 and the Hsp42 chaperone. *Cell Rep.* 16, 1717–1732. doi: 10.1016/j.celrep.2016.07.015

Mathur, V., Taneja, V., Sun, Y., and Liebman, S. W. (2010). Analyzing the birth and propagation of two distinct prions, $[PSI^+]$ and $[\text{Het-s}]_y$, in yeast. *Mol. Biol. Cell* 21, 1449–1461. doi: 10.1091/mbc.E09-11-0927

Mayer, A., Wickner, W., and Haas, A. (1996). Sec18p (NSF)-driven release of Sec17p (α-SNAP) can precede docking and fusion of yeast vacuoles. *Cell* 85, 83–94. doi: 10.1016/s0092-8674(00)81084-3

McClellan, A. J., Scott, M. D., and Frydman, J. (2005). Folding and quality control of the VHL tumor suppressor proceed through distinct chaperone pathways. *Cell* 121, 739–748. doi: 10.1016/j.cell.2005.03.024

Miller, S. B., Ho, C. T., Winkler, J., Khokhrina, M., Neuner, A., Mohamed, M. Y., et al. (2015a). Compartment-specific aggregases direct distinct nuclear and cytoplasmic aggregate deposition. *EMBO J.* 34, 778–797. doi: 10.15252/embj.201489524

Miller, S. B., Mogk, A., and Bukau, B. (2015b). Spatially organized aggregation of misfolded proteins as cellular stress defense strategy. *J. Mol. Biol.* 427, 1564–1574. doi: 10.1016/j.jmb.2015.02.006

Monastyrska, I., Rieter, E., Klionsky, D. J., and Reggiori, F. (2009). Multiple roles of the cytoskeleton in autophagy. *Biol. Rev. Camb. Philos. Soc.* 84, 431–448. doi: 10.1111/j.1469-185x.2009.00082.x

Nair, U., Jotwani, A., Geng, J., Gammoh, N., Richerson, D., Yen, W. L., et al. (2011). SNARE proteins are required for macroautophagy. *Cell* 146, 290–302. doi: 10.1016/j.cell.2011.06.022

Nair, U., and Klionsky, D. J. (2011). Autophagosome biogenesis requires SNAREs. *Autophagy* 7, 1570–1572. doi: 10.4161/auto.7.12.18001

Nyström, T. (2005). Role of oxidative carbonylation in protein quality control and senescence. *EMBO J.* 24, 1311–1317. doi: 10.1038/sj.emboj.7600599

Nyström, T., and Liu, B. (2014). Protein quality control in time and space—links to cellular aging. *FEMS Yeast Res.* 14, 40–48. doi: 10.1111/1567-1364.12095

O'Driscoll, J., Clare, D., and Saibil, H. (2015). Prion aggregate structure in yeast cells is determined by the Hsp104-Hsp110 disaggregase machinery. *J. Cell Biol.* 211, 145–158. doi: 10.1083/jcb.201505104

Ogrodnik, M., Salmonowicz, H., Brown, R., Turkowska, J., Sredniawa, W., Pattabiraman, S., et al. (2014). Dynamic JUNQ inclusion bodies are asymmetrically inherited in mammalian cell lines through the asymmetric partitioning of vimentin. *Proc. Natl. Acad. Sci. U S A* 111, 8049–8054. doi: 10.1073/pnas.1324035111

Ohashi, Y., and Munro, S. (2010). Membrane delivery to the yeast autophagosome from the Golgi-endosomal system. *Mol. Biol. Cell* 21, 3998–4008. doi: 10.1091/mbc.E10-05-0457

Olzscha, H., Schermann, S. M., Woerner, A. C., Pinkert, S., Hecht, M. H., Tartaglia, G. G., et al. (2011). Amyloid-like aggregates sequester numerous metastable proteins with essential cellular functions. *Cell* 144, 67–78. doi: 10.1016/j.cell.2010.11.050

Park, S. H., Kukushkin, Y., Gupta, R., Chen, T., Konagai, A., Hipp, M. S., et al. (2013). PolyQ proteins interfere with nuclear degradation of cytosolic proteins by sequestering the Sis1p chaperone. *Cell* 154, 134–145. doi: 10.1016/j.cell.2013.06.003

Paushkin, S. V., Kushnirov, V. V., Smirnov, V. N., and Ter-Avanesyan, M. D. (1996). Propagation of the yeast prion-like [psi+] determinant is mediated by oligomerization of the SUP35-encoded polypeptide chain release factor. *EMBO J.* 15, 3127–3134.

Peters, L. Z., Karmon, O., David-Kadoch, G., Hazan, R., Yu, T., Glickman, M. H., et al. (2015). The protein quality control machinery regulates its misassembled proteasome subunits. *PLoS Genet.* 11:e1005178. doi: 10.1371/journal.pgen.1005178

Peters, L. Z., Karmon, O., Miodownik, S., and Ben-Aroya, S. (2016). Proteasome storage granules are transiently associated with the insoluble protein deposit in *Saccharomyces cerevisiae*. *J. Cell Sci.* 129, 1190–1197. doi: 10.1242/jcs.179648

Saibil, H. R., Seybert, A., Habermann, A., Winkler, J., Eltsov, M., Perkovic, M., et al. (2012). Heritable yeast prions have a highly organized three-dimensional architecture with interfiber structures. *Proc. Natl. Acad. Sci. U S A* 109, 14906–14911. doi: 10.1073/pnas.1211976109

Satpute-Krishnan, P., Langseth, S. X., and Serio, T. R. (2007). Hsp104-dependent remodeling of prion complexes mediates protein-only inheritance. *PLoS Biol.* 5:e24. doi: 10.1371/journal.pbio.0050024

Shiber, A., Breuer, W., Brandeis, M., and Ravid, T. (2013). Ubiquitin conjugation triggers misfolded protein sequestration into quality control foci when Hsp70 chaperone levels are limiting. *Mol. Biol. Cell* 24, 2076–2087. doi: 10.1091/mbc.E13-01-0010

Shorter, J., and Lindquist, S. (2004). Hsp104 catalyzes formation and elimination of self-replicating Sup35 prion conformers. *Science* 304, 1793–1797. doi: 10.1126/science.1098007

Song, J., Yang, Q., Yang, J., Larsson, L., Hao, X., Zhu, X., et al. (2014). Essential genetic interactors of SIR2 required for spatial sequestration and asymmetrical inheritance of protein aggregates. *PLoS Genet.* 10:e1004539. doi: 10.1371/journal.pgen.1004539

Sontag, E. M., Samant, R. S., and Frydman, J. (2017). Mechanisms and functions of spatial protein quality control. *Annu. Rev. Biochem.* 86, 97–122. doi: 10.1146/annurev-biochem-060815-014616

Sontag, E. M., Vonk, W. I. M., and Frydman, J. (2014). Sorting out the trash: the spatial nature of eukaryotic protein quality control. *Curr. Opin. Cell Biol.* 26, 139–146. doi: 10.1016/j.ceb.2013.12.006

Specht, S., Miller, S. B., Mogk, A., and Bukau, B. (2011). Hsp42 is required for sequestration of protein aggregates into deposition sites in *Saccharomyces cerevisiae*. *J. Cell Biol.* 195, 617–629. doi: 10.1083/jcb.201106037

Speldewinde, S. H., Doronina, V. A., Tuite, M. F., and Grant, C. M. (2017). Disrupting the cortical actin cytoskeleton points to two distinct mechanisms of yeast $[PSI^+]$ prion formation. *PLoS Genet.* 13:e1006708. doi: 10.1371/journal.pgen.1006708

Spokoini, R., Moldavski, O., Nahmias, Y., England, J. L., Schuldiner, M., and Kaganovich, D. (2012). Confinement to organelle-associated inclusion structures mediates asymmetric inheritance of aggregated protein in budding yeast. *Cell Rep.* 2, 738–747. doi: 10.1016/j.celrep.2012.08.024

Suzuki, K. (2013). Selective autophagy in budding yeast. *Cell Death Differ.* 20, 43–48. doi: 10.1038/cdd.2012.73

Suzuki, K., and Ohsumi, Y. (2010). Current knowledge of the pre-autophagosomal structure (PAS). *FEBS Lett.* 584, 1280–1286. doi: 10.1016/j.febslet.2010.02.001

Takahashi, Y., Tsotakos, N., Liu, Y., Young, M. M., Serfass, J., Tang, Z., et al. (2016). The Bif-1-Dynamin 2 membrane fission machinery regulates Atg9-containing

vesicle generation at the Rab11-positive reservoirs. *Oncotarget* 7, 20855–20868. doi: 10.18632/oncotarget.8028

Tanaka, M., Kim, Y. M., Lee, G., Junn, E., Iwatsubo, T., and Mouradian, M. M. (2004). Aggresomes formed by α-synuclein and synphilin-1 are cytoprotective. *J. Biol. Chem.* 279, 4625–4631. doi: 10.1074/jbc.M310994200

Tongaonkar, P., Beck, K., Shinde, U. P., and Madura, K. (1999). Characterization of a temperature-sensitive mutant of a ubiquitin-conjugating enzyme and its use as a heat-inducible degradation signal. *Anal. Biochem.* 272, 263–269. doi: 10.1006/abio.1999.4190

Tyedmers, J. (2012). Patterns of [PSI^+] aggregation allow insights into cellular organization of yeast prion aggregates. *Prion* 6, 191–200. doi: 10.4161/pri.18986

Tyedmers, J., Madariaga, M. L., and Lindquist, S. (2008). Prion switching in response to environmental stress. *PLoS Biol.* 6:e294. doi: 10.1371/journal.pbio.0060294

Tyedmers, J., Mogk, A., and Bukau, B. (2010a). Cellular strategies for controlling protein aggregation. *Nat. Rev. Mol. Cell Biol.* 11, 777–788. doi: 10.1038/nrm2993

Tyedmers, J., Treusch, S., Dong, J., McCaffery, J. M., Bevis, B., and Lindquist, S. (2010b). Prion induction involves an ancient system for the sequestration of aggregated proteins and heritable changes in prion fragmentation. *Proc. Natl. Acad. Sci. U S A* 107, 8633–8638. doi: 10.1073/pnas.1003895107

Wang, Y., Meriin, A. B., Zaarur, N., Romanova, N. V., Chernoff, Y. O., Costello, C. E., et al. (2009). Abnormal proteins can form aggresome in yeast: aggresome-targeting signals and components of the machinery. *FASEB J.* 23, 451–463. doi: 10.1096/fj.08-117614

Wang, K., Yang, Z., Liu, X., Mao, K., Nair, U., and Klionsky, D. J. (2012). Phosphatidylinositol 4-kinases are required for autophagic membrane trafficking. *J. Biol. Chem.* 287, 37964–37972. doi: 10.1074/jbc.M112.371591

Weisberg, S. J., Lyakhovetsky, R., Werdiger, A. C., Gitler, A. D., Soen, Y., and Kaganovich, D. (2012). Compartmentalization of superoxide dismutase 1 (SOD1G93A) aggregates determines their toxicity. *Proc. Natl. Acad. Sci. U S A* 109, 15811–15816. doi: 10.1073/pnas.1205829109

Williams, M., and Kim, K. (2014). From membranes to organelles: emerging roles for dynamin-like proteins in diverse cellular processes. *Eur. J. Cell Biol.* 93, 267–277. doi: 10.1016/j.ejcb.2014.05.002

Winkler, J., Tyedmers, J., Bukau, B., and Mogk, A. (2012). Hsp70 targets Hsp100 chaperones to substrates for protein disaggregation and prion fragmentation. *J. Cell Biol.* 198, 387–404. doi: 10.1083/jcb.201201074

Wolfe, K. J., Ren, H. Y., Trepte, P., and Cyr, D. M. (2013). The Hsp70/90 cochaperone, Sti1, suppresses proteotoxicity by regulating spatial quality control of amyloid-like proteins. *Mol. Biol. Cell* 24, 3588–3602. doi: 10.1091/mbc.E13-06-0315

Yamamoto, H., Kakuta, S., Watanabe, T. M., Kitamura, A., Sekito, T., Kondo-Kakuta, C., et al. (2012). Atg9 vesicles are an important membrane source during early steps of autophagosome formation. *J. Cell Biol.* 198, 219–233. doi: 10.1083/jcb.201202061

Yang, J., Hao, X., Cao, X., Liu, B., and Nyström, T. (2016). Spatial sequestration and detoxification of Huntingtin by the ribosome quality control complex. *Elife* 5:e11792. doi: 10.7554/eLife.11792

Conflict of Interest Statement: The authors declare that the research was conducted in the absence of any commercial or financial relationships that could be construed as a potential conflict of interest.

frontiers in Molecular Neuroscience

REVIEW
published: 23 July 2018
doi: 10.3389/fnmol.2018.00249

Studying Spatial Protein Quality Control, Proteopathies, and Aging Using Different Model Misfolding Proteins in *S. cerevisiae*

*Kara L. Schneider, Thomas Nyström and Per O. Widlund**

Department of Microbiology and Immunology, Institute of Biomedicine, Sahlgrenska Academy, University of Gothenburg, Gothenburg, Sweden

Protein quality control (PQC) is critical to maintain a functioning proteome. Misfolded or toxic proteins are either refolded or degraded by a system of temporal quality control and can also be sequestered into aggregates or inclusions by a system of spatial quality control. Breakdown of this concerted PQC network with age leads to an increased risk for the onset of disease, particularly neurological disease. *Saccharomyces cerevisiae* has been used extensively to elucidate PQC pathways and general evolutionary conservation of the PQC machinery has led to the development of several useful *S. cerevisiae* models of human neurological diseases. Key to both of these types of studies has been the development of several different model misfolding proteins, which are used to challenge and monitor the PQC machinery. In this review, we summarize and compare the model misfolding proteins that have been used to specifically study spatial PQC in *S. cerevisiae*, as well as the misfolding proteins that have been shown to be subject to spatial quality control in *S. cerevisiae* models of human neurological diseases.

Keywords: protein quality control, spatial protein quality control, protein misfolding, misfolding model, inclusions, aging, cell stress, temperature-sensitive

OPEN ACCESS

Edited by:
Ralf J. Braun, University of Bayreuth, Germany

Reviewed by:
Jens Tyedmers, Universitätsklinikum Heidelberg, Germany
Martin Lothar Duennwald, University of Western Ontario, Canada

****Correspondence:***
Per O. Widlund
per.widlund@gu.se

Received: *15 April 2018*
Accepted: *02 July 2018*
Published: *23 July 2018*

Citation:
Schneider KL, Nyström T and Widlund PO (2018) Studying Spatial Protein Quality Control, Proteopathies, and Aging Using Different Model Misfolding Proteins in S. cerevisiae. Front. Mol. Neurosci. 11:249. doi: 10.3389/fnmol.2018.00249

INTRODUCTION

The presence of protein inclusions is a hallmark of many age-related neurological diseases (Kaytor and Warren, 1999; Koo et al., 1999; Paulson, 1999). There is much evidence to suggest that the misfolded proteins generated during progression of these diseases are deposited into inclusions by the cell's protein quality control (PQC) machinery to shield cellular components from their toxic properties (Saudou et al., 1998; Arrasate et al., 2004; Takahashi et al., 2008; Tyedmers et al., 2010).

Though protein deposits are common to many neurological diseases, inclusions can also be seen in aged neuronal cells of healthy animals (Fiori, 1987; Peters et al., 1991), reinforcing the idea that inclusions are a normal response of the PQC machinery to misfolded proteins. However, there are several lines of evidence for an age-related decline in the cells ability to process damaged proteins, which may explain the increased incidence of neurological disease with age (Cuervo and Dice, 2000; Koga et al., 2011; Kruegel et al., 2011; Andersson et al., 2013; Oling et al., 2014; Saez and Vilchez, 2014).

While the observed inclusions vary in form and intracellular location across species ranging from bacteria to humans, the formation of cellular inclusions in response to aberrantly folded proteins is evolutionarily conserved and is a consequence of the cell's ongoing effort to maintain

protein homeostasis, or proteostasis. Organisms across the evolutionary tree have evolved systems of temporal quality control and spatial quality control to maintain a functioning proteome (Hartl and Hayer-Hartl, 2009; Mogk and Bukau, 2017). The chaperones of the temporal quality control system ensure proper folding of newly synthesized proteins, attempt to refold misfolded proteins and promote degradation of those that cannot be effectively refolded (Hill et al., 2017; Josefson et al., 2017; Sontag et al., 2017). A system of spatial quality control runs in parallel to sort and deposit potentially harmful misfolded proteins and its action is most apparent when the temporal quality control system fails or is overloaded. When this occurs, misfolded proteins are partitioned into inclusions which shield the cell from their toxicity and can aid in their eventual clearance (Taylor et al., 2003; Escusa-Toret et al., 2013; Wolfe et al., 2013).

Due to the general conservation of the PQC machinery, several model organisms have been used to study not only the pathways involved in PQC, but also how they manage misfolded proteins that have been identified as important in the development of several human age-related neurological diseases. One of these is the proven model eukaryote, *Saccharomyces cerevisiae*. It is well-suited for the study of PQC, particularly in the context of aging, because aging can be studied in two major contexts: non-proliferative and proliferative cells. Yeast can be grown to stationary phase, where they eventually lose viability. This loss of viability, sometimes called chronological aging, can in many ways mimic aging experienced by differentiated cells like neuronal cells. Furthermore, proliferative cells, like stem cells, can also be modeled since yeast similarly undergo asymmetric cell divisions.

Asymmetric divisions are important in the context of spatial quality control because they allow damage, notably damaged proteins, to be segregated asymmetrically. During asymmetric cell division in yeast, the daughter cell is rejuvenated and one reason for this is that damaged or misfolded proteins are retained in the mother cell as part of the system of spatial quality control (Aguilaniu et al., 2003; Shcheprova et al., 2008). Evidence is emerging that some stem cell types also segregate damage asymmetrically to allow the stem cell lineage to propagate free of damage (Rujano et al., 2006; Fuentealba et al., 2008; Bufalino et al., 2013; Ogrodnik et al., 2014). Since this asymmetrical division of damage is limited to proliferating cells, it is possible that the higher incidence of inclusions in differentiated cells like neurons may be a consequence of the inability of the spatial quality control machinery to remove damage through division. Spatial PQC, therefore, plays a key role in both aging and age-related neurological disease and yeast has been successfully used to study the pathways involved in both contexts.

A key reason for this success has been due to the development of model proteins that either probe how the cell responds to misfolding proteins in general or how they deal with those that are thought to be the main causative agents of human disease. Model misfolding proteins are especially useful in the study of both temporal and spatial quality control as they can be used to track processing by the quality control machinery with minimal perturbation to the system itself. Fluorescently tagged substrates are indispensable, particularly in the study of spatial quality control, as they allow straightforward tracking of aggregate formation and localization by light microscopy. They also allow the study of spatial quality control in relation to temporal control by following aggregates in the cell through time. Several misfolding model proteins have been developed for these purposes. Furthermore, several human disease proteins have also been successfully used in yeast to study both the nature of the toxicity of the misfolded proteins, as well as how the PQC machinery responds to these proteins. Herein, we review the major model proteins used in *S. cerevisiae* to study spatial PQC pathways and the role of spatial quality control in the molecular basis of human disease.

MODEL MISFOLDING PROTEINS

Model misfolding proteins have helped to define the different quality control sites that have been identified in yeast (Kaganovich et al., 2008; Miller et al., 2015; Hill et al., 2017) (**Figure 1**). When induced, they often initially accumulate at stress foci, called CytoQs/Q-bodies/peripheral aggregates, in the cytoplasm or at the surface of organelles including the endoplasmic reticulum, mitochondria, and vacuole (Specht et al., 2011; Spokoini et al., 2012; Escusa-Toret et al., 2013; Miller et al., 2015). During prolonged stress, the aggregates coalesce into larger foci, often called inclusions, which are deposited or collected at several defined sites: the juxtanuclear quality control (JUNQ), the intranuclear quality control (INQ) and the insoluble protein deposit (IPOD) site (Kaganovich et al., 2008; Miller et al., 2015). They also can associate with, and be imported into, mitochondria (Zhou et al., 2014; Ruan et al., 2017). Other sites are likely to exist as some misfolding human disease models do not appear to localize to these defined sites (Tenreiro et al., 2014; Farrawell et al., 2015). The misfolding models are summarized in **Table 1**. We grouped them into three general categories: Temperature-sensitive (Ts) misfolding proteins, continuously misfolding proteins, and human disease proteins. For each category, we will first describe the development of model proteins for *S. cerevisiae* and then discuss how they have been used to elucidate spatial quality control pathways.

TEMPERATURE-SENSITIVE MISFOLDING PROTEINS

Luciferase, FlucSM/DM

Photinus pyralis luciferase was an early model substrate used in the study of PQC. It was selected to elucidate the cellular chaperone machinery in *Escherichia coli* because it was thermolabile, could be reactivated *in vivo*, and activity could readily be monitored by luminescence assay (Schröder et al., 1993). A fluorescently tagged version was later used to study spatial quality control in *E. coli* (Winkler et al., 2010) before versions were adapted for use in *S. cerevisiae* (Specht et al., 2011).

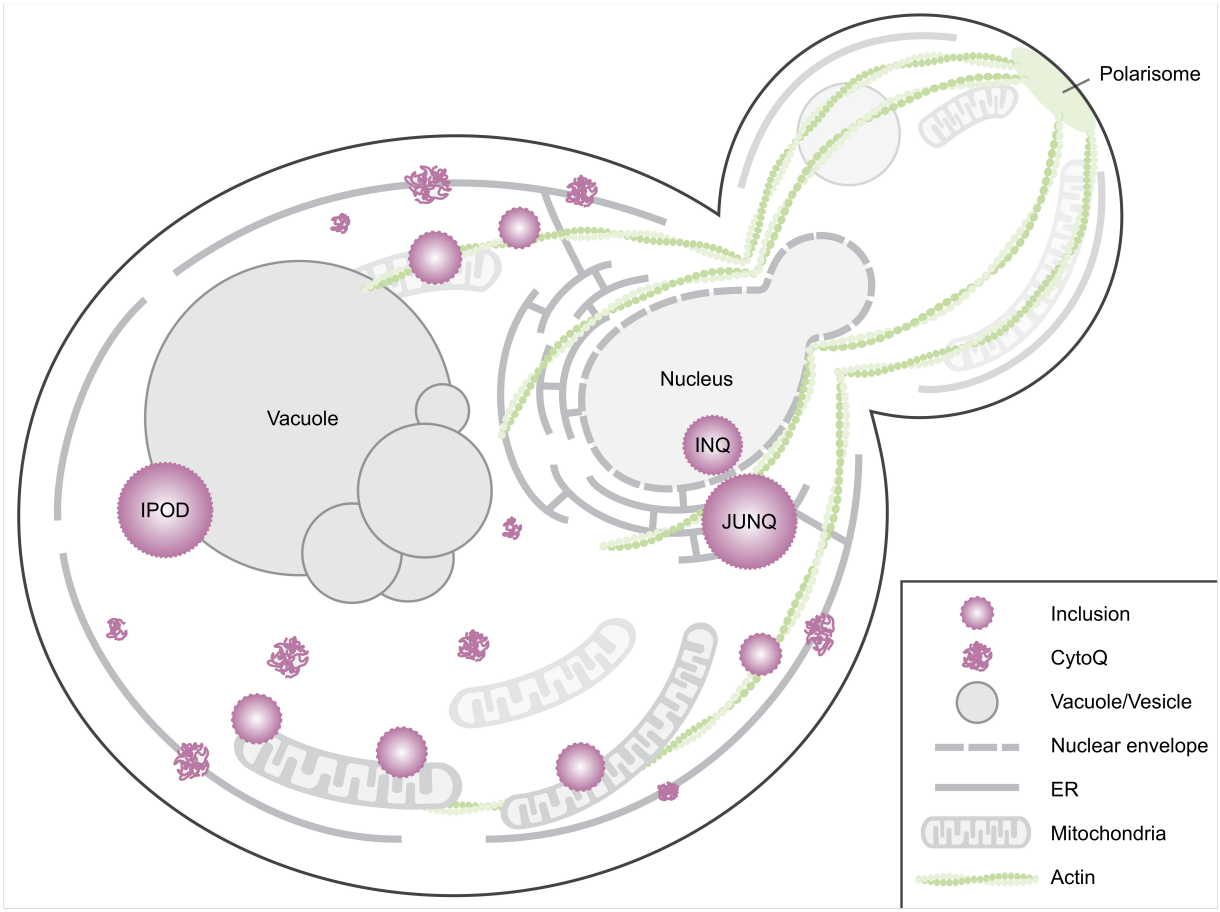

FIGURE 1 | Spatial protein quality control sites in *Saccharomyces cerevisiae*. When induced to misfold, proteins aggregate in the cytosol and on the ER membrane (Escusa-Toret et al., 2013). These initial cytosolic aggregates are called CytoQ (Miller et al., 2015), stress foci (Spokoini et al., 2012), peripheral aggregates (Specht et al., 2011), cytosolic puncta (Kaganovich et al., 2008) or Q-bodies (Escusa-Toret et al., 2013). These coalesce into larger structures, usually referred to as inclusions. Smaller inclusions have been observed tethered to actin cables (Liu et al., 2010; Song et al., 2014) or are captured by mitochondria (Zhou et al., 2014; Böckler et al., 2017). Yeast cells have several distinct larger inclusions including, but not limited to, the intranuclear quality control site (INQ), the juxtanuclear quality control site (JUNQ), and the perivacuolar IPOD site (Kaganovich et al., 2008; Miller et al., 2015). Other IPOD-like peripheral inclusions likely exist as some aggregates of model substrates do not co-localize with the IPOD, e.g., the non-amyloidogenic disease protein OPTN (Kryndushkin et al., 2012). An additional site, the age-associated protein deposit site (APOD, not depicted here) has been identified in aged cells (Saarikangas and Barral, 2015).

Mutant versions of Luciferase, FlucSM/DM were developed to be more susceptible to heat denaturation (Gupta et al., 2011). *S. cerevisiae* compatible constructs were recently developed (Ruan et al., 2017).

Ubc9ts (ubc9-2)

Temperature-sensitive mutants of *S. cerevisiae* genes have been used to study gene function for decades, particularly of essential genes. Many Ts alleles behave as effective nulls and one mechanism for this was shown with the gene product of a Ts allele of the ubiquitin conjugating enzyme, Ubc9. Several mutant ubc9 proteins were shown to be short-lived at the restrictive temperature and the observed rapid breakdown could be suppressed and was dependent on proteasome activity (Betting and Seufert, 1996). A GFP tagged version of ubc9-2 containing the point mutation Y69L was then used to show that misfolding proteins partition between at least two quality control compartments, the JUNQ and IPOD (Kaganovich et al., 2008).

guk1-7, gus1-3, pro3-1, ugp1-3

A screen of a panel of 22 Ts alleles of six essential genes encoding predominantly cytoplasmic proteins showed that a significant fraction was degraded at the restrictive temperature, clearly demonstrating degradation as a major mechanism for Ts phenotypes (Khosrow-Khavar et al., 2012). Four unstable mutants were fluorescently tagged and used as model misfolding substrates: guk1-7, gus1-3, pro3-1, and ugp1-3 (Comyn et al., 2016). A Ts mutant of a guanylate kinase, guk1-7, was selected for further characterization. The temperature sensitivity of guk1-7 is a consequence of four missense mutations. It was shown to co-localize with Hsp104-mCherry and with Hsp42-mCherry foci (Comyn et al., 2016), and based on these markers, they are likely deposited into

TABLE 1 | Fluorescently tagged misfolding model proteins.

Name	Origin	Mutant model	Misfolding	Control	Expression	Fluorescent tag location	Reference
Luciferase	*P. pyralis*	Heat denaturation	Ts	N/A	Constitutive – ACT1	N-terminus	Specht et al., 2011
FlucSM	*P. pyralis*	Heat denaturation/missense	Ts	Fluc	Constitutive	C-terminus	Ruan et al., 2017
ubc9-2	*S. cerevisiae*	Heat denaturation/missense	Ts	UBC9	Induced – GAL	N-terminus	Kaganovich et al., 2008
guk1-7	*S. cerevisiae*	Heat denaturation/missense	Ts	GUK1	Constitutive – TDH3	C-terminus	Comyn et al., 2016
gus1-3	*S. cerevisiae*	Heat denaturation/missense	Ts	GUS1	Constitutive – TDH3	C-terminus	Comyn et al., 2016
pro3-1	*S. cerevisiae*	Heat denaturation/missense	Ts	PRO3	Constitutive – TDH3	C-terminus	Comyn et al., 2016
ugp1-3	*S. cerevisiae*	Heat denaturation/missense	Ts	UGP1	Constitutive – TDH3	C-terminus	Comyn et al., 2016
Actin(E364K)	*D. melanogaster*	Missense	Continuous	None available	Induced – GAL	C-terminus	Kaganovich et al., 2008
VHL	*H. sapiens*	Absent binding partner	Continuous	N/A	Induced – GAL	N-terminus	Kaganovich et al., 2008
ΔssCPY*	*S. cerevisiae*	Missorting	Continuous	N/A	Constitutive – PRC1, Induced – GAL	C-terminus	Park et al., 2007, 2013
ΔssPrA	*S. cerevisiae*	Missorting	Continuous	N/A	Constitutive – TDH3	C-terminus	Prasad et al., 2010
tGnd1	*S. cerevisiae*	Nonsense	Continuous	GND1	Constitutive	C-terminus	Miller et al., 2015
DegAB	*S. cerevisiae*)	Degron (contains degradation signal)	Continuous	N/A	Constitutive – TDH3	N-terminus	Shiber et al., 2013
Htt103Q	*H. sapiens*	Huntington's disease	Continuous	Htt25Q	Induced – GAL	C-terminus	Krobitsch and Lindquist, 2000
β-amyloid	*H. sapiens*	Alzheimer's disease	Continuous	N/A	Induced – GAL	C-terminus	Treusch et al., 2011
Alpha synuclein	*H. sapiens*	Parkinson's disease	Continuous	N/A	Induced – GAL	C-terminus	Outeiro and Lindquist, 2003
FUS	*H. sapiens*	Amyotrophic lateral sclerosis (ALS)	Continuous	N/A	Induced – GAL	C-terminus	Fushimi et al., 2011; Kryndushkin et al., 2011; Sun et al., 2011
TDP-43	*H. sapiens*	Amyotrophic lateral sclerosis (ALS)	Continuous	N/A	Induced – GAL	C-terminus	Johnson et al., 2008; Kryndushkin et al., 2011
OPTN	*H. sapiens*	Amyotrophic lateral sclerosis (ALS)	Continuous	N/A	Induced – GAL	C-terminus	Kryndushkin et al., 2012

References are to the earliest use of the misfolded reporter in the study of spatial quality control.

one or more of the major PQCs like Q-bodies, JUNQ/INQ or IPOD.

QUALITY CONTROL OF TEMPERATURE-SENSITIVE PROTEINS

Many temperature sensitive proteins are not degraded at the restrictive temperature. The conditional lethal phenotype caused by these stable variants are likely due to local perturbations in domain structure caused by the mutations. This local effect is apparent in Ts alleles that encode homomultimeric proteins where intragenic complementation is possible (Sundberg and Davis, 1997). Dominant Ts alleles have been proposed to affect protein structure locally (McMurray, 2014). Indeed, these local effects may generally help to explain the wide range of phenotypes that can be observed with different Ts mutants of the same gene.

In contrast, a significant percentage of temperature-sensitive mutants display a recessive, null phenotype at the restrictive temperature that is often due to degradation of the expressed protein (Khosrow-Khavar et al., 2012). The null phenotype of unstable Ts alleles can often be rescued by removal of one or a combination of genes involved in PQC, indicating that the mutations do not significantly affect protein function, but instead cause partial unfolding that the quality control machinery recognizes, resulting in that protein being targeted for destruction (Betting and Seufert, 1996; Gardner et al., 2005; Khosrow-Khavar et al., 2012). It is this class of Ts mutants that has been adapted for the study of PQC.

Of the Ts substrates adapted, Luciferase is the only one with several well-established assays to monitor enzymatic activity, which is one of the main reasons it was initially chosen as a model substrate (Schröder et al., 1993). When used as a spatial quality control substrate, it has a rather mild aggregation

phenotype that either requires a higher 42°C heat shock or proteasomal inhibition for aggregates to be clearly visible. As a consequence, destabilized versions of luciferase, FlucSM and FlucDM were later engineered to make them more amenable to studies of proteome stress (Gupta et al., 2011). FlucSM expressed in yeast forms clear aggregates at 42°C, but experiments with milder 37°C heat stress have not yet been reported in yeast (Ruan et al., 2017). Luciferase is also the only exogenous Ts substrate used in the study of spatial quality control. This has the potential advantage that it is unlikely to specifically interact with endogenous proteins. However, it may also not be recognized by the PQC machinery in the same way as an endogenous protein, potentially limiting its use in elucidating endogenous spatial quality control pathways.

The remaining substrates are Ts versions of *S. cerevisiae* proteins which have been selected to be unstable at or above 37°C. Ubc9-2 has often been used as a spatial quality control substrate since it was originally used to help define the JUNQ and IPOD deposition sites (Kaganovich et al., 2008). The guk1-7, gus1-3, pro3-1, and ugp1-3 proteins expand the number of available Ts substrates significantly and allow interesting comparisons between processing of endogenous misfolded proteins since they differ in their wild-type gene function, cellular localization and pathways of degradation upon misfolding. At the permissive temperature, these Ts substrates have been reported to have the following localization patterns: ubc9-2, nucleus; guk1-7, nucleus and cytoplasm; gus1-3, cytoplasm and mitochondria; pro3-1, cytoplasm; ugp1-3, cytoplasm and plasma membrane[1]. It is perhaps not surprising that these model proteins show notable differences in the way they are processed by the PQC machinery. For example, degradation of pro3-1 is partially dependent on the E3 ubiquitin ligase San1 for degradation while guk1-7 is significantly less dependent. They also show different responses to deletion of prefoldin subunits. Furthermore, gus1-3 appears to be unique in that it does not appear to depend on the proteasome for degradation (Khosrow-Khavar et al., 2012). **Table 2** summarizes what is known about the processing of the Ts model substrates.

There are further subclasses of Ts proteins that are important to distinguish between, especially in the context of quality control. Some proteins are TL (thermolabile) while others are TSS (temperature sensitive synthesis) (Sadler and Novick, 1965; McMurray, 2014) (**Figure 2**). TL mutants are universally destabilized at the restrictive temperature, whereas TSS mutants are those that only misfold during synthesis. In yeast, a clear distinction between these phenotypes was shown with Ts mutants of Gal80 (Matsumoto et al., 1978). These unique properties can be exploited to examine whether the PQC machinery handles misfolding of newly synthesized or aged proteins differently. Of the Ts proteins used to study spatial quality control, only Ubc9ts has been characterized in this way and was shown to be TL as it could form foci during heat shock even after expression was shut off (Escusa-Toret et al., 2013). For this reason, we cannot generally distinguish between TL and TSS in this review.

[1]https://www.yeastgenome.org/

CONTINUOUSLY MISFOLDING PROTEINS

Actin(E364K)

The actin mutant actin(E364K) was originally isolated in *Drosophila melanogaster* (Drummond et al., 1991) and was later shown to be degraded by the PQC machinery (McClellan et al., 2005). A GFP tagged version localized to quality control compartments seen with ubc9-2 (Kaganovich et al., 2008).

von Hippel–Lindau (VHL)

The von Hippel–Lindau (VHL) tumor-suppressor protein is subject to chaperone mediated folding in mammalian cells (Feldman et al., 1999). Tumor-causing mutations that disrupt VHL binding to Elongin B/C leads to misfolding and degradation by the proteasome (Feldman et al., 1999; Schoenfeld et al., 2000). Wild type VHL was shown to be degraded in yeast due to absence of Elongin B/C and this was similarly dependent on the ubiquitin-proteasome pathway (McClellan et al., 2005). GFP tagged VHL was shown to be subject to spatial quality control in yeast similar to ubc9-2 and actin(E346K) (Kaganovich et al., 2008).

ΔssCPY*

The first mutant version of the vacuolar enzyme carboxypeptidase Y (Y, yscY, CPY, PRC1) was isolated in 1975 (Wolf and Fink, 1975) in a screen with the purpose of investigating the function of the proteinase itself. However, CPY* did not localize to the vacuole, its regular destination, but instead was retained in the ER for proteasome-independent rapid degradation and was found to be misfolded (Finger et al., 1993).

Many derivatives of CPY have been used to study their degradation or PQC pathways, which differ depending on the domains they are fused to, e.g., the fusion to a transmembrane domain to study ER membrane proteins (Stolz and Wolf, 2012). One such derivative is ΔssCPY*, which is a cytoplasmic misfolding substrate made by eliminating the ER-targeting signal sequence from CPY*. Though originally used as a negative control when studying ERAD dependent degradation, (Medicherla et al., 2004) GFP tagged ΔssCPY* was shown to form inclusions and is subject to spatial quality control (Prasad et al., 2010; Park et al., 2013). Based on this construct, a similar cytosolic misfolding protein, ΔssPrA, was made using vacuolar proteinase A (PEP4) (Prasad et al., 2010).

tGnd1

A dosage suppressor screen using a high copy (2 μ) genomic library was performed to identify factors involved in stabilization of the misfolded model ΔssCPY* (Heck et al., 2010). The recovered hits were found to express truncated proteins, one of which was a truncated form of Gnd1, a phosphogluconate dehydrogenase. The truncation proved to be a competing PQC substrate. Fluorescently tagged tGnd1 was shown to localize to JUNQ/INQ and CytoQ deposits (Miller et al., 2015).

TABLE 2 | Spatial quality control pathways implicated in processing of the misfolding model substrates, as well as dependence on the proteasome for degradation.

Name	Degradation	Ubr1 dependent?	San1 dependent?	Sorted to JUNQ/INQ?	Sorted to IPOD?	Reference
Luciferase	Proteasome	Yes	N/D	Yes	No	Nillegoda et al., 2010; Miller et al., 2015
FlucSM/DM	Proteasome	N/D	N/D	N/D	N/D	Gupta et al., 2011; Ruan et al., 2017
ubc9-2	Proteasome	N/D	N/D	Yes	Yes	Betting and Seufert, 1996; Kaganovich et al., 2008
guk1-7	Proteasome	Yes	No	Yes[1]	N/D	Khosrow-Khavar et al., 2012; Comyn et al., 2016
gus1-3	Unknown	N/D	N/D	N/D	N/D	Khosrow-Khavar et al., 2012
pro3-1	Proteasome	Yes	Yes	N/D	N/D	Khosrow-Khavar et al., 2012
ugp1-3	Proteasome	Yes	N/D	N/D	N/D	Khosrow-Khavar et al., 2012
Actin(E364K)	Proteasome	N/D	N/D	Yes	Yes	Kaganovich et al., 2008
VHL	Proteasome	N/D	N/D	Yes	Yes	McClellan et al., 2005; Kaganovich et al., 2008
ΔssCPY*	Proteasome	Yes	Yes	Yes	Yes[1]	Eisele and Wolf, 2008; Miller et al., 2015
ΔssPrA	Proteasome	No	Yes	Yes[1]	Yes[1]	Prasad et al., 2010
tGnd1	Proteasome	Yes	Yes	Yes	Yes[1]	Heck et al., 2010; Miller et al., 2015
DegAB	Proteasome	N/D	N/D	Yes	Yes[1]	Furth et al., 2011; Alfassy et al., 2013; Shiber et al., 2013, 2014
Htt103Q	Proteasome, autophagy	N/D	N/D	No	Yes	Kaganovich et al., 2008; Chuang et al., 2016
β-amyloid	Secretory pathway	N/D	N/D	N/D	N/D	Treusch et al., 2011; D'Angelo et al., 2013
Alpha synuclein	Proteasome, autophagy	N/D	N/D	No	No	Outeiro and Lindquist, 2003; Petroi et al., 2012; Tenreiro et al., 2014
FUS	N/D	N/D	N/D	No	Yes, only N-terminal fusion	Kryndushkin et al., 2012
TDP-43	Proteasome, autophagy	N/D	N/D	No	No	Farrawell et al., 2015; Leibiger et al., 2018
OPTN	Proteasome	N/D	N/D	No	Partially	Kryndushkin et al., 2012

N/D, not determined. [1]inferred from relative location.

DegAB

A study of the degradation signal (degron) of the kinetochore protein, Ndc10, showed that it functions autonomously, as it leads to degradation of various other stable proteins when it is attached (Furth et al., 2011). This degron consists of two parts, DegA and DegB, leading to the collective name DegAB (Alfassy et al., 2013). This model degron differs from conventionally used terminally misfolding model substrates for PQC as it does not aggregate spontaneously, is not cytotoxic and can model mildly misfolded PQC substrates, which remain soluble and derive from an endogenous yeast protein (Shiber et al., 2013). A GFP fusion of DegAB, GFP-DegAB, can be used to study spatial PQC and generally forms two inclusions, one of which is juxtanuclear.

QUALITY CONTROL OF CONTINUOUSLY MISFOLDING PROTEINS

All non-thermolabile misfolding proteins presented here are targeted for degradation via the ubiquitin-proteasome pathway (Schoenfeld et al., 2000; McClellan et al., 2005; Park et al., 2007; Heck et al., 2010; Furth et al., 2011). Nonetheless, the factors required for degradation of substrates differ. For example, actin(E364K) and VHL have been compared in the same study and it was shown that Hsp90 is required for VHL degradation but not for actin(E364K) degradation. Additionally, VHL requires the Hsp70 chaperone Ssa1 and its co-chaperone Sti1 for degradation (McClellan et al., 2005). ΔssCPY* and tGnd1 share a requirement for the Ubr1 and San1 E3 ubiquitin ligases for their degradation (Eisele and Wolf, 2008; Heck et al., 2010; Miller et al., 2015). Similarly, DegAB was found to depend on Ssa1 or Ssa2 (Shiber et al., 2013).

Another similarity of all non-thermolabile substrates studied so far in this regard is their spatial sorting in the cell, as they have been observed to at least partially localize to both the JUNQ/INQ and IPOD compartment upon aggregation. Actin(E364K) and VHL both localize to JUNQ/INQ and IPOD but VHL requires heat shock for localization to the IPOD (Kaganovich et al., 2008). Proteasome inhibition alone results in a single nuclear inclusion, most likely the JUNQ/INQ (Kaganovich et al., 2008;

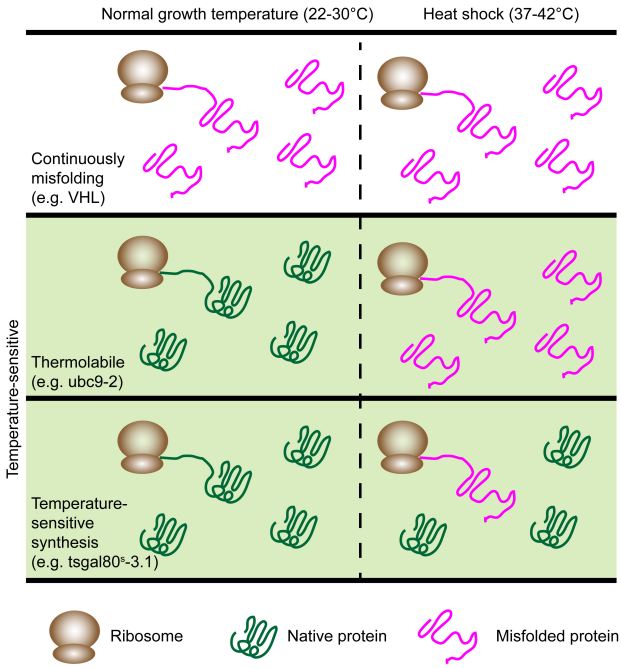

FIGURE 2 | The model proteins have different patterns of misfolding. Continuously misfolding proteins misfold at all temperatures. Ts proteins (green panel) misfold during heat shock and fall into two classes: Thermolabile (TL) and temperature-sensitive synthesis (TSS). TL proteins universally misfold during heat shock while TSS proteins misfold only if synthesized during heat shock. Examples are listed for each category.

Specht et al., 2011; Spokoini et al., 2012; Miller et al., 2015). ΔssCPY* and tGnd1 have been demonstrated to localize to the JUNQ/INQ in the stabilizing ubr1Δ san1Δ background in which these model proteins are no longer, or only marginally, ubiquitinated. This observation lead to the conclusion that ubiquitination is not a requirement for JUNQ/INQ targeting (Miller et al., 2015). In these experiments, tGnd1 is also targeted to a second cytoplasmic focus, which most likely corresponds to the IPOD, while ΔssCPY* appears exclusively targeted to INQ. However, cytoplasmic foci have also been observed for ΔssCPY*. DegAB foci were shown to co-localize with Hsp42 and Hsp104 (Shiber et al., 2013) and detergent solubility properties of DegAB were determined to be similar to those of ΔssCPY* as measured by flow cytometry (Shiber et al., 2014). In summary, there are clear differences in sorting of these model proteins, which makes it reasonable to use more than one misfolding substrate when general conclusions about spatial sorting pathways are to be drawn.

HUMAN DISEASE PROTEINS

Age-associated proteopathies have been increasingly modeled in yeast to gain more nuanced insight into the molecular bases of the diseases while circumventing potential ethical issues such as those with patient samples. The successful introduction of a range of different disease model proteins highlights the versatility and applicability of this model organism in the study of proteostasis, aging, and disease development (Braun et al., 2010). Different types of high-throughput screens with budding yeast are particularly powerful and have been used, in part, to find modifiers of cytotoxicity of disease proteins (Willingham et al., 2003; Cooper et al., 2006; Liang et al., 2008; Elden et al., 2010; Ju et al., 2011; Kayatekin et al., 2014). Importantly, fluorescently tagged versions of several proteins implicated in disease progression have been introduced to study how the spatial quality control machinery handles them and to help determine what contributes to their toxicity in diseased neurons. Here, we focus exclusively on substrates that have been shown to be subject to spatial quality control and aim to provide guidance in the selection of model substrates used to study spatial quality control pathways relevant to these proteopathies. For more thoroughly detailed descriptions of yeast models of human neurodegenerative disease, we refer the reader several excellent reviews (Braun et al., 2010; Pereira et al., 2012; Tenreiro et al., 2013; Braun, 2015; Menezes et al., 2015; Fruhmann et al., 2017). The disease models are summarized below and common constructs are listed in **Table 1**.

Huntington's Disease

Htt103Q/Htt97Q

Yeast models for characterization of Huntingtin (Htt), the protein that is mutated in patients of Huntington's disease, were established by testing variants of exon 1 of the N-terminus of human Huntingtin. These differ in the lengths of the polyglutamine expansions that modify aggregation behavior (Krobitsch and Lindquist, 2000). The Huntingtin model protein commonly used in yeast is Htt103Q, which is named after the number of glutamines in the expansion. A non-expanded variant, Htt25Q, is used as a control. Non-expanded variants, like Htt25Q, display diffuse localization in the cytoplasm, while expansions of 72 glutamines or more cause the proteins to form visible aggregates of varying size and quality (Krobitsch and Lindquist, 2000). Interestingly, it has been reported that an intermediate length huntingtin with a 47 glutamine expansion forms aggregates in yeast upon entry into stationary phase, which supports the use of stationary phase cells as a reasonable model for aged neuronal cells (Cohen et al., 2012). Models with longer expansions, such as Htt103Q, have different patterns of localization, ranging from on major focus per cell to multiple foci, that depend on expression levels and the regions flanking the polyglutamine expansion (Krobitsch and Lindquist, 2000; Duennwald et al., 2006; Wang et al., 2009; Song et al., 2014; Berglund et al., 2017).

Alzheimer's Disease

β-Amyloid

Alzheimer's disease (AD) models focus on one of the proteins implicated in the pathology of AD, the amyloid-β peptide (Aβ), as extracellular amyloid plaques containing Aβ appear in affected individuals. The Aβ peptides arise through cleavage of the amyloid precursor protein (APP) via the amyloidogenic

pathway, resulting in different sizes of Aβ, mostly $A\beta_{40}$ and $A\beta_{42}$ (O'Brien and Wong, 2011). The latter is more aggregation-prone and nucleates plaques in diseased individuals and is therefore often selected as a model. A GFP-$A\beta_{42}$ fusion protein was shown to form aggregates and induced a stress response (Caine et al., 2007). Toxicity models expressing the Aβ peptide were established later by targeting Aβ to the secretory pathway (Treusch et al., 2011; D'Angelo et al., 2013). Expression via an inducible promoter caused cytotoxicity without extensive cell death compared to a less toxic $A\beta_{40}$ peptide control (Treusch et al., 2011).

Parkinson's Disease

Alpha Synuclein

Alpha synuclein (aSyn) is a lipid-binding protein and the main constituent of Lewy Bodies, which are protein deposits occurring in diseased neurons that are affected by Parkinson's Disease (PD) and other disorders. aSyn and derivatives were first investigated in mammalian cells (McLean et al., 2001) and later used to develop a PD model in yeast (Outeiro and Lindquist, 2003). While several PD models have been established in yeast [reviewed in (Menezes et al., 2015)], aSyn is the most commonly used model protein. Expression of aSyn in yeast causes dose-dependent cytotoxicity, a phenotype reminiscent of what is seen in human cells. Toxicity can therefore be modified by inducing different levels of expression by regulatable promoters or by changing plasmid copy number. As with human cells, aSyn has been reported to localize mainly to the plasma membrane and partially to the cytoplasm. However, overexpression causes visible aggregation of aSyn into cytosolic inclusions (Outeiro and Lindquist, 2003).

Amyotrophic Lateral Sclerosis (ALS)

FUS, TDP-43, OPTN

Mutations associated with amyotrophic lateral sclerosis (ALS) appear in the proteins SOD1, FUS, TDP-43, and OPTN which become misfolded and aggregate. Yeast studies have focused on FUS and especially TDP-43. Both proteins act as DNA/RNA-binding proteins and are found in neuronal inclusions of affected individuals. A TDP-43 model in yeast mimics several disease characteristics. Expression from an inducible plasmid causes it to form nuclear inclusions, while higher expression induces mislocalization to the cytoplasm where it forms visible inclusions (Johnson et al., 2008). These cytoplasmic aggregates are toxic to the cell. Similarly, FUS models have shown that expression in yeast is also cytotoxic (Fushimi et al., 2011; Kryndushkin et al., 2011; Sun et al., 2011). The model protein forms numerous cytoplasmic aggregates, which co-localize with and cause formation of RNA processing sites (P-bodies and stress granules) as observed in human cells (Kryndushkin et al., 2011). Another protein known to form inclusions in ALS-affected individuals is optineurin (OPTN). In a recently developed yeast model, wild type OPTN was shown to be toxic, as were versions with disease-causing mutations (Kryndushkin et al., 2012).

QUALITY CONTROL OF HUMAN DISEASE PROTEINS

The disease proteins summarized above do not require stress conditions such as heat shock or proteasome inhibition to induce aggregate formation since they aggregate autonomously. Therefore, they are most commonly expressed using inducible promoters (**Table 1**). Additionally, it should be noted that none of the human misfolding proteins discussed here have orthologs in yeast.

The spatial quality control mechanisms handling several disease model proteins in yeast have not yet been extensively studied, however, it appears that amyloidogenic proteins in general are targeted to the IPOD compartment, which has been shown using Htt mutant proteins (Kaganovich et al., 2008; Escusa-Toret et al., 2013). The aggregates formed by aSyn are likely neither localized to JUNQ nor IPOD, as they did not co-localize with any of the commonly used markers for these quality control compartments (Outeiro and Lindquist, 2003; Tenreiro et al., 2014). In contrast to the other disease model proteins, TDP-43, FUS, and OPTN form non-amyloid aggregates. The spatial quality control mechanisms involved in the transport and processing of TDP-43, FUS, and OPTN have not been extensively investigated in yeast. A study using a mouse cell line concluded that the inclusions visible for TDP-43 and FUS might be distinct from several of the known quality control compartments: aggresome, JUNQ and IPOD (Farrawell et al., 2015). However, both TDP-43 and FUS have been reported to co-localize and physically interact in yeast (Kryndushkin et al., 2011), suggesting involvement of similar spatial PQC mechanisms for both model proteins. Furthermore, a GFP tagged version of FUS localizes to the IPOD while OPTN also shows only partial localization to this quality control site (Kryndushkin et al., 2012). OPTN forms non-amyloid cytoplasmic aggregates, which are distinct from FUS and TDP-43 foci, as they do not exclusively co-localize. OPTN appears to be handled in a unique way by the cell in that a single focus appears early after induction of expression, while upon later time points several small additional foci become visible. The foci only partially overlap with previously characterized model proteins reported to localize to the IPOD, further indicating that additional deposition sites may exist in the cytoplasm.

GENERAL CONSIDERATIONS FOR MODEL SELECTION

When selecting a candidate model misfolding protein, it is useful to consider what type of misfolding is to be modeled, the temperature sensitivity, whether a properly folding control is available, the promoter used for expression and the effects of the fluorescent tag. The categories are listed in **Table 1** and summarized below.

Yeast vs. Non-yeast

Both mutated yeast proteins and non-yeast proteins have been used to study spatial quality control in *S. cerevisiae*. Use of mutated native proteins, such as the frequently used Ubc9ts, has

the general advantage that it most closely mimics a typical error during protein production. The yeast spatial PQC machinery is more likely to properly recognize a misfolded endogenous protein compared to a non-native protein and it is therefore more likely to be sequestered to an "authentic" deposition site in the cell. However, mutated yeast proteins may also cause dominant negative effects, particularly when overexpressed, for example by sequestration of native binding partners. Non-native proteins, particularly those lacking yeast homologs, are less likely to bind endogenous proteins and can therefore be useful alternatives in this regard.

Mutant Model

Aberrant folding of proteins in wild-type cells can happen for several reasons. It is a major consequence of stress, such as with heat-induced denaturation. It can also be a consequence of mutations or a result of errors during protein production. Additionally, changes in expression can also result in a lack of binding partners necessary for proper folding. Model misfolding proteins have been engineered or selected to mimic the misfolding that occurs in these instances so that specific responses by the PQC machinery can be elucidated.

Temperature-Sensitive vs. Continuously Misfolding Reporters

Ts substrates are useful as unfolding can be triggered easily and rapidly by temperature shift so that the immediate response to unfolded proteins can be studied. In the case of TL substrates, it also allows decoupling from translation as one can terminate translation using cycloheximide before temperature shift. However, this temperature shift will also trigger the general heat shock response, which upregulates a range of chaperones. Non-thermolabile proteins do not require this temperature shift; therefore, while chaperones may be induced in response to the continuously misfolding substrate, temperature-induced changes in the levels of molecular chaperones are avoided.

Normally Folding Controls

Negative controls play an important role in studies on PQC as it is important to assess whether observable effects on PQC can be actually attributed to the misfolding protein itself and not to other factors such as their fluorescent tag or dominant negative effects. Negative controls exist for a subset of the human disease models. The Huntingtin models expressed in yeast, Htt103Q or other variants with expanded polyQ stretches, can be compared to a diffusely distributed cytosolic version, Htt25Q, which serves as a wild type control. Similarly, there are comparably less toxic variants of the amyloid beta peptide, which can be used as controls in some experimental setups. Alpha-synuclein aggregation depends on the level of expressed protein. While high expression levels result in aggregation, expression from a low copy number plasmid leaves the protein localized to the plasma membrane and the cytoplasm. A similar principle applies to TDP-43.

Several misfolding proteins can be directly compared to a wild-type control. For example, Ubc9 is used as a control for ubc9-2 (Kaganovich et al., 2008). Corresponding wild-type alleles are also available for guk1-7, gus1-3, pro3-1, and ugp1-3 (Khosrow-Khavar et al., 2012). Wild-type Gnd1 is used as a control for the truncated misfolding tGnd1 (Heck et al., 2010). However, the majority of the continuously misfolding proteins including VHL, actin(E364K), ΔssCPY*, and DegAB do not have obvious normally folding controls.

Promoter

Misfolding substrates have generally been placed behind strong promoters, such as TDH3, with the intent of overloading the temporal quality control system in order to easily visualize aggregates and inclusions. If the model protein of choice is not obviously cytotoxic, constitutively active promoters are useful in that they require no change in experimental conditions (such as a change in carbon source) to induce expression.

Inducible promoters have been commonly used when working with misfolding proteins that are cytotoxic, such as alpha-synuclein (**Table 1**). Thereby, cytotoxic effects of the misfolding protein can be avoided during strain construction and limited to the experiment itself. Additionally, inducible promoters can be useful for misfolding proteins that show a dose-dependent cytotoxicity, as it is easy to compare cytotoxicity when the expression of the misfolding protein is tightly regulated. It is also possible to shut off translation of the misfolding protein at a specific time point without interfering with translation of other proteins with agents such as cycloheximide. This is especially important when the cellular response to any particular misfolding protein is partially or fully dependent on a functional translation machinery.

One major limitation of the constitutive and inducible promoters used for the vast majority of the models covered in this review, is that they are among the strongest promoters characterized in *S. cerevisiae* (Peng et al., 2015). While inclusions can easily be visualized as a result, the high concentration of protein can cause toxicity unrelated to protein misfolding. For example, it can lead to sequestration of native and non-native binding partners and it may result in transport into non-native cellular compartments or organelles. Normally folding controls may mitigate this problem, as they can be used to identify the abnormal or toxic effects of overexpression.

Fluorescent Tagging

Fluorescent tags should, ideally, minimally affect protein function and are therefore generally placed accordingly. Practically, however, the tag will always have some effect regardless of whether it is placed N-terminally, C-terminally, or at an internal site. Even though the proteasome can process N-terminally or C-terminally tagged substrates (Liu et al., 2003), tagging can stabilize certain mutants (Mikalsen et al., 2005; Khosrow-Khavar et al., 2012), perhaps due to shielding of the unfolded domain recognized by the quality control machinery. Tag location will also determine if the misfolding protein exits the ribosome before or after folding of the fluorescent tag can begin, which can affect stability of the model protein or have an effect on the fluorescent tag itself. In fact, certain misfolded proteins have been shown to significantly affect GFP

chromophore formation. This effect was taken advantage of to develop a protein folding assay (Waldo et al., 1999). In this study, fluorescence of GFP tagged test substrates correlated with solubility, indicating that aggregation of their test substrates affected chromophore formation. Therefore, for any substrate, it is important to determine whether the fluorescent signal observed is proportional to the amount of protein present. Along the same lines, the fluorescent signal may not reflect the presence of a misfolded protein as the proteasome can degrade it while leaving the fluorophore intact (Liu et al., 2003). Finally, the tag itself has been shown to influence toxicity of misfolding proteins. Tagging affected toxicity of different huntingtin constructs (Jiang et al., 2017) and the location of the GFP-tag and the design of the linker on FUS and OPTN was shown to influence toxicity and the constructs' aggregation propensities (Kryndushkin et al., 2012).

CONCLUDING REMARKS

Deposition into quality control sites is a common, if not universal, response to misfolding proteins as these sites have been described in a wide range of organisms. Model misfolding proteins have been key tools used in the identification of, and distinction between, these quality control sites. Importantly, the use and characterization of a range of different misfolded proteins in yeast has made it clear that while many are handled similarly, there are often notable differences. For example, several models vary in their dependence on the San1 and Ubr1 E3 ubiquitin ligases for proteasomal degradation, while others do not depend on the proteasome but are degraded or removed in an undefined manner (**Table 2**). Furthermore, human disease models appear to be even more distinct in their processing. The huntingtin model, along with other amyloid aggregates, does not obviously sort to the JUNQ deposition site and ALS model proteins appear to deposit at sites that are distinct from both the JUNQ and IPOD. Similarly, aggregates of the Parkinson's disease model, aSyn, did not colocalize to these defined sites (Tenreiro et al., 2014). Taken together, the evidence points toward the existence of uncharacterized spatial quality control pathways or, at the very least, modifications of defined pathways that have not yet been well characterized. Continued use of model misfolding proteins under varying conditions alone, and in combination, will do much to further define these spatial quality control pathways that play such an important role in the maintenance of proteostasis and prevention of disease progression.

AUTHOR CONTRIBUTIONS

PW designed the review outline. PW and KS wrote the manuscript with guidance and input from TN.

FUNDING

This work was supported by grants from the Swedish Natural Science Research Council (VR) (TN), the Knut and Alice Wallenberg Foundation (Wallenberg Scholar) (TN), and the ERC (Advanced Grant; QualiAge) (TN).

ACKNOWLEDGMENTS

We thank Lisa Larsson Berglund for critical reading of the manuscript and all members of the Nyström lab for useful discussions.

REFERENCES

Aguilaniu, H., Gustafsson, L., Rigoulet, M., and Nyström, T. (2003). Asymmetric inheritance of oxidatively damaged proteins during cytokinesis. *Science* 299, 1751–1753. doi: 10.1126/science.1080418

Alfassy, O. S., Cohen, I., Reiss, Y., Tirosh, B., and Ravid, T. (2013). Placing a disrupted degradation motif at the C terminus of proteasome substrates attenuates degradation without impairing ubiquitylation. *J. Biol. Chem.* 288, 12645–12653. doi: 10.1074/jbc.M410234200

Andersson, V., Hanzén, S., Liu, B., Molin, M., and Nyström, T. (2013). Enhancing protein disaggregation restores proteasome activity in aged cells. *Aging* 5, 802–812. doi: 10.18632/aging.100613

Arrasate, M., Mitra, S., Schweitzer, E. S., Segal, M. R., and Finkbeiner, S. (2004). Inclusion body formation reduces levels of mutant huntingtin and the risk of neuronal death. *Nature* 431, 805–810. doi: 10.1038/nature02998

Berglund, L. L., Hao, X., Liu, B., Grantham, J., and Nyström, T. (2017). Differential effects of soluble and aggregating polyQ proteins on cytotoxicity and type-1 myosin-dependent endocytosis in yeast. *Sci. Rep.* 7:11328. doi: 10.1038/s41598-017-11102-6

Betting, J., and Seufert, W. (1996). A yeast Ubc9 mutant protein with temperature-sensitive in vivo function is subject to conditional proteolysis by a ubiquitin- and proteasome-dependent pathway. *J. Biol. Chem.* 271, 25790–25796. doi: 10.1074/jbc.271.42.25790

Böckler, S., Chelius, X., Hock, N., Klecker, T., Wolter, M., Weiss, M., et al. (2017). Fusion, fission, and transport control asymmetric inheritance of mitochondria and protein aggregates. *J. Cell Biol.* 216, 2481–2498. doi: 10.1038/ng1341

Braun, R. J. (2015). Ubiquitin-dependent proteolysis in yeast cells expressing neurotoxic proteins. *Front. Mol. Neurosci.* 8:8. doi: 10.3389/fnmol.2015.00008

Braun, R. J., Büttner, S., Ring, J., Kroemer, G., and Madeo, F. (2010). Nervous yeast: modeling neurotoxic cell death. *Trends Biochem. Sci.* 35, 135–144. doi: 10.1016/j.tibs.2009.10.005

Bufalino, M. R., DeVeale, B., and van der Kooy, D. (2013). The asymmetric segregation of damaged proteins is stem cell-type dependent. *J. Cell Biol.* 201, 523–530. doi: 10.1083/jcb.201207052

Caine, J., Sankovich, S., Antony, H., Waddington, L., Macreadie, P., Varghese, J., et al. (2007). Alzheimer's Abeta fused to green fluorescent protein induces growth stress and a heat shock response. *FEMS Yeast Res.* 7, 1230–1236. doi: 10.1111/j.1567-1364.2007.00285.x

Chuang, K.-H., Liang, F., Higgins, R., and Wang, Y. (2016). Ubiquilin/Dsk2 promotes inclusion body formation and vacuole (lysosome)-mediated disposal of mutated huntingtin. *Mol. Biol. Cell* 27, 2025–2036. doi: 10.1091/mbc.E16-01-0026

Cohen, A., Ross, L., Nachman, I., and Bar-Nun, S. (2012). Aggregation of polyQ proteins is increased upon yeast aging and affected by Sir2 and Hsf1: novel quantitative biochemical and microscopic assays. *PLoS One* 7:e44785. doi: 10.1371/journal.pone.0044785

Comyn, S. A., Young, B. P., Loewen, C. J., and Mayor, T. (2016). Prefoldin promotes proteasomal degradation of cytosolic proteins with missense mutations by maintaining substrate solubility. *PLoS Genet.* 12:e1006184. doi: 10.1371/journal.pgen.1006184

Cooper, A. A., Gitler, A. D., Cashikar, A., Haynes, C. M., Hill, K. J., Bhullar, B., et al. (2006). Alpha-synuclein blocks ER-Golgi traffic and Rab1 rescues neuron loss in Parkinson's models. *Science* 313, 324–328. doi: 10.1126/science.1129462

Cuervo, A. M., and Dice, J. F. (2000). Age-related decline in chaperone-mediated autophagy. *J. Biol. Chem.* 275, 31505–31513. doi: 10.1074/jbc.M002102200

D'Angelo, F., Vignaud, H., Di Martino, J., Salin, B., Devin, A., Cullin, C., et al. (2013). A yeast model for amyloid-β aggregation exemplifies the role of membrane trafficking and PICALM in cytotoxicity. *Dis. Model. Mech.* 6, 206–216. doi: 10.1242/dmm.010108

Drummond, D. R., Hennessey, E. S., and Sparrow, J. C. (1991). Characterisation of missense mutations in the Act88F gene of Drosophila melanogaster. *Mol. Gen. Genet.* 226, 70–80. doi: 10.1007/BF00273589

Duennwald, M. L., Jagadish, S., Muchowski, P. J., and Lindquist, S. (2006). Flanking sequences profoundly alter polyglutamine toxicity in yeast. *Proc. Natl. Acad. Sci. U.S.A.* 103, 11045–11050. doi: 10.1073/pnas.0604547103

Eisele, F., and Wolf, D. H. (2008). Degradation of misfolded protein in the cytoplasm is mediated by the ubiquitin ligase Ubr1. *FEBS Lett.* 582, 4143–4146. doi: 10.1016/j.febslet.2008.11.015

Elden, A. C., Kim, H.-J., Hart, M. P., Chen-Plotkin, A. S., Johnson, B. S., Fang, X., et al. (2010). Ataxin-2 intermediate-length polyglutamine expansions are associated with increased risk for ALS. *Nature* 466, 1069–1075. doi: 10.1038/nature09320

Escusa-Toret, S., Vonk, W. I. M., and Frydman, J. (2013). Spatial sequestration of misfolded proteins by a dynamic chaperone pathway enhances cellular fitness during stress. *Nat. Cell Biol.* 15, 1231–1243. doi: 10.1038/ncb2838

Farrawell, N. E., Lambert-Smith, I. A., Warraich, S. T., Blair, I. P., Saunders, D. N., Hatters, D. M., et al. (2015). Distinct partitioning of ALS associated TDP-43, FUS and SOD1 mutants into cellular inclusions. *Nature* 5:13416. doi: 10.1038/srep13416

Feldman, D. E., Thulasiraman, V., Ferreyra, R. G., and Frydman, J. (1999). Formation of the VHL-elongin BC tumor suppressor complex is mediated by the chaperonin TRiC. *Mol. Cell* 4, 1051–1061. doi: 10.1016/S1097-2765(00)80233-6

Finger, A., Knop, M., and Wolf, D. H. (1993). Analysis of two mutated vacuolar proteins reveals a degradation pathway in the endoplasmic reticulum or a related compartment of yeast. *Eur. J. Biochem.* 218, 565–574. doi: 10.1111/j.1432-1033.1993.tb18410.x

Fiori, M. G. (1987). Intranuclear inclusions in Schwann cells of aged fowl ciliary ganglia. *J. Anat.* 154, 201–214. doi: 10.1111/(ISSN)1469-7580

Fruhmann, G., Seynnaeve, D., Zheng, J., Ven, K., Molenberghs, S., Wilms, T., et al. (2017). Yeast buddies helping to unravel the complexity of neurodegenerative disorders. *Mech. Ageing Dev.* 161, 288–305. doi: 10.1016/j.mad.2016.05.002

Fuentealba, L. C., Eivers, E., Geissert, D., Taelman, V., and De Robertis, E. M. (2008). Asymmetric mitosis: unequal segregation of proteins destined for degradation. *Proc. Natl. Acad. Sci. U.S.A.* 105, 7732–7737. doi: 10.1073/pnas.0803027105

Furth, N., Gertman, O., Shiber, A., Alfassy, O. S., Cohen, I., Rosenberg, M. M., et al. (2011). Exposure of bipartite hydrophobic signal triggers nuclear quality control of Ndc10 at the endoplasmic reticulum/nuclear envelope. *Mol. Biol. Cell* 22, 4726–4739. doi: 10.1091/mbc.E11-05-0463

Fushimi, K., Long, C., Jayaram, N., Chen, X., Li, L., and Wu, J. Y. (2011). Expression of human FUS/TLS in yeast leads to protein aggregation and cytotoxicity, recapitulating key features of FUS proteinopathy. *Protein Cell* 2, 141–149. doi: 10.1007/s13238-011-1014-5

Gardner, R. G., Nelson, Z. W., and Gottschling, D. E. (2005). Degradation-mediated protein quality control in the nucleus. *Cell* 120, 803–815. doi: 10.1016/j.cell.2005.01.016

Gupta, R., Kasturi, P., Bracher, A., Loew, C., Zheng, M., Villella, A., et al. (2011). Firefly luciferase mutants as sensors of proteome stress. *Nat. Meth.* 8, 879–884. doi: 10.1016/j.molcel.2006.08.017

Hartl, F. U., and Hayer-Hartl, M. (2009). Converging concepts of protein folding in vitro and in vivo. *Nat. Struct. Mol. Biol.* 16, 574–581. doi: 10.1038/nsmb.1591

Heck, J. W., Cheung, S. K., and Hampton, R. Y. (2010). Cytoplasmic protein quality control degradation mediated by parallel actions of the E3 ubiquitin ligases Ubr1 and San1. *Proc. Natl. Acad. Sci. U.S.A.* 107, 1106–1111. doi: 10.1038/35050524

Hill, S. M., Hanzén, S., and Nyström, T. (2017). Restricted access: spatial sequestration of damaged proteins during stress and aging. *EMBO Rep.* 18, 377–391. doi: 10.15252/embr.201643458

Jiang, Y., Di Gregorio, S. E., Duennwald, M. L., and Lajoie, P. (2017). Polyglutamine toxicity in yeast uncovers phenotypic variations between different fluorescent protein fusions. *Traffic* 18, 58–70. doi: 10.1111/tra.12453

Johnson, B. S., McCaffery, J. M., Lindquist, S., and Gitler, A. D. (2008). A yeast TDP-43 proteinopathy model: exploring the molecular determinants of TDP-43 aggregation and cellular toxicity. *Proc. Natl. Acad. Sci. U.S.A.* 105, 6439–6444. doi: 10.1073/pnas.0802082105

Josefson, R., Andersson, R., and Nyström, T. (2017). How and why do toxic conformers of aberrant proteins accumulate during ageing? *Essays Biochem.* 61, 317–324. doi: 10.1042/EBC20160085

Ju, S., Tardiff, D. F., Han, H., Divya, K., Zhong, Q., Maquat, L. E., et al. (2011). A yeast model of FUS/TLS-dependent cytotoxicity. *PLoS Biol.* 9:e1001052. doi: 10.1371/journal.pbio.1001052

Kaganovich, D., Kopito, R., and Frydman, J. (2008). Misfolded proteins partition between two distinct quality control compartments. *Nature* 454, 1088–1095. doi: 10.4161/auto.2.2.2388

Kayatekin, C., Matlack, K. E. S., Hesse, W. R., Guan, Y., Chakrabortee, S., Russ, J., et al. (2014). Prion-like proteins sequester and suppress the toxicity of huntingtin exon 1. *Proc. Natl. Acad. Sci. U.S.A.* 111, 12085–12090. doi: 10.1073/pnas.1412504111

Kaytor, M. D., and Warren, S. T. (1999). Aberrant protein deposition and neurological disease. *J. Biol. Chem.* 274, 37507–37510. doi: 10.1074/jbc.274.53.37507

Khosrow-Khavar, F., Fang, N. N., Ng, A. H. M., Winget, J. M., Comyn, S. A., and Mayor, T. (2012). The yeast ubr1 ubiquitin ligase participates in a prominent pathway that targets cytosolic thermosensitive mutants for degradation. *G3* 2, 619–628. doi: 10.1534/g3.111.001933

Koga, H., Kaushik, S., and Cuervo, A. M. (2011). Protein homeostasis and aging: the importance of exquisite quality control. *Ageing Res. Rev.* 10, 205–215. doi: 10.1016/j.arr.2010.02.001

Koo, E. H., Lansbury, P. T., and Kelly, J. W. (1999). Amyloid diseases: abnormal protein aggregation in neurodegeneration. *Proc. Natl. Acad. Sci. U.S.A.* 96, 9989–9990. doi: 10.1073/pnas.96.18.9989

Krobitsch, S., and Lindquist, S. (2000). Aggregation of huntingtin in yeast varies with the length of the polyglutamine expansion and the expression of chaperone proteins. *Proc. Natl. Acad. Sci. U.S.A.* 97, 1589–1594. doi: 10.1073/pnas.97.4.1589

Kruegel, U., Robison, B., Dange, T., Kahlert, G., Delaney, J. R., Kotireddy, S., et al. (2011). Elevated proteasome capacity extends replicative lifespan in *Saccharomyces cerevisiae*. *PLoS Genet.* 7:e1002253. doi: 10.1371/journal.pgen.1002253

Kryndushkin, D., Ihrke, G., Piermartiri, T. C., and Shewmaker, F. (2012). A yeast model of optineurin proteinopathy reveals a unique aggregation pattern associated with cellular toxicity. *Mol. Microbiol.* 86, 1531–1547. doi: 10.1111/mmi.12075

Kryndushkin, D., Wickner, R. B., and Shewmaker, F. (2011). FUS/TLS forms cytoplasmic aggregates, inhibits cell growth and interacts with TDP-43 in a yeast model of amyotrophic lateral sclerosis. *Protein Cell* 2, 223–236. doi: 10.1007/s13238-011-1525-0

Leibiger, C., Deisel, J., Aufschnaiter, A., Ambros, S., Tereshchenko, M., Verheijen, B. M., et al. (2018). TDP-43 controls lysosomal pathways thereby determining its own clearance and cytotoxicity. *Hum. Mol. Genet.* 27, 1593–1607. doi: 10.1093/hmg/ddy066

Liang, J., Clark-Dixon, C., Wang, S., Flower, T. R., Williams-Hart, T., Zweig, R., et al. (2008). Novel suppressors of alpha-synuclein toxicity identified using yeast. *Hum. Mol. Genet.* 17, 3784–3795. doi: 10.1093/hmg/ddn276

Liu, B., Larsson, L., Caballero, A., Hao, X., Öling, D., Grantham, J., et al. (2010). The polarisome is required for segregation and retrograde transport of protein aggregates. *Cell* 140, 257–267. doi: 10.1016/j.cell.2009.12.031

Liu, C.-W., Corboy, M. J., DeMartino, G. N., and Thomas, P. J. (2003). Endoproteolytic activity of the proteasome. *Science* 299, 408–411. doi: 10.1126/science.1079293

Matsumoto, K., Toh-e, A., and Oshima, Y. (1978). Genetic control of galactokinase synthesis in *Saccharomyces cerevisiae*: evidence for constitutive expression of the positive regulatory gene gal4. *J. Bacteriol.* 134, 446–457.

McClellan, A. J., Scott, M. D., and Frydman, J. (2005). Folding and quality control of the VHL tumor suppressor proceed through distinct chaperone pathways. *Cell* 121, 739–748. doi: 10.1016/j.cell.2005.03.024

McLean, P. J., Kawamata, H., and Hyman, B. T. (2001). Alpha-synuclein-enhanced green fluorescent protein fusion proteins form proteasome sensitive inclusions in primary neurons. *Neuroscience* 104, 901–912. doi: 10.1016/S0306-4522(01)00113-0

McMurray, M. (2014). Lean forward: Genetic analysis of temperature-sensitive mutants unfolds the secrets of oligomeric protein complex assembly. *Bioessays* 36, 836–846. doi: 10.1074/jbc.M112.406710

Medicherla, B., Kostova, Z., Schaefer, A., and Wolf, D. H. (2004). A genomic screen identifies Dsk2p and Rad23p as essential components of ER-associated degradation. *EMBO Rep.* 5, 692–697. doi: 10.1038/414652a

Menezes, R., Tenreiro, S., Macedo, D., Santos, C. N., and Outeiro, T. F. (2015). From the baker to the bedside: yeast models of Parkinson's disease. *Microb. Cell* 2, 262–279. doi: 10.15698/mic2015.08.219

Mikalsen, T., Johannessen, M., and Moens, U. (2005). Sequence- and position-dependent tagging protects extracellular-regulated kinase 3 protein from 26S proteasome-mediated degradation. *Int. J. Biochem. Cell Biol.* 37, 2513–2520. doi: 10.1016/j.biocel.2005.06.007

Miller, S. B., Ho, C. T., Winkler, J., Khokhrina, M., Neuner, A., Mohamed, M. Y., et al. (2015). Compartment-specific aggregases direct distinct nuclear and cytoplasmic aggregate deposition. *EMBO J.* 34, 778–797. doi: 10.15252/embj.201489524

Mogk, A., and Bukau, B. (2017). Role of sHsps in organizing cytosolic protein aggregation and disaggregation. *Cell Stress Chaperones* 22, 493–502. doi: 10.1007/s12192-017-0762-4

Nillegoda, N. B., Theodoraki, M. A., Mandal, A. K., Mayo, K. J., Ren, H. Y., Sultana, R., et al. (2010). Ubr1 and Ubr2 function in a quality control pathway for degradation of unfolded cytosolic proteins. *Mol. Biol. Cell* 21, 2102–2116. doi: 10.1091/mbc.E10-02-0098

O'Brien, R. J., and Wong, P. C. (2011). Amyloid precursor protein processing and Alzheimer's disease. *Annu. Rev. Neurosci.* 34, 185–204. doi: 10.1146/annurev-neuro-061010-113613

Ogrodnik, M., Salmonowicz, H., Brown, R., Turkowska, J., Średniawa, W., Pattabiraman, S., et al. (2014). Dynamic JUNQ inclusion bodies are asymmetrically inherited in mammalian cell lines through the asymmetric partitioning of vimentin. *Proc. Natl. Acad. Sci. U.S.A.* 111, 8049–8054. doi: 10.1073/pnas.1324035111

Oling, D., Eisele, F., Kvint, K., and Nystrom, T. (2014). Opposing roles of Ubp3-dependent deubiquitination regulate replicative life span and heat resistance. *EMBO J.* 33, 747–761. doi: 10.1002/embj.201386822

Outeiro, T. F., and Lindquist, S. (2003). Yeast cells provide insight into alpha-synuclein biology and pathobiology. *Science* 302, 1772–1775. doi: 10.1126/science.1090439

Park, S.-H., Bolender, N., Eisele, F., Kostova, Z., Takeuchi, J., Coffino, P., et al. (2007). The cytoplasmic Hsp70 chaperone machinery subjects misfolded and endoplasmic reticulum import-incompetent proteins to degradation via the ubiquitin-proteasome system. *Mol. Biol. Cell* 18, 153–165. doi: 10.1091/mbc.E06-04-0338

Park, S.-H., Kukushkin, Y., Gupta, R., Chen, T., Konagai, A., Hipp, M. S., et al. (2013). PolyQ proteins interfere with nuclear degradation of cytosolic proteins by sequestering the Sis1p chaperone. *Cell* 154, 134–145. doi: 10.1016/j.cell.2013.06.003

Paulson, H. L. (1999). Protein fate in neurodegenerative proteinopathies: polyglutamine diseases join the (mis)fold. *Am. J. Hum. Genet.* 64, 339–345. doi: 10.1086/302269

Peng, B., Williams, T. C., Henry, M., Nielsen, L. K., and Vickers, C. E. (2015). Controlling heterologous geneexpression in yeast cell factories on di erent carbon substrates and across the diauxic shift: a comparison of yeast promoter activities. *Microb. Cell Fact.* 14:91. doi: 10.1186/s12934-015-0278-5

Pereira, C., Bessa, C., Soares, J., Leão, M., and Saraiva, L. (2012). Contribution of yeast models to neurodegeneration research. *J. Biomed. Biotechnol.* 2012:941232. doi: 10.1155/2012/941232

Peters, A., Josephson, K., and Vincent, S. L. (1991). Effects of aging on the neuroglial cells and pericytes within area 17 of the rhesus monkey cerebral cortex. *Anat. Rec.* 229, 384–398. doi: 10.1002/ar.1092290311

Petroi, D., Popova, B., Taheri-Talesh, N., Irniger, S., Shahpasandzadeh, H., Zweckstetter, M., et al. (2012). Aggregate clearance of α-synuclein in *Saccharomyces cerevisiae* depends more on autophagosome and vacuole function than on the proteasome. *J. Biol. Chem.* 287, 27567–27579. doi: 10.1371/journal.pone.0005515

Prasad, R., Kawaguchi, S., and Ng, D. T. W. (2010). A nucleus-based quality control mechanism for cytosolic proteins. *Mol. Biol. Cell* 21, 2117–2127. doi: 10.1091/mbc.E10-02-0111

Ruan, L., Zhou, C., Jin, E., Kucharavy, A., Zhang, Y., Wen, Z., et al. (2017). Cytosolic proteostasis through importing of misfolded proteins into mitochondria. *Nature* 543, 443–446. doi: 10.1038/nature21695

Rujano, M. A., Bosveld, F., Salomons, F. A., Dijk, F., van Waarde, M. A. W. H., van der Want, J. J. L., et al. (2006). Polarised asymmetric inheritance of accumulated protein damage in higher eukaryotes. *PLoS Biol.* 4:e417. doi: 10.1371/journal.pbio.0040417

Saarikangas, J., and Barral, Y. (2015). Protein aggregates are associated with replicative aging without compromising protein quality control. *eLife* 4:e06197. doi: 10.7554/eLife.06197

Sadler, J. R., and Novick, A. (1965). The properties of repressor and the kinetics of its action. *J. Mol. Biol.* 12, 305–327. doi: 10.1016/S0022-2836(65)80255-8

Saez, I., and Vilchez, D. (2014). The mechanistic links between proteasome activity, aging and age-related diseases. *Curr. Genomics* 15, 38–51. doi: 10.2174/1389202915011403061133 44

Saudou, F., Finkbeiner, S., Devys, D., and Greenberg, M. E. (1998). Huntingtin acts in the nucleus to induce apoptosis but death does not correlate with the formation of intranuclear inclusions. *Cell* 95, 55–66. doi: 10.1016/S0092-8674(00)81782-1

Schoenfeld, A. R., Davidowitz, E. J., and Burk, R. D. (2000). Elongin BC complex prevents degradation of von Hippel-Lindau tumor suppressor gene products. *Proc. Natl. Acad. Sci. U.S.A.* 97, 8507–8512. doi: 10.1073/pnas.97.15.8507

Schröder, H., Langer, T., Hartl, F. U., and Bukau, B. (1993). DnaK, DnaJ and GrpE form a cellular chaperone machinery capable of repairing heat-induced protein damage. *EMBO J.* 12, 4137–4144.

Shcheprova, Z., Baldi, S., Frei, S. B., Gonnet, G., and Barral, Y. (2008). A mechanism for asymmetric segregation of age during yeast budding. *Nature* 454, 728–734. doi: 10.1038/nature07212

Shiber, A., Breuer, W., Brandeis, M., and Ravid, T. (2013). Ubiquitin conjugation triggers misfolded protein sequestration into quality control foci when Hsp70 chaperone levels are limiting. *Mol. Biol. Cell* 24, 2076–2087. doi: 10.1091/mbc.E13-01-0010

Shiber, A., Breuer, W., and Ravid, T. (2014). Flow cytometric quantification and characterization of intracellular protein aggregates in yeast. *Prion* 8, 276–284. doi: 10.4161/19336896.2014.968445

Song, J., Yang, Q., Yang, J., Larsson, L., Hao, X., Zhu, X., et al. (2014). Essential genetic interactors of SIR2 required for spatial sequestration and asymmetrical inheritance of protein aggregates. *PLoS Genet.* 10:e1004539. doi: 10.1371/journal.pgen.1004539.s009

Sontag, E. M., Samant, R. S., and Frydman, J. (2017). Mechanisms and functions of spatial protein quality control. *Annu. Rev. Biochem.* 86, 97–122. doi: 10.1146/annurev-biochem-060815-14616

Specht, S., Miller, S. B. M., Mogk, A., and Bukau, B. (2011). Hsp42 is required for sequestration of protein aggregates into deposition sites in *Saccharomyces cerevisiae*. *J. Cell Biol.* 195, 617–629. doi: 10.1083/jcb.136.1.111

Spokoini, R., Moldavski, O., Nahmias, Y., England, J. L., Schuldiner, M., and Kaganovich, D. (2012). Confinement to organelle-associated inclusion structures mediates asymmetric inheritance of aggregated protein in budding yeast. *Cell Rep.* 2, 738–747. doi: 10.1016/j.celrep.2012.08.024

Stolz, A., and Wolf, D. H. (2012). Use of CPY and its derivatives to study protein quality control in various cell compartments. *Methods Mol. Biol.* 832, 489–504. doi: 10.1007/978-1-61779-474-2_35

Sun, Z., Diaz, Z., Fang, X., Hart, M. P., Chesi, A., Shorter, J., et al. (2011). Molecular determinants and genetic modifiers of aggregation and toxicity for the ALS disease protein FUS/TLS. *PLoS Biol.* 9:e1000614. doi: 10.1371/journal.pbio.1000614

Sundberg, H. A., and Davis, T. N. (1997). A mutational analysis identifies three functional regions of the spindle pole component Spc110p in *Saccharomyces cerevisiae*. *Mol. Biol. Cell* 8, 2575–2590. doi: 10.1091/mbc.8.12.2575

Takahashi, T., Kikuchi, S., Katada, S., Nagai, Y., Nishizawa, M., and Onodera, O. (2008). Soluble polyglutamine oligomers formed prior to inclusion body formation are cytotoxic. *Hum. Mol. Genet.* 17, 345–356. doi: 10.1093/hmg/ddm311

Taylor, J. P., Tanaka, F., Robitschek, J., Sandoval, C. M., Taye, A., Markovic-Plese, S., et al. (2003). Aggresomes protect cells by enhancing the degradation of toxic polyglutamine-containing protein. *Hum. Mol. Genet.* 12, 749–757. doi: 10.1093/hmg/ddg074

Tenreiro, S., Munder, M. C., Alberti, S., and Outeiro, T. F. (2013). Harnessing the power of yeast to unravel the molecular basis of neurodegeneration. *J. Neurochem.* 127, 438–452. doi: 10.1111/jnc.12271

Tenreiro, S., Reimão-Pinto, M. M., Antas, P., Rino, J., Wawrzycka, D., Macedo, D., et al. (2014). Phosphorylation modulates clearance of alpha-synuclein inclusions in a yeast model of Parkinson's disease. *PLoS Genet.* 10:e1004302. doi: 10.1371/journal.pgen.1004302

Treusch, S., Hamamichi, S., Goodman, J. L., Matlack, K. E. S., Chung, C. Y., Baru, V., et al. (2011). Functional links between Aβ toxicity, endocytic trafficking, and Alzheimer's disease risk factors in yeast. *Science* 334, 1241–1245. doi: 10.1126/science.1213210

Tyedmers, J., Mogk, A., and Bukau, B. (2010). Cellular strategies for controlling protein aggregation. *Nat. Rev. Mol. Cell Biol.* 11, 777–788. doi: 10.1038/nrm2993

Waldo, G. S., Standish, B. M., Berendzen, J., and Terwilliger, T. C. (1999). Rapid protein-folding assay using green fluorescent protein. *Nat. Biotechnol.* 17, 691–695. doi: 10.1038/10904

Wang, Y., Meriin, A. B., Zaarur, N., Romanova, N. V., Chernoff, Y. O., Costello, C. E., et al. (2009). Abnormal proteins can form aggresome in yeast: aggresome-targeting signals and components of the machinery. *FASEB J.* 23, 451–463. doi: 10.1096/fj.08-117614

Willingham, S., Outeiro, T. F., DeVit, M. J., Lindquist, S. L., and Muchowski, P. J. (2003). Yeast genes that enhance the toxicity of a mutant huntingtin fragment or alpha-synuclein. *Science* 302, 1769–1772. doi: 10.1126/science.1090389

Winkler, J., Seybert, A., König, L., Pruggnaller, S., Haselmann, U., Sourjik, V., et al. (2010). Quantitative and spatio-temporal featuresof protein aggregation in *Escherichia coli* and consequences on protein quality control and cellular ageing. *EMBO J* 29, 910–923. doi: 10.1038/emboj.2009.412

Wolf, D. H., and Fink, G. R. (1975). Proteinase C (carboxypeptidase Y) mutant of yeast. *J. Bacteriol.* 123, 1150–1156.

Wolfe, K. J., Ren, H. Y., Trepte, P., and Cyr, D. M. (2013). The Hsp70/90 cochaperone, Sti1, suppresses proteotoxicity by regulating spatial quality control of amyloid-like proteins. *Mol. Biol. Cell* 24, 3588–3602. doi: 10.1091/mbc.E13-06-0315

Zhou, C., Slaughter, B. D., Unruh, J. R., Guo, F., Yu, Z., Mickey, K., et al. (2014). Organelle-based aggregation and retention of damaged proteinsin asymmetrically dividing cells. *Cell* 159, 530–542. doi: 10.1016/j.cell.2014.09.026

Conflict of Interest Statement: The authors declare that the research was conducted in the absence of any commercial or financial relationships that could be construed as a potential conflict of interest.

frontiers in Molecular Neuroscience

REVIEW
published: 04 September 2018
doi: 10.3389/fnmol.2018.00318

Studying Huntington's Disease in Yeast: From Mechanisms to Pharmacological Approaches

Sebastian Hofer[1], Katharina Kainz[1], Andreas Zimmermann[1,2], Maria A. Bauer[1], Tobias Pendl[1], Michael Poglitsch[1], Frank Madeo[1,3] and Didac Carmona-Gutierrez[1]**

[1] Institute of Molecular Biosciences, University of Graz, Graz, Austria, [2] Department of Internal Medicine, Medical University of Graz, Graz, Austria, [3] BioTechMed-Graz, Graz, Austria

Huntington's disease (HD) is a neurodegenerative disorder that leads to progressive neuronal loss, provoking impaired motor control, cognitive decline, and dementia. So far, HD remains incurable, and available drugs are effective only for symptomatic management. HD is caused by a mutant form of the huntingtin protein, which harbors an elongated polyglutamine domain and is highly prone to aggregation. However, many aspects underlying the cytotoxicity of mutant huntingtin (mHTT) remain elusive, hindering the efficient development of applicable interventions to counteract HD. An important strategy to obtain molecular insights into human disorders in general is the use of eukaryotic model organisms, which are easy to genetically manipulate and display a high degree of conservation regarding disease-relevant cellular processes. The budding yeast *Saccharomyces cerevisiae* has a long-standing and successful history in modeling a plethora of human maladies and has recently emerged as an effective tool to study neurodegenerative disorders, including HD. Here, we summarize some of the most important contributions of yeast to HD research, specifically concerning the elucidation of mechanistic features of mHTT cytotoxicity and the potential of yeast as a platform to screen for pharmacological agents against HD.

Keywords: Chorea Huntington, huntingtin, drug discovery, disease model, neurodegeneration, apoptosis, aging

OPEN ACCESS

Edited by:
Ralf J. Braun,
University of Bayreuth, Germany

Reviewed by:
Ruben Fernandez-Busnadiego,
Max-Planck-Institut für Biochemie, Germany
Francesca Cicchetti,
Laval University, Canada

****Correspondence:***
Frank Madeo
frank.madeo@uni-graz.at
Didac Carmona-Gutierrez
didac.carmonagutierrez@uni-graz.at

Received: *20 April 2018*
Accepted: *16 August 2018*
Published: *04 September 2018*

Citation:
Hofer S, Kainz K, Zimmermann A, Bauer MA, Pendl T, Poglitsch M, Madeo F and Carmona-Gutierrez D (2018) Studying Huntington's Disease in Yeast: From Mechanisms to Pharmacological Approaches. Front. Mol. Neurosci. 11:318. doi: 10.3389/fnmol.2018.00318

INTRODUCTION

Since the first detailed and widely recognized description of Huntington's disease (HD) by George Huntington in 1872 (Hayden, 1981, 1983), there have been important advances in understanding this malady. However, to date, the underlying molecular mechanisms as well as the cellular and organismal perturbations that occur in HD patients are not fully understood (Reiner et al., 2011; Kumar et al., 2015). In fact, there is still no cure for the disease, and therapeutic approaches are only limited to symptomatic treatments. It is therefore a pending issue to elucidate the causal network behind this clinically well characterized disease (Roos, 2010) to eventually develop therapies that can revert and/or prevent HD. The application of adequate model systems allows for a useful and rapid possibility to tackle both basic mechanistic research and the explorative quest for new therapeutics. In this review, we will summarize the use and potential of the budding yeast *Saccharomyces cerevisiae* as a model organism in HD research. Since manifold reviews have already been published on the topic (Bates and Hockly, 2003; Coughlan and Brodsky, 2005; Outeiro and Giorgini, 2006; Winderickx et al., 2008; Giorgini and Muchowski, 2009; Duennwald, 2011; Mason and Giorgini, 2011; Pereira et al., 2012; Tenreiro et al., 2013; Peffer et al., 2015; Shrestha and Megeney, 2015; Fruhmann et al., 2017), in this work, we will specifically address critical

limitations and delineate the translational power of this tool for both mechanistic insights and drug discovery. In particular, we will focus on discussing studies that highlight the translational and human-relevant potential harbored by HD research conducted in *S. cerevisiae*.

Huntington's Disease

Huntington's disease is one of nine CAG trinucleotide repeat disorders, a group of inherited neurodegenerative diseases (Zoghbi and Orr, 2000; Nakamura et al., 2001) and is caused by a CAG repeat (codes for glutamine, Q) mutation in exon-1 of the huntingtin (HTT) gene, which results in an elongated polyglutamine [or poly(Q)] stretch of the protein – giving rise to the term mutant HTT (mHTT) (McColgan and Tabrizi, 2017). HD is most prevalent in European societies and can nowadays be diagnosed with reliable genetic tests. In European populations, the HD mutation carrier rate is roughly 10.6 − 13.7/100,000 (Walker, 2007; Bates et al., 2015). The disease is inherited in an autosomal dominant manner and its onset occurs at an average age of 45 years with an asymptomatic, subtle, pre-clinical phase preceding the actual clinical stage by up to 15 years (Ross et al., 2014). Cases of hereditary HD can be traced back for several generations, while in rare cases spontaneous occurrence of non-inherited HD can appear due to genetic instability in parents with CAG repeats, whose number is at the high-end of the normal range (up to 35 repeats, see below) (Shaw and Caro, 1982). In fact, it is now believed that up to 10–15% of HD cases are of spontaneous nature (Reiner et al., 2011). Clinical symptoms include cognitive impairments, motor dysfunction, emotional disturbance, neuropsychiatric alterations, and striatal atrophy, ultimately leading to premature death (Walker, 2007). Many of these symptoms were already described by George Huntington and others in the 19th century (Hayden, 1981, 1983). However, despite huge progress in understanding the disease, there exist no causal treatments yet. Most experimental therapeutic approaches aim at reducing the load of the mutant protein, with the so-called anti-sense oligonucleotide therapy being among the most promising against HD. This multifaceted technique employs allele-specific or -unspecific oligonucleotides targeting HTT DNA or mRNA (Zaghloul et al., 2017). This appealing approach has already been successfully employed in the well-established YAC128 mouse model of HD (Stanek et al., 2013). Of note, recent findings have revealed significant neurotoxic potential of mutant HTT (mHTT)-derived small and elongated RNA species, which may be trapped in the nucleus and compromise cellular viability (de Mezer et al., 2011; Bañez-Coronel et al., 2012).

Healthy individuals possess a CAG count below 35 repeats, whereas HD patients harbor an HTT gene with longer poly(Q) tracts: full penetrance of the disease is believed to occur at 40 or more repeats, whereas poly(Q) regions of 36–39 repeats lead to reduced penetrance, with a chance of no, or very late onset of the disease. Thus, in humans, as well as in model organisms, disease onset (and severity to some extent) seems to correlate with the length of the poly(Q) tract (Snell et al., 1993; Penney et al., 1997; Adegbuyiro et al., 2017). Other (genetic) factors, however, modulate HD as well, but cannot compensate for the causal role of elongated poly(Q) regions within the HTT protein (MacDonald et al., 1993; Finkbeiner, 2011; Reiner et al., 2011). These elongations result in structural alterations, which subsequently make the protein prone for misfolding, aggregation, and fragmentation, leading to intranuclear and cytosolic multi-protein inclusion bodies in brain cells (Davies et al., 1997; Bates et al., 2015), which disturb cellular homeostasis. It is a matter of intense debate whether (large) HTT protein aggregates are the toxic elements or represent a detoxified (or even protective) form. This discrepancy and the importance of different intermediate oligomers would go beyond the scope of this review and will not be discussed here in detail, but definitely asks for clarification in the future (Arrasate and Finkbeiner, 2012). Adding to the disease's complexity, HTT is ubiquitously expressed and, contrary to earlier paradigms, more recent advances highlight the fact that HD affects the human body not only at the neuronal, but also at a systemic level (van der Burg et al., 2009).

The cloning of the HTT gene in 1993 led to a boost in HD research. IT-15 (interesting transcript 15) on chromosome four was identified by "The Huntington's Disease Collaborative Research Group" and shown to contain an unstable (CAG) region that is essential for the toxic role of the protein, followed by an adjacent proline-rich region (PRD) (MacDonald et al., 1993). The discovery of a distinct protein (HTT) at the heart of this neurodegenerative disease also sparked the development of genetic models in various vertebrate (rhesus monkey, sheep, Tibetan miniature pig, rodents, zebrafish), invertebrate (*Drosophila melanogaster*, *Caenorhabditis elegans*), and unicellular (*S. cerevisiae*) organisms (Mason and Giorgini, 2011; Xi et al., 2011; Morton and Howland, 2013; Pouladi et al., 2013). In addition to animal- and unicellular-based HD models, genetically tractable *in vitro* cell culture models have been helpful in deducing the molecular basis of neurodegenerative diseases. Especially in recent years, advances in a technique that employs "induced pluripotent stem cells" (iPSCs) are growingly becoming useful and iPSCs have been applied to HD research already since 2008 [Park et al., 2008; reviewed in Tousley and Kegel-Gleason (2016)]. Nowadays, a wide range of different iPSC lines are available, recapitulating most of the pathological features on a cellular scale as seen in human patients and other models (Tousley and Kegel-Gleason, 2016). These iPSC human cell lines will be of great importance, as they allow time- and cost-efficient screens for drug discovery (Tousley and Kegel-Gleason, 2016). Still, tackling the wide range of significant questions related to HD in the most rapid manner will require a combinatory approach that uses all relevant information using different models at hand. For that, in the scope of this review, we will only discuss the usability and limitations of unicellular yeasts as HD models.

The 67 exons of the HTT gene encode a ∼350-kDa protein, including the polymorphic trinucleotide (CAG) track within exon-1 (MacDonald et al., 1993). With the presence of homologs in many species (but not yeast), HTT is believed to have pleiotropic, potentially conserved molecular and physiological functions (Reiner et al., 2011). Interactors of the ubiquitously expressed HTT have been described in

the range of 40 to several hundred proteins, and the list of suggested native functions is long, including its involvement in autophagy, transcriptional regulation, endocytosis, vesicle function, endosomal trafficking, cell division, ciliogenesis, and antiapoptotic processes (Schulte and Littleton, 2011; Saudou and Humbert, 2016). In fact, while the non-physiological gain-of-function mutation phenotype of HTT is the basis for most HD research in model organisms (Bates and Hockly, 2003; Bates et al., 2015), it does not fully account for the molecular pathologic events seen in human HD cells. A loss-of-function toxicity of *physiological* HTT-tasks likely contributes to the observed detrimental phenotypes (Zuccato and Cattaneo, 2014; Bates et al., 2015).

Among the molecular pathologic features of HD are excessive misfolding, aggregation, transcriptional dysregulation, mitochondrial dysfunction, and altered energy metabolism, impairments of the proteasomal and autophagic system, and many more (Roos, 2010). Intriguingly, using a fruitfly model of HD, Ochaba et al. (2014) have recently discovered a housekeeping function of HTT as a scaffold protein in selective autophagy. Selective autophagy is a catabolic process important for the clearance of intracellular content and is heavily implicated in neurodegenerative diseases (Wong and Cuervo, 2010; Johansen and Lamark, 2011). This discovery also holds evidence for a possible two-faceted pathological role of HTT in HD: the mutated protein is likely to be toxic *per se*, but also titrates functional HTT protein, deriving in impaired autophagic competence and a cascade of cellular perturbations (Ochaba et al., 2014).

Adding to the complex molecular features of HD, more recent reports have shed light on different RNA-based toxicity mechanisms. Seemingly, mHTT transcription can lead to short repeated CAG RNA species and nuclear RNA inclusions. Nucleolar stress, alterations in alternative splicing processes, disruption of nuclear functions by binding of diverse factors to elongated repeats, and cellular dysfunction may be the consequences thereof (Martí, 2016). Moreover, so-called RAN (repeat-associated non-ATG) peptides seem to contribute to HD pathology and might comprise another molecular source of mHTT toxicity (Bañez-Coronel et al., 2015).

This combination of increased lethal and decreased vital effects of HTT increases the difficulty of drug development, as both physiological and pathological functions of HTT have to be taken into consideration. Importantly, as opposed to other HD models, the yeast *S. cerevisiae* represents a "clean" cellular room (since it has no HTT homolog) that, however, possesses a conserved regulated cell death (RCD) machinery. This makes yeast a valuable addition to available higher eukaryotic HD models.

Yeast as a Model Organism for Neurodegenerative Diseases

The budding yeast *S. cerevisiae* is a unicellular eukaryote that has accompanied human societies and culture since the distant past. In more recent times, yeast has additionally become an indispensable and strikingly well-characterized tool in (food) industry and research. In fact, it is considered the best studied eukaryotic cell system with over 6,000 known protein-coding genes, which have largely been annotated. A major advantage for early yeast researchers was the fully sequenced genome, published in 1996, and thereafter, the large number of available systematic studies at the genome and proteome levels (Goffeau et al., 1996; Botstein and Fink, 2011; Engel et al., 2013). Only recently, the Nobel Prize in Physiology or Medicine 2016 was awarded to Yoshinori Ohsumi for his work on autophagy, mainly performed in yeast. Of note, this has been the fifth Nobel prize awarded to work performed with yeast in the 21st century (Zimmermann et al., 2016).

Yeast is widely used as a versatile model organism (Botstein and Fink, 2011), including but not limited to the research fields of RCD (Madeo et al., 1999, 2002; Büttner et al., 2011; Munoz et al., 2012; Côrte-Real and Madeo, 2013; Fahrenkrog, 2015; Carmona-Gutierrez et al., 2018), systems biology (Mustacchi et al., 2006), aging (Gershon and Gershon, 2000; Fröhlich and Madeo, 2001; Herker et al., 2004; Kaeberlein et al., 2007; Janssens and Veenhoff, 2016), prion biology (Speldewinde and Grant, 2015, 2017), virus research (Lista et al., 2017; Zhao, 2017), genetics (Forsburg, 2001; Hagihara et al., 2017), autophagy (Reggiori and Klionsky, 2013; Ohsumi, 2014; Yin et al., 2016) as well as of neurodegeneration (Khurana and Lindquist, 2010; Tenreiro and Outeiro, 2010; Ocampo and Barrientos, 2011; Pereira et al., 2012; Shrestha and Megeney, 2015; Stekovic et al., 2017), drug discovery, and drug development (Ma, 2001; Hughes, 2002; Outeiro and Giorgini, 2006; Eisenberg et al., 2009, 2016; Amen and Kaganovich, 2016; Madeo et al., 2018; Zimmermann et al., 2018). Yeast experiments are usually low cost and can be performed in a high-throughput manner. This makes it suitable for large-scale genetic and pharmacological screens. Yeast researchers can draw from rich sources of freely available databases (e.g., SGD, CYGD, yGMV), extensive knock-out, overexpression, and fusion protein strain collections (e.g., EUROSCARF), handy genetic tools and a large research community (Khurana and Lindquist, 2010; Tenreiro and Outeiro, 2010).

Overall, *S. cerevisiae* provides all the features and techniques needed for a valid model organism. To date, no other yeast species has reached a similar degree of research usability. However, in the future, other yeast-based models may become increasingly important for HD research, especially *Schizosaccharomyces pombe* and *Pichia pastoris*. *S. cerevisiae* has traditionally emerged as the most wide-spread yeast model of choice, since it is highly flexible as an organism and has proven to be a valid tool in other neurodegenerative diseases. It is one of the most robust *in vivo* tools for high-throughput drug- and mechanism-screenings. Moreover, *S. cerevisiae* is at the cutting edge of systems biology, with techniques and tools to generate and analyze "big data" ready to be employed. The combination of genetic manipulations with flexible experimental designs and short experimental durations allows researchers to rapidly approach scientific questions and manage research schedules that are not feasible in other model organisms. This tremendous wealth of resources has led to a vast scientific output from studies conducted in this simple eukaryote.

Besides other disorders, tractable *S. cerevisiae* models have been developed and intensively studied for neurodegenerative diseases such as HD (see following paragraphs), Alzheimer's disease (Heinisch and Brandt, 2016; Verduyckt et al., 2016), Parkinson's disease (Menezes et al., 2015; Tenreiro et al., 2017), Friedreich's Ataxia (Babcock et al., 1997), Batten's disease (Pearce and Sherman, 1998; Rajakumar et al., 2017), amyotrophic lateral sclerosis (Johnson et al., 2008; Kryndushkin and Shewmaker, 2011; Leibiger et al., 2018), Niemann-Pick disease (Berger et al., 2005; Rajakumar et al., 2017), and others (Tenreiro and Outeiro, 2010; Pereira et al., 2012; Ring et al., 2017). Importantly, a variety of genes (>1,000) related to human diseases have orthologs in the yeast genome, many of which can be genetically and functionally replaced by their human counterparts (Menezes et al., 2015). The development of so-called "humanized" yeast strains by modifying yeast genes or replacing whole pathways to resemble human cell biology (Kachroo et al., 2015; Laurent et al., 2016; Truong and Boeke, 2017) has added to the importance of this model organism and redefined its role for human-relevant research (Kachroo et al., 2015; Laurent et al., 2016). Although yeast is regarded as a unicellular organism, yeast cells harbor many of the cellular pathways needed for metabolic homeostasis and protein quality control that have been implicated in neurodegeneration (Barrientos, 2003; Ocampo and Barrientos, 2008), including RCD subroutines (Carmona-Gutierrez and Büttner, 2014; Carmona-Gutierrez et al., 2018) and autophagic processes (Zimmermann et al., 2016; Kainz et al., 2017). Furthermore, yeast cells have been shown to interact with each other in complex manners under specific physiological conditions. This has prompted to overcome the classical dogma of yeast populations being a mere accumulation of single independent elements and to reinterpret them as multicellular entities that undergo intercellular communication, ensuring the survival of the clone (Honigberg, 2011; Carmona-Gutierrez and Büttner, 2014). This may further explain the amount of scientific questions with relevance to humans that can be addressed in yeast.

In summary, *S. cerevisiae* represents the yeast species of choice for a manifold of scientific questions. To date, no other yeast has reached a similarly multilayered level of usability. Nonetheless, it can be expected that the future will bring a wider range of HD models in various yeasts, which will then add to the richness of scientific and technical possibilities.

MODELING HD IN YEAST

Despite the high degree of conservation of human disease-associated genes in yeast, S. cerevisiae – as mentioned above – lacks HTT homologs. Therefore, yeast HD models are based on the heterologous expression of human HTT in various versions (**Table 1**). Noteworthy, N-terminal HTT fragments are an intrinsic feature of human HD pathology (Davies et al., 1997) and many yeast HTT-poly(Q) constructs are modeled accordingly, mostly using HTT exon 1. Different models of mHTT will be discussed in the following chapters, using the term "mHTT" as an identifier for variants with elongated poly(Q) tracts. While the pathological threshold for the poly(Q) length has been well studied in humans, as far as we know, it is not known in yeast. Thus "mHTT" mostly refers to constructs with poly(Q) lengths well above the threshold in humans.

Non-toxic Models

Krobitsch and Lindquist (2000) established a poly(Q)-length-dependent model of HTT aggregation in 2000 by fusing the first 68 N-terminal amino acids of wild-type HTT exon-1 containing poly(Q) tracts of varying length (25, 42, 72, 103 glutamines) to a C-terminal GFP (green fluorescent protein)-tag. For stability reasons, they modified the codons within the poly(Q) tract to a mixture of CAG and CAA. They could either rule out or confirm the involvement of various specific chaperones in the aggregation process. Notably, observed effects were consistent for different low/high-copy plasmids with constitutive or inducible (galactose-driven) expression. Remarkably, deletion of HSP104 completely abolished aggregation of Htt103Q. However, this early model did not show cytotoxicity. Later studies revealed a strong dependency of mHTT toxicity on the flanking sequences (Dehay and Bertolotti, 2006; Duennwald et al., 2006a; Jiang et al., 2016), which might explain the lack of cytotoxicity in the model used by Krobitsch and Lindquist (2000). Interestingly, shortly after this study, it was shown that in a similar model redirecting fragmented exon-1-poly(Q)-fusion proteins to the nucleus, nuclear aggregates are formed, which are unaffected by

TABLE 1 | Overview of important yeast HD models and their basic characteristics.

Original and significant publications	Organism	Promotor (Inducer)	Poly(Q) Lengths	Integrated (i)/Plasmid (p)	N-terminal HTT aminoacids	Cytotoxicity	Aggregation
Krobitsch and Lindquist, 2000	*S. cerevisiae*	*GAL1* (galactose)	25, 42, 72, 103	p	68	No	Yes
Muchowski et al., 2000	*S. cerevisiae*	*CUP1* (copper)	20, 39, 53	p	? (exon-1)	No	Yes
Meriin et al., 2002, 2003	*S. cerevisiae*	*GAL1* (galactose)	25, 103	p	17	Yes	Yes
Solans et al., 2006	*S. cerevisiae*	*GAL1* (galactose)	25, 103	i and p	17	Yes	Yes
Ocampo and Barrientos, 2008; Ruetenik et al., 2016	*S. cerevisiae*	*TEF1-7* (β-estradiol)	25, 46, 72, 103	p	17	Yes	Yes
Kaiser et al., 2013; Papsdorf et al., 2015	*S. cerevisiae*	*GPD* (constitutive)	0, 30, 56	p	0	Yes	Yes
Zurawel et al., 2016	*S. pombe*	*P3nmt1* (thiamine repressible)	25, 46, 72, 103	i	? (exon-1)	No	Yes

HSP104 deletion (Cao et al., 2001). From this observation, it can be hypothesized that aggregation of these HTT fragments in yeast is indeed a controllable process and that different mechanisms exist between the nucleus and the cytoplasm. These early reports, indicating crucial roles of the chaperone system in yeast HD cytotoxicity, were then further validated and confirmed in numerous other studies (see below).

Classical Models of HD in *S. cerevisiae* and the Implication of Prions

Also, Muchowski et al. (2000) cloned human HTT exon-1 into the high copy Yep105 vector (*CUP1* promoter, copper-inducible) containing 20, 39, or 53 glutamines, respectively. Coexpression of the chaperones Hsp40 (yeast Ydj1) and Hsp70 (yeast Ssa1 but, conversely, not Ssb1) prevented the formation of large Htt53Q aggregates in favor of smaller, SDS-soluble aggregate forms (Muchowski et al., 2000). The lack of an effect (or at least a greatly diminished effect) seen for Ssb1p coexpression could be explained by the different functions of the two members of the Hsp70 family: Ssa1p acts posttranslationally (Bush and Meyer, 1996), whereas Ssb1p associates to newly formed proteins at the ribosomes (Nelson et al., 1992; Pfund et al., 1998). In a follow-up study, the same model was employed in a genome-wide synthetic-lethal screen, elucidating important roles of protein folding and stress response processes in HD. Consequently, they found that the Hsp40 chaperone genes *APJ1* and *HLJ1* seem to be necessary to suppress mHTT toxicity. Interestingly, the authors could not find correlations between toxicity and aggregation levels (Willingham et al., 2003).

One of the nowadays most extensively used models was developed by Meriin et al. (2002). It was constructed by cloning the first 17 amino acids of HTT exon-1 followed by 25 or 103 glutamines into a pYES2-vector (*GAL1* promoter, galactose-inducible). The sequences were N- and C-terminally flanked by a FLAG- and GFP-tag, respectively. In their original publication, they could show that Htt103Q accumulates in and is toxic to yeast cells. Furthermore, they observed that molecular chaperones were involved in the aggregation process and that toxicity and aggregation were linked in a correlative manner. Moreover, deletion of the prion gene *RNQ1* abolished poly(Q) toxicity. The authors further concluded that *HSP104*, which is also linked to prion formation, was crucially involved in the nucleation of newly formed aggregates, but not in their growth (Meriin et al., 2002). Of note, in Δ*hsp104* strains spreading of prions is diminished, but its overexpression can conversely also modulate prion formation and/or propagation (Jones and Tuite, 2005). Using the same model, Meriin et al. (2003, 2007) went on to study the fate of endocytosis in mHTT-expressing yeast cells and shed light on the recruitment of proteins into the malignant intracellular aggregates. To circumvent expression problems during long experiments (e.g., chronological aging) when using galactose-inducible systems, possibly arising due to plasmid loss, Solans et al. (2006) used the Meriin model and cloned both Htt25Q- and Htt103Q-fusion proteins into the episomal Yep351 and integrative Yip351 plasmids, again controlled by the *GAL1* promoter. The authors described the detrimental impact of Htt103Q on mitochondria and the possibilities to counteract that (Ocampo et al., 2009).

Ends Matter – The Flanking Regions of the Poly(Q) Tract Determine Aggregation and Toxicity

The flanking regions of mHTT exon-1 seem to have a determinant impact on its toxicity. At least in yeast, poly(Q) toxicity of a human exon-1 fusion construct, as used in most models, is largely dependent on the flanking amino acid sequences. Changes in these flanking regions consequently affect both aggregation and cytotoxicity. The native HTT protein harbors a poly-proline region (poly(P)) at the C-terminus of the poly(Q) tract. It has been suggested that this poly(P) region might have evolved as a protective feature that increases the threshold of Q-repeats for aggregation (Darnell et al., 2007). In line, Htt103Q lacking the neighboring poly(P) region led to multiple small intracellular aggregates, aggravated toxicity (Dehay and Bertolotti, 2006; Duennwald et al., 2006a) and increased the growth defect of Htt103Q-expressing cells (Walter et al., 2014). Furthermore, the poly(P) region interacts with type-1 myosins and, intriguingly, in endocytosis-deficient (e.g., Δ*myo5*) cells, the aggregate-prone form Htt103Q is not toxic, while the non-toxic poly(Q) lengths can display significant toxicity. This might represent an explanation for the positive selection of elongated poly(Q)-tracts (Berglund et al., 2017).

Likewise, in yeast, a FLAG-tag – independent of its position at either the N- or C-terminus – is required for Htt103Q toxicity (at least in the W303 strain) (Duennwald et al., 2006a). Of note, replacement of the FLAG-tag with a similar-sized HA-tag did not produce the same growth defects caused by Htt103Q (Duennwald et al., 2006a). The authors of that study speculated that the negatively charged FLAG-tag mimics sumoylation, a feature of human HD and a modulator of toxicity in some models (Steffan et al., 2004).

Very similar results were obtained *in vitro* and in mammalian neuronal cell culture, showing that the importance of flanking regions for mHTT toxicity is not a yeast-specific artifact. Apparently, both N- and C-terminal regions play an important role in mediating the aggregation dynamics, with the N-terminal amino acids favoring amyloid structures and the C-terminal poly(P) sequence slowing the process (Bhattacharyya et al., 2006; Crick et al., 2013). In fact, these *in vitro* observations were confirmed in mammalian neuronal cells, revealing that the poly(P) region ameliorated aggregation and amyloid fibrillation, whereas the 17 N-terminally flanking amino acids promoted it (Shen et al., 2016). Interference with either region can, thus, drastically influence aggregation behavior, phenotypes, and toxicity.

In addition, both the FLAG-tag and the poly(P) region can mediate their effects *in trans*, and other glutamine-rich proteins may affect poly(Q) toxicity (Duennwald et al., 2006b). This strongly argues for protein interaction and recruitment to poly(Q) proteins or aggregates as an important step toward cytotoxicity. Of note, introducing poly(Q) sequences into unrelated genes can render proteins prone for aggregation

(Ordway et al., 1997), suggesting that poly(Q) expansions alone hold important neurodegenerative features.

Importantly, yeast-optimized C-terminal fluorescent proteins (FPs) also affect phenotypes caused by exon1-Htt103Q expression (Jiang et al., 2016). The presence of an FP was essential for elongated poly(Q) phenotypes *per se*, and both aggregation patterns and toxicity were altered by different FPs. From the tested FPs, the blue FP yomTagBFP2 prevented Htt72Q aggregation and toxicity, probably via its strong tendency to self-assemble into oligomers, which could prevent mHTT-specific inclusion body formation (Jiang et al., 2016). Altogether, flanking regions can profoundly modulate cytotoxicity in yeast and other systems (Lakhani et al., 2010). Therefore, their crucial impact on toxic mechanisms must be considered upon working with yeast models of HD.

Recent Advantages in Modeling HD in Yeast

Ocampo and Barrientos (2008) introduced an alternative system, conveniently eliminating the need for the metabolically active galactose as an acute inductor and allowing to control expression both in time and strength by making use of the β-estradiol-inducible *TEF1-7* promoter. This flexible system has a very tight expression control at various growth stages without the need to change the carbon source. Using this system with fragmented exon-1 containing 25, 46, 72, or 103 glutamines, the group studied the mitochondrial role in mHTT toxicity and could translate basic concepts of their findings into a Drosophila model of HD (Ruetenik et al., 2016).

Yet another model was recently developed to study ploidy control and mitochondrial dysfunction (Kaiser et al., 2013; Papsdorf et al., 2015). The authors used a length-dependent model of mHTT toxicity by cloning poly(Q)-tracts of 0, 30, and 56 glutamines into a p425GPD vector [which harbors the strong constitutive *GPD* (glyceraldehyde-3-phosphat dehydrogenase) promoter], preserving the plasmid's C-terminal polylinker region and the eYFP gene (Kaiser et al., 2013).

Models of HD in Non-*Saccharomyces* Yeasts

Being the best and longest studied yeast model organism, *S. cerevisiae* has gained the most attention from researchers studying HD and other neurodegenerative diseases. To date, we are not aware of any other significant yeasts being extensively employed as HD models. However, Zurawel et al. (2016) developed an integrated, thiamine-repressible (P3nmt1 promoter) system, tagged with FLAG (N-terminal) and GFP (C-terminal) in *Schizosaccharomyces pombe*. They observed mainly cytoplasmic aggregation with only a small percentage of nuclear aggregates in Htt103Q-expressing cells. This was accompanied by mild growth defects for Htt72Q and Htt103Q. Notably, while in *S. pombe*, the poly(Q) stretch seemed to be genetically stable, the authors also showed that in *S. cerevisiae*, the Htt97Q variant was the longest poly(Q) tract that could be stably expressed, at least in their setting.

As research progresses, it will be interesting to see whether other yeasts are fruitfully used as HD models. For example, *Pichia pastoris* also provides many well-established genetic tools and is often the species of choice for heterologous protein expression (Gasser et al., 2013). Especially, the capability to reproduce human glycosylation patterns will become interesting (Gasser et al., 2013), regarding its involvement in HTT toxicity.

LIMITATIONS AND CONSIDERATIONS WHEN USING YEAST AS A HD MODEL

As for any model system, the benefits of handiness and cost-efficiency come at the expense of several disadvantages that need to be carefully taken into consideration when studying mHTT in yeast. In this chapter, we will name only the more general ones and omit those specific limitations that are subject to very particular questions.

One of the most obvious restraints of yeast for neurodegeneration research in general is the lack of multicellularity and inflammatory processes as seen in mammals at all levels. Indeed, many features of neurodegeneration depend on inter-cellular communication/interaction (Garden and La Spada, 2012), among them processes like neuroinflammation (Möller, 2010), and vesicle release/transport (Morton et al., 2001; Li et al., 2009). Highly specialized functions of neuronal cells cannot be fully studied in yeast cells, although basic features (e.g., endo- and exocytosis as rudimentary functions of vesicle transport and neurotransmitter release) may be present. In fact, this limitation may be advantageous for specific queries, as disease mechanisms can be studied isolated from each other without inter-tissue effects. Still, one must not dismiss the fact that HTT is expressed in all cells throughout the body, and pathological effects appear not exclusively in the brain. Alterations in peripheral tissues may sometimes be secondary to neuronal dysfunction, but have also been shown to be directly caused by expression in a specific tissue (van der Burg et al., 2009). Thus, although sometimes neglected, yeast may serve as a potent platform to study non-neurological and more general effects of mHTT.

Nonetheless, when studying neurodegenerative diseases in yeast, results should be interpreted with particular care if not validated in higher eukaryotes. Although many biochemical pathways and organelle functions are basically conserved in yeast, some show significant differences. Of note, yeast mitochondria lack a typical complex I and, instead, use three different, simpler NADH dehydrogenases. These are located externally (*NDE1* and *NDE2*) and internally (*NDI1*) to the inner mitochondrial membrane and do not show rotenone-sensitivity (Matus-Ortega et al., 2015). Additionally, none of the three NADH dehydrogenases present in yeast translocates protons, contrary to mammalian mitochondria (Matus-Ortega et al., 2015). Still, heterologous expression has shown significant functional overlap for the yeast NADH dehydrogenases in mammalian systems. For instance, expression of *NDI1* was sufficient to functionally replace complex 1 in cell culture (Yagi et al., 2006) and, moreover, extend lifespan and modulate energy metabolism

of flies (Bahadorani et al., 2010; Sanz et al., 2010) as well as counteract detrimental effects of a Parkinson's disease mouse model (Barber-Singh et al., 2009).

Large-scale yeast genetic screens with heterologous expression of human disease-relevant proteins are an appealing way to study molecular targets and identify potential disease-promoting pathways (Forsburg, 2001; Giorgini et al., 2005). However, genetic knockouts, for instance, may heavily influence cellular metabolism or modify expression levels, often leading to false-positive phenotypes. Thus, extensive low-throughput validation of screen results remains a prerequisite to rule out artifacts. Regarding HD yeast models, this specific problem can be tackled, for example, by simultaneously analyzing GFP signals when using high-throughput flow cytometry-based cell death analyses. If an apparent screen hit diminishing poly(Q) toxicity also lowers the expression level of HTT itself at some stage, it still might be a mechanistic way of action, but often is an unwanted artifact. In addition, the fact that mammalian HTT does not have a direct homolog in yeast, raises justifiable questions about protein handling, localization, and specification of interactions of heterologously expressed HTT. However, as outlined in the chapters before and hereafter, the translatability of findings in yeast models of HD into higher organisms strongly argues for some degree of specificity and, thus, also applicability of this simple organism for HD research. Further, similarities of human HTT, which is a relatively big and complex protein, with the yeast proteins Atg11p, Vac8p, and Atg23p, all important factors in the cytoplasm-to-vacuole targeting clearance pathway, have been noted (Steffan, 2010). This is in line with Ochaba's recent suggestion, that HTT is a key factor in selective autophagy (Ochaba et al., 2014).

In many yeast models of HD, *GAL1*-promoter vectors are applied, which require the use of metabolically active galactose as an inductor for expression. The choice of carbon source in pre-induction medium (e.g., glucose, raffinose, and glycerol) is of utmost importance and can heavily influence the course of an experiment, as it changes (for instance) the mitochondrial status previous to the expression of HTT constructs. In fact, it is evident that the major mechanisms of mHTT toxicity may vary in distinct genetic backgrounds (Serpionov et al., 2017). Additionally, effects associated with mitochondrial function should be cross-validated in different strain backgrounds that are more suitable for mitochondrial studies (e.g., W303, YPH499/500, and D273-10B), since one of the most widely used strains (BY4741) has a known deficiency in respiratory competence (Gaisne et al., 1999). Moreover, the choice of culturing container and environment may also impact molecular processes (not only) related to mitochondria: oxygen availability across the culture depends on both the surface-to-volume ratio and actions to increase turbulences in the cultures (e.g., baffled flasks), and may heavily impact experiments (Bisschops et al., 2015). Finally, under specific circumstances, it might be useful to test a GFP-only vector as an additional control to low-Q-repeat HTT constructs (e.g., Htt25Q), in order to confirm non-toxicity of the actual control and exclude non-sequence-specific expression artifacts (Berglund et al., 2017).

The widely used *GAL1* promoter, which is activated by galactose and repressed by glucose, has very strong and acute expression, while the copper-inducible *CUP1* promoter is suitable for high expression profiles after the diauxic shift (the transition phase when the preferred carbon source gets depleted and metabolism is primed for the use of an alternative one). Expression via these strong inducible promoters causes rather acute toxicity, making them preferable models for screening of putative pharmacological and/or genetic interventions. However, metabolism-dependent systems might not be the model of choice when investigating metabolic or physiological aspects associated with the disease (Ocampo and Barrientos, 2008). Promoters that are constitutively active (e.g., *TEF1*, *SSA1*, and *GPD*) might as well be employed, but differ greatly in their expression profiles (Peng et al., 2015). Interestingly, recently developed synthetic hybrid promoters, bimodulars system composed of an enhancer element (tandem repeats or combinations of upstream activating sequences) and a core promoter, exhibiting new and enhanced expression and control features have not yet found their way into yeast HD research, but could lead to improved models soon (Peng et al., 2015). Generally, a system that allows continuous and controllable protein expression levels via a metabolically inactive inductor (e.g., non-metabolized β-estradiol) represents a great advantage at different levels, including the possibility to freely choose the carbon source, expression start, and control expression levels. Thus, the use of the above mentioned *TEF1-7* promoter model (Ocampo and Barrientos, 2008; Ruetenik et al., 2016) will likely improve the robustness of findings in yeast-based HD studies. This might be of special interest in setups requiring a more gradual and tunable expression instead of an acute expression that declines over time (as seen with the *GAL1*-expression system).

CYTOTOXIC MECHANISMS IN HD YEAST MODELS

Despite its relative simplicity, yeast harbors a significant number of cellular pathways and factors relevant to human neurodegeneration and HD, including conserved mitochondrial regulation (Galluzzi et al., 2016), endoplasmic reticulum (ER) and ER-associated protein degradation (ERAD) biology (Duennwald and Lindquist, 2008), vesicle fusion (Li et al., 2009), endocytosis (Meriin et al., 2003), lysosomal/vacuolar mechanisms (Rajakumar et al., 2017), autophagy (Yin et al., 2016), lipid biology (Klug and Daum, 2014), RCD (Carmona-Gutierrez et al., 2010, 2018), oxidative stress (Sorolla et al., 2011), and cell cycle control (Bocharova et al., 2008). The high degree of conservation enables researchers to reliably model disease mechanisms in a highly controllable environment.

Aggregation as an Intrinsic Feature of HD

One of the key features of neurodegenerative diseases is aggregation (to various degrees) of multiple intra- or extracellular

proteins. In HD, aggregation of mHTT derives from an elongated poly(Q)-stretch in exon-1 (Taylor et al., 2002), which can also be observed in yeast models of HD (Krobitsch and Lindquist, 2000; Meriin et al., 2002; Ocampo and Barrientos, 2011; Kaiser et al., 2013). Recently, the ultrastructural architecture of a GFP-tagged human exon1-97Q construct was explored in yeast (Gruber et al., 2018). Both fibrillar and – to a major part – unstructured inclusions were found, while no detrimental interactions with cellular membranes were seen (Gruber et al., 2018). This stands at odds with previous findings of a similar construct forming amyloid-like fibrils in mammalian cells that interact with endomembranes, preferentially those of the ER (Bäuerlein et al., 2017). This ultrastructural discrepancy of basically similar mHTT constructs has yet to be fully put into biological context and needs further effort to be understood. However, this might also argue for the cellular context being highly relevant for aggregation and, thus, may provide another variable adding to the complexity of cell-specific effects by mHTT in human pathology. As Gruber et al. (2018) have argued, it is indeed conceivable, that the dissimilar chaperone systems of yeast and mammalian cells might be one of the reasons for these differences.

Commonly, yeast models of HD display largely cytosolic distribution of aggregates, although localization of aggregates into the nucleus dependent on yeast metacaspase YCA1 has been described (Sokolov et al., 2006). In line with data from mammalian cells, in yeast, this is accompanied by DNA cleavage, cytotoxicity, and cell cycle defects, which is reminiscent of the phenotype in human neurons (Sokolov et al., 2006; Zheng et al., 2017). Since different localization profiles of HTT aggregates have been described in yeast, this needs further clarification. It is likely that the contribution of the localization to cytotoxicity in yeast is subject to various variables, such as the properties of different constructs, timepoints, experimental setup, and aggregate-subtype. However, transition between or localization to different cellular subtypes is most likely not the sole major determent of toxicity.

Overall, after intense research, it is still not possible to fully capture the whole picture of the interplay between aggregation and toxicity. Still, from a wider point of view, the connection between aggregation processes *per se* and toxicity seems rather clear. There has been a paradigm shift, that the initially identified large aggregates caused by mHTT are not the major mediators of its toxicity. This might be attributed to the limitations of early microscopy. To sum up, it is likely, but not fully understood, that certain species other than the final form of large inclusion bodies cause mHTT-mediated cytotoxicity in yeast (and other models) (Bocharova et al., 2009).

The actual contribution of aggregates to neuronal cytotoxicity in humans has also yet to be fully elucidated. Although many studies suggest a correlation between aggregate formation and HD (Bates, 2003; Arrasate and Finkbeiner, 2012), the causal connection remains a matter of debate. A major reason for that is the fact that in human brain samples, neuronal aggregates are not necessarily overrepresented in those cells (medium spiny projection neurons) or tissues (striatum) that die the earliest or are affected the most (Gutekunst et al., 1999; Kuemmerle et al., 1999).

Huntingtin Aggregation Can Be Modulated by Genetic and Pharmacological Means

Aggregation has been shown to be a (partially) specific process that depends on the poly(Q)-length and can be modified both by genetic and pharmacologic means. Prominent insights into mHTT aggregation were obtained by yeast studies, like the intensively studied involvement of chaperones in the aggregation process. Similarly, yeast has contributed to the identification and characterization of HD-relevant small molecule anti-aggregation agents, including the polyphenol (−)-epigallocatechin-3-gallate or the synthetic chemical compound C2-8 (see Chapter below) (Krobitsch and Lindquist, 2000; Zhang et al., 2005; Ehrnhoefer et al., 2006).

Interestingly, a recent study in yeast has shown different stages of aggregation for both Htt25Q and Htt103Q with significant alterations over time, including the surprising finding that (non-toxic) Htt25Q can form large aggregates as well (Xi et al., 2016). This argues for the concept that – if aggregation promotes toxicity – it is not by aggregation *per se*, but rather via a distinct population of aggregates. In this study, the authors argued for a correlation of mid-sized aggregates with cytotoxicity and could show that factors blocking toxicity of Htt103Q [including elimination of the poly(P) region] also changed the aggregation pattern, including a decrease of mid-sized and large aggregate populations (Xi et al., 2016). A large body of evidence indicates that Hsp40 chaperones can suppress poly(Q) aggregation, an observation already made as early as 2000 from yeast studies (Muchowski et al., 2000). Intriguingly, a recent yeast study revealed that the essential Hsp40 chaperone Sis1 is sequestered into mHTT aggregates, which subsequently compromises proteasomal degradation (Park et al., 2013). The importance of Hsp40 chaperones is further underlined by Drosophila (Kuo et al., 2013) and mouse (Popiel et al., 2012) studies, arguing for this type of chaperones being major players in suppressing poly(Q) aggregation and potential therapeutic targets. Moreover, recent literature shows that many endogenous proteins may be sequestered and, thereby, their function may be impaired by interactions with poly(Q) aggregates in yeast. Notably, additionally to a global reduction, mitochondrial proteins were found to be favorably sequestered by the aggregates, leading to changed mitochondrial morphology (Gruber et al., 2018).

Manifold genetic factors, especially chaperones (for example Hsp104) have been extensively linked to mHTT aggregation from yeast to rodents (Krobitsch and Lindquist, 2000; Lo Bianco et al., 2008; Lee and Goldberg, 2010; Cushman-Nick et al., 2013) (see also Chapter "Yeast as a Model Organism for Neurodegenerative Diseases"). Noteworthy, Hsp104 has also been implicated and studied as a therapeutic agent in other aggregate-associated neurodegenerative diseases, such as Alzheimer's and Parkinson's disease (Vashist et al., 2010). Although metazoan lack Hsp104 orthologs, diverse beneficial effects, including lifespan-extension

of a HD mouse model (Vacher et al., 2005), have been achieved with expression of this chaperone.

A recent study has also implicated increased glycation (achieved by elevated levels of methylglyoxal, the most potent glycation agent) as a mechanism aggravating Htt72Q and Htt103Q aggregation in yeast, Drosophila and human cell lines (Vicente Miranda et al., 2016).

To Clear or Not to Clear? Autophagy and HD in Yeast

Macroautophagy (hereafter referred to as autophagy) is a well-conserved intracellular recycling program and, together with the proteasome, one of the major degradation and proteostatic processes. Several subtypes have been described, that can eliminate damaged or overdue organelles, aggregates, or other cellular content (Yin et al., 2016). Autophagy has been heavily implicated in HD pathology and discussed as a therapeutically targetable pathway to clear aggregates and improve cellular homeostasis (Wong and Cuervo, 2010; Lin and Qin, 2013). Thereby, yeast has played a primary role in characterizing the autophagic process in general (Ohsumi, 2014; Zimmermann et al., 2016) and the autophagic machinery in particular, including the ATG genes, which are essential for autophagic functioning. In yeast, autophagy is needed for the delivery of aggregates to vacuoles (Chuang et al., 2016) and mutant strains Δ*atg8*, Δ*cue5*, and *rsp5-2*, which have autophagy and/or ubiquitylation deficiencies are more sensitive to poly(Q)-expression (Lu et al., 2014). In the same study, yeast experiments revealed the ubiquitin-binding CUE-domain protein Cue5 as an important player in the clearance of aggregates and selective autophagy (Lu et al., 2014). Interestingly, a recent yeast study has corroborated these findings by showing that deletion of the ubiquitin-interacting protein Dsk2 alters the Htt103Q aggregation profile toward a more dispersed distribution of smaller aggregates and Δ*dsk2* strains show elevated sensitivity to poly(Q) cytotoxicity (Chuang et al., 2016). Overall, it seems that HTT clearance in yeast heavily relies on both the ubiquitin proteasome system and autophagy, with many factors involved and time-dependent differences that must be taken into consideration. Moreover, a chaperone network likely contributes and coordinates the formation of inclusion bodies, which are then subject to autophagic degradation (Higgins et al., 2018). Concurringly, strains having defects in the chaperone system (Δ*sse1*, Δ*fes1*, and Δ*ydj1*) show reduced colocalization of HTT and Atg8p, an essential autophagic adapter protein (Higgins et al., 2018).

Elevated autophagic levels increase cellular viability and decrease soluble and aggregated forms of HTT in cell culture, Drosophila and mouse models (Rubinsztein, 2006). Perceptibly, the autophagy-inducer rapamycin, a well-known inhibitor of TOR (target of rapamycin; negative regulator of autophagy), as well as rapamycin-analogs exert protective effects in various HD models (Ravikumar et al., 2004; Sarkar et al., 2007). In other cases though, mHTT seems to increase autophagy in different species (Sarkar and Rubinsztein, 2008). Notably, mTOR activity is reduced (hence autophagy upregulated) by sequestration into HTT aggregates in mouse models and human brain samples (Ravikumar et al., 2004). Nevertheless, increased autophagy in these cases may represent a cellular reaction rather than a causal toxicity mechanism (Carmona-Gutierrez et al., 2018; Galluzzi et al., 2018). We therefore argue for the intensified and reinforced use of yeast as a model system to elucidate the connection and therapeutic potential of autophagy and HD.

A physiological role of native HTT in autophagy has recently been suggested: the weak similarity of HTT to yeast Atg11, Atg23, and Vac8 has led to the hypothesis that HTT might act as a scaffold protein in selective autophagic processes (Steffan, 2010; Ochaba et al., 2014). Still, as mentioned above, the complete native function of HTT remains elusive. The ratio of wild-type HTT and mHTT seems to play a role in the disease manifestation, at least in mice (Leavitt et al., 2001). Certainly, in Htt25Q/103Q coexpression experiments in yeast, the low-Q variant seemed to increase the solubility of Htt103Q, which reduced oxidative stress and toxicity (Saleh et al., 2013). This, however, remains open to debate and needs further studies, as opposite findings have been described in the literature. However, in this particular study, the authors found an expression-dependent dynamic: highly expressed Htt25Q enhanced the solubility of Htt103Q, while at lower levels, it was preferentially sequestered to aggregates itself (Saleh et al., 2013). Therefore, it could be that the interaction of wild type und mHTT follows a complex dynamic, which could explain the contradictory reports.

Discovering Further Toxicity Mechanisms in Yeast

The possibility of feasible genetic screens has been consistently employed upon modeling HD in yeast. For instance, an early study identified 52 genetic enhancers of toxicity, which were predominantly related to stress response and protein folding pathways (Muchowski et al., 2000; Willingham et al., 2003). This is in line with numerous studies on different stress signaling pathways affected by HD (Duennwald, 2015). As an example, the heat shock response (HSR) via the transcription factor Hsf1 is impaired by elongated poly(Q) HTT with extensive two-sided interactions and HSR proteins (e.g., Hsp40 and Hsp70) modulating aggregation and toxicity (Duennwald, 2015) (see above). Furthermore, it is well established that mHTT impairs ER stress response, leading to accumulation of misfolded proteins in the ER and activation of the unfolded protein response (Kouroku et al., 2007; Matus et al., 2008). In line, yeast cells expressing mHTT display an acute and specific ER stress response that is to some extent the consequence of essential ERAD components (Npl4p, Ufd1p, and p97) being trapped in HTT aggregates (Duennwald and Lindquist, 2008). In that study, however, HSR was not activated by elongated poly(Q) expression (Duennwald and Lindquist, 2008). Both pathways (HSR and ERAD) might comprehend druggable targets in the future. Of note, the Golgi stress response is also compromised in HD (Sbodio et al., 2018), and HTT has been implicated in an immediate type of stress response including so-called huntingtin stress bodies, which might be defective in HD (Nath et al., 2015). Another genome-wide knockout screen could

show that polyploidy represents a resistance mechanism against poly(Q) toxicity (Kaiser et al., 2013). In that study, haploid cells were more susceptible to Htt56Q-induced growth defects and proteins within the septin ring (e.g., Cdc10, Shs1) seemed to mislocalize under poly(Q)-stress. Twenty-eight out of the 38 toxicity-modulating screen hits also had an impact on the Htt103Q model, and tetraploid strains (e.g., PY5006, PY5007) were resistant to poly(Q) toxicity (Kaiser et al., 2013). Though, the implications of these findings for human HD pathology have yet to be investigated.

Mitochondria as Central Organelles in HTT Toxicity

Persistent ER stress response is accompanied by oxidative stress and mitochondrial impairment, resulting in cell death (Haynes et al., 2004). Mitochondrial defects in human HD pathology, especially in neurons with high energy demand, are indeed the consequence of multiple perturbations caused by mHTT (Braun, 2012; Farshbaf and Ghaedi, 2017). Similarly, in yeast, mHTT expression leads to detrimental respiratory defects, impairs complex II and III, enhances production of reactive oxygen species and alters mitochondrial morphology (Solans et al., 2006). Furthermore, longer poly(Q) lengths of 72 and 103 glutamines seem to increase the fragments' tendency to associate with mitochondria and impair mitochondrial membrane potential (Ocampo et al., 2009). Congruently, activation of mitochondrial biogenesis (through overexpression of *HAP4*, a regulator of nuclear-encoded mitochondrial genes) counteracts these effects in yeast and Drosophila (Ocampo et al., 2009; Ruetenik et al., 2016). In line with this, poly(Q) toxicity and oxidative stress are aggravated in respiring yeast cells (Sorolla et al., 2011). A pathological feature of HD patients that can also be observed in yeast are metabolic alterations (Aziz, 2007; Papsdorf et al., 2015). In a yeast model, poly(Q) toxicity could be connected to iron metabolism and mitochondria (Papsdorf et al., 2015). Indeed, elevated iron levels have been reported in HD by some studies, but how they affect respective neurons and brains remains controversially discussed (van den Bogaard et al., 2013; Muller and Leavitt, 2014).

Endocytic Processes, Prions, and the Intracellular Localization of Aggregates Are Key-Determinants of Toxicity

In mouse models and human samples of HD, components of the vesicle fusion machinery, endocytosis, and exocytosis are negatively affected (Velier et al., 1998; Morton and Edwardson, 2001; Morton et al., 2001; Trushina et al., 2006; Li et al., 2009). Using yeast, two recent studies have analyzed the involvement of ribosomal quality control and type-1 myosin-dependent endocytosis systems, respectively (Berglund et al., 2017; Zheng et al., 2017). Zheng et al. (2017) showed a positive correlation between Htt103Q nuclear localization and cytotoxicity and could identify several factors involved in the nucleocytoplasmic distribution of Htt103Q. Deletions of the ubiquitin ligase *LTN1* or *RQC1*, a component of the ribosome quality control complex (RQC), promoted nuclear localization via the nuclear pore complexes. This transport mechanism involves the v-SNARE-binding protein Btn2, the overexpression of which blocked nuclear accumulation of Htt103Q (Zheng et al., 2017). Interestingly, Btn2 has been shown to exert anti-prion properties (Wickner et al., 2014), which – given the dependency of mHTT toxicity on Rnq1p and its prion status in yeast – is of special interest and should be further explored. Interestingly, out of six identified suppressors of Htt103Q toxicity (including Hsp40 chaperone Sis1) in an overexpression screen, three possessed Q-rich, prion-like domains, namely Gts1, Mcm1, and Nab3 (Ripaud et al., 2014). The authors found that these proteins could modulate aggregation to more non-toxic forms, preventing the aggregates from interacting with endogenous proteins and increasing the interactions with chaperones (Ripaud et al., 2014). This puts extra emphasis on the importance of prion biology for HD. Additionally, the interaction of Q-rich proteins with HTT and the possible modulation of toxicity thereby, might be an important line of research to understand basic toxic mechanisms of HD.

In a genome-wide screen for poly(Q) toxicity, Berglund et al. (2017) discovered that the 25Q version is toxic in strains with defects in actin- and type-1 myosin-dependent endocytosis. This enhanced toxicity of the soluble HTT variant was abolished in cells expressing the aggregation-prone 103Q version (Berglund et al., 2017). It is tempting to speculate that this may contribute to positive selection of longer poly(Q) tracts. Thus, although yeast lacks a vesicular system as needed for the modeling of neurotransmission defects, basic processes, and alterations caused by mHTT still might be studied fundamentally. Interestingly, endocytosis was reported to play a central role in pathological mechanisms of amyotrophic lateral sclerosis models in yeast and flies (Liu et al., 2017; Leibiger et al., 2018). Hence, it will be also interesting to see in the future, how dysfunctional endocytic processes may be incorporated into the complex picture of cytotoxic mechanisms in HD.

Is RCD Implicated in HTT Toxicity in Yeast?

Neuronal loss (partly) due to RCD is a shared feature of many neurodegenerative diseases (Vila and Przedborski, 2003). Studies on neuronal loss in HD have reported signs of apoptotic and, more recently, also necrotic cell death (Portera-Cailliau et al., 1995; Sawa et al., 2003; Mao et al., 2016). Yeast has a long-standing history in RCD research, including the modeling of mammalian cell death processes (Madeo et al., 1997; Carmona-Gutierrez et al., 2010, 2018) in general and neurodegenerative mechanisms in particular (Pereira et al., 2012). Indeed, prominent RCD subroutines have been characterized, including apoptosis and regulated necrosis. In addition, core components orchestrating RCD are highly conserved (Carmona-Gutierrez and Büttner, 2014; Carmona-Gutierrez et al., 2018). Still, data on RCD mechanisms/pathways in yeast HD models remain rather scarce.

In conclusion, aggregation, elevated ER stress levels, autophagy, and RCD are closely connected (Kouroku et al., 2007;

Matus et al., 2008), and yeast incorporates many conserved pathways and convenient techniques to further elucidate the interplay of these neurodegenerative hallmarks.

YEAST AS A SCREENING PLATFORM FOR DRUG DISCOVERY

One of the most crucial advantages of modeling human diseases in yeast is the possibility of time- and cost-efficient high-throughput screens (Barberis et al., 2005). Beyond the feasibility of uncovering mechanistic insights via genetic screens (see above), yeast offers great potential for drug discovery, also targeting neurodegenerative diseases (Tardiff et al., 2013; Menezes et al., 2015; Park et al., 2016; Porzoor and Macreadie, 2016; **Figures 1**, **2**). Studies in this unicellular eukaryote have led, for example, to the discovery of the anti-aging agents spermidine (Eisenberg et al., 2009) and resveratrol (Howitz et al., 2003). Follow-up and validation studies have often proven the translational potential of yeast findings to higher model organisms (**Table 2**).

Drug Candidate Discovery Through Pharmacological Screens in Yeast

In fact, the use of commercially available libraries and pharmacological approaches to find toxicity-modulating substances were already applied early on in yeast HD research (**Figure 2**). In 2004, it was shown that the intrabody V_L12.3 could reduce aggregation and toxicity in a yeast model with integrated exon-1-Htt25Q/72Q constructs (Colby et al., 2004). Some of these beneficial effects could be later corroborated in cell culture (Southwell et al., 2008) and lentivirus mouse models (Southwell et al., 2009) of HD. However, adverse effects were shown too in a transgenic HD mouse model (Southwell et al., 2009; Butler et al., 2014). Irrespectively, the study helped strengthening the intrabody-concept as a therapeutic approach against HD and other intrabodies (e.g., MW7, C4 sFv, Happ1) against HTT have been tested (Wolfgang et al., 2005; Southwell et al., 2009; Messer and Joshi, 2013).

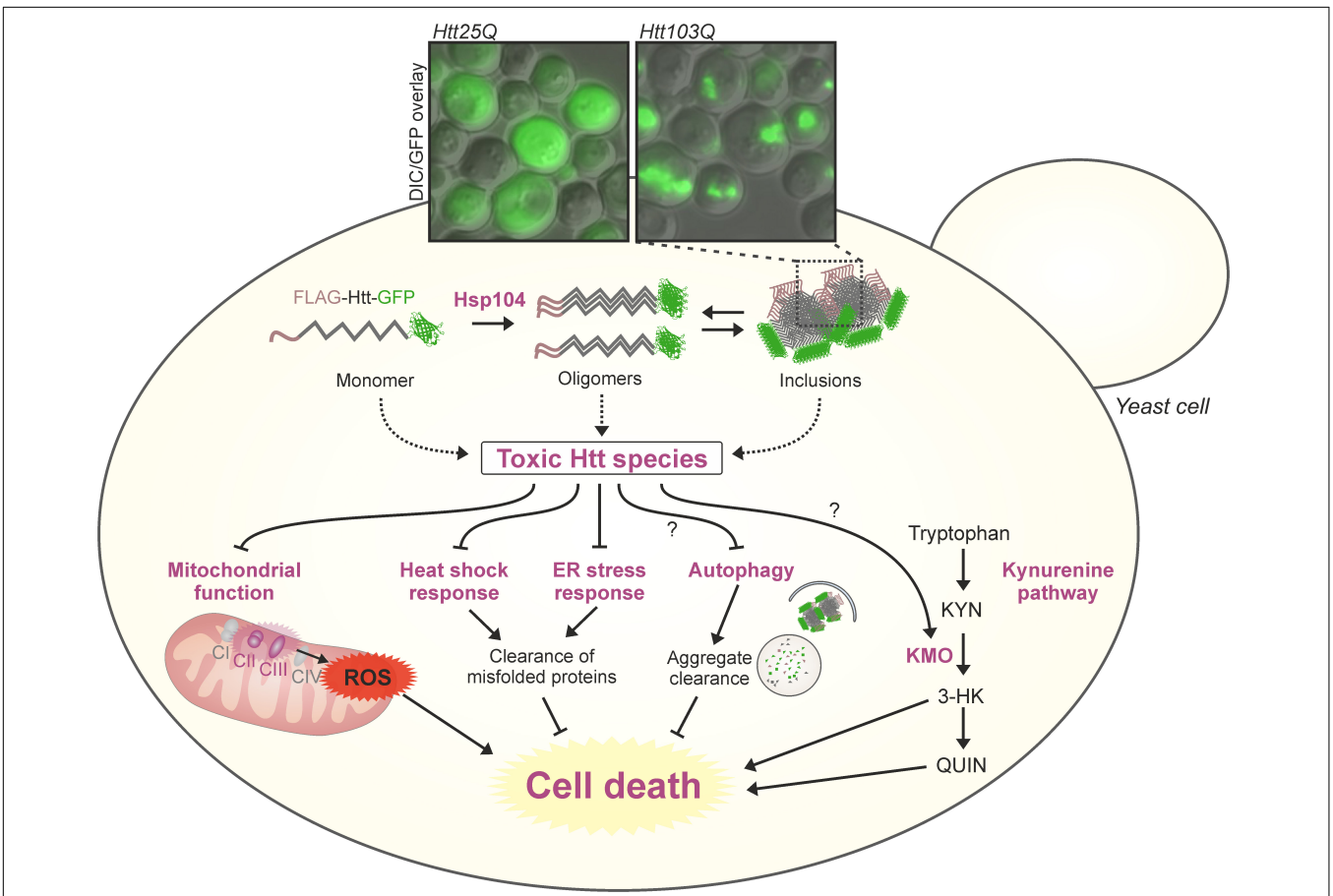

FIGURE 1 | Sights and mechanisms of mHTT toxicity in yeast models of HD. Multiple sources and modulatory pathways of mHTT toxicity have been identified in different models of HD in yeast (dysfunctional mitochondria, aggregation, altered stress responses, kynurenine pathway, and more). The combination of toxic effects leads to increased cell death. The microscopy inset shows pictures of typical aggregation of GFP tagged exon 1-poly(Q) constructs in a widely used *S. cerevisiae* model of HD (Meriin et al., 2002), 24 h after galactose-induction of chronologically aged yeast cells. KMO, kynurenine 3-monooxygenase; ROS, reactive oxygen species.

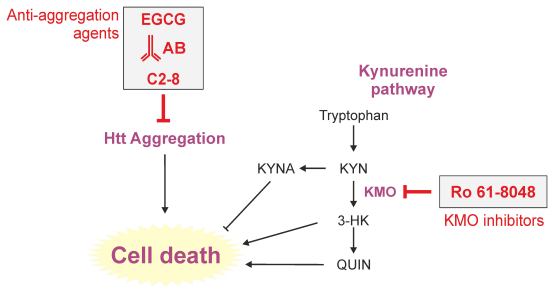

FIGURE 2 | Therapeutic approaches to tackle toxicity and/or aggregation in yeast models of HD. Yeast has long served as a tool to identify pharmacological agents against HD. Here, important processes (aggregation and kynurenine pathway) of HD toxicity in yeast are depicted. Prominent approaches previously used in yeast are the application of the polyphenol epigallocatechin-3-gallate (EGCG), intrabodies or the small molecule C2-8, all in order to reduce intracellular aggregation load. The KMO inhibitor Ro 61-8048 was used to modulate the course of tryptophan degradation via the kynurenine pathway, which is heavily implicated in HD, leading to less cell death. AB (here intrabody), EGCG (epigallocatechin-3-gallate), KMO (kynurenine 3-monooxygenase).

Zhang et al. (2005) used a yeast-based approach including 16,000 substances to identify and further validate an aggregation-inhibiting compound, C2-8 (N-(4-bromophenyl)-3-{[(4-bromophenyl)amino]sulfonyl}benzamide), in Drosophila and mouse tissue. Several chemical compounds showed anti-aggregation properties in yeast, while the structural analog of C2, C2-8, did so in a dose-responsive manner and with low IC_{50} values (50 nM). They found that the compound's aggregation inhibition greatly relies on cellular systems, arguing for cellular targets, and that it prominently affects the polymerization/growth of aggregates, rather than their nucleation/initiation. For screening, a Δ*erg6* mutant strain with increased membrane permeability was employed. Primary hit selection was based upon photometric assessment and/or eGFP fluorescence, which was then microscopically validated. The substance has ultimately led to successful pre-clinical studies in HD mouse models, proving the concept of yeast as an initial screening tool for toxicity modulators (Chopra et al., 2007; Wang et al., 2013). It should be noted that in this study, the use of an Δ*erg6* mutant obeyed the rationale that in yeast, specific cell wall and drug transporters represent obstacles for any non-endogenous substance. In order to ease the transition of drugs into or slow the secretion out of the cell, strains deficient in multi-drug transporters (Δ*pdr5*) (Walter et al., 2014) or increased membrane permeability (Δ*erg6*) (Zhang et al., 2005), for example, are valid approaches, respectively. Yeast ABC (ATP binding cassette transporter) proteins, including pleiotropic drug resistance (PDR; e.g., *PDR5*) and multidrug resistance subfamilies, have been implicated in detoxification of exogenous substances. On the other hand, the deletion of such machineries

TABLE 2 | Basic drug findings in yeast models of HD and their translational validation in cell culture, *Drosophila melanogaster* and rodents.

Compound	Effect	Validation		
		Cell culture	Drosophila	Rodents
Intrabodies (V_L12.3, MW7, C4 sFv, Happ1, Happ3)	V_L12.3 reduces aggregation and toxicity (Colby et al., 2004)	V_L12.3, MW7, Happ1, and Happ3 reduce toxicity and aggregation of HDx-1 (Khoshnan et al., 2002; Southwell et al., 2008)	C4 sFv reduces aggregation and cellular toxicity (Wolfgang et al., 2005)	Happ1 improves neuropathology in transgenic and lentiviral HD mouse models (Southwell et al., 2009) Intrabodies act via different mechanisms and partially show adverse effects in HD mouse models (Southwell et al., 2009; Butler et al., 2014)
C2-8	Aggregation inhibition (Zhang et al., 2005)	Long-term inhibition of elongated poly(Q) aggregation (Zhang et al., 2005)	Dose-dependent suppression of pathogenesis (Zhang et al., 2005)	Reduction of mHTT aggregation, but no improvement of motor dysfunction of striatal neurodegenerative pathology in R6/2 HD transgenic mice (Wang et al., 2013)
Ro 61-8048	Inhibition of kynurenine 3-monooxygenase (KMO) (Giorgini et al., 2005)	–	Inhibition of KMO in a Drosophila model of HD (Campesan et al., 2011)	Inhibition of KMO in a mouse model of HD (Zwilling et al., 2011)
Epigallocatechin-3-gallate (EGCG)	EGCG is a suppressor of mutated huntingtin aggregation and toxicity (Ehrnhoefer et al., 2006)	Protective effect on rat hippocampal neuronal cells (Menard et al., 2013)	Increases fitness and lifespan in Drosophila (Wagner et al., 2015)	EGCG extends lifespan of rats (Niu et al., 2013)
Actinomycin D	Aggregation inhibition (Walter et al., 2014)	Suppresses aggregation of elongated poly(Q) in mammalian cells (Walter et al., 2014)	–	–

EGCG, epigallocatechin-3-gallate; KMO, kynurenine 3-monooxygenase.

may impact cellular physiology at other levels, as efflux pumps are important for mitochondrial homeostasis, secretion processes, organelle biogenesis, stress response, and physiological uptake of substances from the culturing environment (Bauer et al., 2003; Schüller et al., 2003). Thus, studying tested compounds in a transporter-unmodified yeast strain represents a physiologically more intact setting and can also provide useful insights into the bioavailability of drugs in an eukaryotic system (Zimmermann et al., 2018).

The Discovery of the Kynurenine Pathway

Using the same model as Zhang et al. (2005) and Giorgini et al. (2005) performed a loss-of-function genomic suppressor screen and identified an enzyme (kynurenine 3-monooxygenase, KMO; in yeast *BNA4*) in the kynurenine pathway of tryptophan degradation, the deletion of which abolished Htt103Q toxicity. Interestingly, KMO had been previously associated with human HD pathology (Beal et al., 1990, 1992; Pearson and Reynolds, 1992; Stoy et al., 2005). The kynurenine pathway is now well-studied and discussed as a drug target for HD (Thevandavakkam et al., 2010; Wild and Tabrizi, 2014; Jacobs et al., 2017). In their original study, Giorgini et al. (2005) already showed a partial amelioration of growth defects in Htt103Q-expressing yeast cells treated with Ro 61-8048, a small molecule inhibitor of KMO. KMO inhibition leads to an altered product and intermediate profile of tryptophan degradation, reducing cellular stress and cell death. Further on, KMO inhibition has been extensively approached pharmacologically and chemically in pre-clinical rodent and Drosophila HD models (Campesan et al., 2011; Zwilling et al., 2011) and might be tested in early human trials in the near future.

Natural Substance Screens With Yeast HD Models

Shortly after the above-mentioned studies, Ehrnhoefer et al. (2006) screened a natural compound library using a W303 strain containing integrated GFP-tagged exon-1-HTT with either a 25Q or 72Q C-terminal stretch. They could elegantly show that the polyphenol (−)-epigallocatechin-3-gallate (EGCG) is a potent suppressor and modulator of mHTT aggregation and toxicity *in vitro* and *in vivo* in yeast and fly models of HD. Interestingly, the substance seems to inhibit aggregation *per se* in yeast cells, but also promotes the formation of larger aggregates *in vitro*. The substance, which is a major bioactive component in green tea, has become a promising candidate for healthy aging and promotes lifespan extension in worms, flies, and rodents (Zhang et al., 2005; Niu et al., 2013; Wagner et al., 2015; Chu et al., 2017; Pallauf et al., 2017). EGCG has been thoroughly examined in the context of neurodegeneration and several independent studies have shown its anti-aggregation properties (Avramovich-Tirosh et al., 2007; Hudson et al., 2009; Liu et al., 2015; Debnath et al., 2016). Animal and human studies (including phase 2 trials) have already been performed with EGCG, though the applicability in humans has been questioned (Mereles and Hunstein, 2011; Mähler et al., 2013).

Walter et al. (2014) also screened natural compounds against HD toxicity and aggregation. They successfully identified actinomycin D as a potent aggregation inhibitor. The substance was applied in nanomolar concentrations and increased the levels of certain heatshock-proteins (e.g., *HSP104*, *HSP70*, and *HSP26)*. The group could further transfer their findings to mammalian cell culture, implying conserved actions of actinomycin D. Noteworthy, the drug actinomycin D (or dactinomycin) has many approved medical uses and could become an exciting drug lead in HD research.

CONCLUDING REMARKS

Saccharomyces cerevisiae has a long-standing history in basic and applied research (Barnett, 2003), and the areas in which it can be used continue to expand in content and number. Indeed, researchers worldwide still rely on its robustness, handiness, applicability and scientific relevance. It may seem bold to study neurodegeneration in a unicellular fungus, but the richness of findings obtained from yeast studies and their translational potential have clearly proven a point. Although many aspects of neurodegenerative processes lie beyond the capacity of yeast models, numerous important features of age-related and neurodegenerative diseases in general and HD in particular can reliably be modeled and studied in yeast.

In this review, we have given a glimpse of the extensive possibilities and significance of yeast for HD research by summarizing some of the most significant insights gained from yeast experiments. We are aware that this short overview does not grasp every aspect of HD research conducted in yeast, but it conveys the convincing potential of yeast as a tool to help both understand and counteract HD. During the last few years, the knowledge about the disease has developed especially fast (McColgan and Tabrizi, 2017), and we expect an accelerated pace of scientific outcome that is relevant for HD patients in the near future.

What Can Be Expected From Yeast in the 21st Century?

With rapid digitalization and big data science becoming increasingly important in basic research, the possibilities of yeast as an *in vivo* quasi "programmable" cell will continue to be of valuable importance. Especially regarding big data production, network analyses and systems biology, there is yeast, and in particular *S. cerevisiae*, at the forefront of data generation and development. The feasibility of performing complex and powerful screens has already been remarkably proven in the past decades. However, we believe that the potential is not exhausted. Modern screening systems already allow the automatic inoculation, mating, dilution, microscopy, and assessment of various parameters in large strain collections. In the near future, we expect to see various screening applications that employ single-cell-techniques, stratifying data, and zooming into individual cell biology. Small-scale omic-approaches as well as upscaled production suites will also likely contribute to pathway finding and therapeutic production, respectively.

Still, the relevance of yeast is not restricted to a screening tool. Instead, the progressing humanization of yeast strains and the methodologically well-engineered manipulation techniques will yield possibilities for systems biology and especially synthetic biology that go beyond the current state of research. Sophisticated, novel methods, and engineered strains will also facilitate research on neurodegenerative diseases.

In that respect, we are sure that yeast approaches will further accompany the research on HD and continue to provide assistance in deciphering fundamental questions.

AUTHOR CONTRIBUTIONS

SH, FM, and DC-G wrote the manuscript and designed the review. KK, AZ, MB, TP, and MP were involved in the generation of the table and figure and critically revised the manuscript for important intellectual content. All authors contributed to the conception of this review article.

FUNDING

This work was supported by the Austrian Science Fund FWF (Grant Nos. SFB-LIPOTOX F3007, F3012, P23490-B20, P24381, P27893, P29203, P29262, and W1226); the European Commission (Grant No. APOSYS); the Austrian Federal Ministry of Science, Research and Economy (Grant No. BMWFW-80.109/0001-WF/V/3b/2015); BioTechMed-Graz [EPIAge]; and the University of Graz [Unkonventionelle Forschung]. We acknowledge support from NAWI Graz.

REFERENCES

Adegbuyiro, A., Sedighi, F., Pilkington, A. W., Groover, S., and Legleiter, J. (2017). Proteins containing expanded polyglutamine tracts and neurodegenerative disease. *Biochemistry (Mosc.)* 56, 1199–1217. doi: 10.1021/acs.biochem.6b00936

Amen, T., and Kaganovich, D. (2016). Yeast screening platform identifies FDA-approved drugs that reduce Aβ oligomerization. *Microb. Cell* 3, 97–100. doi: 10.15698/mic2016.03.482

Arrasate, M., and Finkbeiner, S. (2012). Protein aggregates in Huntington's disease. *Exp. Neurol.* 238, 1–11. doi: 10.1016/j.expneurol.2011.12.013

Avramovich-Tirosh, Y., Reznichenko, L., Mit, T., Zheng, H., Fridkin, M., Weinreb, O., et al. (2007). Neurorescue activity, APP regulation and amyloid-beta peptide reduction by novel multi-functional brain permeable iron-chelating- antioxidants, M-30 and green tea polyphenol, EGCG. *Curr. Alzheimer Res.* 4, 403–411. doi: 10.2174/156720507781788927

Aziz, N. A. (2007). Hypothalamic dysfunction and neuroendocrine and metabolic alterations in huntington disease: clinical consequences and therapeutic implications. *Rev. Neurosci.* 18, 223–252. doi: 10.1515/REVNEURO.2007.18.3-4.223

Babcock, M., Silva, D., de, Oaks, R., Davis-Kaplan, S., Jiralerspong, S., et al. (1997). Regulation of mitochondrial iron accumulation by Yfh1p, a putative homolog of frataxin. *Science* 276, 1709–1712. doi: 10.1126/science.276.5319.1709

Bahadorani, S., Cho, J., Lo, T., Contreras, H., Lawal, H. O., Krantz, D. E., et al. (2010). Neuronal expression of a single-subunit yeast NADH–ubiquinone oxidoreductase (Ndi1) extends *Drosophila lifespan*. *Aging Cell* 9, 191–202. doi: 10.1111/j.1474-9726.2010.00546.x

Bañez-Coronel, M., Ayhan, F., Tarabochia, A. D., Zu, T., Perez, B. A., Tusi, S. K., et al. (2015). RAN translation in huntington disease. *Neuron* 88, 667–677. doi: 10.1016/j.neuron.2015.10.038

Bañez-Coronel, M., Porta, S., Kagerbauer, B., Mateu-Huertas, E., Pantano, L., Ferrer, I., et al. (2012). A pathogenic mechanism in Huntington's disease involves small CAG-repeated RNAs with neurotoxic activity. *PLoS Genet.* 8:e1002481. doi: 10.1371/journal.pgen.1002481

Barberis, A., Gunde, T., Berset, C., Audetat, S., and Lüthi, U. (2005). Yeast as a screening tool. *Drug Discov. Today Technol.* 2, 187–192. doi: 10.1016/j.ddtec.2005.05.022

Barber-Singh, J., Boo Seo, B., Nakamaru-Ogiso, E., Lau, Y.-S., Matsuno-Yagi, A., and Yagi, T. (2009). Neuroprotective effect of long-term NDI1 gene expression in a chronic mouse model of parkinson disorder. *Rejuvenation Res.* 12, 259–267. doi: 10.1089/rej.2009.0854

Barnett, J. A. (2003). Beginnings of microbiology and biochemistry: the contribution of yeast research. *Microbiol. Read. Engl.* 149, 557–567. doi: 10.1099/mic.0.26089-0

Barrientos, A. (2003). Yeast models of human mitochondrial diseases. *IUBMB Life* 55, 83–95. doi: 10.1002/tbmb.718540876

Bates, G. (2003). Huntingtin aggregation and toxicity in Huntington's disease. *Lancet* 361, 1642–1644. doi: 10.1016/S0140-6736(03)13304-1

Bates, G. P., Dorsey, R., Gusella, J. F., Hayden, M. R., Kay, C., Leavitt, B. R., et al. (2015). Huntington disease. *Nat. Rev. Dis. Primer* 1:15005. doi: 10.1038/nrdp.2015.5

Bates, G. P., and Hockly, E. (2003). Experimental therapeutics in Huntington's disease: are models useful for therapeutic trials? *Curr. Opin. Neurol.* 16, 465–470. doi: 10.1097/01.wco.0000084223.82329.bb

Bauer, B. E., Schüller, C., and Kuchler, K. (2003). "Fungal abc proteins in clinical drug resistance and cellular detoxification," in *ABC Proteins*, Chap. 15, eds I. B. Holland, S. Coole, K. Kuchler, and C. Higgins (London: Academic Press), 295–316. doi: 10.1016/B978-012352551-2/50016-0

Bäuerlein, F. J. B., Saha, I., Mishra, A., Kalemanov, M., Martínez-Sánchez, A., Klein, R., et al. (2017). In situ architecture and cellular interactions of PolyQ inclusions. *Cell* 171, 179.e10–187.e10. doi: 10.1016/j.cell.2017.08.009

Beal, M. F., Matson, W. R., Storey, E., Milbury, P., Ryan, E. A., Ogawa, T., et al. (1992). Kynurenic acid concentrations are reduced in Huntington's disease cerebral cortex. *J. Neurol. Sci.* 108, 80–87. doi: 10.1016/0022-510X(92)90191-M

Beal, M. F., Matson, W. R., Swartz, K. J., Gamache, P. H., and Bird, E. D. (1990). Kynurenine pathway measurements in Huntington's disease striatum: evidence for reduced formation of kynurenic acid. *J. Neurochem.* 55, 1327–1339. doi: 10.1111/j.1471-4159.1990.tb03143.x

Berger, A. C., Hanson, P. K., Wylie Nichols, J., and Corbett, A. H. (2005). A yeast model system for functional analysis of the niemann-pick type C protein 1 Homolog, Ncr1p: a yeast model for NP-C disease. *Traffic* 6, 907–917. doi: 10.1111/j.1600-0854.2005.00327.x

Berglund, L. L., Hao, X., Liu, B., Grantham, J., and Nyström, T. (2017). Differential effects of soluble and aggregating polyQ proteins on cytotoxicity and type-1 myosin-dependent endocytosis in yeast. *Sci. Rep.* 7:11328. doi: 10.1038/s41598-017-11102-6

Bhattacharyya, A., Thakur, A. K., Chellgren, V. M., Thiagarajan, G., Williams, A. D., Chellgren, B. W., et al. (2006). Oligoproline effects on polyglutamine conformation and aggregation. *J. Mol. Biol.* 355, 524–535. doi: 10.1016/j.jmb.2005.10.053

Bisschops, M. M. M., Vos, T., Martínez-Moreno, R., Cortés, P., de la, T., Pronk, J. T., et al. (2015). Oxygen availability strongly affects chronological lifespan and thermotolerance in batch cultures of *Saccharomyces cerevisiae*. *Microb. Cell* 2, 429–444. doi: 10.15698/mic2015.11.238

Bocharova, N., Chave-Cox, R., Sokolov, S., Knorre, D., and Severin, F. (2009). Protein aggregation and neurodegeneration: clues from a yeast model of Huntington's disease. *Biochem. Mosc.* 74, 231–234. doi: 10.1134/S0006297909020163

Bocharova, N. A., Sokolov, S. S., Knorre, D. A., Skulachev, V. P., and Severin, F. F. (2008). Unexpected link between anaphase promoting complex and the toxicity of expanded polyglutamines expressed in yeast. *Cell Cycle Georget. Tex* 7, 3943–3946. doi: 10.4161/cc.7.24.7398

Botstein, D., and Fink, G. R. (2011). Yeast: an experimental organism for 21st century biology. *Genetics* 189, 695–704. doi: 10.1534/genetics.111.130765

Braun, R. J. (2012). Mitochondrion-mediated cell death: dissecting yeast apoptosis for a better understanding of neurodegeneration. *Front. Oncol.* 2:182. doi: 10.3389/fonc.2012.00182

Bush, G. L., and Meyer, D. I. (1996). The refolding activity of the yeast heat shock proteins Ssa1 and Ssa2 defines their role in protein translocation. *J. Cell Biol.* 135, 1229–1237. doi: 10.1083/jcb.135.5.1229

Butler, D. C., Snyder-Keller, A., De Genst, E., and Messer, A. (2014). Differential nuclear localization of complexes may underlie in vivo intrabody efficacy in Huntington's disease. *Protein Eng. Des. Sel.* 27, 359–363. doi: 10.1093/protein/gzu041

Büttner, S., Ruli, D., Vögtle, F.-N., Galluzzi, L., Moitzi, B., Eisenberg, T., et al. (2011). A yeast BH3-only protein mediates the mitochondrial pathway of apoptosis. *EMBO J.* 30, 2779–2792. doi: 10.1038/emboj.2011.197

Campesan, S., Green, E. W., Breda, C., Sathyasaikumar, K. V., Muchowski, P. J., Schwarcz, R., et al. (2011). The kynurenine pathway modulates neurodegeneration in a *Drosophila* model of huntington's disease. *Curr. Biol. CB* 21, 961–966. doi: 10.1016/j.cub.2011.04.028

Cao, F., Levine, J. J., Li, S.-H., and Li, X.-J. (2001). Nuclear aggregation of huntingtin is not prevented by deletion of chaperone Hsp104. *Biochim. Biophys. Acta BBA – Mol. Basis Dis.* 1537, 158–166. doi: 10.1016/S0925-4439(01)00068-0

Carmona-Gutierrez, D., Bauer, M. A., Zimmermann, A., Aguilera, A., Austriaco, N., Ayscough, K., et al. (2018). Guidelines and recommendations on yeast cell death nomenclature. *Microb. Cell* 5, 4–31. doi: 10.15698/mic2018.01.607

Carmona-Gutierrez, D., and Büttner, S. (2014). The many ways to age for a single yeast cell. *Yeast Chichester Engl.* 31, 289–298. doi: 10.1002/yea.3020

Carmona-Gutierrez, D., Eisenberg, T., Büttner, S., Meisinger, C., Kroemer, G., and Madeo, F. (2010). Apoptosis in yeast: triggers, pathways, subroutines. *Cell Death. Differ.* 17, 763–773. doi: 10.1038/cdd.2009.219

Chopra, V., Fox, J. H., Lieberman, G., Dorsey, K., Matson, W., Waldmeier, P., et al. (2007). A small-molecule therapeutic lead for Huntington's disease: preclinical pharmacology and efficacy of C2-8 in the R6/2 transgenic mouse. *Proc. Natl. Acad. Sci. U.S.A.* 104, 16685–16689. doi: 10.1073/pnas.0707842104

Chu, C., Deng, J., Man, Y., and Qu, Y. (2017). Green tea extracts epigallocatechin-3-gallate for different treatments. *BioMed Res. Int.* 2017:9 doi: 10.1155/2017/5615647

Chuang, K.-H., Liang, F., Higgins, R., and Wang, Y. (2016). Ubiquilin/Dsk2 promotes inclusion body formation and vacuole (lysosome)-mediated disposal of mutated huntingtin. *Mol. Biol. Cell* 27, 2025–2036. doi: 10.1091/mbc.E16-01-0026

Colby, D. W., Chu, Y., Cassady, J. P., Duennwald, M., Zazulak, H., Webster, J. M., et al. (2004). Potent inhibition of huntingtin aggregation and cytotoxicity by a disulfide bond-free single-domain intracellular antibody. *Proc. Natl. Acad. Sci. U.S.A.* 101, 17616–17621. doi: 10.1073/pnas.0408134101

Côrte-Real, M., and Madeo, F. (2013). Yeast programed cell death and aging. *Front. Oncol.* 3:3283. doi: 10.3389/fonc.2013.00283

Coughlan, C. M., and Brodsky, J. L. (2005). Use of yeast as a model system to investigate protein conformational diseases. *Mol. Biotechnol.* 30, 171–180. doi: 10.1385/MB:30:2:171

Crick, S. L., Ruff, K. M., Garai, K., Frieden, C., and Pappu, R. V. (2013). Unmasking the roles of N- and C-terminal flanking sequences from exon 1 of huntingtin as modulators of polyglutamine aggregation. *Proc. Natl. Acad. Sci. U.S.A.* 110, 20075–20080. doi: 10.1073/pnas.1320626110

Cushman-Nick, M., Bonini, N. M., and Shorter, J. (2013). Hsp104 suppresses polyglutamine-induced degeneration post onset in a drosophila MJD/SCA3 model. *PLoS Genet.* 9:e1003781. doi: 10.1371/journal.pgen.1003781

Darnell, G., Orgel, J. P. R. O., Pahl, R., and Meredith, S. C. (2007). Flanking polyproline sequences inhibit beta-sheet structure in polyglutamine segments by inducing PPII-like helix structure. *J. Mol. Biol.* 374, 688–704. doi: 10.1016/j.jmb.2007.09.023

Davies, S. W., Turmaine, M., Cozens, B. A., DiFiglia, M., Sharp, A. H., Ross, C. A., et al. (1997). Formation of neuronal intranuclear inclusions underlies the neurological dysfunction in mice transgenic for the HD mutation. *Cell* 90, 537–548. doi: 10.1016/S0092-8674(00)80513-9

de Mezer, M., Wojciechowska, M., Napierala, M., Sobczak, K., and Krzyzosiak, W. J. (2011). Mutant CAG repeats of Huntingtin transcript fold into hairpins, form nuclear foci and are targets for RNA interference. *Nucleic Acids Res.* 39, 3852–3863. doi: 10.1093/nar/gkq1323

Debnath, K., Shekhar, S., Kumar, V., Jana, N. R., and Jana, N. R. (2016). Efficient inhibition of protein aggregation, disintegration of aggregates, and lowering of cytotoxicity by green tea polyphenol-based self-assembled polymer nanoparticles. *ACS Appl. Mater. Interfaces* 8, 20309–20318. doi: 10.1021/acsami.6b06853

Dehay, B., and Bertolotti, A. (2006). Critical role of the proline-rich region in huntingtin for aggregation and cytotoxicity in yeast. *J. Biol. Chem.* 281, 35608–35615. doi: 10.1074/jbc.M605558200

Duennwald, M. L. (2011). Polyglutamine misfolding in yeast: toxic and protective aggregation. *Prion* 5, 285–290. doi: 10.4161/pri.18071

Duennwald, M. L. (2015). Cellular stress responses in protein misfolding diseases. *Future Sci.* 1:FSO42. doi: 10.4155/fso.15.42

Duennwald, M. L., Jagadish, S., Muchowski, P. J., and Lindquist, S. (2006a). Flanking sequences profoundly alter polyglutamine toxicity in yeast. *Proc. Natl. Acad. Sci. U.S.A.* 103, 11045–11050.

Duennwald, M. L., Jagadish, S., Giorgini, F., Muchowski, P. J., and Lindquist, S. (2006b). A network of protein interactions determines polyglutamine toxicity. *Proc. Natl. Acad. Sci. U.S.A.* 103, 11051–11056.

Duennwald, M. L., and Lindquist, S. (2008). Impaired ERAD and ER stress are early and specific events in polyglutamine toxicity. *Genes Dev.* 22, 3308–3319. doi: 10.1101/gad.1673408

Ehrnhoefer, D. E., Duennwald, M., Markovic, P., Wacker, J. L., Engemann, S., Roark, M., et al. (2006). Green tea (−)-epigallocatechin-gallate modulates early events in huntingtin misfolding and reduces toxicity in Huntington's disease models. *Hum. Mol. Genet.* 15, 2743–2751. doi: 10.1093/hmg/ddl210

Eisenberg, T., Abdellatif, M., Schroeder, S., Primessnig, U., Stekovic, S., Pendl, T., et al. (2016). Cardioprotection and lifespan extension by the natural polyamine spermidine. *Nat. Med.* 22, 1428–1438. doi: 10.1038/nm.4222

Eisenberg, T., Knauer, H., Schauer, A., Büttner, S., Ruckenstuhl, C., Carmona-Gutierrez, D., et al. (2009). Induction of autophagy by spermidine promotes longevity. *Nat. Cell Biol.* 11, 1305–1314. doi: 10.1038/ncb1975

Engel, S. R., Dietrich, F. S., Fisk, D. G., Binkley, G., Balakrishnan, R., Costanzo, M. C., et al. (2013). The reference genome sequence of *Saccharomyces cerevisiae*: then and now. *G3 GenesGenomesGenetics* 4, 389–398. doi: 10.1534/g3.113.008995

Fahrenkrog, B. (2015). Histone modifications as regulators of life and death in *Saccharomyces cerevisiae*. *Microb. Cell* 3, 1–13. doi: 10.15698/mic2016.01.472

Farshbaf, M. J., and Ghaedi, K. (2017). Huntington's Disease and mitochondria. *Neurotox. Res.* 32, 518–529. doi: 10.1007/s12640-017-9766-1

Finkbeiner, S. (2011). Huntington's disease. *Cold Spring Harb. Perspect. Biol.* 3:a007476. doi: 10.1101/cshperspect.a007476

Forsburg, S. L. (2001). The art and design of genetic screens: yeast. *Nat. Rev. Genet.* 2, 659–668. doi: 10.1038/35088500

Fröhlich, K. U., and Madeo, F. (2001). Apoptosis in yeast: a new model for aging research. *Exp. Gerontol.* 37, 27–31. doi: 10.1016/S0531-5565(01)00177-2

Fruhmann, G., Seynnaeve, D., Zheng, J., Ven, K., Molenberghs, S., Wilms, T., et al. (2017). Yeast buddies helping to unravel the complexity of neurodegenerative disorders. *Mech. Ageing Dev.* 161, 288–305. doi: 10.1016/j.mad.2016.05.002

Gaisne, M., Bécam, A. M., Verdière, J., and Herbert, C. J. (1999). A "natural" mutation in *Saccharomyces cerevisiae* strains derived from S288c affects the complex regulatory gene HAP1 (CYP1). *Curr. Genet.* 36, 195–200. doi: 10.1007/s002940050490

Galluzzi, L., Kepp, O., and Kroemer, G. (2016). Mitochondrial regulation of cell death: a phylogenetically conserved control. *Microb. Cell* 3, 101–108. doi: 10.15698/mic2016.03.483

Galluzzi, L., Vitale, I., Aaronson, S. A., Abrams, J. M., Adam, D., Agostinis, P., et al. (2018). Molecular mechanisms of cell death: recommendations of the Nomenclature Committee on Cell Death 2018. *Cell Death. Differ.* 25, 486–541. doi: 10.1038/s41418-017-0012-4

Garden, G. A., and La Spada, A. R. (2012). Intercellular (Mis)communication in neurodegenerative disease. *Neuron* 73, 886–901. doi: 10.1016/j.neuron.2012.02.017

Gasser, B., Prielhofer, R., Marx, H., Maurer, M., Nocon, J., Steiger, M., et al. (2013). Pichia pastoris: protein production host and model organism for biomedical research. *Future Microbiol.* 8, 191–208. doi: 10.2217/fmb.12.133

Gershon, H., and Gershon, D. (2000). The budding yeast, *Saccharomyces cerevisiae*, as a model for aging research: a critical review. *Mech. Ageing Dev.* 120, 1–22. doi: 10.1016/S0047-6374(00)00182-2

Giorgini, F., Guidetti, P., Nguyen, Q., Bennett, S. C., and Muchowski, P. J. (2005). A genomic screen in yeast implicates kynurenine 3-monooxygenase as a therapeutic target for Huntington's disease. *Nat. Genet.* 37, 526–531. doi: 10.1038/ng1542

Giorgini, F., and Muchowski, P.J. (2009). "Exploiting yeast genetics to inform therapeutic strategies for huntington's disease," in *Yeast Functional Genomics and Proteomics*, ed. I. Stagljar (Totowa, NJ: Humana Press), 161–174. doi: 10.1007/978-1-59745-540-4_9

Goffeau, A., Barrell, B. G., Bussey, H., Davis, R. W., Dujon, B., Feldmann, H., et al. (1996). Life with 6000 genes. *Science* 274, 546–567. doi: 10.1126/science.274.5287.546

Gruber, A., Hornburg, D., Antonin, M., Krahmer, N., Collado, J., Schaffer, M., et al. (2018). Molecular and structural architecture of polyQ aggregates in yeast. *Proc. Natl. Acad. Sci.U.S.A.* 115, E3446–E3453. doi: 10.1073/pnas.1717978115

Gutekunst, C. A., Li, S. H., Yi, H., Mulroy, J. S., Kuemmerle, S., Jones, R., et al. (1999). Nuclear and neuropil aggregates in Huntington's disease: relationship to neuropathology. *J. Neurosci. Off. J. Soc. Neurosci.* 19, 2522–2534. doi: 10.1523/JNEUROSCI.19-07-02522.1999

Hagihara, K., Kinoshita, K., Ishida, K., Hojo, S., Kameoka, Y., Satoh, R., et al. (2017). A genome-wide screen for FTY720-sensitive mutants reveals genes required for ROS homeostasis. *Microb. Cell* 4, 390–401. doi: 10.15698/mic2017.12.601

Hayden, M. R. (1981). *Huntington's Chorea*. London: Springer. doi: 10.1007/978-1-4471-1308-9

Hayden, M. R. (1983). Reflections on the history of Huntington's chorea. *Trends Neurosci.* 6, 122–124. doi: 10.1016/0166-2236(83)90062-0

Haynes, C. M., Titus, E. A., and Cooper, A. A. (2004). Degradation of misfolded proteins prevents ER-derived oxidative stress and cell death. *Mol. Cell* 15, 767–776. doi: 10.1016/j.molcel.2004.08.025

Heinisch, J. J., and Brandt, R. (2016). Signaling pathways and posttranslational modifications of tau in Alzheimer's disease: the humanization of yeast cells. *Microb. Cell* 3, 135–146. doi: 10.15698/mic2016.04.489

Herker, E., Jungwirth, H., Lehmann, K. A., Maldener, C., Fröhlich, K.-U., Wissing, S., et al. (2004). Chronological aging leads to apoptosis in yeast. *J. Cell Biol.* 164, 501–507. doi: 10.1083/jcb.200310014

Higgins, R., Kabbaj, M.-H., Hatcher, A., and Wang, Y. (2018). The absence of specific yeast heat-shock proteins leads to abnormal aggregation and compromised autophagic clearance of mutant Huntingtin proteins. *PLoS One* 13:e0191490. doi: 10.1371/journal.pone.0191490

Honigberg, S. M. (2011). Cell signals, cell contacts, and the organization of yeast communities. *Eukaryot. Cell* 10, 466–473. doi: 10.1128/EC.00313-10

Howitz, K. T., Bitterman, K. J., Cohen, H. Y., Lamming, D. W., Lavu, S., Wood, J. G., et al. (2003). Small molecule activators of sirtuins extend *Saccharomyces cerevisiae* lifespan. *Nature* 425, 191–196. doi: 10.1038/nature01960

Hudson, S. A., Ecroyd, H., Dehle, F. C., Musgrave, I. F., and Carver, J. A. (2009). (-)-epigallocatechin-3-gallate (EGCG) maintains kappa-casein in its pre-fibrillar state without redirecting its aggregation pathway. *J. Mol. Biol.* 392, 689–700. doi: 10.1016/j.jmb.2009.07.031

Hughes, T. R. (2002). Yeast and drug discovery. *Funct. Integr. Genom.* 2, 199–211. doi: 10.1007/s10142-002-0059-1

Jacobs, K. R., Castellano-González, G., Guillemin, G. J., and Lovejoy, D. B. (2017). Major developments in the design of inhibitors along the kynurenine pathway. *Curr. Med. Chem.* 24, 2471–2495. doi: 10.2174/0929867324666170502123114

Janssens, G. E., and Veenhoff, L. M. (2016). Evidence for the hallmarks of human aging in replicatively aging yeast. *Microb. Cell* 3, 263–274. doi: 10.15698/mic2016.07.510

Jiang, Y., Di Gregorio, S. E., Duennwald, M. L., and Lajoie, P. (2016). Polyglutamine toxicity in yeast uncovers phenotypic variations between different fluorescent protein fusions. *Traffic* 18, 58–70. doi: 10.1111/tra.12453

Johansen, T., and Lamark, T. (2011). Selective autophagy mediated by autophagic adapter proteins. *Autophagy* 7, 279–296. doi: 10.4161/auto.7.3.14487

Johnson, B. S., McCaffery, J. M., Lindquist, S., and Gitler, A. D. (2008). A yeast TDP-43 proteinopathy model: exploring the molecular determinants of TDP-43 aggregation and cellular toxicity. *Proc. Natl. Acad. Sci. U.S.A.* 105, 6439–6444. doi: 10.1073/pnas.0802082105

Jones, G. W., and Tuite, M. F. (2005). Chaperoning prions: the cellular machinery for propagating an infectious protein? *BioEssays* 27, 823–832.

Kachroo, A. H., Laurent, J. M., Yellman, C. M., Meyer, A. G., Wilke, C. O., and Marcotte, E. M. (2015). Systematic humanization of yeast genes reveals conserved functions and genetic modularity. *Science* 348, 921–925. doi: 10.1126/science.aaa0769

Kaeberlein, M., Burtner, C. R., and Kennedy, B. K. (2007). Recent developments in yeast aging. *PLoS Genet.* 3:e84. doi: 10.1371/journal.pgen.0030084

Kainz, K., Tadic, J., Zimmermann, A., Pendl, T., Carmona-Gutierrez, D., Ruckenstuhl, C., et al. (2017). Methods to assess autophagy and chronological aging in yeast. *Methods Enzymol.* 588, 367–394. doi: 10.1016/bs.mie.2016.09.086

Kaiser, C. J. O., Grötzinger, S. W., Eckl, J. M., Papsdorf, K., Jordan, S., and Richter, K. (2013). A network of genes connects polyglutamine toxicity to ploidy control in yeast. *Nat. Commun.* 4:1571. doi: 10.1038/ncomms2575

Khoshnan, A., Ko, J., and Patterson, P. H. (2002). Effects of intracellular expression of anti-huntingtin antibodies of various specificities on mutant huntingtin aggregation and toxicity. *Proc. Natl. Acad. Sci. U.S.A.* 99, 1002–1007. doi: 10.1073/pnas.022631799

Khurana, V., and Lindquist, S. (2010). Modelling neurodegeneration in *Saccharomyces cerevisiae*: why cook with baker's yeast? *Nat. Rev. Neurosci.* 11, 436–449. doi: 10.1038/nrn2809

Klug, L., and Daum, G. (2014). Yeast lipid metabolism at a glance. *FEMS Yeast Res.* 14, 369–388. doi: 10.1111/1567-1364.12141

Kouroku, Y., Fujita, E., Tanida, I., Ueno, T., Isoai, A., Kumagai, H., et al. (2007). ER stress (PERK/eIF2alpha phosphorylation) mediates the polyglutamine-induced LC3 conversion, an essential step for autophagy formation. *Cell Death Differ.* 14, 230–239. doi: 10.1038/sj.cdd.4401984

Krobitsch, S., and Lindquist, S. (2000). Aggregation of huntingtin in yeast varies with the length of the polyglutamine expansion and the expression of chaperone proteins. *Proc. Natl. Acad. Sci. U.S.A.* 97, 1589–1594. doi: 10.1073/pnas.97.4.1589

Kryndushkin, D., and Shewmaker, F. (2011). Modeling ALS and FTLD proteinopathies in yeast. *Prion* 5, 250–257. doi: 10.4161/pri.17229

Kuemmerle, S., Gutekunst, C. A., Klein, A. M., Li, X. J., Li, S. H., Beal, M. F., et al. (1999). Huntington aggregates may not predict neuronal death in Huntington's disease. *Ann. Neurol.* 46, 842–849. doi: 10.1002/1531-8249(199912)46:6<842::AID-ANA6>3.0.CO;2-O

Kumar, A., Kumar Singh, S., Kumar, V., Kumar, D., Agarwal, S., and Rana, M. K. (2015). Huntington's disease: an update of therapeutic strategies. *Gene* 556, 91–97. doi: 10.1016/j.gene.2014.11.022

Kuo, Y., Ren, S., Lao, U., Edgar, B. A., and Wang, T. (2013). Suppression of polyglutamine protein toxicity by co-expression of a heat-shock protein 40 and a heat-shock protein 110. *Cell Death Dis.* 4:e833. doi: 10.1038/cddis.2013.351

Lakhani, V. V., Ding, F., and Dokholyan, N. V. (2010). Polyglutamine induced misfolding of huntingtin exon1 is modulated by the flanking sequences. *PLoS Comput. Biol.* 6:e1000772. doi: 10.1371/journal.pcbi.1000772

Laurent, J. M., Young, J. H., Kachroo, A. H., and Marcotte, E. M. (2016). Efforts to make and apply humanized yeast. *Brief Funct. Genomics* 15, 155–163. doi: 10.1093/bfgp/elv041

Leavitt, B. R., Guttman, J. A., Hodgson, J. G., Kimel, G. H., Singaraja, R., Vogl, A. W., et al. (2001). Wild-type huntingtin reduces the cellular toxicity of mutant huntingtin in vivo. *Am. J. Hum. Genet.* 68, 313–324. doi: 10.1086/318207

Lee, D. H., and Goldberg, A. L. (2010). Hsp104 is essential for the selective degradation in yeast of polyglutamine expanded ataxin-1 but not most misfolded proteins generally. *Biochem. Biophys. Res. Commun.* 391, 1056–1061. doi: 10.1016/j.bbrc.2009.12.018

Leibiger, C., Deisel, J., Aufschnaiter, A., Ambros, S., Tereshchenko, M., Verheijen, B. M., et al. (2018). TDP-43 controls lysosomal pathways thereby determining its own clearance and cytotoxicity. *Hum. Mol. Genet.* 27, 1593–1607. doi: 10.1093/hmg/ddy066

Li, X., Standley, C., Sapp, E., Valencia, A., Qin, Z.-H., Kegel, K. B., et al. (2009). Mutant huntingtin impairs vesicle formation from recycling endosomes by interfering with Rab11 activity. *Mol. Cell. Biol.* 29, 6106–6116. doi: 10.1128/MCB.00420-09

Lin, F., and Qin, Z.-H. (2013). Degradation of misfolded proteins by autophagy: is it a strategy for huntington's disease treatment? *J. Huntingt. Dis.* 2, 149–157. doi: 10.3233/JHD-130052

Lista, M. J., Martins, R. P., Angrand, G., Quillévéré, A., Daskalogianni, C., Voisset, C., et al. (2017). A yeast model for the mechanism of the Epstein-Barr

virus immune evasion identifies a new therapeutic target to interfere with the virus stealthiness. *Microb. Cell* 4, 305–307. doi: 10.15698/mic2017.09.590

Liu, G., Coyne, A. N., Pei, F., Vaughan, S., Chaung, M., Zarnescu, D. C., et al. (2017). Endocytosis regulates TDP-43 toxicity and turnover. *Nat. Commun.* 8:2092. doi: 10.1038/s41467-017-02017-x

Liu, G., Hu, Y., Tunnacliffe, A., and Zheng, Y. (2015). A plant cell model of polyglutamine aggregation: identification and characterisation of macromolecular and small-molecule anti-protein aggregation activity in vivo. *J. Biotechnol.* 207, 39–46. doi: 10.1016/j.jbiotec.2015.05.003

Lo Bianco, C., Shorter, J., Régulier, E., Lashuel, H., Iwatsubo, T., Lindquist, S., et al. (2008). Hsp104 antagonizes alpha-synuclein aggregation and reduces dopaminergic degeneration in a rat model of Parkinson disease. *J. Clin. Invest.* 118, 3087–3097. doi: 10.1172/JCI35781

Lu, K., Psakhye, I., and Jentsch, S. (2014). Autophagic clearance of PolyQ proteins mediated by ubiquitin-Atg8 adaptors of the conserved CUET protein family. *Cell* 158, 549–563. doi: 10.1016/j.cell.2014.05.048

Ma, D. (2001). Applications of yeast in drug discovery. *Prog. Drug Res.* 57, 117–162. doi: 10.1007/978-3-0348-8308-5_3

MacDonald, M. E., Ambrose, C. M., Duyao, M. P., Myers, R. H., Lin, C., Srinidhi, L., et al. (1993). A novel gene containing a trinucleotide repeat that is expanded and unstable on Huntington's disease chromosomes. *Cell* 72, 971–983. doi: 10.1016/0092-8674(93)90585-E

Madeo, F., Eisenberg, T., Pietrocola, F., and Kroemer, G. (2018). Spermidine in health and disease. *Science* 359:eaan2788. doi: 10.1126/science.aan2788

Madeo, F., Fröhlich, E., and Fröhlich, K. U. (1997). A yeast mutant showing diagnostic markers of early and late apoptosis. *J. Cell Biol.* 139, 729–734. doi: 10.1083/jcb.139.3.729

Madeo, F., Fröhlich, E., Ligr, M., Grey, M., Sigrist, S. J., Wolf, D. H., et al. (1999). Oxygen stress: a regulator of apoptosis in yeast. *J. Cell Biol.* 145, 757–767. doi: 10.1083/jcb.145.4.757

Madeo, F., Herker, E., Maldener, C., Wissing, S., Lächelt, S., Herlan, M., et al. (2002). A caspase-related protease regulates apoptosis in yeast. *Mol. Cell* 9, 911–917. doi: 10.1016/S1097-2765(02)00501-4

Mähler, A., Mandel, S., Lorenz, M., Ruegg, U., Wanker, E. E., Boschmann, M., et al. (2013). Epigallocatechin-3-gallate: a useful, effective and safe clinical approach for targeted prevention and individualised treatment of neurological diseases? *EPMA J.* 4:5. doi: 10.1186/1878-5085-4-5

Mao, Y., Chen, X., Xu, M., Fujita, K., Motoki, K., Sasabe, T., et al. (2016). Targeting TEAD/YAP-transcription-dependent necrosis, TRIAD, ameliorates Huntington's disease pathology. *Hum. Mol. Genet.* 25, 4749–4770. doi: 10.1093/hmg/ddw303

Martí, E. (2016). RNA toxicity induced by expanded CAG repeats in Huntington's disease. *Brain Pathol.* 26, 779–786. doi: 10.1111/bpa.12427

Mason, R. P., and Giorgini, F. (2011). Modeling huntington disease in yeast: perspectives and future directions. *Prion* 5, 269–276. doi: 10.4161/pri.18005

Matus, S., Lisbona, F., Torres, M., León, C., Thielen, P., and Hetz, C. (2008). The stress rheostat: an interplay between the unfolded protein response (UPR) and autophagy in neurodegeneration. *Curr. Mol. Med.* 8, 157–172. doi: 10.2174/156652408784221324

Matus-Ortega, M. G., Cárdenas-Monroy, C. A., Flores-Herrera, O., Mendoza-Hernández, G., Miranda, M., González-Pedrajo, B., et al. (2015). New complexes containing the internal alternative NADH dehydrogenase (Ndi1) in mitochondria of Saccharomyces cerevisiae. *Yeast* 32, 629–641. doi: 10.1002/yea.3086

McColgan, P., and Tabrizi, S. J. (2017). Huntington's disease: a clinical review. *Eur. J. Neurol.* 25, 24–34. doi: 10.1111/ene.13413

Menard, C., Bastianetto, S., and Quirion, R. (2013). Neuroprotective effects of resveratrol and epigallocatechin gallate polyphenols are mediated by the activation of protein kinase C gamma. *Front. Cell. Neurosci.* 7:281. doi: 10.3389/fncel.2013.00281

Menezes, R., Tenreiro, S., Macedo, D., Santos, C. N., and Outeiro, T. F. (2015). From the baker to the bedside: yeast models of Parkinson's disease. *Microb. Cell* 2, 262–279. doi: 10.15698/mic2015.08.219

Mereles, D., and Hunstein, W. (2011). Epigallocatechin-3-gallate (EGCG) for clinical trials: more pitfalls than promises? *Int. J. Mol. Sci.* 12, 5592–5603. doi: 10.3390/ijms12095592

Meriin, A. B., Zhang, X., Alexandrov, I. M., Salnikova, A. B., Ter-Avanesian, M. D., Chernoff, Y. O., et al. (2007). Endocytosis machinery is involved in aggregation of proteins with expanded polyglutamine domains. *FASEB J.* 21, 1915–1925. doi: 10.1096/fj.06-6878com

Meriin, A. B., Zhang, X., He, X., Newnam, G. P., Chernoff, Y. O., and Sherman, M. Y. (2002). Huntingtin toxicity in yeast model depends on polyglutamine aggregation mediated by a prion-like protein Rnq1. *J. Cell Biol.* 157, 997–1004. doi: 10.1083/jcb.200112104

Meriin, A. B., Zhang, X., Miliaras, N. B., Kazantsev, A., Chernoff, Y. O., McCaffery, J. M., et al. (2003). Aggregation of expanded polyglutamine domain in yeast leads to defects in endocytosis. *Mol. Cell. Biol.* 23, 7554–7565. doi: 10.1128/MCB.23.21.7554-7565.2003

Messer, A., and Joshi, S. N. (2013). Intrabodies as neuroprotective therapeutics. *Neurotherapeutics* 10, 447–458. doi: 10.1007/s13311-013-0193-6

Möller, T. (2010). Neuroinflammation in huntington's disease. *J. Neural Transm.* 117, 1001–1008. doi: 10.1007/s00702-010-0430-7

Morton, A. J., and Edwardson, J. M. (2001). Progressive depletion of complexin II in a transgenic mouse model of Huntington's disease. *J. Neurochem.* 76, 166–172. doi: 10.1046/j.1471-4159.2001.00059.x

Morton, A. J., Faull, R. L., and Edwardson, J. M. (2001). Abnormalities in the synaptic vesicle fusion machinery in Huntington's disease. *Brain Res. Bull.* 56, 111–117. doi: 10.1016/S0361-9230(01)00611-6

Morton, A. J., and Howland, D. S. (2013). Large genetic animal models of Huntington's disease. *J. Huntingt. Dis.* 2, 3–19.

Muchowski, P. J., Schaffar, G., Sittler, A., Wanker, E. E., Hayer-Hartl, M. K., and Hartl, F. U. (2000). Hsp70 and Hsp40 chaperones can inhibit self-assembly of polyglutamine proteins into amyloid-like fibrils. *Proc. Natl. Acad. Sci. U.S.A.* 97, 7841–7846. doi: 10.1073/pnas.140202897

Muller, M., and Leavitt, B. R. (2014). Iron dysregulation in Huntington's disease. *J. Neurochem.* 130, 328–350. doi: 10.1111/jnc.12739

Munoz, A. J., Wanichthanarak, K., Meza, E., and Petranovic, D. (2012). Systems biology of yeast cell death. *FEMS Yeast Res.* 12, 249–265. doi: 10.1111/j.1567-1364.2011.00781.x

Mustacchi, R., Hohmann, S., and Nielsen, J. (2006). Yeast systems biology to unravel the network of life. *Yeast* 23, 227–238. doi: 10.1002/yea.1357

Nakamura, K., Jeong, S. Y., Uchihara, T., Anno, M., Nagashima, K., Nagashima, T., et al. (2001). SCA17, a novel autosomal dominant cerebellar ataxia caused by an expanded polyglutamine in TATA-binding protein. *Hum. Mol. Genet.* 10, 1441–1448. doi: 10.1093/hmg/10.14.1441

Nath, S., Munsie, L. N., and Truant, R. (2015). A huntingtin-mediated fast stress response halting endosomal trafficking is defective in Huntington's disease. *Hum. Mol. Genet.* 24, 450–462. doi: 10.1093/hmg/ddu460

Nelson, R. J., Ziegelhoffer, T., Nicolet, C., Werner-Washburne, M., and Craig, E. A. (1992). The translation machinery and 70 kd heat shock protein cooperate in protein synthesis. *Cell* 71, 97–105. doi: 10.1016/0092-8674(92)90269-I

Niu, Y., Na, L., Feng, R., Gong, L., Zhao, Y., Li, Q., et al. (2013). The phytochemical, EGCG, extends lifespan by reducing liver and kidney function damage and improving age-associated inflammation and oxidative stress in healthy rats. *Aging Cell* 12, 1041–1049. doi: 10.1111/acel.12133

Ocampo, A., and Barrientos, A. (2008). From the bakery to the brain business: developing inducible yeast models of human neurodegenerative disorders. *BioTechniques* 45, vii–xiv. doi: 10.2144/000112746

Ocampo, A., and Barrientos, A. (2011). Developing yeast models of human neurodegenerative disorders. *Methods Mol. Biol. Clifton NJ* 793, 113–127. doi: 10.1007/978-1-61779-328-8_8

Ocampo, A., Zambrano, A., and Barrientos, A. (2009). Suppression of polyglutamine-induced cytotoxicity in *Saccharomyces cerevisiae* by enhancement of mitochondrial biogenesis. *FASEB J.* 24, 1431–1441. doi: 10.1096/fj.09-148601

Ochaba, J., Lukacsovich, T., Csikos, G., Zheng, S., Margulis, J., Salazar, L., et al. (2014). Potential function for the Huntingtin protein as a scaffold for selective autophagy. *Proc. Natl. Acad. Sci. U.S.A.* 111, 16889–16894. doi: 10.1073/pnas.1420103111

Ohsumi, Y. (2014). Historical landmarks of autophagy research. *Cell Res.* 24, 9–23. doi: 10.1038/cr.2013.169

Ordway, J. M., Tallaksen-Greene, S., Gutekunst, C. A., Bernstein, E. M., Cearley, J. A., Wiener, H. W., et al. (1997). Ectopically expressed CAG

repeats cause intranuclear inclusions and a progressive late onset neurological phenotype in the mouse. *Cell* 91, 753–763. doi: 10.1016/S0092-8674(00)80464-X

Outeiro, T. F., and Giorgini, F. (2006). Yeast as a drug discovery platform in Huntington's and Parkinson's diseases. *Biotechnol. J.* 1, 258–269. doi: 10.1002/biot.200500043

Pallauf, K., Duckstein, N., and Rimbach, G. (2017). A literature review of flavonoids and lifespan in model organisms. *Proc. Nutr. Soc.* 76, 145–162. doi: 10.1017/S0029665116000720

Papsdorf, K., Kaiser, C. J. O., Drazic, A., Grötzinger, S. W., Haeßner, C., Eisenreich, W., et al. (2015). Polyglutamine toxicity in yeast induces metabolic alterations and mitochondrial defects. *BMC Genomics* 16:662. doi: 10.1186/s12864-015-1831-7

Park, I.-H., Arora, N., Huo, H., Maherali, N., Ahfeldt, T., Shimamura, A., et al. (2008). Disease-specific induced pluripotent stem cells. *Cell* 134, 877–886. doi: 10.1016/j.cell.2008.07.041

Park, S.-H., Kukushkin, Y., Gupta, R., Chen, T., Konagai, A., Hipp, M. S., et al. (2013). PolyQ proteins interfere with nuclear degradation of cytosolic proteins by sequestering the sis1p chaperone. *Cell* 154, 134–145. doi: 10.1016/j.cell.2013.06.003

Park, S.-K., Ratia, K., Ba, M., Valencik, M., and Liebman, S. W. (2016). Inhibition of Aβ42 oligomerization in yeast by a PICALM ortholog and certain FDA approved drugs. *Microb. Cell* 3, 53–64. doi: 10.15698/mic2016.02.476

Pearce, D. A., and Sherman, F. (1998). A yeast model for the study of Batten disease. *Proc. Natl. Acad. Sci. U.S.A.* 95, 6915–6918. doi: 10.1073/pnas.95.12.6915

Pearson, S. J., and Reynolds, G. P. (1992). Increased brain concentrations of a neurotoxin, 3-hydroxykynurenine, in Huntington's disease. *Neurosci. Lett.* 144, 199–201. doi: 10.1016/0304-3940(92)90749-W

Peffer, S., Cope, K., and Morano, K. A. (2015). Unraveling protein misfolding diseases using model systems. *Future Sci. OA* 1:FSO41. doi: 10.4155/fso.15.41

Peng, B., Williams, T. C., Henry, M., Nielsen, L. K., and Vickers, C. E. (2015). Controlling heterologous gene expression in yeast cell factories on different carbon substrates and across the diauxic shift: a comparison of yeast promoter activities. *Microb. Cell Fact.* 14:91. doi: 10.1186/s12934-015-0278-5

Penney, J. B., Vonsattel, J. P., MacDonald, M. E., Gusella, J. F., and Myers, R. H. (1997). CAG repeat number governs the development rate of pathology in Huntington's disease. *Ann. Neurol.* 41, 689–692. doi: 10.1002/ana.410410521

Pereira, C., Bessa, C., Soares, J., Leão, M., and Saraiva, L. (2012). Contribution of yeast models to neurodegeneration research. *J. Biomed. Biotechnol.* 2012, 1–12. doi: 10.1155/2012/941232

Pfund, C., Lopez-Hoyo, N., Ziegelhoffer, T., Schilke, B. A., Lopez-Buesa, P., Walter, W. A., et al. (1998). The molecular chaperone Ssb from *Saccharomyces cerevisiae* is a component of the ribosome-nascent chain complex. *EMBO J.* 17, 3981–3989. doi: 10.1093/emboj/17.14.3981

Popiel, H. A., Takeuchi, T., Fujita, H., Yamamoto, K., Ito, C., Yamane, H., et al. (2012). Hsp40 gene therapy exerts therapeutic effects on polyglutamine disease mice via a non-cell autonomous mechanism. *PLoS One* 7:e51069. doi: 10.1371/journal.pone.0051069

Portera-Cailliau, C., Hedreen, J. C., Price, D. L., and Koliatsos, V. E. (1995). Evidence for apoptotic cell death in Huntington disease and excitotoxic animal models. *J. Neurosci. Off. J. Soc. Neurosci.* 15, 3775–3787. doi: 10.1523/JNEUROSCI.15-05-03775.1995

Porzoor, A., and Macreadie, I. (2016). Yeast as a model for studies on Aβ aggregation toxicity in Alzheimer's disease, autophagic responses, and drug screening. *Methods Mol. Biol. Clifton NJ* 1303, 217–226. doi: 10.1007/978-1-4939-2627-5_12

Pouladi, M. A., Morton, A. J., and Hayden, M. R. (2013). Choosing an animal model for the study of Huntington's disease. *Nat. Rev. Neurosci.* 14, 708–721. doi: 10.1038/nrn3570

Rajakumar, T., Munkacsi, A. B., and Sturley, S. L. (2017). Exacerbating and reversing lysosomal storage diseases: from yeast to humans. *Microb. Cell* 4, 278–293. doi: 10.15698/mic2017.09.588

Ravikumar, B., Vacher, C., Berger, Z., Davies, J. E., Luo, S., Oroz, L. G., et al. (2004). Inhibition of mTOR induces autophagy and reduces toxicity of polyglutamine expansions in fly and mouse models of Huntington disease. *Nat. Genet.* 36, 585–595. doi: 10.1038/ng1362

Reggiori, F., and Klionsky, D. J. (2013). Autophagic processes in yeast: mechanism, machinery and regulation. *Genetics* 194, 341–361. doi: 10.1534/genetics.112.149013

Reiner, A., Dragatsis, I., and Dietrich, P. (2011). Genetics and neuropathology of Huntington's disease. *Int. Rev. Neurobiol.* 98, 325–372. doi: 10.1016/B978-0-12-381328-2.00014-6

Ring, J., Rockenfeller, P., Abraham, C., Tadic, J., Poglitsch, M., Schimmel, K., et al. (2017). Mitochondrial energy metabolism is required for lifespan extension by the spastic paraplegia-associated protein spartin. *Microb. Cell* 4, 411–422. doi: 10.15698/mic2017.12.603

Ripaud, L., Chumakova, V., Antonin, M., Hastie, A. R., Pinkert, S., Körner, R., et al. (2014). Overexpression of Q-rich prion-like proteins suppresses polyQ cytotoxicity and alters the polyQ interactome. *Proc. Natl. Acad. Sci. U.S.A.* 111, 18219–18224. doi: 10.1073/pnas.1421313111

Roos, R. A. (2010). Huntington's disease: a clinical review. *Orphanet J. Rare Dis.* 5:40. doi: 10.1186/1750-1172-5-40

Ross, C. A., Aylward, E. H., Wild, E. J., Langbehn, D. R., Long, J. D., Warner, J. H., et al. (2014). Huntington disease: natural history, biomarkers and prospects for therapeutics. *Nat. Rev. Neurol.* 10, 204–216. doi: 10.1038/nrneurol.2014.24

Rubinsztein, D. C. (2006). The roles of intracellular protein-degradation pathways in neurodegeneration. *Nature* 443, 780–786. doi: 10.1038/nature05291

Ruetenik, A. L., Ocampo, A., Ruan, K., Zhu, Y., Li, C., Zhai, R. G., et al. (2016). Attenuation of polyglutamine-induced toxicity by enhancement of mitochondrial OXPHOS in yeast and fly models of aging. *Microb. Cell* 3, 338–351. doi: 10.15698/mic2016.08.518

Saleh, A. A., Bhadra, A. K., and Roy, I. (2013). Cytotoxicity of mutant huntingtin fragment in yeast can be modulated by the expression level of wild type huntingtin fragment. *ACS Chem. Neurosci.* 5, 205–215. doi: 10.1021/cn400171d

Sanz, A., Soikkeli, M., Portero-Otín, M., Wilson, A., Kemppainen, E., McIlroy, G., et al. (2010). Expression of the yeast NADH dehydrogenase Ndi1 in Drosophila confers increased lifespan independently of dietary restriction. *Proc. Natl. Acad. Sci. U.S.A.* 107, 9105–9110. doi: 10.1073/pnas.0911539107

Sarkar, S., Perlstein, E. O., Imarisio, S., Pineau, S., Cordenier, A., Maglathlin, R. L., et al. (2007). Small molecules enhance autophagy and reduce toxicity in Huntington's disease models. *Nat. Chem. Biol.* 3, 331–338. doi: 10.1038/nchembio883

Sarkar, S., and Rubinsztein, D. C. (2008). Huntington's disease: degradation of mutant huntingtin by autophagy. *FEBS J.* 275, 4263–4270. doi: 10.1111/j.1742-4658.2008.06562.x

Saudou, F., and Humbert, S. (2016). The biology of huntingtin. *Neuron* 89, 910–926. doi: 10.1016/j.neuron.2016.02.003

Sawa, A., Tomoda, T., and Bae, B.-I. (2003). Mechanisms of neuronal cell death in Huntington's disease. *Cytogenet. Genome Res.* 100, 287–295. doi: 10.1159/000072864

Sbodio, J. I., Snyder, S. H., and Paul, B. D. (2018). Golgi stress response reprograms cysteine metabolism to confer cytoprotection in Huntington's disease. *Proc. Natl. Acad. Sci. U.S.A.* 115, 780–785. doi: 10.1073/pnas.1717877115

Schüller, C., Bauer, B.E., and Kuchler, K. (2003). "Inventory and evolution of fungal abc protein genes," in *ABC Proteins*, eds B. Holland, S. Cole, K. Kuchler, C. Higgins (London: Academic Press), 279–293.

Schulte, J., and Littleton, J. T. (2011). The biological function of the Huntingtin protein and its relevance to Huntington's Disease pathology. *Curr. Trends Neurol.* 5, 65–78.

Serpionov, G. V., Alexandrov, A. I., and Ter-Avanesyan, M. D. (2017). Distinct mechanisms of mutant huntingtin toxicity in different yeast strains. *FEMS Yeast Res.* 17:pii: fow102. doi: 10.1093/femsyr/fow102

Shaw, M., and Caro, A. (1982). The mutation rate to Huntington's chorea. *J. Med. Genet.* 19, 161–167. doi: 10.1136/jmg.19.3.161

Shen, K., Calamini, B., Fauerbach, J. A., Ma, B., Shahmoradian, S. H., Serrano Lachapel, I. L., et al. (2016). Control of the structural landscape and neuronal proteotoxicity of mutant Huntingtin by domains flanking the polyQ tract. *ELife* 5:e18065. doi: 10.7554/eLife.18065

Shrestha, A., and Megeney, L. (2015). Yeast proteinopathy models: a robust tool for deciphering the basis of neurodegeneration. *Microb. Cell* 2, 458–465. doi: 10.15698/mic2015.12.243

Snell, R. G., MacMillan, J. C., Cheadle, J. P., Fenton, I., Lazarou, L. P., Davies, P., et al. (1993). Relationship between trinucleotide repeat expansion

and phenotypic variation in Huntington's disease. *Nat. Genet.* 4, 393–397. doi: 10.1038/ng0893-393

Sokolov, S., Pozniakovsky, A., Bocharova, N., Knorre, D., and Severin, F. (2006). Expression of an expanded polyglutamine domain in yeast causes death with apoptotic markers. *Biochim. Biophys. Acta BBA – Bioenerg.* 1757, 660–666. doi: 10.1016/j.bbabio.2006.05.004

Solans, A., Zambrano, A., Rodríguez, M., and Barrientos, A. (2006). Cytotoxicity of a mutant huntingtin fragment in yeast involves early alterations in mitochondrial OXPHOS complexes II and III. *Hum. Mol. Genet.* 15, 3063–3081. doi: 10.1093/hmg/ddl248

Sorolla, M. A., Nierga, C., Rodríguez-Colman, M. J., Reverter-Branchat, G., Arenas, A., Tamarit, J., et al. (2011). Sir2 is induced by oxidative stress in a yeast model of Huntington disease and its activation reduces protein aggregation. *Arch. Biochem. Biophys.* 510, 27–34. doi: 10.1016/j.abb.2011.04.002

Southwell, A. L., Khoshnan, A., Dunn, D., Bugg, C. W., Lo, D. C., and Patterson, P. H. (2008). Intrabodies binding the proline-rich domains of mutant huntingtin increase its turnover and reduce neurotoxicity. *J. Neurosci. Off. J. Soc. Neurosci.* 28, 9013–9020. doi: 10.1523/JNEUROSCI.2747-08.2008

Southwell, A. L., Ko, J., and Patterson, P. H. (2009). Intrabody gene therapy ameliorates motor, cognitive and neuropathological symptoms in multiple mouse models of Huntington's disease. *J. Neurosci. Off. J. Soc. Neurosci.* 29:13589. doi: 10.1523/JNEUROSCI.4286-09.2009

Speldewinde, S. H., and Grant, C. M. (2015). Spermidine cures yeast of prions. *Microb. Cell* 3, 46–48. doi: 10.15698/mic2016.01.474

Speldewinde, S. H., and Grant, C. M. (2017). The frequency of yeast [PSI+] prion formation is increased during chronological ageing. *Microb. Cell* 4, 127–132. doi: 10.15698/mic2017.04.568

Stanek, L. M., Yang, W., Angus, S., Sardi, P. S., Hayden, M. R., Hung, G. H., et al. (2013). Antisense oligonucleotide-mediated correction of transcriptional dysregulation is correlated with behavioral benefits in the YAC128 mouse model of Huntington's disease. *J. Huntingt. Dis.* 2, 217–228.

Steffan, J. S. (2010). Does Huntingtin play a role in selective macroautophagy? *Cell Cycle* 9, 3401–3413. doi: 10.4161/cc.9.17.12671

Steffan, J. S., Agrawal, N., Pallos, J., Rockabrand, E., Trotman, L. C., Slepko, N., et al. (2004). SUMO modification of huntingtin and Huntington's disease pathology. *Science* 304, 100–104. doi: 10.1126/science.1092194

Stekovic, S., Ruckenstuhl, C., Royer, P., Winkler-Hermaden, C., Carmona-Gutierrez, D., Fröhlich, K.-U., et al. (2017). The neuroprotective steroid progesterone promotes mitochondrial uncoupling, reduces cytosolic calcium and augments stress resistance in yeast cells. *Microb. Cell* 4, 191–199. doi: 10.15698/mic2017.06.577

Stoy, N., Mackay, G. M., Forrest, C. M., Christofides, J., Egerton, M., Stone, T. W., et al. (2005). Tryptophan metabolism and oxidative stress in patients with Huntington's disease. *J. Neurochem.* 93, 611–623. doi: 10.1111/j.1471-4159.2005.03070.x

Thevandavakkam, M. A., Schwarcz, R., Muchowski, P. J., and Giorgini, F. (2010). Targeting Kynurenine 3-Monooxygenase (KMO): Implications for Therapy in Huntingtons Disease. *CNS Neurol. Disord. Drug Targets* 9, 791–800. doi: 10.2174/187152710793237430

Tardiff, D. F., Jui, N. T., Khurana, V., Tambe, M. A., Thompson, M. L., Chung, C. Y., et al. (2013). Yeast reveal a "druggable" Rsp5/Nedd4 network that ameliorates α-synuclein toxicity in neurons. *Science* 342, 979–983. doi: 10.1126/science.1245321

Taylor, J. P., Hardy, J., and Fischbeck, K. H. (2002). Toxic proteins in neurodegenerative disease. *Science* 296, 1991–1995. doi: 10.1126/science.1067122

Tenreiro, S., Franssens, V., Winderickx, J., and Outeiro, T. F. (2017). Yeast models of Parkinson's disease-associated molecular pathologies. *Curr. Opin. Genet. Dev.* 44, 74–83. doi: 10.1016/j.gde.2017.01.013

Tenreiro, S., Munder, M. C., Alberti, S., and Outeiro, T. F. (2013). Harnessing the power of yeast to unravel the molecular basis of neurodegeneration. *J. Neurochem.* 127, 438–452. doi: 10.1111/jnc.12271

Tenreiro, S., and Outeiro, T. F. (2010). Simple is good: yeast models of neurodegeneration: yeast as a model for neurodegeneration. *FEMS Yeast Res.* 10, 970–979. doi: 10.1111/j.1567-1364.2010.00649.x

Tousley, A., and Kegel-Gleason, K. B. (2016). Induced pluripotent stem cells in huntington's disease research: progress and opportunity. *J. Huntingt. Dis.* 5, 99–131. doi: 10.3233/JHD-160199

Truong, D. M., and Boeke, J. D. (2017). Resetting the yeast epigenome with human nucleosomes. *Cell* 171, 1508.e13–1519.e13. doi: 10.1016/j.cell.2017.10.043

Trushina, E., Singh, R. D., Dyer, R. B., Cao, S., Shah, V. H., Parton, R. G., et al. (2006). Mutant huntingtin inhibits clathrin-independent endocytosis and causes accumulation of cholesterol in vitro and in vivo. *Hum. Mol. Genet.* 15, 3578–3591. doi: 10.1093/hmg/ddl434

Vacher, C., Garcia-Oroz, L., and Rubinsztein, D. C. (2005). Overexpression of yeast hsp104 reduces polyglutamine aggregation and prolongs survival of a transgenic mouse model of Huntington's disease. *Hum. Mol. Genet.* 14, 3425–3433. doi: 10.1093/hmg/ddi372

van den Bogaard, S. J. A., Dumas, E. M., and Roos, R. A. C. (2013). The role of iron imaging in Huntington's disease. *Int. Rev. Neurobiol.* 110, 241–250. doi: 10.1016/B978-0-12-410502-7.00011-9

van der Burg, J. M. M., Björkqvist, M., and Brundin, P. (2009). Beyond the brain: widespread pathology in Huntington's disease. *Lancet Neurol.* 8, 765–774. doi: 10.1016/S1474-4422(09)70178-4

Vashist, S., Cushman, M., and Shorter, J. (2010). Applying Hsp104 to protein-misfolding disorders. *Biochem. Cell Biol. Biochim. Biol. Cell.* 88, 1–13. doi: 10.1139/o09-121

Velier, J., Kim, M., Schwarz, C., Kim, T. W., Sapp, E., Chase, K., et al. (1998). Wild-type and mutant huntingtins function in vesicle trafficking in the secretory and endocytic pathways. *Exp. Neurol.* 152, 34–40. doi: 10.1006/exnr.1998.6832

Verduyckt, M., Vignaud, H., Bynens, T., Van den Brande, J., Franssens, V., Cullin, C., et al. (2016). Yeast as a model for Alzheimer's disease: latest studies and advanced strategies. *Methods Mol. Biol. Clifton NJ* 1303, 197–215. doi: 10.1007/978-1-4939-2627-5_11

Vicente Miranda, H., Gomes, M. A., Branco-Santos, J., Breda, C., Lázaro, D. F., Lopes, L. V., et al. (2016). Glycation potentiates neurodegeneration in models of Huntington's disease. *Sci. Rep.* 6:36798. doi: 10.1038/srep36798

Vila, M., and Przedborski, S. (2003). Neurological diseases: targeting programmed cell death in neurodegenerative diseases. *Nat. Rev. Neurosci.* 4, 365–375. doi: 10.1038/nrn1100

Wagner, A. E., Piegholdt, S., Rabe, D., Baenas, N., Schloesser, A., Eggersdorfer, M., et al. (2015). Epigallocatechin gallate affects glucose metabolism and increases fitness and lifespan in *Drosophila melanogaster*. *Oncotarget* 6, 30568–30578. doi: 10.18632/oncotarget.5215

Walker, F. O. (2007). Huntington's disease. *Lancet* 369, 218–228. doi: 10.1016/S0140-6736(07)60111-1

Walter, G. M., Raveh, A., Mok, S.-A., McQuade, T. J., Arevang, C. J., Schultz, P. J., et al. (2014). High-throughput screen of natural product extracts in A yeast model of polyglutamine proteotoxicity. *Chem. Biol. Drug Des.* 83, 440–449. doi: 10.1111/cbdd.12259

Wang, N., Lu, X.-H., Sandoval, S. V., and Yang, X. W. (2013). An independent study of the preclinical efficacy of C2-8 in the R6/2 transgenic mouse model of Huntington's disease. *J. Huntingt. Dis.* 2, 443–451. doi: 10.3233/JHD-130074

Wickner, R. B., Bezsonov, E., and Bateman, D. A. (2014). Normal levels of the antiprion proteins Btn2 and Cur1 cure most newly formed [URE3] prion variants. *Proc. Natl. Acad. Sci. U.S.A.* 111, E2711–E2720. doi: 10.1073/pnas.1409582111

Wild, E. J., and Tabrizi, S. J. (2014). Targets for future clinical trials in Huntington's disease: What's in the pipeline? *Mov. Disord.* 29, 1434–1445. doi: 10.1002/mds.26007

Willingham, S., Outeiro, T. F., DeVit, M. J., Lindquist, S. L., and Muchowski, P. J. (2003). Yeast genes that enhance the toxicity of a mutant huntingtin fragment or alpha-synuclein. *Science* 302, 1769–1772. doi: 10.1126/science.1090389

Winderickx, J., Delay, C., De Vos, A., Klinger, H., Pellens, K., Vanhelmont, T., et al. (2008). Protein folding diseases and neurodegeneration: lessons learned from yeast. *Biochim. Biophys. Acta BBA – Mol. Cell Res.* 1783, 1381–1395. doi: 10.1016/j.bbamcr.2008.01.020

Wolfgang, W. J., Miller, T. W., Webster, J. M., Huston, J. S., Thompson, L. M., Marsh, J. L., et al. (2005). Suppression of Huntington's disease pathology in *Drosophila* by human single-chain Fv antibodies. *Proc. Natl. Acad. Sci. U.S.A.* 102, 11563–11568. doi: 10.1073/pnas.0505321102

Wong, E., and Cuervo, A. M. (2010). Autophagy gone awry in neurodegenerative diseases. *Nat. Neurosci.* 13, 805–811. doi: 10.1038/nn.2575

Xi, W., Wang, X., Laue, T. M., and Denis, C. L. (2016). Multiple discrete soluble aggregates influence polyglutamine toxicity in a Huntington's disease model system. *Sci. Rep.* 6:34916. doi: 10.1038/srep34916

Xi, Y., Noble, S., and Ekker, M. (2011). Modeling neurodegeneration in zebrafish. *Curr. Neurol. Neurosci. Rep.* 11, 274–282. doi: 10.1007/s11910-011-0182-2

Yagi, T., Seo, B. B., Nakamaru-Ogiso, E., Marella, M., Barber-Singh, J., Yamashita, T., et al. (2006). Can a single subunit yeast NADH dehydrogenase (Ndi1) remedy diseases caused by respiratory complex I defects? *Rejuvenation Res.* 9, 191–197.

Yin, Z., Pascual, C., and Klionsky, D. J. (2016). Autophagy: machinery and regulation. *Microb. Cell* 3, 588–596. doi: 10.15698/mic2016.12.546

Zaghloul, E. M., Gissberg, O., Moreno, P. M. D., Siggens, L., Hällbrink, M., Jørgensen, A. S., et al. (2017). CTG repeat-targeting oligonucleotides for down-regulating Huntingtin expression. *Nucleic Acids Res.* 45, 5153–5169. doi: 10.1093/nar/gkx111

Zhang, X., Smith, D. L., Meriin, A. B., Engemann, S., Russel, D. E., Roark, M., et al. (2005). A potent small molecule inhibits polyglutamine aggregation in Huntington's disease neurons and suppresses neurodegeneration in vivo. *Proc. Natl. Acad. Sci. U.S.A.* 102, 892–897. doi: 10.1073/pnas.0408936102

Zhao, R. Y. (2017). Yeast for virus research. *Microb. Cell* 4, 311–330. doi: 10.15698/mic2017.10.592

Zheng, J., Yang, J., Choe, Y.-J., Hao, X., Cao, X., Zhao, Q., et al. (2017). Role of the ribosomal quality control machinery in nucleocytoplasmic translocation of polyQ-expanded huntingtin exon-1. *Biochem. Biophys. Res. Commun.* 493, 708–717. doi: 10.1016/j.bbrc.2017.08.126

Zimmermann, A., Hofer, S., Pendl, T., Kainz, K., Madeo, F., and Carmona-Gutierrez, D. (2018). Yeast as a tool to identify anti-aging compounds. *FEMS Yeast Res.* 18:foy020. doi: 10.1093/femsyr/foy020

Zimmermann, A., Kainz, K., Andryushkova, A., Hofer, S., Madeo, F., and Carmona-Gutierrez, D. (2016). Autophagy: one more Nobel Prize for yeast. *Microb. Cell* 3, 579–581. doi: 10.15698/mic2016.12.544

Zoghbi, H. Y., and Orr, H. T. (2000). Glutamine repeats and neurodegeneration. *Annu. Rev. Neurosci.* 23, 217–247. doi: 10.1146/annurev.neuro.23.1.217

Zuccato, C., and Cattaneo, E. (2014). "Huntington's disease," in *Neurotrophic Factors*, eds G. R. Lewin and B. D. Carter (Berlin: Springer), 357–409. doi: 10.1007/978-3-642-45106-5_14

Zurawel, A. A., Kabeche, R., DiGregorio, S. E., Deng, L., Menon, K. M., Opalko, H., et al. (2016). CAG expansions are genetically stable and form nontoxic aggregates in cells lacking endogenous polyglutamine proteins. *MBio* 7, e1367–e1316. doi: 10.1128/mBio.01367-16

Zwilling, D., Huang, S.-Y., Sathyasaikumar, K. V., Notarangelo, F. M., Guidetti, P., Wu, H.-Q., et al. (2011). Kynurenine 3-monooxygenase inhibition in blood ameliorates neurodegeneration. *Cell* 145, 863–874. doi: 10.1016/j.cell.2011.05.020

Conflict of Interest Statement: The authors declare that the research was conducted in the absence of any commercial or financial relationships that could be construed as a potential conflict of interest.

frontiers in Molecular Neuroscience

MINI REVIEW
published: 19 September 2018
doi: 10.3389/fnmol.2018.00329

A Mitochondria-Associated Oxidative Stress Perspective on Huntington's Disease

Ju Zheng[1,2,3], *Joris Winderickx*[2], *Vanessa Franssens*[2]* *and Beidong Liu*[3,4,5]*

[1]Department of Biology, Southern University of Science and Technology, Shenzhen, China, [2]Department of Biology, Functional Biology, KU Leuven, Heverlee, Belgium, [3]Department of Chemistry and Molecular Biology, University of Gothenburg, Gothenburg, Sweden, [4]State Key Laboratory of Subtropical Silviculture, School of Forestry and Biotechnology, Zhejiang A&F University, Hangzhou, China, [5]Center for Large-scale Cell-based Screening, Faculty of Science, University of Gothenburg, Gothenburg, Sweden

Huntington's disease (HD) is genetically caused by mutation of the Huntingtin (*HTT*) gene. At present, the mechanisms underlying the defect of *HTT* and the development of HD remain largely unclear. However, increasing evidence shows the presence of enhanced oxidative stress in HD patients. In this review article, we focus on the role of oxidative stress in the pathogenesis of HD and discuss mediators and potential mechanisms involved in mutant HTT-mediated oxidative stress generation and progression. Furthermore, we emphasize the role of the unicellular organism *Saccharomyces cerevisiae* in investigating mutant HTT-induced oxidative stress. Overall, this review article provides an overview of the latest findings regarding oxidative stress in HD and potential therapeutic targets for HD.

Keywords: Huntington's disease, Huntingtin, neurodegeneration, yeast, oxidative stress

OPEN ACCESS

Edited by:
Ralf J. Braun,
University of Bayreuth, Germany

Reviewed by:
Johannes Herrmann,
Technische Universität Kaiserslautern, Germany
Martin Lothar Duennwald,
University of Western Ontario, Canada

***Correspondence:**
Vanessa Franssens
vanessa.franssens@kuleuven.be
Beidong Liu
beidong.liu@cmb.gu.se

Received: *13 April 2018*
Accepted: *24 August 2018*
Published: *19 September 2018*

Citation:
Zheng J, Winderickx J, Franssens V and Liu B (2018) A Mitochondria-Associated Oxidative Stress Perspective on Huntington's Disease. Front. Mol. Neurosci. 11:329. doi: 10.3389/fnmol.2018.00329

INTRODUCTION

Huntington's Disease

Huntington's disease (HD) is a neurodegenerative disorder inherited in an autosomal dominant pattern. The symptoms in affected individuals include emotional problems, psychiatric disturbances and a decline in the ability to control movements and thinking.

Mutation of the Huntingtin (*HTT*) gene causes HD. An expansion of CAG repeats was found in the DNA sequence of mutant *HTT*, resulting in a polyQ expansion in the encoded mutant HTT protein (MacDonald et al., 1993). This polyQ expansion of HTT has been proven to trigger misfolding/aggregation of HTT and cytotoxicity to cells (DiFiglia et al., 1997; Penney et al., 1997; Krobitsch and Lindquist, 2000). The CAG-segment in the *HTT* gene is repeated approximately 25 times in healthy individuals. In contrast, individuals with 40–50 CAG repeats in the *HTT* gene usually develop adult-onset HD and the presence of more than 60 CAG repeats of *HTT* tends to result in the development of juvenile HD (MacDonald et al., 1993; Langbehn et al., 2004). Despite the well-studied genetic cause of HD, the mechanisms by which polyQ expansion induces cytotoxicity and neuronal death are not yet fully understood. Expression of the N-terminal fragment of HTT with a polyQ expansion results in polyQ protein aggregation and produces neurological symptoms (Lunkes et al., 2002). Therefore, both full-length and truncated HTT containing a polyQ expansion exceeding 36Q are defined as mutant HTT (mHTT) in this review article. As the proline-rich region is critical for polyQ expansion-induced

toxicity in a yeast model (Dehay and Bertolotti, 2006; Duennwald et al., 2006), we will emphasize the presence/absence of the proline-rich region within a mHTT fragment in the yeast model.

In addition to the effect of polyQ-expanded HTT, CAG repeats within HTT mRNA were also identified as a toxic species. Importantly, the toxic effect of CAG repeat within mRNA are also length dependent. CAG repeats in mRNA may serve as a template for formation of RNA foci (Jain and Vale, 2017). Furthermore, expanded CAG repeats sequester functional proteins and cause gene expression perturbations (Martí, 2016). Moreover, non-polyQ-expanded homomeric proteins were reported to accumulate in the HD human brain and were demonstrated to be toxic to neural cells in a consistent, length-dependent manner (Bañez-Coronel et al., 2015).

Oxidative Stress

Cells possess complicated mechanisms to ensure their proper functioning. These mechanisms are responsible for the elimination of harmful by-products generated during biological processes. However, when these cellular systems fail to maintain the balance between generations of toxic by-products and scavenging, stress occurs, and this may result in cellular cytotoxicity. Oxidative stress is the imbalance between reactive oxygen species (ROS)/reactive nitrogen species (RNS) generation and the biological antioxidant defense system. ROS/RNS are very active species that interact with a number of cellular macromolecules, resulting in a reversible alteration of their molecular structure and function that causes a subsequent cellular response. Accumulation of ROS/RNS in cells leads to damage of proteins, DNA and lipids and further damages tissues and organs, and these changes contribute to the pathogenesis of many diseases (Sies, 1991; Yu, 1994; Weidinger and Kozlov, 2015).

Endogenous ROS mainly originates from mitochondria during the synthesis of ATP and the transfer of electrons, derived from the mitochondrial respiratory reactions, to the electron transport chain. Part of the electrons generated during this process interact with O_2, thereby generating superoxide. It was estimated that approximately 2% of the total amount of O_2 that is consumed by mitochondria is involved in ROS generation (Chance et al., 1979; Sabharwal and Schumacker, 2014). In addition, ROS is also produced by NADPH oxidase (NOX) within the cytoplasm (Valencia et al., 2012).

In this review article, we address the ROS production upon expression of mutant HTT and how this increased ROS level contributes to cytotoxicity and neuronal death.

MITOCHONDRIAL DYSFUNCTION CONTRIBUTES TO HD PATHOGENESIS

Although the mechanisms underlying HD are still unclear, there is evidence showing that mitochondrial dysfunction indeed plays a crucial role in the pathogenesis of HD (Lin and Beal, 2006; Quintanilla and Johnson, 2009; Damiano et al., 2010; Costa and Scorrano, 2012; Guedes-Dias et al., 2016; Carmo et al., 2018). Here, we highlight the major findings regarding the role of mitochondrial loss or dysfunction in HD pathogenesis (**Figure 1**).

Evidence for Mitochondrial Dysfunction in HD Pathology

Oxidative stress causes damage to mitochondrial DNA (mtDNA) during ageing. In addition, researchers have provided evidence that mtDNA damage is implicated in the pathogenesis of HD (Polidori et al., 1999; Yang et al., 2008). In this respect, an increase in both the basal levels of mitochondria-generated ROS and mtDNA lesions and a simultaneous decrease in spare respiratory capacity were observed in striatal cells expressing mHTT. As mtDNA is a major target of the oxidative stress associated with mHTT, researchers found that the abundance of mtDNA decreases dramatically in mHTT cells compared to wild-type cells (Siddiqui et al., 2012). In addition, mtDNA depletion in leukocytes was reported in patients with polyQ diseases, and the level of mtDNA content was negatively correlated to the number of polyQ repeats in the mHTT (Liu et al., 2008). A mitochondrial biology study showed that a selective mtDNA depletion coincides with an increased vulnerability of the striatum in transgenic HD mice (Hering et al., 2015). In addition, the copy number of mtDNA is significantly lower in peripheral HD leukocytes and transgenic HD R6/2 mice (Petersen et al., 2014). Moreover, expression of mHTT impairs the mitochondrial disulfide relay system (MDRS), which is accompanied by a decreased copy number of mtDNA and the accumulation of mtDNA deletions (Napoli et al., 2013).

Mitochondria are key organelles that participate in the regulation of intracellular Ca^{2+} homeostasis (Giacomello et al., 2007). When the Ca^{2+} level in the cytosol is high, the extra Ca^{2+} is sequestered into inactive calcium-phosphate complexes. On the other hand, when the Ca^{2+} level is low, Ca^{2+} is released back into the cytosol (Nicholls and Budd, 2000; Nicholls, 2005). Researchers found that calcium transport between the mitochondria and cytoplasm occurs through the ryanodine receptor (RyR), an endoplasmic reticulum-resident Ca^{2+} channel. Inhibitors of the RyR attenuated cell death induced by mHTT, while co-expression of the RyR enhanced HTT toxicity (**Figure 2**). Furthermore, Ca^{2+} leakage was observed in striatal and cortical neurons from R6/2 HD model mice (Suzuki et al., 2012). These observations show that maintaining an appropriate Ca^{2+} concentration within the cytoplasm is vital for cell viability. However, failure of the Ca^{2+} homeostasis buffering system or an overload of Ca^{2+} can lead to the opening of a non-specific pore in the inner mitochondrial membrane, known as the mitochondrial permeability transition pore (mPTP). The opening of the mPTP can disturb the ATP level within mitochondria. Since a proper ATP level is critical for cells to function properly, opening the mPTP potentially kills the cell (Krieger and Duchen, 2002; Halestrap, 2006; Rasola et al., 2010).

Increasing evidence shows that a defect in mitochondrial Ca^{2+} handling contributes to HD pathogenesis (Brustovetsky, 2016). Lower membrane potential and higher sensitivity to calcium loads were found in lymphoblast mitochondria from

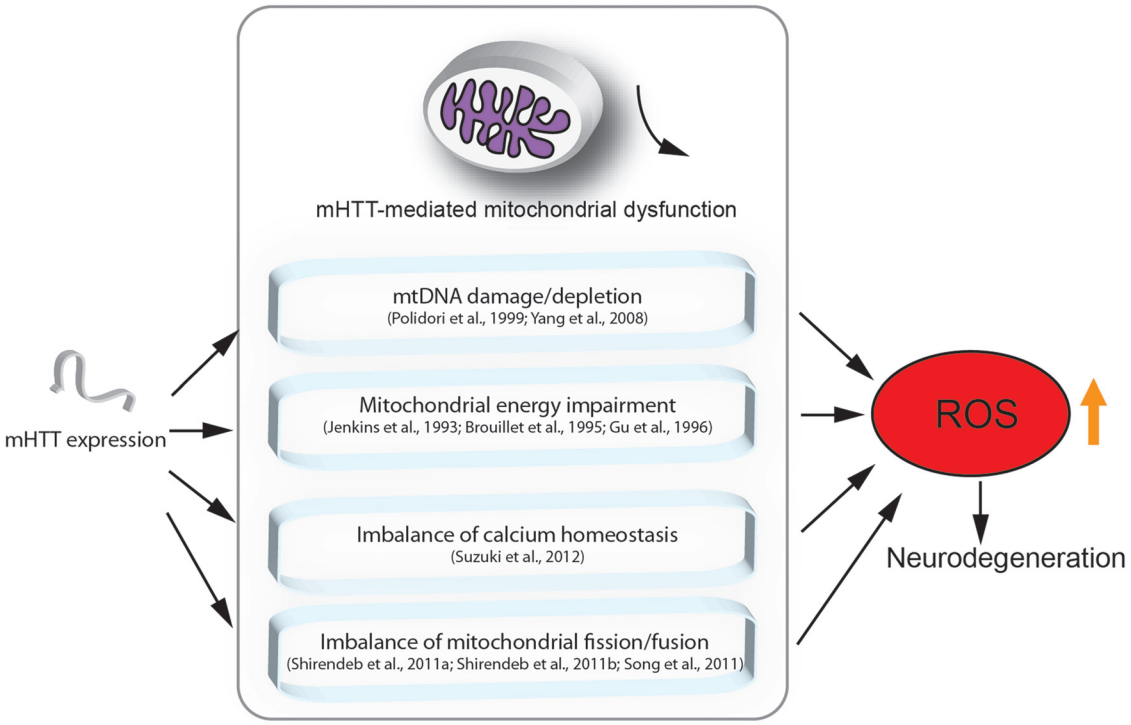

FIGURE 1 | Mutant HTT (mHTT) induced mitochondria-mediated reactive oxygen species (ROS) accumulation. This figure summarizes the mitochondria-associated dysfunction caused by expression of mHTT. mHTT directly contacts the mitochondrial membrane and disturbs calcium homeostasis (Suzuki et al., 2012). mHTT causes mitochondrial dysfunction by damaging mitochondrial DNA (mtDNA; Polidori et al., 1999; Yang et al., 2008). mHTT interrupts mitochondrial fission/fusion and interferes with mitochondrial energy metabolism (Jenkins et al., 1993; Brouillet et al., 1995; Gu et al., 1996; Shirendeb et al., 2011a; Song et al., 2011). Mitochondrial defects result in ROS accumulation, which further leads to apoptosis and cell death.

HD patients and brain mitochondria from transgenic mice expressing mHTT (Panov et al., 2002). Another study showed that mHTT interacts with the outer mitochondrial membrane and directly induces opening of the mPTP, which is accompanied by a significant release of cytochrome *c* (Choo et al., 2004). This release of cytochrome *c* has been shown to initiate apoptosis (Green and Reed, 1998). Addition of cyclosporin A, an inhibitor of the mPTP, prevented the release of cytochrome *c* (**Figure 2**). Moreover, a defect in calcium handling not only resulted in the opening of the mPTP but also caused higher levels of mtDNA damage in HD cells. The same effect was observed with elevated superoxide production, suggesting a new link between an imbalance in mitochondrial Ca^{2+} signaling and elevated oxidative DNA damage in HD (Wang et al., 2013). In addition, it was also shown that the first 17 amino acids and the polyQ repeat region of HTT, cause mitochondrial dysfunction in a calcium-homeostasis disrupted manner (Rockabrand et al., 2007). Furthermore, loss of mitochondrial integrity was observed during ageing and disease progression (Hughes and Gottschling, 2012; Szklarczyk et al., 2014), and the integrity of the mitochondrial cristae were found to be disrupted in HD, which was potentially caused by the oligomerization of OPA1, an optic atrophy protein (Hering et al., 2017). Overall, these results indicate that the imbalance in calcium homeostasis and mitochondrial dysfunction contribute to HD pathogenesis.

Mediators of mHTT-Mediated Mitochondrial Dysfunction

It has been hypothesized that the cytotoxicity mediated by polyQ expansion of mHTT is caused by altering the expression level of cellular factors (McCampbell et al., 2000; Schaffar et al., 2004). The tumor suppressor protein, p53, was found to interact with mHTT, and the mHTT-p53 interaction represses the transcription of genes regulated by p53 (Steffan et al., 2000). Furthermore, activation of p53 increased both mHTT mRNA and protein expression, thereby suggesting that p53 is a modulator of the processes involved in HD development (Feng et al., 2006). On the other hand, suppression of p53 reversed the mHTT-induced mitochondrial depolarization and cytotoxicity in HD cells (Bae et al., 2005), indicating that p53 plays an important role in mediating mitochondrial dysfunction caused by mHTT. Moreover, an interaction between mHTT and the mitochondrial protein import complex TIM23 was reported. This mHTT-TIM23 interaction causes a mitochondrial protein import defect and induces neuronal death (Yano et al., 2014).

Other studies also demonstrated that ROS production in HD is mediated by PGC-1α, a transcriptional co-regulator of

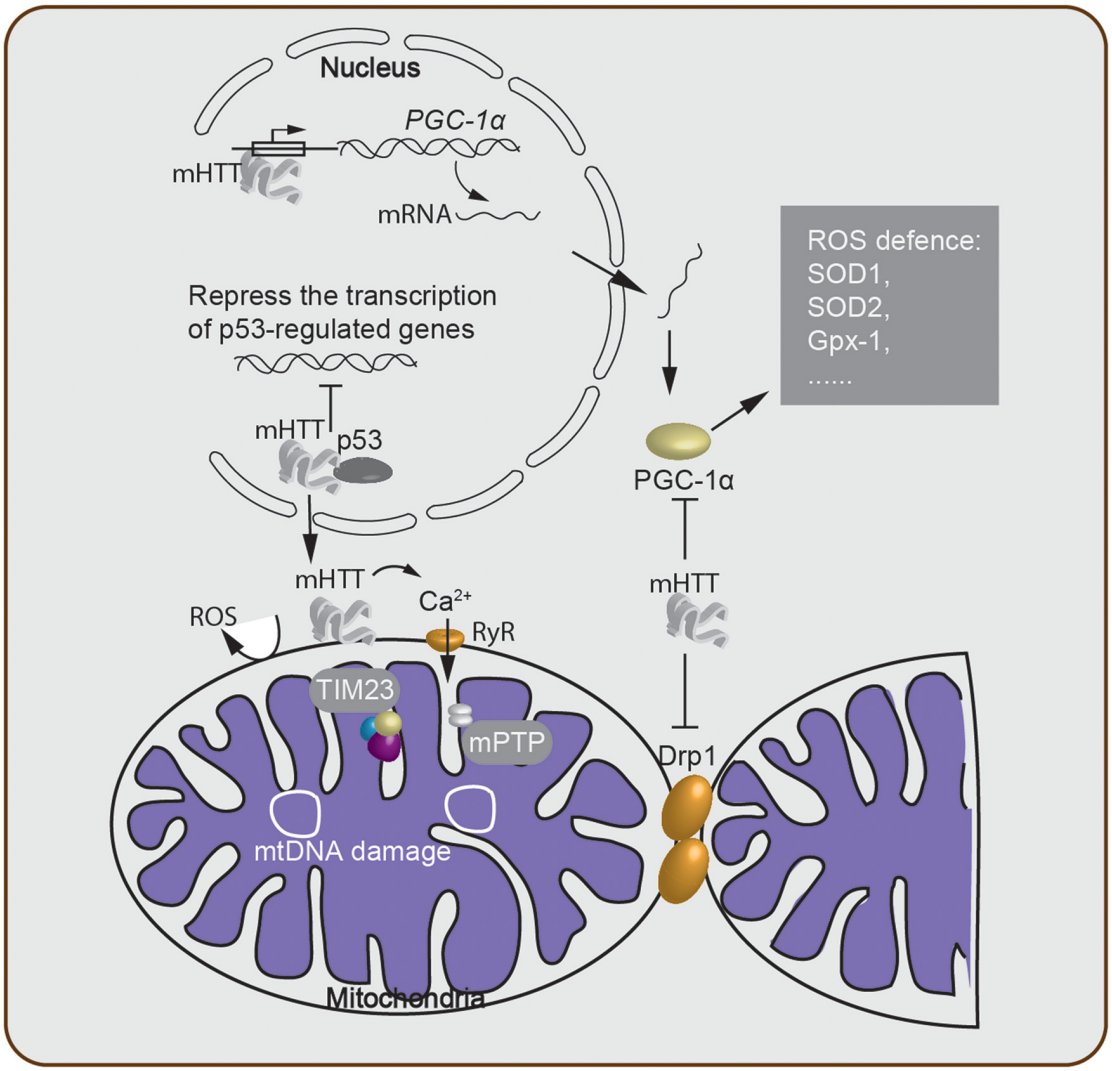

FIGURE 2 | Oxidative stress-associated cellular processes involved in Huntington's disease (HD) pathogenesis. mHTT acts within the nucleus and either suppresses transcription of critical genes and downregulates mitochondrial function or directly alters the expression level of mitochondrial biogenesis-associated proteins such as PGC-1α. This alteration of the PGC-1α protein level then further regulates the ROS defense system in the cytosol. The mHTT-mitochondria interaction generates ROS through many processes, including Ca^{2+} leakage through the ryanodine receptor (RyR). Failure of Ca^{2+} homeostasis triggers the opening of the mitochondrial permeability transition pore (mPTP), which disturbs the ATP level and enables release of cytochrome *c*. Meanwhile, mitochondrial protein import is impaired due to the binding of mHTT to the TIM23 complex. mtDNA damage and depletion within the mitochondria elevate ROS production. Lastly, cytosolic mHTT inhibits mitochondrial fission–fusion by interacting with Drp1.

mitochondrial biogenesis, metabolism, and antioxidant defenses (Johri et al., 2013). mHTT caused an increase in PGC-1α-mediated oxidative stress via multiple mechanisms (**Figure 2**): (1) mHTT binds to the promoter sequences of PGC-1α and reduces the transcription level of PGC-1α (Chaturvedi et al., 2012). (2) mHTT binds directly to PGC-1α, suppresses the activity of PGC-1α, which in turn, reduces the expression level of downstream targets of PGC-1α, including mitochondrial uncoupling proteins and antioxidants such as copper/zinc superoxide dismutase (SOD1), manganese SOD (SOD2), and glutathione peroxidase (Gpx-1; St-Pierre et al., 2006). SODs are major antioxidant enzymes that scavenge O_{2-} radicals in the antioxidant system (Gandhi and Abramov, 2012; Kim et al., 2015). Thus, the lower expression level of SOD1, the more SOD2 and Gpx-1 contribute to the mitochondrial dysfunction, which enhances the pathology of HD. (3) mHTT interacts with Drp1 (Shirendeb et al., 2011b), thereby interfering with the mitochondrial dynamics by disrupting the balance of the mitochondrial fission–fusion processes (Shirendeb et al., 2011a; Song et al., 2011). Indeed, overexpression of PGC-1α rescued HD neurodegeneration partially by attenuating oxidative stress (Tsunemi et al., 2012). A recent study revealed that a variant of PGC-1α is associated with an earlier age onset of HD (Weydt et al., 2014). Furthermore, mice lacking PGC-1α show

mitochondrial function impairment and HD features such as uncontrolled movement and striatal degeneration (Lin et al., 2004). Taken together, this evidence indicates that PGC-1α is a key factor in mediating neuronal death through oxidative stress induced by mHTT.

mHTT-INDUCED OXIDATIVE STRESS AND POTENTIAL THERAPEUTIC TARGETS FOR HD

Multiple pathways that contribute to oxidative stress in HD have been described, including elevated NOX activity, oxidation of mitochondrial enzymes, the disturbance of active vitamin B6 and the activation of the antioxidant defense system (**Table 1**).

NOX, which produces ROS, has been used as an indicator for the ROS level *in vivo*. Researchers detected higher levels of brain NOX activity in post mortem HD cortex and striatum than in controls, particularly, NOX2, which localizes at plasma membrane lipid rafts, directly responsible for ROS level and survival in HD mice (Valencia et al., 2012). Conversely, NOX activity, ROS level and neuronal cell death were significantly reduced when cells were treated with NOX inhibitors (Valencia et al., 2012).

Oxidative modification of proteins is a main aspect of ROS-mediated cytotoxicity *in vivo*, which encouraged researchers to explore the unique oxidative proteins in HD individuals. Indeed, by comparing HD and control samples, Sorolla et al. (2010) identified 13 proteins that were oxidatively modified, including mitochondrial enzymes. Modification of these enzymes decreased their catalytic activity, consistent with the observation of energy deficiency in HD (Sorolla et al., 2010). More importantly, oxidation of pyridoxal kinase and antiquitin 1 decreased the availability of pyridoxal 5-phosphate, the active form of vitamin B6, leading to neurotransmitter disturbances, which is critical in HD pathology (Sorolla et al., 2010). Another study that focused on the proteomic levels of post mortem human brain samples obtained from striatum and cortex identified a significant increase in the level of antioxidant defense proteins, including peroxiredoxins (Prxs) 1, 2 and 6 and Gpx-1 and 6 in individuals with HD (Sorolla et al., 2008). Energy metabolism defects have been consistently proposed to contribute to the pathogenesis of HD (Jenkins et al., 1993; Brouillet et al., 1995; Gu et al., 1996). These findings suggest that oxidative stress and damage to specific macromolecules are increased in HD patients and that the antioxidant defense system alleviates oxidative stress and damage during the HD progression.

Thus far, the connection between oxidative stress and HD is not yet fully understood. It has been suggested that mHTT induces cytotoxicity through the kynurenine pathway (Giorgini et al., 2005; Stoy et al., 2005). In this respect, it has been shown that inhibition of the kynurenine pathway reduces the production of quinolinic acid (QUIN), ROS level, and cytotoxicity induced by mHTT (Giorgini et al., 2005). QUIN triggers striatal neuronal death via a cascade of events including oxidative stress, which is closely related to mitochondrial dysfunction. Recently, Jamwal et al. (2015) observed that spermidine, a molecule with free radical scavenging and anti-inflammatory properties, significantly attenuated the pathological alterations caused by QUIN treatment in rats (Jamwal et al., 2015). Similarly, sulforaphane has been proven to be effective in preventing mitochondrial dysfunction induced by QUIN in the rat striatum (Luis-García et al., 2016). Therefore, it is well worth examining the potential neuroprotective role of spermidine and sulforaphane in HD.

Furthermore, expression of mHTT triggered a decrease in the expression of the antioxidant protein Prx1. The same study also showed that treatment by dimercaptopropanol, a thiol-based antioxidant, rescued the cytotoxicity induced by mHTT and the expression level of Prx1 (Pitts et al., 2012). These results suggest that mHTT can exert its toxic effect by disturbing the ROS clearance system and document the potential of thiol-based antioxidants as drugs for HD treatment. However, some of the antioxidants do not seem to attenuate HD symptoms, which is likely because HD-induced ROS damage mainly occurs at the mitochondria. Indeed, inducing a synthetic mitochondria-specific antioxidant XJB-5-131, which targets mitochondria, remarkably suppressed oxidative mtDNA damage, restored the copy number of mtDNA, and alleviated the pathophysiology in HD animals (Xun et al., 2012; Polyzos et al., 2016). In addition, oxidation of cysteines within mHTT promoted the formation of soluble HTT oligomers, which are mediators of HD pathogenesis, and thereby interfered with the clearance of soluble mHTT, leading to enhanced mHTT cytotoxicity (Fox et al., 2011).

YEAST MODELS PROVIDE INSIGHTS INTO OXIDATIVE STRESS IN HD

Yeast lacks an HTT ortholog, and thus, its value for studying cellular communication is limited due to the absence of axonal and synaptic structures within a yeast bud (Khurana and Lindquist, 2010), as well as the lack of neural transmitters and the corresponding receptors (Khurana and Lindquist, 2010). As such, the suitability of the yeast model should be carefully taken into consideration before application to the study of HD. However, expression of mHTT fragment in yeast reproduces two major features of HD (i.e., protein aggregation and mHTT fragment-induced cytotoxicity). Moreover, many findings in yeast models were confirmed in higher model systems, such as mammalian cell lines, *C. elegans*, mice and even human patients. The insights gained from the studies in yeast have contributed greatly to our understanding of the pathogenesis of HD (Winderickx et al., 2008; Khurana and Lindquist, 2010; Mason and Giorgini, 2011; Fruhmann et al., 2017). As most mediators and pathways of energy metabolism are highly conserved in eukaryotes, it is not surprising to see that mHTT fragment induces oxidative stress in yeast. Here, we discuss the oxidative stress response of mHTT fragment and related findings in yeast models.

A toxic version of the mHTT fragment expression system lacking the proline-rich region in yeast established by the lab of Sherman and Lindquist (Krobitsch and Lindquist, 2000;

TABLE 1 | Major published oxidative stress-associated processes and mediators of Huntington's disease (HD) pathogenesis.

Processes and mediators	Model system	Type of mHTT	Description and consequence	References
mtDNA damage	Mouse; Striatal immortalized neuronal cell	Human HTT exon1: 115–150Q; 111Q	mHTT increases mitochondria-generated ROS and decreases mtDNA abundance.	Yang et al. (2008) and Siddiqui et al. (2012)
mtDNA depletion	Mouse and human HD patient	Human HTT exon1: 144Q; ∼160Q	mHTT results in a lower copy number of mtDNA and increases the vulnerability of the striatum.	Petersen et al. (2014) and Hering et al. (2015)
Ca^{2+} imbalance	Rat cortical neuron	Truncated N-terminal HTT: 150Q	mHTT induces Ca^{2+} leakage through the Ca^{2+} channel RyR, further resulting in opening of the mPTP, which contributes to mitochondrial oxidative stress.	Suzuki et al. (2012)
p53	HEK293 cell; Mouse and human HD patient	Human HTT exon1$^{+/-}$ proline-rich region: 103Q; N-terminal HTT: 86Q	p53 promotes expression of mHTT and mediates mHTT-induced mitochondrial dysfunction; the mHTT-p53 interaction suppresses transcription of p53-regulated genes.	Steffan et al. (2000) and Bae et al. (2005)
PGC-1α	Mouse and striatal cell culture	Human HTT exon1 and Mouse HTT: 111Q	mHTT reduces PGC-1α transcription and activity and suppresses downstream targets of PGC-1α, such as ROS defense factors.	Chaturvedi et al. (2012)
Drp1	Human HD patient; mouse; rat cortical neuron	Human mutant HTT; full-length human mHTT: 97Q; Human HTT exon1: 46 and 97Q	mHTT interacts with Drp1, disrupting the balance of the mitochondrial fission–fusion processes.	Shirendeb et al. (2011a,b) and Song et al. (2011)
NOX	Human HD patient and mouse	Mouse HTT: 140Q	Higher levels of brain NOX activity are observed in HD, whereas NOX inhibitors reduce the ROS level and neuronal death.	Valencia et al. (2012)
Mitochondrial enzymes	Human HD patient and mouse	Human HTT exon1: 94Q	Mitochondrial enzymes are oxidatively modified, with decreased catalytic activity and energy deficiency in individuals with HD.	Sorolla et al. (2010)
Vitamin B6	Human HD patient and mouse	Human HTT exon1: 94Q	Oxidation of pyridoxal kinase and antiquitin 1 decreased the availability of active vitamin B6, leading to the disturbances of neurotransmitters.	Sorolla et al. (2010)
Kynurenine pathway	Yeast	Human HTT exon1 lacking proline-rich region: 103Q	mHTT induces cytotoxicity through the kynurenine pathway and its intermediate product QUIN, which triggers striatal neuronal death via a cascade of events, such as oxidative stress.	Giorgini et al. (2005), Stoy et al. (2005) and Jamwal et al. (2015)
Prx1	PC12 cell	Human HTT exon1: 103Q	mHTT affects expression of the antioxidant protein Prx1, disturbing the ROS clearance system.	Pitts et al. (2012)
GPxs	Yeast	Human HTT exon1 lacking proline-rich region: 103Q	These antioxidant enzymes protect against ROS production and suppress mHTT toxicity.	Mason et al. (2013)
RQC	Yeast	Human HTT exon1 precence/absence of proline-rich region: 103Q	RQC system regulates mHTT compartmentalization and nucleocytoplasmic translocation that is associated with polyQ cytotoxicity.	Yang et al. (2016) and Zheng et al. (2017)

Meriin et al., 2002; Willingham et al., 2003) revealed numerous molecular insights into mHTT fragment-induced toxicity, including findings regard to oxidative stress. In this yeast model, ROS accumulation was enhanced, and abnormal mitochondrial morphology and distribution in cells expressing mHTT fragment were observed. These findings revealed that the polyQ-mitochondria interaction interferes with mitochondrial function and increases ROS production (Solans et al., 2006). Screening the yeast deletion collection for suppressors of mHTT fragment-induced toxicity revealed that kynurenine 3-monooxygenase (Bna4) deficiency rescues cell viability (Giorgini et al., 2005). Metabolites of the kynurenine pathway have been shown to induce oxidative stress and neurological disorders (Pawlak et al., 2009; Parasram, 2018), which is associated with HD pathophysiology (Stoy et al., 2005). Another suppressor screening with gene overexpression, instead of loss-of-function, identified GPxs as potent suppressors of mHTT fragment toxicity (Mason et al., 2013). GPx is an antioxidant enzyme that protects against ROS, thus, enhancing the GPxs capacity can alleviate mHTT fragment toxicity (**Table 1**). Treatment with ebselen, which mimics the antioxidant effects of GPx, showed a strong protective effect on HD model organisms (Mason et al., 2013). These findings shed light on the clinical potential of ebselen and other antioxidants for HD therapy. Another study in yeast also demonstrated a role for Sir2 in protecting cells from ROS. Sir2 levels increased dramatically when yeast cells suffer from oxidative stress from mHTT fragment expression or the environment. However, enhancing

Sir2 expression by a Sir2 activator decreased mHTT fragment aggregation and the mHTT fragment-induced stress. On the other hand, SIR2 knock-out cells showed significant oxidative stress even in the early exponential phase (Sorolla et al., 2011). Overexpression of Hap4, a protein that regulates many genes encoding mitochondrial proteins in yeast, prevented respiratory defects and ameliorated polyQ expansion-induced cytotoxicity (Ocampo et al., 2010). Together, these studies demonstrate that mHTT fragment induces oxidative stress in yeast and that preventing such oxidative stress can be a good strategy to handle mHTT fragment cytotoxicity.

Recently, a technique that combines automated yeast genetics and high-content microscopy has been applied to study mHTT fragment localization, protein-protein interaction and aggregate morphology in yeast. Taking advantage of this powerful screening approach, Yang et al identified that both the ribosome quality control (RQC) system and Hsf1 regulate the compartmentalization of mHTT fragment containing the proline-rich region (Yang et al., 2016). A follow-up study by Zheng et al. (2017) demonstrated that the RQC system indeed regulates the nucleocytoplasmic translocation of mHTT exon-1 lacking the proline-rich region and that a defective RQC system leads to enhanced cytotoxicity of mHTT fragment. Interestingly, it has been shown that oxidative stress can cause damage to rRNAs inside the ribosome, and oxidized rRNA inhibits protein synthesis in the ribosome (Willi et al., 2018). In this respect, mHTT-induced oxidative stress might be a driving force for the impairment of RQC system.

CONCLUDING REMARKS

More than two decades have passed since the first identification of the *HTT* gene, and mutation of this gene is responsible for HD pathogenesis. The mechanisms responsible for the development of the single gene mutation that induce this neurodegenerative disease are not yet fully understood, and to date, no effective therapeutic target has been developed. The major findings point towards a close relationship between HD pathogenesis and oxidative stress.

Although multiple factors are involved in regulating mHTT-mediated oxidative stress, there are indications that mitochondria play a key role. Both mtDNA damage and mtDNA depletion have been detected upon expression of mHTT (Yang et al., 2008; Napoli et al., 2013). Given the core role of mitochondria in respiration and energy production, mtDNA damage or depletion leads to increased levels of oxidative stress. Moreover, a defect in mitochondrial calcium handling was observed in HD patients (Panov et al., 2002). Failure of keeping a mitochondrial calcium balance triggers the opening of the mPTP and the subsequent events lead to the final stage of cell death. The connection between oxidative stress and HD is also supported by the interaction of mHTT with p53 or PGC-1α, which modulates the activity of mitochondria. NOX activity, oxidation of mitochondrial enzymes, the disturbance of active vitamin B6 and the activation of antioxidant defense system are also implicated in sensing oxidative stress from mHTT.

Increased oxidative stress is detected during HD pathogenesis, and the published literatures reviewed here favors the idea that expression of mHTT is the primary cause of HD and that mHTT induces cellular dysfunction via multiple pathways, including oxidative stress. In this aspect, oxidative stress is likely a downstream consequence of HD pathogenesis. Moreover, other neurodegenerative disorders such as Alzheimer's disease and Parkinson's disease are controlled by multiple genes that are associated with oxidative stress (Gandhi and Abramov, 2012; Kim et al., 2015).

Despite the intensive studies on HD pathogenesis and evidence showing that oxidative stress occurs during this process, the major pathways and the sequence of oxidative stress-associated events in HD pathogenesis are still not known. Future studies that strengthen the understanding of oxidative stress in HD pathogenesis will provide insights into drug development and identification of therapeutic targets, for instance, clarifying the connections among the known pathways involved in mHTT-induced oxidative stress, identifying oxidative stress associated key factors in HD pathogenesis, and determining the major aspects as well as the order of pathologic events that contribute to HD development. Overall, this review article provides an overview of the current studies linking oxidative stress and HD development.

AUTHOR CONTRIBUTIONS

BL, VF and JW conceived and outlined the article and JZ wrote the manuscript with the help from VF, JW and BL.

FUNDING

This work was supported by the Fund for Scientific Research Flanders (FWO-Vlaanderen to JW) and an FWO postdoctoral fellowship (to VF). This work was also supported by grants from the Swedish Cancer Society (Cancerfonden, CAN 2012/601, CAN 2015/406 and CAN 2017/643, to BL), the Swedish Natural Research Council (VR 2011-5923 and VR 2015-04984, to BL), and the Carl Trygger Foundation (Carl Tryggers Stiftelse för Vetenskaplig Forskning, CTS 14: 295, to BL). Additional support came from the People Programme (Marie Curie Actions) of the European Union's Seventh Framework Programme (FP7/2007–2013) under REA grant agreement n° 608743.

REFERENCES

Bae, B.-I., Xu, H., Igarashi, S., Fujimuro, M., Agrawal, N., Taya, Y., et al. (2005). p53 mediates cellular dysfunction and behavioral abnormalities in Huntington's disease. *Neuron* 47, 29–41. doi: 10.1016/j.neuron.2005.06.005

Bañez-Coronel, M., Ayhan, F., Tarabochia, A. D., Zu, T., Perez, B. A., Tusi, S. K., et al. (2015). RAN translation in Huntington disease. *Neuron* 88, 667–677. doi: 10.1016/j.neuron.2015.10.038

Brouillet, E., Hantraye, P., Ferrante, R. J., Dolan, R., Leroy-willig, A., Kowall, N. W., et al. (1995). Chronic mitochondrial energy impairment

produces selective striatal degeneration and abnormal choreiform movements in primates. *Proc. Natl. Acad. Sci. U S A* 92, 7105–7109. doi: 10.1073/pnas.92.15.7105

Brustovetsky, N. (2016). Mutant huntingtin and elusive defects in oxidative metabolism and mitochondrial calcium handling. *Mol Neurobiol.* 53, 2944–2953. doi: 10.1007/s12035-015-9188-0

Carmo, C., Naia, L., Lopes, C., and Rego, A. C. (2018). Mitochondrial dysfunction in Huntington's disease. *Adv. Exp. Med. Biol.* 1049, 59–83. doi: 10.1007/978-3-319-71779-1_3

Chance, B., Sies, H., and Boveris, A. (1979). Hydroperoxide metabolism in mammalian organs. *Physiol. Rev.* 59, 527–605. doi: 10.1152/physrev.1979.59.3.527

Chaturvedi, R. K., Hennessey, T., Johri, A., Tiwari, S. K., Mishra, D., Agarwal, S., et al. (2012). Transducer of regulated CREB-binding proteins (TORCs) transcription and function is impaired in Huntington's disease. *Hum. Mol. Genet.* 21, 3474–3488. doi: 10.1093/hmg/dds178

Choo, Y. S., Johnson, G. V., MacDonald, M., Detloff, P. J., and Lesort, M. (2004). Mutant huntingtin directly increases susceptibility of mitochondria to the calcium-induced permeability transition and cytochrome c release. *Hum. Mol. Genet.* 13, 1407–1420. doi: 10.1093/hmg/ddh162

Costa, V., and Scorrano, L. (2012). Shaping the role of mitochondria in the pathogenesis of Huntington's disease. *EMBO J.* 31, 1853–1864. doi: 10.1038/emboj.2012.65

Damiano, M., Galvan, L., Déglon, N., and Brouillet, E. (2010). Mitochondria in Huntington's disease. *Biochim. Biophys. Acta* 1802, 52–61. doi: 10.1016/j.bbadis.2009.07.012

Dehay, B., and Bertolotti, A. (2006). Critical role of the proline-rich region in Huntingtin for aggregation and cytotoxicity in yeast. *J. Biol. Chem.* 281, 35608–35615. doi: 10.1074/jbc.m605558200

DiFiglia, M., Sapp, E., Chase, K. O., Davies, S. W., Bates, G. P., Vonsattel, J. P., et al. (1997). Aggregation of huntingtin in neuronal intranuclear inclusions and dystrophic neurites in brain. *Science* 277, 1990–1993. doi: 10.1126/science.277.5334.1990

Duennwald, M. L., Jagadish, S., Giorgini, F., Muchowski, P. J., and Lindquist, S. (2006). A network of protein interactions determines polyglutamine toxicity. *Proc. Natl. Acad. Sci. U S A.* 103, 11051–11056. doi: 10.1073/pnas.0604548103

Feng, Z., Jin, S., Zupnick, A., Hoh, J., De Stanchina, E., Lowe, S., et al. (2006). p53 tumor suppressor protein regulates the levels of huntingtin gene expression. *Oncogene* 25, 1–7. doi: 10.1038/sj.onc.1209021

Fox, J. H., Connor, T., Stiles, M., Kama, J., Lu, Z., Dorsey, K., et al. (2011). Cysteine oxidation within N-terminal mutant huntingtin promotes oligomerization and delays clearance of soluble protein. *J. Biol. Chem.* 286, 18320–18330. doi: 10.1074/jbc.m110.199448

Fruhmann, G., Seynnaeve, D., Zheng, J., Ven, K., Molenberghs, S., Wilms, T., et al. (2017). Yeast buddies helping to unravel the complexity of neurodegenerative disorders. *Mech. Ageing. Dev.* 161, 288–305. doi: 10.1016/j.mad.2016.05.002

Gandhi, S., and Abramov, A. Y. (2012). Mechanism of oxidative stress in neurodegeneration. *Oxid. Med. Cell. Longev.* 2012, 1–11. doi: 10.1155/2012/428010

Giacomello, M., Drago, I., Pizzo, P., and Pozzan, T. (2007). Mitochondrial Ca^{2+} as a key regulator of cell life and death. *Cell Death Differ.* 14, 1267–1274. doi: 10.1038/sj.cdd.4402147

Giorgini, F., Guidetti, P., Nguyen, Q., Bennett, S. C., and Muchowski, P. J. (2005). A genomic screen in yeast implicates kynurenine 3-monooxygenase as a therapeutic target for Huntington disease. *Nat. Genet.* 37, 526–531. doi: 10.1038/ng1542

Green, D. R., and Reed, J. C. (1998). Mitochondria and apoptosis. *Science* 281, 1309–1312. doi: 10.1126/science.281.5381.1309

Gu, M., Gashc, M. T., Mann, V. M., Javoy-Agid, F., Cooper, J. M., and Schapira, A. H. V. (1996). Mitochondrial defect in Huntington's disease caudate nucleus. *Annals of Neurol.* 39, 385–389. doi: 10.1002/ana.410390317

Guedes-Dias, P., Pinho, B. R., Soares, T. R., De, P. J., Duchen, M. R., and Oliveira, J. M. (2016). Mitochondrial dynamics and quality control in Huntington's disease. *Neurobiol. Dis.* 90, 51–57. doi: 10.1016/j.nbd.2015.09.008

Halestrap, A. P. (2006). Calcium, mitochondria and reperfusion injury: a pore way to die. *Biochem. Soc. Trans.* 34, 232–237. doi: 10.1042/bst20060232

Hering, T., Birth, N., Taanman, J.-W., and Orth, M. (2015). Selective striatal mtDNA depletion in end-stage Huntington's disease R6/2 mice. *Exp. Neurol.* 266, 22–29. doi: 10.1016/j.expneurol.2015.02.004

Hering, T., Kojer, K., Birth, N., Hallitsch, J., Taanman, J.-W., and Orth, M. (2017). Mitochondrial cristae remodelling is associated with disrupted OPA1 oligomerisation in the Huntington's disease R6/2 fragment model. *Exp. Neurol.* 288, 167–175. doi: 10.1016/j.expneurol.2016.10.017

Hughes, A. L., and Gottschling, D. E. (2012). An early-age increase in vacuolar pH limits mitochondrial function and lifespan in yeast. *Nature* 492, 261–265. doi: 10.1038/nature11654

Jain, A., and Vale, R. D. (2017). RNA phase transitions in repeat expansion disorders. *Nature* 546, 243–247. doi: 10.1038/nature22386

Jamwal, S., Singh, S., Kaur, N., and Kumar, P. (2015). Protective effect of spermidine against excitotoxic neuronal death induced by quinolinic acid in rats: possible neurotransmitters and neuroinflammatory mechanism. *Neurotox. Res.* 28, 171–184. doi: 10.1007/s12640-015-9535-y

Jenkins, B. G., Koroshetz, W. J., Beal, M. F., and Rosen, B. R. (1993). Evidence for impairment of energy metabolism *in vivo* in Huntington's disease using localized 1H NMR spectroscopy. *Neurology* 43, 2689–2695. doi: 10.1212/wnl.43.12.2689

Johri, A., Chandra, A., and Beal, M. F. (2013). PGC-1α, mitochondrial dysfunction and Huntington's disease. *Free Radic. Biol. Med.* 62, 37–46. doi: 10.1016/j.freeradbiomed.2013.04.016

Khurana, V., and Lindquist, S. (2010). Modelling neurodegeneration in *Saccharomyces cerevisiae*: why cook with baker's yeast? *Nat. Rev. Neurosci.* 11, 436–449. doi: 10.1038/nrn2809

Kim, G. H., Kim, J. E., Rhie, S. J., and Yoon, S. (2015). The role of oxidative stress in neurodegenerative diseases. *Exp. Neurobiol.* 24, 325–340. doi: 10.5607/en.2015.24.4.325

Krieger, C., and Duchen, M. R. (2002). Mitochondria, Ca^{2+} and neurodegenerative disease. *Eur. J. Pharmacol.* 447, 177–188. doi: 10.1016/S0014-2999(02)01842-3

Krobitsch, S., and Lindquist, S. (2000). Aggregation of huntingtin in yeast varies with the length of the polyglutamine expansion and the expression of chaperone proteins. *Proc. Natl. Acad. Sci. U S A* 97, 1589–1594. doi: 10.1073/pnas.97.4.1589

Langbehn, D. R., Brinkman, R. R., Falush, D., Paulsen, J. S., and Hayden, M. R. (2004). A new model for prediction of the age of onset and penetrance for Huntington's disease based on CAG length. *Clin. Genet.* 65, 267–277. doi: 10.1111/j.1399-0004.2004.00241.x

Lin, J., Wu, P.-H., Tarr, P. T., Lindenberg, K. S., St-Pierre, J., Zhang, C.-Y., et al. (2004). Defects in adaptive energy metabolism with CNS-linked hyperactivity in *PGC-1α* null mice. *Cell* 119, 121–135. doi: 10.1016/j.cell.2004.09.013

Lin, M. T., and Beal, M. F. (2006). Mitochondrial dysfunction and oxidative stress in neurodegenerative diseases. *Nature* 443, 787–795. doi: 10.1038/nature05292

Liu, C.-S., Cheng, W.-L., Kuo, S.-J., Li, J.-Y., Soong, B.-W., and Wei, Y.-H. (2008). Depletion of mitochondrial DNA in leukocytes of patients with poly-Q diseases. *J. Neurol. Sci.* 264, 18–21. doi: 10.1016/j.jns.2007.07.016

Luis-García, E. R., Limón-Pacheco, J. H., Serrano-García, N., Hernández-Pérez, A. D., Pedraza-Chaverri, J., and Orozco-Ibarra, M. (2016). Sulforaphane prevents quinolinic acid-induced mitochondrial dysfunction in rat striatum. *J. Biochem. Mol. Toxicol.* 31, 1–7. doi: 10.1002/jbt.21837

Lunkes, A., Lindenberg, K. S., Ben-Haïem, L., Weber, C., Devys, D., Landwehrmeyer, G. B., et al. (2002). Proteases acting on mutant huntingtin generate cleaved products that differentially build up cytoplasmic and nuclear inclusions. *Mol. Cell* 10, 259–269. doi: 10.1016/s1097-2765(02)00602-0

MacDonald, M. E., Ambrose, C. M., Duyao, M. P., Myers, R. H., Lin, C., Srinidhi, L., et al. (1993). A novel gene containing a trinucleotide repeat that is expanded and unstable on Huntington's disease chromosomes. *Cell* 72, 971–983. doi: 10.1016/0092-8674(93)90585-e

Martí, E. (2016). RNA toxicity induced by expanded CAG repeats in Huntington's disease. *Brain Pathol.* 26, 779–786. doi: 10.1111/bpa.12427

Mason, R. P., and Giorgini, F. (2011). Modeling Huntington disease in yeast: perspectives and future directions. *Prion* 5, 269–276. doi: 10.4161/pri.18005

Mason, R. P., Casu, M., Butler, N., Breda, C., Campesan, S., Clapp, J., et al. (2013). Glutathione peroxidase activity is neuroprotective in models of Huntington's disease. *Nat. Genet.* 45, 1249–1254. doi: 10.1038/ng.2732

McCampbell, A., Taylor, J. P., Taye, A. A., Robitschek, J., Li, M., Walcott, J., et al. (2000). CREB-binding protein sequestration by expanded polyglutamine. *Hum. Mol. Genet.* 9, 2197–2202. doi: 10.1093/hmg/9.14.2197

Meriin, A. B., Zhang, X., He, X., Newnam, G. P., Chernoff, Y. O., and Sherman, M. Y. (2002). Huntingtin toxicity in yeast model depends on polyglutamine aggregation mediated by a prion-like protein Rnq1. *J. Cell. Biol.* 157, 997–1004. doi: 10.1083/jcb.200112104

Napoli, E., Wong, S., Hung, C., Ross-Inta, C., Bomdica, P., and Giulivi, C. (2013). Defective mitochondrial disulfide relay system, altered mitochondrial morphology and function in Huntington's disease. *Hum. Mol. Genet.* 22, 989–1004. doi: 10.1093/hmg/dds503

Nicholls, D. G. (2005). Mitochondria and calcium signaling. *Cell Calcium* 38, 311–317. doi: 10.1016/j.ceca.2005.06.011

Nicholls, D. G., and Budd, S. L. (2000). Mitochondria and neuronal survival. *Physiol. Rev.* 80, 315–360. doi: 10.1152/physrev.2000.80.1.315

Ocampo, A., Zambrano, A., and Barrientos, A. (2010). Suppression of polyglutamine-induced cytotoxicity in saccharomyces cerevisiae by enhancement of mitochondrial biogenesis. *FASEB J.* 24, 1431–1441. doi: 10.1096/fj.09-148601

Panov, A. V., Gutekunst, C.-A., Leavitt, B. R., Hayden, M. R., Burke, J. R., Strittmatter, W. J., et al. (2002). Early mitochondrial calcium defects in Huntington's disease are a direct effect of polyglutamines. *Nat. Neurosci.* 5, 731–736. doi: 10.1038/nn884

Parasram, K. (2018). Phytochemical treatments target kynurenine pathway induced oxidative stress. *Redox Rep.* 23, 25–28. doi: 10.1080/13510002.2017.1343223

Pawlak, K., Domaniewski, T., Mysliwiec, M., and Pawlak, D. (2009). The kynurenines are associated with oxidative stress, inflammation and the prevalence of cardiovascular disease in patients with end-stage renal diseases. *Atherosclerosis* 204, 309–314. doi: 10.1016/j.atherosclerosis.2008.08.014

Penney, J. B. Jr, Vonsattel, J. P., Macdonald, M. E., Gusella, J. F., and Myers, R. H. (1997). CAG repeat number governs the development rate of pathology in Huntington's disease. *Ann. Neurol.* 41, 689–692. doi: 10.1002/ana.410410521

Petersen, M. H., Budtz-Jørgensen, E., Sørensen, S. A., Nielsen, J. E., Hjermind, L. E., Vinther-Jensen, T., et al. (2014). Reduction in mitochondrial DNA copy number in peripheral leukocytes after onset of Huntington's disease. *Mitochondrion* 17, 14–21. doi: 10.1016/j.mito.2014.05.001

Pitts, A., Dailey, K., Newington, J. T., Chien, A., Arseneault, R., Cann, T., et al. (2012). Dithiol-based compounds maintain expression of antioxidant protein peroxiredoxin 1 that counteracts toxicity of mutant huntingtin. *J. Biol Chem.* 287, 22717–22729. doi: 10.1074/jbc.m111.334565

Polidori, M. C., Mecocci, P., Browne, S. E., Senin, U., and Beal, M. F. (1999). Oxidative damage to mitochondrial DNA in Huntington's disease parietal cortex. *Neurosci. Lett.* 272, 53–56. doi: 10.1016/s0304-3940(99)00578-9

Polyzos, A., Holt, A., Brown, C., Cosme, C., Wipf, P., Gomezmarin, A., et al. (2016). Mitochondrial targeting of XJB-5-131 attenuates or improves pathophysiology in HdhQ150 animals with well-developed disease phenotypes. *Hum. Mol. Genet.* 25, 1792–1802. doi: 10.1093/hmg/ddw051

Quintanilla, R. A., and Johnson, G. V. (2009). Role of mitochondrial dysfunction in the pathogenesis of Huntington's disease. *Brain. Res Bull.* 80, 242–247. doi: 10.1016/j.brainresbull.2009.07.010

Rasola, A., Sciacovelli, M., Pantic, B., and Bernardi, P. (2010). Signal transduction to the permeability transition pore. *FEBS Lett.* 584, 1989–1996. doi: 10.1016/j.febslet.2010.02.022

Rockabrand, E., Slepko, N., Pantalone, A., Nukala, V. N., Kazantsev, A., Marsh, J. L., et al. (2007). The first 17 amino acids of Huntingtin modulate its sub-cellular localization, aggregation and effects on calcium homeostasis. *Hum. Mol. Genet.* 16, 61–77. doi: 10.1093/hmg/ddl440

Sabharwal, S. S., and Schumacker, P. T. (2014). Mitochondrial ROS in cancer: initiators, amplifiers or an Achilles' heel? *Nat. Rev. Cancer* 14, 709–721. doi: 10.1038/nrc3803

Schaffar, G., Breuer, P., Boteva, R., Behrends, C., Tzvetkov, N., Strippel, N., et al. (2004). Cellular toxicity of polyglutamine expansion proteins: mechanism of transcription factor deactivation. *Mol. Cell* 15, 95–105. doi: 10.1016/j.molcel.2004.06.029

Shirendeb, U., Reddy, A. P., Manczak, M., Calkins, M. J., Mao, P., Tagle, D. A., et al. (2011a). Abnormal mitochondrial dynamics, mitochondrial loss and mutant huntingtin oligomers in Huntington's disease: implications for selective neuronal damage. *Hum. Mol. Genet.* 20, 1438–1455. doi: 10.1093/hmg/ddr024

Shirendeb, U. P., Calkins, M. J., Manczak, M., Anekonda, V., Dufour, B., McBride, J. L., et al. (2011b). Mutant huntingtin's interaction with mitochondrial protein Drp1 impairs mitochondrial biogenesis and causes defective axonal transport and synaptic degeneration in Huntington's disease. *Hum. Mol. Genet.* 21, 406–420. doi: 10.1093/hmg/ddr475

Siddiqui, A., Rivera-Sánchez, S., Castro, M. d. R., Acevedo-Torres, K., Rane, A., Torres-Ramos, C. A., et al. (2012). Mitochondrial DNA damage is associated with reduced mitochondrial bioenergetics in Huntington's disease. *Free Radic. Biol. Med.* 53, 1478–1488. doi: 10.1016/j.freeradbiomed.2012.06.008

Sies, H. (1991). Oxidative stress: from basic research to clinical application. *Am. J. Med.* 91, S31–S38. doi: 10.1016/0002-9343(91)90281-2

Solans, A., Zambrano, A., Rodríguez, M., and Barrientos, A. (2006). Cytotoxicity of a mutant Huntingtin fragment in yeast involves early alterations in mitochondrial OXPHOS complexes II and III. *Hum. Mol. Genet.* 15, 3063–3081. doi: 10.1093/hmg/ddl248

Song, W., Chen, J., Petrilli, A., Liot, G., Klinglmayr, E., Zhou, Y., et al. (2011). Mutant huntingtin binds the mitochondrial fission GTPase dynamin-related protein-1 and increases its enzymatic activity. *Nat. Med.* 17, 377–382. doi: 10.1038/nm.2313

Sorolla, M. A., Nierga, C., Rodríguez-Colman, M. J., Reverter-Branchat, G., Arenas, A., Tamarit, J., et al. (2011). Sir2 is induced by oxidative stress in a yeast model of Huntington disease and its activation reduces protein aggregation. *Arch. Biochem. Biophys.* 510, 27–34. doi: 10.1016/j.abb.2011.04.002

Sorolla, M. A., Reverter-Branchat, G., Tamarit, J., Ferrer, I., Ros, J., and Cabiscol, E. (2008). Proteomic and oxidative stress analysis in human brain samples of Huntington disease. *Free Radic. Biol. Med.* 45, 667–678. doi: 10.1016/j.freeradbiomed.2008.05.014

Sorolla, M. A., Rodríguez-Colman, M. J., Tamarit, J., Ortega, Z., Lucas, J. J., Ferrer, I., et al. (2010). Protein oxidation in Huntington disease affects energy production and vitamin B6 metabolism. *Free Radic. Biol. Med.* 49, 612–621. doi: 10.1016/j.freeradbiomed.2010.05.016

Steffan, J. S., Kazantsev, A., Spasic-Boskovic, O., Greenwald, M., Zhu, Y.-Z., Gohler, H., et al. (2000). The Huntington's disease protein interacts with p53 and CREB-binding protein and represses transcription. *Proc. Natl. Acad. Sci. U S A* 97, 6763–6768. doi: 10.1073/pnas.100110097

Stoy, N., Mackay, G. M., Forrest, C. M., Christofides, J., Egerton, M., Stone, T. W., et al. (2005). Tryptophan metabolism and oxidative stress in patients with Huntington's disease. *J. Neurochem.* 93, 611–623. doi: 10.1111/j.1471-4159.2005.03070.x

St-Pierre, J., Drori, S., Uldry, M., Silvaggi, J. M., Rhee, J., Jäger, S., et al. (2006). Suppression of reactive oxygen species and neurodegeneration by the PGC-1 transcriptional coactivators. *Cell* 127, 397–408. doi: 10.1016/j.cell.2006.09.024

Suzuki, M., Nagai, Y., Wada, K., and Koike, T. (2012). Calcium leak through ryanodine receptor is involved in neuronal death induced by mutant huntingtin. *Biochem. Biophys. Res. Commun.* 429, 18–23. doi: 10.1016/j.bbrc.2012.10.107

Szklarczyk, R., Nooteboom, M., and Osiewacz, H. D. (2014). Control of mitochondrial integrity in ageing and disease. *Philos. Trans. R. Soc. Lond. B. Biol. Sci.* 369:20130439. doi: 10.1098/rstb.2013.0439

Tsunemi, T., Ashe, T. D., Morrison, B. E., Soriano, K. R., Au, J., Roque, R. A. V., et al. (2012). PGC-1α rescues Huntington's disease proteotoxicity by preventing oxidative stress and promoting TFEB function. *Sci. Transl. Med.* 4:142ra97. doi: 10.1126/scitranslmed.3003799

Valencia, A., Sapp, E., Kimm, J. S., McClory, H., Reeves, P. B., Alexander, J., et al. (2012). Elevated NADPH oxidase activity contributes to oxidative stress and cell death in Huntington's disease. *Hum. Mol. Genet.* 22, 1112–1131. doi: 10.1093/hmg/dds516

Wang, J.-Q., Chen, Q., Wang, X., Wang, Q.-C., Wang, Y., Cheng, H.-P., et al. (2013). Dysregulation of mitochondrial calcium signaling and superoxide flashes cause mitochondrial genomic DNA damage in Huntington disease. *J. Biol. Chem.* 288, 3070–3084. doi: 10.1074/jbc.m112.407726

Weidinger, A., and Kozlov, A. V. (2015). Biological activities of reactive oxygen and nitrogen species: oxidative stress *versus* signal transduction. *Biomolecules* 5, 472–484. doi: 10.3390/biom5020472

Weydt, P., Soyal, S. M., Landwehrmeyer, G. B., and Patsch, W. (2014). A single nucleotide polymorphism in the coding region of PGC-1α is a male-specific modifier of Huntington disease age-at-onset in a large European cohort. *BMC Neurol.* 14:1. doi: 10.1186/1471-2377-14-1

Willi, J., Küpfer, P., Evéquoz, D., Fernandez, G., Katz, A., Leumann, C., et al. (2018). Oxidative stress damages rRNA inside the ribosome and differentially affects the catalytic center. *Nucleic. Acids Res.* 46, 1945–1957. doi: 10.1093/nar/gkx1308

Willingham, S., Outeiro, T. F., DeVit, M. J., Lindquist, S. L., and Muchowski, P. J. (2003). Yeast genes that enhance the toxicity of a mutant huntingtin fragment or α-synuclein. *Science* 302, 1769–1772. doi: 10.1126/science.1090389

Winderickx, J., Delay, C., De Vos, A., Klinger, H., Pellens, K., Vanhelmont, T., et al. (2008). Protein folding diseases and neurodegeneration: lessons learned from yeast. *Biochim. Biophys. Acta* 1783, 1381–1395. doi: 10.1016/j.bbamcr.2008.01.020

Xun, Z., Rivera-Sánchez, S., Ayala-Peña, S., Lim, J., Budworth, H., Skoda, E. M., et al. (2012). Targeting of XJB-5-131 to mitochondria suppresses oxidative DNA damage and motor decline in a mouse model of Huntington's disease. *Cell Rep.* 2, 1137–1142. doi: 10.1016/j.celrep.2012.10.001

Yang, J., Hao, X., Cao, X., Liu, B., and Nyström, T. (2016). Spatial sequestration and detoxification of Huntingtin by the ribosome quality control complex. *Elife* 5:e11792. doi: 10.7554/elife.11792

Yang, J.-L., Weissman, L., Bohr, V. A., and Mattson, M. P. (2008). Mitochondrial DNA damage and repair in neurodegenerative disorders. *DNA Repair* 7, 1110–1120. doi: 10.1016/j.dnarep.2008.03.012

Yano, H., Baranov, S. V., Baranova, O. V., Kim, J., Pan, Y., Yablonska, S., et al. (2014). Inhibition of mitochondrial protein import by mutant huntingtin. *Nat. Neurosci.* 17, 822–831. doi: 10.1038/nn.3721

Yu, B. P. (1994). Cellular defenses against damage from reactive oxygen species. *Physiol. Rev.* 74, 139–162. doi: 10.1152/physrev.1994.74.1.139

Zheng, J., Yang, J., Choe, Y.-J., Hao, X., Cao, X., Zhao, Q., et al. (2017). Role of the ribosomal quality control machinery in nucleocytoplasmic translocation of polyQ-expanded Huntingtin exon-1. *Biochem. Biophys. Res. Commun.* 493, 708–717. doi: 10.1016/j.bbrc.2017.08.126

Conflict of Interest Statement: The authors declare that the research was conducted in the absence of any commercial or financial relationships that could be construed as a potential conflict of interest.

frontiers in Molecular Neuroscience

REVIEW
published: 30 October 2018
doi: 10.3389/fnmol.2018.00394

ALS Yeast Models—Past Success Stories and New Opportunities

*Sonja E. Di Gregorio and Martin L. Duennwald**

Schulich School of Medicine and Dentistry, Pathology and Laboratory Medicine, Western University, London, ON, Canada

In the past two decades, yeast models have delivered profound insights into basic mechanisms of protein misfolding and the dysfunction of key cellular pathways associated with amyotrophic lateral sclerosis (ALS). Expressing ALS-associated proteins, such as superoxide dismutase (SOD1), TAR DNA binding protein 43 (TDP-43) and Fused in sarcoma (FUS), in yeast recapitulates major hallmarks of ALS pathology, including protein aggregation, mislocalization and cellular toxicity. Results from yeast have consistently been recapitulated in other model systems and even specimens from human patients, thus providing evidence for the power and validity of ALS yeast models. Focusing on impaired ribonucleic acid (RNA) metabolism and protein misfolding and their cytotoxic consequences in ALS, we summarize exemplary discoveries that originated from work in yeast. We also propose previously unexplored experimental strategies to modernize ALS yeast models, which will help to decipher the basic pathomechanisms underlying ALS and thus, possibly contribute to finding a cure.

Keywords: ALS, yeast, protein misfolding, neurodegeneration, proteinopathy

OPEN ACCESS

Edited by:
Ralf J. Braun,
University of Bayreuth, Germany

Reviewed by:
Beidong Liu,
University of Gothenburg, Sweden
Aaron D. Gitler,
Stanford University, United States

***Correspondence:**
Martin L. Duennwald
martin.duennwald@schulich.uwo.ca

Received: *22 June 2018*
Accepted: *10 October 2018*
Published: *30 October 2018*

Citation:
Di Gregorio SE and Duennwald ML (2018) ALS Yeast Models—Past Success Stories and New Opportunities. Front. Mol. Neurosci. 11:394. doi: 10.3389/fnmol.2018.00394

ALS

Amyotrophic lateral sclerosis (ALS) is a heterogeneous neurodegenerative disease caused by loss of the upper motor neurons, i.e., neurons that extend from the cortex to the brain stem and the spinal cord and lower motor neurons, i.e., neurons that connect the brainstem or spinal cord to muscle (Hardiman et al., 2017). Progressive loss of these neuron populations can manifest in two distinct early ALS symptoms: patients diagnosed with spinal-onset display a significant weakness of the limbs, whereas bulbar-onset leads to difficulty swallowing (dysphagia) and difficulty speaking (dysarthria; Hardiman et al., 2017). As the disease progresses, symptoms converge and death due to respiratory failure usually occurs within 3–5 years post diagnosis.

There is a substantial magnitude of heterogeneity of symptoms, variation of the age of onset and of disease progression in ALS. Comorbidity is observed with non-motor neuropathology in 50% of cases, with at least 13% of patients presenting concomitant behavioral variant frontotemporal dementia (FTD), which identifies ALS as a spectrum disorder rather than one single disease (Strong et al., 2017). ALS can also be grouped into either sporadic ALS (sALS), i.e., there is no family history, which accounts for ∼90% of all ALS cases, or familial ALS (fALS), i.e., ALS is inherited within families, which accounts for the remaining ∼10% of all ALS cases (Chen et al., 2013). The global incidence rate of the disease is approximately 1–2 new cases per 100,000 individuals with an overall prevalence averaging at 4–6 cases per 100,000 individuals (Chen et al., 2013). Despite considerable research efforts, the molecular mechanisms underpinning ALS remain mostly unknown and there is no cure. The substantial heterogeneity of ALS poses a

significant problem in deciphering unifying ALS pathomechanisms. Yet basic cellular pathways, such as dysregulated ribonucleic acid (RNA) metabolism and protein misfolding and the associated toxicity appear to be highly common and key contributing factors to ALS pathogenesis.

IMPAIRED RNA METABOLISM IN ALS

RNA metabolism is a broad term encompassing the entire life cycle of all cellular RNAs, such as messenger RNA (mRNA), micro RNA (miRNA) and transfer RNA (tRNA). This includes RNA synthesis, modifications, folding and unfolding, processing and degradation, all of which are tightly regulated by multiple cellular pathways. RNA is synthesized from a DNA template by the process of transcription. Transcription is carried out in three steps of initiation, elongation and termination in a tightly controlled manner. Following termination, the synthesized RNA strand (hnRNA) must undergo post-transcriptional modifications before it can be translated at the ribosome in the case of mRNAs or processed into functional miRNAs or tRNAs. Finally, intervening introns are excised from the transcript to generate mature mRNAs (Krishnamurthy and Hampsey, 2009; Sainsbury et al., 2015). Modified mRNAs are then transported out of the nucleus and into the cytoplasm by a set of protein factors (Rodriguez et al., 2004). These messenger ribonucleoproteins diffuse through the nuclear pore complex and the protein factors are gradually removed to prepare the transcript for translation into protein by the ribosome. All RNAs can be degraded at any stage of their life cycle, allowing for dynamic regulation in the cell.

Perturbed RNA metabolism, particularly mRNA metabolism, plays a crucial role in the development of many neurodegenerative disorders, including ALS. Defects at all stages of the mRNA life cycle are prevalent in ALS and are mainly driven by disease-specific mutations in RNA binding proteins (RBPs). There are 10 RBPs with known ALS mutations in their encoding genes: ANG, EWSR1, Fused in sarcoma (FUS), hnRNPA1, hnRNPA2B1, RGNEF, SETX, TAF15, TIA-1 and TAR DNA binding protein 43 (TDP-43; **Table 1**). These mutations lead to a broad range of deficits in RNA metabolism, including impaired transcription of both mRNAs and miRNAs, post-transcriptional modifications and RNA editing. Many of the RBPs affected in ALS participate in the formation of stress granules (SGs) under cellular stress to halt non-essential translation and to sequester and preserve specific mRNAs.

For example, TAF15 is a component of the TFIID complex that is essential for RNA polymerase II transcription (Bertolotti et al., 1996; Kwon et al., 2013). Mutations in the gene encoding TAF15 have been uncovered in ALS patients but are not present in unaffected controls (Couthouis et al., 2011; Ticozzi et al., 2011). An overarching theme amongst ALS RBPs is their structural similarities. TAF15 shares sequence and domain homology with both TDP-43 and FUS and all three proteins may at least partially overlap in function. Both FUS and TAF15 belong to the FET family of heterogeneous nuclear ribonucleoproteins (hnRNPs) and like TDP-43 and FUS, TAF15 functions in alternative splicing and transcription. Furthermore, the majority of TAF15 ALS mutations are located within the glycine-rich region or prion-like-domain at the C-terminus of the protein, with similar ALS-associated mutations found in TDP-43 and FUS. Finally, TAF15 also mislocalizes from the nucleus into the cytoplasm and is found in cytoplasmic inclusions, a common pathological hallmark in ALS proteinopathy, which is also well-established for TDP-43 and FUS.

PROTEIN MISFOLDING IN ALS

Protein misfolding describes the conversion of proteins from their normal, mostly soluble and functional three-dimensional conformations into aberrant, often insoluble, non-functional conformations (Soto, 2003; Soto and Estrada, 2008; Sweeney et al., 2017). This can result in a toxic gain-of-function or loss-of-function of the disease gene or protein, or a combination of both, which cause neurodegeneration. Most neurodegenerative diseases, such as Alzheimer's disease, Parkinson's disease, Huntington's disease and ALS are protein misfolding diseases. Genetic mutations can cause a protein to misfold, e.g., the misfolded huntingtin protein in Huntington's disease. However, in Parkinson's, Alzheimer's and ALS, most cases cannot be associated with any known mutations. Environmental insults, such as changes in pH and exposure to toxic chemicals or oxidative stress, can lead to protein misfolding that may contribute to neurodegeneration. Finally, the highest risk factor for most neurodegenerative diseases is advanced age, indicating that the physiological changes associated with aging contribute to disease-related protein misfolding.

Like most neurodegenerative diseases, ALS is characterized by protein misfolding and protein aggregation in affected neurons (Sweeney et al., 2017). These misfolded proteins and aggregates, containing proteins, such as TDP-43, FUS, C9orf72, superoxide dismutase (SOD1) and many others, are well-established pathological hallmarks of ALS (Okamoto et al., 1991; Watanabe et al., 2001; Arai et al., 2006; Neumann et al., 2006; Mackenzie et al., 2007; Kwiatkowski et al., 2009; Vance et al., 2009; Al-Sarraj et al., 2011). Yet it remains unclear how these misfolded and aggregated proteins execute neurotoxic functions and contribute to the ALS-specific pattern of neurodegeneration. Like many other neurodegenerative diseases, ALS is characterized by the highly selective demise of specific neurons, mostly motor neurons, while other neurons remain unaffected (Saxena and Caroni, 2011). This implies that the affected neurons are unable to avert the toxic consequences of ALS-specific protein misfolding and aggregation and that the defensive mechanisms that normally combat protein misfolding are ineffective. By contrast, unaffected neurons seem to be able to avert the toxic consequences of protein misfolding or even protein misfolding itself.

The newly discovered liquid-to-solid phase transition of the ALS protein FUS has added an additional layer of complexity to the well-known aspects of protein misfolding (Murakami et al., 2015; Patel et al., 2015; Monahan et al., 2017; Qamar et al., 2018). Phase transition begins with the single monomer of an

TABLE 1 | A list of the most common genes implicated in amyotrophic lateral sclerosis (ALS) and other neurodegenerative disorders. Known biological functions of each protein are listed.

Protein	RNA binding protein	Normal function	Disease	Reference
TDP-43	Yes	RNA metabolism	ALS (FTLD/ALS)	Sreedharan et al. (2008) and Kirby et al. (2010)
FUS	Yes	RNA metabolism	ALS (FTLD/ALS)	Kwiatkowski et al. (2009) and Vance et al. (2009)
SOD1	No	Oxidative stress	ALS	Rosen et al. (1993) and Andersen (2006)
C9orf72	Yes	RNA metabolism/RNA processing, nucleocytoplasmic transport	ALS, FTLD/ALS, FTD	DeJesus-Hernandez et al. (2011) and Renton et al. (2011)
Ataxin-2	No	Caspase activation, TDP-43 modification	ALS, PD, Ataxias	Elden et al. (2010)
Tau	No	Microtubule homeostasis	FTD, AD, Tauopathy	Lin et al. (2017)
OPTN	No	Autophagy	ALS	Maruyama et al. (2010)
PFN1	No	Cytoskeleton, actin polymerization	ALS	Wu et al. (2012)
hnRNPA1, hnRNPA2B1	Yes	RNA metabolism and transport	ALS, FTLD/ALS, FTD	Kim et al. (2013)
VAPB	No	Vesicle trafficking	ALS	Nishimura et al. (2004, 2005)
VCP	No	Protein degradation	ALS, FTLD/ALS, FTD, MJD, HD, PD	Johnson et al. (2010)
SETX	Yes	DNA/RNA Helicase, RNA Metabolism	ALS	Chen et al. (2004)
DCTN1	No	Axonal transport	ALS, FTLD/ALS	Münch et al. (2004, 2005)
NEFH	No	Neurofilament component	ALS	Figlewicz et al. (1994)
ALS2	No	Rho GEF, Vesicle transport	Juvenile ALS	Hadano et al. (2001) and Yang et al. (2001)
CHMP2B	No	Vesicle transport	ALS, FTD	Parkinson et al. (2006) and Cox et al. (2010)
ANG	Yes	RNA metabolism	ALS, FTLD/ALS	Greenway et al. (2004, 2006)
UBQLN2	No	Targeting misfolded proteins to proteasome, autophagy	ALS, FTLD/ALS	Deng et al. (2011)
SQSTM1	No	Autophagy, NFkB activator	ALS, FTLD/ALS	Fecto et al. (2011)
TUBA4A	No	Microtubule component	ALS	Smith et al. (2014)
7TBK1	No	NFkB activator, vesicle transport, autophagy	ALS	Cirulli et al. (2015) and Freischmidt et al. (2015)
C21orf2	No	Cilia formation, DNA repair	ALS	van Rheenen et al. (2016)
NEK1	No	Cilia formation, DNA repair	ALS	Kenna et al. (2016)
CHCHD10	No	Oxidative Phosphorylation	ALS, FTLD/ALS, FTD	Bannwarth et al. (2014) and Johnson et al. (2014)
TAF 15	Yes	RNA Metabolism	ALS	Couthouis et al. (2011)

intrinsically disordered protein harboring a prion-like domain (PrLD; St. George-Hyslop et al., 2018). The monomers exist in liquid-liquid phase separation under physiological conditions as spherical droplet structures. These structures are an example of a non-membrane bound compartment distinguished from the cytoplasm or the nucleoplasm by their condensed liquid state. When multiple FUS droplets come into contact, they quickly fuse and arrange into a larger droplet. This is governed by relatively weak, transient and homotypic interactions between the aggregation-prone domains of the protein. Patel et al. (2015) have shown that larger droplet formations of multiple droplets carry the potential to undergo aberrant liquid-solid phase transition which results in the formation of solid, fibrous aggregates. ALS-associated mutations in FUS can expedite this process (Patel et al., 2015).

Neurodegeneration is closely linked to prion-like conversion of properly folded to misfolded proteins and the spreading of neuropathology from cell to cell (Scheckel and Aguzzi, 2018). The concept of prion and prion-like-behavior is rooted in earlier work on the mammalian prion PrP and yeast prions. Domains of low-sequence complexity form compartments unbound by membranes, similar to the liquid-solid phase transition of FUS (Brangwynne et al., 2009; Kato et al., 2012; Patel et al., 2015). Yeast prions contain low complexity domains that readily transition into solid, aggregate fibers rather than a liquid state (Liebman and Chernoff, 2012). Thus, comparable domains in proteins were coined "prion-like." Low complexity PrLDs are common in RNA/DNA binding proteins, such as FUS and TAR DNA binding protein 43 (TDP-43), and many other known ALS proteins (Gitler and Shorter, 2011). It is plausible that prion-like conversion and seeding mechanisms of protein misfolding is central to the spreading of ALS pathology, e.g., from neuron to neuron.

CELL STRESS RESPONSES—FROM HUMANS TO YEAST

There are three major cellular stress response programs regulating protein quality control that protect cells from the toxic effects of protein misfolding: (1) the heat shock response (HSR); (2) the antioxidant response (AR) both of which act in the cytoplasm; and (3) the unfolded protein response (UPR) which acts in the endoplasmic reticulum and secretory pathway.

The HSR is a highly conserved pathway activated to prevent or repair the damages caused by heat and other stressors (Richter et al., 2010). In humans and yeast the HSR is regulated primarily by the transcription factor heat shock

factor 1 (Hsf1), which is responsible for transient induction of the expression of heat shock stress proteins (Hsps) and molecular chaperones (Wu, 1984; Wu et al., 1986; Richter et al., 2010). Oxidative stress contributes to the pathogenesis of neurodegenerative diseases (Kim et al., 2015). Oxidative stress is defined as the imbalance between reactive oxygen species (ROS) and reactive nitrogen species (NOS) and the defensive cellular AR (Camhi et al., 1995). Prolonged damage to the cell can be inflicted by ROS on nucleic acids, proteins and membrane lipids. Oxidative stress is a major contributor to many neurodegenerative diseases. The UPR collectively describes multiple pathways dedicated to maintaining proteostasis in the ER and secretory pathway (Hetz and Papa, 2018). These processes are constitutively active at basal levels, however, in the presence of accumulated misfolded proteins in the ER, quality control mechanisms become overwhelmed leading to ER stress. This leads to rapid activation of the UPR, via three central signal proteins, the protein kinase-like ER kinase (PERK), activating transcription factor 6 (ATF6) and inositol-requiring enzyme-1 (Ire1a), which results in strong induction of the expression of proteins involved in protein folding, ER-associated degradation (ERAD), vesicular trafficking, ER redox control, amino acid metabolism, lipid synthesis and autophagy. Only the Ire1 UPR signaling pathway is conserved from yeast to human cells.

Previous work in cultured cells and transgenic mice, strongly indicates that all three stress response pathways are malfunctioning and contribute to ALS pathogenesis (Atkin et al., 2008; Wang et al., 2011). Yet what role the dysregulation of these stress response pathways plays in human ALS neurons, particularly in those neurons strongly affected in ALS, has not yet been examined in a systematic manner.

YEAST MODELS—OPPORTUNITIES AND LIMITATIONS

The contributions from studies in yeast to our understanding of basic mechanisms underlying ALS and identifying key proteins has been substantial. *Saccharomyces cerevisiae* (yeast) is a single-celled organism and was the first eukaryote to have its genome fully sequenced (Goffeau et al., 1996). Nearly a third of yeast genes have a direct human ortholog and more than two thirds have significant homology with human genes (Laurent et al., 2016). Approximately 500 genes implicated in human disease have a direct ortholog in yeast, implicating the tractability of yeast as a model to study human disease (Kryndushkin and Shewmaker, 2011). The strengths of the yeast model arise from our considerable understanding of basic cell biology, genetics and biochemistry.

A multitude of genetic, microscopic and biochemical tools have been developed, such as high-throughput screens, which are not yet possible to this the same extent in any other model eukaryotic organism. These screens are highly versatile and allow the detection of novel genetic and protein-protein interactions. Over-expression and deletion libraries of the entire yeast genome allow identifying and characterizing modifiers of a target misfolded protein. Such studies have elucidated previously unexplored mechanisms in many neurodegenerative disorders, including ALS (Yeger-Lotem et al., 2009; Elden et al., 2010; Khurana and Lindquist, 2010; Treusch et al., 2011; Kim et al., 2014).

The cellular processes that involve protein misfolding and in turn the cellular response to protein misfolding, i.e., cellular stress response pathways, are highly conserved between humans and yeast (Winderickx et al., 2008). As a consequence, many yeast models of protein misfolding diseases recapitulate the general patterns of mislocalization, aggregation and cellular quality control mechanisms (**Figure 1**; Winderickx et al., 2008). Additionally, cellular quality control mechanisms, including the HSR and the UPR, are heavily conserved. While the focus of this review article is on impaired RNA metabolism and protein misfolding, yeast models also recapitulate many other essential mechanisms of eukaryotic biology. Cell cycle regulation, organelle function, and DNA metabolism are all examples of highly tractable process that can be aptly studied in yeast (**Figure 2**).

Using yeast as a living test-tube undoubtedly has a firm place in our experimental repertoire to explore neurodegenerative diseases, yet some caveats should be considered when assessing the suitability of yeast models. For instance, certain cellular mechanisms, such as cytoskeletal regulation and certain aspects of RNA metabolism, are not highly conserved between yeast and human neurons (Lemmens et al., 2010; Kevenaar and Hoogenraad, 2015). The simplification of such systems can therefore be problematic if not properly considered. For example, yeast do not contain neurofilaments, which are heteropolymers that form the neuronal cytoskeleton along with microfilaments and tubulin. While neurofilaments seem to contribute to ALS pathogenesis (Mendonça et al., 2005; Petzold, 2005; Gnanapavan et al., 2013), it might thus be problematic to study neurofilament-associated aspects of cytoskeleton disorganization in ALS yeast models. Similarly, certain aspects of RNA metabolism, i.e., RNA transport, degradation and translation, differ in yeast and mammalian cells (Lemmens et al., 2010). Only a small number of yeast genes possess introns and there are notable differences in the intron region of pre-mRNA that are essential for splicing between yeast and human cells. Also, yeast does not possess the miRNA processing machinery characteristic of human cells. Considering the substantial amount of RNA metabolism regulators implicated in ALS (**Tables 1**, **2**), it is important to understand these limitations when using yeast models. Yet, many of the core aspects of RNA metabolism, particularly mRNA processing, are similar between yeast and humans and, thus, some ALS-related RNA mechanisms can most likely be evaluated in yeast models.

Clearly, the suitability of the yeast model depends on what research question is explored (**Figure 2**). It seems obvious that there are certain questions that cannot be answered within this single-celled organism, e.g., macro-physiological or tissue-specific processes, such as inflammation and prion-like cell to cell spreading from cell to cell. Also, exploring highly specialized neuronal functions, such as synaptic communication and axonal transport in ALS make effective studies difficult in yeast models.

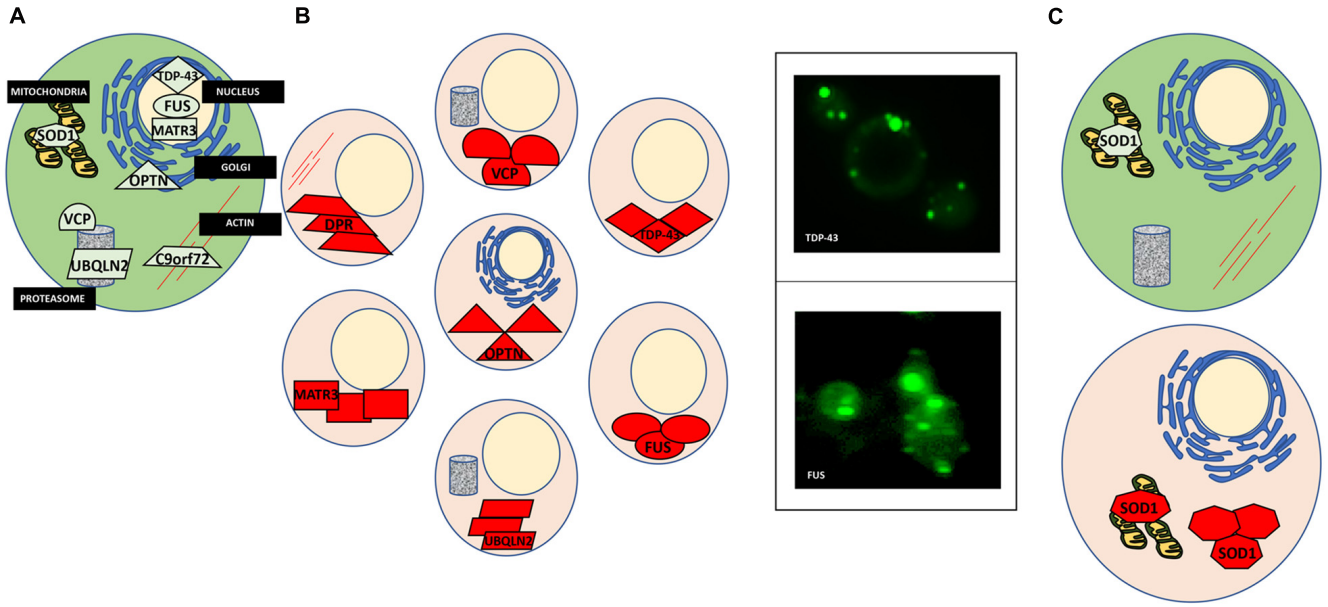

FIGURE 1 | Protein misfolding in amyotrophic lateral sclerosis (ALS). **(A)** A normal cell depicting natively folded proteins in their proper location compared to ALS cells where proteins are found mislocalized and aggregated. **(B)** TAR DNA binding protein 43 (TDP-43) is mislocalized from the nucleus and aggregated within the cytosol (top left). Yeast models of ALS recapitulate these features of TDP-43 proteinopathy (top right). GFP-tagged TDP-43 wild-type expressed in yeast is found in cytoplasmic inclusions throughout the cell. Fused in sarcoma (FUS) proteinopathy is similar to that of TDP-43 (bottom left and right). **(C)** Superoxide dismutase (SOD1) is localized to the mitochondria and throughout the cytosol. In ALS, misfolded SOD1 is found aggregated at these locations.

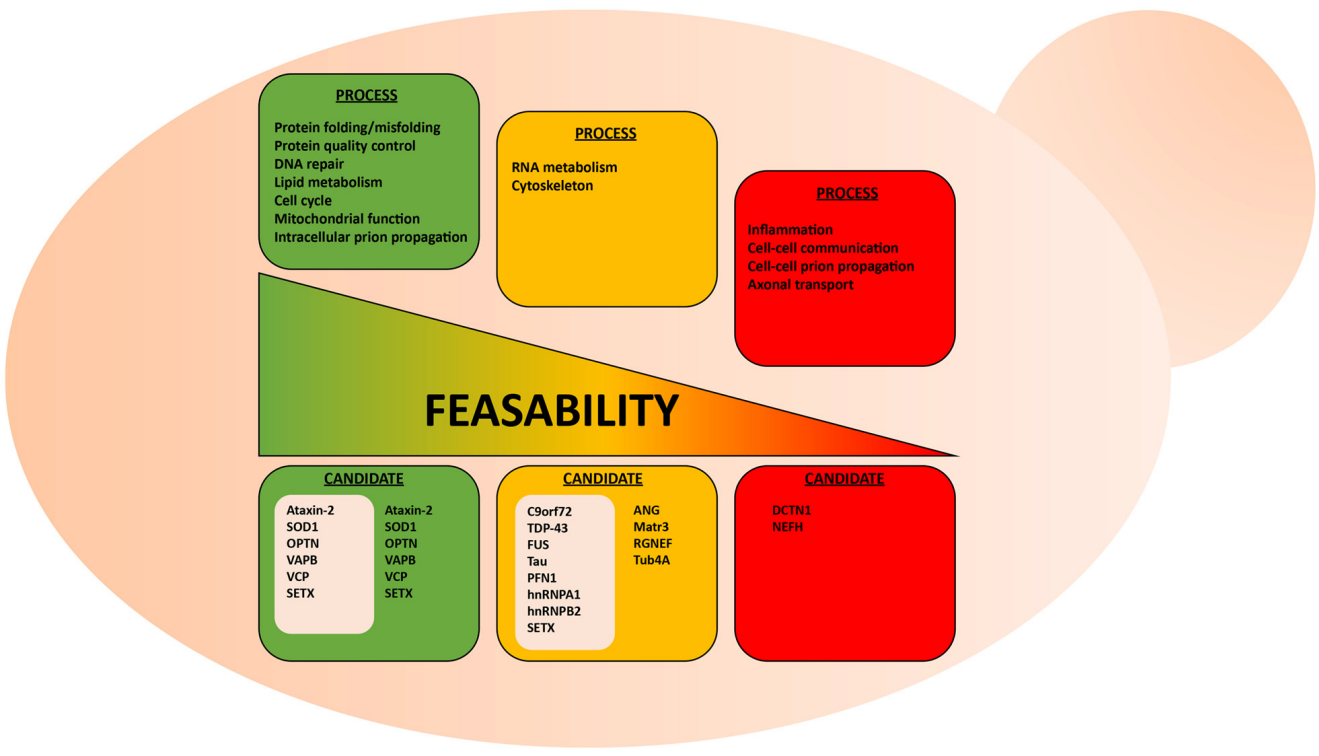

FIGURE 2 | Suitability of the yeast model system to study various aspects of ALS. Highly conserved biological processes, such as protein misfolding and protein quality control, are better suited for studies in yeast. Here, examples of conserved and non-conserved processes are listed for candidate ALS proteins already studied in yeast. These ALS proteins are grouped in gray-colored boxes.

TABLE 2 | Published ALS yeast models and their characteristics.

Human ALS protein (wild-type and mutants)	Toxicity	Aggregation	Reference
TDP-43 G294A, Q331K, M337V, Q343R, N345K, R361S, N390D	Yes	Yes	Johnson et al. (2009), Armakola et al. (2011), Braun et al. (2011), Kryndushkin and Shewmaker (2011), Sun et al. (2011), Jackrel et al. (2014), Liu et al. (2017) and Leibiger et al. (2018)
FUS R524S, P525L	Yes	Yes	Fushimi et al. (2011), Ju et al. (2011), Kryndushkin and Shewmaker (2011), Kryndushkin et al. (2011), Sun et al. (2011), Daigle et al. (2013) and Jackrel et al. (2014)
SOD1 A3V, G36R, H47Q, G92A, S133N	No	No	Nishida et al. (1994), Rabizadeh et al. (1995), Corson et al. (1998), Gunther et al. (2004), Bastow et al. (2011) and Bastow et al. (2016)
C9orf72 (GA)50, (GR)100, (PA)50, (PR)50	Yes	Not assessed	Jovičić et al. (2015) and Chai and Gitler (2018)
Ataxin-2 Q22, Q79	No	Not assessed	Ralser et al. (2005), Nonhoff et al. (2007), Elden et al. (2010) and Bonini and Gitler (2011)
OPTN E50K, E478G	Yes	Yes	Kryndushkin et al. (2012)
PFN1 C71G, T109M, M114T, E117G, G118V, R136W, H120E	No	No assessed	Figley et al. (2014)
hnRNPA1, hnRNPA2B1 hnRNPA1 D262V, hnRNPA1 D262N, hnRNPA2B1 D290V	Yes	Yes	Kim et al. (2013)
VAPB P56S	Wild-type—Yes P56S—not assessed	Yes	Suzuki et al. (2009), Nakamichi et al. (2011)
VCP R155C, A232E, T761E, K524A	No	Wild-type, T761E, K524A—No R155C and A232E—Yes	Takata et al. (2012)
SETX	No	No	Richard et al. (2013), Bennett and La Spada (2018)
ANG	Yes	Yes	Jo et al. (2017)
TAF 15	Yes	Yes	Couthouis et al. (2011)
UBQLN2 (essential domain only)	No	Not assessed	Gilpin et al. (2015)

Wild-type and ALS-associated mutant proteins that have been expressed in yeast are listed and categorized based on toxicity and aggregation phenotypes. Toxicity refers to growth defects of yeast cells expressing ALS proteins. Aggregation refers to fluorescent microscopically assessed inclusions or foci. Note, that even though there is a strong correlated between aggregation and toxicity of ALS proteins in yeast, this does not equate with a causative relation.

YEAST MODELS OF ALS

We count more than 13 published ALS yeast models, i.e., yeast expressing different ALS-associated protein (**Table 2**, Van Damme et al., 2017). Many of these are not yet developed to the extent of the TDP-43 and FUS models, however, important commonalities between these models are emerging. **Figure 1** illustrates the aggregation and mislocalization of ALS proteins, a hallmark of pathology that is consistently recapitulated in yeast. It is noteworthy that even though in all listed examples in **Tables 1**, **2** lists all of these ALS yeast models, the associated proteins, and major findings. A major similarity between all these proteins, regardless of their diverse biological function, is protein misfolding and many of them have RNA binding function.

Of the 10 known RBPs involved in ALS, nine of them have been successfully modeled in yeast. ANG is involved in the processing of ribosomal RNA and has been shown to act as stress-activated RNase that promotes SG assembly by cleaving tRNA and inhibiting translation (Shapiro et al., 1986; Harper and Vallee, 1989). The yeast proteome does not contain any ANG homolog and ANG expression is highly toxic in yeast, both of which are common features of many ALS yeast models (e.g., TDP-43 and FUS but not SOD1, which has a yeast homolog). Yeast high-throughput screens using human libraries identified genetic modifiers of ANG toxicity (Jo et al., 2017), i.e., potent suppressors of ANG toxicity. Deletion of a subset of these suppressor genes also attenuated protein aggregation in these models. Four of the suppressors uncovered novel interactions between ANG and the ALS protein OPTN.

Another RBP that has been studied in yeast is SETX, an RNA/DNA helicase. SETX has been shown to function as an RNA Polymerase II transcription terminator by resolving R-loops and allowing the 5′-3′exoribonuclease Xrn2 to degrade the RNA transcript following extended pausing at G-rich sites (Skourti-Stathaki et al., 2011). Interactor screens in the yeast-2-hybrid system revealed an interaction between SETX and Rpr45, a component of the exosome complex important for RNA turnover and quality control (Richard et al., 2013). This interaction depends upon sumoylation of SETX. ALS mutants of SETX were also examined, however, it was found that ALS-associated mutations did not disrupt interaction with Rpr45. Following up on these findings, the authors demonstrated co-localization of SETX and Rpr45 in the nucleus in mammalian cell lines. This occurred as a response to induced DNA damage, suggesting a new role for the exosome is DNA repair that may have implications in ALS (Richard et al., 2013).

The most prominent ALS yeast model is the TDP-43. TDP-43 is a DNA/RBP involved in RNA metabolism and one of the most common genetic causes of ALS (Chen et al., 2013). Over 40 ALS mutations have been discovered in TDP-43 which accounts for 4%–5% of fALS and 2% of sALS. Notably, almost all identified mutations are missense mutations in the glycine-rich C-terminal region, also known as a PrLD. This region is important for protein-protein interactions and likely a central contributor to TDP-43 misfolding (Gitler and Shorter, 2011). TDP-43 is the most common component of hallmark ALS cytoplasmic inclusions independent of mutated forms of the protein (Mackenzie and Rademakers, 2008). Approximately 97% of ALS patients demonstrate TDP-43 proteinopathy, where the protein is found mislocalized, i.e., expelled from the nucleus and misfolded into aggregates in the cytoplasm, a phenomenon coined TDP-43 proteinopathy.

Yeast as a model of TDP-43 proteinopathy has proven quite useful, recapitulating the major characteristics of the misfolded protein in the disease (Johnson et al., 2009; Armakola et al., 2011; Kryndushkin and Shewmaker, 2011; Sun et al., 2011). When expressed in yeast, TDP-43 is found outside the nucleus in soluble aggregates in the cytosol (**Figure 1B**). Many of the ALS-associated mutants have also been modeled in yeast and compared to the wild-type TDP-43 protein. These studies revealed that ALS mutations increased the propensity of TDP-43 to aggregate and increased toxicity (Johnson et al., 2009; Armakola et al., 2011; Kryndushkin and Shewmaker, 2011; Sun et al., 2011). Additionally, TDP-43 is toxic in yeast in a dose-dependent manner, making it a highly suitable candidate for high-throughput screens to identify genes and proteins that modulate its toxicity. From these screens many previously undescribed genetic interactions of TDP-43 have been identified, the most significant being the modulation of TDP-43 toxicity by ATAXIN-2 (ATXN2), the polyQ protein mutated in spinocerebellar ataxia type 2 (SCA2). A study by Gitler and co-workers revealed that PBP1, the yeast homolog of ATXN2, is a potent enhancer of TDP-43 toxicity when overexpressed simultaneously in yeast (Elden et al., 2010). Concurrently, when expressed in strains genetically deleted for gene encoding Pbp1, TDP-43 toxicity was reduced. Also, the upregulation of Pbp1 increased the number of fluorescent foci of fluorescent protein-tagged TDP-43 in yeast. These critical findings established the importance of ATXN2 as a common contributor to ALS and provided yet another example of proteins misfolding across multiple neurodegenerative disorders, as ATXN2 can also contribute to Parkinson's disease and mutations in ATXN2 cause SCA2 (Imbert et al., 1996; Pulst et al., 1996; Sanpei et al., 1996; Lorenzetti et al., 1997; Infante et al., 2004; Nanetti et al., 2009; Fischbeck and Pulst, 2011). Importantly, subsequent studies in human cell culture, fly and mouse models have confirmed these results from yeast (Bonini and Gitler, 2011).

Similarly, wild-type and ALS mutants of FUS, another misfolded RBP in ALS, have also been successfully studied in yeast. As with TDP-43, FUS is mislocalized from the nucleus and found aggregated in the cytoplasm in ALS post-mortem tissues (FUS proteinopathy) and mammalian cell models (Mackenzie et al., 2011; Shang and Huang, 2016; Sharma et al., 2016). This holds true in yeast, as FUS is found outside of the nucleus and sequestered into aggregates in the cytosol (**Figure 1B**; Fushimi et al., 2011; Ju et al., 2011; Kryndushkin and Shewmaker, 2011; Kryndushkin et al., 2011; Sun et al., 2011). Like TDP-43, FUS also contains a glycine-rich region and NLS where most ALS-associated mutations occur. Studies in yeast have helped delineate which domains contribute to protein misfolding, aggregation, and the formation of aberrant protein-protein interactions (Sun et al., 2011). In addition, studies in yeast revealed that FUS induces the formation of RNA granules and localizes there along with other components such as Pbp1. Furthermore, deletion of the RNA recognition motif in FUS did not alter aggregation, however, rescued toxicity in yeast, demonstrating that the ability of FUS to bind RNA is required for FUS toxicity, providing an fascinating example of the interplay between protein misfolding and RNA metabolism in ALS (Sun et al., 2011).

hnRNPs, A2B1 and A1, are additional examples of an RBPs with a PrLDs implicated in ALS (Kim et al., 2013). These proteins function in partnership with TDP-43 in pre-mRNA splicing, mRNA transport, transcript stability and translation regulation (Martinez et al., 2016). As with TDP-43 and FUS, the disease-causing mutations fall within the PrLD of each protein and are predicted to enhance aggregation propensity. As a result, they are recruited to SGs and cytoplasmic inclusions similar to other ALS RBPs (Martinez et al., 2016). Kim et al. (2013) characterized a yeast model expressing A2B1 wild-type and the D290V mutant and found that both variants are highly toxic and form fluorescent foci in yeast. HnRNPA1 wild-type and two mutants, D262V and D262N, were also characterized in yeast with similar phenotypes. They found that both hnRNPs demonstrated greater toxicity in yeast than either TDP-43 or FUS and their mutants. Unlike ALS mutants of TDP-43 and FUS, hnRNP toxicity was not increased in the mutants. Considering the prevalence of RBPs with PrLDs and the role these domains play in driving the development of ALS, there is a strong basis to conclude that both RNA metabolism and protein misfolding are strongly linked (Kim et al., 2013).

VAPB is involved with vesicular trafficking, a process known to be involved in ALS and many other neurodegenerative disorders (Suzuki et al., 2009; Nakamichi et al., 2011). Importantly, several proteins involved in autophagy and protein degradation, such as OPTN and VCP, have also been previously studied in yeast (Kryndushkin et al., 2012; Takata et al., 2012).

Mutations in the gene encoding Copper, Zink SOD1, a conserved cytosolic ROS scavenger, were the first identified genetic causes of fALS, and until the discovery of TDP-43 and FUS in 2006, SOD1 was the only known ALS gene. There is an extensive body of literature dedicated to the study of SOD1 wild-type and over 160 known ALS mutations (Rosen et al., 1993; Bunton-Stasyshyn et al., 2015). Unlike TDP-43 and FUS, SOD1 mutations are scattered throughout the entire protein and likely affect more than one of its biochemical properties and biological functions (Cleveland and Rothstein, 2001). SOD1 and a subset of ALS-linked mutations have been introduced into yeast (**Tables 1**, **2**, Nishida et al., 1994; Gunther et al., 2004; Bastow

et al., 2016). Intriguingly, neither the wild-type protein or any of the currently modeled ALS mutations in yeast demonstrate any severe growth defect (Nishida et al., 1994; Rabizadeh et al., 1995; Corson et al., 1998; Gunther et al., 2004; Bastow et al., 2011, 2016). Deletion of the yeast SOD1 homolog revealed that human SOD1 could fully complement the biological function of yeast SOD1 (Martins and English, 2014). This lead to the discovery that many of the mutated SOD1 proteins in ALS retain full enzymatic function (Bastow et al., 2016). There is, however, a marked propensity for the wild-type SOD1 protein and even more so for ALS-associated SOD1 mutants to selectively aggregate close to mitochondria where the protein may confer a toxic function that is not yet fully understood (**Figure 1C**; Vijayvergiya et al., 2005). The relationship between the ALS mutations and the apparent toxicity remains enigmatic and seems quite distinct from other ALS proteins studied in yeast. Also, experiments in yeast and other model systems demonstrated interference by mutant SOD1 with ER-Golgi transport. Unlike TDP-43 and FUS, where aggregation propensity correlates with growth defects, yeast models of SOD1 do not reveal toxicity in the presence of mitochondrial inclusions (**Figure 1C**; Nishida et al., 1994; Gunther et al., 2004; Bastow et al., 2011, 2016). All these results challenge a simple correlation between protein misfolding or aggregation and toxicity for SOD1 and its ALS-associated mutants. Traditionally, aggregation has been considered detrimental to the cell. Yet increasing evidence suggests that sequestering misfolded proteins can also be protective and facilitated by cellular protein quality control mechanisms, e.g., molecular chaperones (Chen et al., 2011; Takalo et al., 2013). It is also known that SOD1 localizes to intermembrane compartment of the mitochondria and exerts a protective function against ROS, thus cautioning the proper distinction between normal localization and aberrant aggregation (Chen et al., 2011; Fischer et al., 2011). Continued work in yeast and other model systems will further delineate the intricate relationships between SOD1 and its ALS-associated mutations and their toxicity, localization, misfolding and aggregation.

In 2011, the discovery of intronic, hexanucleotide repeats of the C9Orf72 gene revealed the most common cause of fALS-FTD (Renton et al., 2011; Freibaum and Taylor, 2017). The GGGGCC repeats lower expression of the C9Orf72 protein product and accumulation of repeat-containing RNA may sequester RBPs to confer a toxic gain of function. Importantly, unconventional translation of RNA containing the GGGGCC repeats produces aberrant dipeptide repeat (DPR) proteins that accumulate in motor neurons and may seed the early stages of the disease (**Figure 1A**; Freibaum and Taylor, 2017). There are five different DPRs: glycine–alanine (GA), glycine–arginine (GR), proline–alanine (PA), proline–arginine (PR) and glycine–proline (GP). All five DPRs have been modeled in yeast and other model systems. As in human cells and *Drosophila*, the GR and PR DPRs are toxic in yeast (Jovičić et al., 2015; Chai and Gitler, 2018). This phenotype was exploited by Gitler and colleagues to investigate the specific causes of toxicity in high throughput-enhancer and suppressor screens in yeast. These studies revealed 133 gene deletions that supressed the toxicity phenotype associated with the expression of GR_{100}, a construct with 100 DPRs. Many of these modifiers are related to ribosome biogenesis. These deletions had not been identified in previous screens for genetic modifiers of other ALS proteins (e.g., FUS or TDP-43), suggesting a DPR-specific mechanism of toxicity (Jovičić et al., 2015; Chai and Gitler, 2018).

THE FUTURE OF ALS STUDIES IN YEAST

Despite the considerable body of ALS yeast literature, we argue that there remains a largely untapped potential of this model system. Many of the complex mechanisms underlying ALS onset might be rooted in protein-protein interactions. Yeast is an excellent platform for the discovery of novel interactors but also for the characterization of such relationships. The Split-ubiquitin assay is one effective alternative to the classical yeast-two-hybrid system that can detect protein interactions without translocation to the nucleus and proteins bound to the cell membrane (Johnsson and Varshavsky, 1994; Müller and Johnsson, 2008). Many methods such as pull-down assays that detect protein-protein interactions are also highly suitable for studies in yeast with its well-described proteome (Xing et al., 2016). In addition, the interplay between different ALS-associated proteins and mutations remains poorly understood. Future protein-protein interaction and genetic studies in yeast present the ideal scenario to retrieve novel information of the basic biology of these interactions. For instance, it will be important to explore how the misfolding of one ALS protein, modulates the misfolding of another, for example, how TDP-43 misfolding modulates SOD1 misfolding and toxicity.

Studies on yeast prions have been tremendously successful in deciphering basic mechanisms underlying prion propagation and prion maintenance (Liebman and Chernoff, 2012). Yeast prions are self-perpetuating protein aggregates or conformers that confer a transmissible and heritable phenotype in a non-Mendelian inheritance pattern (Liebman and Chernoff, 2012). Considering what is already known about ALS proteins containing PrLDs (e.g., TDP-43 and FUS), and the newly proposed mechanism of phase transition of the FUS protein, similar investigations in yeast can probably enhance our understanding of protein misfolding in ALS. For example, very little is known about the events that precede the formation of hallmark inclusions in ALS that contain both FUS and TDP-43. Future studies in yeast could delineate the nature of recruitment of these proteins to inclusions.

Additionally, as we recently reviewed in detail, yeast is also a very suitable model to study the aspects of aging, which play an important role in most neurodegeneration, including ALS (Di Gregorio and Duennwald, 2018). In brief, there are two distinguished paradigms of yeast aging models: chronological and replicative aging. Chronological aging describes the length of time a yeast cell can remain viable and replicative aging describes the number of cellular divisions a mother cell can undergo before senescence. Yeast growth follows the classical "S"-curve stages of divisions, beginning with the lag phase, transitioning into the log phase, and finally the stationary phase (cells cease

dividing). Yeast cells are "aged" following the diauxic shift that occurs toward the end of the log phase. Thus, "young" cells are still in lag and early log phase. These wild-type phases are defined by different metabolic profiles and rates of division. Importantly, aged yeast cells recapitulate many of the important aspects of mammalian cell counterparts and specifically, aged yeast more closely resemble neurons: older yeast cells undergo G1 cell cycle arrest, show increased ROS and autophagy, and metabolically switch to oxidative phosphorylation. All these are commonalities between aged yeast and neuronal cells. Thus, studying ALS-associated protein misfolding in aged yeast model may reveal how aging contributes to protein misfolding and the associated toxicity.

Yeast models can also serve to study the impact of different metabolic states, e.g., energy production by glycolysis compared to oxidative phosphorylation. Different yeast metabolic states can be induced by simply altering the carbon source in their media. Glucose is the primary carbon source preferred by yeast and induces glycolysis and anerobic fermentation (Otterstedt et al., 2004). In contrast, providing a non-fermentable carbon source, such as glycerol, will switch yeast cells to a respiratory metabolism with oxidative phosphorylation carried out by mitochondria as the major source of ATP (Otterstedt et al., 2004). This metabolic switch also increases ROS levels and arrest or significantly slow down cell division (Otterstedt et al., 2004). All these changes create many untapped opportunities to study the impact on oxidative stress and respiratory metabolism and mitochondrial dysfunction in ALS by simply expressing ALS proteins in cells grown in glycerol (Braun et al., 2011).

A surprisingly understudied area of ALS research is that of cellular stress responses. It seems plausible that at some point the cells' quality control arsenal fails in ALS-affected neurons and this ultimately gives way to cell death. As we have previously outlined, there are three distinguished, yet interconnected responses that become activated upon cell stress: the HSR, the antioxidative stress response, and the UPR. Yeast present an excellent platform to study cellular stress responses in a quick and effective manner. In fact, the tools to do so have already been optimized and used with great success in yeast (Jonikas et al., 2009; Brandman et al., 2012). Reporter constructs for each response have been developed and expressed in yeast that rely simply on the stress response sequence target of each response's respective transcriptional activator (Jonikas et al., 2009; Brandman et al., 2012).

AUTHOR CONTRIBUTIONS

Both authors wrote the article.

REFERENCES

Al-Sarraj, S., King, A., Troakes, C., Smith, B., Maekawa, S., Bodi, I., et al. (2011). p62 positive, TDP-43 negative, neuronal cytoplasmic and intranuclear inclusions in the cerebellum and hippocampus define the pathology of C9orf72-linked FTLD and MND/ALS. *Acta Neuropathol.* 122, 691–702. doi: 10.1007/s00401-011-0911-2

Andersen, P. M. (2006). Amyotrophic lateral sclerosis associated with mutations in the CuZn superoxide dismutase gene. *Curr. Neurol. Neurosci. Rep.* 6, 37–46. doi: 10.1007/s11910-996-0008-9

Arai, T., Hasegawa, M., Akiyama, H., Ikeda, K., Nonaka, T., Mori, H., et al. (2006). TDP-43 is a component of ubiquitin-positive tau-negative inclusions in frontotemporal lobar degeneration and amyotrophic lateral sclerosis. *Biochem. Biophys. Res. Commun.* 351, 602–611. doi: 10.1016/j.bbrc.2006.10.093

Armakola, M., Hart, M. P., and Gitler, A. D. (2011). TDP-43 toxicity in yeast. *Methods* 53, 238–245. doi: 10.1016/j.ymeth.2010.11.006

Atkin, J. D., Farg, M. A., Walker, A. K., Mclean, C., Tomas, D., and Horne, M. K. (2008). Endoplasmic reticulum stress and induction of the unfolded protein response in human sporadic amyotrophic lateral sclerosis. *Neurobiol. Dis.* 30, 400–407. doi: 10.1016/j.nbd.2008.02.009

Bannwarth, S., Ait-El-Mkadem, S., Chaussenot, A., Genin, E. C., Lacas-Gervais, S., Fragaki, K., et al. (2014). Reply: mutations in the CHCHD10 gene are a common cause of familial amyotrophic lateral sclerosis. *Brain* 137:e312. doi: 10.1093/brain/awu267

Bastow, E. L., Gourlay, C. W., and Tuite, M. F. (2011). Using yeast models to probe the molecular basis of amyotrophic lateral sclerosis. *Biochem. Soc. Trans.* 39, 1482–1487. doi: 10.1042/bst0391482

Bastow, E. L., Peswani, A. R., Tarrant, D. S. J., Pentland, D. R., Chen, X., Morgan, A., et al. (2016). New links between SOD1 and metabolic dysfunction from a yeast model of amyotrophic lateral sclerosis. *J. Cell Sci.* 129, 4118–4129. doi: 10.1242/jcs.190298

Bennett, C. L., and La Spada, A. R. (2018). Senataxin, a novel helicase at the interface of RNA transcriptome regulation and neurobiology: from normal function to pathological roles in motor neuron disease and cerebellar degeneration. *Adv. Neurobiol.* 20, 265–281. doi: 10.1007/978-3-319-89689-2_10

Bertolotti, A., Lutz, Y., Heard, D. J., Chambon, P., and Tora, L. (1996). hTAF(II)68, a novel RNA/ssDNA-binding protein with homology to the pro-oncoproteins TLS/FUS and EWS is associated with both TFIID and RNA polymerase II. *EMBO J.* 15, 5022–5031. doi: 10.1002/j.1460-2075.1996.tb00882.x

Bonini, N. M., and Gitler, A. D. (2011). Model organisms reveal insight into human neurodegenerative disease: ataxin-2 intermediate-length polyglutamine expansions are a risk factor for ALS. *J. Mol. Neurosci.* 45, 676–683. doi: 10.1007/s12031-011-9548-9

Brandman, O., Stewart-Ornstein, J., Wong, D., Larson, A., Williams, C. C., Li, G. W., et al. (2012). A ribosome-bound quality control complex triggers degradation of nascent peptides and signals translation stress. *Cell* 151, 1042–1054. doi: 10.1016/j.cell.2012.10.044

Brangwynne, C. P., Eckmann, C. R., Courson, D. S., Rybarska, A., Hoege, C., Gharakhani, J., et al. (2009). Germline P granules are liquid droplets that localize by controlled dissolution/condensation. *Science* 324, 1729–1732. doi: 10.1126/science.1172046

Braun, R. J., Sommer, C., Carmona-Gutierrez, D., Khoury, C. M., Ring, J., Buttner, S., et al. (2011). Neurotoxic 43-kDa TAR DNA-binding protein (TDP-43) triggers mitochondrion-dependent programmed cell death in yeast. *J. Biol. Chem.* 286, 19958–19972. doi: 10.1074/jbc.m110.194852

Bunton-Stasyshyn, R. K., Saccon, R. A., Fratta, P., and Fisher, E. M. (2015). SOD1 function and its implications for amyotrophic lateral sclerosis pathology: new and renascent themes. *Neuroscientist* 21, 519–529. doi: 10.1177/1073858414561795

Camhi, S. L., Lee, P., and Choi, A. M. (1995). The oxidative stress response. *New Horiz.* 3, 170–182.

Chai, N., and Gitler, A. D. (2018). Yeast screen for modifiers of C9orf72 poly(glycine-arginine) dipeptide repeat toxicity. *FEMS Yeast Res.* 18:4. doi: 10.1093/femsyr/foy024

Chen, Y.-Z., Bennett, C. L., Huynh, H. M., Blair, I. P., Puls, I., Irobi, J., et al. (2004). DNA/RNA helicase gene mutations in a form of juvenile amyotrophic lateral sclerosis (ALS4). *Am. J. Hum. Genet.* 74, 1128–1135. doi: 10.1086/421054

Chen, B., Retzlaff, M., Roos, T., and Frydman, J. (2011). Cellular strategies of protein quality control. *Cold Spring Harb. Perspect. Biol.* 3:a004374. doi: 10.1101/cshperspect.a004374

Chen, S., Sayana, P., Zhang, X., and Le, W. (2013). Genetics of amyotrophic lateral sclerosis: an update. *Mol. Neurodegener.* 8:28. doi: 10.1186/1750-1326-8-28

Cirulli, E. T., Lasseigne, B. N., Petrovski, S., Sapp, P. C., Dion, P. A., Leblond, C. S., et al. (2015). Exome sequencing in amyotrophic lateral sclerosis identifies risk genes and pathways. *Science* 347, 1436–1441. doi: 10.1126/science.aaa3650

Cleveland, D. W., and Rothstein, J. D. (2001). From Charcot to Lou Gehrig: deciphering selective motor neuron death in ALS. *Nat. Rev. Neurosci.* 2, 806–819. doi: 10.1038/35097565

Corson, L. B., Strain, J. J., Culotta, V. C., and Cleveland, D. W. (1998). Chaperone-facilitated copper binding is a property common to several classes of familial amyotrophic lateral sclerosis-linked superoxide dismutase mutants. *Proc. Natl. Acad. Sci. U S A* 95, 6361–6366. doi: 10.1073/pnas.95.11.6361

Couthouis, J., Hart, M. P., Shorter, J., Dejesus-Hernandez, M., Erion, R., Oristano, R., et al. (2011). A yeast functional screen predicts new candidate ALS disease genes. *Proc. Natl. Acad. Sci. U S A* 108, 20881–20890. doi: 10.1073/pnas.1109434108

Cox, L. E., Ferraiuolo, L., Goodall, E. F., Heath, P. R., Higginbottom, A., Mortiboys, H., et al. (2010). Mutations in CHMP2B in lower motor neuron predominant amyotrophic lateral sclerosis (ALS). *PLoS One* 5:e9872. doi: 10.1371/journal.pone.0009872

Daigle, J. G., Lanson, N. A. Jr., Smith, R. B., Casci, I., Maltare, A., Monaghan, J., et al. (2013). RNA-binding ability of FUS regulates neurodegeneration, cytoplasmic mislocalization and incorporation into stress granules associated with FUS carrying ALS-linked mutations. *Hum. Mol. Genet.* 22, 1193–1205. doi: 10.1093/hmg/dds526

DeJesus-Hernandez, M., Mackenzie, I. R., Boeve, B. F., Boxer, A. L., Baker, M., Rutherford, N. J., et al. (2011). Expanded GGGGCC hexanucleotide repeat in noncoding region of C9ORF72 causes chromosome 9p-linked FTD and ALS. *Neuron* 72, 245–256. doi: 10.1016/j.neuron.2011.09.011

Deng, H. X., Chen, W., Hong, S. T., Boycott, K. M., Gorrie, G. H., Siddique, N., et al. (2011). Mutations in UBQLN2 cause dominant X-linked juvenile and adult-onset alS and ALS/dementia. *Nature* 477, 211–215. doi: 10.1038/nature10353

Di Gregorio, S. E., and Duennwald, M. L. (2018). Yeast as a model to study protein misfolding in aged cells. *FEMS Yeast Res.* 18:6. doi: 10.1093/femsyr/foy054

Elden, A. C., Kim, H. J., Hart, M. P., Chen-Plotkin, A. S., Johnson, B. S., Fang, X., et al. (2010). Ataxin-2 intermediate-length polyglutamine expansions are associated with increased risk for ALS. *Nature* 466, 1069–1075. doi: 10.1038/nature09320

Fecto, F., Yan, J., Vemula, S. P., Liu, E., Yang, Y., Chen, W., et al. (2011). SQSTM1 mutations in familial and sporadic amyotrophic lateral sclerosis. *Arch. Neurol.* 68, 1440–1446. doi: 10.1001/archneurol.2011.250

Figlewicz, D. A., Krizus, A., Martinoli, M. G., Meininger, V., Dib, M., Rouleau, G. A., et al. (1994). Variants of the heavy neurofilament subunit are associated with the development of amyotrophic lateral sclerosis. *Hum. Mol. Genet.* 3, 1757–1761. doi: 10.1093/hmg/3.10.1757

Figley, M. D., Bieri, G., Kolaitis, R. M., Taylor, J. P., and Gitler, A. D. (2014). Profilin 1 associates with stress granules and ALS-linked mutations alter stress granule dynamics. *J. Neurosci.* 34, 8083–8097. doi: 10.1523/jneurosci.0543-14.2014

Fischbeck, K. H., and Pulst, S. M. (2011). Amyotrophic lateral sclerosis and spinocerebellar ataxia 2. *Neurology* 76, 2050–2051. doi: 10.1212/wnl.0b013e31821f4498

Fischer, L. R., Igoudjil, A., Magrane, J., Li, Y., Hansen, J. M., Manfredi, G., et al. (2011). SOD1 targeted to the mitochondrial intermembrane space prevents motor neuropathy in the Sod1 knockout mouse. *Brain* 134, 196–209. doi: 10.1093/brain/awq314

Freibaum, B. D., and Taylor, J. P. (2017). The role of dipeptide repeats in C9ORF72-Related ALS-FTD. *Front. Mol. Neurosci.* 10:35. doi: 10.3389/fnmol.2017.00035

Freischmidt, A., Wieland, T., Richter, B., Ruf, W., Schaeffer, V., Muller, K., et al. (2015). Haploinsufficiency of TBK1 causes familial ALS and fronto-temporal dementia. *Nat. Neurosci.* 18, 631–636. doi: 10.1038/nn.4000

Fushimi, K., Long, C., Jayaram, N., Chen, X., Li, L., and Wu, J. Y. (2011). Expression of human FUS/TLS in yeast leads to protein aggregation and cytotoxicity, recapitulating key features of FUS proteinopathy. *Protein Cell* 2, 141–149. doi: 10.1007/s13238-011-1014-5

Gilpin, K. M., Chang, L., and Monteiro, M. J. (2015). ALS-linked mutations in ubiquilin-2 or hnRNPA1 reduce interaction between ubiquilin-2 and hnRNPA1. *Hum. Mol. Genet.* 24, 2565–2577. doi: 10.1093/hmg/ddv020

Gitler, A. D., and Shorter, J. (2011). RNA-binding proteins with prion-like domains in ALS and FTLD-U. *Prion* 5, 179–187. doi: 10.4161/pri.5.3.17230

Gnanapavan, S., Grant, D., Morant, S., Furby, J., Hayton, T., Teunissen, C. E., et al. (2013). Biomarker report from the phase II lamotrigine trial in secondary progressive MS—neurofilament as a surrogate of disease progression. *PLoS One* 8:e70019. doi: 10.1371/journal.pone.0070019

Goffeau, A., Barrell, B. G., Bussey, H., Davis, R. W., Dujon, B., Feldmann, H., et al. (1996). Life with 6000 genes. *Science* 274, 563–567. doi: 10.1126/science.274.5287.546

Greenway, M. J., Alexander, M. D., Ennis, S., Traynor, B. J., Corr, B., Frost, E., et al. (2004). A novel candidate region for ALS on chromosome 14q11.2. *Neurology* 63, 1936–1938. doi: 10.1212/01.wnl.0000144344.39103.f6

Greenway, M. J., Andersen, P. M., Russ, C., Ennis, S., Cashman, S., Donaghy, C., et al. (2006). ANG mutations segregate with familial and 'sporadic' amyotrophic lateral sclerosis. *Nat. Genet.* 38, 411–413. doi: 10.1038/ng1742

Gunther, M. R., Vangilder, R., Fang, J., and Beattie, D. S. (2004). Expression of a familial amyotrophic lateral sclerosis-associated mutant human superoxide dismutase in yeast leads to decreased mitochondrial electron transport. *Arch. Biochem. Biophys.* 431, 207–214. doi: 10.1016/j.abb.2004.08.009

Hadano, S., Hand, C. K., Osuga, H., Yanagisawa, Y., Otomo, A., Devon, R. S., et al. (2001). A gene encoding a putative GTPase regulator is mutated in familial amyotrophic lateral sclerosis 2. *Nat. Genet.* 29, 166–173. doi: 10.1038/ng1001-166

Hardiman, O., Al-Chalabi, A., Chio, A., Corr, E. M., Logroscino, G., Robberecht, W., et al. (2017). Amyotrophic lateral sclerosis. *Nat. Rev. Dis. Primers* 3:17071. doi: 10.1038/nrdp.2017.71

Harper, J. W., and Vallee, B. L. (1989). A covalent angiogenin/ribonuclease hybrid with a fourth disulfide bond generated by regional mutagenesis. *Biochemistry* 28, 1875–1884. doi: 10.1021/bi00430a067

Hetz, C., and Papa, F. R. (2018). The unfolded protein response and cell fate control. *Mol. Cell* 69, 169–181. doi: 10.1016/j.molcel.2017.06.017

Imbert, G., Saudou, F., Yvert, G., Devys, D., Trottier, Y., Garnier, J. M., et al. (1996). Cloning of the gene for spinocerebellar ataxia 2 reveals a locus with high sensitivity to expanded CAG/glutamine repeats. *Nat. Genet.* 14, 285–291. doi: 10.1038/ng1196-285

Infante, J., Berciano, J., Volpini, V., Corral, J., Polo, J. M., Pascual, J., et al. (2004). Spinocerebellar ataxia type 2 with Levodopa-responsive parkinsonism culminating in motor neuron disease. *Mov. Disord.* 19, 848–852. doi: 10.1002/mds.20090

Jackrel, M. E., Desantis, M. E., Martinez, B. A., Castellano, L. M., Stewart, R. M., Caldwell, K. A., et al. (2014). Potentiated Hsp104 variants antagonize diverse proteotoxic misfolding events. *Cell* 156, 170–182. doi: 10.1016/j.cell.2013.11.047

Jo, M., Chung, A. Y., Yachie, N., Seo, M., Jeon, H., Nam, Y., et al. (2017). Yeast genetic interaction screen of human genes associated with amyotrophic lateral sclerosis: identification of MAP2K5 kinase as a potential drug target. *Genome Res.* 27, 1487–1500. doi: 10.1101/gr.211649.116

Johnson, J. O., Glynn, S. M., Gibbs, J. R., Nalls, M. A., Sabatelli, M., Restagno, G., et al. (2014). Mutations in the CHCHD10 gene are a common cause of familial amyotrophic lateral sclerosis. *Brain* 137:e311. doi: 10.1093/brain/awu265

Johnson, J. O., Mandrioli, J., Benatar, M., Abramzon, Y., Van Deerlin, V. M., Trojanowski, J. Q., et al. (2010). Exome sequencing reveals VCP mutations as a cause of familial ALS. *Neuron* 68, 857–864. doi: 10.1016/j.neuron.2010.11.036

Johnson, B. S., Snead, D., Lee, J. J., Mccaffery, J. M., Shorter, J., and Gitler, A. D. (2009). TDP-43 is intrinsically aggregation-prone and amyotrophic lateral sclerosis-linked mutations accelerate aggregation and increase toxicity. *J. Biol. Chem.* 284, 20329–20339. doi: 10.1074/jbc.a109.010264

Johnsson, N., and Varshavsky, A. (1994). Split ubiquitin as a sensor of protein interactions *in vivo*. *Proc. Natl. Acad. Sci. U S A* 91, 10340–10344. doi: 10.1073/pnas.91.22.10340

Jonikas, M. C., Collins, S. R., Denic, V., Oh, E., Quan, E. M., Schmid, V., et al. (2009). Comprehensive characterization of genes required for protein folding in the endoplasmic reticulum. *Science* 323, 1693–1697. doi: 10.1126/science.1167983

Jovičić, A., Mertens, J., Boeynaems, S., Bogaert, E., Chai, N., Yamada, S. B., et al. (2015). Modifiers of C9orf72 dipeptide repeat toxicity connect nucleocytoplasmic transport defects to FTD/ALS. *Nat. Neurosci.* 18, 1226–1229. doi: 10.1038/nn.4085

Ju, S., Tardiff, D. F., Han, H., Divya, K., Zhong, Q., Maquat, L. E., et al. (2011). A yeast model of FUS/TLS-dependent cytotoxicity. *PLoS Biol.* 9:e1001052. doi: 10.1371/journal.pbio.1001052

Kato, M., Han, T. W., Xie, S., Shi, K., Du, X., Wu, L. C., et al. (2012). Cell-free formation of RNA granules: low complexity sequence domains form dynamic fibers within hydrogels. *Cell* 149, 753–767. doi: 10.1016/j.cell.2012.04.017

Kenna, K. P., Van Doormaal, P. T., Dekker, A. M., Ticozzi, N., Kenna, B. J., Diekstra, F. P., et al. (2016). *NEK1* variants confer susceptibility to amyotrophic lateral sclerosis. *Nat. Genet.* 48, 1037–1042. doi: 10.1038/ng.3626

Kevenaar, J. T., and Hoogenraad, C. C. (2015). The axonal cytoskeleton: from organization to function. *Front. Mol. Neurosci.* 8:44. doi: 10.3389/fnmol.2015.00044

Khurana, V., and Lindquist, S. (2010). Modelling neurodegeneration in Saccharomyces cerevisiae: why cook with baker's yeast? *Nat. Rev. Neurosci.* 11, 436–449. doi: 10.1038/nrn2809

Kim, G. H., Kim, J. E., Rhie, S. J., and Yoon, S. (2015). The role of oxidative stress in neurodegenerative diseases. *Exp. Neurobiol.* 24, 325–340. doi: 10.5607/en.2015.24.4.325

Kim, H. J., Kim, N. C., Wang, Y. D., Scarborough, E. A., Moore, J., Diaz, Z., et al. (2013). Mutations in prion-like domains in hnRNPA2B1 and hnRNPA1 cause multisystem proteinopathy and ALS. *Nature* 495, 467–473. doi: 10.1038/nature11922

Kim, H. J., Raphael, A. R., Ladow, E. S., Mcgurk, L., Weber, R. A., Trojanowski, J. Q., et al. (2014). Therapeutic modulation of eIF2α phosphorylation rescues TDP-43 toxicity in amyotrophic lateral sclerosis disease models. *Nat. Genet.* 46, 152–160. doi: 10.1038/ng.2853

Kirby, J., Goodall, E. F., Smith, W., Highley, J. R., Masanzu, R., Hartley, J. A., et al. (2010). Broad clinical phenotypes associated with TAR-DNA binding protein (TARDBP) mutations in amyotrophic lateral sclerosis. *Neurogenetics* 11, 217–225. doi: 10.1007/s10048-009-0218-9

Krishnamurthy, S., and Hampsey, M. (2009). Eukaryotic transcription initiation. *Curr. Biol.* 19, R153–R156. doi: 10.1016/j.cub.2008.11.052

Kryndushkin, D., Ihrke, G., Piermartiri, T. C., and Shewmaker, F. (2012). A yeast model of optineurin proteinopathy reveals a unique aggregation pattern associated with cellular toxicity. *Mol. Microbiol.* 86, 1531–1547. doi: 10.1111/mmi.12075

Kryndushkin, D., and Shewmaker, F. (2011). Modeling ALS and FTLD proteinopathies in yeast: an efficient approach for studying protein aggregation and toxicity. *Prion* 5, 250–257. doi: 10.4161/pri.17229

Kryndushkin, D., Wickner, R. B., and Shewmaker, F. (2011). FUS/TLS forms cytoplasmic aggregates, inhibits cell growth and interacts with TDP-43 in a yeast model of amyotrophic lateral sclerosis. *Protein Cell* 2, 223–236. doi: 10.1007/s13238-011-1525-0

Kwiatkowski, T. J.Jr., Bosco, D. A., Leclerc, A. L., Tamrazian, E., Vanderburg, C. R., Russ, C., et al. (2009). Mutations in the FUS/TLS gene on chromosome 16 cause familial amyotrophic lateral sclerosis. *Science* 323, 1205–1208. doi: 10.1126/science.1166066

Kwon, I., Kato, M., Xiang, S., Wu, L., Theodoropoulos, P., Mirzaei, H., et al. (2013). Phosphorylation-regulated binding of RNA polymerase II to fibrous polymers of low-complexity domains. *Cell* 155, 1049–1060. doi: 10.1016/j.cell.2013.10.033

Laurent, J. M., Young, J. H., Kachroo, A. H., and Marcotte, E. M. (2016). Efforts to make and apply humanized yeast. *Brief. Funct. Genomics* 15, 155–163. doi: 10.1093/bfgp/elv041

Leibiger, C., Deisel, J., Aufschnaiter, A., Ambros, S., Tereshchenko, M., Verheijen, B. M., et al. (2018). TDP-43 controls lysosomal pathways thereby determining its own clearance and cytotoxicity. *Hum. Mol. Genet.* 27, 1593–1607. doi: 10.1093/hmg/ddy066

Lemmens, R., Moore, M. J., Al-Chalabi, A., Brown, R. H.Jr., and Robberecht, W. (2010). RNA metabolism and the pathogenesis of motor neuron diseases. *Trends Neurosci.* 33, 249–258. doi: 10.1016/j.tins.2010.02.003

Liebman, S. W., and Chernoff, Y. O. (2012). Prions in yeast. *Genetics* 191, 1041–1072. doi: 10.1534/genetics.111.137760

Lin, H.-C., Lin, C.-H., Chen, P.-L., Cheng, S.-J., and Chen, P.-H. (2017). Intrafamilial phenotypic heterogeneity in a Taiwanese family with a *MAPT* p.R5H mutation: a case report and literature review. *BMC Neurol.* 17:186. doi: 10.1186/s12883-017-0966-3

Liu, G., Coyne, A. N., Pei, F., Vaughan, S., Chaung, M., Zarnescu, D. C., et al. (2017). Endocytosis regulates TDP-43 toxicity and turnover. *Nat. Commun.* 8:2092. doi: 10.1038/s41467-017-02017-x

Lorenzetti, D., Bohlega, S., and Zoghbi, H. Y. (1997). The expansion of the CAG repeat in ataxin-2 is a frequent cause of autosomal dominant spinocerebellar ataxia. *Neurology* 49, 1009–1013. doi: 10.1212/wnl.49.4.1009

Mackenzie, I. R. A., Ansorge, O., Strong, M., Bilbao, J., Zinman, L., Ang, L. C., et al. (2011). Pathological heterogeneity in amyotrophic lateral sclerosis with FUS mutations: two distinct patterns correlating with disease severity and mutation. *Acta Neuropathol.* 122, 87–98. doi: 10.1007/s00401-011-0838-7

Mackenzie, I. R., Bigio, E. H., Ince, P. G., Geser, F., Neumann, M., Cairns, N. J., et al. (2007). Pathological TDP-43 distinguishes sporadic amyotrophic lateral sclerosis from amyotrophic lateral sclerosis with SOD1 mutations. *Ann. Neurol.* 61, 427–434. doi: 10.1002/ana.21147

Mackenzie, I. R. A., and Rademakers, R. (2008). The role of TDP-43 in amyotrophic lateral sclerosis and frontotemporal dementia. *Curr. Opin. Neurol.* 21, 693–700. doi: 10.1097/WCO.0b013e3283168d1d

Martinez, F. J., Pratt, G. A., Van Nostrand, E. L., Batra, R., Huelga, S. C., Kapeli, K., et al. (2016). Protein-RNA networks regulated by normal and ALS-associated mutant HNRNPA2B1 in the nervous system. *Neuron* 92, 780–795. doi: 10.1016/j.neuron.2016.09.050

Martins, D., and English, A. M. (2014). SOD1 oxidation and formation of soluble aggregates in yeast: relevance to sporadic ALS development. *Redox Biol.* 2, 632–639. doi: 10.1016/j.redox.2014.03.005

Maruyama, H., Morino, H., Ito, H., Izumi, Y., Kato, H., Watanabe, Y., et al. (2010). Mutations of optineurin in amyotrophic lateral sclerosis. *Nature* 465, 223–226. doi: 10.1038/nature08971

Mendonça, D. M. F., Chimelli, L., and Martinez, A. M. B. (2005). Quantitative evidence for neurofilament heavy subunit aggregation in motor neurons of spinal cords of patients with amyotrophic lateral sclerosis. *Braz. J. Med. Biol. Res.* 38, 925–933. doi: 10.1590/s0100-879x2005000600015

Monahan, Z., Ryan, V. H., Janke, A. M., Burke, K. A., Rhoads, S. N., Zerze, G. H., et al. (2017). Phosphorylation of the FUS low-complexity domain disrupts phase separation, aggregation, and toxicity. *EMBO J.* 36, 2951–2967. doi: 10.15252/embj.201696394

Müller, J., and Johnsson, N. (2008). Split-ubiquitin and the split-protein sensors: chessman for the endgame. *Chembiochem* 9, 2029–2038. doi: 10.1002/cbic.200800190

Münch, C., Rosenbohm, A., Sperfeld, A. D., Uttner, I., Reske, S., Krause, B. J., et al. (2005). Heterozygous R1101K mutation of the DCTN1 gene in a family with ALS and FTD. *Ann. Neurol.* 58, 777–780. doi: 10.1002/ana.20631

Münch, C., Sedlmeier, R., Meyer, T., Homberg, V., Sperfeld, A. D., Kurt, A., et al. (2004). Point mutations of the p150 subunit of dynactin (DCTN1) gene in ALS. *Neurology* 63, 724–726. doi: 10.1212/01.wnl.0000134608.83927.b1

Murakami, T., Qamar, S., Lin, J. Q., Schierle, G. S., Rees, E., Miyashita, A., et al. (2015). ALS/FTD mutation-induced phase transition of FUS liquid droplets and reversible hydrogels into irreversible hydrogels impairs RNP granule function. *Neuron* 88, 678–690. doi: 10.1016/j.neuron.2015.10.030

Nakamichi, S., Yamanaka, K., Suzuki, M., Watanabe, T., and Kagiwada, S. (2011). Human VAPA and the yeast VAP Scs2p with an altered proline distribution can phenocopy amyotrophic lateral sclerosis-associated VAPB(P56S). *Biochem. Biophys. Res. Commun.* 404, 605–609. doi: 10.1016/j.bbrc.2010.12.011

Nanetti, L., Fancellu, R., Tomasello, C., Gellera, C., Pareyson, D., and Mariotti, C. (2009). Rare association of motor neuron disease and spinocerebellar ataxia type 2 (SCA2): a new case and review of the literature. *J. Neurol.* 256, 1926–1928. doi: 10.1007/s00415-009-5237-9

Neumann, M., Sampathu, D. M., Kwong, L. K., Truax, A. C., Micsenyi, M. C., Chou, T. T., et al. (2006). Ubiquitinated TDP-43 in frontotemporal lobar degeneration and amyotrophic lateral sclerosis. *Science* 314, 130–133. doi: 10.1126/science.1134108

Nishida, C. R., Gralla, E. B., and Valentine, J. S. (1994). Characterization of three yeast copper-zinc superoxide dismutase mutants analogous to those coded for in familial amyotrophic lateral sclerosis. *Proc. Natl. Acad. Sci. U S A* 91, 9906–9910. doi: 10.1073/pnas.91.21.9906

Nishimura, A. L., Al-Chalabi, A., and Zatz, M. (2005). A common founder for amyotrophic lateral sclerosis type 8 (ALS8) in the Brazilian population. *Hum. Genet.* 118, 499–500. doi: 10.1007/s00439-005-0031-y

Nishimura, A. L., Mitne-Neto, M., Silva, H. C., Richieri-Costa, A., Middleton, S., Cascio, D., et al. (2004). A mutation in the vesicle-trafficking protein VAPB causes late-onset spinal muscular atrophy and amyotrophic lateral sclerosis. *Am. J. Hum. Genet.* 75, 822–831. doi: 10.1086/425287

Nonhoff, U., Ralser, M., Welzel, F., Piccini, I., Balzereit, D., Yaspo, M. L., et al. (2007). Ataxin-2 interacts with the DEAD/H-box RNA helicase DDX6 and interferes with P-bodies and stress granules. *Mol. Biol. Cell* 18, 1385–1396. doi: 10.1091/mbc.e06-12-1120

Okamoto, K., Hirai, S., Yamazaki, T., Sun, X. Y., and Nakazato, Y. (1991). New ubiquitin-positive intraneuronal inclusions in the extra-motor cortices in patients with amyotrophic lateral sclerosis. *Neurosci. Lett.* 129, 233–236. doi: 10.1016/0304-3940(91)90469-a

Otterstedt, K., Larsson, C., Bill, R. M., StÅHlberg, A., Boles, E., Hohmann, S., et al. (2004). Switching the mode of metabolism in the yeast Saccharomyces cerevisiae. *EMBO Rep.* 5, 532–537. doi: 10.1038/sj.embor.7400132

Parkinson, N., Ince, P. G., Smith, M. O., Highley, R., Skibinski, G., Andersen, P. M., et al. (2006). ALS phenotypes with mutations in *CHMP2B* (charged multivesicular body protein 2B). *Neurology* 67, 1074–1077. doi: 10.1212/01.wnl.0000231510.89311.8b

Patel, A., Lee, H. O., Jawerth, L., Maharana, S., Jahnel, M., Hein, M. Y., et al. (2015). A liquid-to-solid phase transition of the ALS protein FUS accelerated by disease mutation. *Cell* 162, 1066–1077. doi: 10.1016/j.cell.2015.07.047

Petzold, A. (2005). Neurofilament phosphoforms: surrogate markers for axonal injury, degeneration and loss. *J. Neurol. Sci.* 233, 183–198. doi: 10.1016/j.jns.2005.03.015

Pulst, S. M., Nechiporuk, A., Nechiporuk, T., Gispert, S., Chen, X. N., Lopes-Cendes, I., et al. (1996). Moderate expansion of a normally biallelic trinucleotide repeat in spinocerebellar ataxia type 2. *Nat. Genet.* 14, 269–276. doi: 10.1038/ng1196-269

Qamar, S., Wang, G., Randle, S. J., Ruggeri, F. S., Varela, J. A., Lin, J. Q., et al. (2018). FUS phase separation is modulated by a molecular chaperone and methylation of arginine cation-π interactions. *Cell* 173, 720.e15–734.e15. doi: 10.1016/j.cell.2018.03.056

Rabizadeh, S., Gralla, E. B., Borchelt, D. R., Gwinn, R., Valentine, J. S., Sisodia, S., et al. (1995). Mutations associated with amyotrophic lateral sclerosis convert superoxide dismutase from an antiapoptotic gene to a proapoptotic gene: studies in yeast and neural cells. *Proc. Natl. Acad. Sci. U S A* 92, 3024–3028. doi: 10.1073/pnas.92.7.3024

Ralser, M., Nonhoff, U., Albrecht, M., Lengauer, T., Wanker, E. E., Lehrach, H., et al. (2005). Ataxin-2 and huntingtin interact with endophilin-A complexes to function in plastin-associated pathways. *Hum. Mol. Genet.* 14, 2893–2909. doi: 10.1093/hmg/ddi321

Renton, A. E., Majounie, E., Waite, A., Simón-Sánchez, J., Rollinson, S., Gibbs, J. R., et al. (2011). A hexanucleotide repeat expansion in C9Orf72 is the cause of chromosome 9P21-linked ALS-FTD. *Neuron* 72, 257–268. doi: 10.1016/j.neuron.2011.09.010

Richard, P., Feng, S., and Manley, J. L. (2013). A SUMO-dependent interaction between Senataxin and the exosome, disrupted in the neurodegenerative disease AOA2, targets the exosome to sites of transcription-induced DNA damage. *Genes Dev.* 27, 2227–2232. doi: 10.1101/gad.224923.113

Richter, K., Haslbeck, M., and Buchner, J. (2010). The heat shock response: life on the verge of death. *Mol. Cell* 40, 253–266. doi: 10.1016/j.molcel.2010.10.006

Rodriguez, M. S., Dargemont, C., and Stutz, F. (2004). Nuclear export of RNA. *Biol. Cell* 96, 639–655. doi: 10.1016/j.biolcel.2004.04.014

Rosen, D. R., Siddique, T., Patterson, D., Figlewicz, D. A., Sapp, P., Hentati, A., et al. (1993). Mutations in Cu/Zn superoxide dismutase gene are associated with familial amyotrophic lateral sclerosis. *Nature* 362, 59–62. doi: 10.1136/jmg.30.6.532-b

Sainsbury, S., Bernecky, C., and Cramer, P. (2015). Structural basis of transcription initiation by RNA polymerase II. *Nat. Rev. Mol. Cell Biol.* 16, 129–143. doi: 10.1038/nrm3952

Sanpei, K., Takano, H., Igarashi, S., Sato, T., Oyake, M., Sasaki, H., et al. (1996). Identification of the spinocerebellar ataxia type 2 gene using a direct identification of repeat expansion and cloning technique, DIRECT. *Nat. Genet.* 14, 277–284. doi: 10.1038/ng1196-277

Saxena, S., and Caroni, P. (2011). Selective neuronal vulnerability in neurodegenerative diseases: from stressor thresholds to degeneration. *Neuron* 71, 35–48. doi: 10.1016/j.neuron.2011.06.031

Scheckel, C., and Aguzzi, A. (2018). Prions, prionoids and protein misfolding disorders. *Nat. Rev. Genet.* 19, 405–418. doi: 10.1038/s41576-018-0011-4

Shang, Y., and Huang, E. J. (2016). Mechanisms of FUS mutations in familial amyotrophic lateral sclerosis. *Brain Res.* 1647, 65–78. doi: 10.1016/j.brainres.2016.03.036

Shapiro, R., Riordan, J. F., and Vallee, B. L. (1986). Characteristic ribonucleolytic activity of human angiogenin. *Biochemistry* 25, 3527–3532. doi: 10.1021/bi00360a008

Sharma, A., Lyashchenko, A. K., Lu, L., Nasrabady, S. E., Elmaleh, M., Mendelsohn, M., et al. (2016). ALS-associated mutant FUS induces selective motor neuron degeneration through toxic gain of function. *Nat. Commun.* 7:10465. doi: 10.1038/ncomms10465

Skourti-Stathaki, K., Proudfoot, N. J., and Gromak, N. (2011). Human senataxin resolves RNA/DNA hybrids formed at transcriptional pause sites to promote Xrn2-dependent termination. *Mol. Cell* 42, 794–805. doi: 10.1016/j.molcel.2011.04.026

Smith, B. N., Ticozzi, N., Fallini, C., Gkazi, A. S., Topp, S., Kenna, K. P., et al. (2014). Exome-wide rare variant analysis identifies TUBA4A mutations associated with familial ALS. *Neuron* 84, 324–331. doi: 10.1016/j.neuron.2014.09.027

Soto, C. (2003). Unfolding the role of protein misfolding in neurodegenerative diseases. *Nat. Rev. Neurosci.* 4, 49–60. doi: 10.1038/nrn1007

Soto, C., and Estrada, L. D. (2008). Protein misfolding and neurodegeneration. *Arch. Neurol.* 65, 184–189. doi: 10.1001/archneurol.2007.56

Sreedharan, J., Blair, I. P., Tripathi, V. B., Hu, X., Vance, C., Rogelj, B., et al. (2008). TDP-43 mutations in familial and sporadic amyotrophic lateral sclerosis. *Science* 319, 1668–1672. doi: 10.1126/science.1154584

St. George-Hyslop, P., Lin, J. Q., Miyashita, A., Phillips, E. C., Qamar, S., Randle, S. J., et al. (2018). The physiological and pathological biophysics of phase separation and gelation of RNA binding proteins in amyotrophic lateral sclerosis and fronto-temporal lobar degeneration. *Brain Res.* 1693, 11–23. doi: 10.1016/j.brainres.2018.04.036

Strong, M. J., Abrahams, S., Goldstein, L. H., Woolley, S., Mclaughlin, P., Snowden, J., et al. (2017). Amyotrophic lateral sclerosis—frontotemporal spectrum disorder (ALS-FTSD): revised diagnostic criteria. *Amyotroph. Lateral Scler. Frontotemporal. Degener.* 18, 153–174. doi: 10.1080/21678421.2016.1267768

Sun, Z., Diaz, Z., Fang, X., Hart, M. P., Chesi, A., Shorter, J., et al. (2011). Molecular determinants and genetic modifiers of aggregation and toxicity for the ALS disease protein FUS/TLS. *PLoS Biol.* 9:e1000614. doi: 10.1371/journal.pbio.1000614

Suzuki, H., Kanekura, K., Levine, T. P., Kohno, K., Olkkonen, V. M., Aiso, S., et al. (2009). ALS-linked P56S-VAPB, an aggregated loss-of-function mutant of VAPB, predisposes motor neurons to ER stress-related death by inducing aggregation of co-expressed wild-type VAPB. *J. Neurochem.* 108, 973–985. doi: 10.1111/j.0022-3042.2008.05857.x

Sweeney, P., Park, H., Baumann, M., Dunlop, J., Frydman, J., Kopito, R., et al. (2017). Protein misfolding in neurodegenerative diseases: implications and strategies. *Transl. Neurodegener.* 6:6. doi: 10.1186/s40035-017-0077-5

Takalo, M., Salminen, A., Soininen, H., Hiltunen, M., and Haapasalo, A. (2013). Protein aggregation and degradation mechanisms in neurodegenerative diseases. *Am. J. Neurodegener. Dis.* 2, 1–14.

Takata, T., Kimura, Y., Ohnuma, Y., Kawawaki, J., Kakiyama, Y., Tanaka, K., et al. (2012). Rescue of growth defects of yeast cdc48 mutants by pathogenic IBMPFD-VCPs. *J. Struct. Biol.* 179, 93–103. doi: 10.1016/j.jsb.2012.06.005

Ticozzi, N., Vance, C., Leclerc, A. L., Keagle, P., Glass, J. D., McKenna-Yasek, D., et al. (2011). Mutational analysis reveals the FUS homolog TAF15 as a candidate gene for familial amyotrophic lateral sclerosis. *Am. J. Med. Genet. B Neuropsychiatr. Genet.* 156B, 285–290. doi: 10.1002/ajmg.b.31158

Treusch, S., Hamamichi, S., Goodman, J. L., Matlack, K. E., Chung, C. Y., Baru, V., et al. (2011). Functional links between Aβ toxicity, endocytic trafficking, and Alzheimer's disease risk factors in yeast. *Science* 334, 1241–1245. doi: 10.1126/science.1213210

Van Damme, P., Robberecht, W., and Van Den Bosch, L. (2017). Modelling amyotrophic lateral sclerosis: progress and possibilities. *Dis. Model. Mech.* 10, 537–549. doi: 10.1242/dmm.029058

van Rheenen, W., Shatunov, A., Dekker, A. M., McLaughlin, R. L., Diekstra, F. P., Pulit, S. L., et al. (2016). Genome-wide association analyses identify new risk

variants and the genetic architecture of amyotrophic lateral sclerosis. *Nat. Genet.* 48, 1043–1048. doi: 10.1038/ng.3622

Vance, C., Rogelj, B., Hortobágyi, T., De Vos, K. J., Nishimura, A. L., Sreedharan, J., et al. (2009). Mutations in FUS, an RNA processing protein, cause familial amyotrophic lateral sclerosis type 6. *Science* 323, 1208–1211. doi: 10.1126/science.1165942

Vijayvergiya, C., Beal, M. F., Buck, J., and Manfredi, G. (2005). Mutant superoxide dismutase 1 forms aggregates in the brain mitochondrial matrix of amyotrophic lateral sclerosis mice. *J. Neurosci.* 25, 2463–2470. doi: 10.1523/JNEUROSCI.4385-04.2005

Wang, L., Popko, B., and Roos, R. P. (2011). The unfolded protein response in familial amyotrophic lateral sclerosis. *Hum. Mol. Genet.* 20, 1008–1015. doi: 10.1093/hmg/ddq546

Watanabe, M., Dykes-Hoberg, M., Culotta, V. C., Price, D. L., Wong, P. C., and Rothstein, J. D. (2001). Histological evidence of protein aggregation in mutant SOD1 transgenic mice and in amyotrophic lateral sclerosis neural tissues. *Neurobiol. Dis.* 8, 933–941. doi: 10.1006/nbdi.2001.0443

Winderickx, J., Delay, C., De Vos, A., Klinger, H., Pellens, K., Vanhelmont, T., et al. (2008). Protein folding diseases and neurodegeneration: lessons learned from yeast. *Biochim. Biophys. Acta* 1783, 1381–1395. doi: 10.1016/j.bbamcr.2008.01.020

Wu, C. (1984). Two protein-binding sites in chromatin implicated in the activation of heat-shock genes. *Nature* 309, 229–234. doi: 10.1038/309229a0

Wu, C.-H., Fallini, C., Ticozzi, N., Keagle, P. J., Sapp, P. C., Piotrowska, K., et al. (2012). Mutations in the profilin 1 gene cause familial amyotrophic lateral sclerosis. *Nature* 488, 499–503. doi: 10.1038/nature11280

Wu, B. J., Kingston, R. E., and Morimoto, R. I. (1986). Human HSP70 promoter contains at least two distinct regulatory domains. *Proc. Natl. Acad. Sci. U S A* 83, 629–633. doi: 10.1073/pnas.83.3.629

Xing, S., Wallmeroth, N., Berendzen, K. W., and Grefen, C. (2016). Techniques for the analysis of protein-protein interactions *in vivo*. *Plant Physiol.* 171, 727–758. doi: 10.1104/pp.16.00470

Yang, Y., Hentati, A., Deng, H. X., Dabbagh, O., Sasaki, T., Hirano, M., et al. (2001). The gene encoding alsin, a protein with three guanine-nucleotide exchange factor domains, is mutated in a form of recessive amyotrophic lateral sclerosis. *Nat. Genet.* 29, 160–165. doi: 10.1038/ng1101-352b

Yeger-Lotem, E., Riva, L., Su, L. J., Gitler, A. D., Cashikar, A. G., King, O. D., et al. (2009). Bridging high-throughput genetic and transcriptional data reveals cellular responses to α-synuclein toxicity. *Nat. Genet.* 41, 316–323. doi: 10.1038/ng.337

Conflict of Interest Statement: The authors declare that the research was conducted in the absence of any commercial or financial relationships that could be construed as a potential conflict of interest.

frontiers in Molecular Neuroscience

REVIEW
published: 02 November 2018
doi: 10.3389/fnmol.2018.00400

Exploiting Post-mitotic Yeast Cultures to Model Neurodegeneration

Andrea Ruetenik[1,2] *and Antonio Barrientos*[1,2,3]*

[1] Department of Neurology, School of Medicine, University of Miami Miller School of Medicine, Miami, FL, United States, [2] Neuroscience Graduate Program, School of Medicine, University of Miami Miller School of Medicine, Miami, FL, United States, [3] Department of Biochemistry, School of Medicine, University of Miami Miller School of Medicine, Miami, FL, United States

Over the last few decades, the budding yeast *Saccharomyces cerevisiae* has been extensively used as a valuable organism to explore mechanisms of aging and human age-associated neurodegenerative disorders. Yeast models can be used to study loss of function of disease-related conserved genes and to investigate gain of function activities, frequently proteotoxicity, exerted by non-conserved human mutant proteins responsible for neurodegeneration. Most published models of proteotoxicity have used rapidly dividing cells and suffer from a high level of protein expression resulting in acute growth arrest or cell death. This contrasts with the slow development of neurodegenerative proteotoxicity during aging and the characteristic post-mitotic state of the affected cell type, the neuron. Here, we will review the efforts to create and characterize yeast models of neurodegeneration using the chronological life span model of aging, and the specific information they can provide regarding the chronology of physiological events leading to neurotoxic proteotoxicity-induced cell death and the identification of new pathways involved.

Keywords: inducible yeast model, *Saccharomyces cerevisiae*, chronological life span, neurodegenerative disorder, mitochondria, proteotoxicity, reactive oxygen species

OPEN ACCESS

Edited by:
Ralf J. Braun,
University of Bayreuth, Germany

Reviewed by:
Per Olov Ingvar Widlund,
University of Gothenburg, Sweden
Dina Petranovic,
Chalmers University of Technology, Sweden

***Correspondence:**
Antonio Barrientos
abarrientos@med.miami.edu

Received: *08 June 2018*
Accepted: *12 October 2018*
Published: *02 November 2018*

Citation:
Ruetenik A and Barrientos A (2018) Exploiting Post-mitotic Yeast Cultures to Model Neurodegeneration. Front. Mol. Neurosci. 11:400. doi: 10.3389/fnmol.2018.00400

NEURODEGENERATIVE DISEASES MODELED IN YEAST

The unicellular yeast *Saccharomyces cerevisiae,* known as baker's yeast or brewer's yeast, has been extensively used in the areas of biotechnology and biomedicine. Over the last century, *S. cerevisiae* has been used as a valuable organism for studying the principles of microbiology, characterizing biochemical pathways and understanding the biology of more complex eukaryotic organisms (Botstein, 1991). A multiplicity of basic cellular activities are conserved from yeast to humans, including DNA replication, recombination and repair, RNA transcription and translation, intracellular trafficking, enzymatic activities of general metabolism and mitochondrial biogenesis, protein quality control pathways, nutrient sensing, and stress resistance pathways (reviewed in Barrientos, 2003). Therefore, knowledge gained in yeast has been fundamental to understanding the physiology of human cells and the pathophysiology of human diseases.

Over the last two decades, yeast has been used to model the human aging process and complex neurodegenerative disorders, including amyotrophic lateral sclerosis (ALS), Parkinson's disease (PD), and Huntington's disease (HD) (reviewed in Miller-Fleming et al., 2008). In humans, these neurodegenerative disorders are characterized by the progressive, selective loss of

neurons in different areas of the brain associated with the misfolding of disease-specific proteins. Although yeast cells are less complex than human neurons, basic metabolic pathways involved in neurodegeneration are well-conserved in *S. cerevisiae*, as mentioned earlier.

Constructing a yeast model of a human neurodegenerative disorder does not present major technical difficulties *per se* but requires a carefully designed multistep plan (**Figure 1**). A major goal is that the yeast model of a particular disease must recapitulate the crucial events preceding cell death that are manifested during the course of the human disorder.

The strategies that are usually followed in the construction of yeast models of human neurodegenerative diseases depend on genetic and pathophysiological constraints. In some cases, human disorders result from a loss of function of the disease gene encoded protein. In these cases, when the human disease gene is conserved from yeast to humans, functional complementation studies will allow determining whether the human disease gene product partially or fully replaces the function of the yeast gene product. If complementation occurs, human disease gene mutant alleles are expressed in yeast and tested for functionality as for mutations in the Cu–Zn superoxide dismutase gene responsible for ALS (Gunther et al., 2004). If complementation does not occur, the disease mutations, frequently involving conserved protein residues, are alternatively introduced in the yeast protein and subsequently analyzed as it has been reported for mutations in the adenine nucleotide translocator (*ANT1*) responsible for cases of external progressive ophthalmoplegia (Fontanesi et al., 2004).

In age-associated neurodegenerative disorders such as Alzheimer's disease (AD), PD, or HD, the human disease genes are restricted to vertebrates. In these diseases, however, a gain of function of the disease mutant proteins greatly contributed to pathogenicity. Mutant forms of the proteins huntingtin (htt) and α-synuclein, responsible for HD and some familiar forms of PD, respectively, undergo misfolding and damage several cellular structures thus leading to cell death. Yeast models of these disorders are constructed by expressing the human disease gene in yeast thus providing paradigms where the toxic effect of the misfolded protein on the cellular physiology and metabolism can be conveniently studied (Outeiro and Lindquist, 2003; Willingham et al., 2003; Ocampo et al., 2010).

THE YEAST CHRONOLOGICAL LIFE SPAN ASSAY: A BETTER SYSTEM TO MODEL NEURODEGENERATION?

Yeast Aging

The ideal yeast models of age-associated neurodegeneration should incorporate the concept of cellular aging. Yeast has two life spans; a replicative life span (RLS), defined as the number of daughters produced by each dividing mother cell, and a chronological life span (CLS), defined as the capacity of stationary (Go) cultures to maintain viability over time. The CLS assay, initially established by Valter Longo (University of Southern California) (Longo et al., 1996, 2012; Fabrizio et al., 2001; Fabrizio and Longo, 2007), has been proposed to reflect aging in post-mitotic mammalian cells, such as neurons (Chen et al., 2005; Braun et al., 2009). Despite the different level of complexity between yeast and human post-mitotic cells, yeast models of aging have been instrumental for the identification of essential conserved pathways that influence healthspan and life span. For example, studies aiming to understand the molecular mechanisms of calorie-restriction (CR)-mediated longevity, allowed for the identification of several longevity genes (reviewed in Ruetenik et al., 2016). In yeast, CR down-regulates the conserved Ras/cAMP/PKA, TOR, and Sch9 signaling pathways that integrate the nutrient and other environmental cues to regulate cell growth, division and life span (Wei et al., 2008). Deletion of *RAS2*, *TOR1,* or *SCH9* enhances cellular protection against thermal and oxidative stresses and extends yeast CLS (Longo and Finch, 2003). Inhibition of these pathways converges on the activation of stress resistance transcription factors that will induce the expression of cell protection systems (e.g., catalase and superoxide dismutase -SOD2) and accumulation of stored nutrients (trehalose and glycogen). The key components of these pathways also regulate stress resistance and life span in higher eukaryotes (Fontana et al., 2010). For example, both Akt and S6K, homologs of yeast *SCH9*, regulate life span in higher eukaryotes and inhibition of Tor/S6K signaling extends life span in worms, flies, and mice (Paradis et al., 1999; Hertweck et al., 2004; Kapahi et al., 2004; Selman et al., 2009). Also, mice deficient in elements of the Ras pathway have extended health and life span (Yan et al., 2007; Enns et al., 2009). The longevity pathways play an essential role in the regulation of mitochondrial biogenesis and function, crucial for the management of neuronal life and death, in yeast and higher eukaryotes including mammals (Bonawitz et al., 2007; Anderson and Prolla, 2009). For example, deletion of the *TOR1* gene extends yeast CLS in part by increasing mitochondrial mass and respiration (Bonawitz et al., 2007) and by promoting adaptive mitochondrial reactive oxygen species (ROS) signaling (Pan et al., 2011). The Ras/cAMP/PKA pathway senses excessive ROS to signal to the Hap2,3,4,5 transcriptional system and down-regulate mitochondrial biogenesis (Dejean et al., 2002; Chevtzoff et al., 2009). Also in mammals, modulation of mitochondrial biogenesis and metabolism through the Tor, Akt1, and Ras pathways involves the transcriptional co-activator PGC-1α (Anderson and Prolla, 2009). PGC-1α transcriptional activity appears to be induced in the oxidative stress response and CR through a shared mechanism, suggesting that in mammals, regulation of mitochondrial function is a critical element in both cell survival and longevity (Anderson et al., 2008).

Therefore, the yeast CLS model of aging is expected to be an informative paradigm regarding connections between aging and neurodegeneration, at least for those diseases originating from proteotoxic stress.

The CLS Assay

Chronological life span determination must be conducted in exact conditions to ensure reproducibility. CLS is classically determined in cells grown in liquid synthetic complete media containing 2% glucose (SDC) supplemented with standard

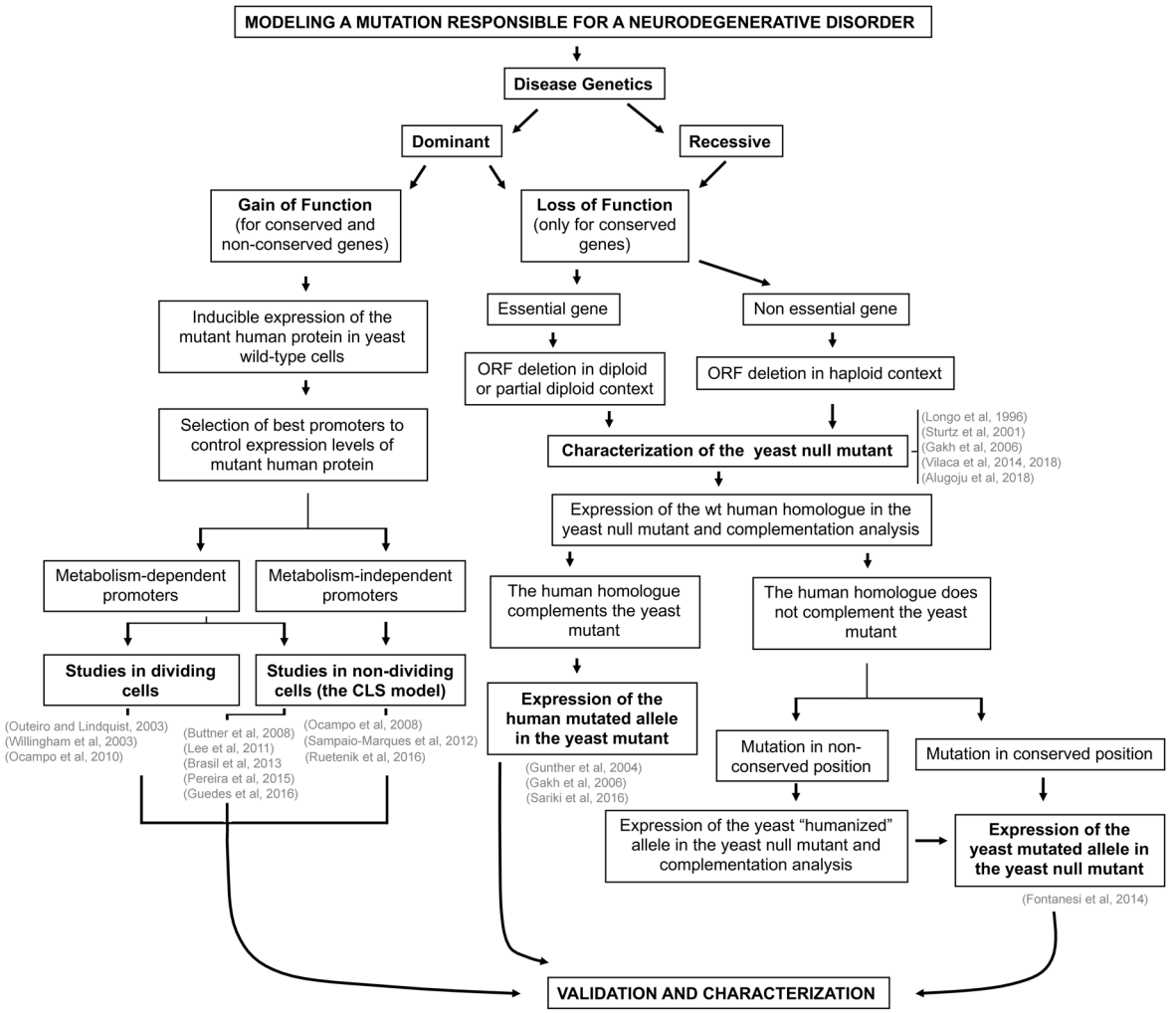

FIGURE 1 | Scheme depicting the strategic planning for the creation of yeast models of neurodegenerative disorders. The strategies used for the construction of yeast models of human monogenic neurodegenerative diseases depend on genetic and pathophysiological constraints. Whether the disease is dominant or recessive, whether the phenotype results from a gain or a loss of function of the protein involved, and whether the gene is functionally conserved or not from yeast to humans are determinants of the kind of yeast model that can be generated. References located in the relevant text boxes provide actual examples in the literature of yeast models of neurodegenerative disorders. See full explanation in the text. Figure modified from Fontanesi et al. (2009).

amounts of amino acids and nucleotide bases as previously described (Sherman, 1991; Ocampo and Barrientos, 2011). The assay is depicted in **Figure 2** and briefly explained in the figure legend. During CLS, multiple approaches can be implemented to analyze the progression or decline of physiological features over time, how they are influenced by the expression of toxic proteins, and how they correlate with survival. As an example, an array of assays that can be implemented to analyze mitochondrial function and ROS production is presented in **Figure 3**.

Strain Background

When preparing yeast models of aging and neurodegeneration it is important to consider the strain background. Several laboratory strains commonly used in aging research are genetically and physiologically heterogeneous (Mortimer and Johnston, 1986; van Dijken et al., 2000), which is reflected in some manner in their CLS (Fabrizio and Longo, 2007; Ocampo and Barrientos, 2011; Ocampo et al., 2012). For example, two different yeast genetic backgrounds commonly used in this field are the short-lived strains BY4741 (Powers et al., 2006; Murakami et al., 2008; Burtner et al., 2009) and DBY2006 (Bonawitz et al., 2007; Pan and Shadel, 2009). Many commonly used strains, including BY4741, CEN.PK113-7D and DBY2006, are S288c derivatives that carry a mutation affecting Hap1, a heme-dependent regulator of a number of genes involved in electron-transfer reactions (Gaisne et al., 1999). This contributes to their reduced ability to respire compared with strains carrying a wild-type *HAP1* gene such as W303, although other genetic differences between the strains may also contribute (Ocampo et al., 2012). As a consequence, when the cells are grown in synthetic medium containing 2% glucose, the CLS of BY4741 (∼8 days), CEN.PK113-7D (∼9 days), and DBY2006 (∼3 days) is shorter

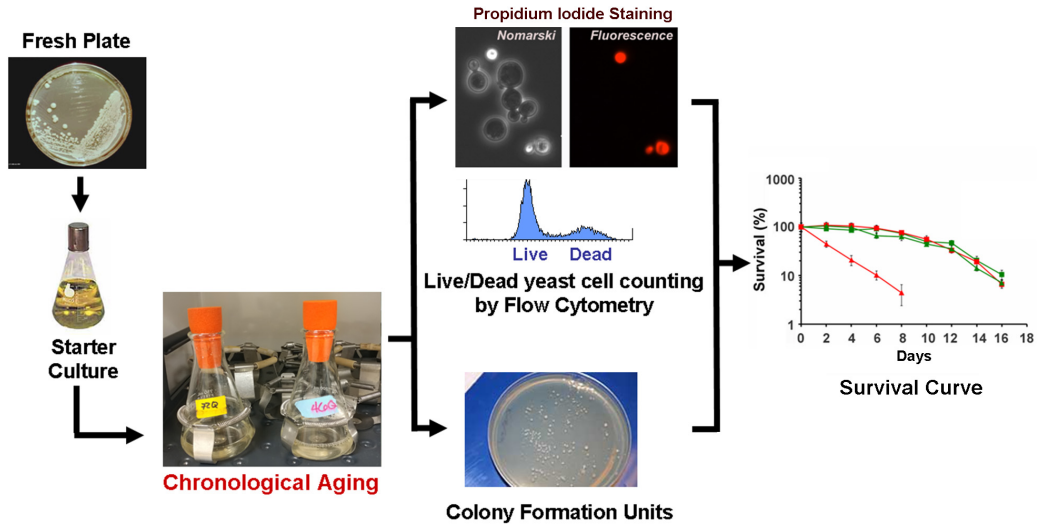

FIGURE 2 | The chronological life span (CLS) assay. In a typical CLS assay, yeast strains from frozen stocks (–80°C) are patched onto YPD agar plates (2% glucose) and incubated at 30°C. The following day, cells are inoculated into 10 ml of SDC media and grown overnight. After 24 h, cells are inoculated into 50 ml of synthetic (SDC) media in 250-ml flasks to an optical density at 600 nm (OD_{600}) of 0.250. Cultures are then grown with shaking (250 rpm) at 30°C. We recommend that all flasks are capped using Bio-Silico plugs that ensure sterility and maximize airflow (Hirschmann, Louisville, KY, United States). Maximum cell density is normally reached after 48 h of growth in SDC, therefore we consider 3 days after inoculation as Day 0 of CLS. Subsequently, cellular viability is determined every other day by either a clonogenic approach using the colony formation unit (CFU) assay of propidium iodide staining and flow cytometry analyses (PI-FCM) as described (Ocampo and Barrientos, 2012; Ocampo et al., 2012). The data obtained from viability analysis is then used to construct survival curves.

than of W303 yeast (∼10.5 days), and the effect of mutations affecting nutrient-sensing and stress-resistance pathways are not exactly equal (for a comparison of CLS in different yeast strains, see, Ocampo and Barrientos, 2011; Ocampo et al., 2012; Chen and Petranovic, 2015). Therefore, the use of at least two different strain backgrounds is always advised to obtain interpretable results.

External Modulators of Yeast CLS

Various external conditions have been found to shorten or extend yeast CLS in wild-type cells. Those need to be taken into account when designing the CLS assays with yeast models of neurodegenerative diseases and when interpreting the results obtained. For example, the CLS on the type of medium in which cells are initially grown. Yeast grown in synthetic medium containing dextrose survive for a few days (from 6 to 11 depending on the yeast strain), which is a very short, high-metabolic post-diauxic phase (Sinclair et al., 1998; Longo, 1999). In contrast, wild-type yeast grown in YPD, and maintained on expired YPD medium, can survive for several weeks, and thus have a prolonged period of hypometabolism in stationary phase (Sinclair et al., 1998; Longo, 1999 and reviewed in Chen et al., 2005). Yeast cultures even have slightly longer survival if they are pre-grown in YPEG (respiratory media) (MacLean et al., 2001). Additional modulators of CLS include: pH of the growth culture medium (Burtner et al., 2009; Longo et al., 2012; Ocampo et al., 2012), amino acid content (Johnson and Johnson, 2014; Maruyama et al., 2016), nitrogen source (Hess et al., 2006; Santos et al., 2015), osmolarity (Kaeberlein et al., 2002; Smith et al., 2007; Murakami et al., 2008), and temperature (Smith et al., 2007). All these factors need to be carefully controlled and maintained constant through experimentation since they are significant sources of experimental variability.

CLS STUDIES USING YEAST MODELS OF NEURODEGENERATIVE DISEASE

Although, the CLS assay has been used extensively to study and identify modifiers of normal yeast aging, proportionately few studies have employed the CLS assay to study yeast models of neurodegenerative disease. This represents a vast missed opportunity. A summary of studies conducted to date using the CLS assay to evaluate the toxicity of disease-related proteins in a wild-type yeast background as well as studies that attempted to find toxicity suppressors in these models using the CLS assay are listed in **Table 1**. In this section, we will briefly introduce the main findings of these studies, the study limitations, and our advice for future work. As seen in **Table 1**, the majority of these studies also quantified yeast viability throughout the CLS assay using only the colony formation unit (CFU) assay method, which, as explained previously may affect the strength of the interpretations that can be made from these studies if not combined with the parallel use of the PI–FCM method.

Huntington's Disease (HD) and Other Polyglutamine (PolyQ) Disorders

Polyglutamine (PolyQ) diseases are caused by a CAG codon repeat expansion in disease-specific genes resulting in the expression of misfolding/aggregation-prone proteins with

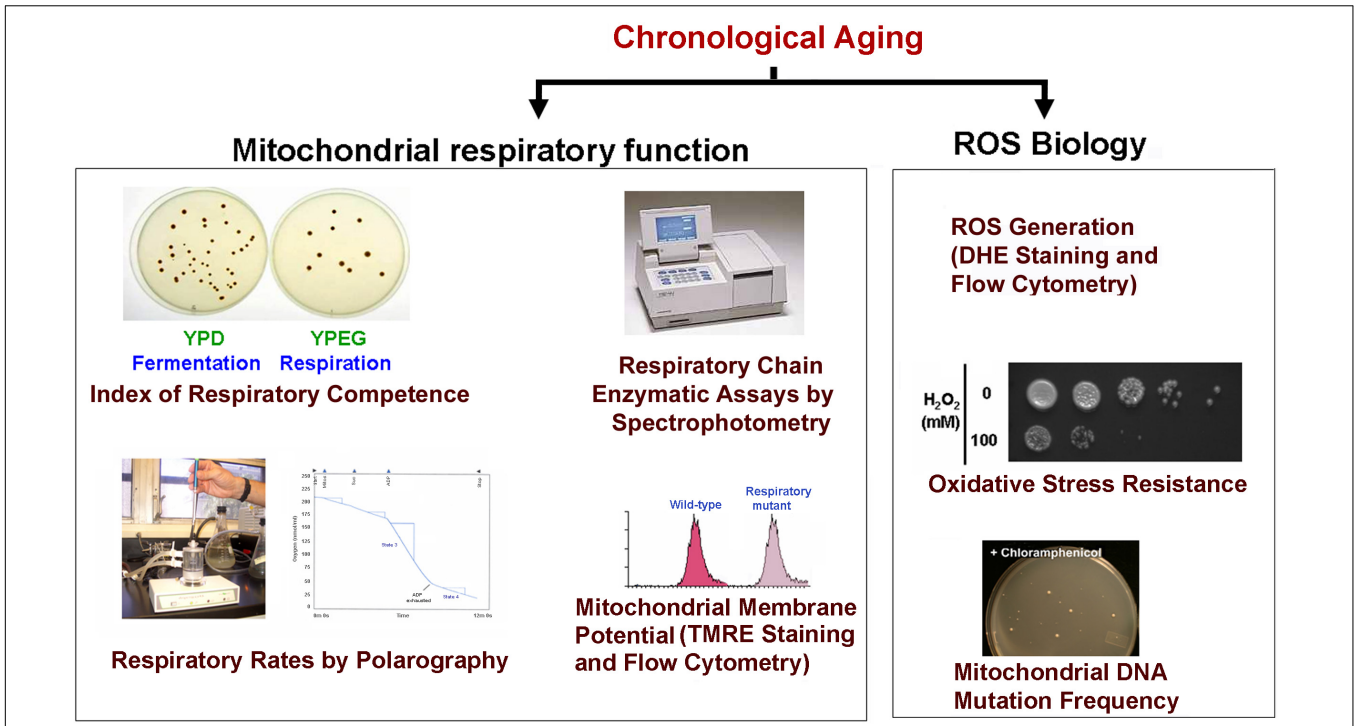

FIGURE 3 | Scheme of some of the experiments used to monitor mitochondrial damage during CLS. During CLS of wild-type yeast cultures expressing or not the toxic proteins are collected at different time points and analyzed for markers of mitochondrial function including: (1) The index of respiratory competence (Parrella and Longo, 2008) or proportion of cells that are able to form colonies in media containing respiratory (glycerol) versus fermentable (glucose) carbon sources. (2) Endogenous cell respiration measured polarographically and mitochondrial respiratory chain (MRC) enzymatic activities measured spectrophotometrically (Barrientos et al., 2009). (3) Mitochondrial membrane potential estimated *in vivo* by flow cytometry using the fluorescent probe tetramethylrhodamine ethyl ester (TMRE) (Ocampo et al., 2010). (4) Oxidative stress and damage: mitochondrial and cellular reactive oxygen species (ROS) production can be measured in whole cells by using the oxidant-sensitive fluorescent probes, MitoSOX Red and dihydroethidium (DHE) as described (Ocampo et al., 2012). Additionally, resistance to oxidative stress can be determined by exposing cells to high H_2O_2 concentrations (up to 100 mM) for 1 h prior to testing growth in complete solid media. Also, mtDNA point mutation frequency can be estimated by counting the proportion of cells that acquire resistance to specific antibiotics (chloramphenicol or erythromycin). Cells are plated in respiratory media supplemented with the drugs as described (O'Rourke et al., 2002).

expanded polyQ stretches. These include HD, characterized by intranuclear and cytoplasmic htt inclusions, and six types of spinocerebellar ataxias (Shao and Diamond, 2007). Mitochondrial dysfunction, altered mitochondrial integrity and dynamics and impaired axonal trafficking have been associated with the pathogenesis of polyQ diseases in human patients and several research model organisms (Panov et al., 2002; Trushina et al., 2004; Cui et al., 2006; Lin and Beal, 2006; Wang et al., 2009). Mutant htt may also damage neurons directly by inducing mitochondrial depolarization and altering calcium homeostasis in patients and in mouse models (Panov et al., 2002). Additionally, mutant htt has been shown to alter mitochondrial function indirectly by inhibiting the expression of the transcriptional co-activator PGC-1α, which regulates mitochondrial biogenesis and respiration (Cui et al., 2006).

Yeast Models in Dividing Cells

In yeast, expression of htt exon I fragments comprising the polyQ stretches faithfully recapitulates htt misfolding/aggregation in a polyQ length-dependent manner, as shown by the pioneering work of Dr. Susan Lindquist (Krobitsch and Lindquist, 2000). These models were constructed by placing polyQ expression under the control of a galactose-inducible promoter. Cells were transferred from glucose (or raffinose) to galactose-containing media to induce strong polyQ expression and acute cytotoxicity. Upon polyQ toxicity, several pathways, including ER stress, cytoskeletal disturbances, oxidative stress, and mitochondrial dysfunction were found to contribute to growth arrest and cell death (Meriin et al., 2002; Muchowski et al., 2002; Solans et al., 2006; Duennwald and Lindquist, 2008; Ocampo et al., 2010). These models have been used extensively to search for suppressors of polyQ toxicity. Toxicity can be reduced by enhancing the clearance pathways for the removal of cytoplasmic aggregate-prone proteins by increasing autophagy (Sarkar et al., 2009), activating the ubiquitin–proteasome system (Bauer and Nukina, 2009) or repairing the endoplasmic reticulum-associated degradation (ERAD) pathway (Duennwald and Lindquist, 2008). Toxicity is ameliorated by modulating the chaperone systems involved in protein refolding, aggregation and disaggregation, thus shifting the balance toward the non-toxic species (Krobitsch and Lindquist, 2000; Vacher et al., 2005). Suppression of polyQ toxicity is also achieved by protecting the cells against events downstream from polyQ misfolding and oligomerization, including suppression of cytoskeletal instability

TABLE 1 | Yeast models of neurodegenerative disorders established in the context of the chronological life span model of aging.

Disorder	Protein involved	Inducible expression system	Toxic?	Select assays reported	Strain and growth phases studied	CLS evaluation method	Interventions tested for CLS	Reference
Huntington's disease	Huntingtin	β-Estradiol inducible 103Q-htt expression *TEF1-7* promoter	Yes	103Q expression by fluorescence microscopy Cell respiration Serial dilution growth test Oxidative phosphorylation inhibitors	W303 Exponential Stationary	CFU Live/dead staining	Glucose restriction *HAP4* overexpression Growth in respiratory media	Ruetenik et al., 2016
Alzheimer's disease	Amyloid-β	Constitutive expression of Amyloid-β with ER targeting signal under multiple promoter types	Yes	CLS (constant pH, oxygen) Serial dilution growth test ROS levels Amyloid oligomerization by immunoblot and immunostaining Proteome activity assay Mitochondrial function Transcriptional and lipid composition response to amyloid-β expression Oxygen limitation Glycogen/trehalose levels	CEN.PK113-7D Exponential Diauxic shift Stationary	CFU Serial dilution Live/dead staining	Glucose restriction	Chen and Petranovic, 2015; Chen et al., 2017
	Mutant ubiquitin (UBB^{+1})	Constitutive expression of UBB^{+1} under *TEF1* promoter in single or multi-copy vectors	No	Proteolytic activity assay Induced protein misfolding challenge ROS levels by DHR123 staining TUNEL assay Caspase activation Heat shock/oxidative stress resistance Transcript levels by rtPCR Knockout of *Atg1*	CEN.PK 113-11C Exponential Stationary	CFU Serial dilution Live/dead staining	N/A	Munoz-Arellano et al., 2018
Parkinson's disease	α-Synuclein	Galactose inducible expression of wild-type and A53T mutant α-synuclein at different intensities	Yes	ROS levels by DHE staining Annexin V/PI/TUNEL staining	BY4741 Stationary	CFU Live/dead staining	*aif1*, *yca1*, *nma111* deletion Depletion of mtDNA	Buttner et al., 2008
		Constitutive expression of α-synuclein under *TPI* promoter	Yes	Autophagy activity assay Autophagic activity by western blotting	BY4741 Stationary	CFU	Glucose restriction *tor1* deletion	Guedes et al., 2016
		Doxycycline induction at different times during CLS, Galactose induction at stationary phase Constitutive expression of wild-type and mutant α-synuclein	Yes	ROS levels by DHE staining Autophagy/mitophagy induction by mRNA levels, activity assay, and confocal microscopy Sod1/2 activity Mitochondrial function	BY4741 and W303 Exponential Diauxic shift Stationary	CFU Live/dead staining	*atg11* and *atg32* deletion Chloroquine supplementation	Sampaio-Marques et al., 2012
		Chromosomally integrated α-synuclein under *FAA2* promoter	Yes	ROS levels by DCFH staining Oxidative stress resistance	BY4741 Stationary	CFU	Triclabendazole or Albendazole supplementation	Lee et al., 2011
	Synphilin-1	Constitutively expressed wild-type and mutant synphilin-1 under *TPI1* promoter	Yes	Protein processing by immunoblotting Aggregate formation by fluorescent microscopy Serial dilution growth test ROS levels by DHE staining Annexin V/PI staining	BY4741 Exponential Stationary	CFU	*sir2* deletion	Buttner et al., 2010
	DJ-1	Single deletion of multiple yeast DJ-1 family members	Yes	Autophagic activity by GFP-Atg8 reporter and fluorescent microscopy Heat shock resistance Carbon starvation Rapamycin treatment Gene expression changes upon DJ-1 knockout	BY4742 and BY4743 Exponential Stationary	CFU	N/A	Miller-Fleming et al., 2014

(Continued)

TABLE 1 | Continued

Disorder	Protein involved	Inducible expression system	Toxic?	Select assays reported	Strain and growth phases studied	CLS evaluation method	Interventions tested for CLS	Reference
	Parkin	Constitutive expression of Parkin under *GPD* promoter	No	Oxidative stress resistance Parkin localization by immunoblotting Pink1 overexpression Autophagy disruption Parkin localization and aggregation by fluorescent microscopy	W303 Stationary	CFU	Growth in respiratory media	Pereira et al., 2015
Congenital neuronal ceroid lipofuscinosis, Alzheimer's disease risk, others	Pep4	*pep4* deletion strain	Yes	Serial dilution growth test Stress resistance tests ROS levels by H_2DCFDA staining Mitochondrial morphology	BY4741 Exponential Stationary	CFU Live/dead staining	Quercetin supplementation	Alugoju et al., 2018
Familial amyotrophic lateral sclerosis (ALS)	SOD1	Wild-type and AV4 mutant human *SOD1* under yeast *SOD1* promoter	No	SOD1 activity assay Intracellular oxidation analysis Protein carbonylation assay	BY4741 Exponential Stationary	CFU	*gsh1* deletion	Brasil et al., 2013
		SOD1 and *SOD2* deletion strains	Yes	Oxygen consumption, amino acid requirements	DBY746 and W303 Exponential Diauxic shift Stationary	CFU	Low aeration *coq3 deletion*	Longo et al., 1996
		SOD1 deletion strains	Yes	Mitochondrial fractionation for protein localization SOD enzymatic activity	DBY746 and W303 Exponential Stationary	Serial dilution	*CCS1* overexpression	Sturtz et al., 2001
Fronto-temporal lobar degeneratio/n (FTLD-U), ALS	TDP-43	Galactose inducible expression of wild-type or mutant *TDP-43*	Yes	ROS levels by DHE staining Aggregation formation by fluorescent microscopy Annexin V/PI staining Respiratory capacity	BY4741 Exponential Stationary	CFU	Depletion of mtDNA Deletion/inhibition of respiratory complexes	Braun et al., 2011
Ataxia with oculomotor apraxia type 2 (AOA2) Amyotrophic lateral sclerosis 4 (ALS4)	Sen1	Multiple genetically modified mutant *sen1* strains	Yes	Serial dilution growth test Mitochondrial function by fluorescent microscopy and flow cytometry ROS levels by DHE and H_2DCFDA staining Stress resistance Transcriptome analysis of Sen1 mutants Annexin V/PI staining	BY4741 Exponential Stationary	CFU	N/A	Sariki et al., 2016
Friedreich ataxia	Frataxin (Yfh1p)	Wild-type or mutant *YFH1* expressed into *yfh1* deletion strain under endogenous *YFH1* promoter	Yes	Serial dilution growth test Oxiblot Iron challenge ROS damage Growth in low oxygen	BY4741 Exponential Stationary	CFU	N/A	Gakh et al., 2006
Niemann–Pick type C	NPC1	*ncr1* deleted yeast cells	Yes	Sphingolipid analysis B-Galactosidase activity Oxidative stress resistance Mitochondrial function Mitochondrial network by fluorescent microscopy Serial dilution growth test	BY4741 Exponential Post-diauxic shift Stationary	CFU	Deletion of *SIT4, CDC55, PKH1,* or *SCH9* Treatment with myriocin	Vilaca et al., 2014, 2018

CFU, colony formation unit; CLS, chronological life span.

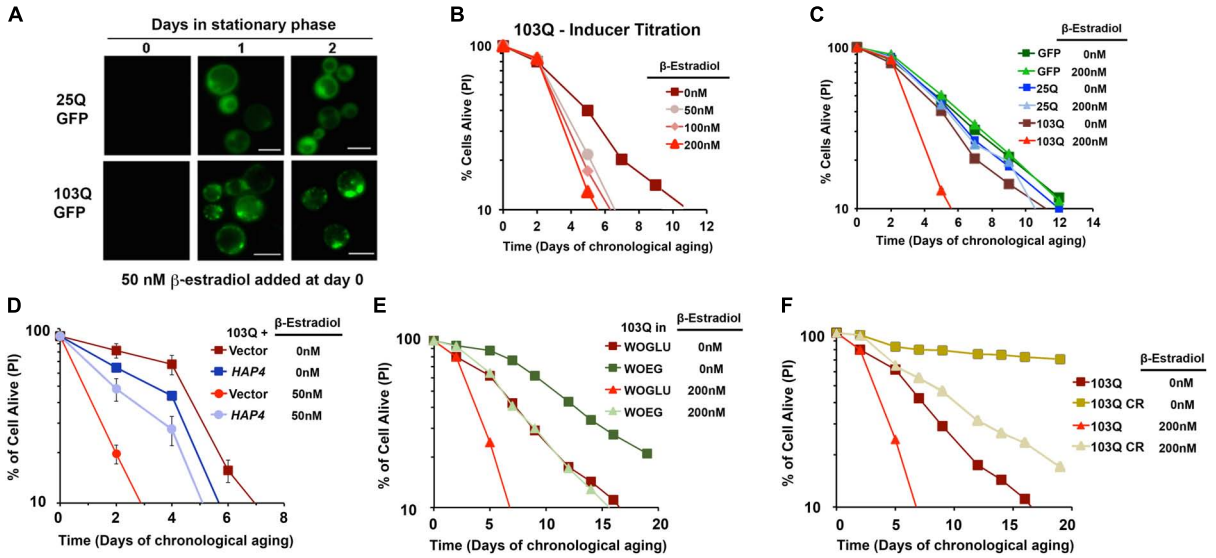

FIGURE 4 | β-Estradiol inducible yeast models of polyglutamine disorders. **(A)** Chronology of polyQ-GFP protein accumulation, followed by fluorescence microscopy, in cells induced with 50 nM β-estradiol. The bar is 5 μm. **(B,C)** Yeast CLS. Survival of wild-type cells expressing 25Q or 103Q from a β-estradiol-inducible promoter activated with the indicated amounts of inducer or supplemented with the solvent (ethanol) was estimated by propidium iodide (PI) staining and flow cytometry analysis of 10,000 cells. Data are average of three samples in % of cells alive at day 0. In **(C)** a β-estradiol titration was performed. **(D)** Effect of increased mitochondrial biogenesis by *HAP4* overexpression on CLS of yeast expressing 103Q from day 0 in the stationary phase. Error bars represent SEM for three independent experiments. **(E)** Effect of growth in synthetic medium containing ethanol and glycerol as non-fermentable (respiratory) carbon sources (WOEG) on 103Q yeast CLS compared to synthetic medium containing glucose as fermentable carbon source (WOGLU). SD <1 for all samples, $n = 3$. **(F)** Effect of calorie restriction (CR) modeled by growing the cells in the presence of 0.5% glucose vs. non-CR (2% glucose) in 103Q yeast CLS. SD <1 for all samples, $n = 3$. This figure was constructed using panels previously published in Ruetenik et al. (2016) with permission since they were published under the terms of the Creative Commons Attribution (CC BY) license.

(Kaminosono et al., 2008), suppression of the kynurenine pathway to limit the accumulation of toxic metabolites that increase ROS generation (Giorgini et al., 2005) and protection of mitochondrial integrity and function (Ocampo et al., 2010). These yeast models have been also used for genome-wide screens to identify genes that enhance polyQ toxicity. The identified genes clustered in the functionally related cellular processes of response to stress, protein folding, and ubiquitin-dependent protein catabolism (Willingham et al., 2003).

Yeast Models in Non-dividing Cells

To ascertain how polyQ toxicity modulates aging, we have studied suppressors of mutant htt toxicity using the CLS assay in a yeast model of HD by expressing 103Q starting at day 0 of the stationary phase using an inducible β-estradiol expression system (**Figure 4**) (Ruetenik et al., 2016). In the CLS assay, in standard synthetic media growth conditions, we observed that overexpression of this 103Q htt fragment through induction with 50 nM β-estradiol resulted in a severe shortening of CLS compared to control cells (Ruetenik et al., 2016) (**Figure 4**).

In previous studies with this yeast model, using exponentially-growing cells, we had discovered that the 103Q mutant htt fragment associates with the mitochondrial membrane and disrupts several key mitochondrial functions (Solans et al., 2004; Ocampo et al., 2010). In an independent study, aiming to understand the determinants of CLS in wild-type yeast, we reported that there are mitochondrial respiratory thresholds during the exponential phase of growth, below which yeast CLS is shortened (Ocampo et al., 2012). We were therefore interested in assessing whether increasing the mitochondrial respiratory capacity in our inducible yeast model of HD from culture initiation could partially or entirely suppress the toxicity of 103Q overexpression in the CLS assay. To test this hypothesis, we explored three separate interventions that had previously been shown to increase mitochondrial respiration during exponential growth and to increase overall CLS. The first intervention, was the constitutive overexpression of *HAP4*, the catalytic subunit of the master transcriptional regulator complex that controls the expression of nuclear genes coding for mitochondrial proteins, which we had previously shown increases mitochondrial respiration in dividing cells when overexpressed (Ocampo et al., 2010). We next tested two nutritional modulators of yeast CLS that increase mitochondrial respiration: growth in media containing non-fermentable carbon sources, and glucose restriction. As expected, each of these three interventions did increase mitochondrial respiration exponential growth phase compared to cells, and these interventions did not decrease 103Q expression compared to controls. Importantly, all three of these interventions tested robustly extended the CLS of yeast overexpressing 103Q beyond that of cells overexpressing 103Q without the interventions (Ruetenik et al., 2016) (**Figure 4**). Therefore, the results in our HD yeast model suggest that treatments targeting mitochondrial

biogenesis, and specifically mitochondrial respiration, may be beneficial in the treatment of HD patients to delay neuronal death.

Alzheimer's Disease (AD)

Chen and Petranovic (2015) employed the CLS assay to study yeast models of AD and how overexpression of amyloid β peptides affects yeast CLS. In these experiments, the authors studied two different amyloid precursor protein cleavage products, Aβ40 and Aβ42. Importantly, Aβ42 has been found to be more prone to aggregation in previous studies by other groups, and it has been hypothesized that mutations that lead to an increase in Aβ42 production may be one of the primary causes of familial AD (Hampel et al., 2010). The experiments by Chen and Petranovic (2015) explored the effects of the constitutive overexpression, at various levels, of either Aβ40 or Aβ42, both with targeting signals directing the peptides to the endoplasmic reticulum (ER) secretory pathway. CLS studies were conducted at a constant pH of 5.0 and dissolved oxygen levels were kept above 30%, all other conditions being standard. In these conditions, overexpression of ER-targeted Aβ40 or Aβ42 both shortened CLS compared to cells without Aβ expression, with Aβ42 overexpression causing the most robust CLS shortening. Propidium iodide live/dead staining further confirmed these findings, revealing that overexpression of the ER-targeted Aβ42 peptide significantly increased the proportion of dead cells throughout the stationary phase compared to control cells (Chen and Petranovic, 2015). In a second publication by this group, a glucose restriction from the standard 2% concentration to 1% glucose at culture initiation was found to robustly increase CLS in the same model system, measured through propidium iodide staining (Chen et al., 2017).

Munoz-Arellano et al. (2018) have also recently studied the consequences of the expression of the loss-of-function ubiquitin variant UBB^{+1} in yeast using the CLS model. This UBB^{+1} variant, found to be neurotoxic in high levels, specifically accumulate and co-aggregate with the tangles and plaques of AD, as well as in HD and some other diseases of protein misfolding, while, in non-diseased cells the UBB^{+1} variant is degraded albeit inefficiently. UBB^{+1} has a high affinity for the proteasome and thus can make it inefficient to degrading other ubiquitinated moieties. To examine the effects of UBB^{+1} on aging cell health, Munoz-Arellano et al. (2018) expressed UBB^{+1} both at low and high levels. Whereas high expression of UBB^{+1} had no effect on yeast CLS, low UBB^{+1} levels greatly extended CLS, through a mechanism that included reduction of ROS levels and attenuation of apoptosis markers compared to control and high UBB^{+1} expressing cells. Altering the ubiquitin–proteasome system capacity by low UBB^{+1} expression was also found to protect cells against the adverse effects of protein misfolding induced through amino acid analogs (Munoz-Arellano et al., 2018). Further exploitation of this UBB^{+1} yeast model might help to identify additional factors that together with UBB^{+1} may contribute to the neurotoxic proteinotaphy disease initiation and/or progression.

Parkinson's Disease (PD) and Other α-Synucleopathies

α-Synuclein (α-syn) is a presynaptic brain protein. Mainly cytosolic, α-synuclein can bind membranes and participate in vesicle trafficking. Misfolded/aggregated α-synuclein is the major constituent of cytoplasmic inclusions called Lewy bodies, a pathological hallmark of α-synucleinopathies (Uversky, 2008). This group of diseases includes PD, multiple system atrophy, and dementia. Mutant α-synuclein, as well as increased α-synuclein levels due to gene duplication, can cause PD. OXPHOS dysfunction and excessive ROS generation have been linked to PD (Schapira et al., 1990; Bender et al., 2006; Kraytsberg et al., 2006; Henchcliffe and Beal, 2008).

Yeast Models in Dividing Cells

Yeast models of α-synucleinopathies consist of overexpression of mutant or wild-type forms of α-synuclein (Outeiro and Lindquist, 2003). α-Synuclein misfolding-aggregation cause growth arrest and induces toxicity and cell death in an expression level-dependent manner (Outeiro and Lindquist, 2003). α-Synuclein toxicity in yeast is characterized by altered lipid metabolism, disrupted vesicular trafficking, ER stress, oxidative stress, impaired protein degradation, and mitochondrion-dependent cell death (Outeiro and Lindquist, 2003; Willingham et al., 2003; Kritzer et al., 2009; Yeger-Lotem et al., 2009; Auluck et al., 2010; Donmez et al., 2012). These yeast models have been also used for genome-wide screens to identify genes that enhance α-synuclein toxicity. Different from what it was found in yeast models of polyQ toxicity, the identified genes clustered in the processes of lipid metabolism and vesicle-mediated transport (Willingham et al., 2003).

Yeast Models in Non-dividing Cells

Whereas studies in growing cells have provided valuable mechanistic and physiological insight into α-synuclein toxicity, they need to be complemented with studies in non-dividing yeast cells to explore how α-synuclein toxicity modulates aging and *vice versa*. Of the neurodegenerative diseases, PD has been the most extensively studied using yeast models and the CLS assay. Of these studies, four have explored the effects of α-synuclein overexpression using different expression systems. The earliest of these studies, by Buttner et al. (2008), used a galactose-inducible system in which wild-type α-synuclein or α-synuclein with the toxic A53T point mutation, a cause of hereditary PD, was highly expressed in yeast at the beginning of the stationary phase. In this system, the overexpression of each form of α-synuclein was highly toxic in the CLS assay, with only about 20% of cells expressing either protein remaining alive by day 3 of the stationary phase, compared to about 70% of cells alive in the empty vector control cells. There was no significant difference seen in cell death between the expression of wild-type or A53T α-synuclein. Deletion of three proteins of interest involved in the apoptotic pathway was found to have no effect on either wild-type or A53T α-synuclein toxicity in the CLS assay. Finally, the authors expressed wild-type or A53T α-synuclein in yeast cells lacking mitochondrial DNA in the CLS assay. Surprisingly, ablation of mitochondrial DNA eliminated the toxic effects of α-synuclein

overexpression in yeast cells in the stationary phase, indicating that the α-synuclein toxicity seen in the CLS assay is dependent on functional mitochondria (Buttner et al., 2008).

In another study, Sampaio-Marques et al. (2012) explored α-synuclein-induced toxicity in the CLS assay using a Tet-On system to induce wild-type α-synuclein expression during exponential growth, the diauxic shift, or the stationary phase of the CLS, and then continued following the yeast life span. Overexpression of α-synuclein was found to be toxic when induced at all stages of growth, but CLS, evaluated through CFU, was shortened most significantly when α-synuclein was induced starting in the stationary phase. These results indicate that aged cells may be particularly vulnerable to high levels of α-synuclein. Interestingly, when α-synuclein was induced at day 0 of the stationary phase, post-exponential phase and diauxic shift, and autophagy was inhibited using the pharmacological drug chloroquine, yeast CLS was greatly extended past that of cells overexpressing α-synuclein alone. However, a chloroquine-only treatment group without α-synuclein expression was not included, making this result difficult to interpret, as autophagy may play a significant role in the survival of wild-type cells in the CLS assay as well. As found by Buttner et al. (2008), when expressed from a high-overexpression galactose-inducible system, both wild-type or A53T α-synuclein expression were highly toxic to cells in stationary growth, reducing the number of viable cells to only 10% of the initial amount after 30 h of expression, compared to 100% remaining viable in cells with empty vector or overexpressing an α-synuclein A30P mutant protein (Sampaio-Marques et al., 2012). Under moderate expression throughout cell life, controlled by a constitutive *TPI1* promoter, expression of all three forms of α-synuclein showed toxicity compared to vector control cells, with A53T α-synuclein shortening CLS the most, and A30P moderately reducing yeast CLS. Unexpectedly, when the three forms of α-synuclein were expressed in cells lacking *Atg11*, which encodes a protein involved in autophagy coordination, under the *TPI1* constitutive promoter, only the A30P mutant, thought to be the less toxic form of α-synuclein from previous experiments, was found to have a shortened CLS. No toxicity was seen through overexpression of any form of α-synuclein in a mitophagy-deficient *atg32* deletion strain, indicating that mitophagy is specifically essential for α-synuclein induced CLS shortening (Sampaio-Marques et al., 2012).

Two more recent studies have explored exogenous modulators on α-synuclein toxicity. First, a small study by Lee et al. (2011), presented a screen of the Prestwick and NIH chemical libraries for drugs that protect *S. cerevisiae* from sugar-induced cell death (SICD). SICD is triggered when stationary-phase yeast cells are transferred from spent rich medium into water with 2% glucose and no other nutrients, a paradigm that induces the generation of large amounts of ROS. The authors found that triclabendazole, a drug commonly used to treat liver fluke infections in cattle and humans, and approved for veterinary use in the United States, partially protects against SICD. Further tests found that treatment from culture initiation with triclabendazole, also suppresses the toxicity induced by constitutively expressed α-synuclein. Treatment with triclabendazole increased the average CLS, measured by CFU, of cells overexpressing α-synuclein to 194% of the CLS of cells overexpressing α-synuclein with DMSO control (Lee et al., 2011). Triclabendazole is believed to be effective against liver fluke infections by inhibiting β-tubulin. However, triclabenzadole was found to extend the life span of wild-type yeast cells *over* a DMSO control at concentrations that did not affect microtubule morphology (Lee et al., 2011), consistently with the fact that two drugs known to target microtubules in yeast, benomyl and nocodazole did not extend yeast life span (Lee et al., 2011). Because triclabenzadole effectively protected stationary-phase yeast cells from hydrogen peroxide-induced toxicity, the authors concluded that its protection of yeast cells from α-synuclein-induced cell could involve oxidative stress attenuation (Lee et al., 2011).

Most recently, a study by Guedes et al. (2017), reported that glucose restriction to 0.5% extends CLS in yeast overexpressing wild-type α-synuclein from the constitutive *TPI1* promoter. A similar effect was observed upon deletion of *Tor1*, the target of rapamycin, and both interventions were associated with decreased autophagy, which was maintained at homeostatic levels. Maintenance of autophagy in α-synuclein-expressing cells under CR or upon *tor1* deletion was proposed to be achieved by decreasing levels and activity of the yeast sirtuin Sir2 (Guedes et al., 2017).

Synphilin-1

In addition to α-synuclein, additional proteins that have been implicated in PD have been studied using the CLS assay. One of these proteins is Synphilin-1, a known interactor of α-synuclein that was first found using a yeast two-hybrid screen.

Interestingly, while studying this protein, Buttner et al. (2010) observed that whereas overexpression of α-synuclein is much more toxic to yeast than synphilin-1 when overexpressed during exponential growth (dividing cells), expression of synphilin-1 or expression of α-synuclein through the constitutive *TPI1* promoter shortened CLS to a similar extent. Furthermore, co-expression of synphilin-1 along with α-synuclein showed induced higher toxicity to yeast in the stationary phase, shortening their CLS more that expression of either of the proteins alone, thus highlighting the relevance of CLS studies to model neurodegeneration. When synphilin-1 and α-synuclein were expressed in a yeast strain lacking *sir2*, a gene implicated in the process of yeast replicative aging, the toxicity and CLS-shortening induced by expression of the proteins individually or in combination was decreased significantly, although toxicity was still higher when synphilin-1 and α-synuclein were expressed together.

Human DJ-1 Protein

It is also known as PD protein 7 and a member of the DJ-1 superfamily of proteins. DJ-1 has been previously shown to inhibit the aggregation of α-synuclein (Shendelman et al., 2004) and mutations in human DJ-1 have been implicated in a form of autosomal recessive early-onset parkinsonism (Bonifati et al., 2003). DJ-1 plays some role in protection from oxidative stress, but how it functions is still unclear. Since yeast contains

homologs of proteins belonging to the DJ-1 superfamily, Miller-Fleming et al. (2014) studied how deleting these proteins in yeast would affect cell viability during the CLS assay. In wild-type yeast cells, without the expression of α-synuclein, single deletion of multiple DJ-1 family member homologs in yeast shortened CLS (Miller-Fleming et al., 2014). However, the synergistic effect that deletion of these DJ-1 family members may have on α-synuclein toxicity was not studied in this model.

Mutations in *PRKN* or *PARK2*

The coding for the protein Parkin, have been also associated with an autosomal recessive form of juvenile PD (Kitada et al., 1998). Parkin is an E3 ubiquitin ligase, which plays essential roles in mitochondrial quality control and turnover. A yeast model to study the function of the Parkin protein was recently developed, in which wild-type Parkin was constitutively expressed in wild-type yeast cells and grown either in standard glucose media or non-fermentable media containing ethanol and glycerol (Pereira et al., 2015). In standard glucose media, no difference between CLS length was seen between cells with or without Parkin expression. However, when grown in non-fermentable media, cells overexpressing Parkin displayed an extended CLS (Pereira et al., 2015). The effects of Parkin overexpression concomitantly with α-synuclein expression are yet to be studied in the yeast CLS assay.

Familial Amyotrophic Lateral Sclerosis (ALS)

Mutations in the Gene *SOD1*

The coding for the mostly cytosolic form of the Cu–Zn superoxide dismutase, was one of the first genetic causes of familial ALS to be discovered, thus the effects of the deletion and overexpression of the SOD1 protein and SOD1 mutants have been a general research focus and have also been studied using the CLS assay. Across species, mitochondria contain a small fraction of SOD1 in the intermembrane space (Sturtz et al., 2001) and a matrix-located Mn-SOD known as SOD2 (Longo et al., 1996). In the original study by Longo et al. (1996) exploring the role of *SOD1* and *SOD2* in superoxide detoxification and its effect on CLS, single and double deletion yeast were grown in standard conditions and then transferred to sterile water upon entrance into the stationary phase. In these conditions, the Δ*sod2* strain showed slightly shortened CLS compared to wild-type cells, the Δ*sod1* strain showed a moderately shortened CLS, and Δ*sod1*Δ*sod2* yeast displayed a severely reduced CLS. Interestingly, in low aeration conditions in sterile water, the Δ*sod1* strain showed a decreased level of toxicity compared to normoxia, while the Δ*sod2* mutant displayed enhanced toxicity compared to normoxia. The CLS shortening observed from the Δ*sod1*Δ*sod2* strain remained the most extreme. Deletion of *COQ3*, a required gene in the synthesis of coenzyme Q, eliminated the respiratory capacity of the yeast cells, and appeared protective against the deletions of *sod1* and *sod2*, however, the cells quickly died during the diauxic shift of the CLS assay, as respiration is required for entrance into the stationary phase (Longo et al., 1996).

As mentioned earlier, although SOD1 is synthesized in the cytosol, a ∼5% fraction of SOD1 and its copper chaperone Ccs1 are transported into the mitochondria to mature within the mitochondrial intermembrane space (Sturtz et al., 2001). Overexpression of the copper chaperone for SOD1, *CCS*, was found to increase the mitochondrial localization of the SOD1 protein, and notably, yeast cells in which mitochondrial SOD1 was enriched had extended CLS compared to yeast in which SOD1 was expressed without this mitochondrial enrichment (Sturtz et al., 2001). These results suggest that minimizing mitochondrial ROS generation is essential to maintain wild-type life span, although because multiple reports have also documented ROS signaling during exponential growth phase that promotes stress resistance that subsequently extends CLS (Pan et al., 2011; Ocampo et al., 2012), a critical ROS homeostasis needs to be maintained for optimal chronological aging.

Brasil et al. (2013) also studied the effects of *SOD1* or *SOD1* mutant overexpression in wild-type yeast cells. This group specifically studied the differences between overexpression of wild-type *SOD1* and the *SOD1* AV4 mutant, the mutation that has been most commonly associated with familial forms of ALS. As glutathione levels within the cell have also been found to be associated with mutant SOD1 toxicity, and overexpression has been previously seen to reduce mutant SOD1 aggregation, the authors also overexpressed both the wild-type and AV4 SOD1 variants in cells lacking the protein that acts as the first step in glutathione synthesis. In the CLS assay, when cells were transferred to sterile water and kept at 37°C during the stationary phase, overexpression of either wild-type or the AV4 SOD1 mutant significantly extended CLS, though the extension by the AV4 mutant was significantly shorter than that of wild-type SOD1. However, when overexpressed in the strain lacking glutathione synthesis, the protective effects of SOD1 overexpression were abolished entirely, and overexpression of the AV4 mutant shortened CLS (Brasil et al., 2013).

Senataxin (SETX)

SETX, which plays a vital role in maintaining RNA transcriptome homeostasis, is an RNA helicase implicated in two neurodegenerative disorders. Dominantly inherited mutations were identified in rare juvenile-onset, motor neuron disease pedigrees in a familial form of ALS (ALS4), whereas recessive mutations were found to cause a severe early-onset ataxia with oculomotor apraxia (AOA2) that is the second most common recessive ataxia after Freidreich's ataxia (Bennett and La Spada, 2015). Senataxin dysfunction has been studied through the CLS assay by targeting its yeast homolog, Sen1. Specifically, a yeast strain missing the N-terminal region of the Sen1 protein was seen to have a severely shortened CLS in standard conditions compared to wild-type cells. This N-terminal region was previously seen to be necessary for protein–protein interactions (Sariki et al., 2016).

TAR DNA-Binding Protein 43 (TDP-43)

It is associated with a spectrum of neurodegenerative diseases, including ALS. TDP-43 has been shown to bind both DNA and RNA and have multiple functions in transcriptional repression,

pre-mRNA splicing and translational regulation (Sephton et al., 2011). Yeast overexpressing human TDP-43 protein has been used to model dementia and motor neuron disorders, including ALS, in which this protein has been discovered in inclusion bodies. In this yeast model, expression of TDP-43 or TDP-43 mutants was driven by a galactose-inducible promoter on a low-copy-number plasmid, resulting in an intermediate level of expression when induced. In dividing cells, it has been shown that TDP-43 turnover and toxicity depend in part upon the endocytosis pathway (Liu et al., 2017). As seen in ALS patient tissues, TDP-43 inhibits endocytosis, and co-localizes strongly with endocytic proteins. Furthermore, impairing endocytosis increases TDP-43 toxicity, aggregation, and protein levels, whereas enhancing endocytosis reverses these phenotypes (Liu et al., 2017; Leibiger et al., 2018). In non-dividing cells, induction of TDP-43 expression (wild-type or the TDP-43 Q331K variant implicated in ALS) at the beginning of the stationary phase, shortened CLS compared to vector-carrying control cells. Curtailed CLS was similar for both TDP-43 variants by the third day of stationary phase, although TDP-43 Q331K resulted in a much faster decrease in cell viability at early time points. Conversely, when a high-copy-number plasmid was used, induction of wild-type TDP-43 resulted in a high degree of toxicity that quickly reduced cell viability to ∼20% 12 h after induction compared to control cells that remained near 100% viable at this time (Braun et al., 2011). When mitochondrial DNA was depleted, this severe toxic phenotype from wild-type TDP-43 overexpression was partially suppressed (Braun et al., 2011), as previously reported for yeast cells expressing α-synuclein (Buttner et al., 2008). Therefore, mitochondrial respiration has been proposed to play a major role in TDP-43- and α-synuclein-induced cytotoxicities in stationary-phase yeast cells. These results are interesting and would fit with the reported mitochondrial metabolic abnormalities often seen in patients suffering from neurodegenerative disorders. They are also intriguing because although respiratory defects in yeast (even absence of respiration) are less detrimental when produced experimentally only in the stationary phase, once yeast have accumulated nutrient stores during growth and undergone their metabolic remodeling during the diauxic shift, a minimum 40%-residual cell respiration during exponential growth is required for normal CLS (Ocampo et al., 2012).

Other Neurological Disorders

A handful of other neurological disorders have also been modeled in yeast and studied using the CLS assay.

Friedreich Ataxia

Friedreich ataxia is a hereditary autosomal recessive disease that causes severe neurological dysfunction (Rotig et al., 1997). The disease is caused by lowered expression of the human mitochondrial protein frataxin, which is conserved in yeast. In all organisms, frataxin plays an essential role in iron homeostasis and therefore in critical mitochondrial functions such as heme biosynthesis and iron–sulfur cluster assembly (Rotig et al., 1997). Gakh et al. (2006) studied how different mutations in yeast frataxin affected CLS. Their results showed that mutations that resulted in the inability of frataxin to oxidize iron or the inability to mineralize iron, both significantly reduced yeast CLS with similar severity (Gakh et al., 2006). Thus, both these functions seem equally important to preserving cell viability during CLS.

Niemann–Pick Type C (NPC)

Loss of function mutations in human *NPC1* cause the rare, but very severe neurodegenerative disorder called Niemann–Pick type C (NPC). Human NPC1 and its yeast homolog Ncr1 are sphingolipid transporters that localize to vacuole membrane and to the ER. The yeast *ncr1* deletion strain has been studied in the CLS assay. Yeast lacking Ncr1 display a premature aging phenotype (cells grown in standard synthetic media at 26°C) and higher sensitivity to oxidative stress associated with mitochondrial dysfunction and accumulation of long-chain bases (Vilaca et al., 2014). Importantly, deletion of the ceramide-activated protein phosphatases *Pkh1, Sit4* and its activator *cdc55* suppressed *ncr1*-deletion phenotypes but downregulation of *de novo* sphingolipid biosynthesis had no protective effect, suggesting that long-chain bases accumulation and shorten CLS may result from an increased turnover of complex sphingolipids (Vilaca et al., 2014, 2018).

Cathepsin D-Related Diseases

The loss of human protein cathepsin D has been linked to several neurodegenerative disorders. Cathepsin D is a protease required for efficient lysosomal protein breakdown, calcineurin signaling, and endosomal sorting (Aufschnaiter et al., 2017). The yeast homolog of cathepsin D is the vacuolar aspartyl protease (proteinase A) named Pep4. A *pep4* deletion yeast strain was found to accumulate ROS and to have shorter CLS in standard conditions. Pointing toward a deleterious oxidative stress in the deletion strain, supplementation of the culture media with quercetin, a dietary flavonoid with antioxidant properties, found in a variety of variety of fruits and vegetables, increased CLS in the Δ*pep4* strain although a positive effect was also observed in wild-type yeast (Alugoju et al., 2018).

GENE EXPRESSION SYSTEMS AND CLS MODELS

Inducible Gene Expression Systems: Advantages and Limitations

To date, most inducible yeast models of (gain of function) neurodegenerative diseases have been created by heterologous expression of human genes under the control of the strong *GAL1* promoter, which is activated by galactose and repressed by glucose. Although these models have provided a significant amount of information, the lack of regulation of expression levels, generally resulting in high levels of expression, often leads to acute toxicity. These acute effects can be advantageous when screening for drugs or genetic suppressors of cytotoxicity but are not the ideal system for analyzing metabolic or physiological disturbances leading to cytotoxicity. Additionally, gene expression under the control of a galactose-inducible promoter introduces a metabolic constraint, since gene

expression is induced upon transferring the cells to media containing 2% galactose, which is a fermentable carbon source. This system would prevent studies in non-fermentable, respiratory conditions that can be relevant to the study. For example, the use of metabolism-independent inducers would allow for the study of cell toxicities in situations in which the cells are forced to exclusively respire, creating a better model of the highly oxidative neuronal metabolism. Besides, the use of metabolism-independent inducers allows studies in non-dividing post-mitotic cells using the yeast stationary phase model of aging or CLS (Sinclair et al., 1998), the focus of this manuscript. As explained in the previous sections, in this post-mitotic state, energetic dependence on mitochondrial respiration and concomitant ROS production highly resemble the situation in which neuronal cells age.

To create refined inducible yeast models of neurodegenerative disorders, researchers have tested several systems (**Table 2**). Sampaio-Marques and colleagues used a Tet-On inducible system to study how age traits potentiate the cytotoxic effects of α-synuclein. In these models, α-synuclein expression was induced from a Tet-On promoter in different phases of yeast growth (exponential, diauxic, or stationary) and CLS was then determined (Sampaio-Marques et al., 2012). The Tet-on system is highly regulatable although tend to be leaky. Importantly, even at low concentrations, the inducer of the system, tetracyclines, are known inhibitors of mitochondrial translation and can therefore provoke mitochondrial proteotoxic stress, leading to changes in nuclear gene expression and altered mitochondrial dynamics and function, which will introduce a confounding variable in experimental settings (Moullan et al., 2015). The use of newly developed tetracycline-based systems that are more sensitive could be an alternative to minimize the dose of the antibiotic that needs to be used; however, even if no apparent mitochondrial toxicity is detected, widespread gene expression changes may sensitize cells to the intended tetracycline-controlled loss or gain of function, still confounding the results (Chatzispyrou et al., 2015).

In our laboratory, we have focused on modeling HD, based on the expression of polyQ domains of normal and pathological length under the control of different promoters, to test for their advantages and drawbacks. We tested the *CUP1* promoter, two different β-estradiol-inducible *GAL1* promoter systems and the *GAL1* promoter in a Δ*gal1* mutant background (Ocampo and Barrientos, 2008, 2012) (**Table 2**). Evaluation and comparison of the different systems was performed to assess their tightness, regulation of expression levels, self-toxicity, and effects on metabolism. The use of copper is not recommended since it can promote the generation of ROS. Models created using the *GAL1* promoter in cells in which their galactose metabolism is disabled by disrupting the endogenous *GAL1* gene are a good choice, since they are highly regulatable, metabolically gratuitous, and non-toxic. We have opted to more extensively use β-estradiol inducible models, which are strongly regulated and are based on the constitutive expression of a transactivator fusion protein GAL4.ER.VP16, which is formed by a *GAL4* DNA binding domain, a β-estradiol receptor domain and a VP16 (virus protein 16) transcriptional activator that can activate transcription of a gene placed under the control of a galactose-inducible promoter (*GAL1*pr). These models have been further optimized to eliminate VP16 toxicity by using a weak constitutive promoter (an attenuated version of the *TEF1* promoter) for the expression of the GAL4.ER.VP16 transactivator (Ruetenik et al., 2016). In the absence of the β-estradiol hormone, the fusion protein in this system is repressed by the yeast chaperones from the Hsp90 family (Louvion et al., 1993). Upon media supplementation with β-estradiol, the fusion protein is de-repressed, binds to *GAL1*pr through the *GAL4* DNA binding domain and the VP16 recruits the transcriptional machinery to start transcription of the gene of interest. This system has been already used successfully to create models of neurotoxic proteotoxicity expressing polyglutamine domains (Ruetenik et al., 2016) in the context of chronological aging. Using an alternative galactose-independent transactivator could further improve the β-estradiol inducible models. In this line, the recently developed LexA-ER-AD β-estradiol -inducible system, based on a heterologous DNA-binding domain (LexA) and non-toxic activation domains, can be used as an alternative (Ottoz et al., 2014).

Alternative Culture Models for the Study of Chronological Life Span

In the classical CLS assays, the age-dependent viability of non-dividing cells is estimated in conditions that involved starvation of exogenous nutrients and reliance on storage carbohydrates, glycogen and trehalose (Cao et al., 2016). However, because many terminally differentiated human cell types rarely starve and some, such as neurons, can consume a large amount of energy (Bourre, 2006), it has been considered imperative to develop a yeast model to study CLS, in which nutrients are not limited, but cell division stops and metabolism remains highly active. With this goal in mind, uncoupling metabolism from cell division, Nagarajan et al. (2014) have promoted the study of CLS in immobilized cells using bioreactors, a technology that has been extensively used in brewing and bioethanol production (Verbelen et al., 2006). To model CLS under nutrient-replete conditions, the authors encapsulated cells in a matrix made of calcium alginate to form beads that were packed into bioreactors and fed *ad libitum* (Nagarajan et al., 2014). In these conditions, cells stopped dividing, retained high glycolytic flux but decreased expression of genes in the tricarboxylic acid cycle, stored large amounts of glycogen, had enhanced expression of stress resistance genes and maintained >95% viability over prolonged culture (17 days). Therefore, yeast metabolism in bioreactors is very different from metabolism in batch cultures, where yeast cells depend on respiration to survive the diauxic shift and reach the stationary phase (Ocampo et al., 2012). Respiratory-competent cells grown in batch liquid cultures in the presence of 2% glucose use both fermentation of stored carbohydrates and respiration for survival once they reach the stationary phase (Ocampo et al., 2012). However, when yeast is grown in liquid cultures containing only 0.5% glucose (what is considered as a model of calorie restriction), their stress resistance is enhanced, accumulation of stored carbohydrates is increased and CLS is extended by 3–4 fold (above 1 month) while their requirement of oxidative metabolism

TABLE 2 | Inducible gene expression systems used for the construction of yeast models of neurodegeneration.

Promoter	Description/induction	Properties	Reference
*CUP1*pr	*CUP1* codes for metallothionein, a protein that binds copper and mediates resistance to high concentrations of copper and cadmium (Butt et al., 1984). – Induction with Copper (0 to 2 mM $CuSO_4$)	– Tight regulation – Weak promoter – Copper may add toxicity, in combination to expression of toxic proteins.	Ocampo and Barrientos, 2008
*GAL1*pr	– Induction by galactose (usually 2%) – Gratuitous induction can be achieved in a Δ*gal1* strain, in which galactose metabolism is deactivated. Cell can be grown in the presence of any carbon source supplemented with low doses of galactose.	– Strong expression – Gratuitous induction is highly regulatable (0.01 and 0.1% galactose are sufficient to induce expression)	Outeiro and Lindquist, 2003; Willingham et al., 2003
Tet-On promoter	Induction by doxycycline (2 μg/ml)	– Highly regulatable – Basal activity may be significant (leaky promoter). – Doxycycline is a potential mitochondrial translation inhibitor.	Sampaio-Marques et al., 2012
GAL4.ER.VP16 transactivator plus *GAL1*pr	Induction by β-estradiol (5–100 nM)	– Highly regulatable – Expression can be achieved in multiple growth conditions. – To prevent toxicity caused by excess VP16, it is necessary to use weak constitutive promoters (e.g., attenuated *TEF1-7*pr) for the expression of the GAL4.ER.VP16 transactivator. – A galactose-independent LexA-ER-VP6 β-estradiol –inducible system can be used as an alternative (Ottoz et al., 2014)	Ocampo and Barrientos, 2008; Ruetenik et al., 2016

Regulated promoters enable control over the timing and level of gene expression, which is an essential feature to consider for the generation of yeast models of neurodegeneration. They are suitable when expression of genes is desired at a specific stage of cell growth, or to prevent the build-up of cytotoxic effects induced by the protein being expressed. The table lists the inducible expression systems so far used for the generation of yeast models of neurodegeneration, and briefly describe their advantages and drawbacks.

for survival is abolished (Ocampo et al., 2012). Immobilized yeast under calorie-unrestricted bioreactor conditions also exhibits long CLS in the absence of respiration, which is precluded by glucose repression and low O_2 tension (Nagarajan et al., 2014). In conclusion, the pattern of gene expression and the metabolism of immobilized cells grown in bioreactors is similar to that of stationary phase liquid cultures initially grown in the presence of low glucose concentrations. Despite the value of immobilized yeast cultures, the classical liquid cultures may be easier to implement in most research laboratories and offer the possibility to modulate media composition to allow aging cells to use fermentative and respiratory metabolisms.

CONCLUDING REMARKS

Yeast models of neurodegenerative disorders have traditionally used rapidly dividing cells and expression of human disease genes. Although some disease genes are conserved along evolution, some of those responsible for age-associated neurodegenerative disorders are restricted to vertebrates. While many features of the disease cannot be modeled in yeast (e.g., neuron type specificity or loss of function activities), yeast models have proven to provide a robust paradigm for the elucidation of pathways leading to cell death upon deletion or overexpression of conserved genes, or upon heterologous expression of human disease genes. The refinement of yeast models by the incorporation of neurotoxic gene expression controlled by metabolism-independent promoters has allowed the study of neurotoxic proteotoxicity in non-dividing yeast using the CLS model of aging. Although relatively few studies using the yeast CLS model are found so far in the literature, they are expected to exponentially increase as they can be a source of information regarding the chronology of physiological events leading to neurotoxic proteotoxicity-induced cell death and the identification of new pathways involved. Importantly, the yeast CLS model has been instrumental for the identification of pathways that modulate life span in yeast and higher organisms. Therefore, inducible yeast models of neurodegeneration in the context of CLS will allow testing whether and how life span modulators (e.g., nutrient-sensing and stress-resistance pathways) postpone the physiological effects and cell death induced by neurotoxic proteins.

AUTHOR CONTRIBUTIONS

All authors listed have made a substantial, direct and intellectual contribution to the work, and approved it for publication.

FUNDING

This work was supported by a Research grant from The Army Research Office (ARO) # W911NF-16-1-0311 (to AB), a Merit award from the Veterans Administration (VA-) Biomedical

Laboratory Research and Development 1I01BX003303-01 (to AB) and an HD Human Biology Project Fellowship from the Huntington's Disease Society of America (HDSA) # GR009606 (to AR).

ACKNOWLEDGMENTS

We thank Julia Denissova for her help with the construction of **Table 1**.

REFERENCES

Alugoju, P., Janardhanshetty, S. S., Subaramanian, S., Periyasamy, L., and Dyavaiah, M. (2018). Quercetin protects yeast *Saccharomyces cerevisiae pep4* mutant from oxidative and apoptotic stress and extends chronological lifespan. *Curr. Microbiol.* 75, 519–530. doi: 10.1007/s00284-017-1412-x

Anderson, R., and Prolla, T. (2009). PGC-1alpha in aging and anti-aging interventions. *Biochim. Biophys. Acta* 1790, 1059–1066. doi: 10.1016/j.bbagen.2009.04.005

Anderson, R. M., Barger, J. L., Edwards, M. G., Braun, K. H., O'connor, C. E., Prolla, T. A., et al. (2008). Dynamic regulation of PGC-1alpha localization and turnover implicates mitochondrial adaptation in calorie restriction and the stress response. *Aging Cell* 7, 101–111. doi: 10.1111/j.1474-9726.2007.00357.x

Aufschnaiter, A., Kohler, V., and Buttner, S. (2017). Taking out the garbage: cathepsin D and calcineurin in neurodegeneration. *Neural Regen. Res.* 12, 1776–1779. doi: 10.4103/1673-5374.219031

Auluck, P. K., Caraveo, G., and Lindquist, S. (2010). alpha-Synuclein: membrane interactions and toxicity in Parkinson's disease. *Annu. Rev. Cell Dev. Biol.* 26, 211–233. doi: 10.1146/annurev.cellbio.042308.113313

Barrientos, A. (2003). Yeast models of human mitochondrial diseases. *IUBMB Life* 55, 83–95. doi: 10.1002/tbmb.718540876

Barrientos, A., Fontanesi, F., and Diaz, F. (2009). Evaluation of the mitochondrial respiratory chain and oxidative phosphorylation system using polarography and spectrophotometric enzyme assays. *Curr. Protoc. Hum. Genet.* 63, 19.3.1–19.3.14. doi: 10.1002/0471142905.hg1903s63

Bauer, P. O., and Nukina, N. (2009). Enhanced degradation of mutant huntingtin by rho kinase inhibition is mediated through activation of proteasome and macroautophagy. *Autophagy* 5, 747–748. doi: 10.4161/auto.5.5.8704

Bender, A., Krishnan, K. J., Morris, C. M., Taylor, G. A., Reeve, A. K., Perry, R. H., et al. (2006). High levels of mitochondrial DNA deletions in *Substantia nigra* neurons in aging and Parkinson disease. *Nat. Genet.* 38, 515–517. doi: 10.1038/ng1769

Bennett, C. L., and La Spada, A. R. (2015). Unwinding the role of senataxin in neurodegeneration. *Discov. Med.* 19, 127–136.

Bonawitz, N. D., Chatenay-Lapointe, M., Pan, Y., and Shadel, G. S. (2007). Reduced TOR signaling extends chronological life span via increased respiration and upregulation of mitochondrial gene expression. *Cell Metab.* 5, 265–277. doi: 10.1016/j.cmet.2007.02.009

Bonifati, V., Rizzu, P., Van Baren, M. J., Schaap, O., Breedveld, G. J., Krieger, E., et al. (2003). Mutations in the DJ-1 gene associated with autosomal recessive early-onset parkinsonism. *Science* 299, 256–259. doi: 10.1126/science.1077209

Botstein, D. (1991). Why yeast? *Hosp. Pract.* 26, 157–161. doi: 10.1080/21548331.1991.11705312

Bourre, J. M. (2006). Effects of nutrients (in food) on the structure and function of the nervous system: update on dietary requirements for brain. Part 2: macronutrients. *J. Nutr. Health Aging* 10, 386–399.

Brasil, A. A., Belati, A., Mannarino, S. C., Panek, A. D., Eleutherio, E. C., and Pereira, M. D. (2013). The involvement of GSH in the activation of human Sod1 linked to FALS in chronologically aged yeast cells. *FEMS Yeast Res.* 13, 433–440. doi: 10.1111/1567-1364.12045

Braun, R. J., Buttner, S., Ring, J., Kroemer, G., and Madeo, F. (2009). Nervous yeast: modeling neurotoxic cell death. *Trends Biochem. Sci.* 35, 135–144. doi: 10.1016/j.tibs.2009.10.005

Braun, R. J., Sommer, C., Carmona-Gutierrez, D., Khoury, C. M., Ring, J., Buttner, S., et al. (2011). Neurotoxic 43-kDa TAR DNA-binding protein (TDP-43) triggers mitochondrion-dependent programmed cell death in yeast. *J. Biol. Chem.* 286, 19958–19972. doi: 10.1074/jbc.M110.194852

Burtner, C. R., Murakami, C. J., Kennedy, B. K., and Kaeberlein, M. (2009). A molecular mechanism of chronological aging in yeast. *Cell Cycle* 8, 1256–1270. doi: 10.4161/cc.8.8.8287

Butt, T. R., Sternberg, E. J., Gorman, J. A., Clark, P., Hamer, D., Rosenberg, M., et al. (1984). Copper metallothionein of yeast, structure of the gene, and regulation of expression. *Proc. Natl. Acad. Sci. U.S.A.* 81, 3332–3336. doi: 10.1073/pnas.81.11.3332

Buttner, S., Bitto, A., Ring, J., Augsten, M., Zabrocki, P., Eisenberg, T., et al. (2008). Functional mitochondria are required for alpha-synuclein toxicity in aging yeast. *J. Biol. Chem.* 283, 7554–7560. doi: 10.1074/jbc.M708477200

Buttner, S., Delay, C., Franssens, V., Bammens, T., Ruli, D., Zaunschirm, S., et al. (2010). Synphilin-1 enhances alpha-synuclein aggregation in yeast and contributes to cellular stress and cell death in a Sir2-dependent manner. *PLoS One* 5:e13700. doi: 10.1371/journal.pone.0013700

Cao, L., Tang, Y., Quan, Z., Zhang, Z., Oliver, S. G., and Zhang, N. (2016). Chronological Llfespan in yeast is dependent on the accumulation of storage carbohydrates mediated by Yak1, Mck1 and Rim15 Kinases. *PLoS Genet.* 12:e1006458. doi: 10.1371/journal.pgen.1006458

Chatzispyrou, I. A., Held, N. M., Mouchiroud, L., Auwerx, J., and Houtkooper, R. H. (2015). Tetracycline antibiotics impair mitochondrial function and its experimental use confounds research. *Cancer Res.* 75, 4446–4449. doi: 10.1158/0008-5472.CAN-15-1626

Chen, Q., Ding, Q., and Keller, J. N. (2005). The stationary phase model of aging in yeast for the study of oxidative stress and age-related neurodegeneration. *Biogerontology* 6, 1–13. doi: 10.1007/s10522-004-7379-6

Chen, X., Bisschops, M. M. M., Agarwal, N. R., Ji, B., Shanmugavel, K. P., and Petranovic, D. (2017). Interplay of energetics and ER stress exacerbates Alzheimer's amyloid-beta (Abeta) toxicity in yeast. *Front. Mol. Neurosci.* 10:232. doi: 10.3389/fnmol.2017.00232

Chen, X., and Petranovic, D. (2015). Amyloid-beta peptide-induced cytotoxicity and mitochondrial dysfunction in yeast. *FEMS Yeast Res.* 15:fov061. doi: 10.1093/femsyr/fov061

Chevtzoff, C., Yoboue, E. D., Galinier, A., Casteilla, L., Daignan-Fornier, B., Rigoulet, M., et al. (2009). Reactive oxygen species mediated regulation of mitochondrial biogenesis in the yeast *Saccharomyces cerevisiae*. *J. Biol. Chem.* 285, 1733–1742. doi: 10.1074/jbc.M109.019570

Cui, L., Jeong, H., Borovecki, F., Parkhurst, C. N., Tanese, N., and Krainc, D. (2006). Transcriptional repression of PGC-1alpha by mutant huntingtin leads to mitochondrial dysfunction and neurodegeneration. *Cell* 127, 59–69. doi: 10.1016/j.cell.2006.09.015

Dejean, L., Beauvoit, B., Bunoust, O., Guerin, B., and Rigoulet, M. (2002). Activation of Ras cascade increases the mitochondrial enzyme content of respiratory competent yeast. *Biochem. Biophys. Res. Commun.* 293, 1383–1388. doi: 10.1016/S0006-291X(02)00391-1

Donmez, G., Arun, A., Chung, C. Y., Mclean, P. J., Lindquist, S., and Guarente, L. (2012). SIRT1 protects against alpha-synuclein aggregation by activating molecular chaperones. *J. Neurosci.* 32, 124–132. doi: 10.1523/JNEUROSCI.3442-11.2012

Duennwald, M. L., and Lindquist, S. (2008). Impaired ERAD and ER stress are early and specific events in polyglutamine toxicity. *Genes Dev.* 22, 3308–3319. doi: 10.1101/gad.1673408

Enns, L. C., Morton, J. F., Treuting, P. R., Emond, M. J., Wolf, N. S., Dai, D. F., et al. (2009). Disruption of protein kinase A in mice enhances healthy aging. *PLoS One* 4:e5963. doi: 10.1371/journal.pone.0005963

Fabrizio, P., and Longo, V. D. (2007). The chronological life span of *Saccharomyces cerevisiae*. *Methods Mol. Biol.* 371, 89–95. doi: 10.1007/978-1-59745-361-5_8

Fabrizio, P., Pozza, F., Pletcher, S. D., Gendron, C. M., and Longo, V. D. (2001). Regulation of longevity and stress resistance by Sch9 in yeast. *Science* 292, 288–290. doi: 10.1126/science.1059497

Fontana, L., Partridge, L., and Longo, V. D. (2010). Extending healthy life span–from yeast to humans. *Science* 328, 321–326. doi: 10.1126/science.1172539

Fontanesi, F., Diaz, F., and Barrientos, A. (2009). Evaluation of the mitochondrial respiratory chain and oxidative phosphorylation system using yeast models

of OXPHOS deficiencies. *Curr. Protoc. Hum. Genet.* 63, 19.5.1–19.5.20. doi: 10.1002/0471142905.hg1905s63

Fontanesi, F., Palmieri, L., Scarcia, P., Lodi, T., Donnini, C., Limongelli, A., et al. (2004). Mutations in *AAC2*, equivalent to human adPEO-associated *ANT1* mutations, lead to defective oxidative phosphorylation in *Saccharomyces cerevisiae* and affect mitochondrial DNA stability. *Hum. Mol. Genet.* 13, 923–934. doi: 10.1093/hmg/ddh108

Gaisne, M., Becam, A. M., Verdiere, J., and Herbert, C. J. (1999). A 'natural' mutation in *Saccharomyces cerevisiae* strains derived from S288c affects the complex regulatory gene *HAP1* (*CYP1*). *Curr. Genet.* 36, 195–200. doi: 10.1007/s002940050490

Gakh, O., Park, S., Liu, G., Macomber, L., Imlay, J. A., Ferreira, G. C., et al. (2006). Mitochondrial iron detoxification is a primary function of frataxin that limits oxidative damage and preserves cell longevity. *Hum. Mol. Genet.* 15, 467–479. doi: 10.1093/hmg/ddi461

Giorgini, F., Guidetti, P., Nguyen, Q., Bennett, S. C., and Muchowski, P. J. (2005). A genomic screen in yeast implicates kynurenine 3-monooxygenase as a therapeutic target for Huntington disease. *Nat. Genet.* 37, 526–531. doi: 10.1038/ng1542

Guedes, A., Ludovico, P., and Sampaio-Marques, B. (2016). Caloric restriction alleviates alpha-synuclein toxicity in aged yeast cells by controlling the opposite roles of Tor1 and Sir2 on autophagy. *Mech. Ageing Dev.* 161(Pt B), 270–276. doi: 10.1016/j.mad.2016.04.006

Guedes, A., Ludovico, P., and Sampaio-Marques, B. (2017). Caloric restriction alleviates alpha-synuclein toxicity in aged yeast cells by controlling the opposite roles of Tor1 and Sir2 on autophagy. *Mech. Ageing Dev.* 161, 270–276. doi: 10.1016/j.mad.2016.04.006

Gunther, M. R., Vangilder, R., Fang, J., and Beattie, D. S. (2004). Expression of a familial amyotrophic lateral sclerosis-associated mutant human superoxide dismutase in yeast leads to decreased mitochondrial electron transport. *Arch. Biochem. Biophys.* 431, 207–214. doi: 10.1016/j.abb.2004.08.009

Hampel, H., Shen, Y., Walsh, D. M., Aisen, P., Shaw, L. M., Zetterberg, H., et al. (2010). Biological markers of amyloid beta-related mechanisms in Alzheimer's disease. *Exp. Neurol.* 223, 334–346. doi: 10.1016/j.expneurol.2009.09.024

Henchcliffe, C., and Beal, M. F. (2008). Mitochondrial biology and oxidative stress in Parkinson disease pathogenesis. *Nat. Clin. Pract. Neurol.* 4, 600–609. doi: 10.1038/ncpneuro0924

Hertweck, M., Gobel, C., and Baumeister, R. (2004). *C. elegans* SGK-1 is the critical component in the Akt/PKB kinase complex to control stress response and life span. *Dev. Cell* 6, 577–588. doi: 10.1016/S1534-5807(04)00095-4

Hess, D. C., Lu, W., Rabinowitz, J. D., and Botstein, D. (2006). Ammonium toxicity and potassium limitation in yeast. *PLoS Biol.* 4:e351. doi: 10.1371/journal.pbio.0040351

Johnson, J. E., and Johnson, F. B. (2014). Methionine restriction activates the retrograde response and confers both stress tolerance and lifespan extension to yeast, mouse and human cells. *PLoS One* 9:e97729. doi: 10.1371/journal.pone.0097729

Kaeberlein, M., Andalis, A. A., Fink, G. R., and Guarente, L. (2002). High osmolarity extends life span in *Saccharomyces cerevisiae* by a mechanism related to calorie restriction. *Mol. Cell. Biol.* 22, 8056–8066. doi: 10.1128/MCB.22.22.8056-8066.2002

Kaminosono, S., Saito, T., Oyama, F., Ohshima, T., Asada, A., Nagai, Y., et al. (2008). Suppression of mutant Huntingtin aggregate formation by Cdk5/p35 through the effect on microtubule stability. *J. Neurosci.* 28, 8747–8755. doi: 10.1523/JNEUROSCI.0973-08.2008

Kapahi, P., Zid, B. M., Harper, T., Koslover, D., Sapin, V., and Benzer, S. (2004). Regulation of lifespan in *Drosophila* by modulation of genes in the TOR signaling pathway. *Curr. Biol.* 14, 885–890. doi: 10.1016/j.cub.2004.03.059

Kitada, T., Asakawa, S., Hattori, N., Matsumine, H., Yamamura, Y., Minoshima, S., et al. (1998). Mutations in the parkin gene cause autosomal recessive juvenile parkinsonism. *Nature* 392, 605–608. doi: 10.1038/33416

Kraytsberg, Y., Kudryavtseva, E., Mckee, A. C., Geula, C., Kowall, N. W., and Khrapko, K. (2006). Mitochondrial DNA deletions are abundant and cause functional impairment in aged human *Substantia nigra* neurons. *Nat. Genet.* 38, 518–520. doi: 10.1038/ng1778

Kritzer, J. A., Hamamichi, S., Mccaffery, J. M., Santagata, S., Naumann, T. A., Caldwell, K. A., et al. (2009). Rapid selection of cyclic peptides that reduce alpha-synuclein toxicity in yeast and animal models. *Nat. Chem. Biol.* 5, 655–663. doi: 10.1038/nchembio.193

Krobitsch, S., and Lindquist, S. (2000). Aggregation of huntingtin in yeast varies with the length of the polyglutamine expansion and the expression of chaperone proteins. *Proc. Natl. Acad. Sci. U.S.A.* 97, 1589–1594. doi: 10.1073/pnas.97.4.1589

Lee, Y. J., Burlet, E., Wang, S., Xu, B., Huang, S., Galiano, F. J., et al. (2011). Triclabendazole protects yeast and mammalian cells from oxidative stress: identification of a potential neuroprotective compound. *Biochem. Biophys. Res. Commun.* 414, 205–208. doi: 10.1016/j.bbrc.2011.09.057

Leibiger, C., Deisel, J., Aufschnaiter, A., Ambros, S., Tereshchenko, M., Verheijen, B. M., et al. (2018). TDP-43 controls lysosomal pathways thereby determining its own clearance and cytotoxicity. *Hum. Mol. Genet.* 27, 1593–1607. doi: 10.1093/hmg/ddy066

Lin, M. T., and Beal, M. F. (2006). Mitochondrial dysfunction and oxidative stress in neurodegenerative diseases. *Nature* 443, 787–795. doi: 10.1038/nature05292

Liu, G., Coyne, A. N., Pei, F., Vaughan, S., Chaung, M., Zarnescu, D. C., et al. (2017). Endocytosis regulates TDP-43 toxicity and turnover. *Nat. Commun.* 8:2092. doi: 10.1038/s41467-017-02017-x

Longo, V. D. (1999). Mutations in signal transduction proteins increase stress resistance and longevity in yeast, nematodes, fruit flies, and mammalian neuronal cells. *Neurobiol. Aging* 20, 479–486. doi: 10.1016/S0197-4580(99)00089-5

Longo, V. D., and Finch, C. E. (2003). Evolutionary medicine: from dwarf model systems to healthy centenarians? *Science* 299, 1342–1346.

Longo, V. D., Gralla, E. B., and Valentine, J. S. (1996). Superoxide dismutase activity is essential for stationary phase survival in *Saccharomyces cerevisiae*. Mitochondrial production of toxic oxygen species in vivo. *J. Biol. Chem.* 271, 12275–12280. doi: 10.1074/jbc.271.21.12275

Longo, V. D., Shadel, G. S., Kaeberlein, M., and Kennedy, B. (2012). Replicative and chronological aging in *Saccharomyces cerevisiae*. *Cell* 16, 18–31. doi: 10.1016/j.cmet.2012.06.002

Louvion, J. F., Havaux-Copf, B., and Picard, D. (1993). Fusion of GAL4-VP16 to a steroid-binding domain provides a tool for gratuitous induction of galactose-responsive genes in yeast. *Gene* 131, 129–134. doi: 10.1016/0378-1119(93)90681-R

MacLean, M., Harris, N., and Piper, P. W. (2001). Chronological lifespan of stationary phase yeast cells; a model for investigating the factors that might influence the ageing of postmitotic tissues in higher organisms. *Yeast* 18, 499–509. doi: 10.1002/yea.701

Maruyama, Y., Ito, T., Kodama, H., and Matsuura, A. (2016). Availability of amino acids extends chronological lifespan by suppressing hyper-acidification of the environment in *Saccharomyces cerevisiae*. *PLoS One* 11:e0151894. doi: 10.1371/journal.pone.0151894

Meriin, A. B., Zhang, X., He, X., Newnam, G. P., Chernoff, Y. O., and Sherman, M. Y. (2002). Huntington toxicity in yeast model depends on polyglutamine aggregation mediated by a prion-like protein Rnq1. *J. Cell Biol.* 157, 997–1004. doi: 10.1083/jcb.200112104

Miller-Fleming, L., Antas, P., Pais, T. F., Smalley, J. L., Giorgini, F., and Outeiro, T. F. (2014). Yeast DJ-1 superfamily members are required for diauxic-shift reprogramming and cell survival in stationary phase. *Proc. Natl. Acad. Sci. U.S.A.* 111, 7012–7017. doi: 10.1073/pnas.1319221111

Miller-Fleming, L., Giorgini, F., and Outeiro, T. F. (2008). Yeast as a model for studying human neurodegenerative disorders. *Biotechnol. J.* 3, 325–338. doi: 10.1002/biot.200700217

Mortimer, R. K., and Johnston, J. R. (1986). Genealogy of principal strains of the yeast genetic stock center. *Genetics* 113, 35–43.

Moullan, N., Mouchiroud, L., Wang, X., Ryu, D., Williams, E. G., Mottis, A., et al. (2015). Tetracyclines disturb mitochondrial function across eukaryotic models: a call for caution in biomedical research. *Cell Rep.* 10, 00180–00181. doi: 10.1016/j.celrep.2015.02.034

Muchowski, P. J., Ning, K., D'souza-Schorey, C., and Fields, S. (2002). Requirement of an intact microtubule cytoskeleton for aggregation and inclusion body formation by a mutant huntingtin fragment. *Proc. Natl. Acad. Sci. U.S.A.* 99, 727–732. doi: 10.1073/pnas.022628699

Munoz-Arellano, A. J., Chen, X., Molt, A., Meza, E., and Petranovic, D. (2018). Different expression levels of human mutant ubiquitin B(+1) (UBB(+1)) can

modify chronological lifespan or stress resistance of *Saccharomyces cerevisiae*. *Front. Mol. Neurosci.* 11:200. doi: 10.3389/fnmol.2018.00200

Murakami, C. J., Burtner, C. R., Kennedy, B. K., and Kaeberlein, M. (2008). A method for high-throughput quantitative analysis of yeast chronological life span. *J. Gerontol. A Biol. Sci. Med. Sci.* 63, 113–121. doi: 10.1093/gerona/63.2.113

Nagarajan, S., Kruckeberg, A. L., Schmidt, K. H., Kroll, E., Hamilton, M., Mcinnerney, K., et al. (2014). Uncoupling reproduction from metabolism extends chronological lifespan in yeast. *Proc. Natl. Acad. Sci. U.S.A.* 111, E1538–E1547. doi: 10.1073/pnas.1323918111

Ocampo, A., and Barrientos, A. (2008). From the bakery to the brain business: developing inducible yeast models of human neurodegenerative disorders. *Biotechniques* 45, vii–xiv. doi: 10.2144/000112746

Ocampo, A., and Barrientos, A. (2011). Quick and reliable assessment of chronological life span in yeast cell populations by flow cytometry. *Mech. Ageing Dev.* 132, 315–323. doi: 10.1016/j.mad.2011.06.007

Ocampo, A., and Barrientos, A. (2012). Developing yeast models of human neurodegenerative disorders. *Methods Mol. Biol.* 793, 113–127. doi: 10.1007/978-1-61779-328-8_8

Ocampo, A., Liu, J., Schroeder, E. A., Shadel, G. S., and Barrientos, A. (2012). Mitochondrial respiratory thresholds regulate yeast chronological life span and its extension by caloric restriction. *Cell Metab.* 16, 55–67. doi: 10.1016/j.cmet.2012.05.013

Ocampo, A., Zambrano, A., and Barrientos, A. (2010). Suppression of polyglutamine-induced cytotoxicity in *Saccharomyces cerevisiae* by enhancement of mitochondrial biogenesis. *FASEB J.* 24, 1431–1441. doi: 10.1096/fj.09-148601

O'Rourke, T. W., Doudican, N. A., Mackereth, M. D., Doetsch, P. W., and Shadel, G. S. (2002). Mitochondrial dysfunction due to oxidative mitochondrial DNA damage is reduced through cooperative actions of diverse proteins. *Mol. Cell Biol.* 22, 4086–4093. doi: 10.1128/MCB.22.12.4086-4093.2002

Ottoz, D. S., Rudolf, F., and Stelling, J. (2014). Inducible, tightly regulated and growth condition-independent transcription factor in *Saccharomyces cerevisiae*. *Nucleic Acids Res.* 42:e130. doi: 10.1093/nar/gku616

Outeiro, T. F., and Lindquist, S. (2003). Yeast cells provide insight into alpha-synuclein biology and pathobiology. *Science* 302, 1772–1775. doi: 10.1126/science.1090439

Pan, Y., Schroeder, E. A., Ocampo, A., Barrientos, A., and Shadel, G. S. (2011). Regulation of yeast chronological life span by TORC1 via adaptive mitochondrial ROS signaling. *Cell Metab.* 13, 668–678. doi: 10.1016/j.cmet.2011.03.018

Pan, Y., and Shadel, G. S. (2009). Extension of chronological life span by reduced TOR signaling requires down-regulation of Sch9p and involves increased mitochondrial OXPHOS complex density. *Aging* 1, 131–145. doi: 10.18632/aging.100016

Panov, A. V., Gutekunst, C. A., Leavitt, B. R., Hayden, M. R., Burke, J. R., Strittmatter, W. J., et al. (2002). Early mitochondrial calcium defects in Huntington's disease are a direct effect of polyglutamines. *Nat. Neurosci.* 5, 731–736. doi: 10.1038/nn884

Paradis, S., Ailion, M., Toker, A., Thomas, J. H., and Ruvkun, G. (1999). A PDK1 homolog is necessary and sufficient to transduce AGE-1 PI3 kinase signals that regulate diapause in *Caenorhabditis elegans*. *Genes Dev.* 13, 1438–1452. doi: 10.1101/gad.13.11.1438

Parrella, E., and Longo, V. D. (2008). The chronological life span of *Saccharomyces cerevisiae* to study mitochondrial dysfunction and disease. *Methods* 46, 256–262. doi: 10.1016/j.ymeth.2008.10.004

Pereira, C., Costa, V., Martins, L. M., and Saraiva, L. (2015). A yeast model of the Parkinson's disease-associated protein Parkin. *Exp. Cell Res.* 333, 73–79. doi: 10.1016/j.yexcr.2015.02.018

Powers, R. W. III, Kaeberlein, M., Caldwell, S. D., Kennedy, B. K., and Fields, S. (2006). Extension of chronological life span in yeast by decreased TOR pathway signaling. *Genes Dev.* 20, 174–184. doi: 10.1101/gad.1381406

Rotig, A., De Lonlay, P., Chretien, D., Foury, F., Koenig, M., Sidi, D., et al. (1997). Aconitase and mitochondrial iron-sulphur protein deficiency in Friedreich ataxia. *Nat. Genet.* 17, 215–217. doi: 10.1038/ng1097-215

Ruetenik, A. L., Ocampo, A., Ruan, K., Zhu, Y., Li, C., Zhai, R. G., et al. (2016). Attenuation of polyglutamine-induced toxicity by enhancement of mitochondrial OXPHOS in yeast and fly models of aging. *Microb. Cell* 3, 338–351. doi: 10.15698/mic2016.08.518

Sampaio-Marques, B., Felgueiras, C., Silva, A., Rodrigues, M., Tenreiro, S., Franssens, V., et al. (2012). SNCA (alpha-synuclein)-induced toxicity in yeast cells is dependent on sirtuin 2 (Sir2)-mediated mitophagy. *Autophagy* 8, 1494–1509. doi: 10.4161/auto.21275

Santos, J., Leitao-Correia, F., Sousa, M. J., and Leao, C. (2015). Ammonium is a key determinant on the dietary restriction of yeast chronological aging in culture medium. *Oncotarget* 6, 6511–6523. doi: 10.18632/oncotarget.2989

Sariki, S. K., Sahu, P. K., Golla, U., Singh, V., Azad, G. K., and Tomar, R. S. (2016). Sen1, the homolog of human Senataxin, is critical for cell survival through regulation of redox homeostasis, mitochondrial function, and the TOR pathway in *Saccharomyces cerevisiae*. *FEBS J.* 283, 4056–4083. doi: 10.1111/febs.13917

Sarkar, S., Ravikumar, B., Floto, R. A., and Rubinsztein, D. C. (2009). Rapamycin and mTOR-independent autophagy inducers ameliorate toxicity of polyglutamine-expanded huntingtin and related proteinopathies. *Cell Death Differ.* 16, 46–56. doi: 10.1038/cdd.2008.110

Schapira, A. H., Cooper, J. M., Dexter, D., Clark, J. B., Jenner, P., and Marsden, C. D. (1990). Mitochondrial complex I deficiency in Parkinson's disease. *J. Neurochem.* 54, 823–827. doi: 10.1111/j.1471-4159.1990.tb02325.x

Selman, C., Tullet, J. M., Wieser, D., Irvine, E., Lingard, S. J., Choudhury, A. I., et al. (2009). Ribosomal protein S6 kinase 1 signaling regulates mammalian life span. *Science* 326, 140–144. doi: 10.1126/science.1177221

Sephton, C. F., Cenik, C., Kucukural, A., Dammer, E. B., Cenik, B., Han, Y., et al. (2011). Identification of neuronal RNA targets of TDP-43-containing ribonucleoprotein complexes. *J. Biol. Chem.* 286, 1204–1215. doi: 10.1074/jbc.M110.190884

Shao, J., and Diamond, M. I. (2007). Polyglutamine diseases: emerging concepts in pathogenesis and therapy. *Hum. Mol. Genet.* 16, R115–R123. doi: 10.1093/hmg/ddm213

Shendelman, S., Jonason, A., Martinat, C., Leete, T., and Abeliovich, A. (2004). DJ-1 is a redox-dependent molecular chaperone that inhibits alpha-synuclein aggregate formation. *PLoS Biol.* 2:e362. doi: 10.1371/journal.pbio.0020362

Sherman, F. (1991). Getting started with yeast. *Methods Enzymol.* 194, 3–21. doi: 10.1016/0076-6879(91)94004-V

Sinclair, D., Mills, K., and Guarente, L. (1998). Aging in *Saccharomyces cerevisiae*. *Annu. Rev. Microbiol.* 52, 533–560. doi: 10.1146/annurev.micro.52.1.533

Smith, D. L. Jr., Mcclure, J. M., Matecic, M., and Smith, J. S. (2007). Calorie restriction extends the chronological lifespan of *Saccharomyces cerevisiae* independently of the Sirtuins. *Aging Cell* 6, 649–662. doi: 10.1111/j.1474-9726.2007.00326.x

Solans, A., Zambrano, A., and Barrientos, A. (2004). Cytochrome c oxidase deficiency: from yeast to human. *Preclinica* 2, 336–348.

Solans, A., Zambrano, A., Rodriguez, M., and Barrientos, A. (2006). Cytotoxicity of a mutant huntingtin fragment in yeast involves early alterations in mitochondrial OXPHOS complexes II and III. *Hum. Mol. Genet.* 15, 3063–3081. doi: 10.1093/hmg/ddl248

Sturtz, L. A., Diekert, K., Jensen, L. T., Lill, R., and Culotta, V. C. (2001). A fraction of yeast Cu, Zn-superoxide dismutase and its metallochaperone, CCS, localize to the intermembrane space of mitochondria. A physiological role for SOD1 in guarding against mitochondrial oxidative damage. *J. Biol. Chem.* 276, 38084–38089.

Trushina, E., Dyer, R. B., Badger, J. D. II, Ure, D., Eide, L., Tran, D. D., et al. (2004). Mutant huntingtin impairs axonal trafficking in mammalian neurons in vivo and in vitro. *Mol. Cell Biol.* 24, 8195–8209. doi: 10.1128/MCB.24.18.8195-8209.2004

Uversky, V. N. (2008). Alpha-synuclein misfolding and neurodegenerative diseases. *Curr. Protein Pept. Sci.* 9, 507–540. doi: 10.2174/138920308785915218

Vacher, C., Garcia-Oroz, L., and Rubinsztein, D. C. (2005). Overexpression of yeast hsp104 reduces polyglutamine aggregation and prolongs survival of a transgenic mouse model of Huntington's disease. *Hum. Mol. Genet.* 14, 3425–3433. doi: 10.1093/hmg/ddi372

van Dijken, J. P., Bauer, J., Brambilla, L., Duboc, P., Francois, J. M., Gancedo, C., et al. (2000). An interlaboratory comparison of physiological and genetic

properties of four *Saccharomyces cerevisiae* strains. *Enzyme Microb. Technol.* 26, 706–714. doi: 10.1016/S0141-0229(00)00162-9

Verbelen, P. J., De Schutter, D. P., Delvaux, F., Verstrepen, K. J., and Delvaux, F. R. (2006). Immobilized yeast cell systems for continuous fermentation applications. *Biotechnol. Lett.* 28, 1515–1525. doi: 10.1007/s10529-006-9132-5

Vilaca, R., Barros, I., Matmati, N., Silva, E., Martins, T., Teixeira, V., et al. (2018). The ceramide activated protein phosphatase Sit4 impairs sphingolipid dynamics, mitochondrial function and lifespan in a yeast model of Niemann-Pick type C1. *Biochim. Biophys. Acta* 1864, 79–88. doi: 10.1016/j.bbadis.2017.10.010

Vilaca, R., Silva, E., Nadais, A., Teixeira, V., Matmati, N., Gaifem, J., et al. (2014). Sphingolipid signalling mediates mitochondrial dysfunctions and reduced chronological lifespan in the yeast model of Niemann-Pick type C1. *Mol. Microbiol.* 91, 438–451. doi: 10.1111/mmi.12470

Wang, H., Lim, P. J., Karbowski, M., and Monteiro, M. J. (2009). Effects of overexpression of huntingtin proteins on mitochondrial integrity. *Hum. Mol. Genet.* 18, 737–752. doi: 10.1093/hmg/ddn404

Wei, M., Fabrizio, P., Hu, J., Ge, H., Cheng, C., Li, L., et al. (2008). Life span extension by calorie restriction depends on Rim15 and transcription factors downstream of Ras/PKA, Tor, and Sch9. *PLoS Genet.* 4:e13. doi: 10.1371/journal.pgen.0040013

Willingham, S., Outeiro, T. F., Devit, M. J., Lindquist, S. L., and Muchowski, P. J. (2003). Yeast genes that enhance the toxicity of a mutant huntingtin fragment or alpha-synuclein. *Science* 302, 1769–1772. doi: 10.1126/science.1090389

Yan, L., Vatner, D. E., O'connor, J. P., Ivessa, A., Ge, H., Chen, W., et al. (2007). Type 5 adenylyl cyclase disruption increases longevity and protects against stress. *Cell* 130, 247–258. doi: 10.1016/j.cell.2007.05.038

Yeger-Lotem, E., Riva, L., Su, L. J., Gitler, A. D., Cashikar, A. G., King, O. D., et al. (2009). Bridging high-throughput genetic and transcriptional data reveals cellular responses to alpha-synuclein toxicity. *Nat. Genet.* 41, 316–323. doi: 10.1038/ng.337

Conflict of Interest Statement: The authors declare that the research was conducted in the absence of any commercial or financial relationships that could be construed as a potential conflict of interest.

frontiers in Molecular Neuroscience

ORIGINAL RESEARCH
published: 05 November 2018
doi: 10.3389/fnmol.2018.00406

The Impact of ESCRT on Aβ$_{1-42}$ Induced Membrane Lesions in a Yeast Model for Alzheimer's Disease

Gernot Fruhmann[1†], Christelle Marchal[2†‡], Hélène Vignaud[2], Mathias Verduyckt[1], Nicolas Talarek[3], Claudio De Virgilio[4], Joris Winderickx[1] and Christophe Cullin[2]**

[1] Functional Biology, KU Leuven, Leuven, Belgium, [2] Institut de Chimie et Biologie des Membranes et des Nano-objets, University of Bordeaux, CNRS UMR 5248, Pessac, France, [3] Institut de Génétique Moléculaire de Montpellier, University of Montpellier, CNRS, Montpellier, France, [4] Department of Biology, Université de Fribourg, Fribourg, Switzerland

Aβ metabolism plays a pivotal role in Alzheimer's disease. Here, we used a yeast model to monitor Aβ$_{42}$ toxicity when entering the secretory pathway and demonstrate that processing in, and exit from the endoplasmic reticulum (ER) is required to unleash the full Aβ$_{42}$ toxic potential. Consistent with previously reported data, our data suggests that Aβ$_{42}$ interacts with mitochondria, thereby enhancing formation of reactive oxygen species and eventually leading to cell demise. We used our model to search for genes that modulate this deleterious effect, either by reducing or enhancing Aβ$_{42}$ toxicity, based on screening of the yeast knockout collection. This revealed a reduced Aβ$_{42}$ toxicity not only in strains hampered in ER-Golgi traffic and mitochondrial functioning but also in strains lacking genes connected to the cell cycle and the DNA replication stress response. On the other hand, increased Aβ$_{42}$ toxicity was observed in strains affected in the actin cytoskeleton organization, endocytosis and the formation of multivesicular bodies, including key factors of the ESCRT machinery. Since the latter was shown to be required for the repair of membrane lesions in mammalian systems, we studied this aspect in more detail in our yeast model. Our data demonstrated that Aβ$_{42}$ heavily disturbed the plasma membrane integrity in a strain lacking the ESCRT-III accessory factor Bro1, a phenotype that came along with a severe growth defect and enhanced loading of lipid droplets. Thus, it appears that also in yeast ESCRT is required for membrane repair, thereby counteracting one of the deleterious effects induced by the expression of Aβ$_{42}$. Combined, our studies once more validated the use of yeast as a model to investigate fundamental mechanisms underlying the etiology of neurodegenerative disorders.

Keywords: Aβ$_{42}$, amyloid beta, Alzheimer's disease, ESCRT, membrane repair, *Saccharomyces cerevisiae*, yeast

OPEN ACCESS

Edited by:
Ralf J. Braun,
University of Bayreuth, Germany

Reviewed by:
Md. Golam Sharoar,
University of Connecticut Health Center, United States
Markus Babst,
The University of Utah, United States

****Correspondence:***
Joris Winderickx
joris.winderickx@kuleuven.be
Christophe Cullin
christophe.cullin@u-bordeaux.fr

[†]These authors have contributed equally to this work

[‡]Co-first authorship

Received: *13 April 2018*
Accepted: *16 October 2018*
Published: *05 November 2018*

Citation:
Fruhmann G, Marchal C, Vignaud H, Verduyckt M, Talarek N, De Virgilio C, Winderickx J and Cullin C (2018) The Impact of ESCRT on Aβ$_{1-42}$ Induced Membrane Lesions in a Yeast Model for Alzheimer's Disease. Front. Mol. Neurosci. 11:406. doi: 10.3389/fnmol.2018.00406

INTRODUCTION

Amyloid β$_{1-42}$ (referred to as Aβ$_{42}$) is an intensively investigated peptide involved in Alzheimer's disease (AD) but beyond its role as a possibly malignant factor, the physiological functions of Aβ$_{42}$ are still speculative. It has been shown that it has a role in activity dependent synaptic vesicle release and there is evidence that it might act as an antimicrobial agent in the brain, but besides that, not much is known about its physiological function (Pearson and Peers, 2006;

Abramov et al., 2009; Kagan et al., 2012; Kumar et al., 2016). Thus, although several efforts have been put in investigating its role in AD, still most of its functions remain elusive. In humans, the membrane bound amyloid precursor protein, APP, is processed in two possible ways: it can enter the non-amyloidogenic pathway or it might be cleaved by β- and γ-secretases in the amyloidogenic pathway thus producing Aβ peptides of lengths between 37 and 43 amino acids (LaFerla et al., 2007). In AD, these peptides are then secreted and form inert extracellular plaques, but monomers and especially small oligomers are transported to several intracellular organelles where they reveal their toxic potential. For instance, strong evidence was found for that $A\beta_{42}$ perturbs proper function of mitochondria through blocking respiration at complex IV, resulting in cells producing more reactive oxygen species (ROS) and eventually apoptotic cell death (Wang et al., 2010; Ittner and Gotz, 2011; Benilova et al., 2012; Jackrel et al., 2014; Alexandrov et al., 2016; Vicente Miranda et al., 2016).

In the past decade, yeast was established as a model organism for studying fundamental aspects related to neurodegenerative disorders such as Huntington's, Parkinson's, or AD (Winderickx et al., 2008; Franssens et al., 2010; Swinnen et al., 2011; Porzoor and Macreadie, 2013; Jiang et al., 2016; Verduyckt et al., 2016; Fruhmann et al., 2017). Since most of the overall cellular architecture and most basic biochemical processes are conserved between mammalian cells and yeast, and given the fact that about 20–30 per cent of all human genes have orthologs in *Saccharomyces cerevisiae* (Foury, 1997; Hamza et al., 2015; Liu et al., 2017), it is obvious that certain disease mechanisms can be studied in this easy to handle model organism. In connection to AD and $A\beta_{42}$, we and others reported that expression of this peptide triggers toxicity in yeast when targeted to the secretory pathway as to mimic its multi-compartment trafficking observed in mammalian systems. This led to the observation that $A\beta_{42}$ expression in yeast alters endocytosis of plasma membrane resident proteins (Treusch et al., 2011; D'Angelo et al., 2013), induces ER-stress and the unfolded protein response (Chen et al., 2017) and triggers mitochondrial dysfunction (D'Angelo et al., 2013; Chen and Petranovic, 2015; Chen et al., 2017). In the studies presented in this paper, we used previously reported constructs (D'Angelo et al., 2013; Vignaud et al., 2013) where the yeast mating type α-prepro factor directs $A\beta_{42}$ into the Golgi. Here, the α-prepro factor is cleaved off, followed by transport of the peptide to the plasma membrane. In addition, the constructs contain a C-terminal linker-GFP tag in order to ensure stable expression and easy localization of $A\beta_{42}$ in the yeast cells. Besides the wild-type $A\beta_{42}$ and the clinical arctic mutant, we also expressed two synthetic mutants generated by random mutagenesis and previously shown to be either more toxic ($A\beta_{42}$G37C) to, or to be moderately toxic ($A\beta_{42}$L34T) compared to $A\beta_{42}$wt (D'Angelo et al., 2013; Vignaud et al., 2013). Using these constructs, we performed genome-wide screenings as to identify $A\beta_{42}$ toxicity modulators. We confirm the previously reported $A\beta_{42}$ toxicity phenotypes and in addition demonstrate that $A\beta_{42}$ introduces membrane lesions that require the ESCRT system in order to become repaired.

MATERIALS AND METHODS

Yeast Strains, Plasmids, and Media

We used the haploid *Saccharomyces cerevisiae* strain BY4741 MATa *his3Δ1 leu2Δ0 met15Δ0 ura3Δ0* and BY4742 MATα *his3Δ1 leu2Δ0 lys2Δ0 ura3Δ0* for all specified experiments. All deletion strains were obtained from the commercial EUROSCARF knock-out library (Y.K.O. collection). For a full list of strains used in this study see **Table 1**.

The pYe plasmids with the galactose inducible, episomal $\alpha A\beta_{42}$-linker-GFP isoforms, the similar $A\beta_{42}$-GFP construct without the α-prepro sequence and the control constructs for expressing of either GFP (ev-GFP) or a α-prepro-GFP fusion (ev-αGFP) were described previously (Tong et al., 2001). The p426-GAL vector (Addgene) was used as additional empty vector (ev) control. For a full list of plasmids used in this study see **Table 2**.

Standard yeast techniques were applied. We used minimal medium containing Yeast Nitrogen Base (YNB) without ammonium sulfate (FORMEDIUM). Supplements were ammonium sulfate (5 g/L; VWR), histidine (100 mg/L; MP Biomedicals), methionine (20 mg/L; Acros Organics), leucine (30 mg/L; FORMEDIUM) and lysine (30 mg/L; FORMEDIUM). Synthetic Drop-Out (SD) medium was used for microscopy and contained YNB with ammonium sulfate and was depleted for either uracil or uracil and leucine (FORMEDIUM). For solid media, 1.5% Difco-agar (BD) was added. Pre-cultures were grown on medium supplemented with 4% glucose and gene expression was induced by washing the cells with medium without sugar followed by transfer to medium supplemented with 2% galactose.

Synthetic Genetic Array and Suppressor screening

The synthetic genetic array (SGA) screening was essentially performed as previously described in Tong et al. (2001). The query strain (MATα *can1Δ::STE*pr-*HIS5*sp *lyp1Δ his3Δ1 leu2Δ0 met15Δ0 ura3Δ0 LYS2*) expressing $\alpha A\beta_{42}$wt-linker-GFP (further designated as $\alpha A\beta_{42}$wt), the $\alpha A\beta_{42}$G37C-linker-GFP (designated $\alpha A\beta_{42}$G37C) or the ev-αGFP was mated with the non-essential deletion mutant array (MATa *target_gene::kanMX4 his3Δ1 leu2Δ0 met15Δ0 ura3Δ0*) on SD plates lacking uracil. Diploids were selected on SD medium lacking uracil but containing G418 (geneticin). Next, sporulation was induced by plating diploids onto sporulation medium containing G418. Then, haploids were selected in two steps. First, spores were plated onto YNB lacking arginine, lysine, and histidine but containing canavanine and thialysine, which ensures uptake of canavanine. This allowed growth of MATa haploids only. In a second step, the selected haploids were grown on YNB lacking uracil, arginine, lysine, and histidine but containing canavanine, thialysine and G418 to select for haploid knock-out mutants still carrying the $\alpha A\beta_{42}$wt, $\alpha A\beta_{42}$G37C, or ev-αGFP plasmids. Growth analysis was performed with the ScreenMill software (Dittmar et al., 2010).

TABLE 1 | Yeast strains used in this study.

Name	Genotype	Source
Query strain (SGA)	MATα *can1Δ::STEpr-HIS5sp lyp1Δ his3Δ1 leu2Δ0 met15Δ0 ura3Δ0 LYS2*	Tong et al., 2001
Deletion mutant strains (SGA)	MATa *Target_gene::kanMX4 his3Δ1 leu2Δ0 met15Δ0 ura3Δ0*	Tong et al., 2001
BY4741	MATa *his3Δ1 leu2Δ0 met15Δ0 ura3Δ0*	Openbiosystems
BY4742	MATα *his3Δ1 leu2Δ0 lys2Δ0 ura3Δ0*	Openbiosystems
JW 12 918	MATa *his3Δ1 leu2Δ0 met15Δ0 ura3Δ0 erv29::kanMX*	Y.K.O. collection
JW 23 168	MATα *his3Δ1 leu2Δ0 lys2Δ0 ura3Δ0 hse1Δ::kanMX*	Y.K.O. collection
JW 23 771	MATα *his3Δ1 leu2Δ0 lys2Δ0 ura3Δ0 vps27::kanMX*	Y.K.O. collection
JW 20 178	MATα *his3Δ1 leu2Δ0 lys2Δ0 ura3Δ0 srn2::kanMX*	Y.K.O. collection
JW 21 184	MATα *his3Δ1 leu2Δ0 lys2Δ0 ura3Δ0 mvb12::kanMX*	Y.K.O. collection
JW 21 335	MATα *his3Δ1 leu2Δ0 lys2Δ0 ura3Δ0 stp22::kanMX*	Y.K.O. collection
JW 22 115	MATα *his3Δ1 leu2Δ0 lys2Δ0 ura3Δ0 vps28::kanMX*	Y.K.O. collection
JW 23 142	MATα *his3Δ1 leu2Δ0 lys2Δ0 ura3Δ0 vps25::kanMX*	Y.K.O. collection
JW 21 849	MATα *his3Δ1 leu2Δ0 lys2Δ0 ura3Δ0 vps36::kanMX*	Y.K.O. collection
JW 22 164	MATα *his3Δ1 leu2Δ0 lys2Δ0 ura3Δ0 snf8::kanMX*	Y.K.O. collection
JW 20 891	MATα *his3Δ1 leu2Δ0 lys2Δ0 ura3Δ0 doa4::kanMX*	Y.K.O. collection
JW 22 100	MATα *his3Δ1 leu2Δ0 lys2Δ0 ura3Δ0 bro1::kanMX*	Y.K.O. collection
JW 22 220	MATα *his3Δ1 leu2Δ0 lys2Δ0 ura3Δ0 vps4::kanMX*	Y.K.O. collection
JW 22 777	MATα *his3Δ1 leu2Δ0 lys2Δ0 ura3Δ0 did2::kanMX*	Y.K.O. collection
JW 24 370	MATα *his3Δ1 leu2Δ0 lys2Δ0 ura3Δ0 vps60::kanMX*	Y.K.O. collection
JW 21 424	MATα *his3Δ1 leu2Δ0 lys2Δ0 ura3Δ0 vta1::kanMX*	Y.K.O. collection
JW 23 123	MATα *his3Δ1 leu2Δ0 lys2Δ0 ura3Δ0 chm7::kanMX*	Y.K.O. collection
JW 20 444	MATα *his3Δ1 leu2Δ0 lys2Δ0 ura3Δ0 ist1::kanMX*	Y.K.O. collection
JW 20 124	MATα *his3Δ1 leu2Δ0 lys2Δ0 ura3Δ0 snf7::kanMX*	Y.K.O. collection
JW 21 479	MATα *his3Δ1 leu2Δ0 lys2Δ0 ura3Δ0 vps24::kanMX*	Y.K.O. collection
JW 22 806	MATα *his3Δ1 leu2Δ0 lys2Δ0 ura3Δ0 vps20::kanMX*	Y.K.O. collection
JW 11 560	MATα *his3Δ1 leu2Δ0 lys2Δ0 ura3Δ0 did4::kanMX*	Y.K.O. collection

TABLE 2 | Plasmids used in this study.

Name	Backbone	Marker	Insert	Source
$\alpha A\beta_{42}$wt	pYe-GAL10 2U	*URA3*	*α-prepro-*$A\beta_{42}$*wt-linker-GFP*	D'Angelo et al., 2013
$\alpha A\beta_{42}$arc	pYe-GAL10 2U	*URA3*	*α-prepro-*$A\beta_{42}$*arc-linker-GFP*	D'Angelo et al., 2013
$\alpha A\beta_{42}$G37C	pYe-GAL10 2U	*URA3*	*α-prepro-*$A\beta_{42}$*G37C-linker-GFP*	D'Angelo et al., 2013
$\alpha A\beta_{42}$G37C-HDEL	pYe-GAL10 2U	*URA3*	*α-prepro-*$A\beta_{42}$*G37C-linker-GFP-HDEL*	Christophe Cullin
$\alpha A\beta_{42}$L34T	pYe-GAL10 2U	*URA3*	*α prepro-*$A\beta_{42}$*L34T-linker-GFP*	D'Angelo et al., 2013
ev-αGFP	pYe-GAL10 2U	*URA3*	*α-prepro-GFP*	D'Angelo et al., 2013
ev-GFP	pYe-GAL10 2U	*URA3*	*GFP*	D'Angelo et al., 2013
Ev	p426-GAL1	*URA3*		Mumberg et al., 1994
pHS12-mCherry	pHS12-ADH1	*LEU2*	*COX4*	Addgene
pYX242-mCherry	pYX242-TPI	*LEU2*	*Kar2*$_{(1-135)}$*-mCherry-HDEL*	Swinnen et al., 2014

In a second so-called suppressor screening, the Euroscarf collection of deletion strains was pooled transformed with αAβ42G37C. Transformants were plated on minimal medium lacking uracil. After incubation, transformants were selected that grew similar as the isogenic wild-type carrying the empty vector control, also when replica plated on SD medium supplemented with casamino acids. Transformants were then used for bar-code PCR sequencing as to identify their corresponding ORF deletion.

Electron Microscopy

Electron microscopic analysis of yeast cells was done similar as previously described (Lefebvre-Legendre et al., 2005). Briefly, pellets of yeast cells were placed on the surface of a copper

EM grid (400 mesh) coated with formvar. Grids were immersed in liquid propane held at −180°C by liquid nitrogen and then transferred in a 4% osmium tetroxide solution in dry acetone at −82°C for 72 h. They were warmed progressively to RT, and washed three times with dry acetone and stained with 1% uranyl acetate. After washing in dry acetone, the grids were infiltrated with araldite (Fluka). Ultra-thin sections were contrasted with lead citrate and observed in an electron microscope (80 kV; 7650; Hitachi) at the EM facility of the Bordeaux Imaging Center.

Growth Profile Analysis and Spot Assays

Cells were grown under non-inducing conditions in 96-well plates shaking at 30°C in a Multiskan GO or Multiskan FC microplate spectrophotometer (Thermo Scientific) to an $OD_{595\ nm}$ or $OD_{600\ nm}$, respectively, of 0.5 to 0.9. Cells were washed with minimal medium containing galactose and diluted to an $OD_{595\ nm}$ or $OD_{600\ nm}$, respectively, of 0.5 after which growth was monitored every 2 h by OD measurement. Four different transformants were taken per experiment and at least three independent experiments were performed. Growth curves were analyzed with GraphPad Prism v7.03, error bars represent standard deviations.

For spot assays, serial dilutions of precultures were spotted on solid medium containing either glucose or galactose and cells were grown at 30°C. The plates were scanned at days 3 to 6.

Cytometry and Fluorescence Microscopy

To monitor plasma membrane disruption with propidium iodide (PI) staining and the formation of ROS by dihydroethidium (DHE) staining, cells were grown in SD medium lacking uracil and containing 4% glucose. Once in exponential phase, the cells were washed with and re-suspended in SD medium without uracil but containing 2% galactose as to induce expression of $\alpha A\beta_{42}$-linker-GFP and control constructs. Flow cytometric analysis was performed on at least four independent transformants with a Guava easyCyte 8HT benchtop flow cytometer (Millipore) after staining with 5 μM PI for 30 min at 30°C and subsequent washing. Data were analyzed with FlowJo v10 and GraphPad Prism 7.03 software packages. Gates were set in FlowJo v10 with single stained ev-αGFP samples. Further statistical analysis was done in GraphPad Prism v7.03. Error bars represent standard deviations and asterisks the significance calculated with an ordinary Two-way ANOVA.

For the FM4-64/CMAC (Thermo Fisher) and Nile Red (Acros) stainings, the cells were grown as described above. After pre-incubating the cells with CAMAC at 30°C for 30 min, FM4-64 stainings were performed as described before (Zabrocki et al., 2005). For the Nile Red staining, the cells were fixed with formaldehyde (4% final concentration) and stained with 2% Nile Red (60 μg/mL stock) for 30 min with shaking at 30°C. Then, the cells were washed twice with PBS and either stored at 4°C or taken immediately for fluorescence microscopy.

For epifluorescence pictures, cells were pre-grown in selective glucose (4%) containing SD medium to exponential phase. After transfer to SD medium containing 2% galactose to induce expression of $\alpha A\beta_{42}$-linker-GFP, the cells were grown at 30°C and pictures were taken after different time intervals using a Leica DM4000B or a DMi8 microscope. For Hoechst stainings, the cells were incubated with 20 nM Hoechst 33342 (Sigma-Aldrich) for 10 min. Pictures were deconvolved with Huygens Essential software (v18.04.0p4 64, Scientific Volume Imaging B.V.) and further processed with the standard FIJI software package (v1.51n) (Schindelin et al., 2012).

Immunological Techniques

Cultures were grown to exponential phase in 4% glucose containing SD medium, transferred to 2% galactose containing medium and grown overnight. Then, three OD units were harvested by centrifugation and protein extracts were prepared by using an alkaline lysis method. The cells were permeabilized with 0.185 M NaOH plus 2% β-mercaptoethanol. After 10 min incubation on ice, trichloroacetic acid (TCA) was added to a final concentration of 5%, followed by an additional 10 min incubation step on ice. Precipitates were collected by centrifugation for 5 min at 13000 *g* and pellets were resuspended in 50 μL of sample buffer (4% sodium dodecyl sulfate, 0.1 M Tris-HCl pH 6.8, 4 mM EDTA, 20% glycerol, 2% β-mercaptoethanol, and 0.02% bromophenol blue) plus 25 μL of 1 M Tris-Base. Samples were separated by standard SDS-PAGE on 12% polyacrylamide gels and further analyzed using standard Western blotting techniques. An anti-GFP primary antibody (Sigma-Aldrich) and anti-Mouse (GAM)-HRP conjugated secondary antibody (Biorad) were used. The ECL method (SuperSignal West Pico or Femto, Thermo Scientific) was used for detection and visualization of the blots was performed with a UVP Biospectrum® Multispectral Imaging System.

RESULTS

αAβ$_{42}$-Linker-GFP Is Toxic in an AD Yeast Model

To date, the exact molecular basis of how $A\beta_{42}$ impacts cell functions remains largely elusive. To address this question, we used a yeast model transformed with plasmids carrying the galactose-inducible *GAL10* promoter to control expression of wild-type or mutant $A\beta_{42}$ that is N-terminally fused to the α-prepro sequence and C-terminally to a linker and GFP (in this paper referred to as $\alpha A\beta_{42}$; **Figure 1A**) (D'Angelo et al., 2013; Vignaud et al., 2013). Besides the wild-type $\alpha A\beta_{42}$ ($\alpha A\beta_{42}$wt), we additionally expressed the clinical E22G arctic mutant ($\alpha A\beta_{42}$arc) that is associated to a familial form of AD as well as the previously described synthetic mutants $\alpha A\beta_{42}$G37C and $\alpha A\beta_{42}$L34T (**Figure 1A**) (D'Angelo et al., 2013; Vignaud et al., 2013). We used three control vectors, i.e., an empty vector allowing for the expression of an α-prepro fused GFP (ev-αGFP), GFP alone (ev-GFP) or an empty vector just carrying the galactose promotor (ev). To disperse concerns about the processing efficacy of the α-prepro factor in the Golgi system, we tested both the BY4741 MATa and BY4742 MATα strains with all control vectors and the aforementioned wild-type and mutant $\alpha A\beta_{42}$-linker-GFP constructs (**Figures 1B–D** and **Supplementary Figure S1**). Albeit the strains transformed with the ev-αGFP control grew somewhat

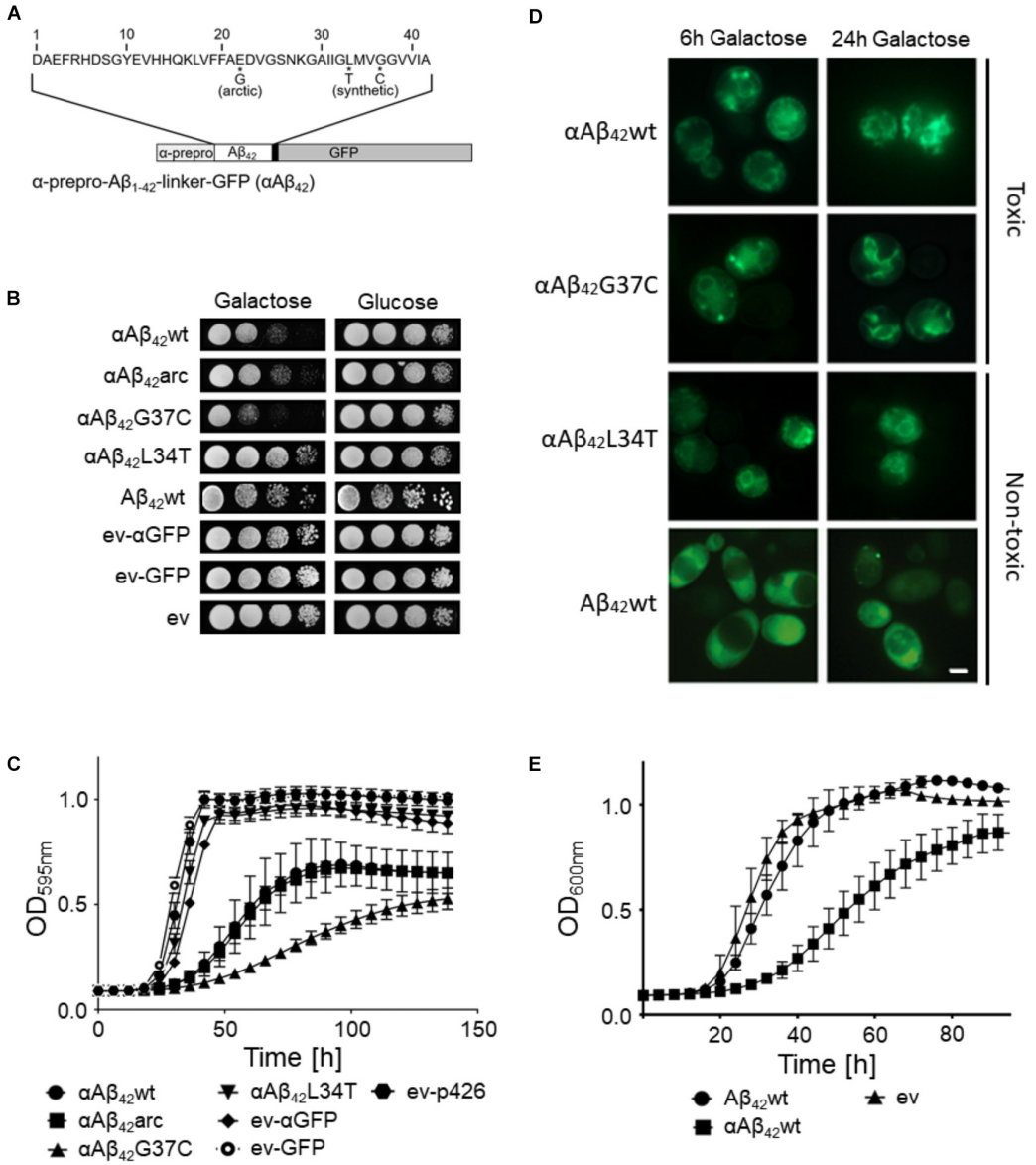

FIGURE 1 | Toxicity profiles of wild-type or mutant $\alpha A\beta_{42}$ in the haploid *Saccharomyces cerevisiae* strains BY4741. **(A)** Schematic representation of the α-prepro-$A\beta_{42}$-linker-GFP construct with indication of the mutants used in this study. **(B)** Spot assays under inducing (galactose) and repressing (glucose) conditions and **(C)** growth profiles under inducing conditions of the BY4741 wild-type strain transformed with constructs allowing for expression of $\alpha A\beta_{42}$wt, $\alpha A\beta_{42}$arc, $\alpha A\beta_{42}$G37C, $\alpha A\beta_{42}$L34T, $A\beta_{42}$wt and control vectors (ev-αGFP, ev-GFP, ev) as indicated. Error bars in the growth profiles represent the standard deviation of at least four independent transformants. **(D)** Fluorescence microscopy pictures show localization of α-prepro fused $A\beta_{42}$ mutants to the ER 6 and 24 h after induction on galactose-containing medium. 24 h after induction of gene expression the toxic $\alpha A\beta_{42}$ isoforms show a more "patchy" pattern while the non-toxic $\alpha A\beta_{42}$L34T still localizes at the ER. The $A\beta_{42}$wt construct lacking the α-prepro sequence is seen in the cytoplasm. The scale bar represents 2 μm. **(E)** Growth profiles of the BY4741 wild-type strain transformed with an empty vector (ev) or constructs allowing for expression of $\alpha A\beta_{42}$wt and $A\beta_{42}$wt.

slower than those transformed with ev-GFP or ev (**Figures 1B,C** and **Supplementary Figure S1A**), both spot assays and growth analysis in liquid medium confirmed that wild-type or mutant $\alpha A\beta_{42}$ instigated a significantly higher level of toxicity that was similar in the BY4741 and the BY4742 strains (**Figures 1B,C** and **Supplementary Figure S1**). The synthetic $\alpha A\beta_{42}$G37C mutant was the most toxic followed by $\alpha A\beta_{42}$wt and $\alpha A\beta_{42}$arc. The synthetic $\alpha A\beta_{42}$L34T mutant, on the other hand, did not yield a toxic phenotype and these transformants grew similar as those expressing ev-αGFP, thereby confirming previously reported data (Vignaud et al., 2013).

Fluorescence microscopy showed that all $\alpha A\beta_{42}$ constructs clearly stained the perinuclear ER and to a lesser extent the cortical ER and that particularly the cells expressing the toxic

$\alpha A\beta_{42}$ forms often displayed ER-associated foci and filamentous structures (**Figure 1D**). These were previously believed to be vesicles (D'Angelo et al., 2013), but recent studies suggests that these may as well-represent ER-aggregates or clustering of ER membranes, both indicative for ER stress (Varadarajan et al., 2012, 2013; Vevea et al., 2015). In contrast, when the $A\beta_{42}$wt was expressed from a construct that lacks the α-prepro sequence, the GFP fusion was mainly found to be distributed in the cytoplasm though some cells presented foci after prolonged induction (**Figure 1D**). Despite of these foci, the expression of the $A\beta_{42}$wt construct without the α-prepro sequence only triggered a small growth retardation (**Figures 1B,E**). This nicely demonstrates that the processing in the ER/Golgi system is required to unleash the full toxic capacity of $\alpha A\beta_{42}$.

Retention of $\alpha A\beta_{42}$ in the ER Diminishes Its Toxicity

Previously, we reported that the processing of the $\alpha A\beta_{42}$-linker-GFP fusion constructs in the ER/Golgi system yields three distinct isoforms when performing Western blot analysis, i.e., the α-prepro precursor (41 kDa), the glycosylated precursor (50 kDa), and the matured $A\beta_{42}$-linker-GFP form (34 kDa) (D'Angelo et al., 2013; Vignaud et al., 2013). Given that the latter is shuttled into the secretory pathway, we wondered if retention of the $\alpha A\beta_{42}$-linker-GFP fusion in the endoplasmic reticulum (ER) would affect its toxic capacity. To this end, we introduced a HDEL retention signal at the C-terminal end of the construct. The yeast HDEL sequence is equivalent to the mammalian KDEL retention signal that shuttles the KDEL containing proteins back to the ER lumen (Dean and Pelham, 1990; Lewis and Pelham, 1990; Ruan et al., 2017). Consistently, microscopic analysis demonstrated that while both $\alpha A\beta_{42}$G37C and $\alpha A\beta_{42}$G37C-HDEL are equally present at the perinuclear ER, the latter accumulated more in the peripheral cortical ER (**Figure 2A**). Also, Western blot analysis showed that in case of expression of $\alpha A\beta_{42}$G37C-HDEL, both the non-processed $\alpha A\beta_{42}$G37C precursor as well as the glycosylated version accumulated, while the fully processed $A\beta_{42}$G37C was significantly reduced (**Figure 2B**). Next, a growth analysis was performed. This revealed that the strain expressing $\alpha A\beta_{42}$G37C-HDEL construct grew much better than that with $\alpha A\beta_{42}$G37C, thereby displaying a level of toxicity comparable to a strain with the $\alpha A\beta_{42}$arc mutant (**Figure 2C**).

In order to confirm these results with a different approach, we expressed $\alpha A\beta_{42}$wt, $\alpha A\beta_{42}$arc, as well as the super-toxic $\alpha A\beta_{42}$G37C mutant in a BY4741 strain deleted for *ERV29*, which encodes a transmembrane factor involved in COP-II dependent vesicle formation and in trafficking of the α-prepro factor from the ER to the Golgi apparatus (Belden and Barlowe, 2001). Upon deletion of *ERV29*, $\alpha A\beta_{42}$ gets stuck in the ER and cannot transit to the Golgi. Strikingly, cytotoxicity of all tested mutants was indeed significantly diminished in this *erv29*Δ strain and even the super-toxic $\alpha A\beta_{42}$G37C mutant almost completely lost its toxic power (**Figures 2D,E**). Thus, the data above confirm that $\alpha A\beta_{42}$ needs to be fully processed and exit the ER in order to gain its full toxic potential.

$\alpha A\beta_{42}$ Affects Mitochondrial Functioning

Since $\alpha A\beta_{42}$ confers toxicity by entering the secretory pathway, we wanted to know more about the targets and processes being affected. Therefore, we first focused on mitochondria given that previous studies have associated $A\beta_{42}$ to mitochondrial dysfunction in yeast (Chen and Petranovic, 2015; Chen et al., 2017; Hu et al., 2018). To this end, we co-expressed $\alpha A\beta_{42}$wt, $\alpha A\beta_{42}$arc, $\alpha A\beta_{42}$G37C, $\alpha A\beta_{42}$L34T or the ev-αGFP together with a mCherry labeled mitochondrial marker Cox4 in wild-type cells. As illustrated in **Figure 3A**, this suggests a toxicity dependent co-localization since $\alpha A\beta_{42}$wt and even more $\alpha A\beta_{42}$G37C seem to partially co-localize with mitochondria. We then performed a DHE staining to estimate the ROS levels as marker for mitochondrial dysfunction and a PI staining to monitor the amount of cells with disrupted plasma membranes as marker for cell demise (**Figures 3B,C** and **Supplementary Figure S2**). As expected, and consistent with previously reported data (Chen and Petranovic, 2015; Chen et al., 2017), also these aspects correlated to the observed $\alpha A\beta_{42}$ instigated toxicity. Although our data on co-localization suggest that $\alpha A\beta_{42}$ may directly interfere with mitochondrial functioning, we cannot exclude that these effects on mitochondrial function or morphology are indirect, for instance due alterations in ER-mitochondrial communication via ERMES contact sites.

Identification of Additional Processes Underlying $\alpha A\beta_{42}$ Toxicity

To decipher which additional processes sustain the $\alpha A\beta_{42}$ toxicity, we performed two unbiased genetic screens. In a first screening setup, we aimed to identify alleviators of $A\beta_{42}$G37C toxicity. Therefore, we transformed a pooled Euroscarf knock-out (KO) library with the $\alpha A\beta_{42}$G37C-linker-GFP construct and looked for transformants that grew similar as the empty vector control. Out of 90,000 transformants obtained when plated on repressive glucose containing medium, only 465 were able to form visible colonies after 72 h on galactose-containing medium where the expression of the super-toxic $A\beta_{42}$ mutant is induced. Each colony was then plated on SD medium supplemented with casamino acids to manually confirm the suppressive effect on $\alpha A\beta_{42}$ toxicity. Of the 465 initial clones, 268 were still able to grow. Finally, we characterized each KO strain by sequencing the PCR amplicon of its bar-code region. This led us to identify 113 different KO strains. In the second screening setup, we performed an unbiased SGA analysis with the full gene knock-out library using either $\alpha A\beta_{42}$wt, the super-toxic $\alpha A\beta_{42}$G37C mutant and the ev-GFP control. The additional use of the empty vector control and $\alpha A\beta_{42}$wt, which displays a more moderate toxicity phenotype, allowed for more complete results since not only suppressors but also toxicity aggravators could be scored. With this SGA screen, we identified 87 additional KO strains that modulated $\alpha A\beta_{42}$ toxicity, one of which contains a deletion in the overlapping genes *INP52/RRT16*. Finally, the 200 KO strains that were identified by either one of the screening procedures (**Table 3** and **Supplementary Table S1**) were also transformed individually with a construct allowing for the expression of $\alpha A\beta_{42}$arc, which has an intermediate toxicity similar to that

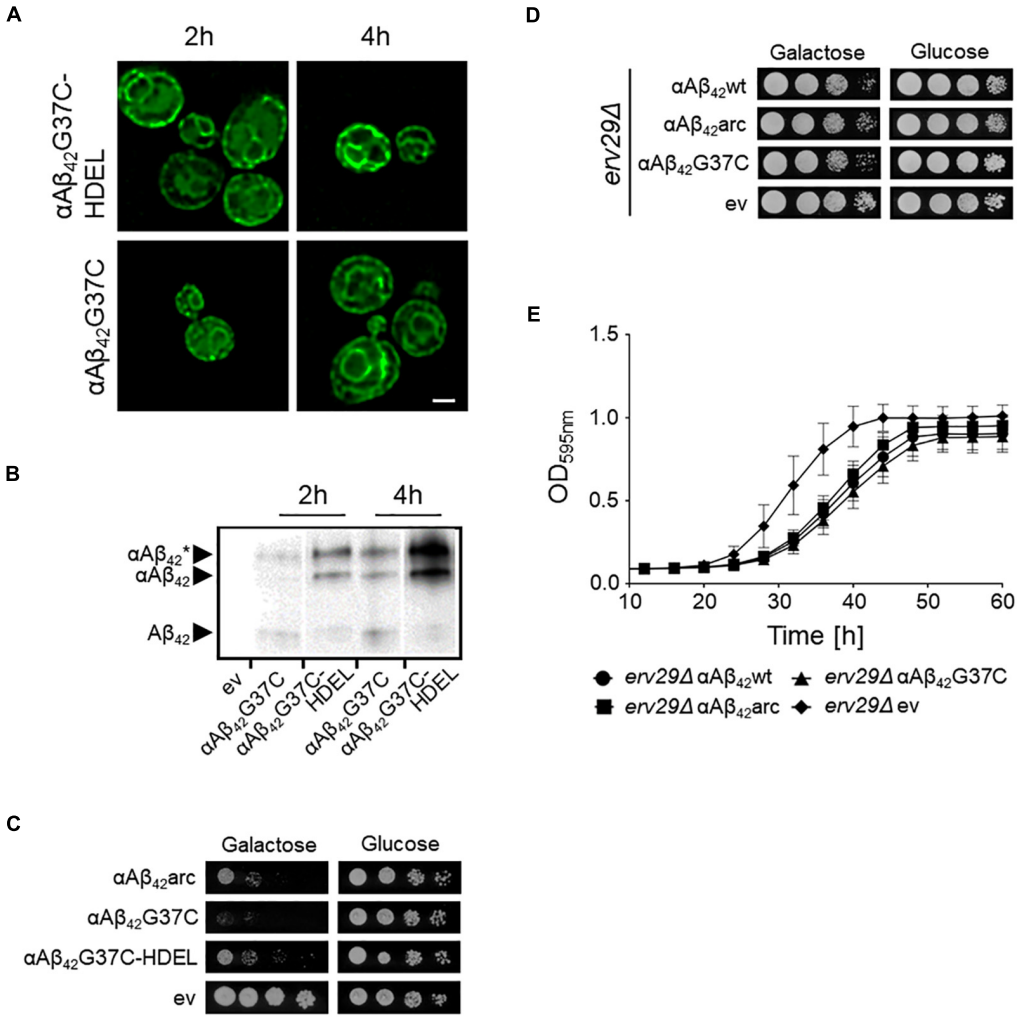

FIGURE 2 | Retention of $\alpha A\beta_{42}$ in the ER and the consequence for toxicity. **(A)** Fluorescence microscopy pictures showing $\alpha A\beta_{42}$G37C and $\alpha A\beta_{42}$G37C-HDEL localization at the perinuclear and cortical ER. Scale bar represents 2 μm. **(B)** Western blot analysis of total protein extracts obtained from cells expressing either $\alpha A\beta_{42}$G37C and $\alpha A\beta_{42}$G37C-HDEL. The different processing isoforms are indicated, i.e., $\alpha A\beta^*_{42}$ indicates glycosylated $\alpha A\beta_{42}$, $\alpha A\beta_{42}$ indicates un-glycosylated $\alpha A\beta_{42}$ and $A\beta_{42}$ indicates fully processed form where the α-prepro sequence is cleaved off. Spot assays under inductive (galactose) and repressive (glucose) conditions of wild-type **(C)** or *erv29*Δ **(D)** cells transformed with the empty vector (ev) or constructs allowing for expression of $\alpha A\beta_{42}$wt, $\alpha A\beta_{42}$arc, $\alpha A\beta_{42}$G37C, or $\alpha A\beta_{42}$G37C-HDEL as indicated. **(E)** Growth profiles of *erv29*Δ transformed with the empty vector (ev) or constructs allowing for expression of $\alpha A\beta_{42}$wt, $\alpha A\beta_{42}$arc, or $\alpha A\beta_{42}$G37C when grown on galactose-containing medium.

of $\alpha A\beta_{42}$wt and thus is again ideal to provide confirmation of both aggravators and suppressors of toxicity (D'Angelo et al., 2013). This provided an independent confirmation that all the KO strains selected in one of the two genetic screens are indeed involved in modulating $\alpha A\beta_{42}$arc toxicity. For each of the KO strains, the cell density under galactose inducing conditions was monitored allowing to rank KO strains from 0 to 5 depending on the growth capacity in comparison to the wild-type strain transformed $\alpha A\beta_{42}$arc. For 29 KO strains, growth was improved strongly (scored as 5), for 18 KO strains growth was clearly improved (scored as 4) and for 129 KO strains growth was only slightly better (scored as 3). On the other hand, we also identified 2 KO strains in which $\alpha A\beta_{42}$arc toxicity was strongly enhanced (scored as "0") and 17 KO strains that enhanced $\alpha A\beta_{42}$arc toxicity moderately (scored as 1) or weakly (scored as 2) (**Table 3** and **Supplementary Table S1**). Next, a gene ontology (GO) analysis using the SGD Gene Ontology Slim Mapper[1] allowed to sort the KO strains into functional categories depending on the gene deleted (**Table 3**). These included, amongst others, cytoskeleton organization and endocytosis, protein sorting and trafficking, protein ubiquitination, plasma membrane transport, cell cycle, translation, and transcription.

Interestingly, among the many KO strains that alleviated $\alpha A\beta_{42}$arc toxicity we found not only the strain deleted for *ERV29*, which is in line with the data described above, but also strains lacking other genes that impact on ER/Golgi functioning

[1]https://www.yeastgenome.org/cgi-bin/GO/goSlimMapper.pl

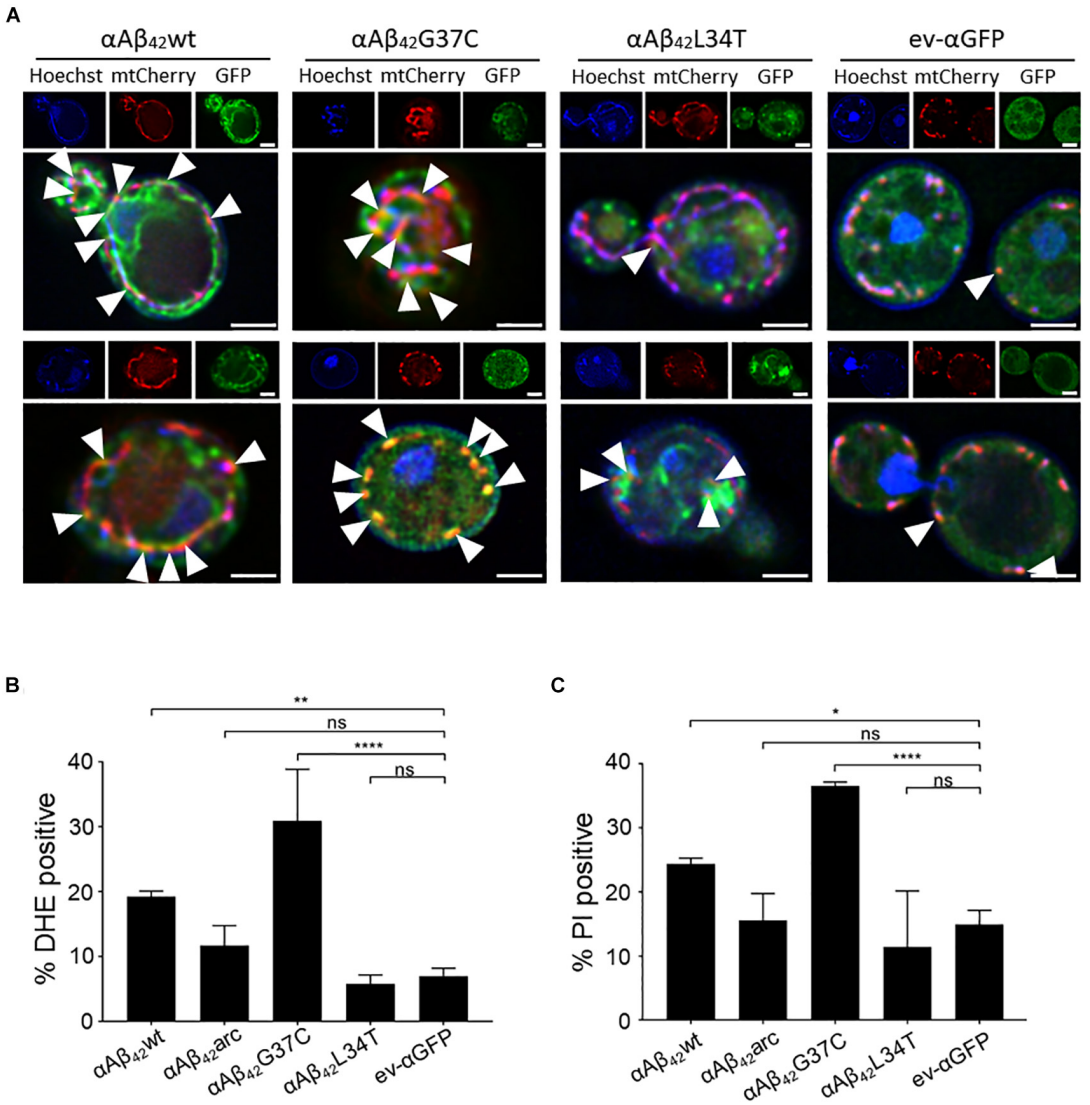

FIGURE 3 | $\alpha A\beta_{42}$ induces mitochondrial dysfunction and cell demise. **(A)** Fluorescence microscopy pictures suggesting partial co-localization of toxic $\alpha A\beta_{42}$ but not of the non-toxic $\alpha A\beta_{42}$L34T nor of the αGFP control (green) with mitochondria (red) in wild-type cells. Hoechst staining (blue) shows mitochondrial as well as nuclear DNA. The white arrowheads indicate sites of co-localization between $\alpha A\beta_{42}$ and mitochondria. Two single cells shown per strain. Scale bars represent 2 μm. Percentage of wild-type yeast cells expressing wild-type or mutant $\alpha A\beta_{42}$ and a control stained with DHE as a marker for ROS-formation **(B)** or PI as a marker for plasma membrane integrity **(C)**. $^{*}P \leq 0.05$; $^{**}P \leq 0.01$; $^{****}P \leq 0.0001$; $^{ns}P > 0.05$.

and traffic, such as the *SPC2* encoded subunit of the peptidase complex, which cleaves the signal sequence from proteins targeted to the ER, *EMP24*, which encodes a component of the p24 complex that mediates ER-to-Golgi transport of GPI anchored proteins, or *ARF2* and *YPT31*, which both encode GTPases required for intra-Golgi traffic. Also found were several strains lacking genes encoding mitochondrial functions and this included *AIF1* that codes for the mitochondrial cell death effector, indicative that $\alpha A\beta_{42}$ actively induces programmed cell death pathways. Furthermore, the fact that we retrieved the KO strains for *ATG1*, *ATG2,* and *ATG20* suggests that $\alpha A\beta_{42}$ may overstimulate the autophagy and the cytoplasm-to-vacuole targeting pathways (Kim and Klionsky, 2000; Nice et al., 2002). Finally, it was recently shown by transcriptome analysis that $A\beta_{42}$ impacts on lipid metabolism with *INO1* being most significantly upregulated (Chen et al., 2017). We found the KO strain lacking *ITC1* to reduce $\alpha A\beta_{42}$ toxicity. *ITC1* encodes a subunit of ATP-dependent Isw2p-Itc1p chromatin remodeling complex that is required for repression of *INO1*. In addition, also KO strains lacking genes involved sphingolipid and ceramide metabolism were retrieved, i.e., *FAA1*, *SUR1*, *YDC1*. Overall, these data confirm that the noxious effect of $\alpha A\beta_{42}$ is associated to changes in lipid metabolism.

The KO strains that aggravated $\alpha A\beta_{42}$ toxicity were often missing functions associated to maintenance and organization of the actin cytoskeleton, endocytosis and the multivesicular

TABLE 3 | $\alpha A\beta_{42}$ toxicity modifiers.

GO term	Enhancers	Suppressors
Biological process unknown	**FMP41** (2), **MTC3** (2), YBR113W (2), YHL005C (2), YJL169W (2)	GL081W (3), ICY1 (3), IRC10 (3), MRX11 (3), NBA1 (3), NRP1 (3), PHM7 (3), PRM9 (3), RRT16 (3), TDA8 (3), URN1 (3), YBR209W (3), YBR284W (3), YCR085W (3), YCR099C (3), YDR042C (3), YER067C-A (3), YER186C (3), YGL101W (3), YGR259C (3), YIL014C-A (3), YKL066W (3), YL043W (3), YLR042C (3), YLR279W (3), **YLR283W** (3), YML096W (3), YML119W (3), YMR102C (3), YMR153C-A (3), YMR160W (3), YMR178W (3), YMR244W (3), YMR316C-A (3), YMR317W (3), YNL146W (3), YOR263C (3), YPL257W (3), YGL109W (4), YJL007C (4), YMR114C (4), YNL338W (4), YNR071C (4), YGL072C (5), YLR149C (5), YML084W (5), YMR103C (5), YOR296W (5), YPL247C (5)
Cell cycle	**END3** (2), **RIM8** (2), **CCR4** (2)	**CLN1** (3), **DIA2** (3), **FYV5** (3), **GAS2** (3), **MAM1** (3), **NFI1** (3), **PCL1** (3), **PEA2** (3), **REC114** (3), **PRM3** (3), **SMK1** (3), **SRC1** (3), **SSO2** (3), **SSP1** (3), **TEC1** (3), **TEP1** (3), **TOF1** (3), **YOR338W** (3), **BDF2** (4), **ITC1** (4), **REI1** (4), **XRN1** (4), **ADA2** (5), **CLB3** (5), **CSM4** (5), **STE24** (5), **YHP1** (5), **ZDS1** (5)
Cell morphology	**END3** (2)	**GAS2** (3), **GPD2** (3), **PEA2** (3), **SMK1** (3), **SSP1** (3), **TEP1** (3), **REI1** (4)
Cytoskeleton	SAC6 (0), **BEM2** (2), **END3** (2), **RVS167** (0), **SLA1** (2) TDA2 (2)	**ABP1** (3), **PCL1** (3), **PEA2** (3), **SLM2** (3), **WHI2** (3), **CLB3** (5), **PFD1** (5)
DNA	**CCR4** (2), **SLX8** (2)	**ADA2** (5), **CSM4** (5), **DIA2** (3), HCS1 (3), **RAD34** (3), **REC114** (3), **RPB9** (3), **SLX5** (3), **TEC1** (3), **TOF1** (3)
Mitochondria	**MTC3** (2), **FMP41** (2), **RTG1** (2), **SAM37** (2)	**HEM25** (3), MRX5 (3), **AIM25** (3), **YLR283W** (3), **GUF1** (3), **AIF1** (3), **ODC1** (3), **MDL2** (3), **YME1** (3), **SUE1** (3), **PKP1** (4), **FMP25** (4), **RSM25** (5), **FMP30** (5)
Metabolism	**TDA9** (2)	ALD2 (3), ALD3 (3), CPA1 (3), **FAA1** (3), FAA3 (3), FAU1 (3), **GPD2** (3), LEU4 (3), NMA1 (3), SNO2 (3), SUR1 (3), YDC1 (3), IGD1 (4), **FMP30** (5), HIS1 (5), **PSK2** (5), SPE2 (5)
Organelle organization	**SAM37** (2), **RIM8** (2)	**ABP1** (3), **AIM25** (3), **ATG1** (3), ATG2 (3), **ATG20** (3), DID2 (3), **DJP1** (3), IWR1 (3), **MAM1** (3), **NGR1** (3), **PEA2** (3), **PEX6** (3), **PRM3** (3), **REC114** (3), SPC2 (3), **SRC1** (3), **SSO2** (3)**TOF1** (3), VPS68 (3), **WHI2** (3), **YME1** (3), **BDF2** (4), **FMP25** (4), **ADA2** (5), **CLB3** (5), **CSM4** (5) **SCD6** (5)
Other	**BEM2** (2), **END3** (2), **RIM8** (2), **RTG1** (2)	ADH6 (3), APE2 (3), ARF2 (3), **DIA2** (3), FDO1 (3), **FYV5** (3), IGO2 (3), **ODC1** (3), OXP1 (3), **PEX6** (3), PML39 (3), **SLM2** (3), **GAS2** (3), **SMK1** (3), **SSO2** (3), **SSP1** (3), **SUE1** (3), **TEC1** (3), **TEP1** (3), TVP18 (3), YML082W (3), **YOR338W** (3), ECM4 (4), PDE2 (4), YGR111W (4)
Protein modification	**SNF7** (1), HPM1 (2), **PKR1** (2), **RIM8** (2), **SAM37** (2), **SLA1** (2), **SLX8** (2), **UMP1** (2), **VPS24** (2)	**ABP1** (3), **ATG1** (3), **CLN1** (3), CPS1 (3), CUL3 (3), CUR1 (3), **DIA2** (3), **NFI1** (3), **HRT3** (3), **MAM1** (3), **PCL1** (3), **SLX5** (3), **SMK1** (3), SPC2 (3), **SSP1** (3), TUL1 (3), **YME1** (3), **FMP25** (4), **PKP1** (4), **XRN1** (4), **ADA2** (5), **CLB3** (5), **PFD1** (5), **PSK2** (5), **STE24** (5)
RNA	**CCR4** (2)	DEG1 (3), HIT1 (4), NGL2 (3), **RPB4** (3), RPS8A (3), **XRN1** (4), CBC2 (5), MSL1 (5), SNT309 (5), **TSR3** (5)
Stress response	**SNF7** (1), **PKR1** (2), **PMP3** (2), **RTG1** (2), **RVS167** (0), **SLX8** (2), **UMP1** (2)	**AIF1** (3), **AIM25** (3), CUR1 (3), **FYV5** (3), HYR1 (3), **MDL2** (3), MIG1 (3), **PEA2** (3), **RAD34** (3), **RPB4** (3), **RPB9** (3), **SLX5** (3), SMF3 (3), **TOF1** (3), YCR102C (3), **ITC1** (4), TRK1 (5), **WHI2** (3), **ADA2 (5), YAR1 (5)**
Transcription	**CCR4** (2), **RTG1** (2), **TDA9** (2)	CAF120 (3), FUI1 (3), GAT2 (3), **ITC1** (4), MIG1 (3), **RPB4** (3), **RPB9** (3), **TEC1** (3), **YOR338W** (3), FZF1 (4), STP1 (4), **XRN1** (4), **ADA2** (5), MBF1 (5), **PFD1** (5), **YHP1** (5)
Translation	RPS7A (2)	**GUF1** (3), **NGR1** (3), **RPB4** (3), RPS7B (3), RPS8A (3), HIT1 (4), **REI1** (4), **PSK2** (5), RPL2B (5), **RSM25** (5), **SCD6** (5), **TSR3** (5), **YAR1 (5)**
Transport (not vesicular)	**SNF7** (1), **PMP3** (2), **SAM37** (2), VPS24 (2)	ATO3 (3), **DJP1** (3), **FAA1** (3), FUI1 (3), GFD1 (5), **HEM25** (3), IWR1 (3), **MDL2** (3), MSN5 (3), NRT1 (3), **PEX6** (3), PUT4 (3), **RPB4** (3), SMF3 (3), **YME1** (3), YOL163W (3), FZF1 (4), **REI1** (4),**YAR1 (5)**, **ZDS1** (5)
Vesicles/trafficking	**RVS167** (0), **SNF7** (1), **END3 (2), RIM8** (2), **SLA1** (2), **VPS24** (2)	**ATG20** (3), DID2 (3), EMP24 (3), **PRM3** (3), **SLM2** (3), **SSO2** (3), VPS68 (3), **WHI2** (3), YPT31 (3), SLM6 (4), ERV29 (5)

Enhancers and suppressors of the $\alpha A\beta_{42}$ instigated toxicity are shown. Genes are sorted according to the Gene Ontology (GO) terms. Category "Mitochondria" was manually added according to GO terms list. Genes that occur in more than 1 GO-term category are in bold. The numbers between brackets refer to the growth scores ranging from 0 (worst growth) to 5 (best growth). See main text for details.

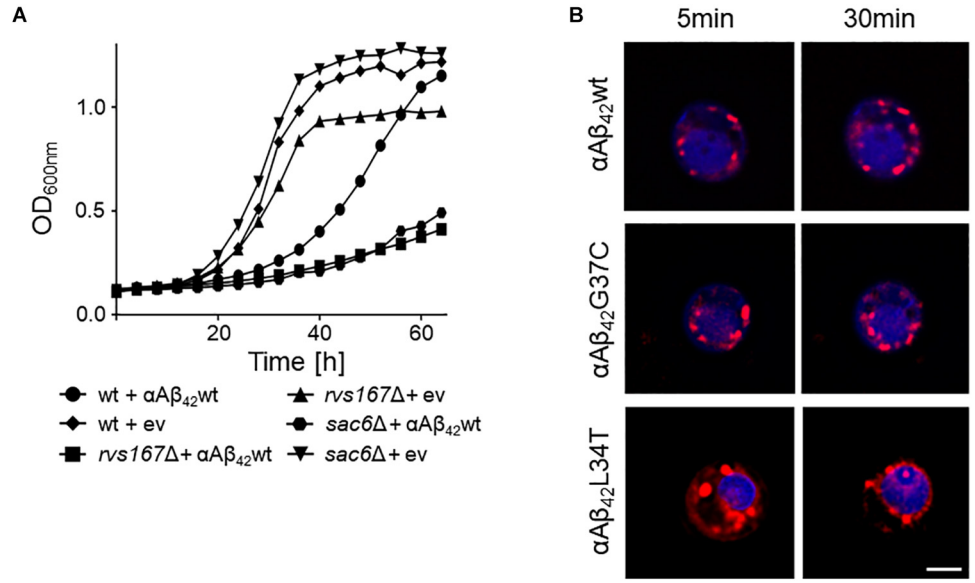

FIGURE 4 | Interference of $\alpha A\beta_{42}$ with endocytosis. **(A)** Growth profiles of wild-type cells and *rvs167*Δ or *sac6*Δ cells transformed with the empty vector (ev) or a construct allowing for expression of $\alpha A\beta_{42}$wt when grown on galactose-containing medium. **(B)** Fluorescence microscopy pictures of strains expressing the toxic $\alpha A\beta_{42}$wt and $\alpha A\beta_{42}$G37C or the non-toxic $\alpha A\beta_{42}$L34T stained with the endocytosis tracker FM4-64 (red) and CMAC (blue), a dye to stain the vacuolar lumen. The scale bar represents 2 μm.

body (MVB) pathway. The two strains with the strongest enhanced toxicity were those carrying a deletion of *SAC6* or *RVS167*. Sac6 is an actin-bundling protein that is required for endocytosis (Penalver et al., 1997; Gheorghe et al., 2008). Rvs167 is a homolog of mammalian amphiphysin that interacts with actin as well and that functions in the internalization step of endocytosis (Lombardi and Riezman, 2001). As illustrated for the expression of $\alpha A\beta_{42}$wt, we indeed observed a similar severe growth phenotype in both the *sac6*Δ and *rvs167*Δ mutants as compared to the isogenic wild-type strain (**Figure 4A**). To further confirm the link between endocytosis and $\alpha A\beta_{42}$ toxicity, we also monitored the uptake of the endocytosis tracker FM4-64 by wild-type cells expressing either the toxic $\alpha A\beta_{42}$wt and $\alpha A\beta_{42}$G37C and non-toxic $\alpha A\beta_{42}$L34T isoforms after 4 h induction on galactose-containing medium. As shown, FM4-64 already stained the vacuolar membrane within 30 min in cells expressing the non-toxic construct while no, or only a minimal staining of the vacuolar membrane was observed in cells expressing the toxic $\alpha A\beta_{42}$ species, even not after 60 min of incubation (**Figure 4B**). This demonstrates that the latter have a direct impact on the endocytic process.

$\alpha A\beta_{42}$ Enhances the Occurrence of Plasma Membrane Lesions and Formation of Lipid Droplets

Closely connected to endocytosis, we noticed that our screening retrieved some ESCRT components, which function in the MVB pathway that is required for the turnover of plasma membrane proteins and lipids. The first step in MVB formation is the binding of ESCRT-0 (Hse1 and Vps27) and ESCRT-I (involving Vps28, Mvb12, Srn2, and Stp22) to ubiquitinated MVB cargoes. Next, the ESCRT-II complex (involving Vps25, Vps36, and Snf8) mediates the recruitment of ESCRT-III accessory factors (Bro1 and Doa4), which in turn loads general ESCRT-III factors (Vps20, Snf7, Did4, Chm7, Ist1, and Vps24) to direct the continued sorting of cargoes into invaginating vesicles during MVB formation. ESCRT-III dissociation factors (Vps4, Vps60, Did2, and Vta1) mediate the release and recycling of all involved factors (Hurley, 2010; Babst, 2011). All the 21 corresponding genes are not essential and could therefore be tested for their implications in $\alpha A\beta_{42}$ toxicity. After transformation of the corresponding KO strains with either $\alpha A\beta_{42}$wt, $\alpha A\beta_{42}$G37C or the ev-αGFP control construct, we evaluated the impact of the deletions on $\alpha A\beta_{42}$ toxicity through spot assays. This revealed that for several components of the MVB pathway their deletion significantly aggravated $\alpha A\beta_{42}$ toxicity. This included the ESCRTIII components Did4, the ESCRTIII accessory components Bro1 and Doa4 as well as the ESCRTIII dissociation mediator Vps4 (**Supplementary Figures S3, S4**). Recent studies in mammalian cells have demonstrated that besides its role in the MVB pathway, ESCRT plays key roles in a variety of other processes, including membrane lesion repair (Jimenez et al., 2014; Sundquist and Ullman, 2015; Campsteijn et al., 2016; Denais et al., 2016; Raab et al., 2016). It is well-established that $A\beta_{42}$ can introduce membrane lesions and different non-excluding mechanisms were proposed, including membrane lipid interaction, alterations in membrane fluidity, pore formation, or lipid oxidation (Eckert et al., 2000; Muller et al., 2001; Ambroggio et al., 2005; Rauk, 2008; Axelsen et al., 2011; Viola and Klein, 2015). We speculated that $\alpha A\beta_{42}$ would also trigger membrane lesions in our yeast system. To test this, we analyzed

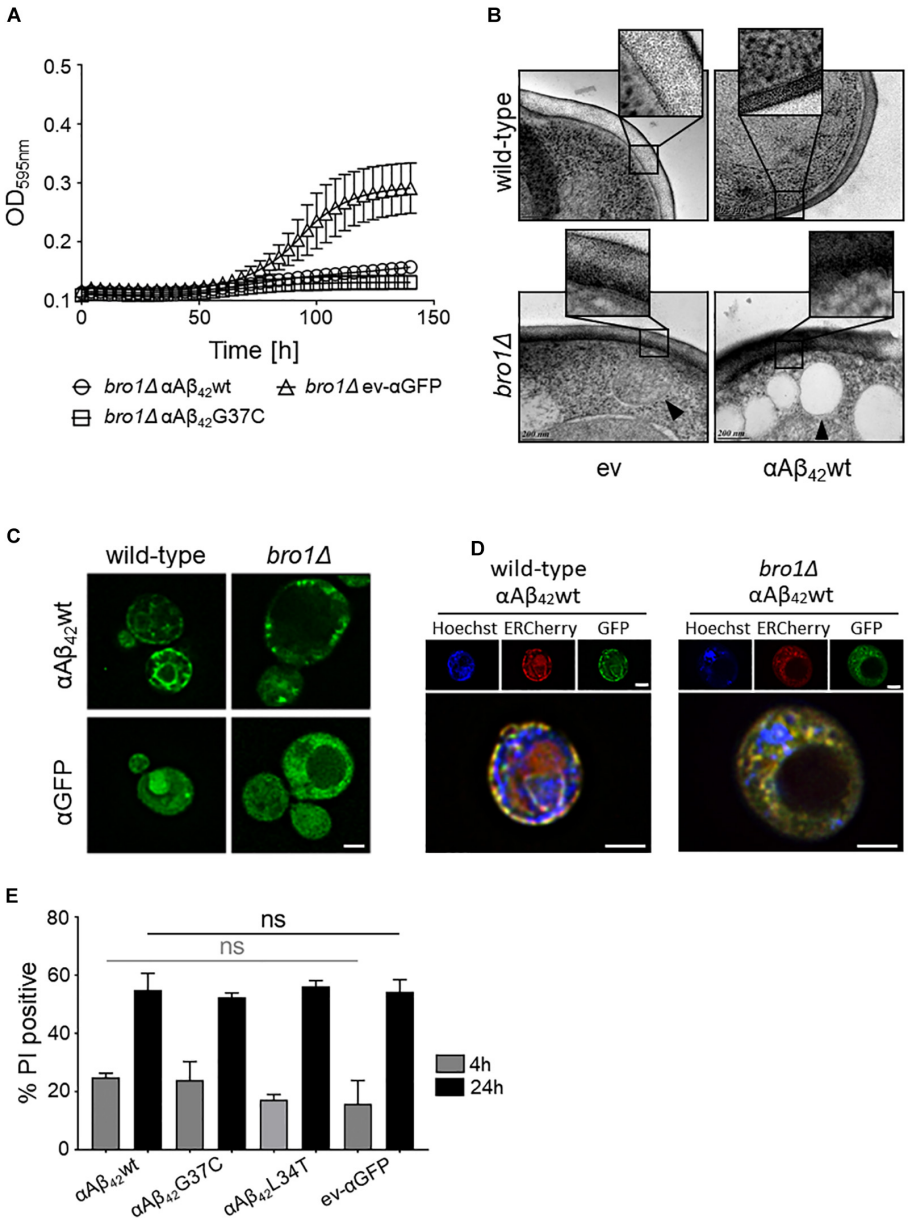

FIGURE 5 | The role of Bro1 for membrane lesion repair. **(A)** Growth profile on galactose-containing medium of a strain deleted for the ESCRT-III accessory factor *BRO1* transformed with an empty vector (ev-αGFP) or constructs allowing for expression of $\alpha A\beta_{42}$wt or $\alpha A\beta_{42}$G37C. Cryo-EM pictures **(B)** and fluorescence microscopy pictures **(C)** of wild-type and *bro1*Δ cells transformed with an empty vector (ev) or expressing $\alpha A\beta_{42}$wt and grown for 6 h on galactose-containing medium. The indents in panel **(B)** zoom in on the plasma membrane and cell wall. The black arrowhead in **(B)** indicates a lipid droplet. Scale bars for cryo-EM pictures represent 200 nm. **(D)** BY4742 wild-type and a *bro1*Δ strains transformed with a plasmids carrying $\alpha A\beta_{42}$wt and additionally a plasmid allowing the expression of $Kar2_{(1-135)}$-mCherry-HDEL (ERCherry), a marker for the ER. DNA was stained with Hoechst. Cells were grown in medium allowing for gene expression for 6 h prior to microscopy. Scale bars for fluorescence pictures represent 2 μm. **(E)** PI staining of cells deleted for *BRO1* transformed with constructs allowing for expression of $\alpha A\beta_{42}$wt, $\alpha A\beta_{42}$L34T, $\alpha A\beta_{42}$G37C, or αGFP after 4 or 24 h growth on galactose-containing medium. Error bars represent standard deviations of at least four independent transformants.

the plasma membrane integrity of wild-type and *bro1*Δ cells by cryo-EM. We chose the *bro1*Δ strain because here $\alpha A\beta_{42}$wt and $\alpha A\beta_{42}$G37C was almost lethal (**Figure 5A**) and because Bro1 is the yeast ortholog of human Alix, a proposed biomarker for AD (Sun et al., 2015). Consistent with our hypothesis, the cryo-EM study showed that the plasma membrane of *bro1*Δ cells expressing $\alpha A\beta_{42}$wt seemed heavily corrugated while the *bro1*Δ cells transformed with empty vector displayed a more modest phenotype. In the wild-type strain, the plasma membrane remained ostensibly smooth even upon expression of $\alpha A\beta_{42}$wt (**Figure 5B**). However, although we did not quantify, the observed membrane corrugating effects of specifically the *bro1*Δ

strain expressing $\alpha A\beta_{42}$wt are strikingly obvious. Moreover, when compared to the wild-type cells, the ER morphology in the *bro1*Δ mutant was completely different and appeared to be deteriorated. Indeed, only a minimal perinuclear and cortical ER was detected and the cells displayed the $\alpha A\beta_{42}$-linker-GFP fusion mostly in filamentous structures and foci (**Figures 5C,D**). Thus, expression of $\alpha A\beta_{42}$wt seems to dramatically affect all membranous structures evidencing that Bro1, and by extension the ESCRT system, is absolutely required for the repair of membrane lesions induced by $\alpha A\beta_{42}$. In line with this essential requirement of ESCRT, we observed that while still seeing a tendency of increased PI uptake after 4 h induction for those *bro1*Δ cells expressing toxic $\alpha A\beta_{42}$, a maximal PI uptake in all *bro1*Δ transformants is seen after 24 h, even for those strains expressing the non-toxic $\alpha A\beta_{42}$L34T mutant or the ev-αGFP control (**Figure 5E**).

The cryo-EM study also pointed to the formation of cortical vesicle-like structures, which we believe may correspond to lipid droplets. Since previous studies have shown that the formation of lipid droplets denotes an adaptive response to a chronic lipid imbalance (Vevea et al., 2015; Garcia et al., 2018), which is likely to occur in *bro1*Δ strain because of hampered MVB formation and lipid turnover, we decided to perform a Nile Red staining to visualize the droplets. While during the first hours of induction on galactose-containing medium we observed an overall enhanced lipid droplet biogenesis in all *bro1*Δ strains as compared to the respective wild-type strains, the increase was persistent and especially more dense droplets were seen with *bro1*Δ cells expressing $\alpha A\beta_{42}$G37C or $\alpha A\beta_{42}$wt (**Figure 6A**). This observation confirms previously reported data on an increased lipid droplet load in an $A\beta_{42}$ wild-type strain (Chen et al., 2017).

The perturbation of lipid homeostasis has also been linked to defects in the ER and mitochondria (Vevea et al., 2015), and the latter incited us to monitor the level of ROS in the *bro1*Δ strains. As shown, and comparable to the PI uptake, we found similar high levels of ROS in all strains tested indicative that this is a characteristic mainly associated to the deletion of *BRO1* itself (**Figure 6B**).

DISCUSSION

During the past decades, several studies validated the use of yeast to decipher the pathobiology underlying a variety of human disorders. Especially for degenerative protein folding diseases, like Huntington's, Parkinson's, or Alzheimer's disease, this led to the discovery of processes and molecular pathways contributing to cell demise (Winderickx et al., 2008; Franssens et al., 2010; Swinnen et al., 2011; Porzoor and Macreadie, 2013; Tenreiro et al., 2013, 2017; Chen and Petranovic, 2016; Jiang et al., 2016; Verduyckt et al., 2016; Fruhmann et al., 2017). The insight gained from these studies were not only relevant in the context of disease, but they also clarified fundamental aspects on how a cell manages to maintain proteostasis and the consequences in case this system fails. In this paper, we used a previously reported model to study the repercussions when the APP-derived peptide $A\beta_{42}$ is expressed in yeast (D'Angelo et al., 2013; Vignaud et al., 2013). Though this model makes use of a GFP fusion, the use of the super-toxic $A\beta_{42}$G37C and the non-toxic $A\beta_{42}$L34T mutants clearly demonstrated that the properties of the GFP fusion are dictated by the $A\beta_{42}$ peptide moiety. Furthermore, by comparing constructs with or without an N-terminal fusion with the α-prepro sequence and conditions that retain the α-prepro in the ER, it became obvious that the processing in the ER/Golgi system and the subsequent shuttling into the secretory pathway is essential to unleash the full toxic capacity of the $A\beta_{42}$-linker-GFP fusion. Our data also contradict the argument that the $\alpha A\beta_{42}$ instigated toxicity would simply be due to an overload of the ER/Golgi processing system because both wild-type and mutant $\alpha A\beta_{42}$ are processed in the same manner (D'Angelo et al., 2013; Vignaud et al., 2013) and no toxicity is seen in case of expression of mutant $\alpha A\beta_{42}$L34T.

The use of our yeast model allowed us to confirm some data previously reported. This included the impact of $\alpha A\beta_{42}$ on endocytosis (Treusch et al., 2011; D'Angelo et al., 2013), where we now show that strains with a deletion of *SAC6* or *RVS167* display an increased $\alpha A\beta_{42}$ toxicity, as well as the impact on mitochondrial functioning (D'Angelo et al., 2013; Chen and Petranovic, 2015; Chen et al., 2017), which we illustrated by co-localization studies and the observation that $\alpha A\beta_{42}$ enhances ROS formation. These data are relevant because, indeed, changes in endocytic capacity and mitochondrial dysfunction are typically seen in the pathogenesis of AD and have been observed in other AD models as well (Thomas et al., 2011; Wang et al., 2011; Avetisyan et al., 2016; Schreij et al., 2016; Dixit et al., 2017; Shoshan-Barmatz et al., 2018; Xu et al., 2018). However, the observed partial co-localization of toxic $\alpha A\beta_{42}$ with mitochondria may either indicate a direct interaction of the peptide with this organelle or it may simply be a reflection of the interaction between the ER and mitochondria through the membrane contact sites known as ERMES (Kornmann et al., 2009). This aspect needs to be analyzed in more detail. Interestingly, mitochondria associated membranes (MAMs), the mammalian counterpart of ERMES, have already been implicated in AD (Area-Gomez and Schon, 2016; Paillusson et al., 2016). Closely related to the observed mitochondrial dysfunction is our observation that deletion of *AIF1*, encoding a cell death effector, has a protective effect on the $\alpha A\beta_{42}$ expressing yeast cells. This suggests that $\alpha A\beta_{42}$ may induce an apoptotic-like program in yeast, which fits the finding that neuronal cells die through apoptosis in AD (Ohyagi et al., 2005; Shoshan-Barmatz et al., 2018). Our data also show that particularly the expression of the toxic $\alpha A\beta_{42}$ isoforms is linked to the formation of ER-associated foci and filamentous structures. Though we did not study these structures in detail and previously believed these to represent vesicles (D'Angelo et al., 2013), it is well-possible that they may in fact be ER aggregates or clustering of ER membranes, which are both indicative for ER stress (Varadarajan et al., 2012, 2013; Vevea et al., 2015). Also ER stress is associated to AD (Gerakis and Hetz, 2018) and several links between ER stress and mitochondrial dysfunction have been proposed in this neurodegenerative disorder (Costa et al., 2012; Barbero-Camps et al., 2014; Erpapazoglou et al., 2017).

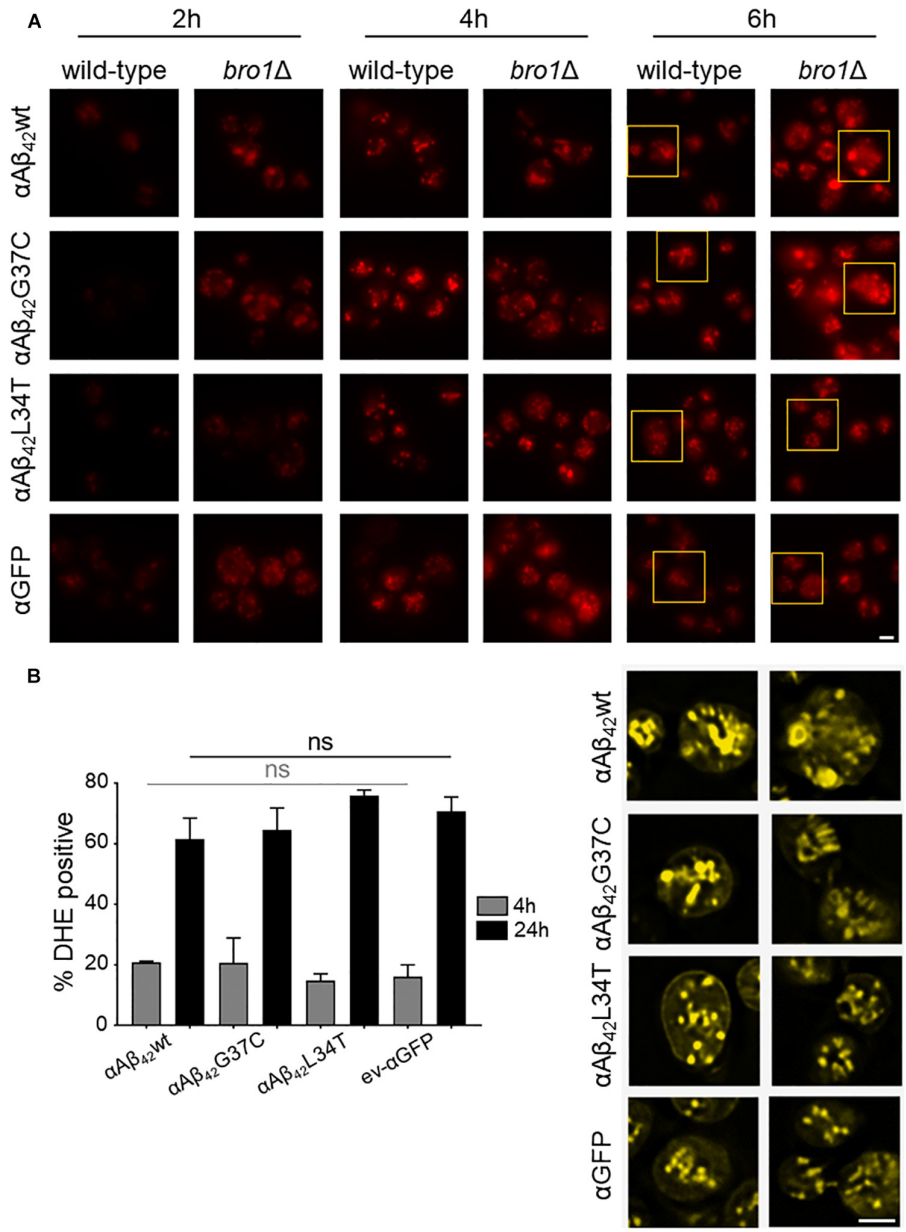

FIGURE 6 | $\alpha A\beta_{42}$ instigated lipid droplet biogenesis. **(A)** Nile Red stainings (top panel), a marker for lipid droplets, of wild-type and the *bro1*Δ cells expressing $\alpha A\beta_{42}$wt, $\alpha A\beta_{42}$G37C, or $\alpha A\beta_{42}$L34T or αGFP after 2, 4, or 6 h growth on galactose-containing medium. The bottom panel (yellow) shows magnifications and deconvolved parts of the top-panel pictures at time point of 6 h. Note that due to deconvolution the picture intensities are enhanced. Scale bars represent 2 μm. **(B)** DHE staining of cells deleted for *BRO1* transformed with constructs allowing for expression of $\alpha A\beta_{42}$wt, $\alpha A\beta_{42}$L34T, $\alpha A\beta_{42}$G37C, or αGFP after 4 or 24 h growth on galactose-containing medium. Error bars represent standard deviations of at least four independent transformants.

One of the most striking observations made in our studies is the role of ESCRT in modulating the $\alpha A\beta_{42}$ toxicity. The ESCRT system functions in the MVB pathway and several studies have linked this role of ESCRT to AD. Neurons of AD transgenic mice were shown to display enlarged MVBs as compared to the neurons of wild-type mice, and ESCRT was demonstrated to modulate intracellular $A\beta_{42}$ accumulation by directing APP to lysosomal degradation and by enhancing $A\beta_{42}$ secretion. In addition, ESCRT components were found associated with amyloid plaques in transgenic mice and to granular structures hippocampal neurons of AD diseased human brain (Yamazaki et al., 2010; Edgar et al., 2015; Willen et al., 2017). However, apart from its function in the MVB pathway, ESCRT is also required for the repair of membrane lesions. Here, both cryo-EM and PI-staining give a strong impression of the presence of such lesions at the plasma membrane of cells lacking the ESCRT component Bro1, probably explaining in part the sick phenotype of the *bro1*Δ mutant. As such, our data strongly

suggest that the role of ESCRT for plasma membrane repair, which so far was only demonstrated in mammalian cells, is evolutionary well-conserved. Interestingly, we found that the disruption of the plasma membrane integrity in the *bro1*Δ strain is dramatically exacerbated upon expression of $\alpha A\beta_{42}$ and that this came along with the deterioration of the ER and an almost lethal phenotype. This is intriguing for several reasons. It demonstrates that when the fully processed $A\beta_{42}$-linker-GFP arrives at the plasma membrane, the peptide further aggravates plasma membrane disruption, which given the observed effect on the ER, might well be involving fusion of secretory vesicles that contain disordered membranes. The fact that our screens retrieved the KO strain lacking *SSO2* as suppressor of $\alpha A\beta_{42}$ toxicity favors the last possibility. Indeed, *SSO2* encodes a plasma membrane t-SNARE that is required for fusion secretory vesicles (Grote et al., 2000). Moreover, the data recapitulate observations made for AD where, as mentioned, $A\beta_{42}$ was shown to introduce membrane lesions via different non-excluding mechanisms, including membrane lipid interaction, alterations in membrane fluidity, pore formation, or lipid oxidation (Eckert et al., 2000; Muller et al., 2001; Ambroggio et al., 2005; Rauk, 2008; Axelsen et al., 2011; Viola and Klein, 2015).

Given the effect of $A\beta_{42}$ on plasma membrane integrity, the presence of this peptide also impacts on the overall cellular lipid homeostasis. In fact, extensive lipid alterations are implicated in the AD disease pathology but it is still a matter of debate whether such alterations are the cause or the consequence of AD (Grosgen et al., 2010; Xiang et al., 2015; El Gaamouch et al., 2016). In yeast, the expression of $A\beta_{42}$ has been linked to a transcriptional upshift of key regulators of lipid metabolism as well as an enhanced formation of lipid droplets (Chen et al., 2017). Our screens with the yeast deletion collection and our Nile Red stainings support the link between $A\beta_{42}$ and lipid metabolism. Intriguingly, a recent study demonstrated lipid droplet formation to be an adaptive response to an acute lipid imbalance in yeast cells. The same study then also showed that the biogenesis of these droplets occurs at ER aggregates (Vevea et al., 2015), which we believe to correspond to the ER-associated foci and filamentous structures seen when yeast cells express toxic forms of $\alpha A\beta_{42}$, as mentioned. Notably, also in transgenic mouse models of AD an enhanced lipid droplet formation is observed (Hamilton et al., 2010; Yang et al., 2014), again underscoring the relevance of the data obtained in yeast.

AUTHOR CONTRIBUTIONS

GF, CM, HV, MV, and NT performed experiments and analyzed data. GF and JW wrote the draft. CDV, CC, and JW contributed conception and design of the studies. CC and JW corrected and edited the draft.

FUNDING

This work was financially supported by the KU Leuven and the FWO Vlaanderen (Project No. G0A6315N). CDV was supported by the Swiss National Science Foundation and the Canton of Fribourg.

ACKNOWLEDGMENTS

We want to thank Joëlle Rosseels, Dorien Vliegen, and Elodie Cougouille for technical and experimental support. We also want to thank Dr. B. Salin and to the Bordeaux Imaging Center (BIC) for performing TEM experiments.

SUPPLEMENTARY MATERIAL

The Supplementary Material for this article can be found online at: https://www.frontiersin.org/articles/10.3389/fnmol.2018.00406/full#supplementary-material

REFERENCES

Abramov, E., Dolev, I., Fogel, H., Ciccotosto, G. D., Ruff, E. (2009). Amyloid-β as a positive endogenous regulator of release probability at hippocampal synapses. *Nat. Neurosci.* 12, 1567–1576. doi: 10.1038/nn.2433

Alexandrov, A. I., Serpionov, G. V., Kushnirov, V. V., and Ter-Avanesyan, M. D. (2016). Wild type huntingtin toxicity in yeast: Implications for the role of amyloid cross-seeding in polyQ diseases. *Prion* 10, 221–227. doi: 10.1080/19336896.2016.1176659

Ambroggio, E. E., Kim, D. H., Separovic, F., Barrow, C. J., Barnham, K. J., Bagatolli, L. A., et al. (2005). Surface behavior and lipid interaction of Alzheimer β-amyloid peptide 1-42: a membrane-disrupting peptide. *Biophys. J.* 88, 2706–2713. doi: 10.1529/biophysj.104.055582

Area-Gomez, E., and Schon, E. A. (2016). Mitochondria-associated ER membranes and Alzheimer disease. *Curr. Opin. Genet. Dev.* 38, 90–96. doi: 10.1016/j.gde.2016.04.006

Avetisyan, A. V., Samokhin, A. N., Alexandrova, I. Y., Zinovkin, R. A., Simonyan, R. A., and Bobkova, N. V. (2016). Mitochondrial dysfunction in neocortex and hippocampus of olfactory bulbectomized mice, a model of Alzheimer's disease. *Biochemistry (Mosc)* 81, 615–623. doi: 10.1134/S0006297916060080

Axelsen, P. H., Komatsu, H., and Murray, I. V. (2011). Oxidative stress and cell membranes in the pathogenesis of Alzheimer's disease. *Physiology (Bethesda)* 26, 54–69. doi: 10.1152/physiol.00024.2010

Babst, M. (2011). MVB vesicle formation: ESCRT-dependent, ESCRT-independent and everything in between. *Curr. Opin. Cell Biol.* 23, 452–457. doi: 10.1016/j.ceb.2011.04.008

Barbero-Camps, E., Fernandez, A., Baulies, A., Martinez, L., Fernandez-Checa, J. C., and Colell, A. (2014). Endoplasmic reticulum stress mediates amyloid beta neurotoxicity via mitochondrial cholesterol trafficking. *Am. J. Pathol.* 184, 2066–2081. doi: 10.1016/j.ajpath.2014.03.014

Belden, W. J., and Barlowe, C. (2001). Role of Erv29p in collecting soluble secretory proteins into ER-derived transport vesicles. *Science* 294, 1528–1531. doi: 10.1126/science.1065224

Benilova, I., Karran, E., and De Strooper, B. (2012). The toxic Aβ oligomer and Alzheimer's disease: an emperor in need of clothes. *Nat. Neurosci.* 15, 349–357. doi: 10.1038/nn.3028

Campsteijn, C., Vietri, M., and Stenmark, H. (2016). Novel ESCRT functions in cell biology: spiraling out of control? *Curr. Opin. Cell Biol.* 41, 1–8. doi: 10.1016/j.ceb.2016.03.008

Chen, X., Bisschops, M. M. M., Agarwal, N. R., Ji, B., Shanmugavel, K. P., and Petranovic, D. (2017). Interplay of energetics and ER stress exacerbates

Alzheimer's amyloid-beta (Abeta) toxicity in yeast. *Front. Mol. Neurosci.* 10:232. doi: 10.3389/fnmol.2017.00232

Chen, X., and Petranovic, D. (2015). Amyloid-β peptide-induced cytotoxicity and mitochondrial dysfunction in yeast. *FEMS Yeast Res.* 15, 1–21. doi: 10.1093/femsyr/fov061

Chen, X., and Petranovic, D. (2016). Role of frameshift ubiquitin B protein in Alzheimer's disease. *Wiley Interdiscip. Rev. Syst. Biol. Med.* 8, 300–313. doi: 10.1002/wsbm.1340

Costa, R. O., Ferreiro, E., Martins, I., Santana, I., Cardoso, S. M., Oliveira, C. R., et al. (2012). Amyloid beta-induced ER stress is enhanced under mitochondrial dysfunction conditions. *Neurobiol. Aging* 33, 824.e825-e816. doi: 10.1016/j.neurobiolaging.2011.04.011

D'Angelo, F., Vignaud, H., Di Martino, J., Salin, B., Devin, A., Cullin, C., et al. (2013). A yeast model for amyloid-beta aggregation exemplifies the role of membrane trafficking and PICALM in cytotoxicity. *Dis. Model Mech.* 6, 206–216. doi: 10.1242/dmm.010108

Dean, N., and Pelham, H. R. (1990). Recycling of proteins from the golgi compartment to the ER in yeast. *J. Cell Biol.* 111, 369–377. doi: 10.1083/jcb.111.2.369

Denais, C. M., Gilbert, R. M., Isermann, P., McGregor, A. L., te Lindert, M., Weigelin, B., et al. (2016). Nuclear envelope rupture and repair during cancer cell migration. *Science (New York, N.Y.)* 352, 353–358. doi: 10.1126/science.aad7297

Dittmar, J. C., Reid, R. J., and Rothstein, R. (2010). ScreenMill: a freely available software suite for growth measurement, analysis and visualization of high-throughput screen data. *BMC Bioinformatics* 11:353. doi: 10.1186/1471-2105-11-353

Dixit, S., Fessel, J. P., and Harrison, F. E. (2017). Mitochondrial dysfunction in the APP/PSEN1 mouse model of Alzheimer's disease and a novel protective role for ascorbate. *Free Radic. Biol. Med.* 112, 515–523. doi: 10.1016/j.freeradbiomed.2017.08.021

Eckert, G. P., Cairns, N. J., Maras, A., Gattaz, W. F., and Muller, W. E. (2000). Cholesterol modulates the membrane-disordering effects of beta-amyloid peptides in the hippocampus: specific changes in Alzheimer's disease. *Dement. Geriatr. Cogn. Disord.* 11, 181–186. doi: 10.1159/000017234

Edgar, J. R., Willen, K., Gouras, G. K., and Futter, C. E. (2015). ESCRTs regulate amyloid precursor protein sorting in multivesicular bodies and intracellular amyloid-beta accumulation. *J. Cell Sci.* 128, 2520–2528. doi: 10.1242/jcs.170233

El Gaamouch, F., Jing, P., Xia, J., and Cai, D. (2016). Alzheimer's disease risk genes and lipid regulators. *J. Alzheimers Dis.* 53, 15–29. doi: 10.3233/JAD-160169

Erpapazoglou, Z., Mouton-Liger, F., and Corti, O. (2017). From dysfunctional endoplasmic reticulum-mitochondria coupling to neurodegeneration. *Neurochem. Int.* 109, 171–183. doi: 10.1016/j.neuint.2017.03.021

Foury, F. (1997). Human genetic diseases: a cross-talk between man and yeast. *Gene* 195, 1–10. doi: 10.1016/S0378-1119(97)00140-6

Franssens, V., Boelen, E., Anandhakumar, J., Vanhelmont, T., Buttner, S., and Winderickx, J. (2010). Yeast unfolds the road map toward alpha-synuclein-induced cell death. *Cell Death Differ.* 17, 746–753. doi: 10.1038/cdd.2009.203

Fruhmann, G., Seynnaeve, D., Zheng, J., Ven, K., Molenberghs, S., Wilms, T., et al. (2017). Yeast buddies helping to unravel the complexity of neurodegenerative disorders. *Mech. Ageing Dev.* 161(Pt B), 288–305. doi: 10.1016/j.mad.2016.05.002

Garcia, E. J., Vevea, J. D., and Pon, L. A. (2018). Lipid droplet autophagy during energy mobilization, lipid homeostasis and protein quality control. *Front. Biosci. (Landmark Ed)* 23, 1552–1563. doi: 10.2741/4660

Gerakis, Y., and Hetz, C. (2018). Emerging roles of ER stress in the etiology and pathogenesis of Alzheimer's disease. *FEBS J.* 285, 995–1011. doi: 10.1111/febs.14332

Gheorghe, D. M., Aghamohammadzadeh, S., Smaczynska-de, R. II, Allwood, E. G., Winder, S. J., and Ayscough, K. R. (2008). Interactions between the yeast SM22 homologue Scp1 and actin demonstrate the importance of actin bundling in endocytosis. *J. Biol. Chem.* 283, 15037–15046. doi: 10.1074/jbc.M710332200

Grosgen, S., Grimm, M. O., Friess, P., and Hartmann, T. (2010). Role of amyloid beta in lipid homeostasis. *Biochim. Biophys. Acta* 1801, 966–974. doi: 10.1016/j.bbalip.2010.05.002

Grote, E., Carr, C. M., and Novick, P. J. (2000). Ordering the final events in yeast exocytosis. *J. Cell Biol.* 151, 439–452. doi: 10.1083/jcb.151.2.439

Hamilton, L. K., Aumont, A., Julien, C., Vadnais, A., Calon, F., and Fernandes, K. J. (2010). Widespread deficits in adult neurogenesis precede plaque and tangle formation in the 3xTg mouse model of Alzheimer's disease. *Eur. J. Neurosci.* 32, 905–920. doi: 10.1111/j.1460-9568.2010.07379.x

Hamza, A., Tammpere, E., Kofoed, M., Keong, C., Chiang, J., Giaever, G., et al. (2015). Complementation of yeast genes with human genes as an experimental platform for functional testing of human genetic variants. *Genetics* 201, 1263–1274. doi: 10.1534/genetics.115.181099

Hu, W., Wang, Z., and Zheng, H. (2018). Mitochondrial accumulation of amyloid beta (Abeta) peptides requires TOMM22 as a main Abeta receptor in yeast. *J. Biol. Chem.* 293, 12681–12689. doi: 10.1074/jbc.RA118.002713

Hurley, J. H. (2010). The ESCRT complexes. *Crit. Rev. Biochem. Mol. Biol.* 45, 463–487. doi: 10.3109/10409238.2010.502516

Ittner, L. M., and Gotz, J. (2011). Amyloid-beta and tau–a toxic pas de deux in Alzheimer's disease. *Nat. Rev. Neurosci.* 12, 65–72. doi: 10.1038/nrn2967

Jackrel, M. E., DeSantis, M. E., Martinez, B. A., Castellano, L. M., Stewart, R. M., Caldwell, K. A., et al. (2014). Potentiated Hsp104 variants antagonize diverse proteotoxic misfolding events. *Cell* 156, 170–182. doi: 10.1016/j.cell.2013.11.047

Jiang, Y., Chadwick, S. R., and Lajoie, P. (2016). Endoplasmic reticulum stress: The cause and solution to Huntington's disease? *Brain Res.* 1648, 650–657. doi: 10.1016/j.brainres.2016.03.034

Jimenez, A. J., Maiuri, P., Lafaurie-Janvore, J., Divoux, S., Piel, M., and Perez, F. (2014). ESCRT machinery is required for plasma membrane repair. *Science* 343:1247136. doi: 10.1126/science.1247136

Kagan, B. L., Jang, H., Capone, R., Teran Arce, F., Ramachandran, S., Lal, R., et al. (2012). Antimicrobial properties of amyloid peptides. *Mol. Pharm.* 9, 708–717. doi: 10.1021/mp200419b

Kim, J., and Klionsky, D. J. (2000). Autophagy, cytoplasm-to-vacuole targeting pathway, and pexophagy in yeast and mammalian cells. *Annu. Rev. Biochem.* 69, 303–342. doi: 10.1146/annurev.biochem.69.1.303

Kornmann, B., Currie, E., Collins, S. R., Schuldiner, M., Nunnari, J., Weissman, J. S., et al. (2009). An ER-mitochondria tethering complex revealed by a synthetic biology screen. *Science* 325, 477–481. doi: 10.1126/science.1175088

Kumar, D. K., Choi, S. H., Washicosky, K. J., Eimer, W. A., Tucker, S., Ghofrani, J., et al. (2016). Amyloid-beta peptide protects against microbial infection in mouse and worm models of Alzheimer's disease. *Sci. Transl. Med.* 8:340ra372. doi: 10.1126/scitranslmed.aaf1059

LaFerla, F. M., Green, K. N., and Oddo, S. (2007). Intracellular amyloid-β in Alzheimer's disease. *Nat. Rev. Neurosci.* 8, 499–509. doi: 10.1038/nrn2168

Lefebvre-Legendre, L., Salin, B., Schaeffer, J., Brethes, D., Dautant, A., Ackerman, S. H., et al. (2005). Failure to assemble the alpha 3 beta 3 subcomplex of the ATP synthase leads to accumulation of the alpha and beta subunits within inclusion bodies and the loss of mitochondrial cristae in *Saccharomyces cerevisiae*. *J. Biol. Chem.* 280, 18386–18392. doi: 10.1074/jbc.M410789200

Lewis, M. J., and Pelham, H. R. B. (1990). A human homologue of the yeast HDEL receptor. *Nature* 348, 162–163. doi: 10.1038/348162a0

Liu, W., Li, L., Ye, H., Chen, H., Shen, W., Zhong, Y., et al. (2017). From *Saccharomyces cerevisiae* to human: the important gene co-expression modules. *Biomed. Rep.* 7, 153–158. doi: 10.3892/br.2017.941

Lombardi, R., and Riezman, H. (2001). Rvs161p and Rvs167p, the two yeast amphiphysin homologs, function together in vivo. *J. Biol. Chem.* 276, 6016–6022. doi: 10.1074/jbc.M008735200

Muller, W. E., Kirsch, C., and Eckert, G. P. (2001). Membrane-disordering effects of beta-amyloid peptides. *Biochem. Soc. Trans.* 29(Pt 4), 617–623. doi: 10.1042/bst0290617

Mumberg, D., Müller, R., and Funk, M. (1994). Regulatable promoters of Saccharomyces cerevisiae: comparison of transcriptional activity and their use for heterologous expression. *Nucleic Acids Res.* 22, 5767–5768. doi: 10.1093/nar/22.25.5767

Nice, D. C., Sato, T. K., Stromhaug, P. E., Emr, S. D., and Klionsky, D. J. (2002). Cooperative binding of the cytoplasm to vacuole targeting pathway proteins, Cvt13 and Cvt20, to phosphatidylinositol 3-phosphate at the pre-autophagosomal structure is required for selective autophagy. *J. Biol. Chem.* 277, 30198–30207. doi: 10.1074/jbc.M204736200

Ohyagi, Y., Asahara, H., Chui, D. H., Tsuruta, Y., Sakae, N., Miyoshi, K., et al. (2005). Intracellular Abeta42 activates p53 promoter: a pathway to

neurodegeneration in Alzheimer's disease. *FASEB J.* 19, 255–257. doi: 10.1096/fj.04-2637fje

Paillusson, S., Stoica, R., Gomez-Suaga, P., Lau, D. H. W., Mueller, S., Miller, T., et al. (2016). There's something wrong with my MAM; the ER-mitochondria axis and neurodegenerative diseases. *Trends Neurosci.* 39, 146–157. doi: 10.1016/j.tins.2016.01.008

Pearson, H. A., and Peers, C. (2006). Physiological roles for amyloid beta peptides. *J. Physiol.* 575, 5–10. doi: 10.1113/jphysiol.2006.111203

Penalver, E., Ojeda, L., Moreno, E., and Lagunas, R. (1997). Role of the cytoskeleton in endocytosis of the yeast maltose transporter. *Yeast* 13, 541–549. doi: 10.1002/(SICI)1097-0061(199705)13:6<541::AID-YEA112>3.0.CO;2-4

Porzoor, A., and Macreadie, I. G. (2013). Application of yeast to study the tau and amyloid-beta abnormalities of Alzheimer's disease. *J. Alzheimers Dis.* 35, 217–225. doi: 10.3233/JAD-122035

Raab, M., Gentili, M., de Belly, H., Thiam, H. R., Vargas, P., Jimenez, A. J., et al. (2016). ESCRT III repairs nuclear envelope ruptures during cell migration to limit DNA damage and cell death. *Science (New York, N.Y.)* 352, 359–362. doi: 10.1126/science.aad7611

Rauk, A. (2008). Why is the amyloid beta peptide of Alzheimer's disease neurotoxic? *Dalton Trans.* 1273–1282. doi: 10.1039/b718601k

Ruan, L., Zhou, C., Jin, E., Kucharavy, A., Zhang, Y., Wen, Z., et al. (2017). Cytosolic proteostasis through importing of misfolded proteins into mitochondria. *Nature* 543, 443–446. doi: 10.1038/nature21695

Schindelin, J., Arganda-Carreras, I., Frise, E., Kaynig, V., Longair, M., Pietzsch, T., et al. (2012). Fiji: an open-source platform for biological-image analysis. *Nat. Methods* 9, 676–682. doi: 10.1038/nmeth.2019

Schreij, A. M., Fon, E. A., and McPherson, P. S. (2016). Endocytic membrane trafficking and neurodegenerative disease. *Cell Mol. Life Sci.* 73, 1529–1545. doi: 10.1007/s00018-015-2105-x

Shoshan-Barmatz, V., Nahon-Crystal, E., Shteinfer-Kuzmine, A., and Gupta, R. (2018). VDAC1, mitochondrial dysfunction, and Alzheimer's disease. *Pharmacol. Res.* 131, 87–101. doi: 10.1016/j.phrs.2018.03.010

Sun, Y., Rong, X., Lu, W., Peng, Y., Li, J., Xu, S., et al. (2015). Translational study of Alzheimer's disease (AD) biomarkers from brain tissues in AbetaPP/PS1 mice and serum of AD patients. *J. Alzheimers Dis.* 45, 269–282. doi: 10.3233/JAD-142805

Sundquist, W. I., and Ullman, K. S. (2015). Cell biology. an escrt to seal the envelope. *Science (New York, N.Y.)* 348, 1314–1315. doi: 10.1126/science.aac7083

Swinnen, E., Buttner, S., Outeiro, T. F., Galas, M. C., Madeo, F., Winderickx, J., et al. (2011). Aggresome formation and segregation of inclusions influence toxicity of alpha-synuclein and synphilin-1 in yeast. *Biochem. Soc. Trans.* 39, 1476–1481. doi: 10.1042/BST0391476

Swinnen, E., Wilms, T., Idkowiak-Baldys, J., Smets, B., De Snijder, P., Accardo, S., et al. (2014). The protein kinase Sch9 is a key regulator of sphingolipid metabolism in *Saccharomyces cerevisiae*. *Mol. Biol. Cell* 25, 196–211. doi: 10.1091/mbc.E13-06-0340

Tenreiro, S., Franssens, V., Winderickx, J., and Outeiro, T. F. (2017). Yeast models of Parkinson's disease-associated molecular pathologies. *Curr. Opin. Genet. Dev.* 44, 74–83. doi: 10.1016/j.gde.2017.01.013

Tenreiro, S., Munder, M. C., Alberti, S., and Outeiro, T. F. (2013). Harnessing the power of yeast to unravel the molecular basis of neurodegeneration. *J. Neurochem.* 127, 438–452. doi: 10.1111/jnc.12271

Thomas, R. S., Lelos, M. J., Good, M. A., and Kidd, E. J. (2011). Clathrin-mediated endocytic proteins are upregulated in the cortex of the Tg2576 mouse model of Alzheimer's disease-like amyloid pathology. *Biochem. Biophys. Res. Commun.* 415, 656–661. doi: 10.1016/j.bbrc.2011.10.131

Tong, A. H., Evangelista, M., Parsons, A. B., Xu, H., Bader, G. D., Page, N., et al. (2001). Systematic genetic analysis with ordered arrays of yeast deletion mutants. *Science* 294, 2364–2368. doi: 10.1126/science.1065810

Treusch, S., Hamamichi, S., Goodman, J. L., Matlack, K. E. S., Chung, C. Y., Baru, V., et al. (2011). Functional links between a toxicity, endocytic trafficking, and Alzheimer's disease risk factors in yeast. *Science* 334, 1241–1245. doi: 10.1126/science.1213210

Varadarajan, S., Bampton, E. T., Smalley, J. L., Tanaka, K., Caves, R. E., Butterworth, M., et al. (2012). A novel cellular stress response characterised by a rapid reorganisation of membranes of the endoplasmic reticulum. *Cell Death Differ.* 19, 1896–1907. doi: 10.1038/cdd.2012.108

Varadarajan, S., Tanaka, K., Smalley, J. L., Bampton, E. T., Pellecchia, M., Dinsdale, D., et al. (2013). Endoplasmic reticulum membrane reorganization is regulated by ionic homeostasis. *PLoS One* 8:e56603. doi: 10.1371/journal.pone.0056603

Verduyckt, M., Vignaud, H., Bynens, T., Van den Brande, J., Franssens, V., Cullin, C., et al. (2016). Yeast as a model for Alzheimer's disease: latest studies and advanced strategies. *Methods Mol. Biol.* 1303, 197–215. doi: 10.1007/978-1-4939-2627-5_11

Vevea, J. D., Garcia, E. J., Chan, R. B., Zhou, B., Schultz, M., Di Paolo, G., et al. (2015). Role for lipid droplet biogenesis and microlipophagy in adaptation to lipid imbalance in yeast. *Dev. Cell* 35, 584–599. doi: 10.1016/j.devcel.2015.11.010

Vicente Miranda, H., Gomes, M. A., Branco-Santos, J., Breda, C., Lázaro, D. F., Lopes, L. V., et al. (2016). Glycation potentiates neurodegeneration in models of Huntington's disease. *Sci. Rep.* 6:36798. doi: 10.1038/srep36798

Vignaud, H., Bobo, C., Lascu, I., Sörgjerd, K. M., Zako, T., Maeda, M., et al. (2013). A structure-toxicity study of Aß42 reveals a new anti-parallel aggregation pathway. *PLoS One* 8:e80262. doi: 10.1371/journal.pone.0080262

Viola, K. L., and Klein, W. L. (2015). Amyloid β oligomers in Alzheimer's disease pathogenesis, treatment, and diagnosis. *Acta Neuropathol.* 129, 183–206. doi: 10.1007/s00401-015-1386-3

Wang, D., Yuen, E. Y., Zhou, Y., Yan, Z., and Xiang, Y. K. (2011). Amyloid beta peptide-(1-42) induces internalization and degradation of beta2 adrenergic receptors in prefrontal cortical neurons. *J. Biol. Chem.* 286, 31852–31863. doi: 10.1074/jbc.M111.244335

Wang, H., Ma, J., Tan, Y., Wang, Z., Sheng, C., Chen, S., et al. (2010). Amyloid-β1-42 induces reactive oxygen species-mediated autophagic cell death in U87 and SH-SY5Y Cells. *J. Alzheimer's Dis.* 21, 597–610. doi: 10.3233/JAD-2010-091207

Willen, K., Edgar, J. R., Hasegawa, T., Tanaka, N., Futter, C. E., and Gouras, G. K. (2017). Abeta accumulation causes MVB enlargement and is modelled by dominant negative VPS4A. *Mol. Neurodegener.* 12:61. doi: 10.1186/s13024-017-0203-y

Winderickx, J., Delay, C., De Vos, A., Klinger, H., Pellens, K., Vanhelmont, T., et al. (2008). Protein folding diseases and neurodegeneration: lessons learned from yeast. *Biochim. Biophys. Acta* 1783, 1381–1395. doi: 10.1016/j.bbamcr.2008.01.020

Xiang, Y., Lam, S. M., and Shui, G. (2015). What can lipidomics tell us about the pathogenesis of Alzheimer disease? *Biol. Chem.* 396, 1281–1291. doi: 10.1515/hsz-2015-0207

Xu, W., Fang, F., Ding, J., and Wu, C. (2018). Dysregulation of Rab5-mediated endocytic pathways in Alzheimer's disease. *Traffic* 19, 253–262. doi: 10.1111/tra.12547

Yamazaki, Y., Takahashi, T., Hiji, M., Kurashige, T., Izumi, Y., Yamawaki, T., et al. (2010). Immunopositivity for ESCRT-III subunit CHMP2B in granulovacuolar degeneration of neurons in the Alzheimer's disease hippocampus. *Neurosci. Lett.* 477, 86–90. doi: 10.1016/j.neulet.2010.04.038

Yang, D. S., Stavrides, P., Saito, M., Kumar, A., Rodriguez-Navarro, J. A., Pawlik, M., et al. (2014). Defective macroautophagic turnover of brain lipids in the TgCRND8 Alzheimer mouse model: prevention by correcting lysosomal proteolytic deficits. *Brain* 137(Pt 12), 3300–3318. doi: 10.1093/brain/awu278

Zabrocki, P., Pellens, K., Vanhelmont, T., Vandebroek, T., Griffioen, G., Wera, S., et al. (2005). Characterization of alpha-synuclein aggregation and synergistic toxicity with protein tau in yeast. *FEBS J.* 272, 1386–1400. doi: 10.1111/j.1742-4658.2005.04571.x

Conflict of Interest Statement: The authors declare that the research was conducted in the absence of any commercial or financial relationships that could be construed as a potential conflict of interest.

frontiers in Molecular Neuroscience

REVIEW
published: 11 December 2018
doi: 10.3389/fnmol.2018.00453

Yeast Models of Prion-Like Proteins That Cause Amyotrophic Lateral Sclerosis Reveal Pathogenic Mechanisms

*Zachary T. Monahan, Shannon N. Rhoads, Debra S. Yee and Frank P. Shewmaker**

Department of Pharmacology and Molecular Therapeutics, Uniformed Services University, Bethesda, MD, United States

Many proteins involved in the pathogenic mechanisms of amyotrophic lateral sclerosis (ALS) are remarkably similar to proteins that form prions in the yeast *Saccharomyces cerevisiae*. These ALS-associated proteins are not orthologs of yeast prion proteins, but are similar in having long, intrinsically disordered domains that are rich in hydrophilic amino acids. These so-called prion-like domains are particularly aggregation-prone and are hypothesized to participate in the mislocalization and misfolding processes that occur in the motor neurons of ALS patients. Methods developed for characterizing yeast prions have been adapted to studying ALS-linked proteins containing prion-like domains. These yeast models have yielded major discoveries, including identification of new ALS genetic risk factors, new ALS-causing gene mutations and insights into how disease mutations enhance protein aggregation.

Keywords: prion, FUS, TAF15, HNRNPA2B1, EWSR1, TDP-43, amyloid, ALS

OPEN ACCESS

Edited by:
Stephen Moss,
Tufts University School of Medicine, United States

Reviewed by:
Michela Ferrucci,
University of Pisa, Italy
Martin Lothar Duennwald,
University of Western Ontario, Canada

****Correspondence:***
Frank P. Shewmaker
frank.shewmaker@usuhs.edu

Received: *03 August 2018*
Accepted: *23 November 2018*
Published: *11 December 2018*

Citation:
Monahan ZT, Rhoads SN, Yee DS and Shewmaker FP (2018) Yeast Models of Prion-Like Proteins That Cause Amyotrophic Lateral Sclerosis Reveal Pathogenic Mechanisms. Front. Mol. Neurosci. 11:453. doi: 10.3389/fnmol.2018.00453

INTRODUCTION

Neurodegenerative diseases are defined by irreversible loss of neurons. Clinically, these diseases manifest as dementias and movement disorders, depending on the subset of neurons that are principally affected. As a whole, the cost of neurodegenerative diseases is staggering. According to the Alzheimer's Association, in 2018, the total expense of treating dementias in the United States was approximately $277 billion. Unlike cancer and viral diseases, which have seen astonishing advances in treatments, no drugs have been developed that reverse or stop progression of neurodegenerative disease. To develop effective treatments, there is need to better understand the fundamental causes of these diseases and develop tractable models for genetic and pharmacological screening.

Amyotrophic lateral sclerosis (ALS) is a neurodegenerative disease that affects upper and lower motor neurons. It primarily manifests as a movement disorder, but it has many clinical and pathological features that overlap with frontotemporal dementia (FTD), which primarily manifests as a dementia. A surprising development in recent years is that diseased neurons from ALS and FTD patients frequently feature the accumulation of specific proteins that resemble yeast prion proteins. The intersection of yeast prions and human disease-associated proteins has led to novel experimental systems using tractable yeast models.

Prions

A common theme among nearly all neurodegenerative diseases is an apparent loss of normal protein quality control, resulting in the accumulation of disease-specific proteins into large

aggregates. Increasingly, a prion-like mechanism is being recognized as potentially underlying this protein aggregation (Polymenidou and Cleveland, 2011). The term "prion" means infectious protein (**Table 1**). However, infectivity does not necessarily result from the protein itself, but from its folded tertiary and quaternary structure. Mechanistically, a prion protein adopts a multimeric, highly-ordered conformation, which can then propagate through healthy cells and tissue by causing similar proteins to adopt the pathological form. This is distinct from protein misfolding into amorphous aggregates within isolated cells because prion propagation is a molecular pathological process that can spread. The accumulation of various proteins into large aggregates are hypothesized to cause neuronal degeneration by causing loss of the proteins' normal functions, as well as causing gain-of-function toxic properties.

For years, infectious forms of the mammalian prion protein, or PrP, were the only protein-only agents thought to be responsible for a human disease (Prusiner, 2013). Collectively, these diseases are known as the transmissible spongiform encephalopathies. The idea that a protein could itself be an infectious agent was initially controversial. However, the protein-only model of infectivity gained significant support from experiments demonstrating the ability to generate infectious prions *in vitro*. Castilla et al. (2005) generated infectious PrP using an *in vitro* amplification protocol from infected brain material. Later work strengthened the protein-only infectivity model by producing prions from bacteria-derived recombinant PrP (Wang et al., 2010; Deleault et al., 2012).

The discovery that the yeast *Saccharomyces cerevisiae*—one of the most widely used eukaryotic model systems—harbored naturally occurring prions completely unrelated to PrP significantly increased the acceptance of the prion hypothesis (Wickner, 1994). In the years since discovery of the first yeast prions (e.g., Rnq1p, Sup35p, Ure2p), dozens of yeast proteins have been proposed to have "prion properties," which broadly means the proteins can stably (but reversibly) exist within a cell population in one of two forms: (1) a soluble and functional form; or (2) a dysfunctional and high-molecular-weight aggregated form, concentrated mostly within discrete, insoluble, punctate ultrastructures. For example, an isogenic yeast strain might be cultured as two distinct populations. In one population a specific prion protein is aggregated within all cells, while in the other population the protein is soluble in all cells. Unlike PrP, yeast prions are generally tolerated by host cells, causing only mild phenotypic effects, which make them tractable experimental models for studying the prion phenomenon. The phenotypes resulting from yeast prions are generally associated with diminished function of the specific prion protein because it is accumulated into aggregates.

Amyloid and Prion Domains

The ability of yeast prion proteins to adopt an alternative, aggregated state is a result of their ability to fold into a multimeric structural motif known as amyloid (**Table 1**). Amyloid is a filamentous protein homopolymer of indefinite length in which the protein subunits stack linearly to form beta sheets that run the length of the polymer. Individual beta strands run perpendicular to the filament's long axis. The amyloid formed *in vitro* by purified recombinantly produced yeast prion proteins is infectious to yeast, thus proving the amyloid/protein-only model of yeast prions (King and Diaz-Avalos, 2004; Tanaka et al., 2004; Brachmann et al., 2005; Patel and Liebman, 2007).

Importantly, amyloid is a well-ordered, folded state, conceptually like a one-dimensional crystal. The significance of this architecture is it tends to be relatively stable, thus resistant to treatments that might normally unfold or solubilize protein aggregates, and it provides a mechanism for self-propagation. The ends of the filaments serve as templates for the autocatalytic conversion of additional protein into the amyloid conformation. The breaking of filaments provides new sites for protein recruitment. Moreover, amyloid filaments of short length (or oligomeric amyloid) can remain relatively soluble and be passed to progeny yeast cells. In fact, for several neurodegenerative diseases, smaller oligomeric assemblies, which are pre-amyloid or amyloid-like, may in fact be the more cytotoxic and infectious species (Espargaró et al., 2016).

In the case of disease, the concern with amyloid is that it has the potential to cause runaway aggregation of a specific protein, while resisting the cellular mechanisms dedicated to clearing misfolded proteins. Also, as with crystal structures, a single protein can adopt multiple slightly different amyloid conformations that differ at the atomic level, and perhaps,

TABLE 1 | Concepts linking yeast prions and subtypes of amyotrophic lateral sclerosis (ALS) and frontotemporal dementia (FTD).

Amyloid	A structurally ordered filamentous aggregate consisting of a single protein in a polymeric arrangement; each end of the filament serves as template for the addition of more protein, providing a molecular mechanism for runaway aggregation. Several ALS-linked proteins can form amyloid with atypical dye-binding properties.
Neuronal cytoplasmic inclusions (NCIs)	Large pathological protein aggregates that commonly form in neurons afflicted by various neurodegenerative diseases. Different diseases frequently have a unique subset of proteins within NCIs. Similar inclusions are observed in yeast cells harboring specific prion proteins.
Prion	An infectious protein. Canonically, a prion protein adopts an alternative structural fold that causes similar protein molecules to adopt the same structure (e.g., amyloid). Most characterized prion proteins are found in fungi, particularly *Saccharomyces cerevisiae*.
Prion domain	The distinct segments of yeast proteins that enable prion formation. These domains are distinguished by their "low-complexity," consisting predominately of hydrophilic, but not charged or hydrophobic, amino acids.
Prion-like domain	Segments found in many mammalian proteins, especially proteins with RNA-related functions, which have sequence composition very similar to yeast prion domains. They are disproportionately present in proteins that aggregate in neurodegenerative diseases.

disease presentation. These are called variants, or strains, and can differ in their biological effects (Prusiner, 1998; Diaz-Avalos et al., 2005). It is important to note that there could be other higher-order filamentous pathogenic structures that differ from canonical amyloid but are likewise able to propagate through template-driven growth.

Most yeast prion proteins assemble into amyloid via their aptly named "prion domains." These are lengthy, intrinsically disordered regions composed disproportionately of just a few amino acids (i.e., low-complexity). They are distinguished by an abundance of polar residues and a paucity of hydrophobic and charged residues (Toombs et al., 2010). Their removal from a prion protein eliminates its ability to be a prion. Numerous human proteins have segments that highly resemble yeast prion domains; they are generally called "prion-like" because it is unknown if they have any prion-facilitating properties *in vivo* (**Table 1**). In recent years, several human proteins with prion-like domains have been implicated in neurodegenerative diseases. Importantly, human prion-like proteins are extremely over-represented in genetic links to neurodegenerative disease (An and Harrison, 2016). Strikingly, many of these prion-like proteins are found in the large pathological aggregates of diseased neurons. In general, prion-like domains facilitate self-assembly into larger complexes and aggregates (March et al., 2016). For example, prion-like domains can be exchanged for true yeast prion domains with a retention of capacity for functional aggregation (Shelkovnikova et al., 2014). This has led to speculation that some of these proteins harboring prion-like domains may contribute to pathology via a mechanism similar to what is observed with naturally occurring yeast prions.

This emerging model suggests that autocatalytic protein propagation, the fundamental phenomenon of prion spread, potentially underlies a much broader collection of neurodegenerative diseases than just the previously described transmissible spongiform encephalopathies. The specific contribution of a prion mechanism to diseases like ALS, Parkinson's, Alzheimer's and chronic traumatic encephalopathy remains controversial, but there is ample evidence supporting the possibility. For example, aggregates of neurodegenerative disease-linked proteins can "infect" cell models causing endogenous proteins to aggregate (Furukawa et al., 2011; Karpowicz et al., 2017; Olsson et al., 2018). Likewise, ALS-linked proteins are capable of being transferred between cultured cells (Feiler et al., 2015; Feuillette et al., 2017). Likewise, the yeast protein Sup35 can propagate as a prion via horizontal transfer between cultured mammalian cells (Krammer et al., 2009; Liu et al., 2017). All of these observations suggest infectious protein aggregates might travel anatomical pathways and cause disease.

Why Use Yeast Models for Human Disease Proteins?

Approximately 6,000 human genes have yeast homologs; about 10% of which can be complemented by (or can complement) their yeast counterpart *in vivo* (Cherry et al., 2012). About 500 human disease genes have yeast orthologs (Kryndushkin and Shewmaker, 2011). The most straightforward approach to looking at human disease genes in yeast is in situations when the gene complements a yeast ortholog. This is the case for SOD1, in which human mutants can be quickly assayed for their ability to complement the yeast ortholog (Kryndushkin and Shewmaker, 2011). Unfortunately, most neurodegenerative disease-causing proteins do not have yeast orthologs, thus making their study more challenging. However, the methodology for studying the aggregation and propagation of yeast prion domains within genetically optimized yeast reporter strains has been refined for over two decades. These yeast models have proven efficient and inexpensive platforms for studying the potential prion-like properties of several neurodegenerative disease-linked proteins. The following sections summarize the modeling of specific ALS-associated prion-like proteins in yeast models.

EXAMPLES OF ALS-LINKED PROTEINS WITH PRION-LIKE DOMAINS MODELED IN YEAST

Many neurodegenerative disease-linked proteins have been modeled in yeast, including Parkinson's, Huntington's and Alzheimer's diseases (Braun, 2015). Likewise, there are yeast models for evaluating ALS-linked proteins, such as SOD1 and OPTN (Rabizadeh et al., 1995; Kryndushkin et al., 2012). However, yeast models of ALS-associated proteins with prion-like domains have proven particularly powerful because of their similarity to naturally occurring yeast prions. Prominent examples include the proteins fused-in-sarcoma (FUS), TAR DNA-binding protein-43 kDa (TDP-43kDa), heterogeneous nuclear ribonucleoprotein (hnRNPA2), TATA-box binding protein associated factor 15 (TAF15) and ewing sarcoma breakpoint region 1 (EWS; **Figure 1**), which are unified by remarkable similarities in architecture. Also, each is found post-mortem within neuronal cytoplasmic inclusions of subsets of patients with ALS or FTD. In cell models and yeast, these proteins (or their mutant forms) generally have dominant gain-of-function toxicity that is at least partially mediated by aggregation via their prion-like domains.

FUS

FUS is a ubiquitously expressed, predominantly nuclear animal protein originally named for its association to liposarcomas (Pérez-Losada et al., 2000). In the past decade, much research on FUS has focused on its relationship to ALS and FTD (Kwiatkowski et al., 2009; Vance et al., 2009). Mutations in FUS cause around 5% of all familial ALS cases, with disease phenotypes inherited in an autosomal dominant fashion (Shang and Huang, 2016). Yeast do not encode a FUS ortholog. Yeast models that ectopically express human FUS (or disease-causing mutants) reveal gain-of-function toxicity that is tightly associated with the degree to which FUS forms aggregates in the yeast cytoplasm (Kryndushkin et al., 2012; Monahan et al., 2017). Aggregation is dependent on the presence of FUS's prion-like domain; truncations lacking the domain are

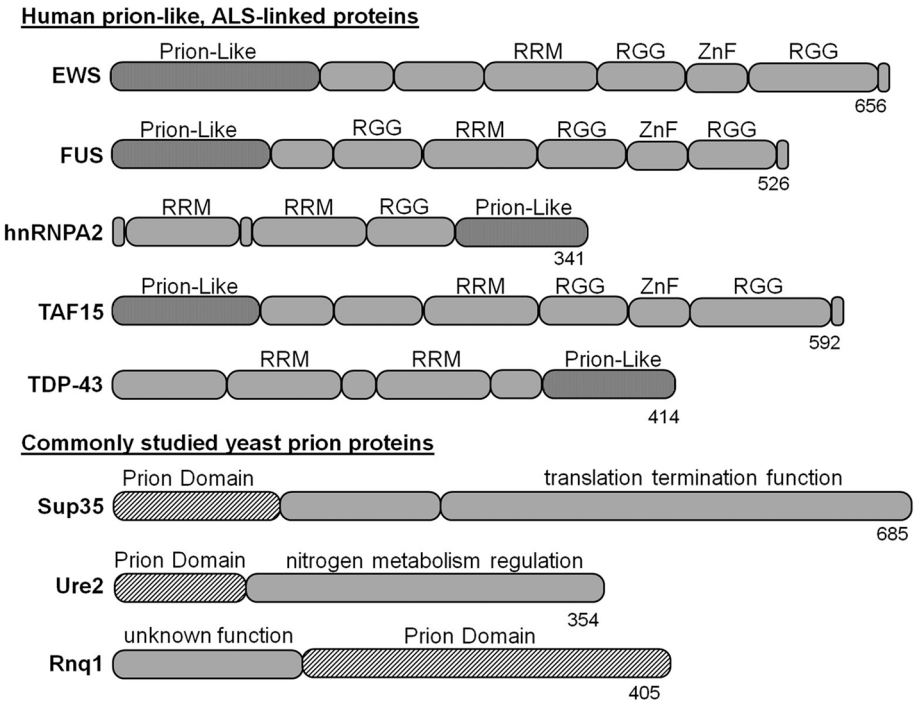

FIGURE 1 | Amyotrophic lateral sclerosis (ALS)-linked proteins with yeast prion-like domains have been modeled in yeast. The prion domains of naturally occurring yeast prion proteins have similar size and composition, but are not homologous to the prion-like domains of ALS-linked proteins. The tools for studying yeast prions have been applied to ectopic expression of human disease proteins to evaluate aggregation and toxicity mechanisms. RRM, RNA recognition motif; RGG, arginine-glycine-glycine rich domain; ZnF, zinc finger domain.

not toxic and remain relatively soluble in yeast cytoplasm (Ju et al., 2011; Kryndushkin et al., 2011; Sun et al., 2011). An important distinction between ectopic FUS and yeast prions like Sup35 is that FUS does not appear to exist as either soluble or aggregated (Kryndushkin et al., 2011), but instead appears to be sufficiently aggregation-prone in yeast cytoplasm that it always forms aggregates.

TDP-43

Like FUS, TDP-43 is an RNA-binding protein associated with several RNA-homeostatic functions. It is mostly localized within the nucleus, but is found in neuronal cytoplasmic inclusions of FTD and ALS patients (Neumann et al., 2006). Most ALS patients have TDP-43 pathology in spinal neurons despite having no mutations in the gene (Mackenzie et al., 2007); however, mutations in TDP-43 are also responsible for a small percentage of ALS (Sreedharan et al., 2008). TDP-43's propensity to aggregate and cause toxicity is well established in yeast models (Johnson et al., 2008; Braun et al., 2011). Yeast do not have a TDP-43 ortholog; ectopic expression of human TDP-43 indicates its carboxy-terminal prion-like domain is critical to both intracellular aggregation and toxicity (Johnson et al., 2008).

hnRNPA2

hnRNPs function in the processing, metabolism and transport of mRNA. Yeast have several proteins with similar functions and domain architecture as human hnRNPs. Two human paralogs have been linked to ALS: hnRNPA2/B1 and hnRNPA1 (Kim et al., 2013). hnRNPA2/B1 can be alternatively spliced into A2 or B1 isoforms; A2 is the major isoform. Recombinant forms of hnRNPA1 and hnRNPA2 form filamentous structures that can self-propagate *in vitro*, and hnRNPA2 has been found in neuronal cytoplasmic inclusions (Kim et al., 2013). hnRNPA2 has a carboxy-terminal prion-like domain that has been extensively modeled in yeast for its intrinsic aggregation propensity. In yeast, known disease-causing mutations enhance prion-like aggregation relative to wild-type protein (Paul et al., 2017; Cascarina et al., 2018).

TAF15

TAF15 is similar to FUS in both primary sequence and domain organization. Likewise, it possesses an amino-terminal prion-like domain. TAF15 is a member of the RNA polymerase II initiation complex, where it has a transcriptional regulatory role. Like FUS, there is no definitive yeast paralog of TAF15. Missense mutations in TAF15 are linked to a very small percentage of ALS patients (Couthouis et al., 2011). These mutations cause TAF15 to accumulate in the cytoplasm of neuronal models (Couthouis et al., 2011). Similarly, when human TAF15 is expressed ectopically in yeast it forms numerous cytoplasmic aggregates and causes mild cytotoxicity (Couthouis et al., 2011; Jackrel and Shorter, 2014).

EWSR1

The EWSR1 gene codes for EWS, a protein similar to both FUS and TAF15 in domain organization. Like FUS, it gets its name from being originally identified in connection to certain types of sarcoma. EWS contains an amino-terminal prion-like domain. Modeling in yeast by Couthouis et al. (2012) revealed EWS is aggregation-prone and toxic when over-expressed, albeit to a lesser extent than TDP-43 and FUS. They also found EWS accumulated in the cytoplasm of spinal cord neurons of patients with ALS. When they sequenced carboxy-terminal exons of EWSR1, two patient-specific mutations were identified that were absent from controls.

THE TOOLS DEVELOPED FOR YEAST PRIONS HAVE YIELDED HIGH-IMPACT DISCOVERIES ABOUT ALS-LINKED PRION-LIKE PROTEINS

Experimentation with yeast prion proteins has largely focused on their ability to stably exist in distinct biophysical states and how interaction with chaperones and other proteins affects their aggregation, propagation and toxicity. ALS-linked proteins in yeast do not generally appear to exist as completely un-aggregated, like true yeast prions can. However, there are interactions with similar sets of chaperones, such as Hsp104 and Hsp40s, which govern how both types of proteins aggregate. These same approaches are adaptable to the study of human prion-like proteins that cause ALS.

Evaluating the Aggregation and Toxicity Potential of Disease-Causing Mutations

Since FUS, TDP-43, hnRNPA2, TAF15 and EWS each form cytoplasmic aggregates when ectopically expressed in yeast—much like naturally occurring yeast prion proteins—it has been straightforward to monitor how specific ALS-linked mutations alter the proteins' intrinsic propensity to aggregate and exert toxicity, especially when coupled with *in vitro* aggregation assays.

FUS

Most ALS-causing mutations in FUS cluster in and near its carboxy-terminal nuclear localization signal (NLS; Dormann et al., 2010). In yeast models, FUS's NLS is insufficient to achieve dramatic nuclear localization (Ju et al., 2011). For this reason, wild-type human FUS can accumulate in the cytoplasm and cause toxicity. Using a yeast model, Sun et al. (2011) found that increasing the potency of FUS's NLS concomitantly reduced cytoplasmic aggregation and cytotoxicity, supporting the idea that increasing nuclear localization offers a therapeutic mechanism. Likewise, the R524S and P525L ALS mutations at the carboxy terminus caused FUS to have slightly greater cytotoxicity in a yeast model (Fushimi et al., 2011), perhaps due to further diminished nuclear localization. However, another study found ALS FUS mutations to not dramatically affect aggregation and toxicity in the yeast model (Sun et al., 2011). Such a negative result is potentially informative. In this case, it suggests that the toxic mechanism of FUS aggregates has at least a component of gain-of-cytoplasmic-function, and FUS-linked toxicity is unlikely to be explained entirely by loss of function elsewhere in the cell (Sharma et al., 2016).

TDP-43

Most ALS-linked mutations in TDP-43 are located in its prion-like domain (Da Cruz and Cleveland, 2011). Mutant TDP-43 tested in yeast revealed that many mutations simultaneously increased aggregation propensity and toxicity (Johnson et al., 2009). However, some mutations did not accelerate TDP-43 misfolding or enhance its toxicity in yeast, which suggests mutations do not necessarily have to alter aggregation propensity to exert pathogenic effects. TDP-43 aggregates were mildly detergent resistant, but did not have the same amyloid characteristics typical of yeast prions (Johnson et al., 2009).

hnRNPA2

Kim et al. (2013) discovered that a single amino acid substitution (D to V) in the prion-like domain of hnRNPA2 was genetically linked to multisystem proteinopathy, an ALS-related disorder. They substituted the core of this prion-like region into the prion-nucleating segment of the yeast prion protein Sup35 (known as [PSI^+] in the prion form; discussed more below). In this context, they found the D to V mutation dramatically and significantly increased prion formation propensity. Thus, not only could this mutated hnRNPA2 sequence promote Sup35's nucleation into a prion, the D to V mutation specifically facilitates prion-like aggregation.

In summary, yeast models reveal that ALS-causing mutations in prion-like proteins often increase the proteins' intrinsic propensity to form solid cytoplasmic aggregates and/or nucleate aggregation. The advantage to using yeast models is scores of mutations can be assayed rapidly before more expensive model systems are selected for further analysis. High throughput genomic sequencing has revealed numerous low-frequency polymorphisms in ALS-linked proteins, thus yeast could be helpful in determining if certain mutations actually contribute to disease.

Evaluating Effects of Post-translational Modifications on Aggregation and Toxicity

The prion-like domain of FUS is extensively phosphorylated in human cell models following various types of stress (Rhoads et al., 2018a,b). There are as many as 12 PIK kinase sites that are phosphorylated following DNA damage. The generation of phosphomimetic substitutions within FUS's prion-like domain have been used to model how phosphorylation could alter the behavior of FUS in a crowded cellular environment (Monahan et al., 2017). From 1 to 12 glutamate substitutions were introduced in place of the serine/threonine phosphorylation sites in the prion-like domain. These phosphomimetic substitutions caused a reduction in toxicity and aggregation in proportion to the

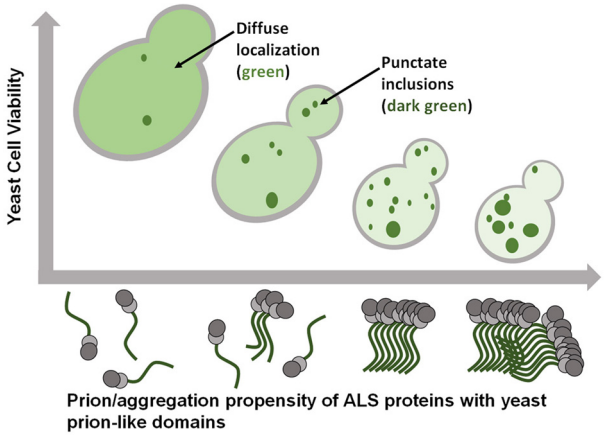

FIGURE 2 | ALS-linked proteins with prion-like domains exhibit gain-of-function toxicity that is tightly associated with the extent of their aggregation. Smaller, more soluble, oligomeric aggregates may be the most toxic species.

number of substitutions, without affecting FUS expression levels. Thus incremental reduction in FUS aggregation led to incremental reduction in FUS toxicity (**Figure 2**). The very precise relationship between these two parameters strongly suggests that FUS aggregation is in fact causally related to cytotoxicity. Additionally, these results are consistent with similar findings reported for both alpha-synuclein in yeast (Tenreiro et al., 2014) and TDP-43 in mammalian cell models (Li et al., 2011).

Excitingly, these results offer context for observations made in post-mortem human tissue interrogated with immunohistochemistry. One critical observation has been the hyperphosphorylated state of disease-associated protein inclusions in tissue from patients with neurodegeneration (Arai et al., 2010), leading to a prevailing model wherein phosphorylation promotes protein aggregation. The use of phosphomimetics in yeast models therefore suggests that the relationship between the phosphorylation and accumulation of pathological proteins may be more nuanced than previously appreciated. If FUS is forming an archetypal amyloid structure with in-register beta sheet, as determined in the lab of Robert Tycko (Murray et al., 2017) then charged groups in the prion-like domain should strongly inhibit amyloid formation.

Quantitative Mutagenesis to Score Prion Propensity of Human Disease Proteins

In recent years, several predictive algorithms (PAPAs) have been developed to identify proteins with yeast prion-like domains (Alberti et al., 2009; Ross et al., 2013; Lancaster et al., 2014). Largely based on their sequence composition, several 100 human proteins with potential prion capability have been identified. As a group, these proteins are very disproportionately linked to neurodegenerative disease (An and Harrison, 2016). FUS, TDP-43, hnRNPA2, TAF15 and EWS are all predicted to have prion-like behavior to various degrees. However, algorithms designed to identify large domains of particular composition may lack the resolution required to determine the effects of single amino acid substitutions.

Simple experiments that detect the yeast prion [PSI$^+$] (prion form of Sup35) can be harnessed to evaluate the nucleation potential of human prion-like proteins. Specifically, prion-like domain sequences are substituted for segments within the Sup35 prion domain (Alberti et al., 2009; **Figure 3**). These fusion proteins can be scored for their prion behavior using the same tools that were developed for characterizing [PSI$^+$], which have sufficient resolution for quantitative analysis of specific mutations. Similar to testing how disease-linked mutations can affect aggregation and toxicity of the full-length ALS proteins, site-directed mutagenesis of the fusion protein can be used to determine how any substitution may specifically affect prion-like protein behavior.

This approach has been extensively performed with hnRNPA1 and hnRNPA2 in the lab of Eric Ross (Cascarina et al., 2018). The intrinsic aggregation propensity of hnRNPA2 was predicted *in silico* and then quantified in a yeast model (Paul et al., 2017). The central region of mutant hnRNPA2's prion-like domain can support prion function of Sup35 when swapped with a segment of Sup35's prion domain (residues 3–40; **Figure 3**; Kim et al., 2013). This hnRNPA2-Sup35 fusion protein was used to quantify how specific amino acid changes affect the prion-like aggregation of hnRNPA2 (Paul et al., 2017). Using this reporter system in combination with a PAPA, Paul et al. (2017) were able to accurately predict the prion effect of nearly every amino acid substitution—disease causing or not—within hnRNPA2's core prion domain. Hydrophobic and aromatic residues promoted aggregation, while charged amino acids were inhibitory (Paul et al., 2017).

The hnRNPA2 yeast model also provided an important conceptual point: the hnRNPA2-Sup35 fusion proteins formed canonical prions, which means they could either remain soluble or form self-propagating amyloid (Cascarina et al., 2018).

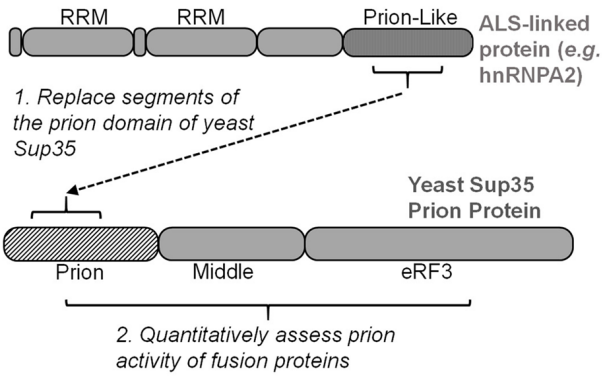

FIGURE 3 | Many yeast strains have been optimized for evaluating and scoring the yeast prion protein Sup35. Inserting segments of ALS-linked prion-like domains into Sup35's prion domain enable quantitative mutagenesis experiments to score prion propensity of amino acid mutations and substitutions. eRF3, eukaryotic release factor 3.

This supports the idea that these human prion-like proteins may similarly form pathological amyloid in diseased neurons. This could therefore explain why the previously mentioned hnRNPA2 D290V mutation causes disease; the loss of a charged residue in a critical amyloid-forming domain fails to inhibit amyloid formation. As new disease-linked mutations are discovered, *in silico* prediction can be coupled with rapid-throughput quantitative yeast prion models to predict amino acid effects on pathogenic aggregation.

Another discovery provided by yeast modeling is that effects of amino-acid substitutions within hnRNPA2's core prion-like domain can indirectly alter aggregation propensity. Cascarina and coworkers discovered that the Q/N content of the core prion-like domain had important effects on proteosome-dependent clearance. While the addition of aromatic amino acids to hnRNPA2's core prion-like domain directly increased aggregation propensity, adding Q/N increased prion formation and aggregation stochastically by inhibiting proteosome turnover (Cascarina et al., 2018).

High-Throughput Screens

Yeast models are powerful for screening because whole-genome libraries can be quickly and inexpensively screened and analyzed. For neurodegenerative disease yeast models, libraries have been screened for genes that alter the toxicity resulting from expression/aggregation of specific disease-causing proteins (Braun et al., 2010). Screens are generally performed with knock down or over-expression libraries to observe changes in protein-induced toxicity. Importantly, the mechanisms of toxicity are unique to the different disease-causing proteins (Figley and Gitler, 2013).

Two large-scale screens of genetic modifiers of FUS toxicity yielded a consistent set of DNA/RNA-binding proteins (Ju et al., 2011; Sun et al., 2011). This corroborates observations that interactions with RNA are integral to FUS-induced toxicity. A yeast RNA helicase, ECM32, was discovered in both screens to suppress FUS-induced toxicity (Daigle et al., 2013). Its human homolog, hUPF1, was likewise found to suppress FUS toxicity (Ju et al., 2011). The yeast homologs of human proteins FBXW7 and EIF4A1 were also identified as suppressors. When tested in human cell lines with ALS-mutant FUS, both FBXW7 and EIF4A1 ameliorated FUS-induced toxicity (Sun et al., 2011).

Yeast two-hybrid screens also continue to be powerful methods to identify and evaluate interacting human proteins. A two-hybrid screen in yeast revealed that FUS interacts with the arginine-methylating protein PRMT1 (Yamaguchi and Kitajo, 2012). Methylation of FUS by PRMTs has subsequently been shown to be critical to mediating FUS subcellular localization (Tradewell et al., 2012; Yamaguchi and Kitajo, 2012).

Genetic screening in the TDP-43 yeast model has led to major ALS discoveries. A yeast deletion library was used to identify the DBR1 gene as a modifier of TDP-43 toxicity (Armakola et al., 2012; Figley and Gitler, 2013). Deletion of yeast DBR1 suppressed TDP-43-induced toxicity. This observation was recapitulated in cell lines and primary neurons, where inhibiting human Dbr1 similarly reduced TDP-43 toxicity. Dbr1 linearizes circular RNA resulting from splicing of pre-mRNA. Accumulation of circular RNA sequesters TDP-43, reducing its accumulation into more toxic aggregates, thus providing a conceptual therapeutic strategy.

Screening of a yeast over-expression library in conjunction with TDP-43 cytotoxicity led to the discovery of major genetic risk factors for ALS (Daigle et al., 2013). Expression of yeast PBP1 was found to specifically enhance TDP-43 cytotoxicity (it did not enhance the toxicity of other neurodegenerative-related proteins). The Pbp1 protein is homologous to human ataxin 2 (ATXN2), which itself causes spinocerebellar ataxia when its polyglutamine tract is expanded from a typical length of ∼22 to >34. Immunohistochemical analysis of ALS patient spinal cord neurons revealed ATXN2 mislocalization. Sequencing of the ATXN2 gene in a large patient cohort revealed that intermediate polyglutamine expansion (∼27–33) was a risk factor in ∼5% of ALS cases. In subsequent studies, when ATXN2 levels were lowered in the central nervous system of a TDP-43-disease mouse model, survival was extended (Becker et al., 2017).

In addition to prion-like domains, many ALS-associated aggregation-prone proteins have RNA recognition motifs (RRMs). To determine if other RRM-containing proteins could be linked to disease, a yeast screen was performed with human RRM proteins (Couthouis et al., 2011). The aggregation and toxicity in yeast of 133 candidate proteins were evaluated, and then "hits" were further refined by bioinformatic sequence analysis of potential prion-like domains. TAF15 was found to aggregate, cause toxicity and have a prion-like domain that ranked highly according to prion-prediction algorithms. TAF15 was sequenced in ALS patients and several mutations were specific to patients and absent in control populations (Couthouis et al., 2011). Also, TAF15 was found to accumulate in the cytoplasm of spinal cord neurons of patients with sporadic ALS. Thus, screening in a yeast model enabled filtering a large pool of potential disease-associated proteins into the best candidates for more thorough analysis, which led to the discovery of a new ALS-linked protein.

Dissecting the Roles of Disaggregases and Chaperones in Suppressing Protein-Aggregate-Induced Cytotoxicity

Hsp104

Work in the lab of James Shorter has identified yeast Hsp104 as having great therapeutic potential against both FUS and TDP-43, as well as other aggregation-prone proteins. Hsp104 is an ATP-dependent hexametric chaperone that disaggregates native prion amyloid in yeast. Its function in yeast prion propagation is critical because it breaks prion amyloid into smaller pieces that get passed to progeny cells (Wegrzyn et al., 2001; Helsen and Glover, 2012). This breaking of amyloid could have therapeutic potential in cases where long-lived cells must rid themselves of terminal protein aggregates. However, mammalian cells mysteriously do not code an Hsp104 homolog, despite no observed problems resulting from Hsp104 ectopic expression in mammalian cell models. In yeast models, Hsp104 has little effect on the aggregation and toxicity of ALS-linked proteins (Jackrel and Shorter, 2015). However, engineered variants of Hsp104 are

capable of solubilizing FUS and TDP-43 aggregates and causing a concomitant reduction in cytotoxicity in yeast models (Jackrel et al., 2014; Tariq et al., 2018). This illustrates a case in which the yeast model system can be used to optimize new molecular technology for disaggregating amyloid-like inclusions.

An additional, subtler point emerges from these experiments. As Hsp104 is critical in disaggregating native yeast prions, the fact that it can also disaggregate ectopically expressed human proteins suggests that the aggregation of these proteins may be governed by prion-like biophysics.

Hsp40 Chaperones: Sis1 and DNAJB1

The yeast Hsp40 chaperone Sis1 interacts specifically with the amyloid forms of several yeast prions (Sondheimer et al., 2001; Higurashi et al., 2008). Work in the lab of Susan Liebman asked how Sis1 might similarly act upon aggregates formed by ALS-linked proteins. When over-expressed, the Sis1 suppresses proteotoxicity caused by both TDP-43 and FUS (Park et al., 2017, 2018). Importantly, this observation translated to mammalian cell models and primary cortical neurons, where increased expression of the human ortholog of Sis1, DNAJB1, could ameliorate TDP-43- and FUS-mediated toxicity (Park et al., 2017). This indicates DNAJB1 could be a therapeutic target of ALS subtypes. Human DNAJB1 can also alter yeast prions when expressed ectopically (Stein et al., 2014), thus yeast strains that are optimized for studying prions can also be used to study human chaperones linked to disease.

Cross Seeding With Heterologous Amyloid

The nucleation of nearly all yeast prion proteins into self-propagating aggregates is influenced by the endogenous yeast prion [PIN$^+$] (also known as [RNQ$^+$]). The [PIN$^+$] prion forms cytoplasmic amyloid that can nucleate the aggregation of heterologous proteins, particularly amyloid-forming prion proteins and polyglutamine expansions. Park and coworkers found that [PIN$^+$] slightly enhances TDP-43 and FUS toxicity in yeast models (Park et al., 2017, 2018). These observations are consistent with TDP-43 and FUS having prion-like properties because it is hypothesized that amyloid structures have some potential to cross-template similar proteins into amyloid conformations. However, there was no evidence that FUS and TDP-43 strongly co-aggregated with the [PIN+] prion. Also, FUS and TDP-43 aggregates were not as resistant as prion proteins to detergent, which would suggest they are not in prion-like amyloid conformations.

The question remains about what conformations these ALS-linked prion-like proteins are forming when aggregated in diseased neurons. *In vitro*, the large aggregates formed by these proteins are described as "amyloid-like," which indicates they appear to form fibrous solid aggregates with mild detergent-resistance and weak or no Thioflavin T reactivity (Johnson et al., 2008; Fushimi et al., 2011). Thioflavin T binding and fluorescence are frequently used to characterize amyloid, so in the absence of a strong Thioflavin T fluorescence, aggregates may be dismissed as non-amyloid. However, there is no molecular explanation that would require this to always be true. For example, recombinant FUS prion-like domain forms archetypal amyloid fibers with cross-beta structure, but are not Thioflavin T responsive (Murray et al., 2017). This indicates that the ALS-linked proteins may be forming a type of amyloid that does not react strongly with Thioflavin T.

LIMITATIONS OF YEAST MODELS

There are limitations to yeast models. What is true for yeast prion domains is not necessarily true for human prion-like domains, so conclusions must be made carefully. For example, it has been hypothesized that prion formation in yeast is naturally beneficial (True et al., 2004; Halfmann et al., 2012), which is not hypothesized for the human ALS proteins with prion-like domains. In fact, nearly all mammalian prion-like proteins are novel since the last common ancestor with yeast (An and Harrison, 2016). This means the similarity in amino-acid composition is a result of convergence, not because the precise properties of yeast prion domains have been conserved through evolutionary time. The differences and similarities between prion and prion-like domains is an ongoing topic of research.

An additional limitation of yeast models is different sets of resident interacting proteins compared to mammalian cells. This is especially important in regards to quality-control proteins like chaperons. Yeast chaperones are integral to propagation of endogenous yeast prions (Masison and Reidy, 2015), but their interactions with ectopically expressed human prion-like proteins is artificial, so may not be informative to human disease. However, as mentioned above, the absence of human protein-quality-control factors can be an advantage; pairing human chaperones with human disease proteins in yeast can be used to evaluate chaperone-mediated changes to aggregation and toxicity. Numerous examples of human chaperones reducing human disease protein gain-of-function toxicity in yeast have been published (De Graeve et al., 2013; Kumar et al., 2018; Park et al., 2018).

CONCLUDING REMARKS

Yeast models have seen widespread adoption for modeling human neurodegenerative diseases like ALS because they are easily manipulated and recapitulate the major properties of more complex eukaryotic cells. Specifically, these yeast models offer insights into the precise relationship between gain-of-function toxicity and protein aggregation. While they do not recapitulate the numerous mechanisms by which neuronal networks may degenerate, yeast models have proven effective in discovering proteins linked to ALS and FTD. Yeast models of prion-like neurodegenerative disease-linked proteins offer a strategy to inexpensively inform subsequent experiments in higher model systems in the goal of ultimately developing therapeutics.

AUTHOR CONTRIBUTIONS

ZM and FS conceived the outline. ZM, SR, DY and FS wrote the article.

FUNDING

This work was supported by the National Institute of General Medical Sciences (NIGMS) of the National Institutes of Health (NIH) under Award Numbers R35GM119790 (Principal investigator—FS) and R01GM118530 (Principal investigator—Nick Fawzi).

REFERENCES

Alberti, S., Halfmann, R., King, O., Kapila, A., and Lindquist, S. (2009). A systematic survey identifies prions and illuminates sequence features of prionogenic proteins. *Cell* 137, 146–158. doi: 10.1016/j.cell.2009.02.044

An, L., and Harrison, P. M. (2016). The evolutionary scope and neurological disease linkage of yeast-prion-like proteins in humans. *Biol. Direct* 11:32. doi: 10.1186/s13062-016-0134-5

Arai, T., Hasegawa, M., Nonoka, T., Kametani, F., Yamashita, M., Hosokawa, M., et al. (2010). Phosphorylated and cleaved TDP-43 in ALS, FTLD and other neurodegenerative disorders and in cellular models of TDP-43 proteinopathy. *Neuropathology* 30, 170–181. doi: 10.1111/j.1440-1789.2009.01089.x

Armakola, M., Higgins, M. J., Figley, M. D., Barmada, S. J., Scarborough, E. A., Diaz, Z., et al. (2012). Inhibition of RNA lariat debranching enzyme suppresses TDP-43 toxicity in ALS disease models. *Nat. Genet.* 44, 1302–1309. doi: 10.3410/f.717962724.793464692

Becker, L. A., Huang, B., Bieri, G., Ma, R., Knowles, D. A., Jafar-Nejad, P., et al. (2017). Therapeutic reduction of ataxin-2 extends lifespan and reduces pathology in TDP-43 mice. *Nature* 544, 367–371. doi: 10.1038/nature22038

Brachmann, A., Baxa, U., and Wickner, R. B. (2005). Prion generation *in vitro*: amyloid of Ure2p is infectious. *EMBO J.* 24, 3082–3092. doi: 10.1038/sj.emboj.7600772

Braun, R. J. (2015). Ubiquitin-dependent proteolysis in yeast cells expressing neurotoxic proteins. *Front. Mol. Neurosci.* 8:8. doi: 10.3389/fnmol.2015.00008

Braun, R. J., Buttner, S., Ring, J., Kroemer, G., and Madeo, F. (2010). Nervous yeast: modeling neurotoxic cell death. *Trends Biochem. Sci.* 35, 135–144. doi: 10.1016/j.tibs.2009.10.005

Braun, R. J., Sommer, C., Carmona-Gutierrez, D., Khoury, C. M., Ring, J., Büttner, S., et al. (2011). Neurotoxic 43-kDa TAR DNA-binding protein (TDP-43) triggers mitochondrion-dependent programmed cell death in yeast. *J Biol. Chem.* 286, 19958–19972. doi: 10.1074/jbc.m110.194852

Cascarina, S. M., Paul, K. R., Machihara, S., and Ross, E. D. (2018). Sequence features governing aggregation or degradation of prion-like proteins. *PLoS Genet.* 14:e1007517. doi: 10.1371/journal.pgen.1007517

Castilla, J., Saá, P., Hetz, C., and Soto, C. (2005). *In vitro* generation of infectious scrapie prions. *Cell* 121, 195–206. doi: 10.1016/j.cell.2005.02.011

Cherry, J. M., Hong, E. L., Amundsen, C., Balakrishnan, R., Binkley, G., Chan, E. T., et al. (2012). Saccharomyces genome database: the genomics resource of budding yeast. *Nucleic. Acids Res.* 40, D700–D705. doi: 10.1093/nar/gkr1029

Couthouis, J., Hart, M. P., Erion, R., King, O. D., Diaz, Z., Nakaya, T., et al. (2012). Evaluating the role of the FUS/TLS-related gene EWSR1 in amyotrophic lateral sclerosis. *Hum. Mol. Genet.* 21, 2899–2911. doi: 10.1093/hmg/dds116

Couthouis, J., Hart, M. P., Shorter, J., DeJesus-Hernandez, M., Erion, R., Oristano, R., et al. (2011). A yeast functional screen predicts new candidate ALS disease genes. *Proc. Natl. Acad. Sci. U S A* 108, 20881–20890. doi: 10.1073/pnas.1109434108

Da Cruz, S., and Cleveland, D. W. (2011). Understanding the role of TDP-43 and FUS/TLS in ALS and beyond. *Curr. Opin. Neurobiol.* 21, 904–919. doi: 10.1016/j.conb.2011.05.029

Daigle, J. G., Lanson, N. A., Smith, R. B., Casci, I., Maltare, A., Monaghan, J., et al. (2013). RNA-binding ability of FUS regulates neurodegeneration, cytoplasmic mislocalization and incorporation into stress granules associated with FUS carrying ALS-linked mutations. *Hum. Mol. Genet.* 22, 1193–1205. doi: 10.1093/hmg/dds526

De Graeve, S., Marinelli, S., Stolz, F., Hendrix, J., Vandamme, J., Engelborghs, Y., et al. (2013). Mammalian ribosomal and chaperone protein RPS3A counteracts α-synuclein aggregation and toxicity in a yeast model system. *Biochem. J.* 455, 295–306. doi: 10.1042/bj20130417

Deleault, N. R., Piro, J. R., Walsh, D. J., Wang, F., Ma, J., Geoghegan, J. C., et al. (2012). Isolation of phosphatidylethanolamine as a solitary cofactor for prion formation in the absence of nucleic acids. *Proc. Natl. Acad. Sci. U S A* 109, 8546–8551. doi: 10.1073/pnas.1204498109

Diaz-Avalos, R., King, C. Y., Wall, J., Simon, M., and Caspar, D. L. (2005). Strain-specific morphologies of yeast prion amyloid fibrils. *Proc. Natl. Acad. Sci. U S A* 102, 10165–10170. doi: 10.1073/pnas.0504599102

Dormann, D., Rodde, R., Edbauer, D., Bentmann, E., Fischer, I., Hruscha, A., et al. (2010). ALS-associated fused in sarcoma (FUS) mutations disrupt Transportin-mediated nuclear import. *EMBO J.* 29, 2841–2857. doi: 10.1038/emboj.2010.143

Espargaró, A., Busquets, M. A., Estelrich, J., and Sabate, R. (2016). Key points concerning amyloid infectivity and prion-like neuronal invasion. *Front. Mol. Neurosci.* 9:29. doi: 10.3389/fnmol.2016.00029

Feiler, M. S., Strobel, B., Freischmidt, A., Helferich, A. M., Kappel, J., Brewer, B. M., et al. (2015). TDP-43 is intercellularly transmitted across axon terminals. *J. Cell Biol.* 211, 897–911. doi: 10.1083/jcb.201504057

Feuillette, S., Delarue, M., Riou, G., Gaffuri, A. L., Wu, J., Lenkei, Z., et al. (2017). Neuron-to-neuron transfer of fus in *Drosophila* primary neuronal culture is enhanced by ALS-associated mutations. *J. Mol. Neurosci.* 62, 114–122. doi: 10.1007/s12031-017-0908-y

Figley, M. D., and Gitler, A. D. (2013). Yeast genetic screen reveals novel therapeutic strategy for ALS. *Rare Dis.* 1:e24420. doi: 10.4161/rdis.24420

Furukawa, Y., Kaneko, K., Watanabe, S., Yamanaka, K., and Nukina, N. (2011). A seeding reaction recapitulates intracellular formation of Sarkosyl-insoluble transactivation response element (TAR) DNA-binding protein-43 inclusions. *J. Biol. Chem.* 286, 18664–18672. doi: 10.1074/jbc.p111.231209

Fushimi, K., Long, C., Jayaram, N., Chen, X., Li, L., and Wu, J. Y. (2011). Expression of human FUS/TLS in yeast leads to protein aggregation and cytotoxicity, recapitulating key features of FUS proteinopathy. *Protein Cell* 2, 141–149. doi: 10.1007/s13238-011-1014-5

Halfmann, R., Jarosz, D. F., Jones, S. K., Chang, A., Lancaster, A. K., and Lindquist, S. (2012). Prions are a common mechanism for phenotypic inheritance in wild yeasts. *Nature* 482, 363–368. doi: 10.1038/nature10875

Helsen, C. W., and Glover, J. R. (2012). A new perspective on Hsp104-mediated propagation and curing of the yeast prion [PSI^{+}]. *Prion* 6, 234–239. doi: 10.4161/pri.19913

Higurashi, T., Hines, J. K., Sahi, C., Aron, R., and Craig, E. A. (2008). Specificity of the J-protein Sis1 in the propagation of 3 yeast prions. *Proc. Natl. Acad. Sci. U S A* 105, 16596–16601. doi: 10.1073/pnas.0808934105

Jackrel, M. E., DeSantis, M. E., Martinez, B. A., Castellano, L. M., Stewart, R. M., Caldwell, K. A., et al. (2014). Potentiated Hsp104 variants antagonize diverse proteotoxic misfolding events. *Cell* 156, 170–182. doi: 10.1016/j.cell.2013.11.047

Jackrel, M. E., and Shorter, J. (2014). Potentiated Hsp104 variants suppress toxicity of diverse neurodegenerative disease-linked proteins. *Dis. Model Mech.* 7, 1175–1184. doi: 10.1242/dmm.016113

Jackrel, M. E., and Shorter, J. (2015). Engineering enhanced protein disaggregases for neurodegenerative disease. *Prion* 9, 90–109. doi: 10.1080/19336896.2015.1020277

Johnson, B. S., McCaffery, J. M., Lindquist, S., and Gitler, A. D. (2008). A yeast TDP-43 proteinopathy model: Exploring the molecular determinants of TDP-43 aggregation and cellular toxicity. *Proc. Natl. Acad. Sci. U S A* 105, 6439–6444. doi: 10.1073/pnas.0802082105

Johnson, B. S., Snead, D., Lee, J. J., McCaffery, J. M., Shorter, J., and Gitler, A. D. (2009). TDP-43 is intrinsically aggregation-prone and amyotrophic lateral sclerosis-linked mutations accelerate aggregation and increase toxicity. *J Biol. Chem.* 284, 20329–20339. doi: 10.1074/jbc.a109.010264

Ju, S., Tardiff, D. F., Han, H., Divya, K., Zhong, Q., Maquat, L. E., et al. (2011). A yeast model of FUS/TLS-dependent cytotoxicity. *PLoS Biol.* 9:e1001052. doi: 10.1371/journal.pbio.1001052

Karpowicz, R. J., Haney, C. M., Mihaila, T. S., Sandler, R. M., Petersson, E. J., and Lee, V. M. (2017). Selective imaging of internalized proteopathic α-synuclein

seeds in primary neurons reveals mechanistic insight into transmission of synucleinopathies. *J. Biol. Chem.* 292, 13482–13497. doi: 10.1074/jbc.m117.780296

Kim, H. J., Kim, N. C., Wang, Y. D., Scarborough, E. A., Moore, J., Diaz, Z., et al. (2013). Mutations in prion-like domains in hnRNPA2B1 and hnRNPA1 cause multisystem proteinopathy and ALS. *Nature* 495, 467–473. doi: 10.1038/nature11922

King, C. Y., and Diaz-Avalos, R. (2004). Protein-only transmission of three yeast prion strains. *Nature* 428, 319–323. doi: 10.1038/nature02391

Krammer, C., Kryndushkin, D., Suhre, M. H., Kremmer, E., Hofmann, A., Pfeifer, A., et al. (2009). The yeast Sup35NM domain propagates as a prion in mammalian cells. *Proc. Natl. Acad. Sci. U S A* 106, 462–467. doi: 10.1073/pnas.0811571106

Kryndushkin, D., Ihrke, G., Piermartiri, T. C., and Shewmaker, F. (2012). A yeast model of optineurin proteinopathy reveals a unique aggregation pattern associated with cellular toxicity. *Mol. Microbiol.* 86, 1531–1547. doi: 10.1111/mmi.12075

Kryndushkin, D., and Shewmaker, F. (2011). Modeling ALS and FTLD proteinopathies in yeast: An efficient approach for studying protein aggregation and toxicity. *Prion* 5, 250–257. doi: 10.4161/pri.5.4.17229

Kryndushkin, D., Wickner, R. B., and Shewmaker, F. (2011). FUS/TLS forms cytoplasmic aggregates, inhibits cell growth and interacts with TDP-43 in a yeast model of amyotrophic lateral sclerosis. *Protein Cell* 2, 223–236. doi: 10.1007/s13238-011-1525-0

Kumar, J., Kline, N. L., and Masison, D. C. (2018). Human DnaJB6 anti-amyloid chaperone protects yeast from polyglutamine toxicity separately from spatial segregation of aggregates. *Mol. Cell Biol.* 38, e00437–e00518. doi: 10.1128/mcb.00437-18

Kwiatkowski, T. J., Bosco, D. A., Leclerc, A. L., Tamrazian, E., Vanderburg, C. R., Russ, C., et al. (2009). Mutations in the FUS/TLS gene on chromosome 16 cause familial amyotrophic lateral sclerosis. *Science* 323, 1205–1208. doi: 10.1126/science.1166066

Lancaster, A. K., Nutter-Upham, A., Lindquist, S., and King, O. D. (2014). PLAAC: a web and command-line application to identify proteins with prion-like amino acid composition. *Bioinformatics* 30, 2501–2502. doi: 10.1093/bioinformatics/btu310

Li, H. Y., Yeh, P. A., Chiu, H. C., Tang, C. Y., and Tu, B. P. (2011). Hyperphosphorylation as a defense mechanism to reduce TDP-43 aggregation. *PLoS One* 6:e23075. doi: 10.1371/journal.pone.0023075

Liu, S., Hossinger, A., Göbbels, S., and Vorberg, I. M. (2017). Prions on the run: How extracellular vesicles serve as delivery vehicles for self-templating protein aggregates. *Prion* 11, 98–112. doi: 10.1080/19336896.2017.1306162

Mackenzie, I. R., Bigio, E. H., Ince, P. G., Geser, F., Neumann, M., Cairns, N. J., et al. (2007). Pathological TDP-43 distinguishes sporadic amyotrophic lateral sclerosis from amyotrophic lateral sclerosis with SOD1 mutations. *Ann. Neurol.* 61, 427–434. doi: 10.1002/ana.21147

March, Z. M., King, O. D., and Shorter, J. (2016). Prion-like domains as epigenetic regulators, scaffolds for subcellular organization and drivers of neurodegenerative disease. *Brain Res.* 1647, 9–18. doi: 10.1016/j.brainres.2016.02.037

Masison, D. C., and Reidy, M. (2015). Yeast prions are useful for studying protein chaperones and protein quality control. *Prion* 9, 174–183. doi: 10.1080/19336896.2015.1027856

Monahan, Z., Ryan, V. H., Janke, A. M., Burke, K. A., Rhoads, S. N., Zerze, G. H., et al. (2017). Phosphorylation of the FUS low-complexity domain disrupts phase separation, aggregation and toxicity. *EMBO J.* 36, 2951–2967. doi: 10.15252/embj.201696394

Murray, D. T., Kato, M., Lin, Y., Thurber, K. R., Hung, I., McKnight, S. L., et al. (2017). Structure of FUS protein fibrils and its relevance to self-assembly and phase separation of low-complexity domains. *Cell* 171, 615.e616–627.e616. doi: 10.1016/j.cell.2017.08.048

Neumann, M., Sampathu, D. M., Kwong, L. K., Truax, A. C., Micsenyi, M. C., Chou, T. T., et al. (2006). Ubiquitinated TDP-43 in frontotemporal lobar degeneration and amyotrophic lateral sclerosis. *Science* 314, 130–133. doi: 10.1126/science.1134108

Olsson, T. T., Klementieva, O., and Gouras, G. K. (2018). Prion-like seeding and nucleation of intracellular amyloid-β. *Neurobiol. Dis.* 113, 1–10. doi: 10.1016/j.nbd.2018.01.015

Park, S. K., Arslan, F., Kanneganti, V., Barmada, S. J., Purushothaman, P., Verma, S. C., et al. (2018). Overexpression of a conserved HSP40 chaperone reduces toxicity of several neurodegenerative disease proteins. *Prion* 12, 16–22. doi: 10.1080/19336896.2017.1423185

Park, S. K., Hong, J. Y., Arslan, F., Kanneganti, V., Patel, B., Tietsort, A., et al. (2017). Overexpression of the essential Sis1 chaperone reduces TDP-43 effects on toxicity and proteolysis. *PLoS Genet.* 13:e1006805. doi: 10.1371/journal.pgen.1006805

Patel, B. K., and Liebman, S. W. (2007). "Prion-proof" for [PIN^+]: infection with *in vitro*-made amyloid aggregates of Rnq1p-(132–405) induces [PIN^+]. *J. Mol. Biol.* 365, 773–782. doi: 10.1016/j.jmb.2006.10.069

Paul, K. R., Molliex, A., Cascarina, S., Boncella, A. E., Taylor, J. P., and Ross, E. D. (2017). Effects of mutations on the aggregation propensity of the human prion-like protein hnRNPA2B1. *Mol. Cell Biol.* 37, e00652–e00716. doi: 10.1128/mcb.00652-16

Pérez-Losada, J., Pintado, B., Gutiérrez-Adán, A., Flores, T., Bañares-González, B., del Campo, J. C., et al. (2000). The chimeric FUS/TLS-CHOP fusion protein specifically induces liposarcomas in transgenic mice. *Oncogene* 19, 2413–2422. doi: 10.1038/sj.onc.1203572

Polymenidou, M., and Cleveland, D. W. (2011). The seeds of neurodegeneration: prion-like spreading in ALS. *Cell* 147, 498–508. doi: 10.1016/j.cell.2011.10.011

Prusiner, S. B. (1998). Prions. *Proc. Natl. Acad. Sci. U S A* 95, 13363–13383. doi: 10.1073/pnas.95.23.13363

Prusiner, S. B. (2013). Biology and genetics of prions causing neurodegeneration. *Annu. Rev. Genet.* 47, 601–623. doi: 10.1146/annurev-genet-110711-155524

Rabizadeh, S., Gralla, E. B., Borchelt, D. R., Gwinn, R., Valentine, J. S., Sisodia, S., et al. (1995). Mutations associated with amyotrophic lateral sclerosis convert superoxide dismutase from an antiapoptotic gene to a proapoptotic gene: studies in yeast and neural cells. *Proc. Natl. Acad. Sci. U S A* 92, 3024–3028. doi: 10.1073/pnas.92.7.3024

Rhoads, S. N., Monahan, Z. T., Yee, D. S., Leung, A. Y., Newcombe, C. G., O'Meally, R. N., et al. (2018a). The prion-like domain of FUS is multiphosphorylated following DNA damage without altering nuclear localization. *Mol. Biol. Cell* 29, 1786–1797. doi: 10.1091/mbc.E17-12-0735

Rhoads, S. N., Monahan, Z. T., Yee, D. S., and Shewmaker, F. P. (2018b). The Role of post-translational modifications on prion-like aggregation and liquid-phase separation of FUS. *Int. J. Mol. Sci.* 19:E886. doi: 10.3390/ijms19030886

Ross, E. D., Maclea, K. S., Anderson, C., and Ben-Hur, A. (2013). A bioinformatics method for identifying Q/N-rich prion-like domains in proteins. *Methods Mol. Biol.* 1017, 219–228. doi: 10.1007/978-1-62703-438-8_16

Shang, Y., and Huang, E. J. (2016). Mechanisms of FUS mutations in familial amyotrophic lateral sclerosis. *Brain Res.* 1647, 65–78. doi: 10.1016/j.brainres.2016.03.036

Sharma, A., Lyashchenko, A. K., Lu, L., Nasrabady, S. E., Elmaleh, M., Mendelsohn, M., et al. (2016). ALS-associated mutant FUS induces selective motor neuron degeneration through toxic gain of function. *Nat. Commun.* 7:10465. doi: 10.1038/ncomms10465

Shelkovnikova, T. A., Robinson, H. K., Southcombe, J. A., Ninkina, N., and Buchman, V. L. (2014). Multistep process of FUS aggregation in the cell cytoplasm involves RNA-dependent and RNA-independent mechanisms. *Hum. Mol. Genet.* 23, 5211–5226. doi: 10.1093/hmg/ddu243

Sondheimer, N., Lopez, N., Craig, E. A., and Lindquist, S. (2001). The role of Sis1 in the maintenance of the [RNQ^+] prion. *EMBO J.* 20, 2435–2442. doi: 10.1093/emboj/20.10.2435

Sreedharan, J., Blair, I. P., Tripathi, V. B., Hu, X., Vance, C., Rogelj, B., et al. (2008). TDP-43 mutations in familial and sporadic amyotrophic lateral sclerosis. *Science* 319, 1668–1672. doi: 10.1126/science.1154584

Stein, K. C., Bengoechea, R., Harms, M. B., Weihl, C. C., and True, H. L. (2014). Myopathy-causing mutations in an HSP40 chaperone disrupt processing of specific client conformers. *J Biol. Chem.* 289, 21120–21130. doi: 10.1074/jbc.m114.572461

Sun, Z., Diaz, Z., Fang, X., Hart, M. P., Chesi, A., Shorter, J., et al. (2011). Molecular determinants and genetic modifiers of aggregation and toxicity for the als disease protein FUS/TLS. *PLoS Biol.* 9:e1000614. doi: 10.1371/journal.pbio.1000614

Tanaka, M., Chien, P., Naber, N., Cooke, R., and Weissman, J. S. (2004). Conformational variations in an infectious protein determine prion strain differences. *Nature* 428, 323–328. doi: 10.1038/nature02392

Tariq, A., Lin, J., Noll, M. M., Torrente, M. P., Mack, K. L., Murillo, O. H., et al. (2018). Potentiating Hsp104 activity via phosphomimetic mutations in the middle domain. *FEMS Yeast Res.* 18:foy042 doi: 10.1093/femsyr/foy042

Tenreiro, S., Reimão-Pinto, M. M., Antas, P., Rino, J., Wawrzycka, D., Macedo, D., et al. (2014). Phosphorylation modulates clearance of alpha-synuclein inclusions in a yeast model of Parkinson's disease. *PLoS Genet.* 10:e1004302. doi: 10.1371/journal.pgen.1004302

Toombs, J. A., McCarty, B. R., and Ross, E. D. (2010). Compositional determinants of prion formation in yeast. *Mol. Cell Biol.* 301, 319–332. doi: 10.1128/mcb.01140-09

Tradewell, M. L., Yu, Z., Tibshirani, M., Boulanger, M. C., Durham, H. D., and Richard, S. (2012). Arginine methylation by PRMT1 regulates nuclear-cytoplasmic localization and toxicity of FUS/TLS harbouring ALS-linked mutations. *Hum. Mol. Genet.* 21, 136–149. doi: 10.1093/hmg/ddr448

True, H. L., Berlin, I., and Lindquist, S. L. (2004). Epigenetic regulation of translation reveals hidden genetic variation to produce complex traits. *Nature* 431, 184–187. doi: 10.1038/nature02885

Vance, C., Rogelj, B., Hortobagyi, T., De Vos, K. J., Nishimura, A. L., Sreedharan, J., et al. (2009). Mutations in FUS, an RNA processing protein, cause familial amyotrophic lateral sclerosis type 6. *Science* 323, 1208–1211. doi: 10.3410/f.1158010.622282

Wang, F., Wang, X., Yuan, C. G., and Ma, J. (2010). Generating a prion with bacterially expressed recombinant prion protein. *Science* 327, 1132–1135. doi: 10.1126/science.1183748

Wegrzyn, R. D., Bapat, K., Newnam, G. P., Zink, A. D., and Chernoff, Y. O. (2001). Mechanism of prion loss after Hsp104 inactivation in yeast. *Mol. Cell Biol.* 21, 4656–4669. doi: 10.1128/mcb.21.14.4656-4669.2001

Wickner, R. B. (1994). [URE3] as an altered URE2 protein: evidence for a prion analog in *Saccharomyces cerevisiae*. *Science* 264, 566–569. doi: 10.1126/science.7909170

Yamaguchi, A., and Kitajo, K. (2012). The effect of PRMT1-mediated arginine methylation on the subcellular localization, stress granules and detergent-insoluble aggregates of FUS/TLS. *PLoS One* 7:e49267. doi: 10.1371/journal.pone.0049267

Conflict of Interest Statement: The authors declare that the research was conducted in the absence of any commercial or financial relationships that could be construed as a potential conflict of interest.

Advantages of publishing in Frontiers

OPEN ACCESS
Articles are free to read for greatest visibility and readership

FAST PUBLICATION
Around 90 days from submission to decision

HIGH QUALITY PEER-REVIEW
Rigorous, collaborative, and constructive peer-review

TRANSPARENT PEER-REVIEW
Editors and reviewers acknowledged by name on published articles

Frontiers
Avenue du Tribunal-Fédéral 34
1005 Lausanne | Switzerland

Visit us: www.frontiersin.org
Contact us: frontiersin.org/about/contact

REPRODUCIBILITY OF RESEARCH
Support open data and methods to enhance research reproducibility

DIGITAL PUBLISHING
Articles designed for optimal readership across devices

FOLLOW US
@frontiersin

IMPACT METRICS
Advanced article metrics track visibility across digital media

EXTENSIVE PROMOTION
Marketing and promotion of impactful research

LOOP RESEARCH NETWORK
Our network increases your article's readership